

# Università degli Studi di Torino

## Doctoral School of Sciences and Innovative Technologies

Earth Sciences Department

# Doctoral Dissertation

*"Hydrologic and erosion response in burned watersheds (Piedmont, Western Italian Alps)"*

Candidate: **Damiano Vacha**

Supervisor: Prof. Giuseppe Mandrone

**XXXIII Cycle**
**2017 - 2020**

# Index

# 1 Introduction

In 2017, an unusually severe wildfire season occurred in Italy and especially in Piedmont (Western Alps). The fact had a considerable media coverage, as the smoke from the fires that hit some mountain and hilly areas reached Torino, the regional capital, making it to the headlines for a long time. In particular, a huge wildfire, extending for more than 4000 hectares, hit the Susa Valley. In this area, in the following spring, a series of flow events took place; the most important of them hit the town of Bussoleno, located in the main valley, downstream of the Comba delle Foglie watershed, causing considerable damage to buildings and infrastructures.

Since future scenarios linked to the effect of climate change predict that forest fire frequency and severity will likely increase, as will the extreme rainfall events, wildfires may constitute a looming issue in the Alpine region too.

What is observed in the USA is that where the fires increase, the statistics report an increasing number of deaths, damages, and force society to face exceptional repair costs. In fact, the impacts of forest fires can lead to new avalanche-prone slopes, a higher risk of rockfall, debris-flow, mudslides, soil erosion and water quality problems. The development of multi-hazard processes can lead to situations in which secondary events have a greater impact than primary ones on the exposed elements, both from the point of view of their potential intensity and of their spatial extension. In such cases, costs of firefighting, restoration of forests and necessary protective measures can seriously rise.

In Italy, the general situation of scarce maintenance of forested areas, especially in the wildland-urban interface contexts, increases the risk that fires may affect areas closer to human settlements, increasing both the primary risk associated with the fire and the secondary risks due to landslides and flows which can reach off-site target. In fact, most of the fires occur in hilly or mountainous areas, where both human settlements and lifelines are at risk.

For these reasons it was decided to approach the problem by analyzing nine burned areas in Piedmont in 2017, integrating field surveys, remote sensing data analysis, use of spatialized models and small-scale tests.

An attempt was made to identify the main processes and to model the erosive phenomena and flow rates of the fire-affected watersheds in the post-disturbance scenario. The applied models were developed in environments and climatic conditions which differ from those found in the Alpine environment. Nonetheless, these models have also found evidence in other regions, and in the present work they are not used to derive data in an absolute sense, but to compare the pre and post-fire scenarios, thus providing relativized results. In addition, the case study of Comba delle Foglie was analyzed in detail, describing its characteristics and the occurred phenomena.

The work is structured as follows: in Chapter 2 the aims and objectives of the work are defined and in Chapter 3 a general overview of post-fire geological hazards is presented. Chapter 4 is dedicated to the analysis of the literature on the topic, while Chapter 5 contains a description of the climate of the years 2017 and 2018. Chapters 6, 7and 8 contain - respectively - the methods used, the results obtained and a discussion of the results. Chapter 9 is reserved for the conclusions, while Chapter 10 contains the list of references.

# 2 Aims and objectives

The aims of this PhD thesis are multiple and originate from the approach to an unusual topic for the study area under examination: this requires facing the problem using a multiscale method to overcome the limitations on the quantity and quality of the available data.

The first step is to analyze the available historical series of fires and landslides to establish whether there are spatially and genetically correlated past events. Thereafter, the first objective is to evaluate the severity of the fires that occurred in 2017: to do this, the analysis of satellite data is crucial, and allows to obtain a large-scale data necessary to correctly compare the impact of the fire in the different areas. The comparison of the severity maps that quantify the effect of the fire on the sub-aerial components immediately after the fire and after months, allows to evaluate the changes occurring in what is called the "recovery phase". In fact, basically, the greatest impact occurs immediately, while with the passage of time the vegetative recovery tends to mitigate the conditions of imbalance, favoring the progressive return toward pre-fire conditions. However, in some cases, the delayed mortality of some tree species can lead to situations in which the severity of fire is greater after a few months compared to the conditions immediately following the fire. For this reason, it is necessary to assess the fire severity evaluating its temporal evolution over the first year following the fire: the task is accomplished by applying the initial and the extended fire severity assessment.

The second task is then to describe the main processes acting in burned areas. The available literature agrees in defining the increase in erosion rates, surface runoff and the development of shallow landslides as the main ones. However, the studies and analyses of these dynamics are generally carried out in environments and climates that are very different from those that characterize the Alpine and subalpine context, since most of them have been conducted in the USA. For this reason, it is necessary to validate these outcomes for the study area.

Following the first two, the third objective is to quantify the influence of fires on the propensity for geo-hydrological hazardous processes. It has been decided to model, through the use of available spatialized data, the erosion and peak discharge rates at the basin scale. Two well-known and widely validated models have been used, the RUSLE and the SCS-CN, modifying their input coefficients to replicate the contribution of the passage of fire. The approach used is deliberately simple, replicable, improvable and easy to implement in a GIS environment. It is also possible to automate it in order to make it available for the rapid production of thematic maps to support authorities and for civil protection purposes.

Moving forward, the fourth task is to conduct a detailed analysis of the Comba delle Foglie watershed, affected by multiple flows in 2018, one of which of considerable magnitude occurred on 7 June. It is

essential to characterize the effects of the fire on the watershed, to reconstruct the sequence of processes and events that occurred and to estimate the deposit volumes. Furthermore, following the application in more detail of the erosion and runoff models, to compare the results obtained with the dimensional parameters of the events occurred and to propose an explanation.

Finally, the fifth objective is to perform some simple fire simulation tests, to begin to experimentally understand the links between the characteristics of the soil, the quantities of fuels and the propagation of heat in depth.

# 3 Post-fire geological hazards

Forest fires are a natural phenomenon that burns vegetation wildland as forests, savannas, grasslands and other environments, occurring in different continents and climatic conditions; the commonly used term wildfire includes all uncontrolled vegetation fires igniting away from built-up areas. Fires are widely recognized as one of the components of the Earth system, with strong influences of carbon cycle, energy balances, climate and ecosystems dynamics (Bowman et al. 2009; Flannigan et al. 2009) and are thought to have naturally occurred in the Mediterranean since the late Devonian (Schmidt and Noack 2000). Since the beginning of land cultivation, the use of fire has contributed to the evolution of humanity and the formation and productivity of cultural landscapes. Some authors claims that fire is a natural and necessary ecological process, a way for perpetuating the spatial and temporal variability of the physical, chemical and biological attributes of the land surface (Shakesby and Doerr 2006; DellaSala and Hanson 2015).

They can affect the vegetation both above and below the ground: for example, ground fires typically ignite in soil thick with organic matter that can feed the flames, like plant roots; on the other hand, surface fires burn in dead or dry vegetation that is lying or growing just above the ground. Crown fires burn in the leaves and canopies of trees and shrubs. Wildfires can start with a natural occurrence or, more often a human-made spark. After the ignition, however, it is often the weather conditions that determine the wildfire growth and behavior. Wind, high temperatures, and little rainfall can all leave trees, shrubs, fallen leaves, and limbs dried out and primed to fuel a fire. Topography plays a big part too, in fact flames burn uphill faster than they burn downhill.

Beside the primary danger caused to people by the fire itself, when wildfire burn near communities, the fires bring with them secondary risks, sometimes even more serious, largely due to changes in the hydrological characteristics of the areas where they occur. Expansion of human development into forested areas, and human settlements localized at the bottom of forested slopes, have created a situation where wildfires can adversely affect lives and property, as can the flooding and landslides that occur in the aftermath of the fires. The reduced infiltration rates deriving from the vegetation loss and the soil exposure, associated with a general reduction of the surface roughness, leads to an increased risk of developing of flashfloods, sediment laden flows (i.e. debris and mud flows), landslides and mudslides. In fact, after a fire, slopes are stripped of vegetation and the root systems within the soil, which favors the transport of material downhill. Channels can quickly be filled with sediment, and culverts can plug; moreover, the increased runoff and the consequent increase in peak discharge in the drainage network means that the channeled waters can easily take over the accumulated sediments and give rise to sudden flows. They can exert great impulsive loads on objects in their path, and may strip vegetation, block drainage ways, and damage infrastructure.

*Figure 3.1 – Aerial view of the juxtaposition between burnt and unaffected areas in the Mompantero pine forest (Courtesy of Gipix Drone).*

The issue is particularly studied in the western United States, and in California, where many cases of disastrous events have been recorded over time. As an example, the Montecito debris flow, occurred in the Santa Barbara County in January 2018 (following the 2017 California wildfire season) caused the death of 23 people, the damaging of 400 houses and an estimated loss of $ 177 million in property damage.

Studies on the risks arising from post-fires geomorphic effects have seen growth since the last twenty years of the 1900s, and have focused on the role of ash deposition, the alteration of the physical properties of soil and rocks, the generation or enhancement of water repellent soils and in the increase in erosion rates after the fire (Parise and Cannon 2011). The effort of the scientific community on these issues has led to the identification of two predominant processes in the generation of post-fire hazards: the erosion and entrainment of material by surface runoff (fig. 3.2) and the infiltration-triggered failure and mobilization of a discrete, shallow landslide mass. These two processes act with different timing: the first originates and reach his maximum likelihood after the very first relevant rainfall events, and may continue for several years although it is unusual for post-fire debris flows to occur beyond the second rainy season. The second process, which is much less common, can occur after several years from the fire, as a consequence of the delayed mortality of the bigger trees; according to the most recent studies, however,

the probability of occurrence of the landslides returns to pre-fire conditions within five years (Rengers et al. 2020).

The decrease in probability of debris flows over time is related to the restoration of the hydrological function, because the vegetation and the soil infiltration parameters return to pre-fire conditions; depending on the characteristics of the soil, the parent rock, the topography and the vegetation, the time required to return to a condition of equilibrium varies from case to case. As an important note, it is worth mentioning another secondary hazard related to post-fire erosive processes, which is the risk of water contamination: in fact, the runoff in recently burned slopes can carry a large quantity of suspended and dissolved elements (such as nitrate, iron, nickel, lead and zinc) into the reservoirs, rivers and wetlands, which causes, amongst others, serious problems for water purification plants (Tecle and Neary 2015).

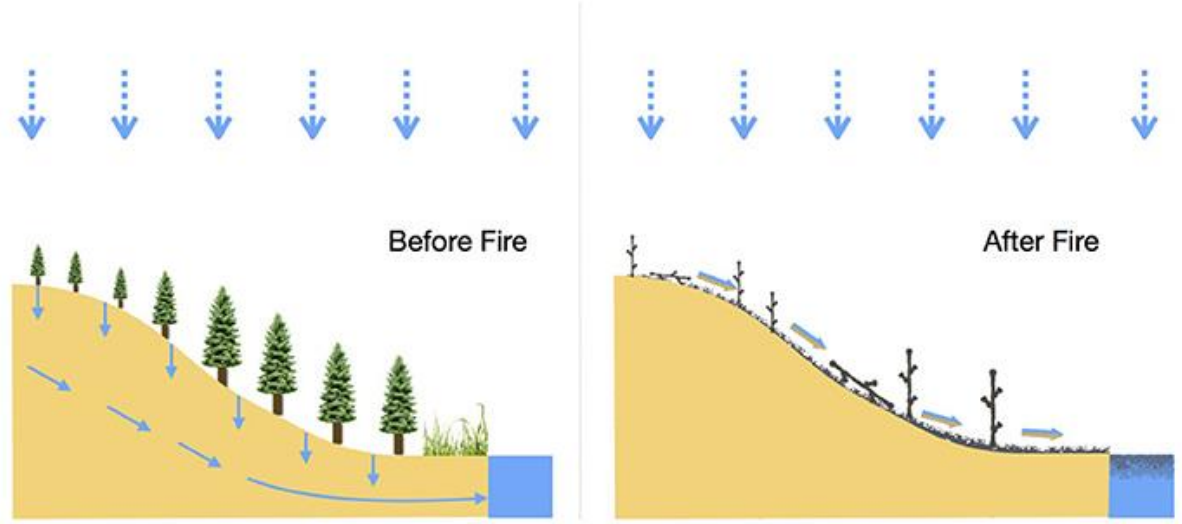


*Figure 3.2 – schematization of the process leading to post-fire increase of peak flow and erosion (Abney and Berhe 2018)*

# 4 Literature review

## 4.1 Wildfires impact

Some impacts associated with fire can be measured directly: for example, if we refer to socio economic effects, we can quantify cost of suppression, cost of rehabilitation, property loss, or human causality.

Concerning the effects of the fire on a landscape, which sum up the effects on different environment components, it is crucial to understand causes, agent, processes and results on every community composing the environment. Some factors determine the ignition of forest fires, some others the spread and the intensity of the fires, and others the fire effect on the soil.

The probability of fire occurrence is mainly determined by the soil and litter moisture and the presence of an ignition source. In turn, fuels humidity values depend on precipitation, temperature, wind and relative humidity. Once the fire has started, the intensity and spreading potential of a forest fire is influenced by other variables, such as vegetation type and structure, fuel amount, topography, wind, slope aspect, humidity (Pezzatti et al. 2009; Boboulos and Purvis 2009; Conedera and Tinner 2010; Girardin and Terrier 2015; Fréjaville et al. 2016). As a consequence, fire effects on soil constitute a very broad spectrum. They can be subdivided into physical, chemical and biological modifications (Neary et al., 1999; Úbeda and Outeiro, 2009; Mataix-Solera et al 2011), varying in magnitude and duration depending on several factors, among which the most important is fire severity that in turn depends on fire intensity. As a result of this great number of factors, and their variability, the effect of a fire can span from little or negligible damage to the most extreme scenario where all aboveground organisms are erased.

A major reason for assessing and quantifying the type and magnitude of those soil properties shift is because they are claimed to be an important indicator of the potential for excess of water runoff, enhanced erosion, landslide susceptibility and a general change in the hydrologic setting of the landscape interested (Robichaud et al. 2000; Wilson et al. 2001; Ruiz-Gallardo et al. 2004; Lewis et al. 2006; Parsons 2003; Ice et al. 2004). As some authors remarked (Robichaud et al. 2000; González-Pelayo et al. 2006) fire and burn severity measure alone are not a reliable predictor of hazardous post-fire processes, as other variables such as topography, soil type, and precipitation are important elements to be accounted for. From a side this fact suggests the need to conduct separate evaluation regarding the fire/burn effect on the soil and the post fire processes, and from the other side push the research in the direction of deepening some aspect which could help to find a reliable and robust link between the two.

## 4.2 Wildfire statistics and trends

Wildfire occurrence is governed by a complex interaction of many variables, such as climate dynamics, environmental characteristics, land use, human actions and others. Globally, the vegetated area annually affected by fire ranges between 300 million and 600 million hectares (Mouillot et al. 2005; Goldammer J. et al. 2017). The global trends in area burned during the twentieth century shows a decrease of the global average area burned by about 7% compared to previous years. Causes are thought to be the increased fire prevention, the detection and fire-fighting efficiency, the abandonment of slash-and-burn cultivation and the increase of permanent agricultural practice in some areas.

During the second half of the past century, a 10% increase in the burned area was registered, and this was attributed to the increased deforestation fires in the tropics and could be the result of a return to a more normal fire regime in areas where fire had been suppressed (Flannigan et al 2009, Doerr and Santin 2016). In the first decades of this century a slight decrease in the global area burned, evaluated in 1% – 2% $yr^{-1}$, was recorded (Giglio et al 2013, Van Lierop et al 2015).

Regional trend for the period 1996–2012 shows for Europe and Australia/New Zealand a strong decline in area burned of 5% $yr^{-1}$. Conversely, for Southeast Asia, the Middle East and boreal North America, the estimated area burned increased by 3–4%. In the whole USA area burned by wildfires experienced an increase by over 5% $yr^{-1}$ (period 1991–2015), with 2015 exceeding 40.000 $km^2$ burned.

Statistics for Europe, up to 2012, reports about 65.000 fires registered every year, with a mean vegetated land surface annually burnt of more than 0,5 million ha. Most of them (more than 85%) affects the European Mediterranean region (San-Miguel-Ayanz et al. 2012).

The 90-95% of the recorded fires are estimated to be caused by humans, either accidentally or intentionally (San-Miguel-Ayanz and Camia 2009; Georg et al. 2013). Main causes are cigarettes, fires getting out of control, flying sparks from trains or during work, arson, hot ashes and power lines. Around 10% of forest fires in the Alps are estimated to be caused by lightning strikes. Amongst the others, a major concern is given by fires affecting wild-land urban interface, usually densely inhabited by tourist in summer. Here there is an increased presence of secondary houses in a context of generalized land abandonment and higher average temperatures, thus the risk of casualties and direct damages to properties is considerably high.

Among European countries Portugal, Spain, Italy, Greece and southern France, are largely the regions more prone to wildfires: statistics covering almost three decades - from 1980 to 2009 - shows an average burned area of about 480.000 ha and 50.000 fires. Looking at general trends for Southern Europe, data shows a substantial increase of fires in the 90's and a decrease since 2000, with marked fluctuation and some outliers (i.e. 2003 and 2005, characterized by an exceptional number of fires due to weather

conditions). The annually burned area generally decreases since 1985, again with strong annual variations. For these countries more than 70% of the occurrences are registered from June to October, while in other countries most of the fires happens in springtime (San-Miguel-Ayanz et al. 2012).

Statistics for the Italian country starting from the eighties of the last century agree with the data on the European and Mediterranean scale; in fact, both the surface covered by fires and their number show a decreasing trend, albeit with some exceptions (for example 2007 and 2017, figg 4.1 and 4.2).

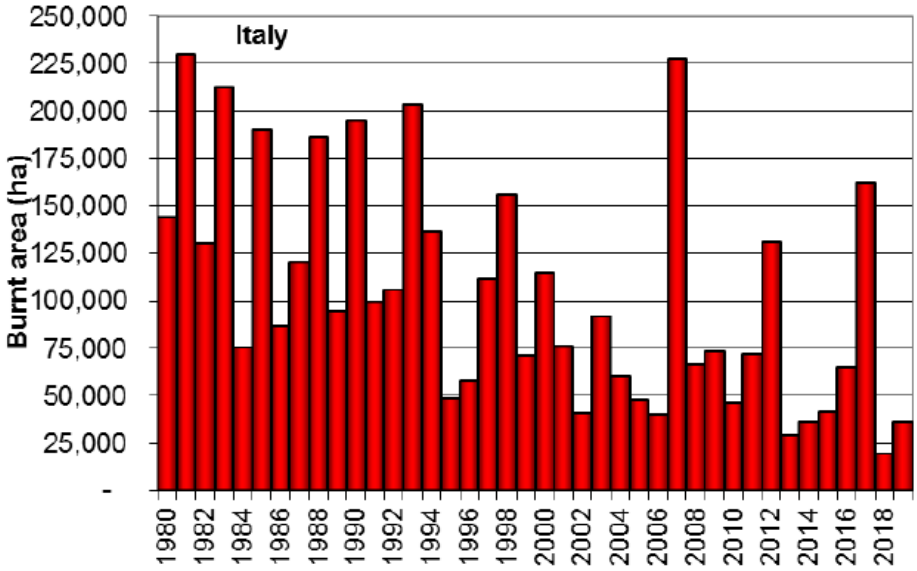


*Figure 4.1 – Burnt area in Italy (1980-2019) (San-Miguel-Ayanz et al., 2020).*

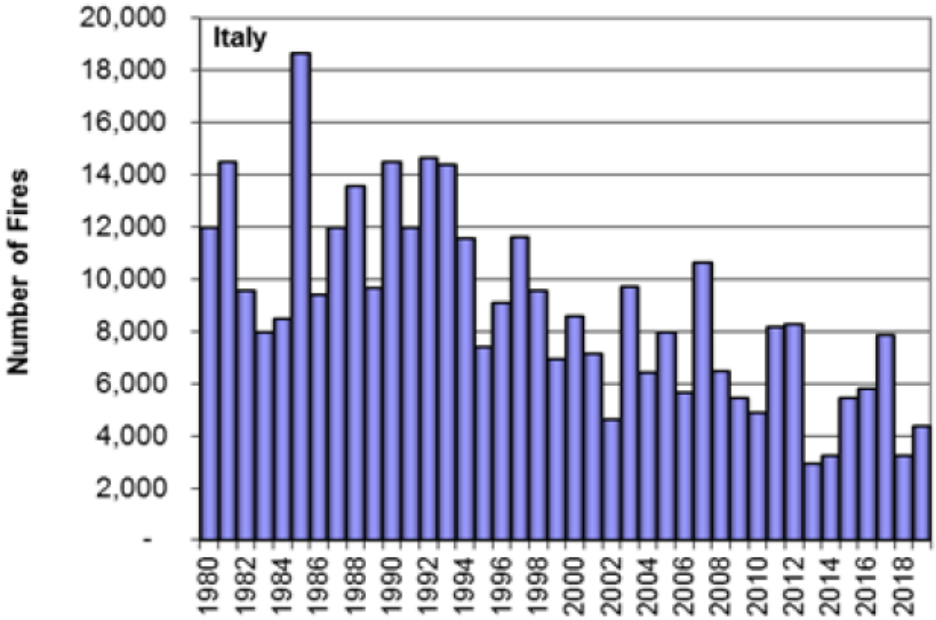


*Figure 4.2 – Number of fires registered in Italy (1980-2019) (San-Miguel-Ayanz et al., 2020).*

Statistics for the Piedmont Region covering the period 1997-2019 (figg 4.3 and 4.4) confirms the overall decreasing trend registered for the National and European data: a slight decrease in fact can be observed both for the burnt surface and number of fires. It is worth to note the exceptional value of the burned area in 2017.

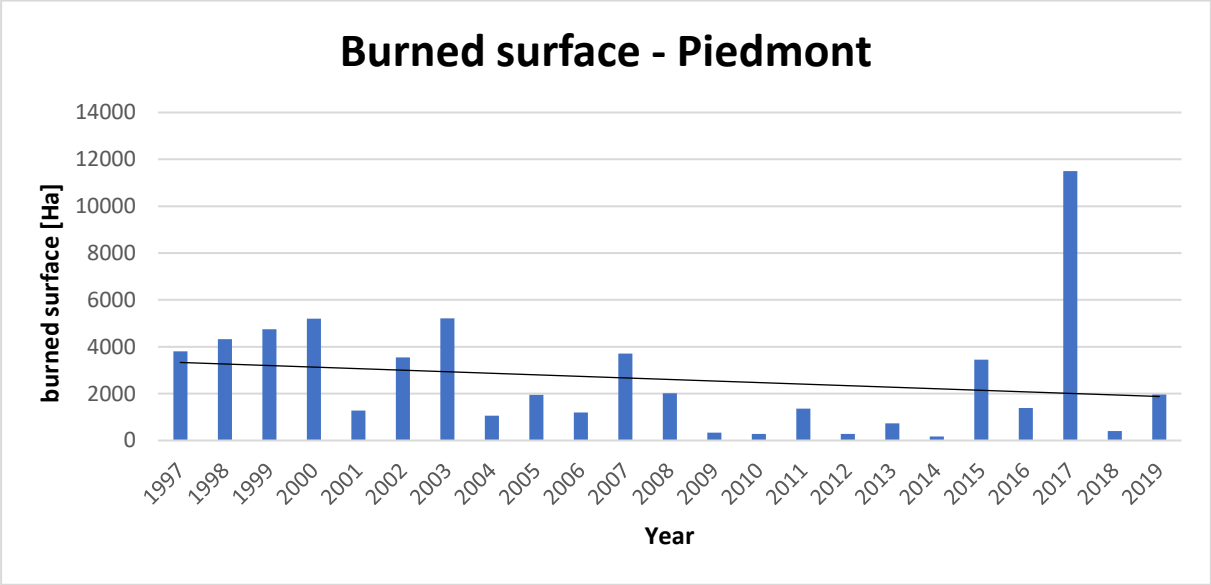


*Figure 4.3 – Burnt area for the Piedmont Region. Source: Corpo Forestale dello stato (1997-2017) and Joint Research Centre (2018-2019).*

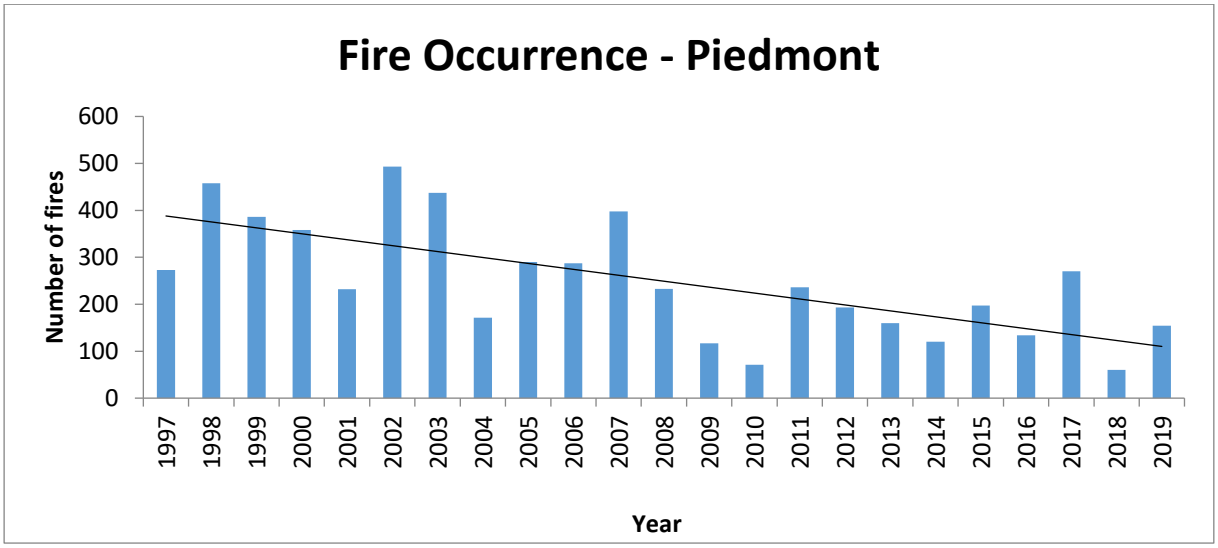


*Figure 4.4 – Number of fires for the Piedmont Region. Source: Corpo Forestale dello Stato (1997-2017) and Joint Research Centre (2018-2019).*

For the near and far future an increasing occurrence of fire is expected, and this tendency is forecasted for many regions worldwide: North and South America, central Asia, southern Europe, southern Africa and Australia (Liu et al. 2010). Also for the Alpine region forest fire frequency and severity is expected to increase in the future (Zumbrunnen et al. 2009; Moreira et al. 2011; Wastl et al. 2012; Arndt et al. 2013, Dupire et al 2019). The occurrence of higher average temperatures associated with longer drought periods, the change in forest management, rural abandonment and increased exploitation of forests for recreational purposes are generally known causes that increase the probability and the intensity of wildfires (e.g. Dupire et al. 2019; Vacchiano et al. 2018; Pezzatti et al. 2013). The risk of wildfire is enhanced in forests dominated by coniferous tree species due to the resin, which is highly flammable, thus leading to a major concern for Alpine region where large portions are populated by Norway spruce (Picea abies) or Scots pine (Pinus sylvestris). Spruce dominated forests at lower altitudes are already suffering from climate change and the temperature and drought expected trend will lead to a worsening of the fires predisposing factors (Muller). Moreover, the fire susceptibility could increase in area historically less endangered; an example from the last decades is the case for the Central-European beech mountain forests in some drought periods (Ascoli et al. 2013a; Maringer et al. 2016). At higher altitude, grasslands and shrub stands of mountain pine (Pinus mugo), when in continuity with forest, could act as a triggering point as they provide a great amount of easily burnable materials. In addition to climate change, many other causes could contribute to the increasing in fire occurrence and spreading: for example storms and bark beetle impact can lead to an increase of available fuel, as well as rural abandonment. Also, as an increase of dry periods is expected, the fire ignition due to lightning could become a problem of major concern. (Conedera et al, 2006)

## 4.3 Wildfire impacts metrics

### 4.3.1 Heat transmission

The energy generated and released during the onset of a fire and the following burning phase is the driving force behind the physical, chemical and biological effects in the soil (De Bano et al. 2010, Neary et al. 2005, Neary and Leonard 2020). The soil thermal transmission phenomena occur by means of radiation, conduction, convection, mass transport, vaporization and condensation.

• Radiation is defined as the transfer of heat from one body to another, not in contact with it, by electromagnetic wave motion. Radiated energy flows outward in all directions from the emitting source until it encounters a material capable of absorbing it (Neary et al. 2005). The net flow of thermal radiative energy for a single frequency, across a surface of an arbitrary orientation, is represented by the spectral radiative energy flux:

$$q_v = \int_0^{4\pi} I_v \cos\theta \, d\Omega$$

Where Ω is the solid angle ($d\Omega = \sin\theta d\theta d\phi$) and $I_v$ is the intensity of radiation expressed as energy per unit area per unit solid angle (Fig 4.5) within a unit frequency interval (DiNenno et al. 2002).

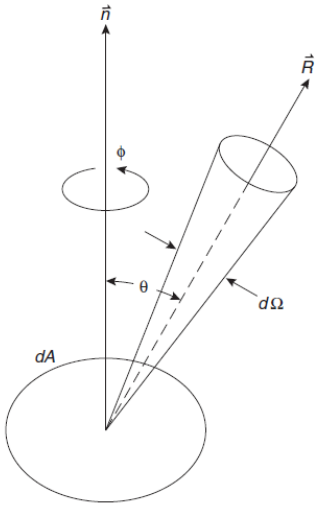


*Figure 4.5 – Coordinate system for radiation intensity (DiNenno et al. 2002).*

• Conduction is the transfer of heat by molecular activity from one part of a substance to another part, or between substances in contact, without appreciable movement or displacement of the substance as a whole (Neary et al 2005). When a temperature gradient exists, heat will be transferred from the higher to the lower temperature region. The rate of the heat flow ($\mathbf{q_k}$) is proportional to the temperature gradient ($\mathbf{dT/dx}$) times the area in which the heat is transferred (**A**) through the thermal conductivity (**k**) of the medium. The rate equation is expressed by the Fourier's Law:

$$qk = -kA\frac{dT}{dx}$$

• Convection is the process whereby heat is transferred from one point to another by the mixing of one portion of a fluid with another fluid. In case of porous media, heat transfer occurs also between fluid and solid phase of the medium. The rate of convection heat transfer (qc) between fluid and solid can be written in the form:

$$qc = \bar{h}_c \, A(T_s - T_{f,\infty})$$

Where $\bar{\boldsymbol{h}}_{\boldsymbol{c}}$ = unit thermal convective conductance at fluid solid interface, W/m²K;

**A** = surface area in contact with fluid, m²;

$\mathbf{T_s}$ = surface temperature, K;

$\mathbf{T_{f,\infty}}$ = temperature of undisturbed fluid far away from heat-transfer surface, K.

Vaporization and condensation are important and very efficient coupled heat transfer mechanisms which can be treated as a part of the convective heat transfer. By comparison, free convection coefficient of water range from 20 to 100 W/m²K while free convection coefficient for condensing water vapor range from 5000 to 100000 W/m²K (Kreith and Black 1980).

Based on current knowledge, heat conduction and convection are the most relevant processes responsible for the soil heating during wildfires, while radiation contribution is marginal. The way these processes affect the soil depends mostly on the quantity of released energy and the duration of the heating. This, in turn, is related to the amount of available fuel and type of fire: crown fires are usually large scale, fast-moving, wind-driven and usually uncontrollable. They often have a deep flame front. Despite this, the fire front usually pass rapidly through the tree canopy causing little soil heating, unless sufficient fuel is accumulated from forest floor to the crowns. Slowly spreading surface fires, on the other hand, are usually small-scale and characterized by a thick flame front. They are capable of combusting a large part of the forest biomass and can substantially transfer heat to the soil. Wind-driven grass fires spread quickly and sometimes over large areas. In these types of fire, the available biomass is limited, so the fire effect on soil is often irrelevant. Smouldering fires are flame-free, slow moving and long lasting unimpressive, but frequently have long burnout times. These affects considerably the soil and subsoil, releasing a remarkable amount of heat within the soil.

The wildfire effect on the vegetation can be measured based on the evaluation of several factors. The definition and description of the principal ones is reported in the following paragraph.

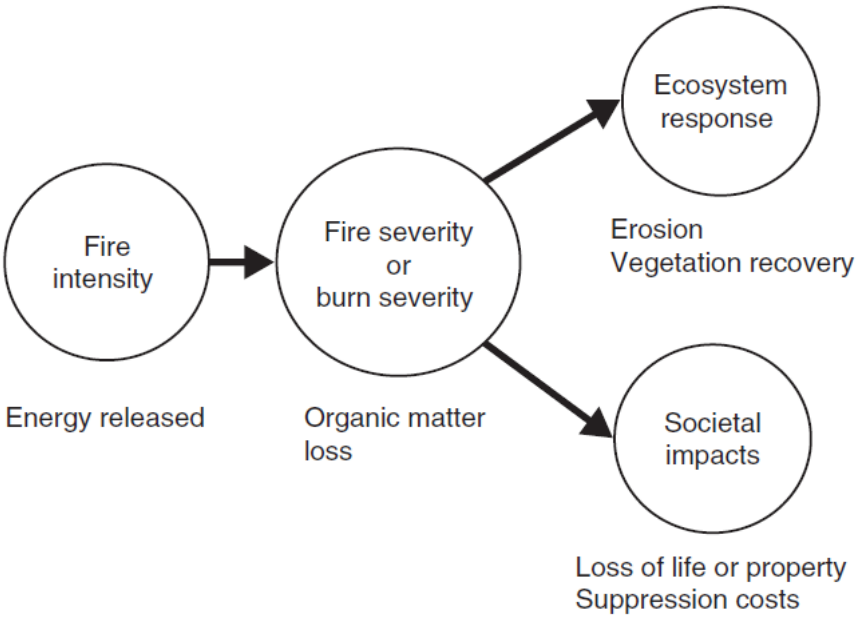


*Figure 4.6 – Relationships between the energy output from a fire, the impact as measured by the loss in organic matter and the ecosystem response and societal impacts (Keeley, 2009).*

## 4.3.2 Fire descriptors

### 4.3.2.1 Fire intensity

Fire intensity describes the physical process which cause the energy release due to combustion of organic matter (Keeley 2009). It can be defined as a measure of the energy flux in a given time, or equally as the volumetric energy multiplied by the velocity at which this energy is propagating. It is expressed in $Wm^{-2}$. This formulation of the radiative energy is appropriate when studying fire impact through remote sensing (Wooster et al. 2003; Dennison et al. 2006).

Byram (1959) proposed a different formulation, used especially when facing the fire propagation, defined as fireline intensity, which is represented by the rate of heat transfer per unit length of the fireline ($kWm^{-1}$). Conceptually this value describes the amount of energy released by convection or radiation in correspondence of the fire front.

Fireline intensity is more suitable for forested landscape, when the relationship between flame length and burning effects on trees or other biological modifications caused by the fires.

When facing impact of fires on soils, such as soil duff consumption or the development of hydrophobic layers into the soil, different metrics parameters can be used: in such cases the temperature at the soil interface and the duration of the heating, or the maximum temperature reached at a certain depth may be closely tied to the physical-chemical effects (DeBano 2000). In fact, a very limited amount of the energy

released after the combustion of aboveground fuels can reach the soil by convection or radiation (Bradstock and Auld 1995).

In summary, fire intensity is defined as the energy released during various fire stages; depending on the different purposes, different expressions can be used from time to time, including reaction intensity, fireline intensity, temperature, residence time, radiant energy and others (Keeley 2009).

#### 4.3.2.2 Fire severity

Fire severity refers to the degree of environmental change caused by the fire (White and Pickett 1985, Simard 1991, Jain et al. 2004, NWCG 2006) or, more operationally, on the loss of vegetation both aboveground (Keeley 2009, Agee 2007, van Wagner 1973, Moreno and Oechel 1989, Tolhurst 1995, Dickinson and Johnson 2001) and below the ground (Wells et al. 1979, Stronach and McNaughton 1989, Neary et al. 1999, Ice et al. 2004).

Ryan and Noste (1985) published one of the first attempt for quantifying this entity, developing an index encompassing a matrix of impacts of the fire on soil and vegetation (Fig. 4.7).

| Fire severity | Description |
|---|---|
| Unburned | Plant parts green and unaltered, no direct effect from heat |
| Scorched | Unburned but plants exhibit leaf loss from radiated heat |
| Light | Canopy trees with green needles although stems scorched |
| | Surface litter, mosses, and herbs charred or consumed |
| | Soil organic layer largely intact and charring limited to a few mm depth |
| Moderate or severe surface burn | Trees with some canopy cover killed, but needles not consumed |
| | All understorey plants charred or consumed |
| | Fine dead twigs on soil surface consumed and logs charred |
| | Pre-fire soil organic layer largely consumed |
| Deep burning or crown fire | Canopy trees killed and needles consumed |
| | Surface litter of all sizes and soil organic layer largely consumed |
| | White ash deposition and charred organic matter to several cm depth |

*Figure 4.7 – Changes in aboveground vegetation and soil organic matter related to fire severity (Keeley, 2009).*

This index appears to capture the fire intensity signals and to be related to fireline intensity, fire residence time and humidity of soil and vegetation. Chatto and Tolhurst (2004), as well as Cram et al. (2006), have found that this index captures the fire intensity signal and appears to be primarily a function of fireline intensity, residence time (heating duration) and soil and plant dryness. Other contributions should be expected by other term such as pre-fire species composition, stand age, topography, substrate, and climate in moving from fire severity to intensity (Keeley 2009). In a similar way, other authors proposed analogous indexes for the fire severity assessment (Buckley 1993, Williams et al. 1998, Catchpole 2000), tailoring them based on the focus of the study. For instance, focusing on soil effects the U.S. BAER (Burned Area Emergency Response) developed a framework, named soil burn severity assessment, for evaluating the link between fire effects and hazardous post-fire processes (erosion, floods and landslides).

Some authors demonstrated a good correlation between satellite remote sensing indexes (especially the Normalized Difference Vegetation Index, NDVI) and fire severity estimated in the field (Turner et al. 1994, Conard et al. 2002, Miller and Yool 2002, Chafer et al. 2004). This correlation appears mostly appropriate for forested areas, so the usage of such index in other context (different vegetation type) must be carefully evaluated (Hammill and Bradstock 2006).

Plant mortality, a measure for the biomass consumption, is also used for estimating fire severity, and is well correlated with fire intensity (Wade 1993, Chappell and Agee 1996, McCaw et al. 1997, Larson and Franklin 2005); numerous studies have shown it is correlated with fire intensity. Since mortality is sometimes evident in the first year after the fire, and because of the influence of resprouting capacity of some plant species, it should be carefully evaluated and used only for non-resprouting species.

#### 4.3.2.3 Burn severity

The term burn severity, which is common in remote sensing application, had an increasing diffusion in the scientific literature in the last years, and its meaning is close to that of fire severity, with whom it shares some metric used for its measurement. In the U.S., BAER context it is used in place of fire severity, while the Glossary of Wildland Fire (NWCG 2006) defines it as the "loss of organic matter in or on the soil surface and aboveground organic matter conversion to ash" (being equal to the BAER definition of soil burn severity (Parsons 2003).

Within the BAER assessment, the differenced Normalized Burn Ratio (dNBR), is used in the so-called Burned Area Reflectance Classification (BARC), resulting in a good correlation with fire severity field validation (Robichaud et al. 2007b). Although several remote sensing studies applies the concepts of the fire severity for field validation (White et al. 1996, Rogan and Franklin 2001, Miller and Yool 2002, Chafer et al. 2004, Hammill and Bradstock 2006, Roldán-Zamarrón et al. 2006), in others the field validation includes parameters belonging to both fire severity and ecosystem response (vanWagtendonk et al. 2004, Cocke et al. 2005, Epting et al. 2005, Chuvieco et al. 2006). An example of this latter case is the protocol called Composite Burn Index (CBI) (Key and Benson 2006), in which fire effects are coupled with information on resprouting of herbs, shrubs and hardwood trees, and seedling colonization. Some authors suggest critical aspects on this approach, stating that although dNBR correlates significantly with fire severity, this signal is not necessarily a good predictor of ecosystem responses (Keeley 2009).

A major reason for post-fire assessments of fire or burn severity is because it is suggested to be an important indicator of the potential for water runoff and erosion increase (Robichaud et al. 2000, Wilson et al. 2001, Ruiz-Gallardo et al. 2004, Lewis et al. 2006) and of changes in soil hydrologic function (Parsons 2003, Ice et al. 2004). Conceptually, this inference is logical based on various types of indirect evidence. For example, loss of biomass exposes more soil surface, which increases the kinetic force of precipitation on the soil surface and the proportion of the overland flow (Moody and Martin 2001).

Further, loss of soil organic matter alters the binding capacity of soil and results in other structural changes that can affect erosional processes (Hubbert et al. 2006). Post-fire modification could also include the formation of hydrophobic layers, even if this aspect seems to be very uneven and not so strongly linked to fire severity (Robichaud 2000, Lewis et al. 2006, Cannon et al. 2001, Doerr et al. 2006).

In general, there is still little direct evidence that fire severity measurements are a reliable indicator of specific changes in hydrologic or other ecosystem functions (Robichaud et al. 2000, González-Pelayo et al. 2006), and some scholars even suggest that fire severity classifications are unsuitable for predicting fire impacts on soil hydrological responses (Doerr et al. 2006). The primary reason is that ecological responses such as erosion, overland water flow and debris flows are affected not only by the fire characteristics, but also by topography, soil type, rates of weathering, fire-free interval, and precipitation (Cannon et al. 2001, Moody and Martin 2001, Nearing et al. 2005). In short, the cause responsible for hydrologic responses to fire is multi-factorial and so each aspect should be clarified separately for a better comprehension of the process.

#### 4.3.2.4 Depth of burn

The relationship of fire intensity to fire severity is hard to define because of difficulties in relating environmental responses to the fire processes (Ryan 2002). It is not always possible to estimate the effects of fire on soil, vegetation, and air measuring or inferring only fire intensity because other factors are involved. The impact of fire on soil can be expected to vary directly with the depth of burn as reflected in the amount of surface litter, organic soil horizons, and woody fuel consumed (Ryan 2002, Neary and DeBano 2005). For example, the depth of lethal heat (approximately 60°C) penetration into the soil can be expected to increase with the increasing depth of surface organic material that is burned, and with the duration of burning. Burn depth can be classified, if no other information is available, on the basis of visual observation of the degree of fuel consumption and charring on residual plant and soil surfaces (Ryan and Noste 1985). Neary and Leonard (2020) gives a summary of the relationships between depth of burn and charring of plant materials in grassland, which can be used as a guide for classification (fig 4.8).

| Burn class | Category | Description |
|---|---|---|
| Unburned | Surface | Fire did not burn on the surface. |
| | Fuels | Some vegetation injury may occur from radiated or convected heat resulting in an increase in dead fuel mass. |
| | Occurrence | A wide range exists in the percent unburned in natural fuels. Under marginal surface fire conditions the area may be >50%. Under severe burning conditions <5% is unburned. 10 to 20% of the area in slash burns is unburned. |
| Light | Surface | Leaf litter is charred or consumed but some plant parts are discernable. Herbaceous stubble extends above the soil surface. Some plant parts may still be standing, bases not deeply burned, and still recognizable. Surface is black after fire. Charring is limited to <0.2 cm into the soil. |
| | Fuels | Typically, 50 to 90% of herbaceous fuels are consumed and much of the remaining fuel is charred. |
| | Occurrence | Burns are spotty to uniform, depending on grass continuity. Light depth of burn occurs in grasslands when soil moisture is high, fuels are sparse, or fires burn under high wind. This is the dominant type of grassland burning. |
| Moderate | Surface | In upland grasslands litter is consumed. Charring extends to <0.5 cm into mineral soil, otherwise soil not altered. Gray or white ash quickly disappears. In grasslands, sedge meadows and prairies growing on organic soils, moderate fires partially burn the root-mat. |
| | Fuels | Herbaceous plants are consumed to the ground-line. |
| | Occurrence | Moderate depth of burn tends to occur when soil moisture is low and fuels are continuous. Then burns tend to be uniform. In discontinuous fuels, high winds are required for high coverage in moderate depth of burn. |
| Deep | Surface | In grasslands growing on mineral soil the litter is completely consumed leaving a fluffy white ash surface that soon disappears. Charring to depth of 1 cm in mineral soil. Soil structure slightly altered. In grasslands growing on deep organic soils, fires burn the root-mat and the underlying peat or muck to varying depths. |
| | Fuels | All above ground fuel is consumed to charcoal and ash. |
| | Occurrence | In uplands, deep depth of burn is limited to areas beneath the occasional log or anthropogenic features (e.g., fences, corrals). In wetland grasslands, deep burns can occur over large areas when the water table is drawn down. |

*Figure 4.8 - Depth of burn classes in grassland (Neary and Leonard 2020).*

## 4.4 Wildfire effects on soil

Wildfires effects concern both the biotic and the abiotic components of the environment. Omitting the post-fire dynamics regarding the vegetation regrowth and recovery, and others ecological implications of wildfires, from a geological hazard perspective the focus has to be set on various slope processes that may arise in the post-fire window. The predisposing causes of this processes, linked to the fire disturbance, are claimed to be litter and vegetation removal, ash deposition, soil physical and chemical alteration and the generation or destruction of water-repellent soils (Parise and Cannon 2012). These, together with rainfall

and geomorphological setting are the key components of the post-fire hazard framework. By modifying soil characteristics and the way it is able to cope with the rainfall, a shift in the ratio between infiltration and overland flow in favor of the latter is induced (at least in the short time); in addition, thanks to the enhanced soil erodibility and erosivity, the overland flow solid transport is increased. The single effects are described in the following paragraphs.

Tree canopies intercept up to 42% of rainfall and reduce rainfall intensity (Hanshaw et al. 2009), they prevent the soil particle detachment during rainfall events, and the roots network improves the mechanical strength of the soil, increases the flow roughness so reducing the overland flow velocity. The rarefaction of the bigger trees crown, the shrubs density and the grass coverage, increase the force of impact exerted by the rain drops on the soil and on the wildfire ash deposits. Moreover, it temporarily reduces the soil-moisture transpiration (Loaiciga et al. 2001). Combustion of litter and duff can also reduce rainfall interception and storage rates, changing the soil-moisture dynamics (Shakesby and Doerr 2006, Parise and Cannon 2012). In addition, the vegetation residuals of combustion, like char, may represent an easily erodible material themselves. The roots of the vegetation increase the geomechanical stability, in particular the shearing resistance of the soil in which they are growing. This of course depends on the root's distribution within the soil and their mechanical performances such as tensile, compressive and bending strength (Schwarz et al 2015, Sanchez-Castillo et al 2017). Moreover, they also act on the soil moisture and matric suction. Several studies focus on the role of roots in the stream banks stability and other channel processes (Thorne 1990, Abernethy 1999, Simon and Collison 2002) and their contribution has been modeled in different ways (Wu et al 1979, Pollen and Simon 2005). The negative effects exerted by the fire on root reinforcement capacity vary depending on fire severity and type of vegetation; in the Alps, for example, the ability of the bigger tree roots to prevent shallow landslides is claimed to be compromised for at least 40 years in case of high severity fires in forest and poor resprouting capacity species (i.e. European beech)(Gehring et al 2019). In grassland the vegetation recovery is usually more rapid, as in most of the cases the fire occurrence is quite unnoticeable after a year (Neary 2020). Despite the fast recovery of these environment, they are subject to erosion, nutrient mobilization, and hydrologic conditions alteration (Ravi et al 2009, Wright et al 1976).

Ash is one of the products that results from the combustion of the fuels (biomass, necromass, soil organic matter) and consists of mineral materials and charred organic components. Its quantity and characteristics depend on fuel load, fuel type and combustion completeness (Bodi et al 2014). It can be either found in discontinue patches or blanketing the soil with a continuous layer. It is believed to being capable to affect infiltration and runoff generation: ash hydraulic conductivity, in facts, spans three order of magnitude and is capable to decrease dramatically after the ash initial hydration. Low and high combustion ash are responsible for a decrease in the hydraulic conductivity due to either a low porosity or the generation of a chemical ash crust (Balfour 2013). The crusting and hardening behavior of ash when wetted (due to the

mineralogical transformation of calcium oxide CaO), found especially in case of high combustion completeness, could have the effect of a lowering in the hydraulic conductivity (Cerda 1998, Balfour and Woods 2013, Bodi et al 2014). Mid-combustion ash, on the contrary, acts as a capillary barrier increasing the water-storage capacity, thus favoring a hydrologic buffering effect (Woods and Balfour 2008, Balfour 2013). Given the high erodibility, moreover, ash can be easily removed by wind, dissolution or water erosion, and it might be removed and redistributed within days or weeks after the fire (Cerdà and Doerr, 2008, Larsen et al 2009, Pereira et al. 2013). Some studies (Mallik et al., 1984; Etiégni and Campbell, 1991) suggested that the downward migration of the ash particles could determine a severe pore clogging, resulting in a sealing effect responsible for the increase in the water runoff at the soil-ash interface, thus leading to an increase in the sediment entrainment. However, recent researches (Cerdà, 1998a, Woods and Balfour, 2008; Larsen et al 2009) proved the ability of ash to reduce soil sealing, and conversely demonstrate that the development of a structural soil seal enhancing runoff is due to the raindrop impacts on the exposed mineral soil after the ash is removed. Other studies agree, having shown that a wide variety of surface cover types (straw mulch, crop residues, leaves, grasses, etc.) can protect against soil sealing (Morin and Benyamini 1977, Poesen 1986, Kinnell et al. 1990, Moss and Watson 1991; Ruan et al. 2001).

Summarizing, the soil-ash sequence act as a two-layer system which can result in an increase, decrease or have no effect on the runoff; this depends on ash depth and type, soil type and rainfall characteristics (Bodi et al 2014). In any case, only on few occasions ash has been claimed as a direct cause of post-fire mass movement such as debris flow (Cannon et al 2001, Smith et al 2012).

Soil physical and chemical alteration due to the fire effect are usually related to a transition to a more friable, less cohesive and more erodible soil. This can be related to the combustion of organic matter in the soil that results in a decrease in the aggregate stability. Moreover, in literature are reported modification of other parameters such as particle-size distribution, bulk density, plasticity and elasticity. (DeBano et al. 1998, Neary et al. 1999, Hubbert et al. 2002, Parise and Cannon 2012). As an example, bulk density is reported to increase as the organo-mineral aggregates collapse because of the pore sealing by the finer particles (Giovannini et al 1988). The reduction or destruction of fungal and microbial activity, which produce cohesive compound as hyphae, is reported as a destabilizing effect (Shakesby and Doerr 2006). The amount of the modifications reported is correlated with the type of soil and the temperature reached within the burned soil horizon (Guerrero et al. 2001) (fig. 4.9).

Aggregate stability, in particular, is a commonly used parameter for assessing the resistance of the soil to external factors. In the literature the effect of fire on this feature is apparently contradictory: in most cases, fire leads to fragmentation of aggregates and loss of stability, while in some other studies no significant changes have been reported; in a few cases an increase in the aggregate stability has been observed (see Matax-Solera et al. 2011 for an extensive review and list of references). For example, high temperature can

fuse the soil particle, generating a coarser texture with less cohesive aggregates; in addition, if the temperature reaches a value above 460 °C clays lose the hydroxyl group which promotes a soil structure weakening (DeBano et al. 1998, Neary et al. 1999, Parise and Cannon 2012). In some soils, the heat exchanged lead to a new aggregation of particles by recrystallization of Fe and Al oxides and thus the wettability of aggregate surfaces may be reduced, causing an increase in aggregate stability (Giovannini and Lucchesi 1983; Giovannini 1994; Mataix-Solera and Doerr 2004).

Another direct effect of the fire is the change in soil wettability: fire, depending on the amount/type of fuels and the temperature reached, can produce water repellent layers in non-repellent soil, or modify either positively and negatively the pre-existing water repellent attitude (De Bano et al 1970, Certini 2005, Shakesby and Doerr 2006). Water repellency has been recorded in many unburned soils, such as eucalypt and coniferous forest (Doerr et al. 2000, Shakesby et al. 2007) and in the chaparral environment of southern California (DeBano 2000b, Cawson et al. 2016). The physico-chemical process responsible for the creation of new repellent layers is the volatilization, and subsequent condensation, of hydrophobic organic substances available in the litter and topsoil. The process is dependent from temperature, oxygen availability and duration of heating (Cawson et al. 2016). Laboratory tests shows little effects for temperatures lower than 175 °C, maximum effect for temperature from 175 to 200 °C and destruction of water repellency from 280 to 400 °C (DeBano 2000). In eucalypt forest, maximum water repellency was found after heating the soil at temperature from 250 to 280 °C, while an additional five-minute heating from 310 to 340 °C was able to destroy the hydrophobic effect. Doubling the heating time, a range of temperature from 290 to 330 °C was enough for erase water repellency (Doerr et al. 2004). Laboratory test results proved very difficult to replicate in the field: some authors reported an increase in water repellency for temperature above 400 °C, other a decrease of the same parameter for temperature below 200 °C. Factor such as soil moisture, oxygen availability, pre-fire conditions and fuel characteristics may represent uncontrolled variables (Vadilonga et al. 2008 Stoof et al. 2011, Cawson et al. 2016).

Other parameters are affected by fire occurrence: soil pH shows a tendential increase due to the organic acid's denaturation. Significant changes are reported at high temperatures (>450 °C). In contrast, fire-induced increase in pH is negligible in carbonated-buffered soils (Certini 2005). Exchangeable capacity is generally decreased, while electrical conductivity is slightly increased (Badia and Marti 2003, Certini 2005).

Soil color is clearly altered after fire: usually fire leads to a color darkening and also ash produced in low and moderate severity fire is black or grey. On the contrary, high severity fire tends to produce brighter ash; shift in colour toward yellow or red is also reported for iron-rich soils. Shift in soil brightness influence the albedo and thus the temperature regime in the soil until the vegetation recovery (Ketterings and Bigham 2000, Certini 2005, Parsons et al 2010).

The biological properties of the soil are affected, too: for example, the microbial mass is usually reduced, and the composition of the microbial community is modified as well, due to the selective effect of fire on some group of microorganism. Soil dwelling invertebrates decrease (less than microorganism because of their mobility) and also the invertebrate community composition is affected (Certini 2005).

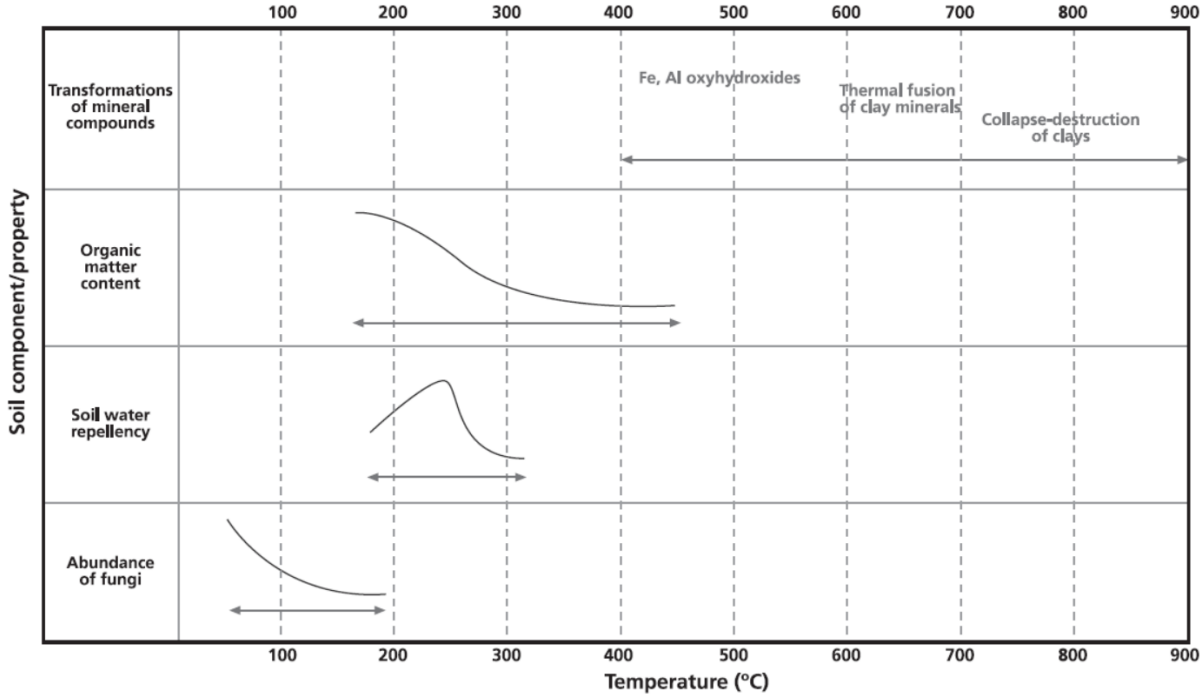


*Figure 4.9 – main soil properties changes at different temperature (Mataix-Solera et al 2011).*

## 4.5 Post-fire geomorphic processes

Wildfire major consequence over a landscape from a geological perspective is the drastic alteration of the pre-fire equilibrium between meteorological external force, slope morphological and hydrological setting, and slope materials characteristics. The result of this system imbalance is a modification in the hydrologic response of watersheds which can be observed even in case of non-exceptional rainfall events. Two major contributes to the slope processes generation are the increased amount of available material, and the increased quantity (and energy) of water reaching the soil surface compared to the pre-fire conditions. As a consequence, a wide range of phenomena can be recorded after fire: they vary in type, magnitude and timing after the fire (fig. 4.10).

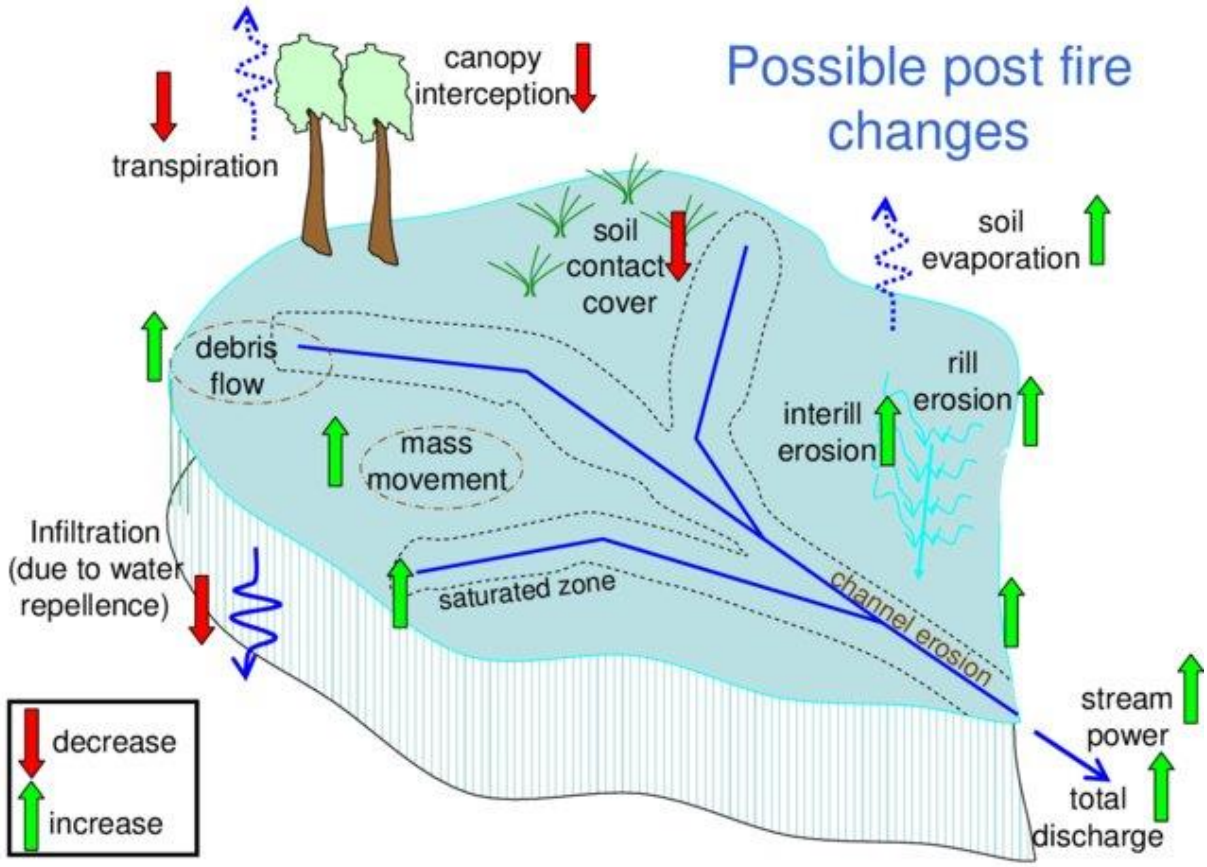


*Figure 4.10 – possible post-fire changes in hydrologic and erosion processes (Smith et al., 2011)*

Post-wildfire processes can be distinguished in two broad categories from a typological perspective: discrete mass movements and surface runoff-dominated processes.

### 4.5.1 Discrete mass movements

The first category includes gravitational phenomena which originates as a consequence of the developing of a failure surface located at a certain depth. Referring to the classification proposed by Varnes (1978), Cruden and Varnes (1996) and lately by Hungr et al., (2014) they can be represented by the "Slides" category and are superimposable to the "landslides" category proposed by Hutchinson (1988) (fig. 4.11).

| Type of movement | Rock | Soil |
|---|---|---|
| Fall | 1. *Rock/ice* fall[a] | 2. *Boulder/debris/silt* fall[a] |
| Topple | 3. Rock block topple[a] | 5. *Gravel/sand/silt* topple[a] |
| | 4. Rock flexural topple | |
| Slide | 6. Rock rotational slide | 11. *Clay/silt* rotational slide |
| | 7. Rock planar slide[a] | 12. *Clay/silt* planar slide |
| | 8. Rock wedge slide[a] | 13. *Gravel/sand/debris* slide[a] |
| | 9. Rock compound slide | 14. *Clay/silt* compound slide |
| | 10. Rock irregular slide[a] | |
| Spread | 15. Rock slope spread | 16. *Sand/silt* liquefaction spread[a] |
| | | 17. Sensitive clay spread[a] |
| Flow | 18. *Rock/ice* avalanche[a] | 19. *Sand/silt/debris* dry flow |
| | | 20. *Sand/silt/debris* flowslide[a] |
| | | 21. Sensitive clay flowslide[a] |
| | | 22. Debris flow[a] |
| | | 23. Mud flow[a] |
| | | 24. Debris flood |
| | | 25. Debris avalanche[a] |
| | | 26. Earthflow |
| | | 27. Peat flow |
| Slope deformation | 28. Mountain slope deformation | 30. Soil slope deformation |
| | 29. Rock slope deformation | 31. Soil creep |
| | | 32. Solifluction |

*Figure 4.11 - Updated Varnes landslide classification system (Hungr et al., 2014).*

These phenomena, after the initiation, may evolve during motion towards other type of processes such as flows or complex ones. These kinds of failure have been reported in literature (Meyer et al., 2001; Cannon and Gartner 2005) although it is very difficult to assess a clear cause-effect relation with fire. This kind of processes are usually shallow and may be favored by a) an increase in soil moisture due to the decreased vegetative cover and a reduced transpiration, b) by a decrease in the soil cohesion related to tree mortality and decay of root stabilizing effect, and c) by an enhanced bank erosion in stream peak flow conditions. The post-fire window in which these processes has been registered is really wide, spanning from the first post-fire rainfall to 1 or 2 years after the fire, and up to 30 years (Megahan 1983, Morton 1989, Swanson 1981, Meyer et al. 2001, May and Gresswell 2003, Wondzell and King 2003, Parise and Cannon 2008).

### 4.5.2 Surface runoff-dominated processes

The second category encompasses a variegated set of processes in which the principal role is exerted by runoff.

In the long term the dominant process is soil erosion: increased rates are reported in many locations worldwide, with authors documenting a median increase of 160 times, reaching values up to 10000 g/m/a (Parise and Cannon 2012, Shakesby and Doerr 2006, Moody and Martin 2009). This process may have

severe effects on the ecosystem, causing aquatic habitat disturbance and soil nutrient losses (Blake et al 2010, Bathurst et al 2007). Above all, the availability of sediment exceeding the normal streamflow carrying capacity increases both the bedload and the suspended materials (Santi et al 2008, Parise and Cannon 2012).

In the short term the combined effect of enhanced erosion and increased runoff is responsible for the generation of 1) flash floods, 2) hyperconcentrated flows and 3) mud/debris flows. Processes 1) and 2) are proper of the bottom of slopes and watersheds and occurs when the overland flow is not retarded by the vegetation and when the infiltration rates are reduced, so that the time of concentration is faster than in the pre-fire conditions. 1) and 2) type of flows behaves as Newtonian fluids, as the viscosity of the fluid is not sufficient for generating a proper debris flow. Effect 3) is the result of a chain of erosional processes and sediment mobilization that encompasses rainsplash, sheetflow and rill erosion until the runoff concentrates in hollows and low order channels (Guilinger et al. 2002). When enough material is eroded, the debris flow may originate (Meyer and Wells 1997, Shakesby and Doerr 2006, Cannon at al 2003, Parise and Cannon 2012). Another particular process can be found either in burned and in unburned areas and is called "firehose effect": it consists of an enhanced erosion of material due to cascading water over steep slopes or morphological steps. When the runoff is increased and the erodibility of the soil is favored by the fire, this phenomenon can be the trigger for debris flows in down valley areas (Calcaterra et al. 2000, Larsen et al. 2006).

# 5 The sin- and post- 2017 Piedmont wildfire season climate

In October and November 2017 nine major wildfire fires broke out in the Piedmont region. Some of them lasted for several days before being extinguished, and the strong wind conditions brought the smoke to the city of Turin, gaining a strong media coverage. The surfaces covered by the fire were 9731 ha, of which 74% covered by forests and 34% of the burnt areas being in protected areas.

*Figure 5.1 - Satellite image acquired in the visible band by the MODIS sensor on NASA's EOS Aqua polar satellite, 11:55 UTC on 25/10/2017.*

The main causes of this anomalous fire season are to be found in the equally anomalous climatic conditions, in particular the absence of rainfall for a long period and the strong wind conditions. The year 2017 in fact was the 3rd warmest in the previous 60 years, with a positive thermal anomaly of about +1.5° C compared to the 1971-2000 climatic average (fig. 5.2). About 700 mm of annual precipitation (regional average) were recorded, with a rainfall deficit of 33% compared to the 1971-2000 average values, making it the 4th driest year in the previous 60 years (fig. 5.3) (Arpa Piemonte 2018).

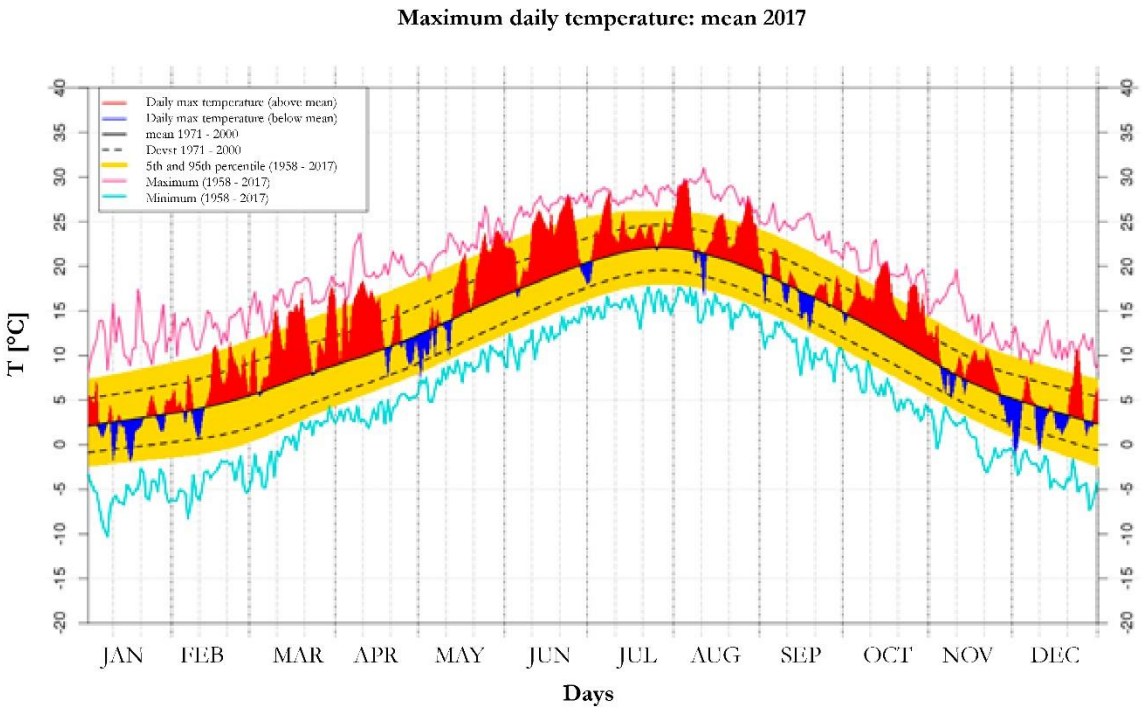


*Figure 5.2 - Trend of the average maximum daily temperature in Piedmont for the year 2017 (values referring to an average point located at 900 m a.s.l.) (redrawn from Arpa Piemonte).*

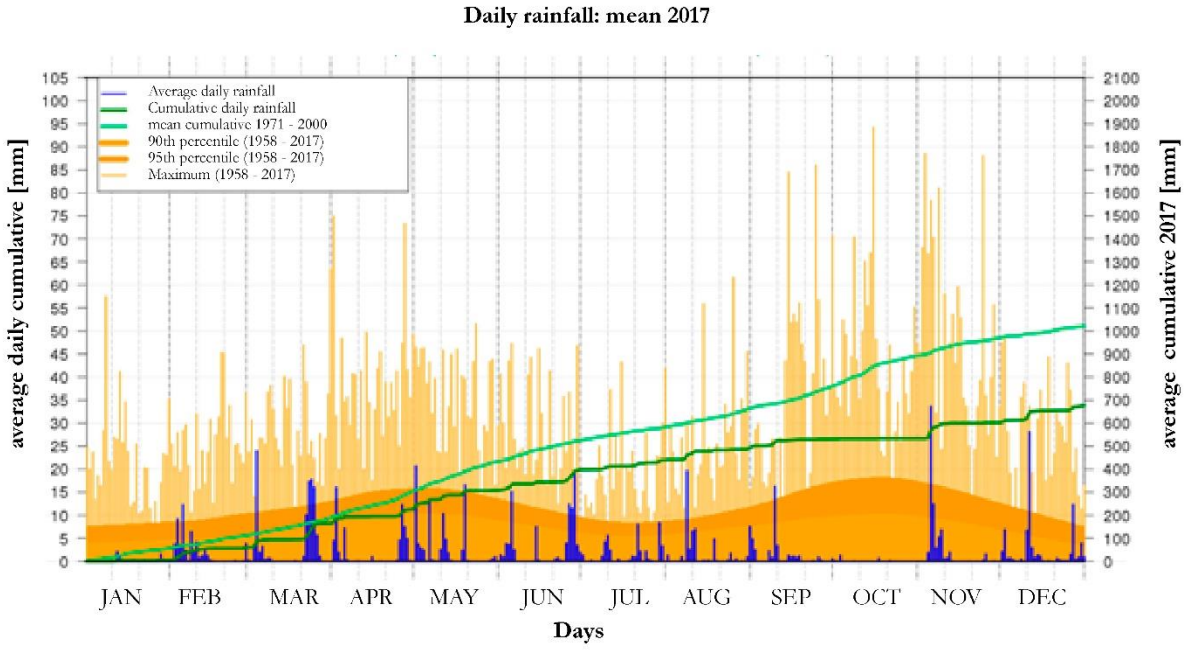


*Figure 5.3 - Trend of the average daily cumulative precipitation in Piedmont for the year 2017 (values referring to an average point located at 900 m a.s.l.) (redrawn from Arpa Piemonte).*

The 2017 autumn season was the second driest in the last 60 years, and in detail the month of October 2017 (fig. 5.4) was the driest of the last 60 years, with an average monthly precipitation of only 3 mm, mainly limited to the mountain reliefs, and a deficit of 98% compared to the 1971-2000 climate. The drought in October aggravated the rainfall deficit already present with over 50 consecutive days without significant rainfall. It was also the hottest month since 1958, with a thermal anomaly of about + 2.9 °C (vs 1971-2000) and +4.5 °C in maximum temperatures.

In addition, eight days with Foehn (hot and dry fall wind) were recorded in October compared to an average of 5 days. The effect of this wind is to cause an exceptional increase in maximum temperatures (it can raise the temperature by 10-20 ° C in a few hours), to reduce the humidity of the fuels, to favor the spread of fires and the transport of smoke at great distances (Arpa Piemonte, 2018).

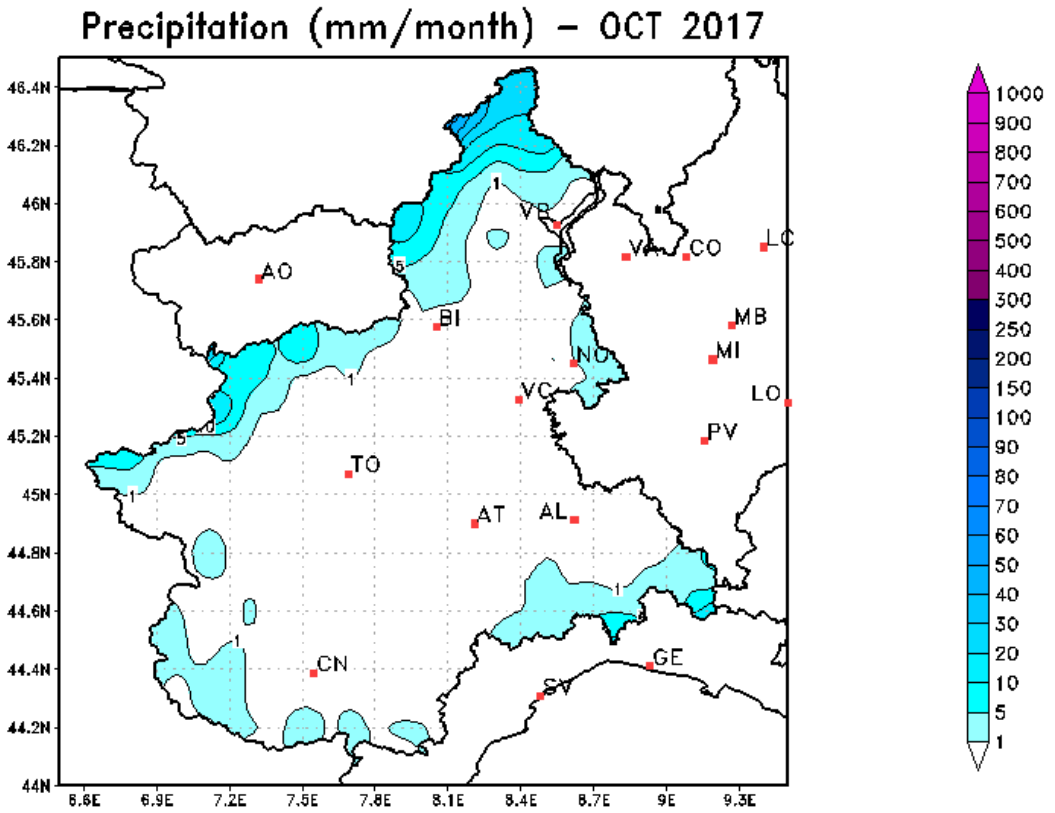


*Figure 5.4 - Monthly precipitation in Piedmont in October 2017 (Arpa Piemonte).*

Year 2018 was the second warmest observed in Piedmont in the entire historical series 1958-2018, with an estimated average positive thermal anomaly of 1.6 ° C compared to the three-year reference period 1971-2000 (fig. 5.5). Analysis of the daily annual trend shows how the positive thermal anomaly has constantly characterized almost the entire year. However, the period between the end of February and the beginning of March was characterized by a marked negative thermal anomaly; in fact the third decade of February was the second coldest of the previous 61 years with an average temperature lower by almost 5° C

compared to the average of this period. The month of April with +3.4 °C had the greatest positive deviation, while January 2018, with a positive anomaly of 2.7° C, was the second warmest January of the last 61 years (Arpa Piemonte, 2019).

Contrary to 2017, the average cumulative rainfall in Piedmont in 2018 was approximately 1380 mm and was higher than the 1971-2000 norm, with a surplus of about 332 mm, which corresponds to 33%; in the 2017/2018 winter season about 274 mm of average precipitation fell, with a pluviometric surplus of about 105 mm (equal to 61%) compared to the climatology of the 1971-2000 period; therefore, the winter 2017/2018 ranks 7th among the winters richest in precipitation of the last 61 years. In particular, January was the month with the highest percentage pluviometric surplus and the second wettest in the 1971-2000 historical series (fig 5.6).

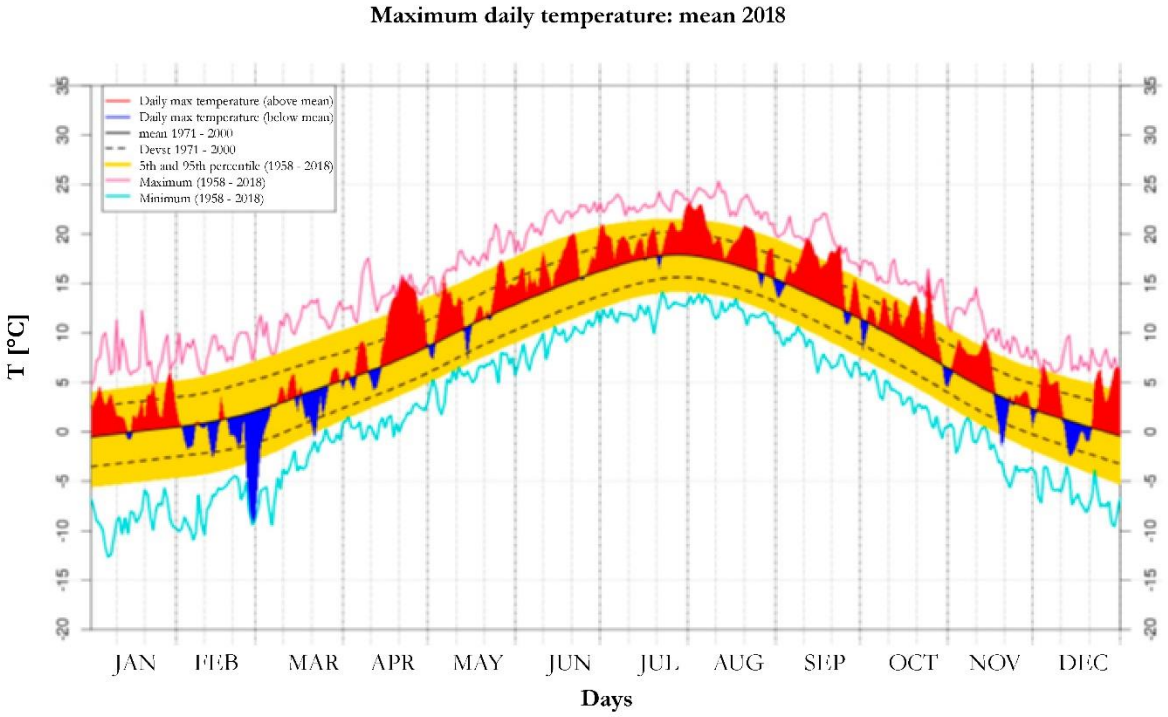


*Figure 5.5 - Trend of the average maximum daily temperature in Piedmont for the year 2018 (values referring to an average point located at 900 m a.s.l.) (redrawn from Arpa Piemonte).*

Later on, in the spring of 2018, Piedmont was affected by a prolonged wet period that led to rainfall well above the climatic norm. In fact, the spring season 2018 was the fifth wettest from 1958, with an average rainfall of about 463 mm and a pluviometric surplus of around 134 mm (equal to 41%) compared to the climatology of the 1971-2000 period. In particular, May 2018 was the seventh wettest May in the previous 60 years with a rainfall surplus of over 60% compared to the reference period 1971-2000 (fig. 5.7).

In the mid Susa Valley, since the beginning of the year there has been an accumulation of precipitation 68% higher than the 1971-2000 climatic norm and, in the period between April 29 and June 7 (40 days) 30 rainy days has been registered (Arpa Piemonte, 2018).

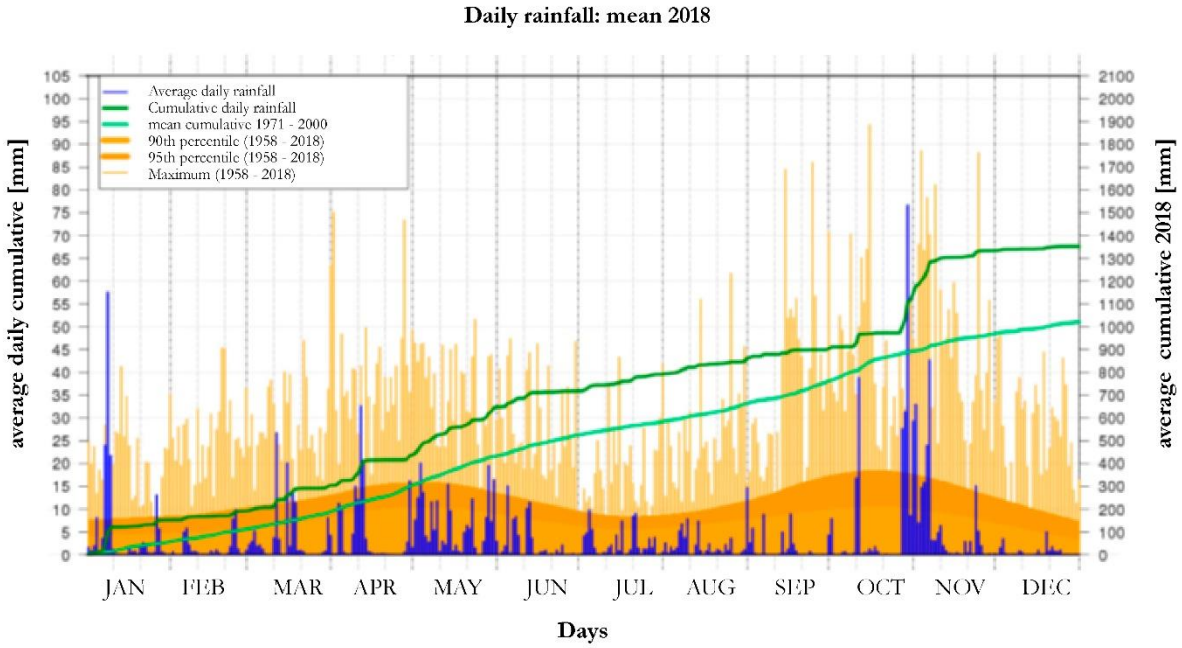


*Figure 5.6 - Trend of the average daily cumulative precipitation in Piedmont for the year 2018 (values referring to an average point located at 900 m a.s.l.) (redrawn from Arpa Piemonte).*

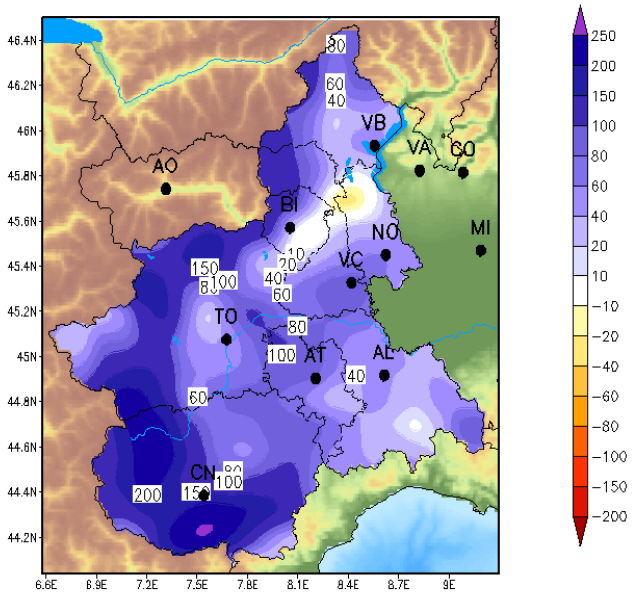


*Figure 5.7 - Anomaly of precipitation in May 2018 in Piedmont (mm) compared to the average of the period 1971-2000 (Arpa Piemonte).*

# 6 Methods

A complete description of a post-wildfire response needs to include the analysis of multiple aspects: local geology and geomorphology, soil characteristics, fire intensity and recurrence, fire severity and fire regimes, precipitation regime, modification of the soil hydraulic and geotechnical properties, soil erosional processes, event magnitude and effects. The effort necessary for describing all these parameters over a large area is not sustainable, especially if the post-fire response is constituted by the onset of infiltration-triggered discrete landslide. Given the absence in the target area of reported or surveyed landslide s.s., the soil hydraulic and geotechnical parameters have been dropped from the evaluation. The focus has been consequently shifted on detailing the post-fire surface runoff - dominated processes. The limited number of surveyed post-fire events does not allow the use of a fully statistical approach, so the problem had to be faced by using deterministic methods. A relevant methodological problem in studying this type of events is the fact that field surveys usually are conducted after the fire, making harder to properly assess and evaluate the pre-fire conditions. Even if controlled burns are executed for having a better control on pre-fire variables, they are affected by a scale effect, thus leading to an increased uncertainty and a bias in the sin- and post-fire measurement. For this reason, the multiscale approach and the data integration is crucial to have a comprehensive and redundant characterization of the processes.

## 6.1 Regional Scale Landslide-wildfires correlation

Landslide locations and features were derived from two regional datasets and integrating recent events information: the SIFraP (Sistema Informativo Frane in Piemonte[1], last updated in 2015) and the Banca Dati Eventi (BDE[2], last updated in 2019). SIFraP database contains the position and attributes of morphological elements, shallow and deep-seated landslides, flows, falls and complex landslides. Data are reported either as punctual, linear or polygonal feature. The entire dataset covers 60 years and contains a total of more than 80.000 entities. BDE database contains geo-referenced reports relating to processes attributable to geo-hydrological phenomena (landslides, river scour and deposition processes, etc.) to which information on the effects and damages are associated. Data are provided as punctual features, and the database contains more than 29.000 events over 1000 years.

Official wildfire perimeters were provided by Carabinieri Forestali, who assess the burned area by on-site inspection. Since wildfire are usually man-made, police force is charged of detect burned areas and, if possible, to identify the ignition point. These data remain in the records for investigation and, if necessary,

[1] Sistema Informativo Frane in Piemonte – Piedmont Landslide Information System
[2] Banca Dati Eventi – Event Database

for a trial. For Piedmont region, the database encompasses wildfire perimeter and ignition point from 1997 to 2017[3] (fig 6.1), and data are represented as polygon and point shapefile in the WGS84 – UTM32N reference system.

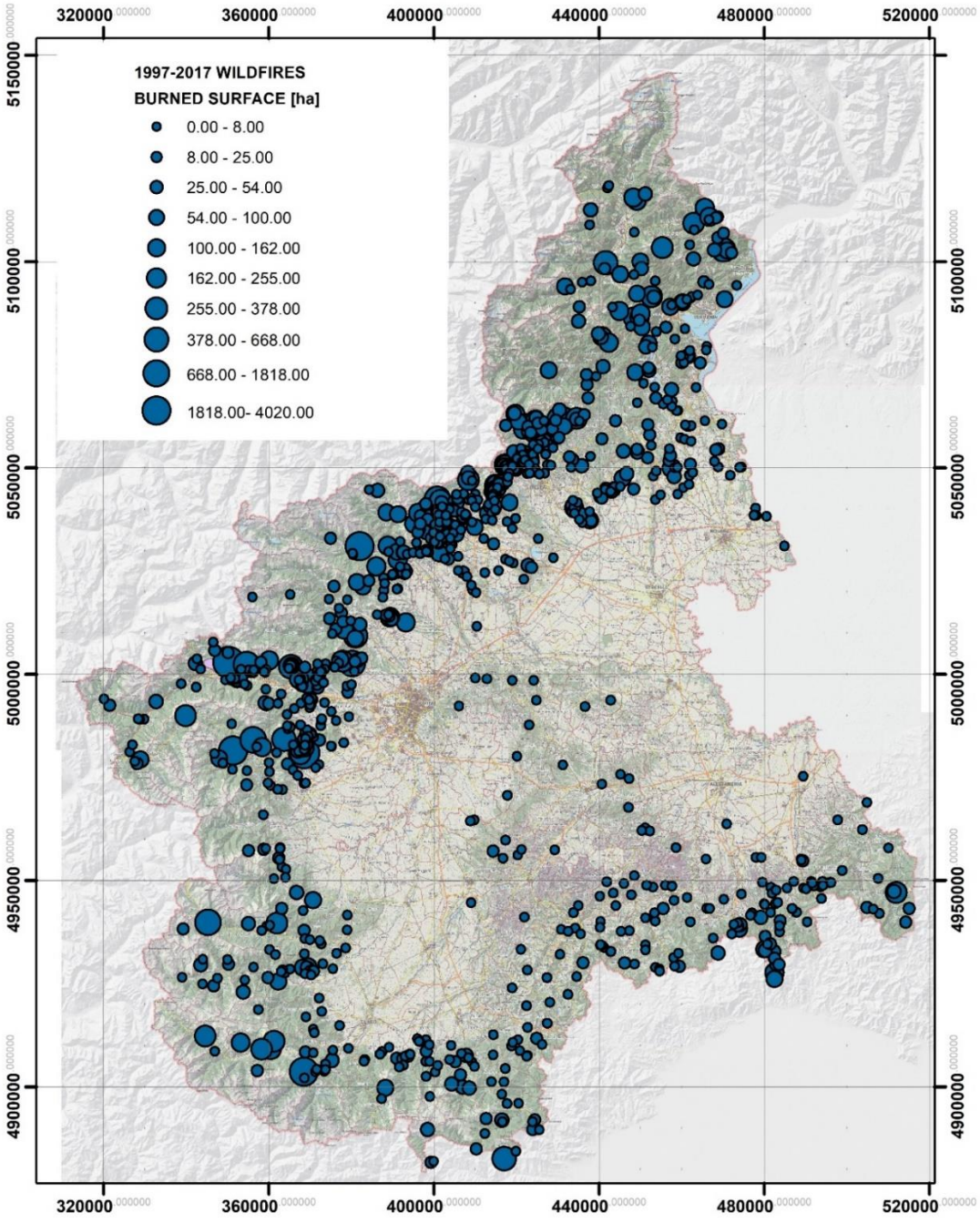


*Figure 6.1 – Burned surfaces from 1997 to 2017 (Regione Piemonte - Incendi boschivi: Aree e punti di innesco).*

[3] Regione Piemonte - Incendi boschivi: Aree e punti di innesco. Piedmont Region – Wildfires: surfaces and ignition points (http://www.datigeo-piem-download.it).

In the database table the following data are reported (Piedmont Region):

*Table 6-1 – wildfires shapefile attribute table*

| ATTRIBUTE | FORMAT | DESCRIPTION |
|---|---|---|
| **ID_COMU** | Numerical | Municipality Id |
| **COD_FASCIC** | Numerical | Dossier number |
| **DATA_INCE** | Date | Ignition date |
| **LOCALITA** | Text | Location name |
| **SUP_TOT** | Numerical | Burned surface (ha) |
| **SUP_BOSC** | Numerical | Burned surface – wooded (ha) |
| **SUP_NOBOSC** | Numerical | Burned surface – not wooded (ha) |
| **WGS84EST** | Numerical | Ignition point Easting (m) |
| **WGS84NORD** | Numerical | Ignition point Northing (m) |
| **ID_INCENDI** | Numerical | Wildfire Id |

Since landslides data derives from heterogeneous sources, data are associated with different attributes, and are given in different formats. For example, the landslide occurrence date, if present, was found to be expressed either in a numerical, text and date format, using moreover different date convention. The first step has been the homogenization of attributes format for ensuring further date treatment and query. After that, data prior to 1997 (year of the older wildfire registered in the dedicated database) were removed, resulting in a dataset containing 17.635 different events. After that, a database query was implemented for selecting landslides belonging to flow or slide type. This output has been then compared to the fire perimeter dataset, selecting landslides occurred within a distance of 1 km from the wildfire boundary. The resulting outcome has been finally filtered for removing errors resulting from landslide occurring upslope with respect to the wildfire boundary or on the other side of the watershed divide (fig. 6.2). The final database has been then arranged for including related wildfire attributes for every landslide, and subdivided in three subsets, reporting polygon, line and point type features, respectively. Recent events (post-2017 wildfire season) were collected through direct field surveys, gathering information on web and newspaper reports and by interviewing local authorities.

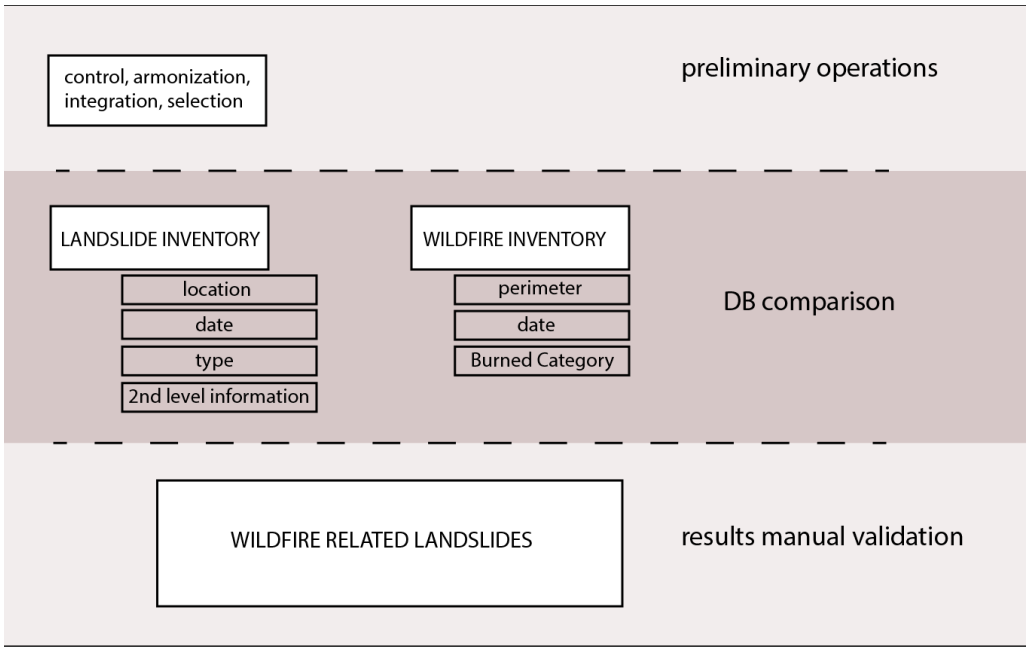


*Figure 6.2– Regional scale landslides-wildfires correlation workflow.*

## 6.2 Watershed scale

The watershed scale analysis is based on the integration of geospatial data treatment and the field surveys outcomes (fig 6.3). The description of the field surveys, the collected data and the processing methodology are explained in the paragraph 6.21, 6.2.2 and 6.2.3.

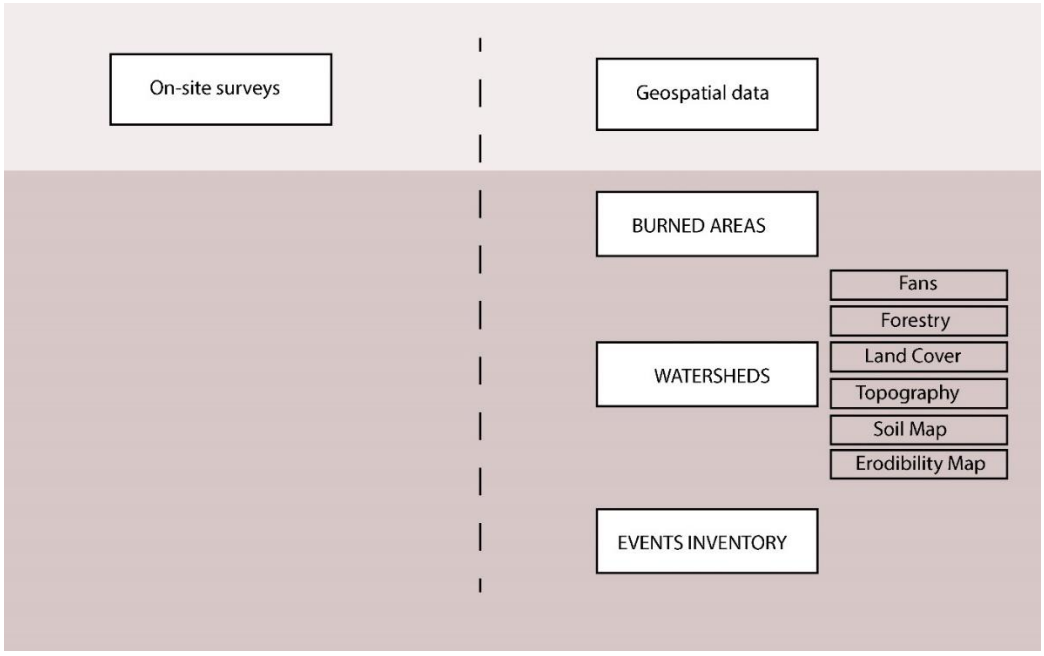


*Figure 6.3 - Watershed scale data treatment workflow.*

### 6.2.1 On site surveys

After the October 2017 forest fires, a campaign of site surveys in the burned areas has been designed and implemented. Surveys has been performed in the framework of the Institutional Technical Table of the Piedmont Region, a task force created for preparing an Emergency Plan for recovery intervention. The team involved Piedmont Region technicians and University of Turin, IPLA[4], Alta Valle di Susa Forestry Consortium, AIB[5] and Carabinieri Forestali as scientific or technical consultant (in the fields of forestry, forest ecology, pedology, geology, hydrogeology, etc.). The plan is devoted to individuating and ranking areas in which the fire has increased the hydrogeological risk, or which are particularly interesting from an environmental and ecological perspective; in these areas high priority of intervention is granted, and post-fire management practice can be authorized and funded with public resources. In less endangered areas the plan provides guidelines for medium and long-term intervention, sustainable with private funding[6].

The first round of surveys has been conducted over the nine wildfire locations, starting at the end of May 2018 and ending by mid-June 2018. The survey plan has been executed six months after the last wildfire because of the climatic conditions; in fact, most of burned areas were covered by snow since December 2017 to March 2018. Following surveys have been repeated in the areas in which more investigation was required after the first observation.

During the on-site inspections, the macroscopic and visual effects of the fire over the vegetation and the landscape has been assessed, with particular focus on the areas surrounding villages, roads and streams. Particular attention was due to the areas in which the preliminary Burn Severity maps indicates higher values. Observations were aimed at investigating the effect of the fires both on the vegetation and the soil. On the vegetation the effects have been evaluated on different vegetation strata, examining soil surface, herbs, shrubs and trees, especially looking at the amount of fuel consumed on the soil surface and its color change, ash coverage, amount of damage on grass and shrubs, height of char on tree trunks and canopy mortality. Geological and geomorphological survey were aimed at individuating relevant signs of an increased slope dynamics and activity, such as enhanced erosion in the upper portions of the watersheds, rills and gully development, evidence of landslide, modification in the drainage network (especially the enhancement in the activity of hollows and low order channels), sediment-laden flow and/or dry ravel deposits.

---

[4] Istituto per le Piante da Legno e l'Ambiente - Institute for Wood Plants and the Environment

[5] Corpo volontari AntiIncendi Boschivi – Forest Fire Volunteer Corps

[6] The national law on forest fires (Law 353/2000, article 10) prohibits, for five years, on forest and grazing land affected by fire, any activity of afforestation and hydrogeological defense supported by public financial resources, except for specific authorization granted for proved situations of hydrogeological risk and when an intervention is urgently required to protect exceptional environments and landscapes.

## 6.2.2 Data collection

For the collection of data, different sources were used, favoring the use of regional open source data. A brief description of each of them is provided in the following paragraphs.

### 6.2.2.1 Burned area

The 2017 wildfires have been selected from the regional database. Their location, extent and main characteristics are reported in fig. 6.4 and table 6-2.

*Table 6-2 – 2017 wildfires overview*

| WILDFIRE ID | WILDFIRE NAME | IGNITION DATE | TOTAL BURNED SURFACE | FOREST SURFACE | NONFOREST SURFACE |
|---|---|---|---|---|---|
| # | | | [ha] | [ha] | [ha] |
| 1 | LOCANA/RIBORDONE | October 22, 2017 | 1569.7673 | 1440.5633 | 129.204 |
| 2 | BUSSOLENO/MOMPANTERO | October 22, 2017 | 4018.5703 | 3102.9065 | 915.6637 |
| 3 | CAPRIE-RUBIANA | October 13, 2017 | 310.7469 | 310.7469 | 0 |
| 4 | CUMIANA/CANTALUPA | October 17, 2017 | 1818.2538 | 1818.2538 | 0 |
| 5 | BELLINO/CASTELDELFINO | October 23, 2017 | 378.0204 | 378.0204 | 0 |
| 6 | SAMBUCO/PIETRAPORZIO | October 19, 2017 | 162.1212 | 111.5919 | 50.5293 |
| 7 | ROURE/PERRERO | October 5, 2017 | 668.6261 | 499.5988 | 169.0272 |
| 8 | TRAVERSELLA | October 25, 2017 | 623.9245 | 250.9528 | 372.9718 |
| 9 | DEMONTE | October 27, 2017 | 219.8098 | 153.8019 | 66.0079 |

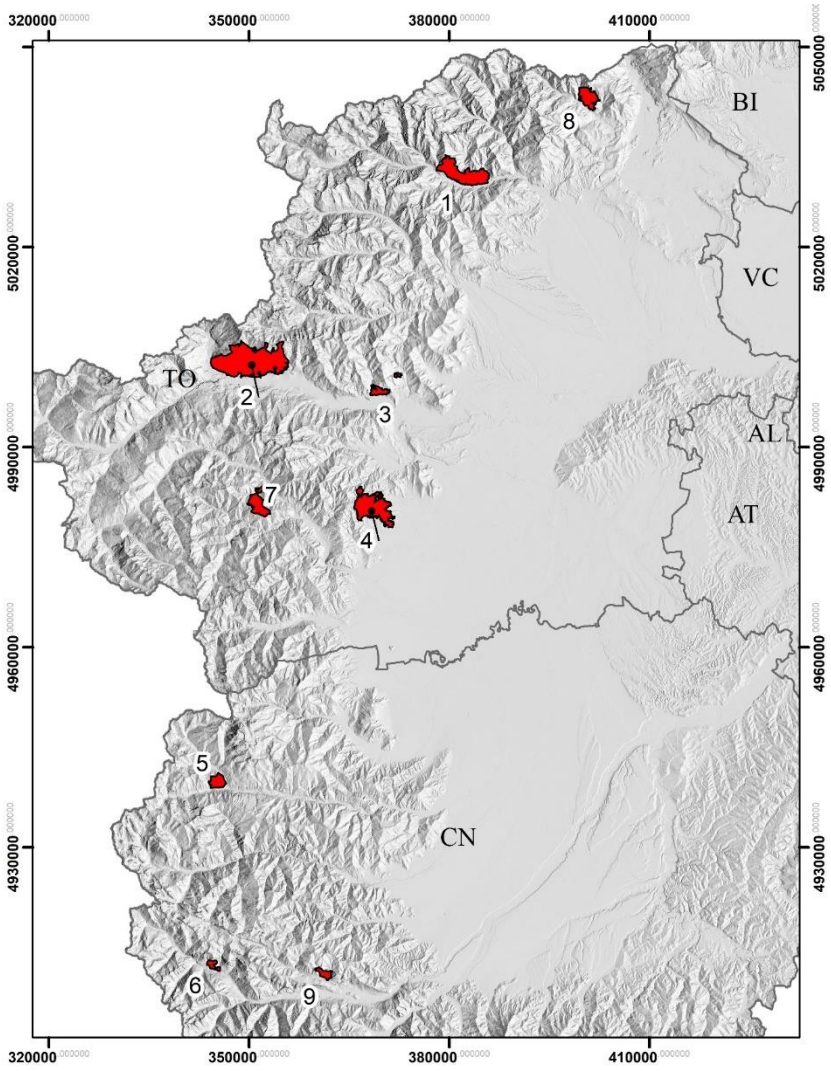


*Figure 6.4 – 2017 wildfires location*

### 6.2.2.2 Catchments

The Piedmont catchments perimeter has been derived from Arpa Piemonte and Regione Piemonte database (Giampani et al., 2013). Morphometrical attributes included in the database are catchment area, fan area and the Melton Index. Based on bedrock lithology, the catchments are classified with a different Clay Weathering Index according to the following scheme (following Tiranti et al. 2008, De Angeli et al. 2011, Marco et al. 2012):

a) *Excellent Clay Maker* – ECM – phyllosilicates rich foliated metamorphic (Calcschists, black shale, argilloschists) and/or clay minerals rich sedimentary rocks;

b) *Good Clay Maker* – GCM – massive calcareous rocks (limestones, dolomites,…);

c) *Bad Clay Maker* – BCM – igneous or massive metamorphic rocks (granitoids, gneiss, greenschists, ultramafic rocks, massive micaschists,…).

These rock classes are distinguished based on the ability to produce, following mechanical and physical disintegration, significant quantities of clays or clay-like minerals in the fine fraction, thus conditioning the prevailing rheology and depositional style, seasonality and the amount of rainfall required for triggering the flows processes (Giampani et al. 2013). On the basis of the morphometrical parameters, lithological classes and triggering rainfall thresholds magnitude and return period of expected phenomena are given (Tiranti 2008, Tiranti et al. 2008, Cremonini et al. 2010, De Angeli et al. 2011).

#### 6.2.2.3 Fans

The Piedmont fan map (1:10000 scale) contains the shape of 2459 fans over the regional territory, spanning from 1 to 340 ha. They have been individuated by Arpa Piemonte based on photointerpretation and orthoimages analysis. The dataset has been downloaded from Arpa Piemonte database in the shapefile format. Shapefile attribute table include parameters such as type, genesis and catchment name. In particular, the attribute "genesis" is helpful to identify the main depositional processes occurring in the catchment. In addition, for some of the catchment (893, bigger than 4 ha), information on the most common processes has been retrieved following the scheme proposed by Marchi et al. (1993), classifying them as Fluvial Fan, Mixed Fan and Debris-Flow Fan.

#### 6.2.2.4 Forest species and forest setting

Forest species and settings were derived from the Forest Map of the Piedmont Region (Camerano et al, 2016) at 1:10,000 scale. According to the current law specifications, forest is defined as land cover by arboreal vegetation, in association or not with shrubby vegetation, natural or artificial, characterized by a surface above 2000 square meter, mean width above 20 meter and coverage above 20%. The dataset has been downloaded from SIFOR (Sistema Informativo Forestale Regionale) database in the shapefile format. A separate dataset mapping arboreal coverage below 20% is provided separately. Shapefile attribute table include parameters such as Forest category, type and subtype, management type, main forest role and purpose and Corine Land Cover (level 3) code.

#### 6.2.2.5 Land Cover

Land Cover data has been derived from Land Cover Map of Piedmont (Regione Piemonte 2010). The dataset is the result of the integration of available spatial data and follows the Corine Land Cover classification scheme.

#### 6.2.2.6 Topography and DTM

Topographic data were derived by Regional Digital Terrain Model (DTM 2009-2011 Piemonte ICE). The digital terrain model has been acquired by using Lidar and has a resolution of 5 meter and a vertical

accuracy of ±0.30 m (±0.60 m in densely forested and urbanized areas). Elevation, Slope and Aspect maps were produced at the same resolution by using Esri® ArcMap 10.2.2.

#### 6.2.2.7 Geology

Geological data were derived from the geological map of Piedmont Region at 1:250000 scale (Piana et al 2017). Geological data derive from revised official and unofficial geological maps and unpublished original data.

#### 6.2.2.8 Soil map and soil erodibility map

Soil maps were derived from Piedmont Soil Map at 1:250000 scale (IPLA 2020, not published). It is an inventory of the principal soil types which incorporates soil order and soil subgroup distribution within each cartographic unit based on USDA soil taxonomy (USDA 1999).

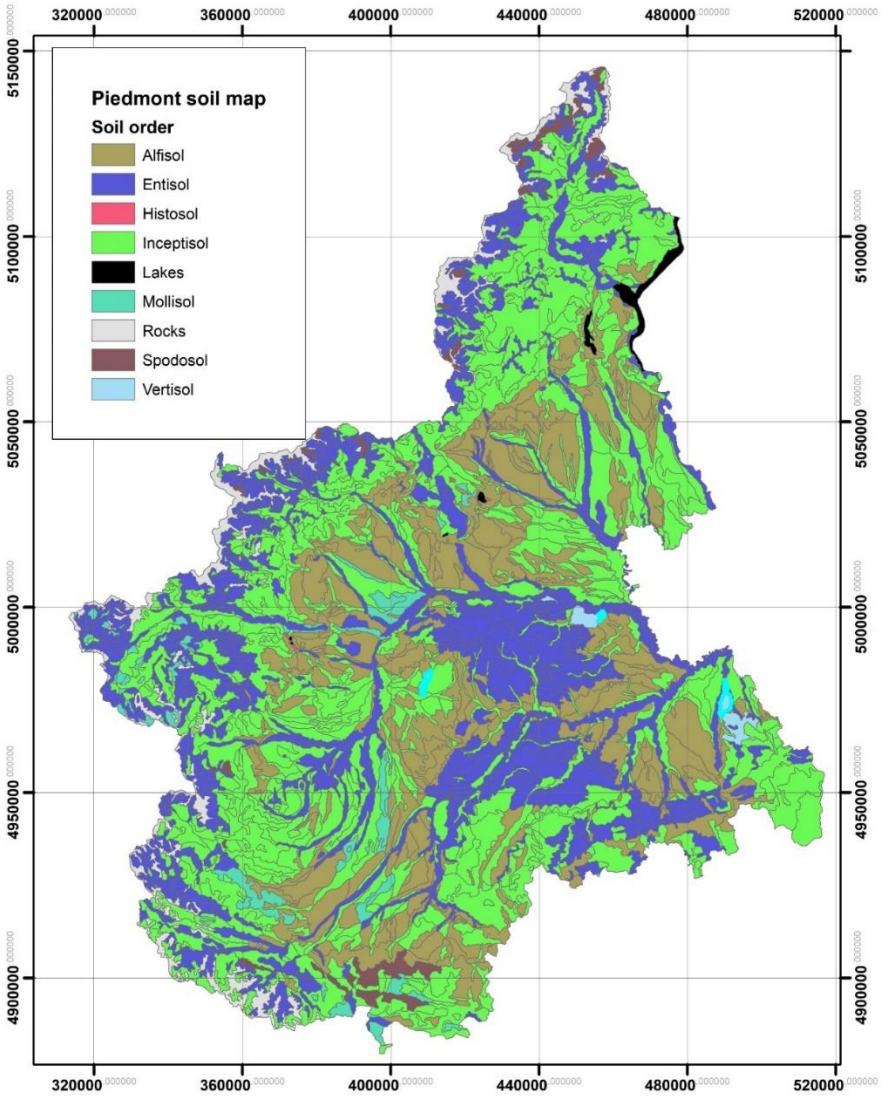


*Figure 6.5 - Piedmont Soil Map (data provided by IPLA, not published).*

Unpublished soil erodibility data, based on 1.250000 soil map, were also provided by Ipla. RUSLE K factor is provided as a raster map with 100 m resolution cells.

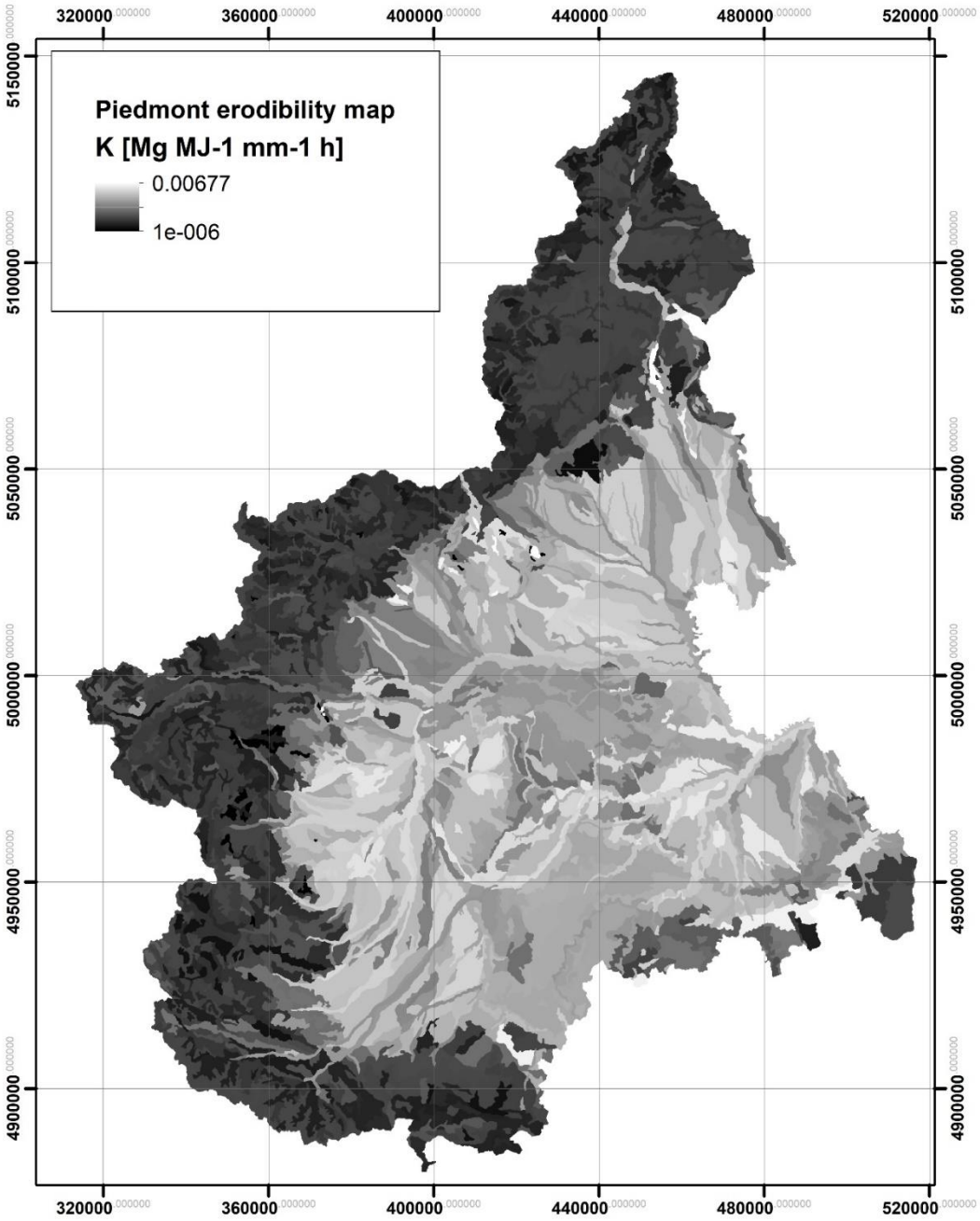


*Figure 6.6 - Piedmont erodibility map, representing RUSLE K factor (data provided by IPLA, not published).*

#### 6.2.2.9 Landslide inventory

Recent events (post-2017 wildfire season) were collected through direct field surveys, gathering information on web and newspaper reports and by interviewing local authorities. A total of 13 events, all of them occurred in 2018, make up the dataset. In the table 6-3 the single events are reported.

*Table 6-3 – Post-2017 wildfire landslides occurrence DF: debris-flow; MF: mud-flow.*

| Watershed | Location | Date | Type | Fire start date | Fire end date |
|---|---|---|---|---|---|
| **Comba delle Foglie** | Bussoleno | 07/06/2018 | DF/MF | 22/10/2017 | 30/10/2017 |
| **Comba delle Foglie** | Bussoleno | 29/04/2018 | DF/MF | 22/10/2017 | 30/10/2017 |
| **Comba delle Foglie** | Bussoleno | 02/05/2018 | DF/MF | 22/10/2017 | 30/10/2017 |
| **Comba delle Foglie** | Bussoleno | 09/05/2018 | DF/MF | 22/10/2017 | 30/10/2017 |
| **Comba delle Foglie** | Bussoleno | 13/05/2018 | DF/MF | 22/10/2017 | 30/10/2017 |
| **Rio della Ravoire** | Mompantero | 09/08/2018 | MF | 22/10/2017 | 30/10/2017 |
| **Rio della Ravoire** | Mompantero | 11/06/2019 | MF | 22/10/2017 | 30/10/2017 |
| **Apparè** | Sparone | 12/06/2018 | MF | 22/10/2017 | 05/11/2017 |
| **Apparè** | Sparone | 12/06/2018 | MF | 22/10/2017 | 05/11/2017 |
| **Carlevaria** | Locana | 11/06/2018 | DF | 22/10/2017 | 05/11/2017 |
| **Locana est** | Locana | 11/06/2018 | DF | 22/10/2017 | 05/11/2017 |
| **Rio Fura** | Locana | 11/06/2018 | DF | 22/10/2017 | 05/11/2017 |
| **Rio Fura** | Locana | 11/06/2018 | DF | 22/10/2017 | 05/11/2017 |

### 6.2.3 Data check and processing

Data processing consist of the treatment of satellite data, forest/land cover maps, wildfire perimeters and watersheds database. The first step is the production of the fire severity maps and the identification of the watersheds affected by the wildfires (fig 6.7). After that, the fire-related erodibility and runoff models have been applied. In the following the detailed procedure is explained.

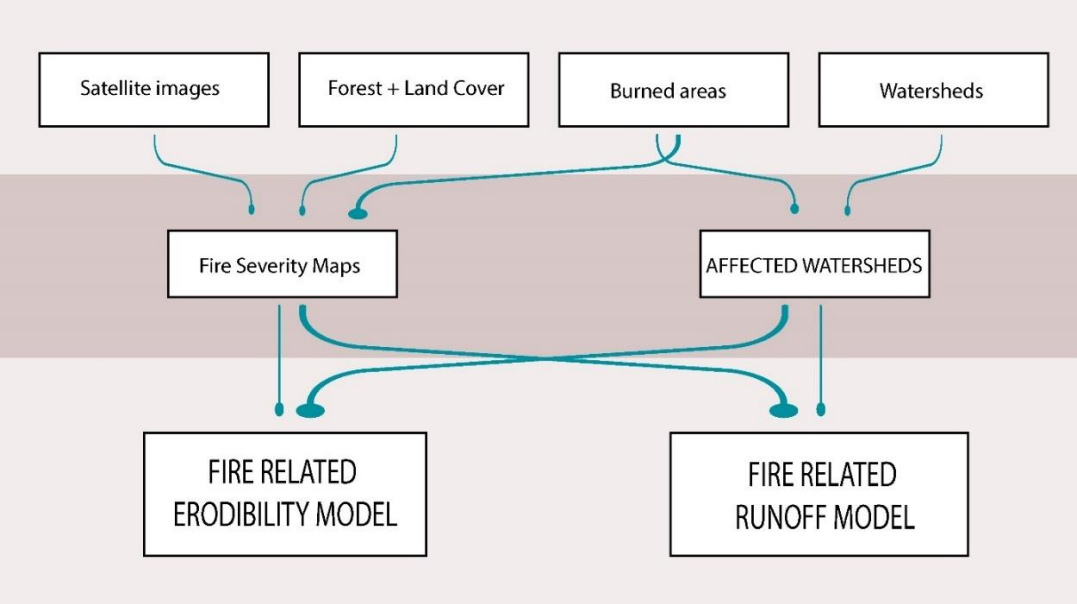


*Figure 6.7 – data processing scheme.*

#### 6.2.3.1 Fire severity maps analysis

Remote sensing images were used to analyse the wildfire process, to check the extent of the burned areas and the burn severity. The fire severity reflects the degree of change induced in the various components of the ecosystem, see paragraph 4.3.1. It is traditionally expressed by classifying the impact of the fire through ordinal quality classes, defined very broadly (eg. low, medium or high severity). In this study, the methodology used for fire severity assessment is based on US FIREMON (Fire Effects Monitoring and Inventory System) framework (Key and Benson 2005).

For the 2017 fires, the fire severity initial assessment has been performed to identify the short-term effects of the fire on burned areas while the results of the "extended assessment", realized by Morresi et al (2021), has been used to evaluate the response of the ecosystem one year after the fire (figg. 6.9 – 6.11). The initial assessment allows to quantify the wildfire impact immediately after the fire, especially regarding the effect on grassland which tend to be obliterated very soon due to the rapid regrowth of the herbaceous species. The extended assessment, in which the burn severity is measured during the first growing season after the fire, allows to assess the direct effects of the fire and the initial response of the forest ecosystem, thus including the delayed mortality of trees, the beginning of the process of renewal, and the colonization of the areas covered by invasive species (Key 2006)(fig. 6.8) . This is crucial for evaluate how the recovery of the vegetation, or conversely its delayed mortality, affects the post-fire hazard evolution; in facts an increased or decreased impact of the erosive processes, and thus the availability of material to be entrained in case of rainfall events, are key mechanism for post-fire triggering of flows.

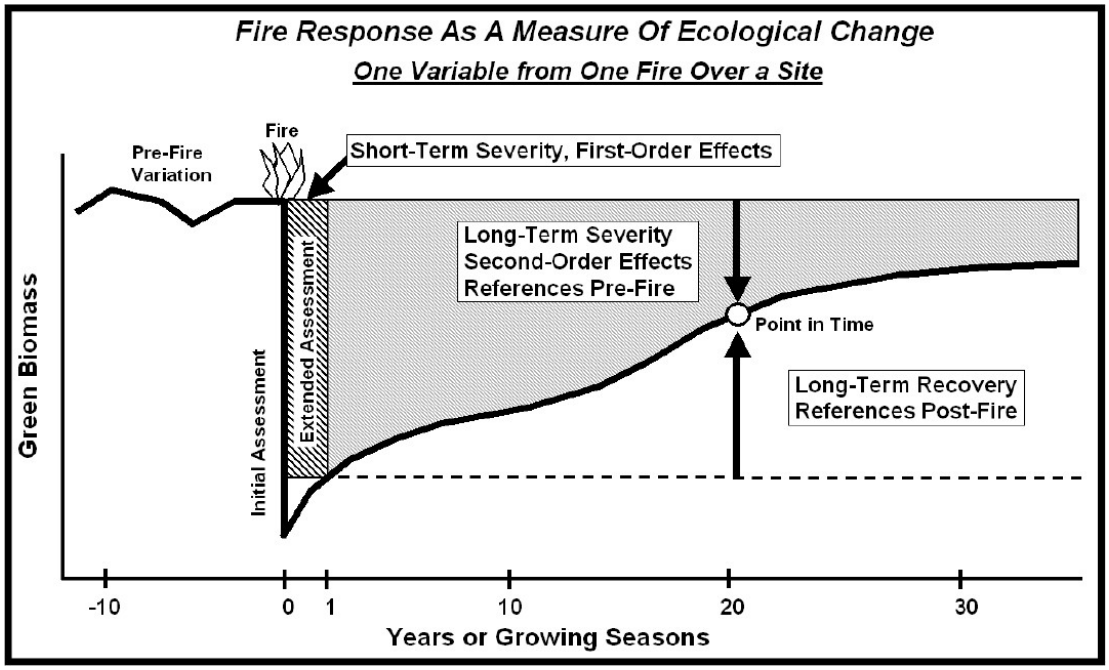


*Figure 6.8 - Conceptual model of burn severity and recovery of the ecosystem over time (Key 2006).*

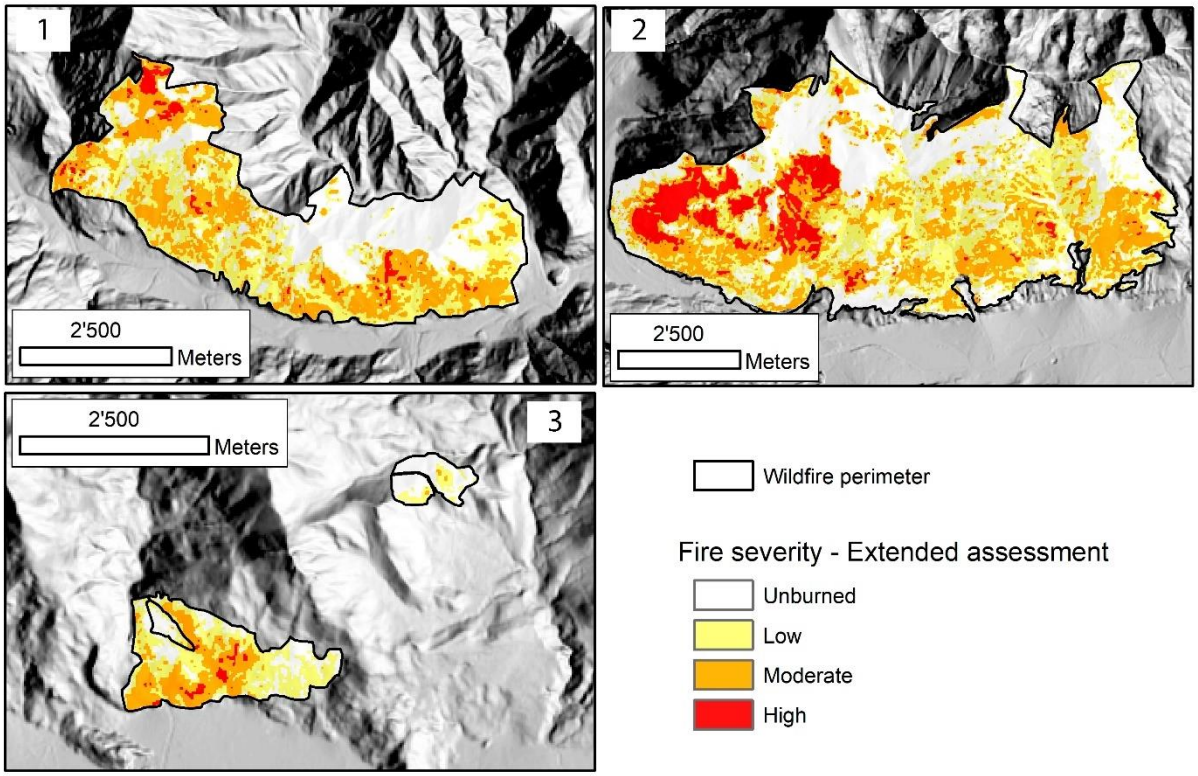


*Figure 6.9 – Fire severity maps, extended assessment, for the Locana/Ribordone (1), Bussoleno/Mompantero (2) and Caprie/Rubiana (3) wildfires (after Morresi et al., 2021)*

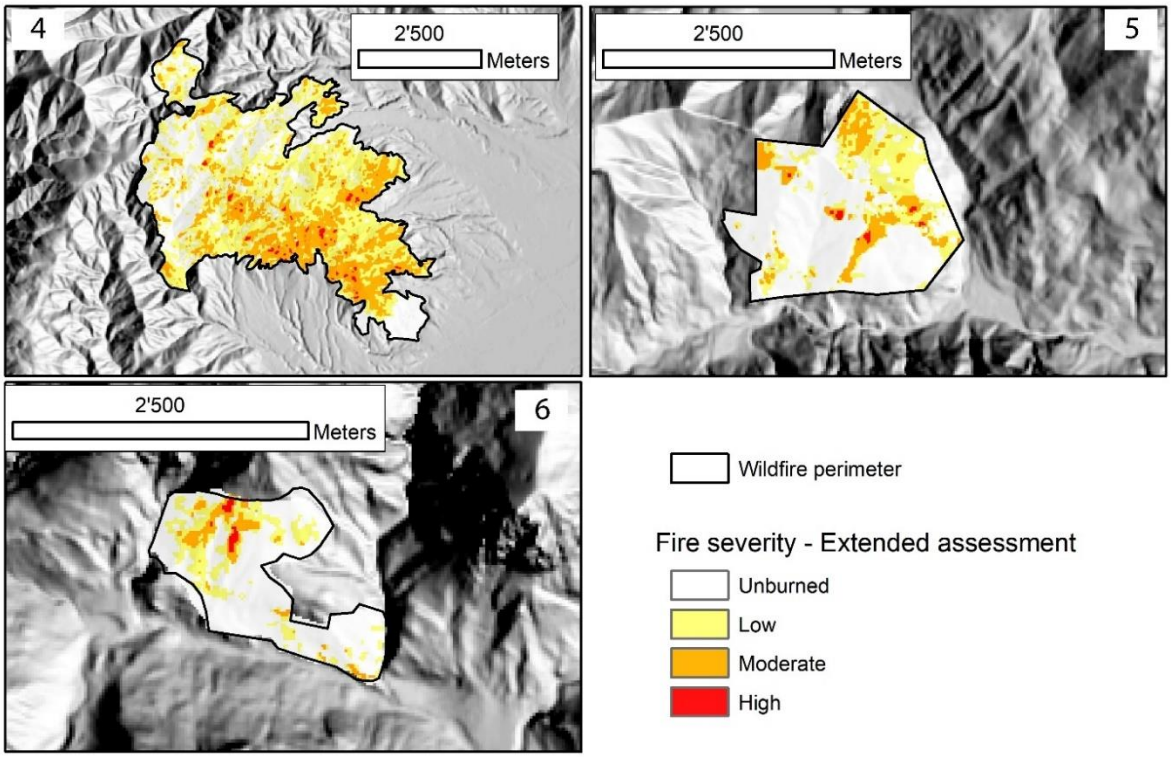


*Figure 6.10 – Fire severity maps, extended assessment, for the Cumiana/Cantalupa (4), Bellino/Casteldelfino (5) and Sambuco/Pietraporzio (6) wildfires (after Morresi et al., 2021)*

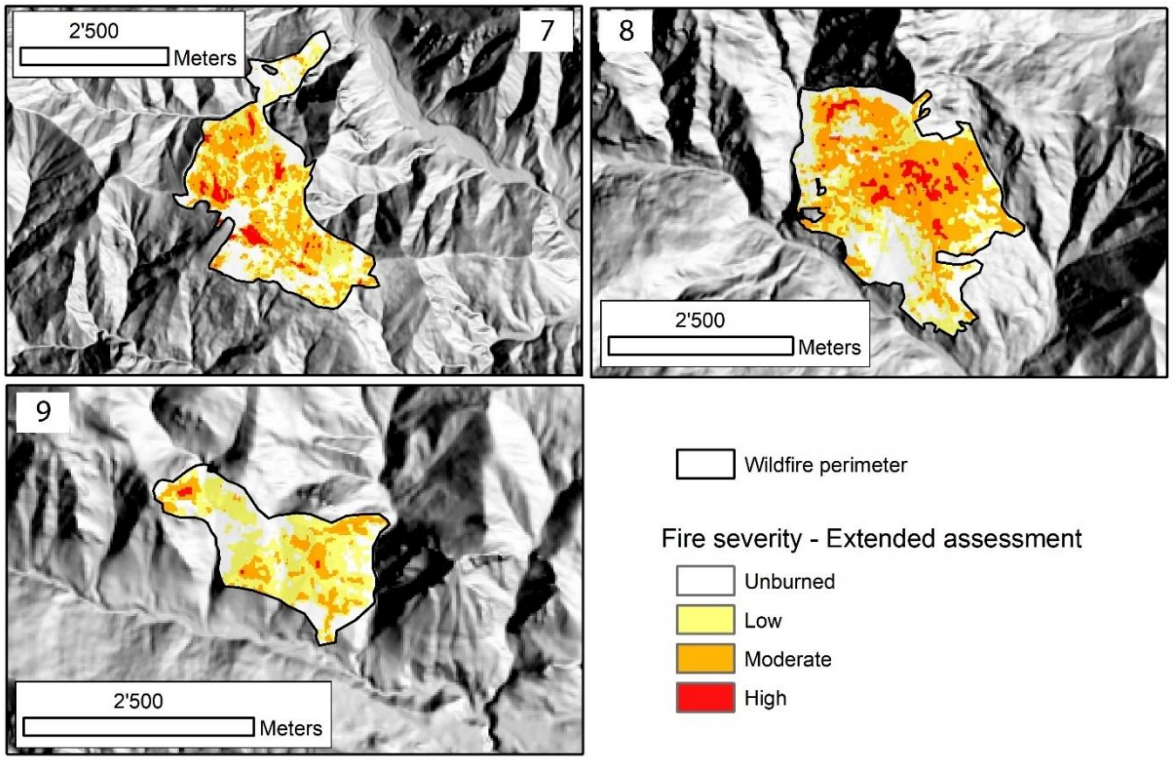


*Figure 6.11– Fire severity maps, extended assessment, for the Roure/Perrero (7), Traversella (8) and Demonte (9) wildfires (after Morresi et al., 2021)*

The analysis of spectral changes was carried out by using images acquired by the European Space Agency (ESA) Sentinel-2A and 2B satellites (S-2A e S-2B). Satellite images, both using bands in the visible wavelength (RGB) and near /shortwave infrared (NIR/SWIR) were downloaded from the Copernicus Open Access Hub[7]. Level 2A products were used if available, otherwise images were first processed for performing the atmospheric, terrain and cirrus correction of Top Of Atmosphere Level 1C input data using Sen2Cor_v2.8 processor[8]. For the fire severity initial assessment images were acquired in October (pre-fire) and November (post-fire) of 2017. By comparison, the extended assessment carried out by Morresi et al (2021) used images acquired in the month of August of 2017 and 2018 respectively for the pre-fire and post-fire.

Normalized Burn Ratio (NBR) index has been calculated at 20 m spatial resolution using surface reflectance in the near infrared (NIR) and in the shortwave infrared (SWIR2), as expressed in the following equation:

$$NBR = (NIR - SWIR)/(NIR + SWIR)$$

For S-2A and S-2B products Bands 8A and Band 12 has been used for NIR and SWIR respectively.

[7] https://scihub.copernicus.eu/
[8] https://step.esa.int/main/snap-supported-plugins/sen2cor/

The Relative delta Normalized Burn Ratio (RdNBR) index (Miller and Thode 2007) has been selected to infer burn severity as it provides relative changes using pre-fire NBR.

$$\mathrm{R}dNBR = \frac{(prefireNBR - postfireNBR)}{\sqrt{|prefireNBR/1000|}}$$

The CBI (Composite Burn Index) is commonly used to define RdNBR thresholds of unburned, low, moderate and high severity classes and to validate burn severity maps (Key and Benson 2006, Miller and Thode, 2007, Miller et al. 2009). The CBI protocol gives a value which is the result of the average value of the severity detected in the field for different layers of vegetation, from undergrowth to arboreal layer (fig. 6.12).

| BI – Long Form | % Burned 100 feet (30 m) diameter from center of plot = | | | | | Fuel Photo Series = | | |
|---|---|---|---|---|---|---|---|---|
| STRATA RATING FACTORS | BURN SEVERITY SCALE | | | | | | | FACTOR SCORES |
| | No Effect | Low | | Moderate | | High | | |
| | 0.0 | 0.5 | 1.0 | 1.5 | 2.0 | 2.5 | 3.0 | |
| **A. SUBSTRATES** | | | | | | | | |
| **% Pre-Fire Cover: Litter =** | **Duff =** | | **Soil/Rock =** | **Pre-Fire Depth (inches): Litter =** | | **Duff =** | **Fuel Bed =** | Σ = |
| Litter/Light Fuel Consumed | Unchanged | -- | 50% litter | -- | 100% litter | >80% light fuel | 98% Light Fuel | |
| Duff | Unchanged | -- | Light char | -- | 50% loss deep char | -- | Consumed | N = |
| Medium Fuel, 3-8 in. | Unchanged | -- | 20% consumed | -- | 40% consumed | -- | >60% loss, deep ch | |
| Heavy Fuel, > 8 in. | Unchanged | -- | 10% loss | -- | 25% loss, deep char | -- | >40% loss, deep ch | $\bar{X}$ = |
| Soil & Rock Cover/Color | Unchanged | -- | 10% change | -- | 40% change | -- | >80% change | |
| **B. HERBS, LOW SHRUBS AND TREES LESS THAN 3 FEET (1 METER):** | | | | | | | | |
| **Pre-Fire Cover =** | | **% Enhanced Growth =** | | | | | | Σ = |
| % Foliage Altered (blk-brn) | Unchanged | -- | 30% | -- | 80% | 95% | 100% + branch loss | |
| Frequency % Living | 100% | -- | 90% | -- | 50% | < 20% | None | N = |
| Colonizers | Unchanged | -- | Low | -- | Moderate | High-Low | Low to None | |
| Spp. Comp. - Rel. Abund. | Unchanged | -- | Little change | -- | Moderate change | -- | High change | $\bar{X}$ = |
| **C. TALL SHRUBS AND TREES 3 to 16 FEET (1 TO 5 METERS):** | | | | | | | | |
| **Pre-Fire Cover =** | | **% Enhanced Growth =** | | | | | | Σ = |
| % Foliage Altered (blk-brn) | 0% | -- | 20% | -- | 60-90% | > 95% | Signifcnt branch loss | |
| Frequency % Living | 100% | -- | 90% | -- | 30% | < 15% | < 1% | N = |
| % Change in Cover | Unchanged | -- | 15% | -- | 70% | 90% | 100% | |
| Spp. Comp. - Rel. Abund. | Unchanged | -- | Little change | -- | Moderate change | -- | High Change | $\bar{X}$ = |
| **D. INTERMEDIATE TREES (SUBCANOPY, POLE-SIZED TREES)** | | | | | | | | |
| **Pre-Fire % Cover =** | **Pre-Fire Number Living =** | | | | **Pre-Fire Number Dead =** | | | Σ = |
| % Green (Unaltered) | 100% | -- | 80% | -- | 40% | < 10% | None | |
| % Black (Torch) | None | -- | 5-20% | -- | 60% | > 85% | 100% + branch loss | N = |
| % Brown (Scorch/Girdle) | None | -- | 5-20% | -- | 40-80% | < 40 or > 80% | None due to torch | |
| % Canopy Mortality | None | -- | 15% | -- | 60% | 80% | %100 | $\bar{X}$ = |
| Char Height | None | -- | 1.5 m | -- | 2.8 m | -- | > 5 m | |
| **Post Fire: %Girdled =** | | **%Felled =** | | **%Tree Mortality =** | | | | |
| **E. BIG TREES (UPPER CANOPY, DOMINANT, CODOMNANT TREES)** | | | | | | | | |
| **Pre-Fire % Cover =** | **Pre-Fire Number Living =** | | | | **Pre-Fire Number Dead =** | | | Σ = |
| % Green (Unaltered) | 100% | -- | 95% | -- | 50% | < 10% | None | |
| % Black (Torch) | None | -- | 5-10% | -- | 50% | > 80% | 100% + branch loss | N = |
| % Brown (Scorch/Girdle) | None | -- | 5-10% | -- | 30-70% | < 30 or > 70% | None due to torch | |
| % Canopy Mortality | None | -- | 10% | -- | 50% | 70% | %100 | $\bar{X}$ = |
| Char Height | None | -- | 1.8 m | -- | 4 m | -- | > 7 m | |
| **Post Fire: %Girdled =** | | **%Felled =** | | **%Tree Mortality =** | | | | |

| Community Notes/Comments: | CBI = Sum of Scores / N Rated: | Sum of Scores | N Rated | CBI |
|---|---|---|---|---|
| | Understory (A+B+C) | | | |
| | Overstory (D+E) | | | |
| | Total Plot (A+B+C+D+E) | | | |

*Figure 6.12 – CBI form (Key and Benson, 2006).*

In this study, CBI survey results provided by Morresi et al. (2021) have been used in the fire severity initial assessment: a linear regression of 251 CBI scores over the 9 wildfire locations has been applied to predict RdNBR thresholds. The coefficient of determination (R2) associated with the regression model is equal to 0.45. The same dataset of CBI scores has been used to predict RdNBR thresholds in the extended assessment (Morresi et al., 2021) giving an R2 equal to 0.89. In table 6-4 RdNBR thresholds determined for the initial and extended assessment are provided.

*Table 6-4 – predicted RdNBR thresholds for the burn severity initial assessment (this work) and the extended assessment (Morresi et al., 2021)*

| Severity Category | CBI score | RdNBR (initial) | RdNBR (extended) |
|---|---|---|---|
| **Unburned** | 0 – 0.1 | <220 | <100 |
| **Low** | 0.1 – 1.24 | 221 - 637 | 101 - 144 |
| **Moderate** | 1.25 – 2.24 | 638 - 999 | 145 - 582 |
| **High** | 2.25 – 3.0 | >=1000 | >=582 |

#### 6.2.3.2 Catchments characterization

Catchments affected by 2017 wildfires, i.e. falling in the official wildfire perimeters, were extracted from Piedmont catchments database (see par 6.2.2.2); for every catchment different parameters were retrieved based on the available spatial data: derived descriptors and statistics belong to different categories, namely morphometry and hydrology, geology and forestry/land-cover (see Appendix 2).

**Morphometry and hydrology**

Main morphological descriptors, related to basin geometry and drainage network, have been derived from 5 m DTM with the help of the Esri ArcGis Hydrology toolbox. Stream network has been calculated based on official watersheds shape, Piedmont Fan map and DTM analysis. First, errors such as sinks were eliminated with the "fill" command. After that "flow direction" was calculated for each pixel using the corrected DTM (see Jenson and Domingue 1988 for reference). "Flow accumulation" was calculated from the flow direction raster, resulting in a grid in which every cell value is equal to the cumulated number of cells that flows into it. The stream network was extracted by considering flow accumulation threshold of 1500 cells. Finally, streams were ordered according to Strahler (1957).

For every watershed, based on DTM the following geometric parameters have been collected: area Aw [$Km^2$], perimeter P [Km], Basin length Lb [km], minimum elevation Emin [m s.l.m.], maximum elevation

Emax [m s.l.m.], mean elevation Emea [m s.l.m.], elevation range Eran [m s.l.m.], minimum slope Smin [°], maximum slope Smax [°], mean slope Smea [°], slope range Sran [°]. Based on produced stream network the following parameters has been retrieved: main channel length Lp [km], average main channel slope LpS [°], total streams length L [km].

Other derived indexes were calculated as follows:

- **Fan to watershed area ratio Af_Aw** [-]: $Af\_Aw = \frac{Af}{A}$ ,

Where **Af** is the fan area, derived from the Piedmont fan map (Giampani et al 2013). The size of alluvial fans depends basically on rates of sediment supply, so it expresses the attitude of the basin to mobilize and transport debris material towards the fan (Regione Piemonte, 2012).

- **Form factor Ff** [-] (Horton 1932): $Ff = \frac{A}{Lb^2}$

Form factor is the ratio of the basin area to the square of basin length. Smaller the value of form factor, more elongated is the basin. For circular watershed, the form factor is 1 and for elongated watershed the Ff value is 0. High Ff watersheds usually have high peak flows of shorter duration, while low Ff watersheds have lower peak flow of longer duration.

- **Circularity ratio Rc** [-] (Miller 1953, Strahler 1964): $Rc = \frac{4\pi A}{P^2}$,

where Rc → 1 indicates a round shape;

0.4 < Rc < 0.5 describes extremely elongated shapes.

Circularity ratio is the ratio of the basin area (A) to the area of a circle having the same perimeter as the basin. Its value is mainly controlled by geology and structure, relief, slope, climate, stream frequency and length. A value of 0 reflects a highly elongated shape and the value of 1 a circular shape.

- **Elongation ratio Re** [-] (Schumm 1956): $Re = \frac{2\sqrt{A}}{Lb\sqrt{\pi}}$

The elongation ratio is the ratio of diameter of a circle of the same area as the basin to the maximum basin length. Re can be discretized as follow: circular (0.9–0.10), oval (0.8–0.9), less elongated (0.7–0.8), elongated (0.5–0.7), and more elongated (< 0.5).

- **Melton Index Me** [-] (Melton 1965): $Me = (Emax - Emin) * A^{-0.5}$

Melton index is frequently used to identify watersheds prone to debris-flow. High Me values indicates a debris-flow attitude of the watershed, while low values indicate a predominancy of flash flood and debris flood phenomena (Marchi et al., 2000).

- **Drainage density Dd** [km/km2] (Strahler 1964): $Dd = \frac{L}{A}$

Drainage density is a measure to analyze the length of different streams per unit area, and is obtained by dividing the total stream length by the total watershed area. It is a measure of the texture of the network and indicates the balance between the erosive power of overland flow and the resistance of surface soils and rocks.

- **Time of concentration Tc** [h] (Kirpich, 1940): $Tc = 0.000325Lp^{0.77} * LpS^{-0.385}$

Time of concentration is defined as the time that a drop of rainwater spends to arrive to the basin outlet section starting from the most hydraulically distant point of the basin, or alternatively as the time from the start of the total runoff to the time of the peak discharge of the total runoff (McCuen 2009). It gives a measure of the time needed for the basin response after a rainfall event.

**Geology**

Watersheds geological characteristics have been derived from the geological map of Piedmont Region (Piana et al 2017), by grouping similar lithological units. Simplified lithological classes are given in table 6-5.

*Table 6-5 – simplified lithological classes description.*

| Legend Class | Description |
|---|---|
| **1** | Carbonate Rich Mudstone, Arenite, Limestone, Conglomerate, Siltstone, Claystone, Mudstone |
| **2** | Chlorite actinolite epidote metamorphic rock, Amphibolite, Schist |
| **3** | fault rocks, breccia |
| **4** | gabbro, metagabbro, diorite |
| **5** | Hornfels |
| **6** | Limestone, Arenite, Carbonate rich mudstone, Impure limestone |
| **7** | Marble, dolomite, pure carbonate mudstone |
| **8** | Migmatite |
| **9** | Rhyolite, Metariolite, Dacite, Orthogneiss |
| **10** | Schist, Mica schist, Gneiss, Quartzite |
| **11** | Serpentinite, Peridotite, Schist |

**Forestry/land-cover**

Land cover data were produced after integrating Land Cover Piemonte dataset (2010) and Forest Map of the Piedmont Region (2016). Forest Map units were grouped based on CLC code, maintaining a separation between forested areas s.s. and vegetated areas with arboreal coverage below 20%. Areas outside the Forest Map has been classified according to Land Cover Piemonte. Bare soil class has been added (table 6-6, 6-7 and 6-8).

*Table 6-6 - forestry and land cover classification and description (part 1)*

| Group | CLC class | Class name | Description |
|---|---|---|---|
| **Urban fabric** | 112 | Discontinuous urban fabric | Areas, substantial part of which are formed mainly by houses, gardens and lawns. |
| **Mine, dump and constructions sites** | 131 | Mineral extraction sites | Areas of quarries |
| **arable land** | 211 | Non-irrigated arable land | Plots of arable landwith rare/sporadic occurrence of scattered greenery. This class includes also fallow lands (3-4 years abandoned). |
| **Permanent crop** | 221 | Vineyards | Areas planted with vines |
| | 222 | Fruit trees and berry plantations | Areas of fruit orchards (apples, plums, pears, cherries, peaches, apricots, etc.) and ligneous crops (walnut, chestnut, hazel, almond, etc.). |
| **Pastures** | 231 | Pastures | Dense, predominantly graminoid grass cover, of floral composition, not under a rotation system. Mainly used for grazing. |
| **Heterogeneous agricultural areas** | 242 | Complex cultivation patterns | Juxtaposition of small parcels of diverse annual crops, pasture and/or permanent crops (arable land, pasture and orchards each occupy less than 75% of the total surface area of the land unit) |
| | 243 | Land principally used for agriculture, with significant areas of natural vegetation | Areas principally used for agriculture, interspersed with significant natural areas (agricultural land occupies between 25 and 75% of the total surface of the land unit) |

*Table 6-7 - forestry and land cover classification and description (part 2)*

| Group | CLC class | Class name | Description |
|---|---|---|---|
| **Forests** | 311 | Broad-leaved forest | Vegetation formation composed principally of trees, including shrub and bush understories, where broadleaved species predominate. |
| | 311b | Broad-leaved forest <20% | Vegetation formation composed principally of trees, including shrub and bush understories, where broadleaved species predominate (less than 20% cover). |
| | 312 | Coniferous forest | Vegetation formation composed principally of trees, including shrub and bush understories, where coniferous species predominate |
| | 312b | Coniferous forest <20% | Vegetation formation composed principally of trees, including shrub and bush understories, where coniferous species predominate (less than 20% cover) |
| | 313 | Mixed forest | Vegetation formation composed principally of trees, including shrub and bush understories, where broadleaved and coniferous species co-dominate. |
| | 313b | Mixed forest <20% | Vegetation formation composed principally of trees, including shrub and bush understories, where broadleaved and coniferous species co-dominate (less than 20% cover). |

*Table 6-8 - forestry and land cover classification and description (part 3).*

| Group | CLC class | Class name | Description |
|---|---|---|---|
| **Scrub and/or herbaceous vegetation associations** | 3211 | Natural grassland prevailingly without trees and shrubs | Areas of natural grasslands without trees and shrubs (less than 15%). They are formed by grasslands of protected areas, alpine grasslands, military training area and abandoned low productivity grassland (e.g. karstic poljes meadows, etc.). |
| | 3212 | Natural grassland with trees and shrubs | Areas of natural grassland with trees and shrubs (between 15-40%). They are formed by grasslands of protected areas, military training areas, alpine grasslands and abandoned low productivity grassland with trees and shrubs. |
| | 322 | Moors and heathland | Vegetation with low and closed cover, dominated by bushes, shrubs and herbaceous plants (heath, briars,broom, gorse, laburnum) |
| | 322b | Moors and heathland <20% | Vegetation with low and closed cover, dominated by bushes, shrubs and herbaceous plants (heath, briars,broom, gorse, laburnum)(Cover less than 20%). |
| | 324 | Transitional woodland-shrub | Bushy or herbaceous vegetation with scattered trees. Can represent either woodland degradation or forest Regeneration/colonisation. |
| **Open spaces with little or no vegetation** | 332 | Bare rocks | Scree, cliffs, rocks and outcrops |
| | 333 | Sparsely vegetated areas | Includes steppes, tundra and badlands. Scattered high-altitude vegetation |
| | 0 | Bare Soil | Bare soil, debris and sediments |

## 6.2.4 Fire-related erodibility model

Fire-related effects on sediment erosion has been assessed implementing, for each watershed, the RUSLE model (Revised Universal Soil Loss Equation – Wischmeier & Smith 1978). The RUSLE empirical model estimates the average annual soil loss caused by surface water erosion through the following equation:

$$A = R * K * L * S * C * P$$

Where A = mean soil loss per year [Mg $ha^{-1}$ $y^{-1}$], *R* = rainfall erosivity factor [MJ mm $h^{-1}$ $ha^{-1}$ $y^{-1}$], *K* = soil erodibility factor [Mg $MJ^{-1}$ $mm^{-1}$ h], *LS* = topographic factor or slope length factor [dimensionless], *C* = soil coverage [dimensionless], and *P* = erosion control practices factor [dimensionless].

The R factor quantifies the mechanical impact energy exerted by a given precipitation, and depends on duration and intensity of the rainfall. Remaining parameters in the equation give a measure of the environmental resistance to erosive phenomena. The K, LS and C factors are assumed to change in areas affected by wildfires as a result of fire effect on soil erodibility, vegetative cover and shift in rill to interrill soil erodibility ratio (Terranova et al. 2009).

It is worth to stress that RUSLE model is intended to quantify soil losses in the long term, so that processes such as gully and channel erosion and sediment transport cannot be modelled. Prediction accuracy for individual storm is very low, as controversial is the application on large spatial scale. Despite this, the model can be used as a solid framework to quantify high-risk erodible areas (Efthimiou et al 2020).

With this regard, the product of K, LS and C factor is used in this work to compare post-fire to pre-fire condition; thus the Erodibility Index EI [Mg $MJ^{-1}$ $mm^{-1}$ h] is introduced to describe the erosion susceptibility:

$$EI = C * K * Ls$$

The application of the methodology has been implemented by using both available data (DTM, rainfall erosivity factor, land cover map and soil erodibility factor) and GIS data processing (fig. 6.13).

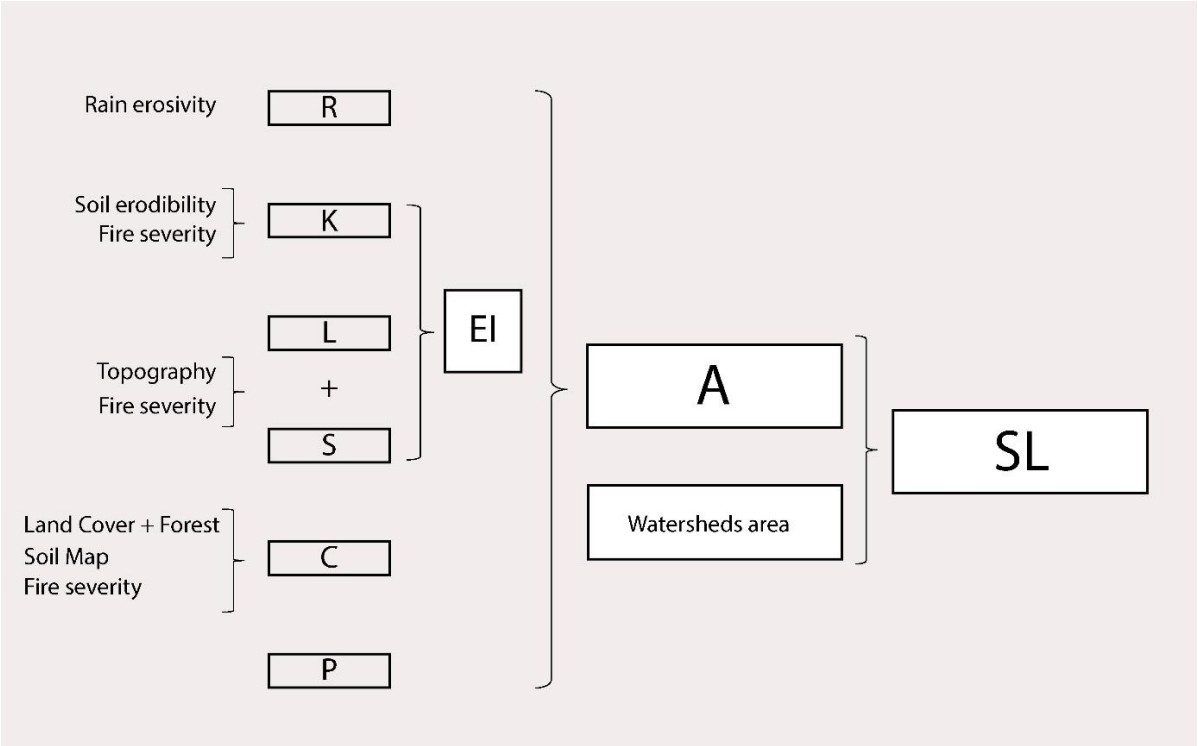


*Figure 6.13 - Fire-related erodibility model scheme*

The R factor has been taken from Panagos et al. (2015a) and downloaded as 500m resolution raster from ESDAC (European Soil Data Centre) repository[9].

The K factor has been taken from piedmont erodibility map (IPLA).

The C factor has been assessed based on Forestry/Land Cover Map and by assigning C values according to Panagos et al. (2015b); values used in this work are the mean values of the range proposed by the authors. Tabulated values for each land cover class are given in table 5-9.

*Table 6-9 – RUSLE cover factor proposed for each land cover class (after Panagos et al., 2015b)*

| CLC class | Class name | C-factor values |
|---|---|---|
| **112** | Discontinuous urban fabric | 0 |
| **131** | Mineral extraction sites | 0 |
| **211** | Non-irrigated arable land | 0.23 |
| **221** | Vineyards | 0.34 |
| **222** | Fruit trees and berry plantations | 0.1 |
| **231** | Pastures | 0.09 |
| **242** | Complex cultivation patterns | 0.147 |
| **243** | Land principally used for agriculture, with significant areas of natural vegetation | 0.124 |
| **311** | Broad-leaved forest | 0.0013 |
| **311b** | Broad-leaved forest <20% | 0.003 |
| **312** | Coniferous forest | 0.0013 |
| **312b** | Coniferous forest <20% | 0.003 |
| **313** | Mixed forest | 0.0013 |
| **313b** | Mixed forest <20% | 0.003 |
| **3211** | Natural grassland prevailingly without trees and shrubs | 0.04 |
| **3212** | Natural grassland with trees and shrubs | 0.03 |
| **322** | Moors and heathland | 0.055 |
| **322b** | Moors and heathland | 0.055 |
| **324** | Transitional woodland-shrub | 0.024 |
| **332** | Bare rocks | 0 |
| **333** | Sparsely vegetated areas | 0.25 |
| **0** | Bare Soil | 1 |

[9] esdac.jrc.ec.europa.eu, European Commission, Joint Research Centre

The LS factor in the original RUSLE model describes the interaction between standard parcel length (L) and slope (S). In this study it is substituted by the unit contributing area Ls, which takes into account the flow convergence (Mitasova et al. 1996, Terranova et al. 2009). Ls is computed for each 5 meters wide DTM cell as follows:

$$Ls = (\mu + 1)(a/a_0)^{\mu}(\sin b/b_0)^{\eta}$$

Where a [m]= the upslope contributing area for each cell (result of the ArcGIS "flowacc" and "resolution" functions), b [%]= slope, $a_0$ [m] = 21.1 m (the standard USLE plot length), $b_o$ [%] = 9 % (the standard USLE plot slope).

The parameter μ is calculated as a function of β, which is the ratio of rill to interrill erosion (Miller et al. 2003, Foster et al. 2003):

$$\mu = {}^{\beta}/_{(1+\beta)}$$

Based on literature, β can be set equal to 0.5 for unburned areas and equal to 1 for high severity burned areas. The parameter η is considered equal to 1.2 following Terranova et al. (2009) and Coschignano et al. (2020). P factor has been considered equal to 1.

#### 6.2.4.1 Pre-fire

Pre-fire mean soil loss per year $A_{pre}$ and Erodibility Index $EI_{pre}$ have been calculated based on the previous equations on a 5 meters resolution raster grid based on DTM cells. Available dataset has been used for $R_{pre}$ and $K_{pre}$ factor, $C_{pre}$ factor has been assigned to each cell and Ls factor has been computed according by setting β=0.5.

A spatially weighted average of calculated $EI_{w\_pre}$ and $A_{w\_pre}$ value has been then computed for every watershed affected by 2017 wildfires. Finally, the value of sediment loss $SL_{pre}$ [Mg $y^{-1}$] for each watershed has been calculated with the following equation:

$$SL_{pre} = A_{\mathrm{pre\_w}} * A_w$$

Where $A_w$= watershed area.

#### 6.2.4.2 Post-fire

Post-fire condition has been modeled for both the initial and the extended assessment by calculating mean soil loss per year $A_{ini}$ and $A_{ext}$ and erodibility Index $EI_{ini}$ and $EI_{ext}$ following the before mentioned procedure.

Parameters $C_{ini}$, $C_{ext}$, $K_{ini}$, $K_{ext}$, $Ls_{ini}$ and $Ls_{ext}$ has been adjusted as a function of fire severity (unburned, low, moderate or high) following Terranova et al. (2009) and Lanorte et al. (2019) as expressed in table 6-10.

*Table 6-10 Adjusted cover factors, erodibility factors and β value (LS factor) for different fire severity classes.*

| Burn Severity class | C factor | K factor | β value (LS) |
|---|---|---|---|
| **Unburned** | $C_{pre}$ | $K_{pre}$ | 0.5 |
| **Low** | 0.01 | 1.6 * $K_{pre}$ | 1 |
| **Moderate** | 0.05 | 1.8 * $K_{pre}$ | 1 |
| **High** | 0.2 (1 in grassland) | 2 * $K_{pre}$ | 1 |

For both the scenarios A and EI values has been subsequently averaged for each watershed following the same pre-fire condition procedure, giving $A_{w\text{-}ini}$, $A_{w\_ext}$, $EI_{w:ini}$ and $EI_{w\_ext}$ values.

Finally, $SL_{ini}$ and $SL_{ext}$ [Mg $y^{-1}$] has been then calculated repeating the pre-fire procedure.

#### 6.2.4.3 Pre-fire vs post-fire

EI values calculated for the pre-fire situation $EI_{w\_pre}$, for the post-fire initial assessment $EI_{w\_ini}$ and for the post-fire extended assessment $EI_{w\_ext}$ have been finally compared by calculating their relative ratios:

$$R\_EI_{\ ini\_pre} = \frac{\mathrm{EI_{w\_ini}}}{\mathrm{EI_{w\_pre}}}$$

$$R\_EI_{\ ext\_pre} = \frac{\mathrm{EI_{w\_ext}}}{\mathrm{EI_{w\_pre}}}$$

$$R\_EI_{\ ext\_ini} = \frac{\mathrm{EI_{w\_ext}}}{\mathrm{EI_{w\_ini}}}$$

In an analogous way, A values calculated for the pre-fire situation $A_{w\_pre}$, for the post-fire initial assessment $A_{w\_ini}$ and for the post-fire extended assessment $A_{w\_ext}$ have been compared by calculating their relative ratios:

$$R\_A_{\ ini\_pre} = \frac{\mathrm{A_{w\_ini}}}{\mathrm{A_{w\_pre}}}$$

$$R\_A_{\ ext\_pre} = \frac{\mathrm{A_{w\_ext}}}{\mathrm{A_{w\_pre}}}$$

### 6.2.5 Fire-related runoff model

The SCS-CN (SCS-USDA 1986) model (fig. 6.15) is a widely used method for estimating the volume of surface runoff from watersheds with a few applications to burned areas (Leopardi et al. 2015;

Coschignano et al. 2019). The infiltration losses are computed as a function of cumulative precipitation, soil cover, land use and antecedent moisture.

The variable relation is expressed by the following equations:

$$Q = \begin{cases} \dfrac{(P - I_a)^2}{P - I_a + S} & P > I_a \\ 0 & P \leq I_a \end{cases}$$

where Q [mm]= the accumulated runoff or rainfall excess at given time, P [mm] = rainfall depth, $I_a$ [mm]= initial abstraction or initial loss and S [mm] = potential maximum retention after runoff begins. $I_a$ is highly variable but generally is correlated with soil and land cover parameters. A commonly assumed empirical relationship links $I_a$ and S:

$$I_a = 0.2S$$

The potential maximum retention S is given by:

$$S = \frac{25400}{CN} - 254$$

Where CN is a dimensionless catchment parameter ranging from 30 to 100 and is derived from data reflecting land cover, hydrologic soil group HSG (A, B, C and D) and antecedent soil moisture condition (SCS - USDA 1986). Lower CN values characterize high infiltration rate and reduced runoff depth, while higher CN values are proper of situation in which the infiltration is reduced, and the runoff is increased.

The HSGs are derived from standard SCS soil classifications ranging from A, which belongs to sand and aggregated silts with high infiltration rates, to D, which refers to soils that swell significantly when wet and have low infiltration rates. HSGs characteristics are reported in table 6-11:

*Table 6-11 – SCS-CN model hydrologic soil groups description.*

| HSG | Surface runoff potential | Description |
|---|---|---|
| **A** | Low | Sand, loamy sand or sandy loam types of soils. Low runoff potential and high infiltration rates even when thoroughly wetted |
| **B** | Moderately low | Silt loam or loam. Moderate infiltration rate when thoroughly wetted. |
| **C** | Moderately high | Sandy clay loam. Low infiltration rates, downward movement impeded |
| **D** | High | Clay loam, silty clay loam, sandy clay, silty clay or clay. Very low infiltration rates |

Curve Numbers suggested values are tabulated as a function of Cover type, Hydrologic condition an HSGs.

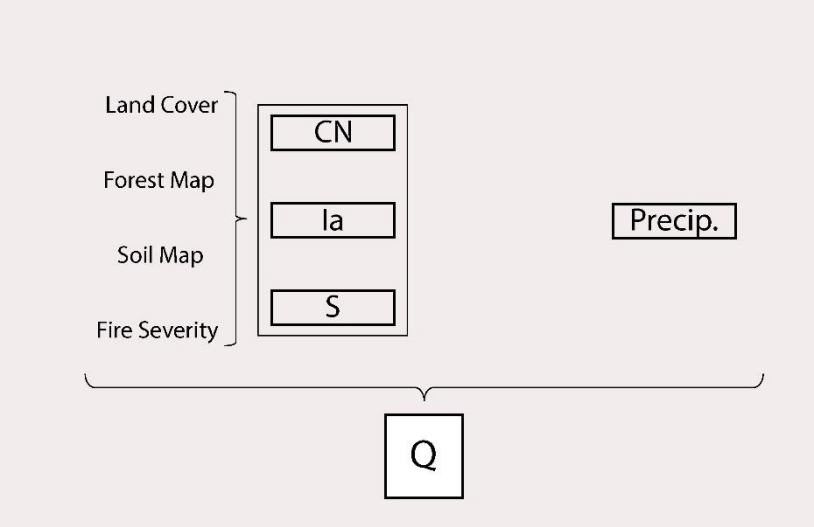


*Figure 6.14 - Fire-related runoff model scheme.*

In the following figure (fig. 6.15), an example of suggested values for natural environment is reported, while the complete CN table is reported in Appendix 1.

| Cover description | | Curve numbers for hydrologic soil group | | | |
|---|---|---|---|---|---|
| Cover type | Hydrologic condition | A | B | C | D |
| Pasture, grassland, or range—continuous forage for grazing. [2] | Poor | 68 | 79 | 86 | 89 |
| | Fair | 49 | 69 | 79 | 84 |
| | Good | 39 | 61 | 74 | 80 |
| Meadow—continuous grass, protected from grazing and generally mowed for hay. | — | 30 | 58 | 71 | 78 |
| Brush—brush-weed-grass mixture with brush the major element. [3] | Poor | 48 | 67 | 77 | 83 |
| | Fair | 35 | 56 | 70 | 77 |
| | Good | 30 [4] | 48 | 65 | 73 |
| Woods—grass combination (orchard or tree farm). [5] | Poor | 57 | 73 | 82 | 86 |
| | Fair | 43 | 65 | 76 | 82 |
| | Good | 32 | 58 | 72 | 79 |
| Woods. [6] | Poor | 45 | 66 | 77 | 83 |
| | Fair | 36 | 60 | 73 | 79 |
| | Good | 30 [4] | 55 | 70 | 77 |
| Farmsteads—buildings, lanes, driveways, and surrounding lots. | — | 59 | 74 | 82 | 86 |

*Figure 6.15 – SCS-CN model runoff curve numbers for non-cultivated surfaces (SCS-USDA 1986, see appendix 2 for the complete table).*

Values for AMCII condition (moderate soil moisture) is given as the base CN and can be adjusted for taking into account near saturated soil moisture condition (AMCIII) or dry antecedent soil moisture condition (AMCI) (Chow et al. 1988):

$$CN_I = \frac{CN_{II}}{2.334 - 0.01334CN_{II}}$$

$$CN_{III} = \frac{CN_{II}}{0.4036 + 0.059CN_{II}}$$

For catchment characterized by heterogeneous soil types and covers, the resulting Curve Number $CN_w$ can be determined by weighting the sub-areas CN values proportionally to their relative spatial extension by applying the following equation:

$$CN_w = \frac{CN_1A_1 + CN_2A_2 + \cdots + CN_iA_i + CN_nA_n}{\sum_{i=1}^{n} A_i}$$

where $CN_i$ is the CN value of the sub-area *i*, *A* is the area of the sub-area *i*, and *n* is the total number of sub-areas.

A weighted average of all CN values in a watershed is commonly used to reduce the number of calculations, ad brings the assumption that CN values and runoff are linearly related, although this is not true (Grove et al 1998). This can lead to an underestimation of runoff absolute values when a wide range of CN values is found. In this study watersheds are generally small though hydrological condition and fire effects are generally not homogeneous. Despite this, the aim of this study is to evaluate the relative difference in the excess runoff from post-fire conditions with respect to pre-fire situation, so the uncertainty arising from application of the weighted average method seems acceptable beyond the possible drawbacks.

#### 6.2.5.1 Pre-fire

*CN* values for the watersheds affected by the 2017 wildfires have been computed by combining information from the land cover map and the hydrologic soil group map, which was produced by assigning a particular hydrologic soil group (A, B, C or D) depending on the predominant soil type.

In detail, CN values have been calculated for homogeneous sub-areas, derived from the intersection between land cover polygons and HSG polygons. Appropriate CN values have been assigned to each feature by following SCS-USDA (1986) under the hypothesis of AMCIII condition, simulating the moisture condition reasonably existing after a prolongated rainfall period.

Subsequently, area-weighted $CNw\_{pre}$ values for the 49 watersheds have been computed according to the aforementioned equations.

After that, $S_{w\_pre}$ and $I_{a\ w\_pre}$ values have been calculated leading to the excess runoff values Q for a chosen design 24h precipitation; a 5 year return period 24h rainfall depth for every watershed has been retrieved from Atlante Piogge Intense webGis service (Arpa Piemonte). Precipitation values given for the Gumbel distribution have been selected at the watersheds centroid and assumed to be uniform at the watershed scale. The 24h – 5 year return period rainfall has been chosen to replicate the rainfall event which caused the Bussoleno debris-flow the June 7, 2018. Selected rainfall values are given in the tables 6-12 -- 6-20.

*Table 6-12 - Design 24h precipitation for the watersheds affected by the Locana/Ribordone wildfire.*

| **Fire n. 1** | **LOCANA/RIBORDONE** | |
|---|---|---|
| **WATERSHED ID** | **WATERSHED NAME** | **P24h_5A [mm]** |
| **1** | Rio Fura | 168.6 |
| **2** | Rio Di Chioso Bosco | 177.6 |
| **3** | R. Montepiano | 164.9 |
| **4** | Carlevaria | 175.2 |
| **5** | Rio Di Bardonetto Inferiore | 175.9 |
| **6** | Ribordone | 166.7 |
| **7** | Eugio | 154.1 |
| **8** | Rio Bocchetta | 172.8 |
| **9** | Rio Di Calsazio | 173.5 |
| **48** | Locana Est | 168.2 |
| **49** | Apparè | 173.2 |

*Table 6-13 - Design 24h precipitation for the watersheds affected by the Bussoleno/Mompantero wildfire.*

| **Fire n. 2** | **BUSSOLENO/MOMPANTERO** | |
|---|---|---|
| **WATERSHED ID** | **WATERSHED NAME** | **P24h_5A [mm]** |
| **10** | Crosiglione | 99.5 |
| **11** | Rio Della Ravoire | 99.1 |
| **12** | Fogasso | 100.3 |
| **13** | Rio Della Codrea | 99.2 |
| **14** | Trinità | 98.1 |
| **15** | Rio Prebech | 111.6 |
| **16** | Moletta | 107.7 |
| **17** | Rio Di Periere | 101.3 |
| **18** | Ravera | 100.3 |
| **19** | Comba Delle Foglie | 102.8 |
| **20** | Rocciamelone | 107.6 |
| **21** | Giandula | 102.4 |
| **22** | I Piani | 98.4 |
| **23** | San Giuseppe | 95.8 |

*Table 6-14 - Design 24h precipitation for the watersheds affected by the Caprie/Rubiana wildfire.*

| **Fire n. 3** | **CAPRIE/RUBIANA** | |
|---|---|---|
| **WATERSHED ID** | **WATERSHED NAME** | **P24h_5A [mm]** |
| **24** | Messa | 145.6 |
| **25** | Sessi | 138.7 |
| **26** | Novaretto | 133.2 |
| **27** | Fra Barbe | 136.9 |

*Table 6-15 - Design 24h precipitation for the watersheds affected by the Cumiana/Cantalupa wildfire.*

| **Fire n. 4** | **CUMIANA/CANTALUPA** | |
|---|---|---|
| **WATERSHED ID** | **WATERSHED NAME** | **P24h_5A [mm]** |
| **28** | 1*Int. Dx. Sangone | 139.8 |
| **29** | Chisola Torrente | 110.9 |
| **30** | Noce Torrente | 120.8 |
| **31** | Chisola Pianura | 104.5 |

*Table 6-16 - Design 24h precipitation for the watersheds affected by the Bellino/Casteldelfino wildfire.*

| **Fire n. 5** | **BELLINO/CASTELDELFINO** | |
|---|---|---|
| **WATERSHED ID** | **WATERSHED NAME** | **P24h_5A [mm]** |
| **32** | Cumbal Della Comu | 86.4 |
| **33** | T. Mas Del Bernard | 89.4 |

*Table 6-17 - Design 24h precipitation for the watersheds affected by the Sambuco/Pietraporzio wildfire.*

| **Fire n. 6** | **SAMBUCO/PIETRAPORZIO** | |
|---|---|---|
| **WATERSHED ID** | **WATERSHED NAME** | **P24h_5A [mm]** |
| **34** | R. Bianco | 98.3 |
| **35** | Sn | 94.1 |
| **36** | Rio Di Castello Pietraporzio | 96.2 |

*Table 6-18 - Design 24h precipitation for the watersheds affected by the Roure/Perrero wildfire.*

| **Fire n. 7** | **ROURE/PERRERO** | |
|---|---|---|
| **WATERSHED ID** | **WATERSHED NAME** | **P24h_5A [mm]** |
| **37** | V.Ne Di Borsetto | 127.4 |
| **38** | S. Martino Sud | 127.7 |
| **39** | Colet | 122.9 |
| **40** | Molotta | 132 |
| **41** | Gernier | 128.1 |

*Table 6-19 - Design 24h precipitation for the watersheds affected by the Traversella wildfire.*

| **Fire n. 8** | **TRAVERSELLA** | |
|---|---|---|
| **WATERSHED ID** | **WATERSHED NAME** | **P24h_5A [mm]** |
| **42** | T.Bersella | 158.8 |
| **43** | Valle Chiara Primo | 176.9 |

*Table 6-20 - Design 24h precipitation for the watersheds affected by the Demonte wildfire.*

| **Fire n. 9** | **DEMONTE** | |
|---|---|---|
| **WATERSHED ID** | **WATERSHED NAME** | **P24h_5A [mm]** |
| **44** | V. Del Saut | 110.8 |
| **45** | Valle Di Monfreis | 108.9 |
| **46** | Sn 2 | 106 |
| **47** | Rio Di Prafioret C. | 108.7 |

#### 6.2.5.2 Post-fire

Post-fire condition has been modeled by computing post-fire *CN* values as a function of fire severity (unburned, low, moderate or high). Empirical relationships reported by Foltz et al. (2009) have been used to adjust pre-fire CN values:

• High burn severity without water repellent soils: $CN_{post} = 91$

• Moderate burn severity without water repellent soils: $CN_{post} = 85$

• Low burn severity: $CN_{post} = CN_{pre} + 5$

Two separate post-fire CN maps have been calculated based on fire severity maps produced for the Initial burn severity assessment and the extended severity assessment respectively. For both the scenarios CN values ($CN_{ini}$ and $CN_{ext}$) have been subsequently averaged for each watershed following the same pre-fire condition procedure giving the value ($CN_{w\_ini}$ and $CN_{w\_ext}$) characteristic of each catchment. $S_{w\_ini}$, $S_{w\_ext}$ $I_{a\ w\_ini}$, $I_{a\ e\_ext}$, $Q_{w\_ini}$ and $Q_{w\_ext}$ have been then calculated repeating the pre-fire procedure.

#### 6.2.5.3 Pre-fire vs post-fire

Excess runoff depth calculated for the pre-fire situation $Q_{pre\_w}$, for the post-fire initial assessment $Q_{ini\_w}$ and for the post-fire extended assessment $Q_{ext\_w}$ has been finally compared by calculating their relative ratios:

$$R\_Q_{\ ini\_pre} = \frac{Q_{w\_ini}}{Q_{w\_pre}}$$

$$R\_Q_{\ ext\_pre} = \frac{Q_{w\_ext}}{Q_{w\_pre}}$$

$$R\_Q_{\ ext\_ini} = \frac{Q_{w\_ext}}{Q_{w\_ini}}$$

## 6.3 The Comba delle Foglie Case Study

The Comba delle Foglie watershed is one of the 14 watersheds affected by the 2017 Bussoleno/Mompantero wildfire. The fire burned 4000 ha on the left of the Dora Riparia river, going up the valley from east to west and affecting the slope almost to the divide. It started on October 22, 2017 and lasted until November 1, 2017. The East–West mountain ridge is mainly formed by rock belonging to two tectonic elements: a) the Upper Unit of the Dora Maira Massif (DM) and b) the Lower Piedmont Zone, represented here by the bassa Val di Susa - Valli di Lanzo - Monte Orsiera unit (SU). DM is one of the nappes of the inner Penninic Domain, characterized a pre-Triassic basement (DMb) and its Mesozoic cover (DMc). The SU consists of oceanic units of the Tethys ocean, which overthrust the DM units with different structural elements (Gasco et al. 2011). Micaschists and gneiss of the DMb, calcschists, marbles and dolomitic marbles belonging to DMc characterize the lower part of the Comba delle Foglie while calcschists, serpentinites, serpentinoschists and chloritoschist belonging to SU outcrop in upper part of the catchment (Carraro et al, 2002) (Fig. 6.16)

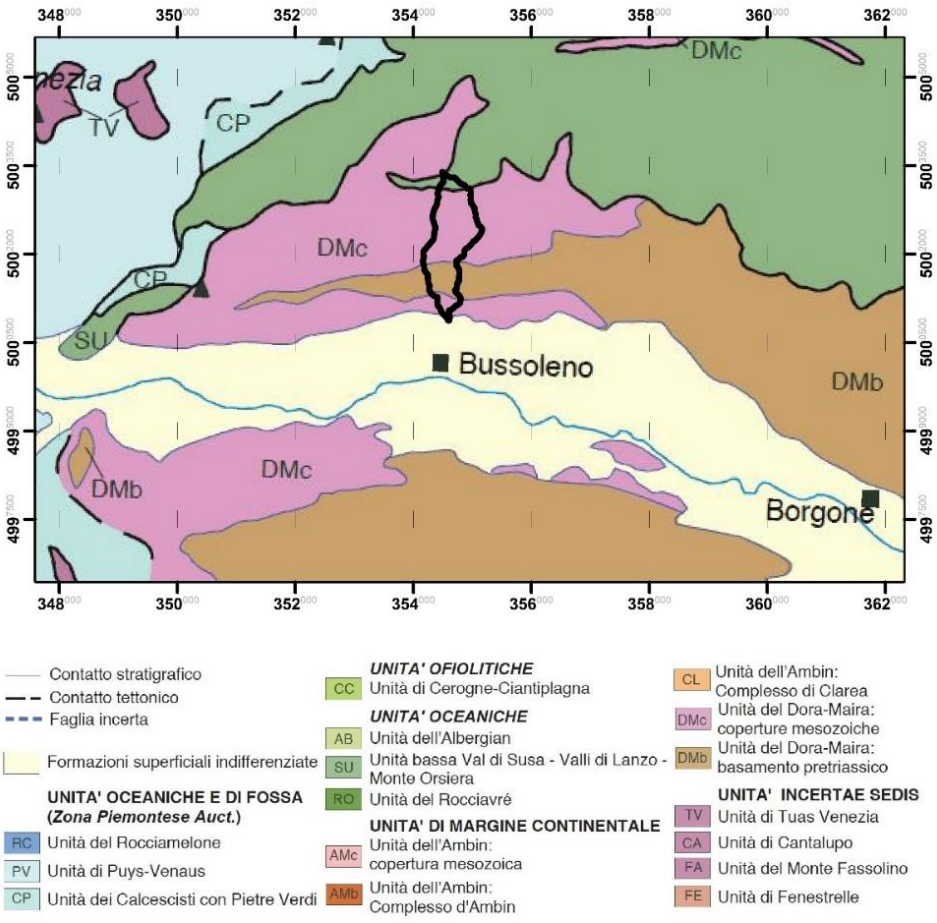


*Figure 6.16 – Tectonic scheme of the Susa valley. Solid line represents the Comba delle Foglie perimeter (Modified after Carraro et al, 2002).*

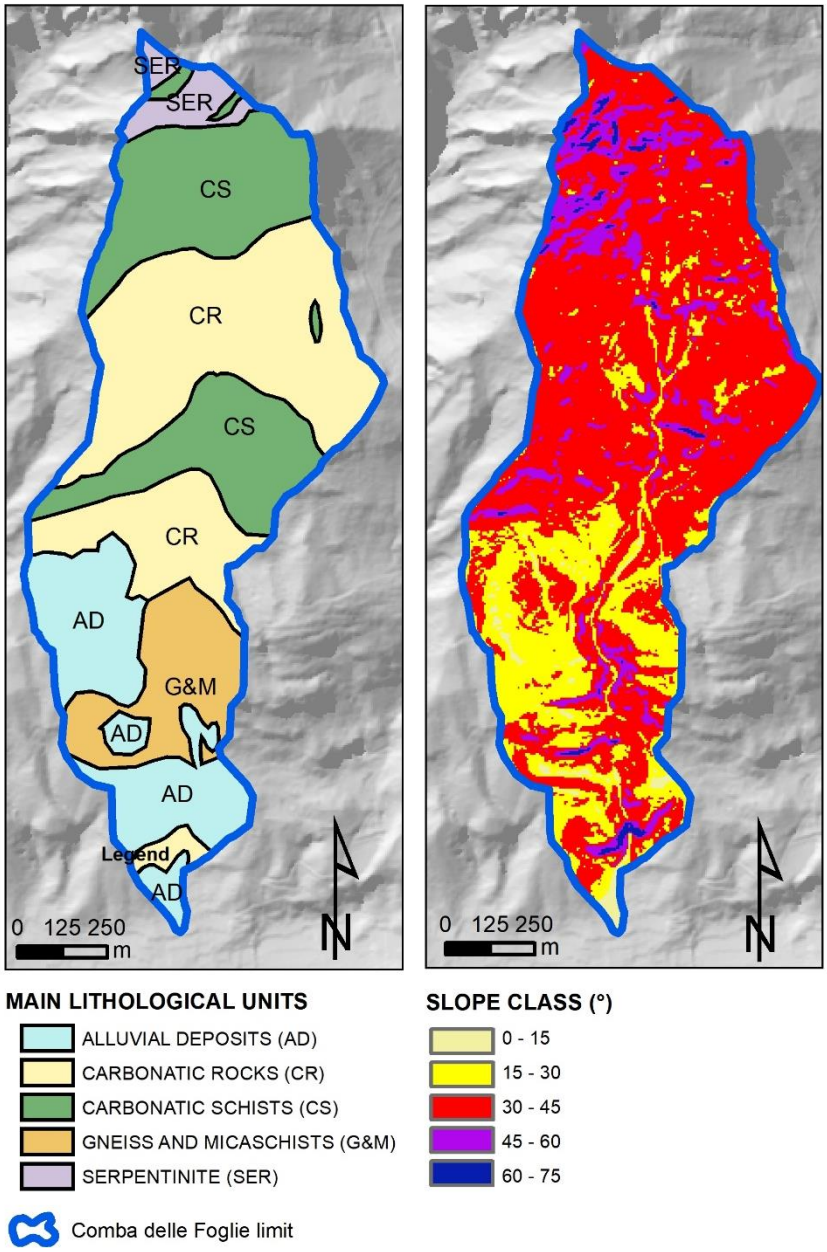


*Figure 6.17 – Main lithological units and slope classes characterizing the Comba delle Foglie watershed.*

Burn severity map for the 2017 wildfire has been produced according to the explained procedure (par. 6.2.3). The same watershed was burned in 2003: the methodology for assessing burn severity has been applied to Landsat 5 pre (Aug 2003) and post-fire (Sept 2003) 30 m resolution images. Reflectance values has been obtained for L5 by converting the digital numbers (DNs) to top-of-atmosphere (TOA) reflectance (Lλ) and then to surface reflectance by applying the Dark Object Subtraction method applied to Band 4 and 7 respectively. No extended assessment was carried out.

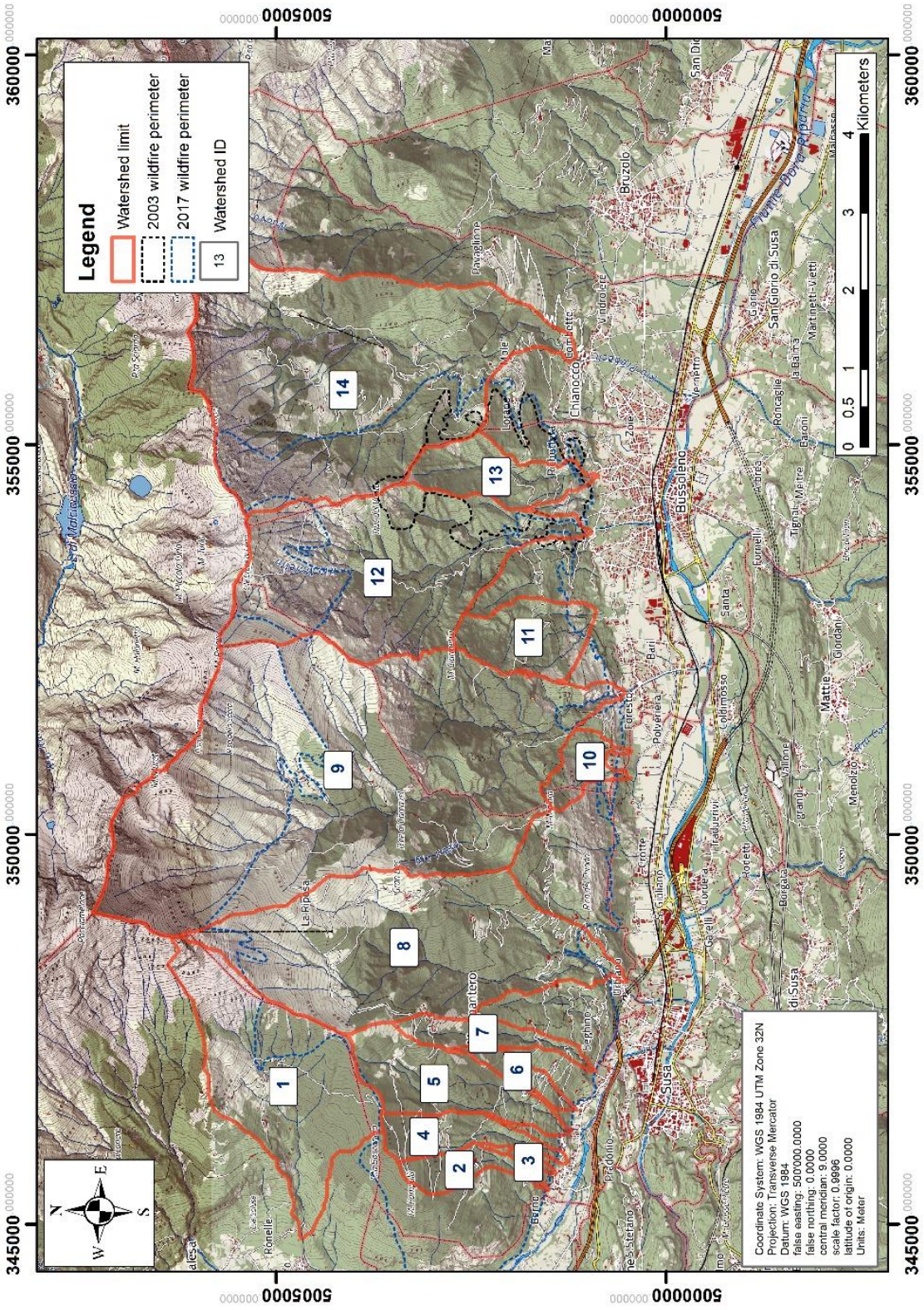


*Figure 6.18 – 2003 and 2017 wildfire perimeters over the Bussoleno/Mompantero area. Watersheds perimeter and code is reported.*

Starting from the spring of 2018, precipitation in the Piedmont area far exceeded the annual averages (see chapter 5), and many sediment-laden floods and debris-flows were registered.

On April 29, 2018 a debris flow hit the northern portion of Bussoleno municipality, coming from Comba delle Foglie watershed, affecting the fan in several positions and causing damages to roads. Traces of enhanced erosion in the stream path were found, while debris, finer material and floated burn residuals were deposited at the upper portion of the fan.

On May 2, 9 and 13, 2018 minor debris-flow and floods events were recorded, without causing relevant damages. On June 7, 2018 a major debris flow, which caused severe damage to roads, buildings and infrastructures was registered. Up to two meters of mud and debris were deposited at the fan outlet. The event caused the complete destruction of two houses, two others were compromised and structural damage to 12 buildings had to be recorded. Gas, water and electrical energy supply were interrupted, and 150 people were evacuated.

*Figure 6.19 – Flow deposits and damages of the June 7 major debris flow at the Comba delle Foglie outlet (Bussoleno).*

Rainfall series from four rain gauges (Arpa Piemonte Network) and radar rainfall intensities estimates were collected. The rain gauges of Prarotto, Pietrastretta, Borgone and Usseglio Malciaussia, between 11:30 and 12:30 UTC recorded 0.4mm, 3.2mm, 0.0mm and 0.2 mm respectively. More consistent rainfall values were registered between 15:00 and 18:30 UTC. However, given the distance and the difference in altitude of the

rain gauges with respect to the basin, as well as in light of the thunderstorm nature of the rainfall, the rainfall data from these measurements cannot be considered completely reliable in this occasion.

The rainfall intensity estimated by radar for the June 7 event showed peaks between 60 and 100 mm/h at 12: 00 UTC. Then between 12:00 and 12:10 about 10 mm fell with an intensity of 60 mm/h. The cumulated rainfall on the ground relative to the interval 11: 55–12: 25 was about 15 mm. These quantities correspond to a return period of 5 years (ARPA Piemonte 2018b).

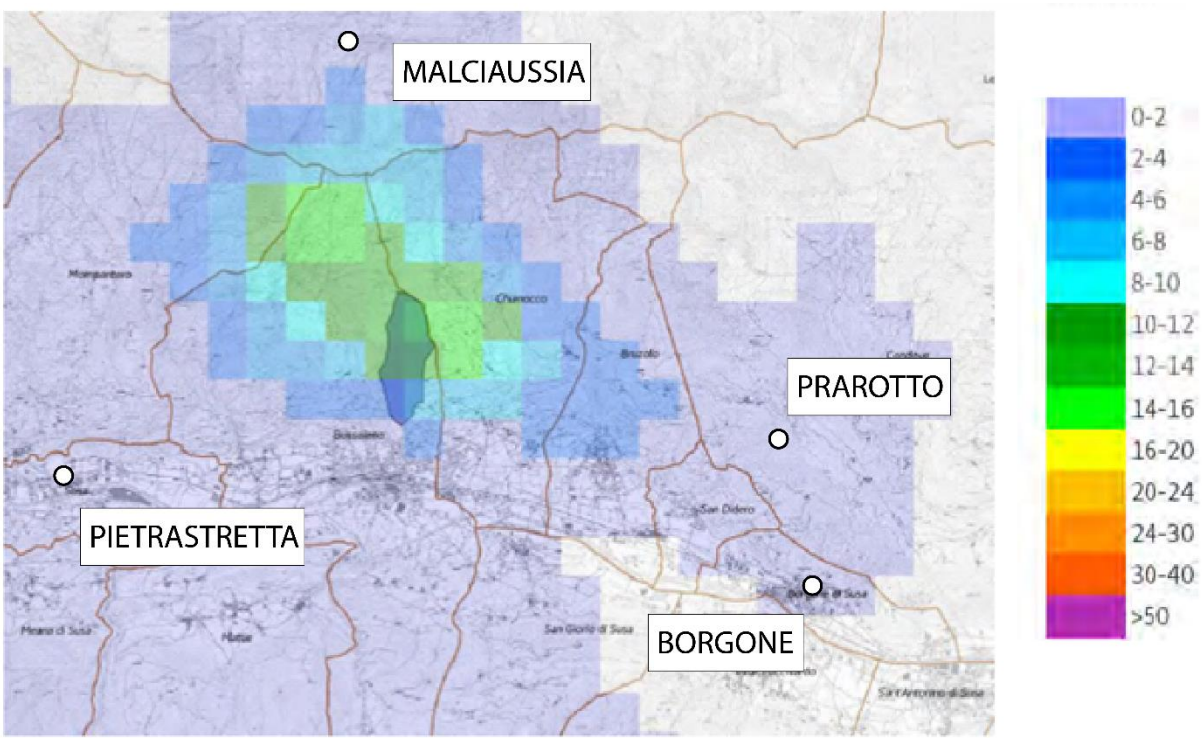


*Figure 6.20 – Cumulated rainfall in the 11:55 – 12:25 UTC of the June 7, 2018. The Comba delle Foglie watershed is highlighted (ARPA Piemonte 2018b). Positions Arpa rain gauges are marked with the white dots.*

### 6.3.1 Field surveys and post-fire watershed response

Field surveys have been carried out on May and June 2018, just after the first minor debris and mud-flow events, to quantify and to map the erosional and depositional features, both on open-slope sectors and over the drainage network. An inventory of the evidence of landslides was also done. Surveys have been repeated immediately after the June 7 debris flow, allowing to have a direct comparison and evidence of the pre- and post-event situation. The June 7 debris flow deposits have been sampled for performing grain size distribution analysis in order to compare deposit and soil textural characteristics. Photogrammetric modelling and Gis elaboration have been carried out to reconstruct pre- and post-event digital terrain models of the bottom of the watershed and of the main deposition area. A dataset of UAV images provided by the Provincial Fire Department was used to produce a 25 cm DTM + Ortophoto of the post-

event scenario; the 5m DTM from Piedmont Region has been then used as a comparison for estimating area and volume of the June 7 debris-flow.

### 6.3.2 Monthly erosion calculation

Sediment erosion has been assessed implementing the RUSLE model at a monthly scale (Revised Universal Soil Loss Equation – Wischmeier & Smith 1978).

The R factor quantify the mechanical impact energy exerted by a given precipitation and depends on duration and intensity of the rainfall. It can be estimated at a monthly scale by calculating the summation of the parameter $EI_{30}$ of every single erosive event k for each considered month.

$$R_{month} = \sum_{k=1}^{n} EI_{30\,k}$$

Following Brown and Foster (1987), $EI_{30}$ for a single rainstorm event is defined as the product of the kinetic energy of rainfall events (E) and its maximum 30-minute intensity ($I_{30}$):

$$EI_{30} = \left(\sum_{r=1}^{m} e_r v_r\right) I_{30}$$

where $e_r$ = unit rainfall energy [MJ ha−1 mm−1], $v_r$ = rainfall volume [mm] during the r-th period of a storm which divided into m parts and $I_{30}$ is the maximum 30-minute rainfall intensity [mm h−1]. The unit rainfall energy $e_r$ is calculated for each time interval as eq xx (Brown and Foster, 1987):

$$e_r = 0.29[1 - 0.72e^{(-0.05i_r)}]$$

where $i_r$ is the rainfall intensity during the time interval [mm h−1].

High resolution rainfall data (10 min time resolution) have been downloaded from Arpa Piemonte database (ANTARES) for three rain gauges located in the surrounding of the watershed, namely Prarotto, Borgone and Malciaussia (table 6-21 and fig 6.21). Rainfall series covers a period of time ranging from September 1, 2017 to August 3, 2018 (i.e. a whole year covering the wildfire occurrence and the reference month in which the fire-severity extended assessment has been performed).

*Table 6-21 – Location of the three rain gauges of Prarotto, Borgone and Malciaussia.*

| Name | City | Elevation (m s.l.m.) | WGS84-UTM32N X (m) | WGS84-UTM32N Y (m) | Basin |
|---|---|---|---|---|---|
| **Prarotto** | Condove | 1440 | 361493 | 5000737 | Dora riparia |
| **Borgone** | Borgone susa | 400 | 361958 | 4997582 | Dora riparia |
| **Malciaussia** | Usseglio | 1800 | 354590 | 5007700 | Stura di lanzo |

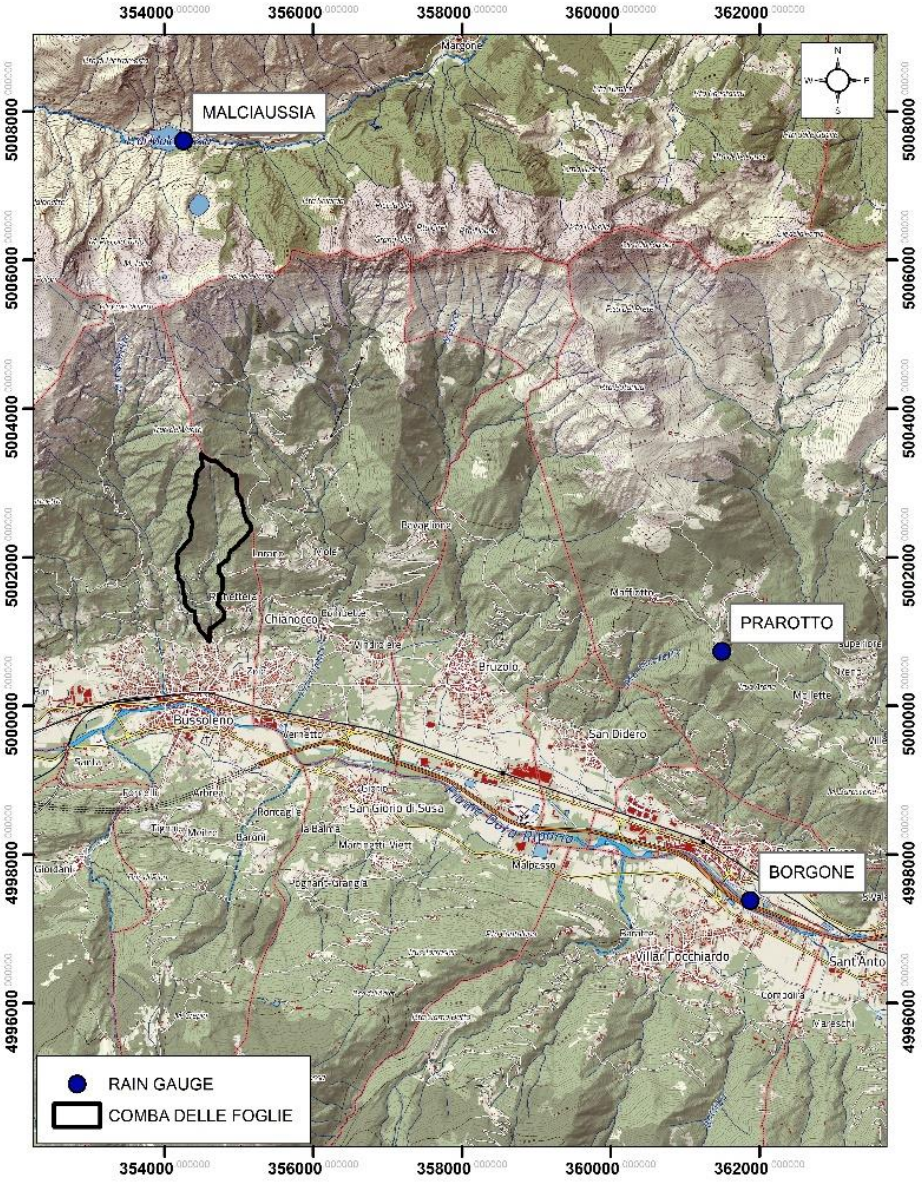


*Figure 6.21 - Location of the three rain gauges of Prarotto, Borgone and Malciaussia with respect to the Comba delle Foglie watershed position.*

The identification of the erosive rainfall (n) events for each station record followed three criteria given by Renard et al. (1997): the cumulative rainfall of an event is greater than 12.7 mm, or the event has at least one peak that is greater than 6.35 mm during a period of 15 min. Individual storms are separated if a rainfall accumulation is less than 1.27 mm during a period of 6 hours. Those criteria have been developed for the USA countries, but are widely accepted also in other areas (Panagos et al., 2015a)

The Rainfall Intensity Summarisation Tool (RIST) software (USDA, 2014) has been used to calculate the R-factor based on the single station annual series. After that, the single monthly R factors has been averaged for applying the RUSLE method at the watershed scale. Results have been compared with average monthly rainfall erosivity calculated at European scale analyzing >17 years of rainfall data by Ballabio et al (2017) and downloaded from ESDAC repository[10].

The remaining parameters in the equation give a measure of the environmental resistance to erosive phenomena.

The erodibility K factor has been determined based on soil textural data. Homogeneous lithological units have been individuated by grouping the geological units derived from 1:50000 geological map (Carraro et al., 2002). Soil samples have been then collected (fig 6.22) and processed in laboratory for determining grain size distribution following standard ASTM procedures. Afterwards, the K factor for each unit has been then calculated based on the following formulae (Renard et al. 1997):

$$K = 0.0034 + 0.0405 * \exp\left[-0.5\left(\frac{logD_g + 1.659}{0.7101}\right)^2\right]$$

$$D_g = \exp\left[\sum f_i \ln\left(\frac{d_i + d_{i-1}}{2}\right)\right]$$

where $D_g$ = geometric mean particle size for each particle size class (clay, silt, sand), $d_i$ = maximum diameter (mm), $d_{i-1}$ = minimum diameter and $f_i$ is the corresponding mass fraction.

LS and C factors have been calculated as described in Par 6.2.4; P value was set to 1.

[10] European Soil Data Centre (ESDAC), esdac.jrc.ec.europa.eu, European Commission, Joint Research Centre

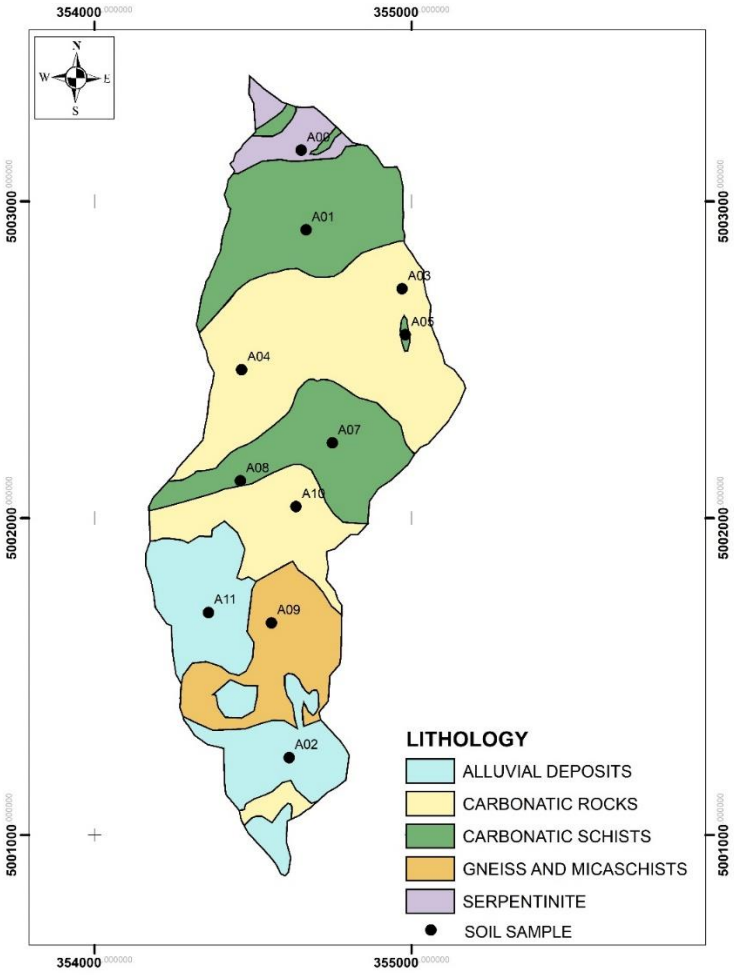


*Figure 6.22 – Location of the soil sampling points in the Comba delle Foglie watersheds.*

### 6.3.3 Peak discharge calculation

The SCS-CN (SCS-USDA 1986) Graphical Peak Discharge method has been applied for computing peak discharge for pre-fire and post-fire conditions (initial and extended assessment). The peak discharge is calculated as:

$$q_p = q_u A Q F_p$$

where $q_p$ = peak discharge [cfs], $q_u$ = unit peak discharge [csm/in], A = drainage area [mi$^2$], Q = excess runoff [in] and $F_p$= pond and swamp adjustment factor [-]

The input required for the Graphical method are the time of concentration Tc [hr], the drainage area A [mi$^2$], the rainfall distribution, the 24-hour rainfall [in], and the watershed CN [-].

CN and excess runoff (Q) for the watershed have been computed according to the methods outlined in par 6.2.5. The watershed CN has been used to determine the initial abstraction (Ia), and then the $I_a/P$ ratio. The obtained value is used for calculating the unit peak discharge as given in following equation:

$$\log(q_u) = c_0 + c_1 \log(T_c) + c_2[\log(T_c)]^2$$

In which C0, C1 and C2 are coefficient which depends on rainfall distribution and $I_a/P$ ratio (fig. 6.23).

| Rainfall type | $I_a/P$ | $C_0$ | $C_1$ | $C_2$ |
|---|---|---|---|---|
| I | 0.10 | 2.30550 | -0.51429 | -0.11750 |
| | 0.20 | 2.23537 | -0.50387 | -0.08929 |
| | 0.25 | 2.18219 | -0.48488 | -0.06589 |
| | 0.30 | 2.10624 | -0.45695 | -0.02835 |
| | 0.35 | 2.00303 | -0.40769 | 0.01983 |
| | 0.40 | 1.87733 | -0.32274 | 0.05754 |
| | 0.45 | 1.76312 | -0.15644 | 0.00453 |
| | 0.50 | 1.67889 | -0.06930 | 0.0 |

*Figure 6.23 – Tabulated C0, C1 and C2 coefficient for a given $I_a/P$ value in case of type I rainfall (SCS-USDA 1986).*

For the Comba delle Foglie watershed the peak discharge $q_p$ has been calculated as in equation for the pre-fire ($q_{p\_pre}$) and post-fire conditions ($q_{p\_ini}$ and $q_{p\_ext}$) as follows:

$$q_{p\_pre} = q_{u\_pre} * A * Q_{pre_w} * F_p$$

$$q_{p\_ini} = q_{u\_ini} * A * Q_{ini\_w} * F_p$$

$$q_{p\_ext} = q_{u\_ext} * A * Q_{ext_w} * F_p$$

## 6.4 Field tests

Experimental tests of controlled burning, simulating a small-scale fire, have been conducted by igniting a known amount of fuel on top of a selected soil. The purpose of the small-scale tests is to evaluate the relationships between the combustion of biomass on the ground and the transfer of heat in the subsoil. In fact, most of the physico-chemical modifications occurring in the soil depend on the temperature gradient and on its temporal duration.

The quantity of energy released by combustion depends on the type of fire (crown vs surface vs ground fires), the type and amount of fuel and the quantity of organic matter in the soil. The heat transfer in the

subsoil depends on the maximum combustion temperature, its duration and the thermophysical characteristics of the geological materials within which the heat pulse propagates (thermal conductivity, volumetric heat capacity, temperature, moisture ...). Of these, the most important physical quantity is thermal conductivity: it defines the ability of a material to transfer heat, corresponding to the amount of heat transferred from a body per unit area. Mathematically, it is expressed by the Fourier's Law of thermal conduction defined using the formula below.

$$q = -\lambda \frac{\delta T}{\delta X}$$

where q is the heat flow in the direction of X, and T is the temperature. The coefficient of proportionality δ is the thermal conductivity (Pasquale et al 2015).

The effective thermal conductivity of soil depends on degree of saturation, grain size, porosity, mineral content, and organic content. In fact, in a heterogeneous and multiphase granular medium it is linked to the thermal conductivity of the single phases that make up the material, that is the conductivity of the grains and intergranular fluids (water and air). As a result, the effective thermal conductivity of the soil components varies across two orders of magnitude: typical ranges for mineral quartz, water, and dry air are respectively 6.15–11.3, 0.58 (at 20° C), and 0.024 W $m^{-1}$ $K^{-1}$ (at 20° C) (Clauser and Huenges 1995, Bristow 1998). The effective thermal conductivity decreases with decreasing grain size, the reduction being more significant for fine grained materials (Midttømme and Roaldset 1998). On contrary, it increases with a decrease in porosity due to a greater fraction of soil material. Also, thermal conductivity decreases with an increase in organic matter content. In addition, effective thermal conductivity shows a nonlinear dependence with temperature: according to Campbell et al. (1994) thermal conductivity of moist soil can be 3 to 5 times greater at 90° C than ambient value, while temperature has a more limited effect on dry soils.

What is commonly seen is that - although heat in moist soil is transported faster and penetrates deeper than in dry soils – the latent heat of vaporization prevents soil temperature from exceeding 95° C until water completely vaporizes; once this threshold is passed, the temperature then typically rises to 200-300° C, or more if heavy fuels are present (Tecle and Neary 2015).

All the fires studied occurred in alpine and pre-alpine areas, on slopes where there are little evolved soils, poor in organic matter, and generally on steep slopes which favor erosive dynamics and scarce accumulation of nutrients. The average grain-size of these soils is generally coarse and the porosity is high; moreover, fires generally started after prolonged dry and windy periods, so it can be assumed with reasonable confidence that the humidity level of the soils in the first horizons was also very low. In fact, the thermal conductivity measures in the summer season, reported in par 7.2.1, shows extremely low

values, with an average of 0.488 W/mK and 0.734 W/mK for the Bussoleno and Mompantero areas, respectively.

The fires have been conducted in the field on a 0.4 x 0.4 m natural soil test area (fig. 6.24) varying the amount of fuel disposed on top of it; the soil is constituted by a sand with gravel and silt (Gravel = 18.28%; Sand = 63.22%; Silt = 17.88%; Clay = 0.62%), with a porosity of 0.58, average saturation of 0.61 and an average apparent density of 1.46 kg/m$^3$.


*Figure 6.24 – Picture and planimetric view of the simulated fire setup. The blue cross indicates the vertical projection of the thermocouples position.*

Thermal conductivity of the soil before each experiment has been measured by using the K2DPro instrument, which is a thermal property analyzer developed by Decagon Devices, compliant to standards ASTM D5334 and IEEE 442. It relies on Transient Line Heat Source methods (Carslaw and Jaeger, 1959 and Kluitenberg et al. 1993) to analyze measurements made during a heating and a cooling interval.

The dual needle SH-1 sensor (1.3 mm diameter x 3 cm long, 6 mm spacing) has been used as it is suitable for solid and granular soils and allows to measure volumetric specific heat, diffusivity, thermal conductivity, and thermal resistivity (accuracy ± 10%). Measurement ranges are reported in the following table:

*Table 6-22 – KD2PRO measurement parameters and ranges.*

| Parameter | Range | Unit |
|---|---|---|
| **Thermal conductivity** | 0.02 to 2.00 | W m$^{-1}$ K$^{-1}$ |
| **Thermal resistivity** | 50 to 5,000 | °C cm W$^{-1}$ |
| **Diffusivity** | 0.1 to 1.0 | mm$^2$ s$^{-1}$ |
| **Volumetric heat capacity** | 0.5 to 4.0 | J m$^{-3}$ k$^{-1}$ |

For the measure, heat is applied to the heated needle for a set time and temperature is measured in the monitoring needle, both during the heating the cooling period. Temperature readings are corrected for ambient temperature and sensor geometrical setup through the equation:

$$T^* = \frac{4\pi(T - T_0)}{q}$$

Then, the resulting data are fitted to the following equations using a non-linear least square procedure (Marquardt, 1963):

$$T^* = b_0 t + b_1 \, Ei(\frac{b_2}{t})$$

$$T^* = b_0 t + b_1 \left\{ Ei\left(\frac{b_2}{t}\right) - Ei\left[\frac{b_2}{t - t_h}\right] \right\}$$

In which Ei is the exponential integral (Abramowitz and Stegun, 1972), $b_o$, $b_1$ and $b_2$ are the constants to be fit, $T_0$ is the temperature at the start of the measurement and q is the heat input. Thermal conductivity and diffusivity are then computed through the following equations:

$$\lambda = \frac{1}{b_1}; \qquad D = \frac{r^2}{4b_2}; \qquad r = \frac{1}{\lambda}; \qquad Cv = \frac{\lambda}{D}$$

The fuel used in the experiment is composed by dry beech wood pellets with a calorific power of 4.5 KWh/kg and dry beech wooden sticks with a calorific power of 4.0 KWh/kg. Before each experiment, a precise quantity of fuel (either pellets or a pellets-wood mixture) has been weighted, then distributed over the soil surface after grass removal. The fires have been ignited in different position of the fuel layer with the aim of firelighters tablet.

Three experiments have been conducted with a fuel load of 9.37 kg/m$^2$, 21.87 kg/m$^2$ (approximatively equivalent to mean dry mass of litter sampled in the Mompantero area, ≈ 18 kg/m$^2$) and 28.12 kg/m$^2$, respectively.

Six type K thermocouple (flexible type, 2 mm diameter, Special class, MgO coating, range: 0 – 1100 °C; Resolution = 0.1 °C) have been placed to record the temperature data: a thermocouples recorded the air temperature just above the fuel layer, one has been placed on the ground-fuel interface and four thermocouples has been inserted horizontally into the soil to provide measurements of temperature changes with time along a vertical axis at varying soil depth (-2, -4, -6 and -8 cm) (fig. 6.25). All the thermocouples have been connected to a data logger (Omega OM-HL-EH-TC) and measurement has been made with a 5 second time step starting from the ignition time and lasting for about 5 hours.

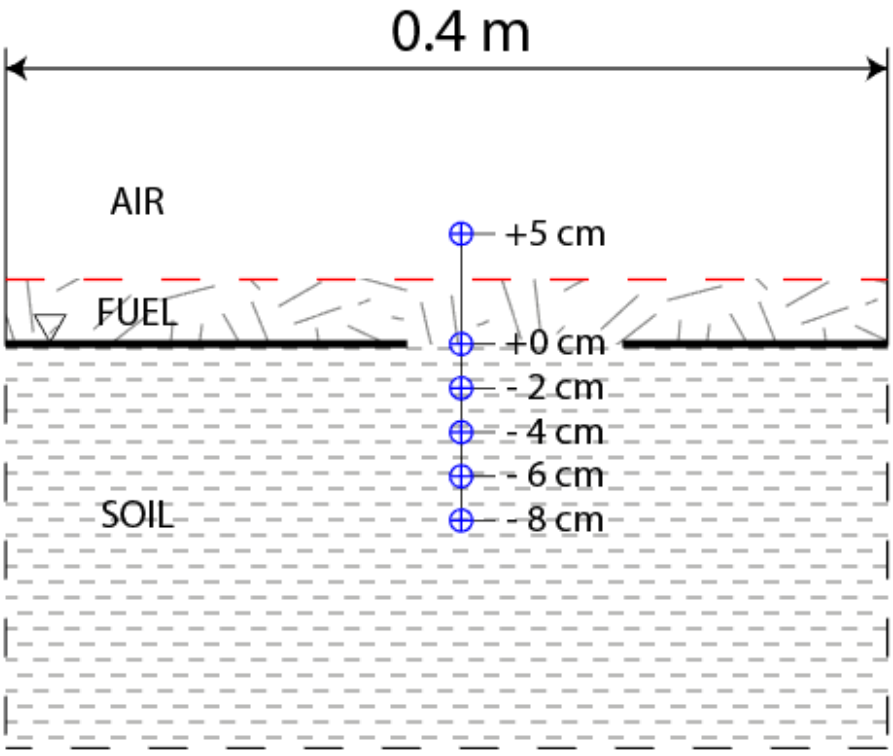


*Figure 6.25 – Vertical cross section of the simulated fire setup. The blue crosses represent the horizontal projection of the six thermocouples.*

Experiments have been conducted in October and November 2020, the air temperature varying between 10° C and 25° C. Initial temperatures of the fuel and soil before the fires therefore differed from one experiment to another. The complete combustion of the fuel has been reached after each experiment.

The experiment no. 2 (fuel load = 21.87 kg/m$^2$) has been modelled in back analysis for deepening the comprehension of the heat propagation in the subsoil. A full 3D meshed model has been implemented in the software FeFlow (DHI), consisting in a finite simulation domain (0.5 m x 0.5 m x 0.213 m) subdivided in slices at progressive depths as reported in fig. 6.26. The simulating domain is considered homogeneous (monophase, porosity = 0) and characterized by a volumetric heat capacity equal to 2.5 MJ m$^{-3}$ k$^{-1}$.

The uppermost layer simulates the heat source, and its temperature follows the heating curve of the thermocouple placed at the soil surface in the physical experiment. The layer 2 and 3 are characterized by a time dependent thermal conductivity value, which has been retrieved through a trial and error procedure to fit the experimental data. All the others layers are characterized by a constant thermal conductivity value, set to 1.6 W m$^{-1}$ k$^{-1}$. The bottom boundary conditions express a constant temperature value equal to 14° C.

The temperature profile at progressive time steps is evaluated by logging data in correspondence of six control point positioned at the same experimental thermocouples depth (0, -2, -4, -6, -8, -10 cm respectively).

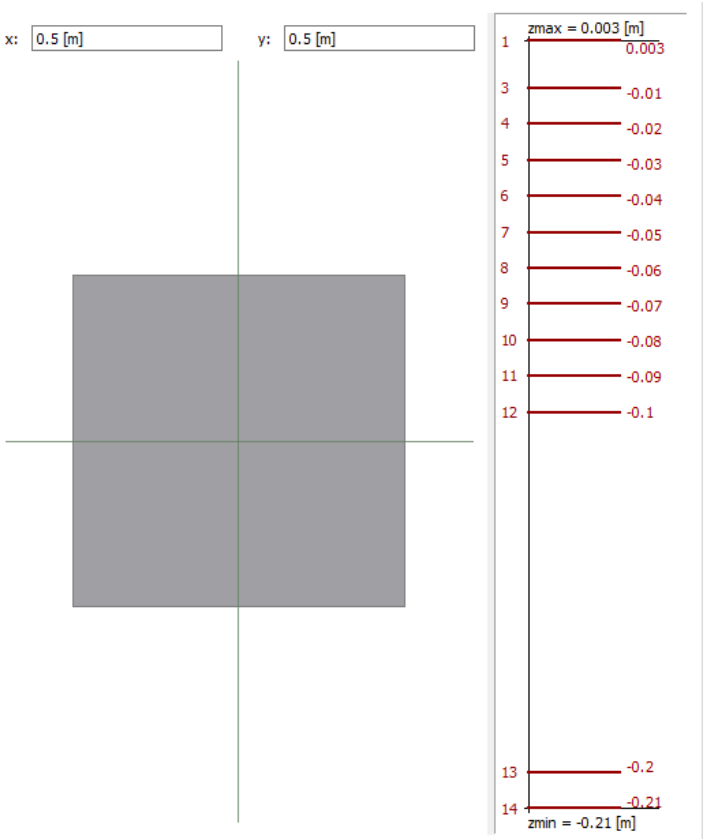


*Figure 6.26 – geometrical parameters of the FEFLOW 3D model.*

# 7 Results

In the following sections the research results are presented: in section 7.1 the evidences of the regional study on the historical series of fires and landslides analysis are presented, while the paragraph 7.2 is focused on the study of the nine wildfires occurred in 2017. In particular the results of the field surveys (7.2.1), the fire severity assessment (7.2.2), the watershed characterization (7.2.3) and the erosion and runoff models outcomes (7.2.4 and 7.2.5) are given. In section 7.3 the results of the Comba delle Foglie case study are presented, and finally section 7.4 is dedicated to the report of the field test outcomes.

## 7.1 Regional Scale landslide-wildfires correlation

Comparing the fire perimeter dataset and the landslide database 7 occurrences have been found having a spatial relationship matching the required criteria (figg 7.1 and 7.2). Unfortunately, no further detail has been found for the majority of the gravitaty-related events. Only for the Pallanzeno debris-flow some key information have been derived from an event report (Arpa Piemonte, 2005); the report describes the characteristics of a multiple flow event having an estimated volume of 4000 $m^3$, originating from the Rio Casella watershed (1.2 $Km^2$). Two primary pulses have been recognized in the field (the first classified as a non-choesive sediment gravity flow, the second as a cohesive sediment gravity flow) in response to a minor rainfall event (15.8 mm in 30 minutes, two years return period). The event triggering has been attributed to the enhanced runoff coming from the surrounding slopes, interested in the month of March 2005 by a large wildfire. In the report, some minor events, due to enhanced erosion of burned biomass and topsoil, are reported to have taken place since March during different rainfall events.

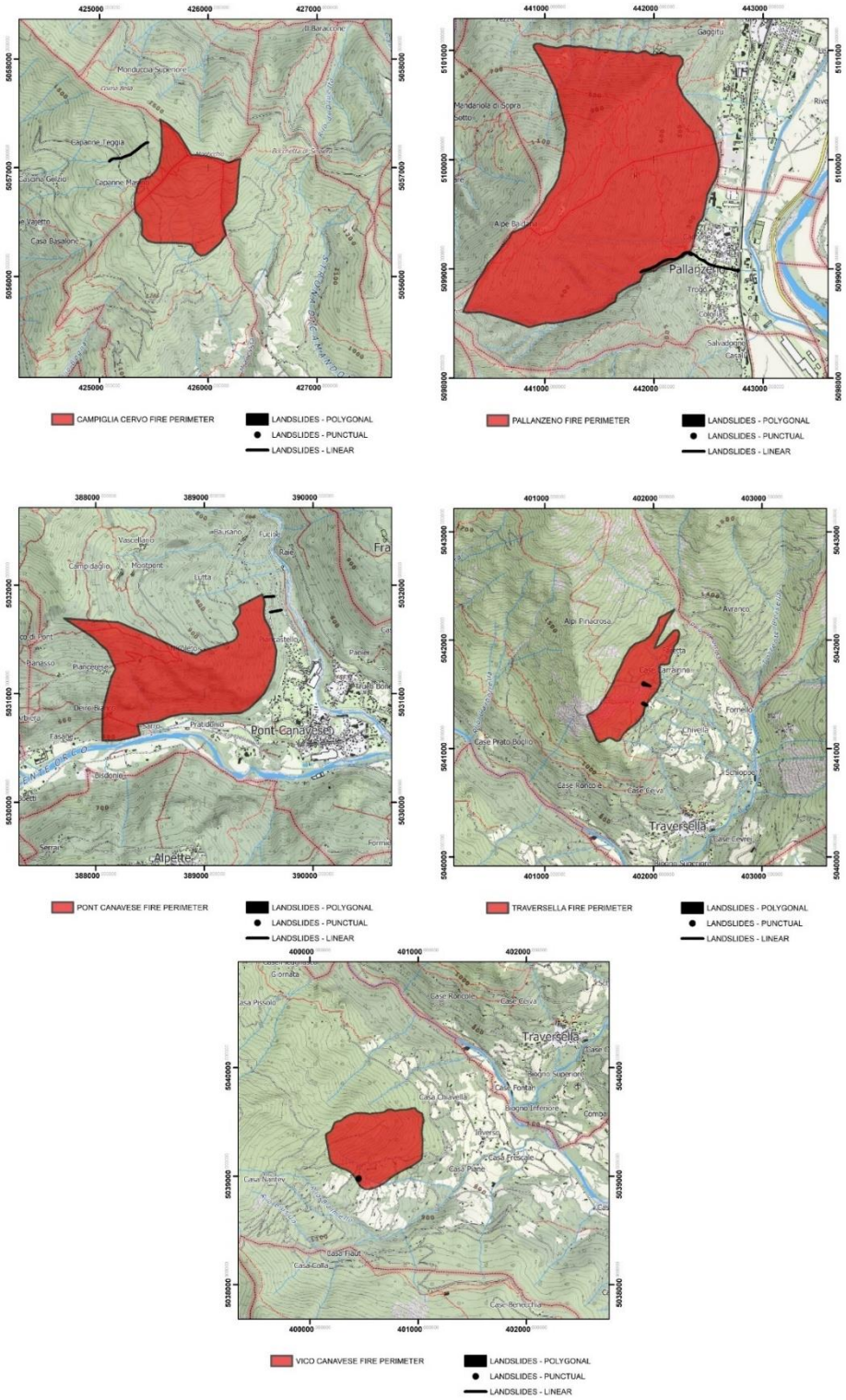


*Figure 7.1 – post-fire landslides positions compared to fire perimeter for the Campiglia Cervo, Pallanzeno, Pont Canavese, Traversella and Vico Canavese wilfires.*

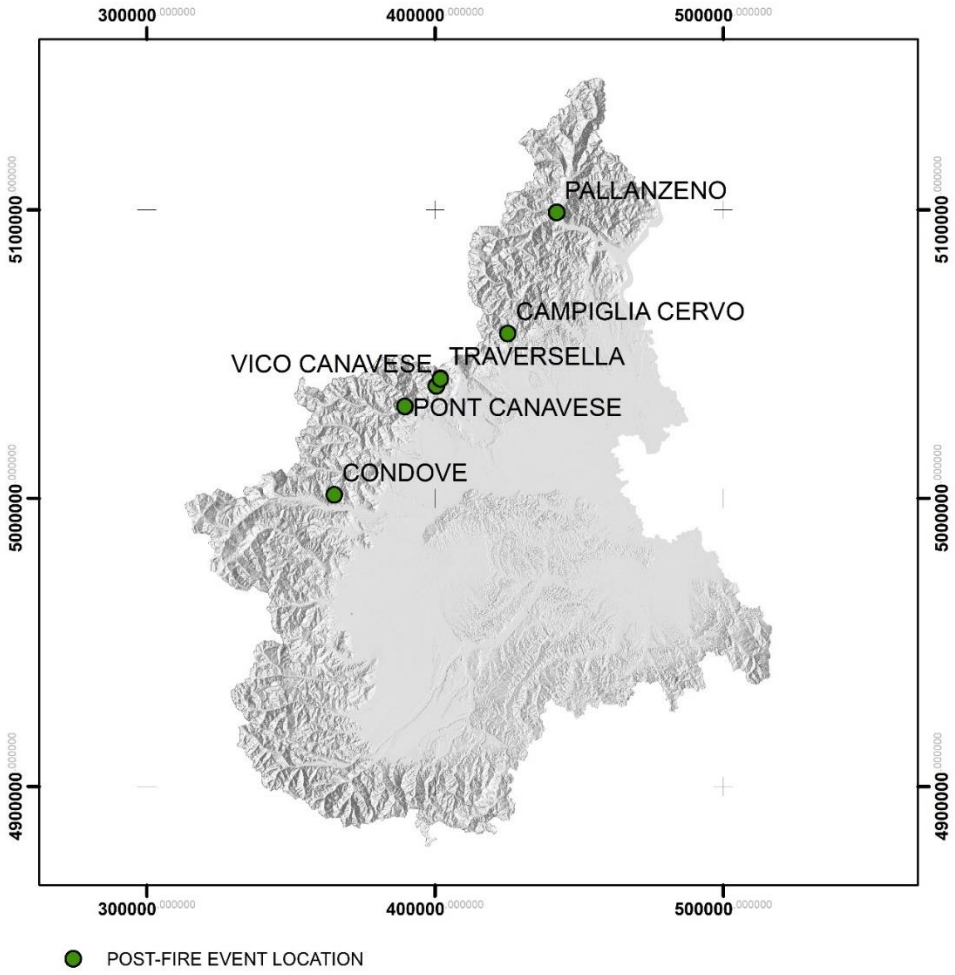


*Figure 7.2 – post-fire landslides location.*

## 7.2 Watershed scale

The following tables recall the names and numbers of the analyzed watersheds, divided for the nine wildfires areas. The results reported in the following sub-paragraphs refer to this classification system.

*Table 7-1 - watersheds affected by the Locana/Ribordone wildfire.*

| **Fire no. 1** | **LOCANA/RIBORDONE** |
|---|---|
| **WATERSHED ID** | **WATERSHED NAME** |
| **1** | Rio Fura |
| **2** | Rio Di Chioso Bosco |
| **3** | R. Montepiano |
| **4** | Carlevaria |
| **5** | Rio Di Bardonetto Inferiore |
| **6** | Ribordone |
| **7** | Eugio |
| **8** | Rio Bocchetta |
| **9** | Rio Di Calsazio |
| **48** | Locana Est |
| **49** | Apparè |

*Table 7-2 - watersheds affected by the Bussoleno/Mompantero wildfire.*

| **Fire no. 2** | **BUSSOLENO/MOMPANTERO** |
|---|---|
| **WATERSHED ID** | **WATERSHED NAME** |
| **10** | Crosiglione |
| **11** | Rio Della Ravoire |
| **12** | Fogasso |
| **13** | Rio Della Codrea |
| **14** | Trinità |
| **15** | Rio Prebech |
| **16** | Moletta |
| **17** | Rio Di Periere |
| **18** | Ravera |
| **19** | Comba Delle Foglie |
| **20** | Rocciamelone |
| **21** | Giandula |
| **22** | I Piani |
| **23** | San Giuseppe |

*Table 7-3 - watersheds affected by the Caprie/Rubiana wildfire.*

| Fire no. 3 | CAPRIE/RUBIANA |
|---|---|
| **WATERSHED ID** | **WATERSHED NAME** |
| **24** | Messa |
| **25** | Sessi |
| **26** | Novaretto |
| **27** | Fra Barbe |

*Table 7-4 - watersheds affected by the Cumiana/Cantalupa wildfire.*

| Fire no. 4 | CUMIANA/CANTALUPA |
|---|---|
| **WATERSHED ID** | **WATERSHED NAME** |
| **28** | 1*Int. Dx. Sangone |
| **29** | Chisola Torrente |
| **30** | Noce Torrente |
| **31** | Chisola Pianura |

*Table 7-5 - watersheds affected by the Bellino/Casteldelfino wildfire.*

| Fire no. 5 | BELLINO/CASTELDELFINO |
|---|---|
| **WATERSHED ID** | **WATERSHED NAME** |
| **32** | Cumbal Della Comu |
| **33** | T. Mas Del Bernard |

*Table 7-6 - watersheds affected by the Sambuco/Pietraporzio wildfire.*

| Fire no. 6 | SAMBUCO/PIETRAPORZIO |
|---|---|
| **WATERSHED ID** | **WATERSHED NAME** |
| **34** | R. Bianco |
| **35** | Sn |
| **36** | Rio Di Castello Pietraporzio |

*Table 7-7 - watersheds affected by the Roure/Perrero wildfire.*

| Fire no. 7 | ROURE/PERRERO |
|---|---|
| **WATERSHED ID** | **WATERSHED NAME** |
| **37** | V.Ne Di Borsetto |
| **38** | S. Martino Sud |
| **39** | Colet |
| **40** | Molotta |
| **41** | Gernier |

*Table 7-8 - watersheds affected by the Traversella wildfire.*

| Fire no. 8 | TRAVERSELLA |
|---|---|
| **WATERSHED ID** | **WATERSHED NAME** |
| **42** | T.Bersella |
| **43** | Valle Chiara Primo |

*Table 7-9 - watersheds affected by the Demonte wildfire.*

| Fire no. 9 | DEMONTE |
|---|---|
| **WATERSHED ID** | **WATERSHED NAME** |
| **44** | V. Del Saut |
| **45** | Valle Di Monfreis |
| **46** | Sn 2 |
| **47** | Rio Di Prafioret C. |

### 7.2.1 On site surveys

The burned areas characteristics surveyed on the field showed a high spatial variability between the nine different fire locations, and within the same fire as well; this can be related to different fire behaviour and intensity, due to different vegetation coverage, soil moisture, topography and wind conditions. In addition, in some areas such as the Comba delle Foglie watershed the 2017 fire affected an area already severely burned in the past. This resulted in a patched distribution of the fire impacts and, as a consequence, in the modifications on the ability to withstand weather forcing and cope with enhanced erosional and depositional dynamics.

The major effects from a hydrogeological perspective have been found in the area of the Bussoleno/Mompantero fire, affected extensively by medium or high burn severity especially on Scots Pine forests. Two sectors showed the most evident signs of post-fire geomorphic dynamics, the Comba delle Foglie watershed and the slope overhanging the Mompantero village. In the first, from which the most severe debris-mud flows originated, extensive phenomena of areal and channelled erosion has been observed, especially in the upper part of the catchment. Traces of the flows transit, such as scour, levee and typical debris flow deposits have been found along the main channel down to the valley outlet. Paragraph 7.3 is dedicated to the detailed discussion of these phenomena.

The Mompantero area showed the most striking effects on the arboreal cover. Large areas of coniferous forest revealed an almost total plant mortality and complete biomass consumption from the ground level to the crown of the trees. On open slopes, evident signs of an extensive erosive dynamic (exerted by rills and gullies) associated with an emphasized stream network re-organization has been found in the upper portion of the slope. Proceeding downvalley significant evidence of transport and deposition processes of material along the drainage axes has been surveyed, even if not comparable to the Comba delle Foglie events in term of volumes. Sediment and combusted material deposits have been found obstructing road crossing and mantling road routes, and some minor events reached the valley bottom in a few occasions.

*Figure 7.3 – Enhanced erosion evidences in the Mompantero coniferous forest (left); sediment, ash and combustion residues in the Mompantero stream network (right).*

The Locana/Ribordone fire, the second largest among those studied, is characterized for about 30% by high or medium burn severity. In the burned area no evident signs of areal erosion have been detected; however, with the spring rainfall season, a series of debris/mud-flows originating from high fire severity sectors were observed. It should be emphasized that the area is historically susceptible to landslide and instability, and the post-fire erosive dynamics may have worsened an already critical situation.

In all the remaining fire locations (Roure/Perrero, Traversella, Cumiana/Cantalupa, Caprie/Rubiana, Bellino/Casteldelfino, Demonte and Sambuco/Pietraporzio) an overall minor fire severity has been detected, and the areas of high and medium severity revealed a minor spatial continuity. No significant erosion or instability phenomena has been found, although in some cases there have been individual falls of rocks mobilized after the fall of the trees to which they were leaning before the fire.

*Figure 7.4 – a large boulder leaning against a tree trunk in the Cantalupa area.*

Some expeditious investigations have been carried out on the site of the Bussoleno/Mompantero fire. Water Drop Penetration Time tests have been conducted in the areas with the greatest fire severity, revealing an extreme spatial heterogeneity of results, although sometimes a weak hydrophobicity was found in the first soil horizon. Furthermore, distributed measurements of thermal conductivity of the superficial soil horizon were carried out, in order to estimate the rate of heat transmission at depth (fig. 7.5, table 7-10 and 7-11). Measurement were taken with KD2Pro Thermal Property Analyzer (Decagon Devices) which uses a proprietary algorithm to fit time and temperature data with exponential integral functions using a non-linear least-squares method.

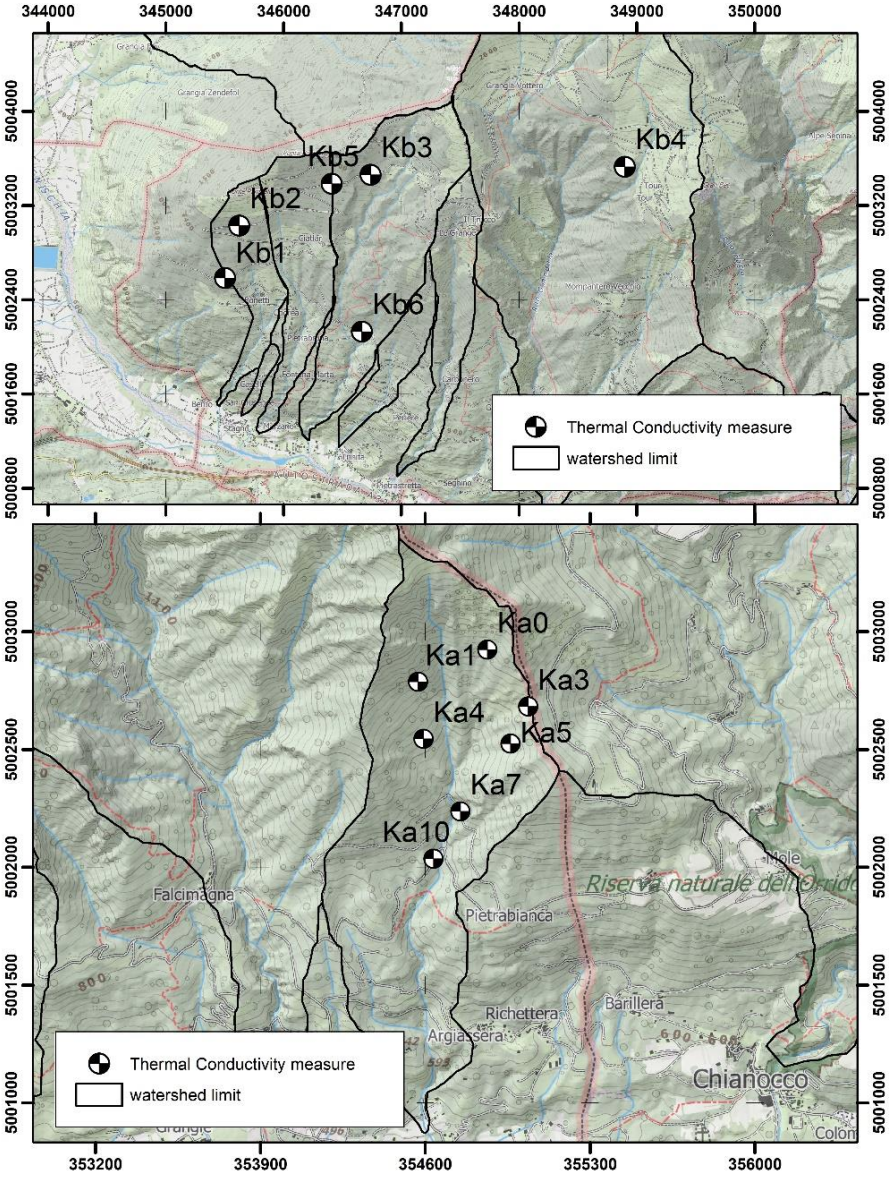


*Figure 7.5 – Thermal conductivity measurements location in the Mompantero (top) and Bussoleno (bottom) areas.*

*Table 7-10 - results of thermal conductivity measurements in the areas of Bussoleno*

| Measure # | λ (W/mK) | T (°C) |
|---|---|---|
| **Ka0** | 0.498 | 20 |
| **Ka1** | 0.251 | 18.98 |
| **Ka3** | 0.813 | 20.31 |
| **Ka4** | 0.62 | 19.59 |
| **Ka5** | 0.395 | 21.13 |
| **Ka7** | 0.179 | 19.25 |
| **Ka10** | 0.658 | 19.58 |
| **Mean** | **0.488** | |

*Table 7-11 - results of thermal conductivity measurements in the areas of Mompantero*

| Measure # | λ (W/mK) | T (°C) |
|---|---|---|
| **Kb1** | 0.743 | 16.26 |
| **Kb2** | 0.335 | 16.75 |
| **Kb3** | 0.628 | 14.17 |
| **Kb4** | 0.809 | 12.03 |
| **Kb5** | 0.583 | 9.99 |
| **Kb6** | 1.306 | 27.9 |
| **Mean** | **0.734** | |

Some empirical in situ shear tests (fig 7.6) were performed in order to have a relative comparison between burned and unburned portions of soil in the Mompantero area (soil textural and geotechnical characteristics are neglected). The method consists in the insertion of a cylindrical soil sampler (Ø=100 mm and h=100 mm) in the ground and in the measure of the force necessary for its shearing along the base area (after the removal of the soil located in frontal sector of the cylinder). The movement is guided thanks to the positioning of a wooden plate above the sampler without applying a normal load. The shearing force is measured by a dynamometer.

Although not completely accurate, the differences in the measure on burned and unburned soil (as close as possible to each other) were so evident that the test could be considered sufficient for a qualitative analysis of the state of the soil. In fact, on average in vegetated unburned soil a force of more than 500 N is required for the sampler to be pulled apart, while an average value of 150 N is found in burned soil.

*Figure 7.6 - empirical shear tests device (left) and Water Drop Penetration Time test for hydrophobicity assessment (right).*

The residual portions of unburned litter in the Mompantero area in tree positions has been sampled in order to estimate the amount of fine fuel present before the fire (fig 7.7 and 7.8, table 7-12).

*Figure 7.7 . Unburned litter profile in the Mompantero forest.*

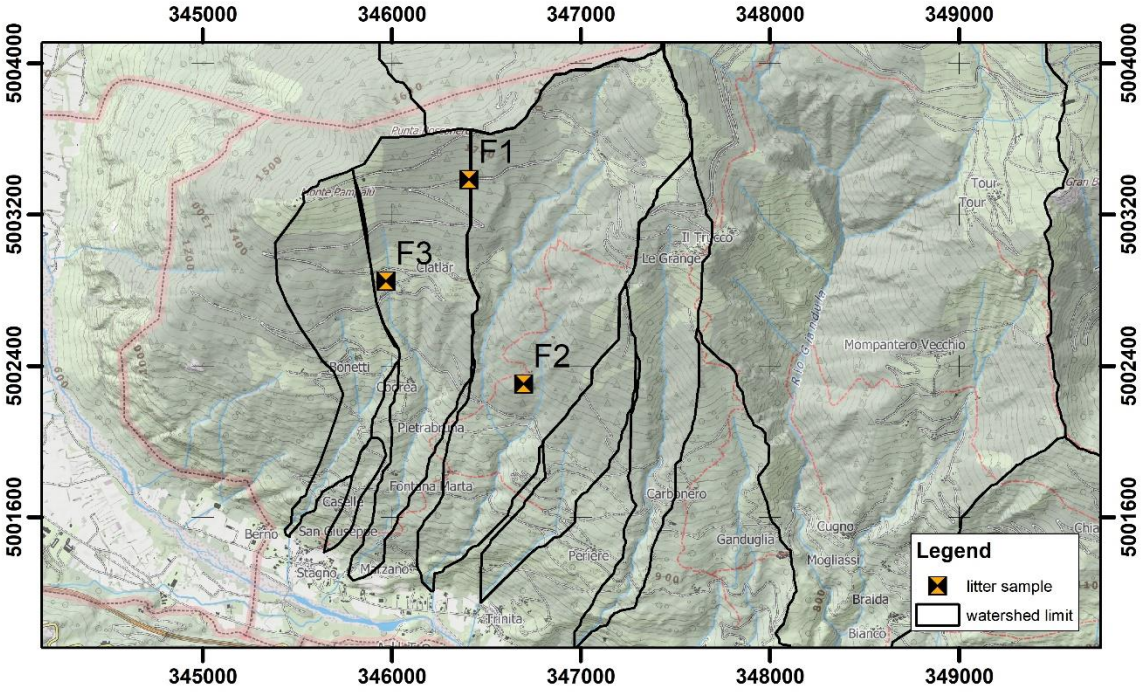


*Figure 7.8 – Unburned litter sampling locations.*

*Table 7-12 – Fuel load measured in the Mompantero area*

| Sample # | Wet fuel load | Dry fuel load |
|---|---|---|
| | [kg/m²] | [kg/m²] |
| **F1** | 15.5 | 5.4 |
| **F2** | 18.9 | 6.15 |
| **F3** | 19.4 | 6.7 |
| **Mean** | 17.93 | 6.08 |

The field surveys have been useful to understand the main processes affecting the considered watersheds as a response to fire and to address the correct modelling approach: in fact, no discrete landslide mass failure has been observed during survey, nor has been reported to the author. This is crucial in excluding these types of phenomena for acting as a source of material for the observed debris and mud-flows generation. Soil modification observed in the field are generally shallow (less than 10 cm) and all of them correlated with overland flow dynamics. Rills, gullies and zero order streams incision are found to be more evident in high burn severity sectors, especially where the three canopy is severely reduced. This allowed to focus the attention on erosive dynamics to the detriment of more purely geotechnical slope processes.

The survey campaign timing anyway brings some drawbacks: since it started some month after the fires occurrence, it did not allow to measure the volume of eroded sediments to validate the proposed model properly, but some indications on the quantity of mobilized sediments derive from the characterization of the phenomenon of Comba delle Foglie. Moreover, the observations made between the various basins can be classified in a relative way, giving a rough susceptibility ranking for supporting the modeling.

*Figure 7.9 – zero-order hollow showing re-incision marks at the expense of burnt soil.*

### 7.2.2 Initial assessment fire severity maps production

The results of the fire severity evaluation in the short term after the fire (initial assessment) show an overall predominance of unburned areas (48.18%). Low, moderate and high severity classes cover a surface percentage of 16.56%, 25.82% and 9.45% respectively (figg. 7.10, 7.11 and 7.12).

If we look at the sum of the areas burned at medium and high severity, the fire nos. 1, 2, 5 and 8 are characterized by the higher values, the area percentage falling in this category being the 63.56%, 51.52%, 35.38% and 53.92% respectively. The other wildfires (nos. 3, 4, 6, 7 and 9) report value of 10.84, 1.70, 2.84, 2.33 and 14.56, respectively.

Comparing these results with the maps produced by Morresi et al. (2021), it is evident a decrease in the overall fire severity in the extended assessment (figg. 7.13, 7.14 and 7.15), despite the fact that in the same wildfire area patches showing an increase, a decrease or an unchanged situation are juxtaposed. Overall, unburned, low, moderate and high severity classes evaluated for the extended assessment cover the 57.41%, 18,04%, 20.25% and 4.30%, respectively.

The areal percentage of the two most severe classes decreases to values of 32.90%, 46.72%, 3.18% and 33.07% for the fires nos. 1, 2, 5 and 8, while for the fires nos. 3, 4, 6, 7 and 9 the values shift to 0.95%, 5.70%, 8.09%, 6.43% and 7.89%, respectively.

Values of areal percentage of the four severity classes characterizing the single watersheds are given in the tables 7-13 – 7-21.

Some watersheds, especially those affected by the Locana/Ribordone and Bussoleno/Mompantero fires, shows a very significant fire severity: for example, the watersheds of Carlevaria, Rio della Ravoire and Comba delle Foglie see more than 80% of their surface affected by medium-high severity in the initial assessment.

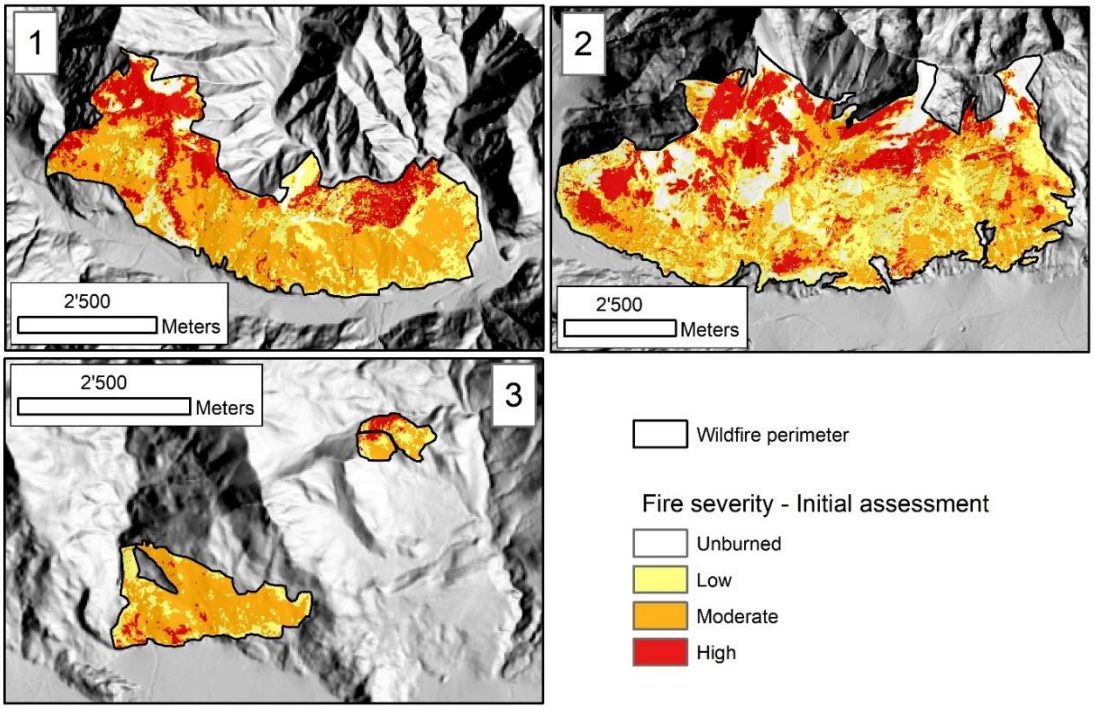


*Figure 7.10 - – Fire severity maps, initial assessment, for the Locana/Ribordone (1), Bussoleno/Mompantero (2) and Caprie/Rubiana (3) wildfires.*

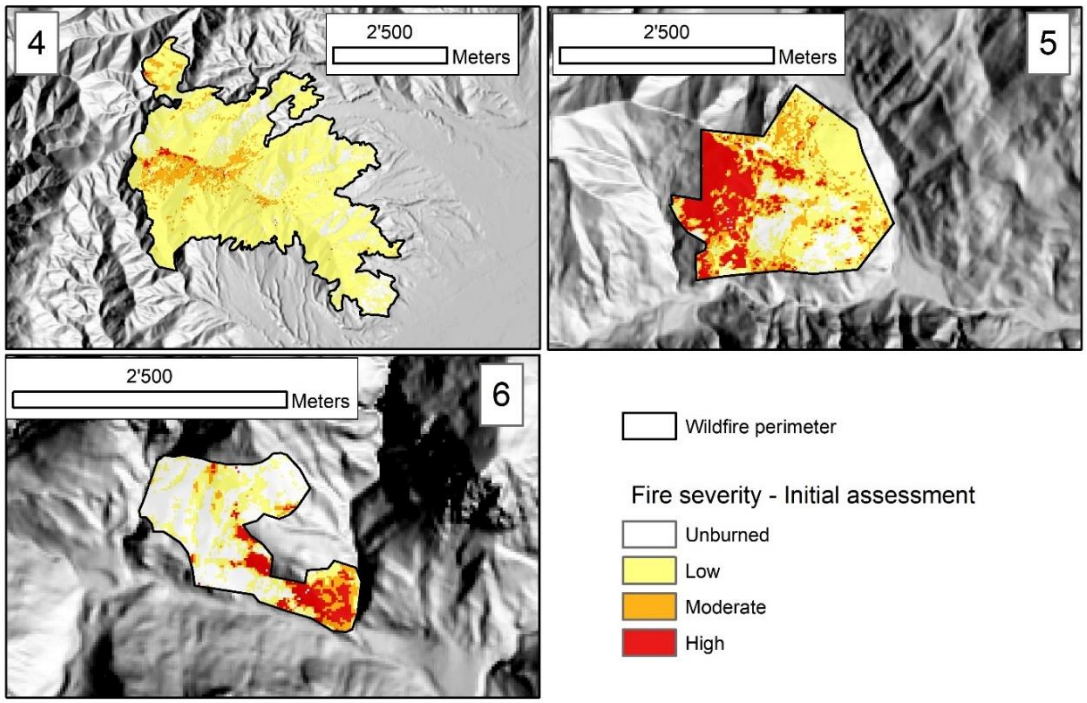


*Figure 7.11 – Fire severity maps, initial assessment, for the Cumiana/Cantalupa (4), Bellino/Casteldelfino (5) and Sambuco/Pietraporzio (6) wildfires.*

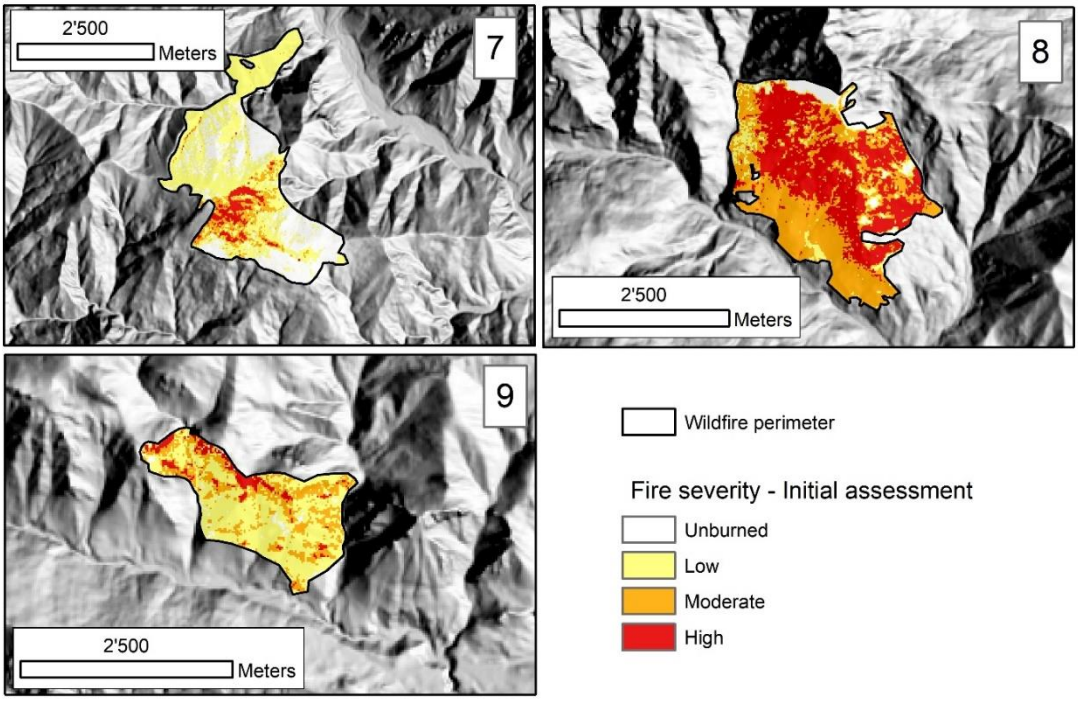


*Figure 7.12 – Fire severity maps, initial assessment, for the Roure/Perrero (7), Traversella (8) and Demonte (9) wildfires.*

*Table 7-13 - relative extension of areas with different fire severity in the Locana/Ribordone wildfire.*

| Fire no. 1 | LOCANA/RIBORDONE | | | |
|---|---|---|---|---|
| Watershed | Fire severity | | | |
| | Unburned | Low | Moderate | High |
| | % | % | % | % |
| Rio Fura | 8.18 | 13.80 | 48.60 | 29.42 |
| Rio Di Chioso Bosco | 0.63 | 30.11 | 67.93 | 1.32 |
| R. Montepiano | 10.49 | 21.15 | 60.82 | 7.54 |
| Carlevaria | 0.37 | 16.66 | 75.19 | 7.78 |
| Rio Di Bardonetto Inferiore | 1.34 | 22.66 | 68.26 | 7.74 |
| Ribordone | 90.55 | 2.81 | 2.93 | 3.71 |
| Eugio | 94.07 | 0.53 | 1.53 | 3.88 |
| Rio Bocchetta | 0.41 | 8.95 | 65.40 | 25.23 |
| Rio Di Calsazio | 0.00 | 14.63 | 84.41 | 0.95 |
| Locana Est | 7.35 | 20.47 | 46.72 | 25.46 |
| Apparè | 2.47 | 33.22 | 64.31 | 0.00 |
| **Mean** | **19.62** | **16.82** | **53.28** | **10.28** |

*Table 7-14 - relative extension of areas with different fire severity in the Bussoleno/Mompantero wildfire.*

| Fire no. 2 | BUSSOLENO/MOMPANTERO | | | |
|---|---|---|---|---|
| Watershed | Fire severity | | | |
| | Unburned | Low | Moderate | High |
| | % | % | % | % |
| **Crosiglione** | 90.04 | 4.38 | 4.73 | 0.85 |
| **Rio Della Ravoire** | 0.97 | 4.84 | 41.48 | 52.72 |
| **Fogasso** | 33.70 | 28.51 | 22.87 | 14.92 |
| **Rio Della Codrea** | 12.97 | 22.25 | 39.48 | 25.30 |
| **Trinitâ** | 7.19 | 37.82 | 45.04 | 9.95 |
| **Rio Prebech** | 81.61 | 9.43 | 6.21 | 2.75 |
| **Moletta** | 34.99 | 22.86 | 27.06 | 15.09 |
| **Rio Di Periere** | 9.46 | 41.63 | 32.30 | 16.62 |
| **Ravera** | 9.21 | 31.68 | 55.14 | 3.98 |
| **Comba Delle Foglie** | 3.13 | 13.64 | 64.28 | 18.94 |
| **Rocciamelone** | 47.71 | 20.52 | 18.61 | 13.17 |
| **Giandula** | 19.73 | 22.26 | 24.57 | 33.44 |
| **I Piani** | 10.47 | 46.17 | 42.89 | 0.48 |
| **San Giuseppe** | 5.54 | 6.03 | 73.02 | 15.41 |
| **Mean** | **26.19** | **22.29** | **35.55** | **15.97** |

*Table 7-15 - relative extension of areas with different fire severity in the Caprie/Rubiana wildfire.*

| Fire no. 3 | CAPRIE/RUBIANA | | | |
|---|---|---|---|---|
| Watershed | Fire severity | | | |
| | Unburned | Low | Moderate | High |
| | % | % | % | % |
| **Messa** | 98.18 | 0.55 | 0.92 | 0.34 |
| **Sessi** | 96.52 | 1.09 | 2.25 | 0.15 |
| **Novaretto** | 62.40 | 12.98 | 24.62 | 0.00 |
| **Fra Barbe** | 81.61 | 3.30 | 15.09 | 0.00 |
| **Mean** | **84.67** | **4.48** | **10.72** | **0.12** |

*Table 7-16 - relative extension of areas with different fire severity in the Cumiana/Cantalupa wildfire.*

| Fire no. 4 | CUMIANA/CANTALUPA | | | |
|---|---|---|---|---|
| Watershed | Fire severity | | | |
| | Unburned | Low | Moderate | High |
| | % | % | % | % |
| 1*Int. Dx. Sangone | 97.59 | 2.09 | 0.31 | 0.02 |
| T. Chisola | 86.92 | 12.13 | 0.86 | 0.10 |
| T. Noce | 68.68 | 25.99 | 5.05 | 0.29 |
| Chisola Pianura | 82.82 | 16.99 | 0.18 | 0.01 |
| **Mean** | **84.00** | **14.30** | **1.60** | **0.11** |

*Table 7-17 - relative extension of areas with different fire severity in the Bellino/Casteldelfino wildfire.*

| Fire no. 5 | BELLINO/CASTELDELFINO | | | |
|---|---|---|---|---|
| Watershed | Fire severity | | | |
| | Unburned | Low | Moderate | High |
| | % | % | % | % |
| Cumbal Della Comu | 19.27 | 24.48 | 21.66 | 34.59 |
| T. Mas Del Bernard | 83.44 | 1.64 | 1.93 | 12.99 |
| **Mean** | **51.36** | **13.06** | **11.80** | **23.79** |

*Table 7-18 - relative extension of areas with different fire severity in the Sambuco/Pietraporzio wildfire..*

| Fire no. 6 | SAMBUCO/PIETRAPORZIO | | | |
|---|---|---|---|---|
| Watershed | Fire severity | | | |
| | Unburned | Low | Moderate | High |
| | % | % | % | % |
| R. Bianco | 98.39 | 0.75 | 0.47 | 0.39 |
| Sn | 56.52 | 35.87 | 6.00 | 1.61 |
| Rio Di Castello Pietraporzio | 97.78 | 2.18 | 0.04 | 0.00 |
| **Mean** | **84.23** | **12.93** | **2.17** | **0.67** |

*Table 7-19 - relative extension of areas with different fire severity in the Roure/Perrero wildfire.*

| Fire no. 7 | ROURE/PERRERO | | | |
|---|---|---|---|---|
| **Watershed** | **Fire severity** | | | |
| | **Unburned** | **Low** | **Moderate** | **High** |
| | **%** | **%** | **%** | **%** |
| **V.Ne Di Borsetto** | 82.43 | 17.29 | 0.23 | 0.04 |
| **S. Martino Sud** | 97.61 | 2.22 | 0.07 | 0.10 |
| **Colet** | 99.78 | 0.22 | 0.00 | 0.00 |
| **Molotta** | 95.18 | 4.35 | 0.47 | 0.00 |
| **Gernier** | 75.08 | 14.18 | 6.81 | 3.94 |
| **Mean** | **90.02** | **7.65** | **1.52** | **0.82** |

*Table 7-20 - relative extension of areas with different fire severity in the Traversella wildfire.*

| Fire no. 8 | TRAVERSELLA | | | |
|---|---|---|---|---|
| **Watershed** | **Fire severity** | | | |
| | **Unburned** | **Low** | **Moderate** | **High** |
| | **%** | **%** | **%** | **%** |
| **T. Bersella** | 85.21 | 1.84 | 5.19 | 7.77 |
| **Valle Chiara Primo** | 5.12 | 0.00 | 45.80 | 49.08 |
| **Mean** | **45.17** | **0.92** | **25.50** | **28.43** |

*Table 7-21 - relative extension of areas with different fire severity in the Demonte wildfire.*

| Fire no. 9 | DEMONTE | | | |
|---|---|---|---|---|
| **Watershed** | **Fire severity** | | | |
| | **Unburned** | **Low** | **Moderate** | **High** |
| | **%** | **%** | **%** | **%** |
| **V. Del Saut** | 83.92 | 8.50 | 4.98 | 2.59 |
| **Valle Di Monfreis** | 91.66 | 4.94 | 3.10 | 0.30 |
| **Sn 2** | 21.96 | 61.53 | 14.26 | 2.25 |
| **Rio Di Prafioret C.** | 10.05 | 59.21 | 21.05 | 9.69 |
| **Mean** | **51.90** | **33.55** | **10.85** | **3.71** |

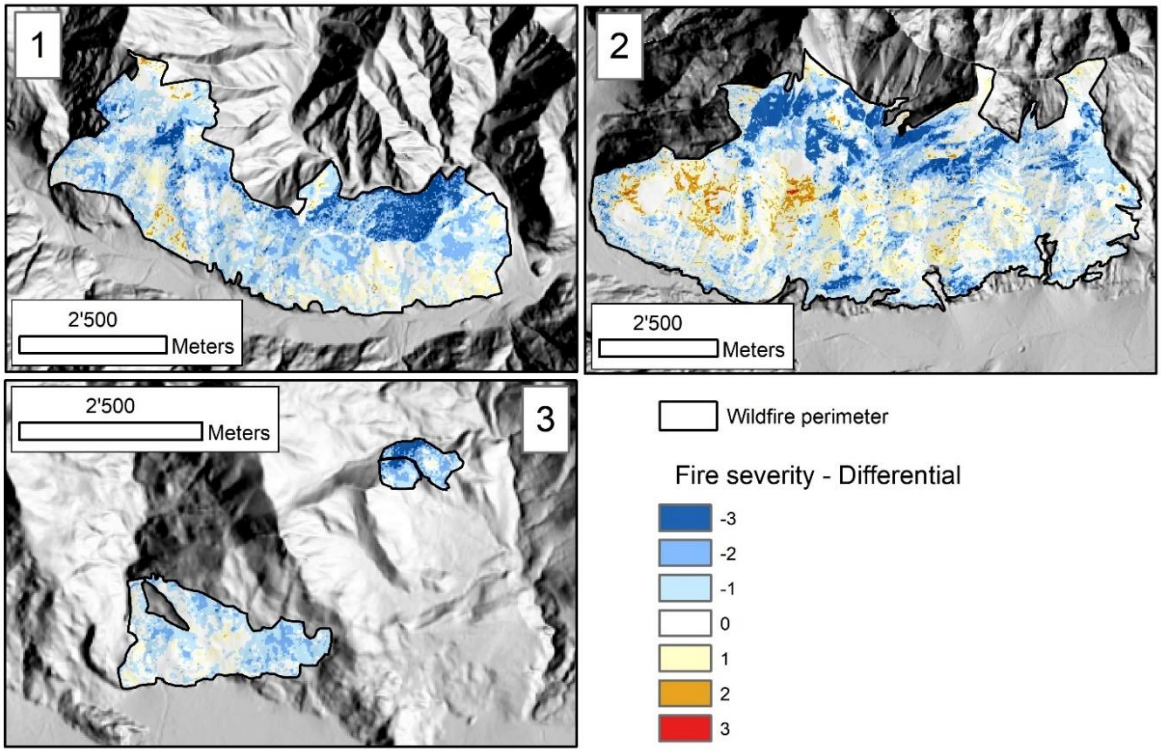


*Figure 7.13 - Fire severity maps differentials between extended and initial assessment, for the Locana/Ribordone (1), Bussoleno/Mompantero (2) and Caprie/Rubiana (3) wildfires. Legend values express the quantity of class incremented (positive, increased fire severity) or decremented (negative, decreased fire severity) in the extended assessment.*

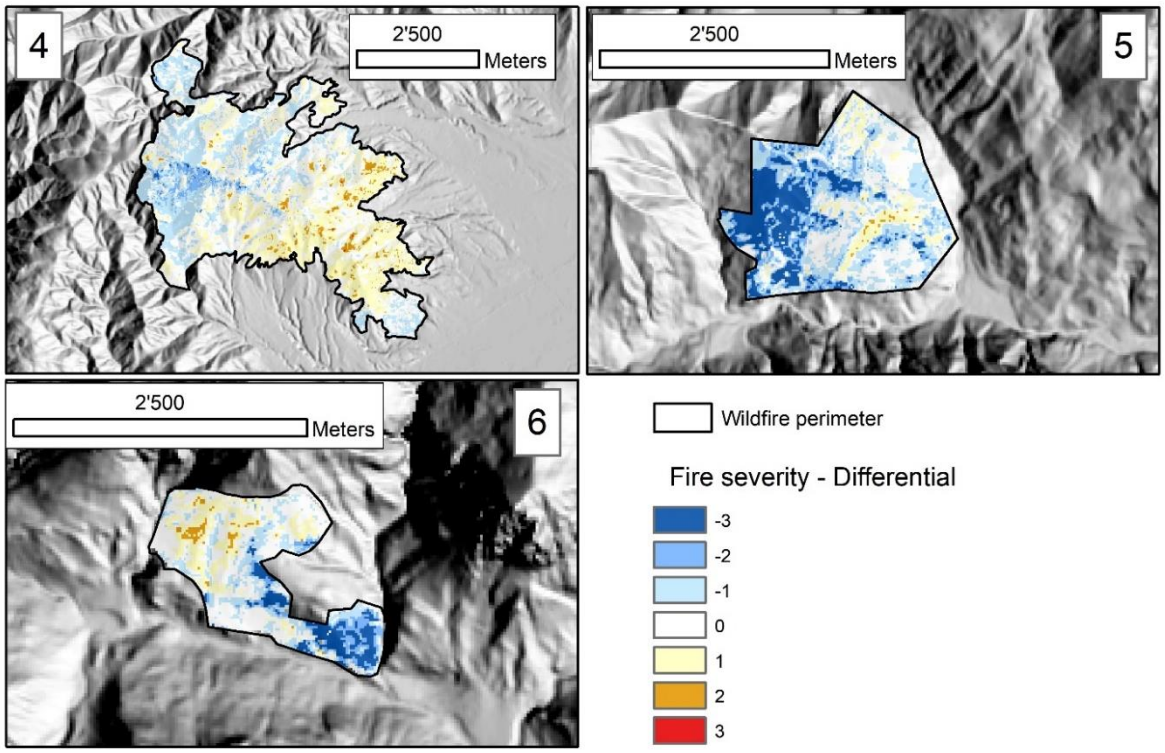


*Figure 7.14 - Fire severity maps differentials between extended and initial assessment, for the Cumiana/Cantalupa (4), Bellino/Casteldelfino (5) and Sambuco/Pietraporzio (6) wildfires. Legend values express the quantity of class incremented (positive, increased fire severity) or decremented (negative, decreased fire severity) in the extended assessment.*

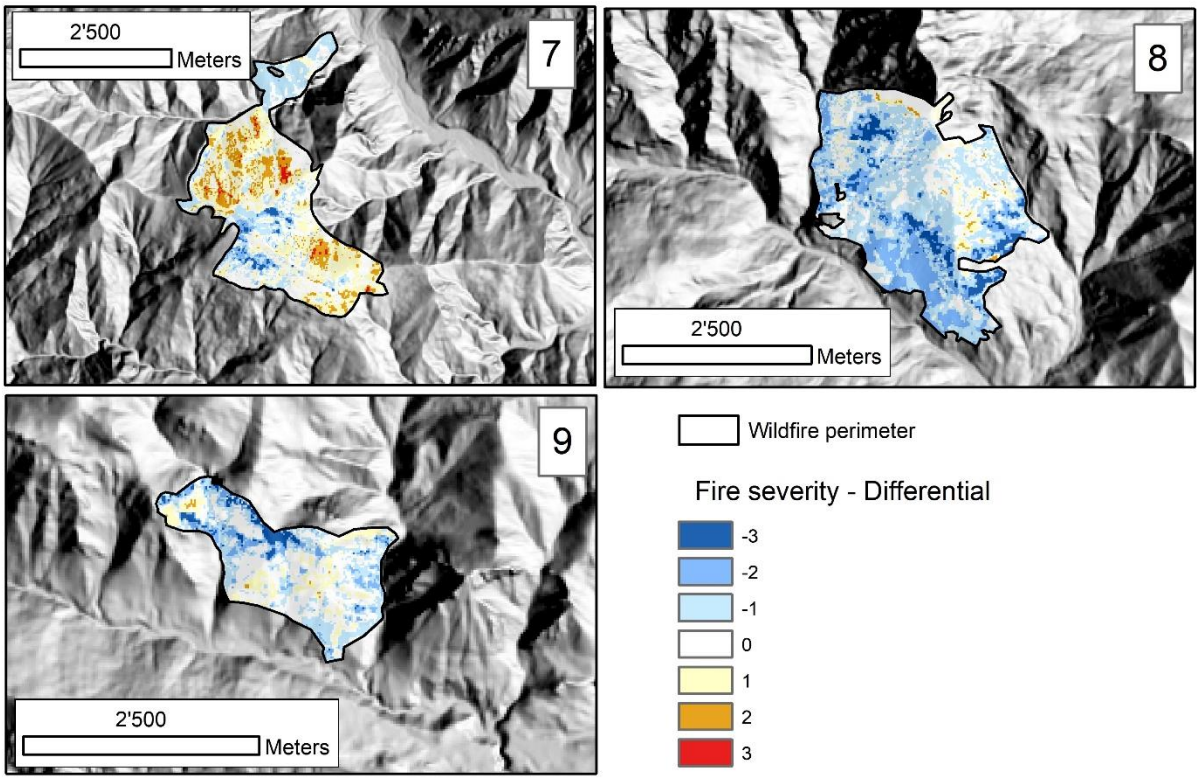


*Figure 7.15 - Fire severity maps differentials between extended and initial assessment, for the Roure/Perrero (7), Traversella (8) and Demonte (9) wildfires. Legend values express the quantity of class incremented (positive, increased fire severity) or decremented (negative, decreased fire severity) in the extended assessment.*

### 7.2.3 Watersheds characterization

**Morphometry and hydrology**

The main morphological descriptors for each watershed have been calculated following methods given in par. 6.2.3. Looking at all 49 watersheds some relevant numbers can be given: watersheds area (Aw) range from 0.06 to 50.74 Km² with an average value of 7.35 Km². The length (Lb) varies between 0.66 and 16.95 Km, averaging 4.02 km. As can be expected from Alpine and pre-Alpine basins, the minimum elevation (Emin) varies between 268 and 1467 m a.s.l. and the maximum (Emax) between 990 and 3535 m a.s.l. The average elevation difference (Eran) is about 1344 m, while the maximum height difference recorded is 3039 m. The slope values are also typical of a mountain environment, with maximum values (Smax) of 85 ° and average values (Smea) of 32 °.

Statistics for all the watersheds give a mean main channel length (Lp) of 3.85 Km, with minimum and maximum values reaching 0.51 and 16.80 Km, respectively. The main channel average slope (LpS) is 29.68°, while mean total streams length (L) is equal to 26.96 Km.

Morphometric parameters global statistics indicate a mean fan to watershed area ratio (Af_Aw) of 5.84, maximum values reaching 42.46. Form factor (Ff) Circularity Ratio (Rc) Elongation Ratio (Re) mean

values are 0.39, 0.56 and 0.67 respectively, indicating generally noticeably elongated watersheds. Drainage density values (Dd) span from a minimum of 1.06 and a maximum of 5.15 km/km², averaging 1.06 km/km². Time of concentration range from 0.05 to 1.24 h, and its mean value is 0.29 h.

Following the classification criteria proposed by Marchi et al. (1993) the catchments have been classified based on the fan slope [°] and Melton Index into three main classes: F (Fluvial, where the main depositional process is the fluvial deposition), DF (Debris-Flow, where the main processes are the gravity-related flows) and M (Mixed, where the fluvial deposition and gravity-related flows coexist). The majority of the analyzed catchments shows a tendency to develop gravity-related flows; just the catchment no. 24 is subject to a characteristic fluvial deposition, while catchment nos. 6 and 25 belongs to the Mixed category (fig. 7.16).

Detailed tables for geometric, hydrological and morphometric parameters are reported in Appendix 2.

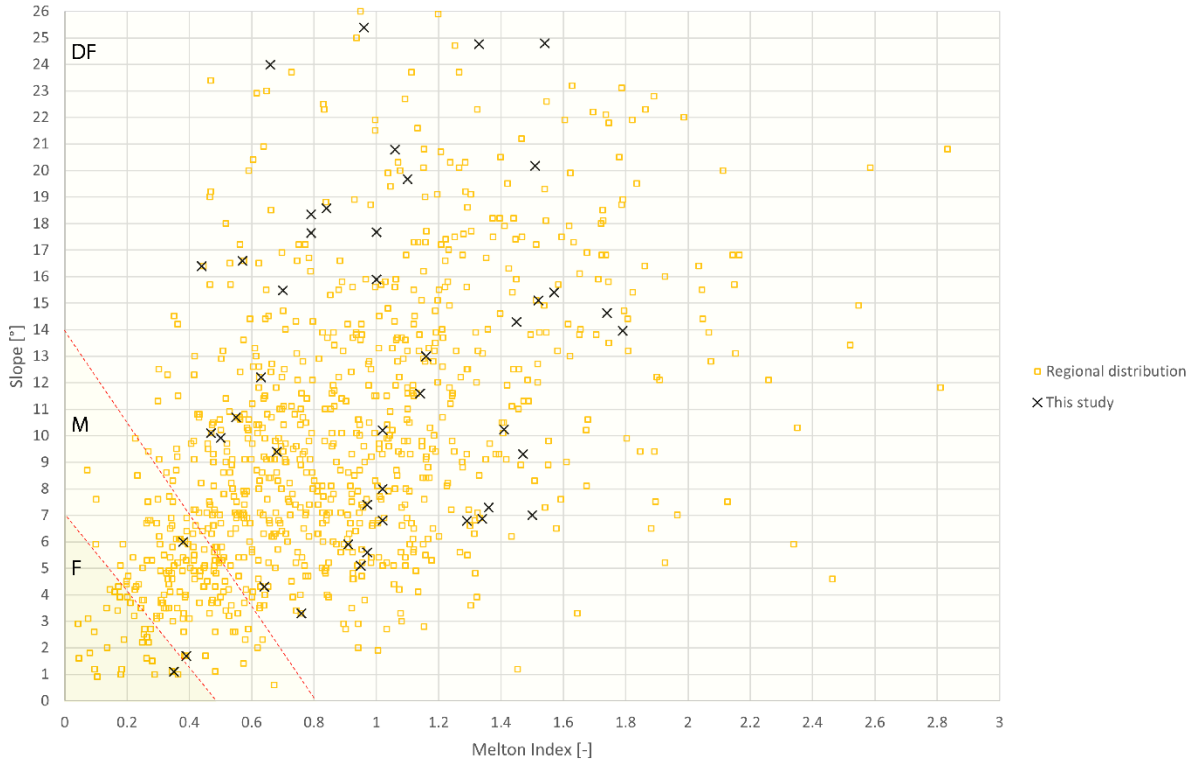


*Figure 7.16 – Melton Index vs fan slope diagram; Dashed lines represent Marchi et al. (1993) thresholds. F: fluvial Fan; M: mixed fan; DF: debris-Flow Fan.*

## Geology

The bedrock of the areas affected by the fires is quite variable and is composed of different formations, spanning from the granite and gneiss of the Gran Paradiso and Dora Maira typical of the fires of Locana, Cumiana, Roure, to the mainly carbonatic (limestone, dolomite) formations of the fires of the Stura Valley, and in part of the Bussoleno area. Calcschists and micaschists characterize the area of the Val Varaita and some sectors in Bussoleno and Mompantero; finally, ophiolites and other various metamorphites characterize burned areas in Caprie and Rubiana and Traversella (fig. 7.17, 7.18 and 7.19).

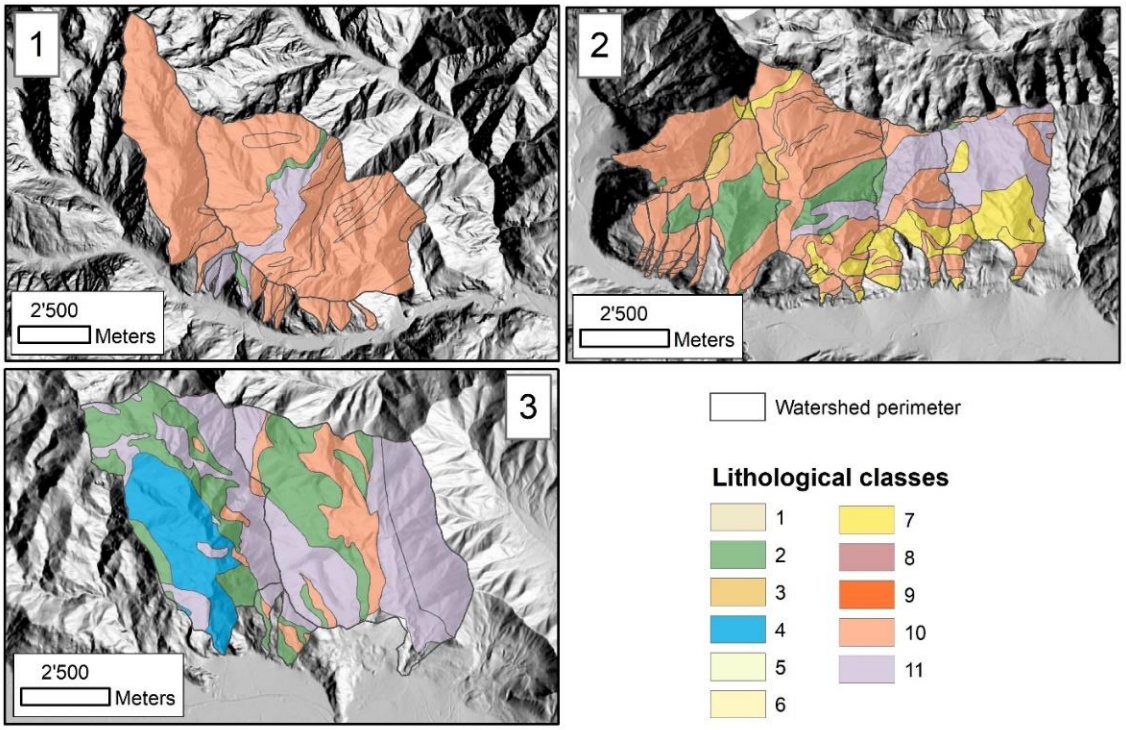


*Figure 7.17 – Lithological maps for the Locana/Ribordone (1), Bussoleno/Mompantero (2) and Caprie/Rubiana (3) wildfires. Legend:* ***1****- Carbonate Rich Mudstone, Arenite, Limestone, Conglomerate, Siltstone, Claystone, Mudstone;* ***2*** *- Chlorite actinolite epidote metamorphic rock, Amphibolite, Schist;* ***3*** *- fault rocks, breccia;* ***4*** *- gabbro, metagabbro, diorite;* ***5*** *– Hornfels;* ***6*** *- Limestone, Arenite, Carbonate rich mudstone, Impure limestone;* ***7*** *- Marble, dolomite, pure carbonate mudstone;* ***8*** *– Migmatite;* ***9*** *- Rhyolite, Metariolite, Dacite, Orthogneiss;* ***10*** *- Schist, Mica schist, Gneiss, Quartzite;* ***11*** *- Serpentinite, Peridotite, Schist.*

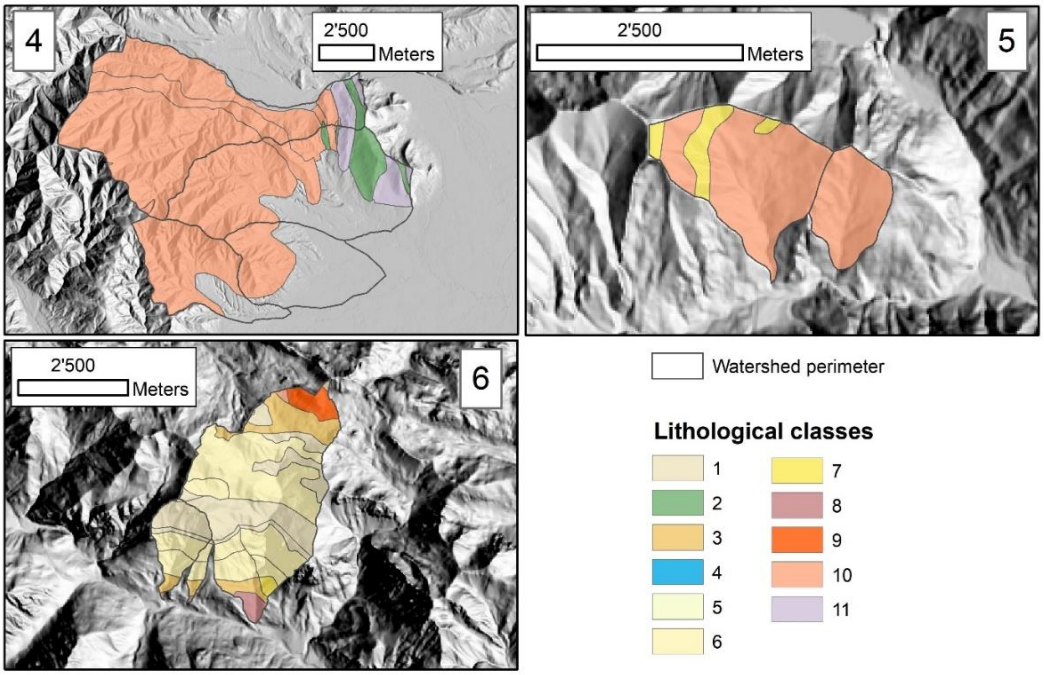


*Figure 7.18 - Lithological maps for the Cumiana/Cantalupa (4), Bellino/Casteldelfino (5) and Sambuco/Pietraporzio (6) wildfires. Legend: **1**- Carbonate Rich Mudstone, Arenite, Limestone, Conglomerate, Siltstone, Claystone, Mudstone; **2** - Chlorite actinolite epidote metamorphic rock, Amphibolite, Schist; **3** - fault rocks, breccia; **4** - gabbro, metagabbro, diorite; **5** – Hornfels; **6** - Limestone, Arenite, Carbonate rich mudstone, Impure limestone; **7** - Marble, dolomite, pure carbonate mudstone; **8** – Migmatite; **9** - Rhyolite, Metariolite, Dacite, Orthogneiss; **10** - Schist, Mica schist, Gneiss, Quartzite; **11** - Serpentinite, Peridotite, Schist.*

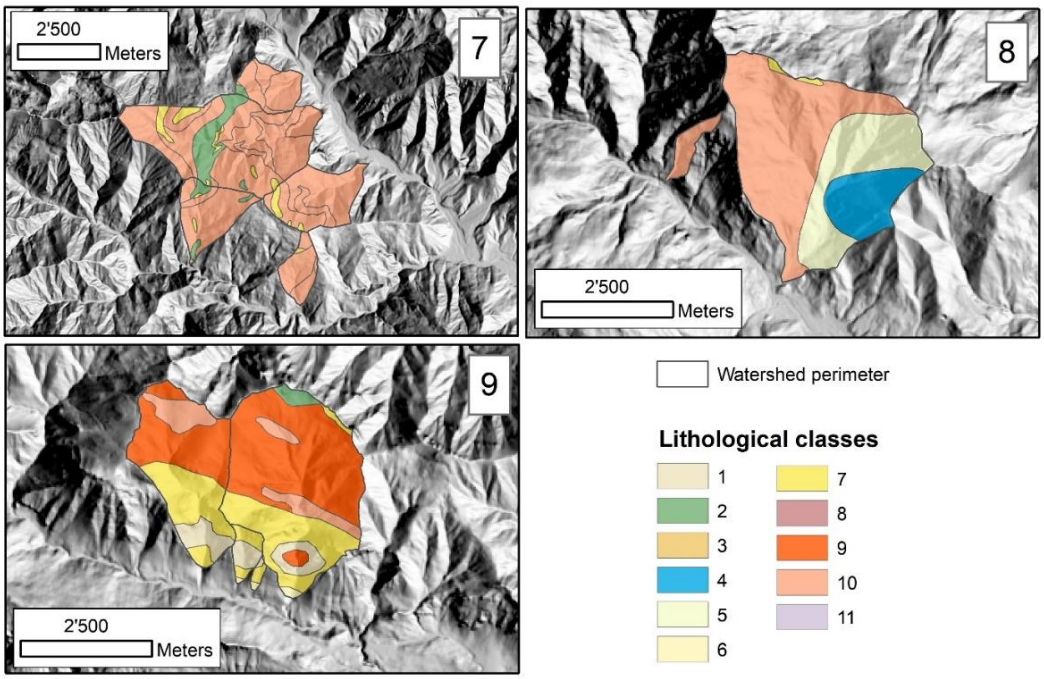


*Figure 7.19 - Lithological maps for the Roure/Perrero (7), Traversella (8) and Demonte (9) wildfires. Legend: **1**- Carbonate Rich Mudstone, Arenite, Limestone, Conglomerate, Siltstone, Claystone, Mudstone; **2** - Chlorite actinolite epidote metamorphic rock, Amphibolite, Schist; **3** - fault rocks, breccia; **4** - gabbro, metagabbro, diorite; **5** – Hornfels; **6** - Limestone, Arenite, Carbonate rich mudstone, Impure limestone; **7** - Marble, dolomite, pure carbonate mudstone; **8** – Migmatite; **9** - Rhyolite, Metariolite, Dacite, Orthogneiss; **10** - Schist, Mica schist, Gneiss, Quartzite; **11** - Serpentinite, Peridotite, Schist.*

**Forestry/land-cover**

Land cover data were produced after integrating Land Cover Piemonte dataset (2010) and Forest Map of the Piedmont Region (2016). Forest Map units were grouped based on CLC code, maintaining a separation between forested areas s.s. and vegetated areas with arboreal coverage below 20%. Areas outside the Forest Map has been classified according to Land Cover Piemonte. Bare soil class has been added (fig. 7.20, 7.21 and 7.22).

Complete cover type table are reported in appendix 3.

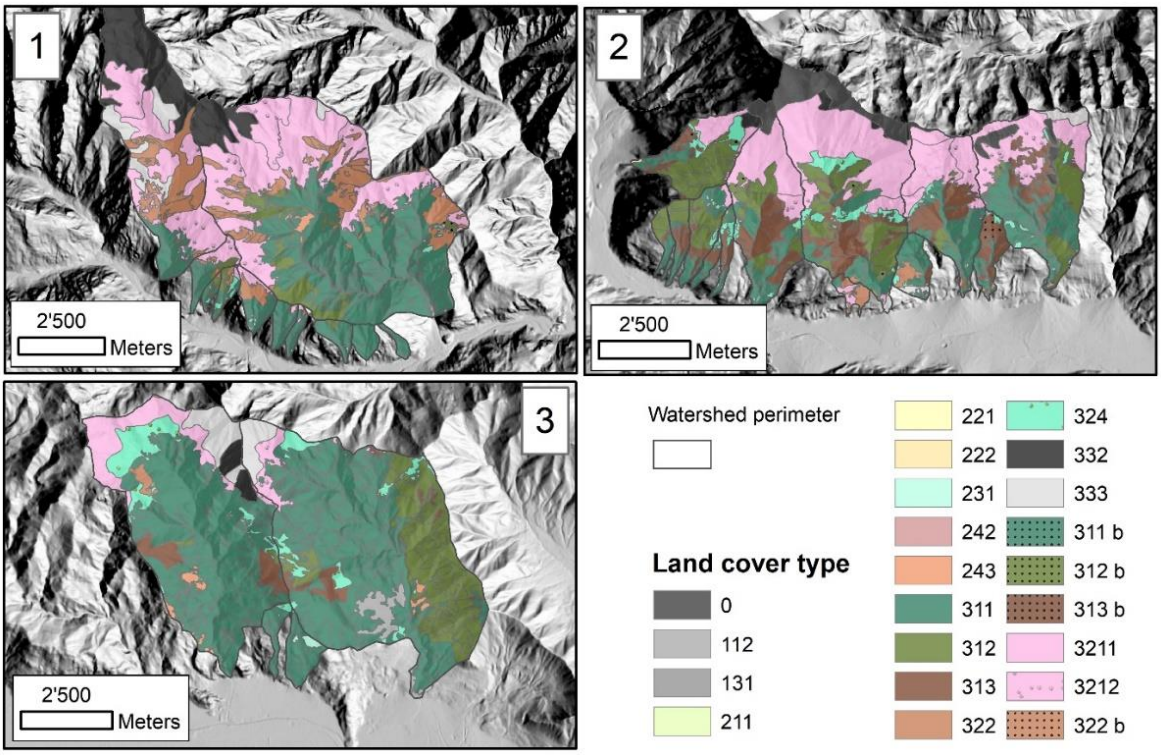


*Figure 7.20 – Land Cover maps for the Locana/Ribordone (1), Bussoleno/Mompantero (2) and Caprie/Rubiana (3) wildfires. Legend:* ***0****- Bare soil;* ***112*** *- Discontinuous urban fabric;* ***131*** *– Mineral extraction sites;* ***211*** *– Non-irrigated arable land;* ***221*** *– Vineyards;* ***222*** *– Fruit trees and berry plantations;* ***231*** *– Pastures;* ***242*** *– Complex cultivation patterns ;* ***243*** *– Land principally used for agriculture, with significant areas of natural vegetation;* ***311*** *– Broad-leaved forest;* ***312*** *– Coniferous forest ;* ***313*** *– Mixed forest;* ***322*** *– Moors and heathland;* ***324*** *– Transitional woodland-shrub ;* ***332*** *– Bare rocks;* ***333*** *– Sparsely vegetated areas;* ***311b*** *– Broad-leaved forest <20%;* ***312b*** *– Coniferous forest <20%;* ***313b*** *– Mixed forest <20%;* ***3211*** *– Natural grassland prevailingly without trees and shrubs;* ***3212*** *– Natural grassland with trees and shrubs ;* ***322b*** *- Moors and heathland <20%.*

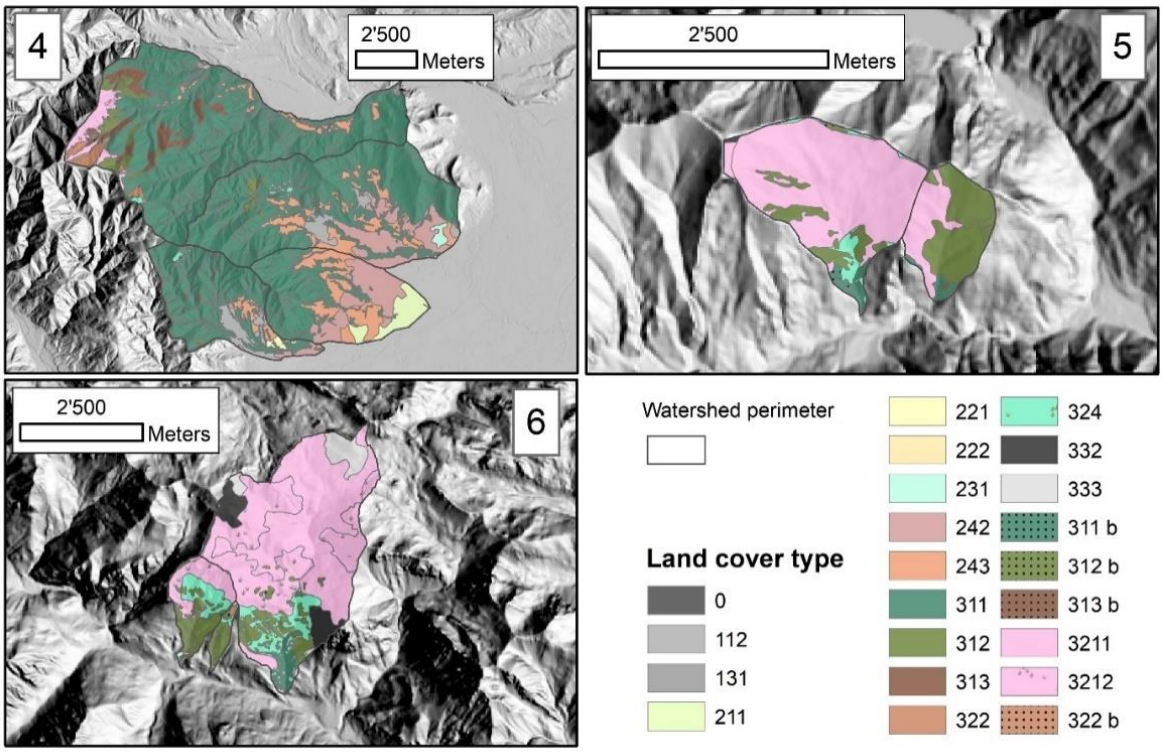


*Figure 7.21 - Land Cover maps for the Cumiana/Cantalupa (4), Bellino/Casteldelfino (5) and Sambuco/Pietraporzio (6) wildfires. Legend:* ***See Fig. 7.20.***

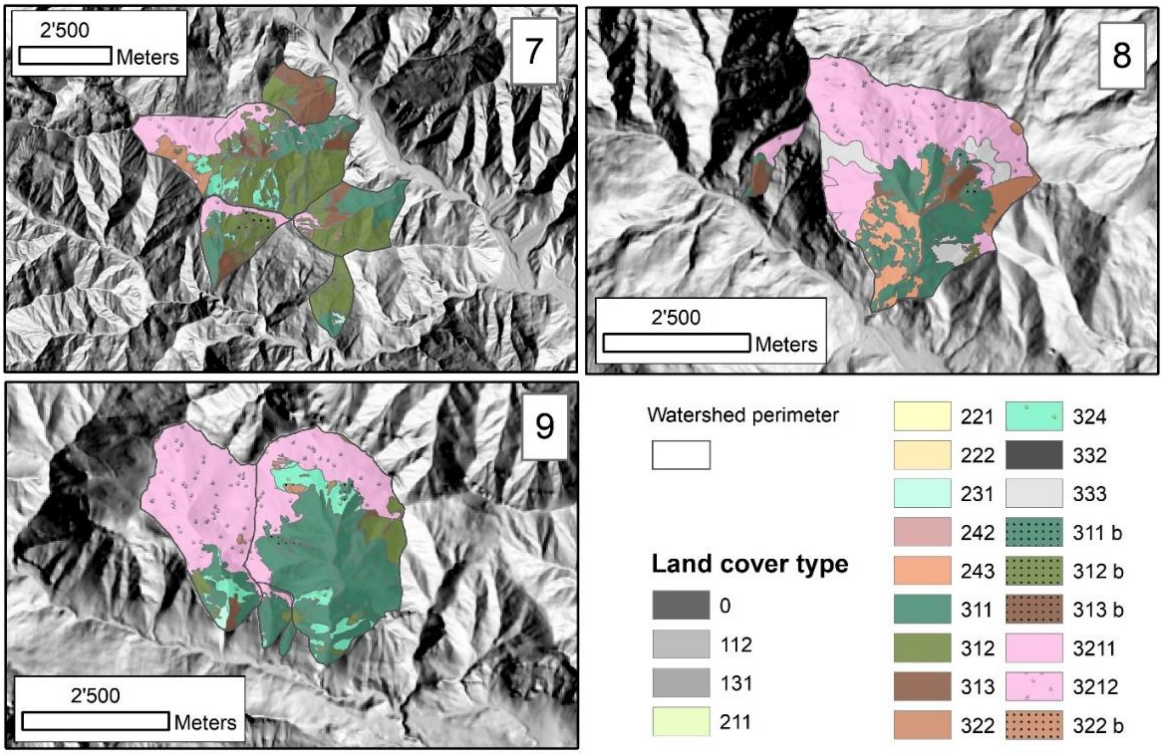


*Figure 7.22 - Land Cover maps for the Roure/Perrero (7), Traversella (8) and Demonte (9) wildfires. Legend:* ***See Fig. 7.20.***

## 7.2.4 Fire-related erodibility model

### 7.2.4.1 Pre-fire

The-Erodibility Index EI [Mg MJ$^{-1}$ mm$^{-1}$ h] is used to compare post-fire to pre-fire erosion susceptibility. Erodibility Index distribution for the pre-fire condition $EI_{pre}$ has been calculated on a 5 meters resolution raster grid and is reported in appendix 4 (fig A4.10, A4.11 and A4.12). Detailed maps of K, LS and C factors are also reported in appendix 4.

In figg. 7.23, 7.24 and 7.25 the spatially averaged value $EI_{w\_pre}$ of the Erosivity Index $EI_{pre}$ calculated for every watershed is presented.

In the pre-fire condition the averaged value of the Erodibility Index at the watershed scale ranges from a minimum value of 1.62E-05 to a maximum of 1.25E-02, the mean value being 7.69E$^{-04}$ Mg MJ$^{-1}$ mm$^{-1}$ h. The majority of the watersheds (87%) has a value below 1.00E$^{-03}$ Mg MJ$^{-1}$ mm$^{-1}$ h, and the only exceptions regards watersheds 6 watersheds in the area of the Bussoleno/Mompantero fire. Particularly relevant values characterize the Rocciamelone, rio Prebech and Crosiglione watersheds.

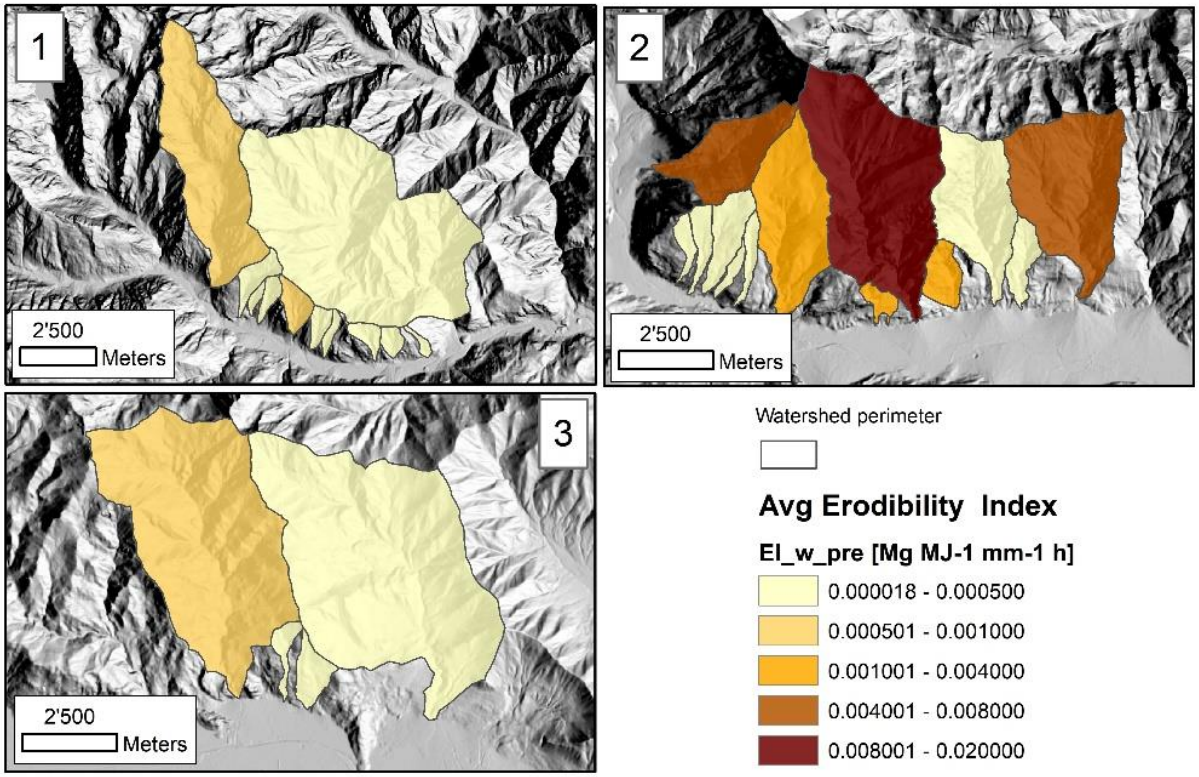


*Figure 7.23 – Pre-fire spatially averaged value of the Erodibility Index, $EI_{w\_pre}$, for the watersheds affected by the Locana/Ribordone (1), Bussoleno/Mompantero (2) and Caprie/Rubiana (3) wildfires.*

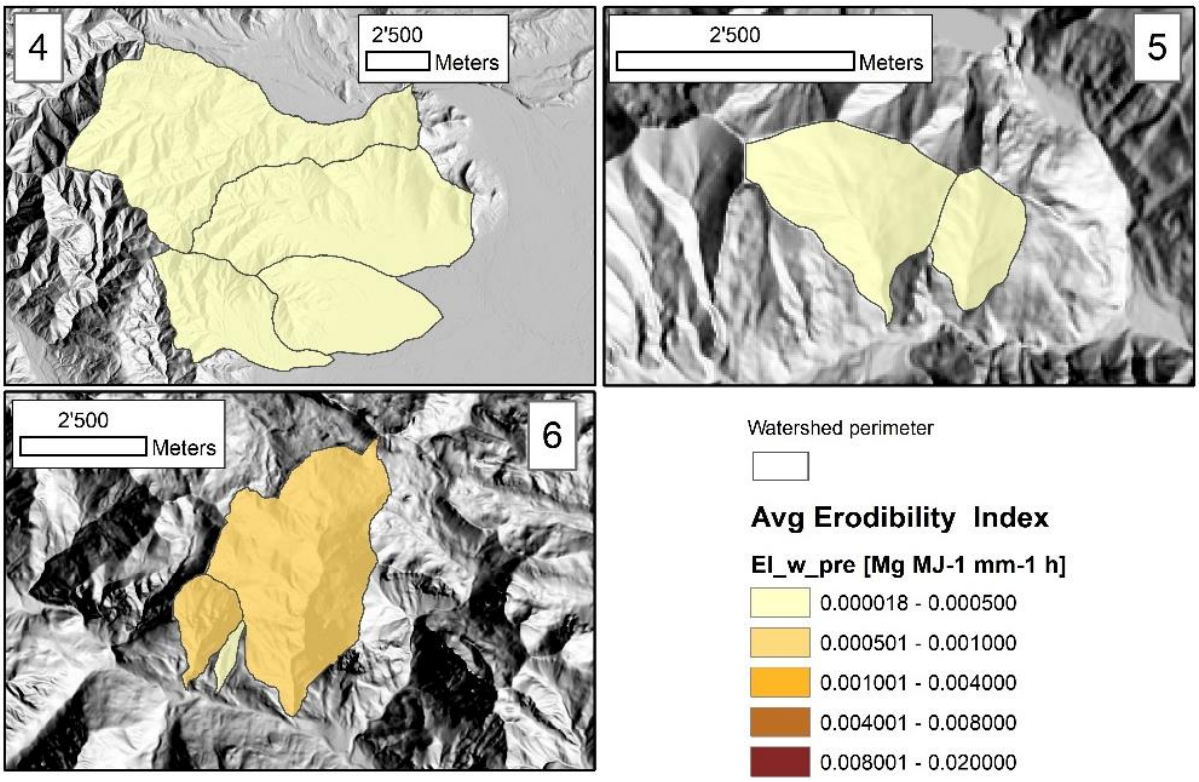


*Figure 7.24 - Pre-fire spatially averaged value of the Erodibility Index, $EI_{w\_pre}$, for the watersheds affected by the Cumiana/Cantalupa (4), Bellino/Casteldelfino (5) and Sambuco/Pietraporzio (6) wildfires.*

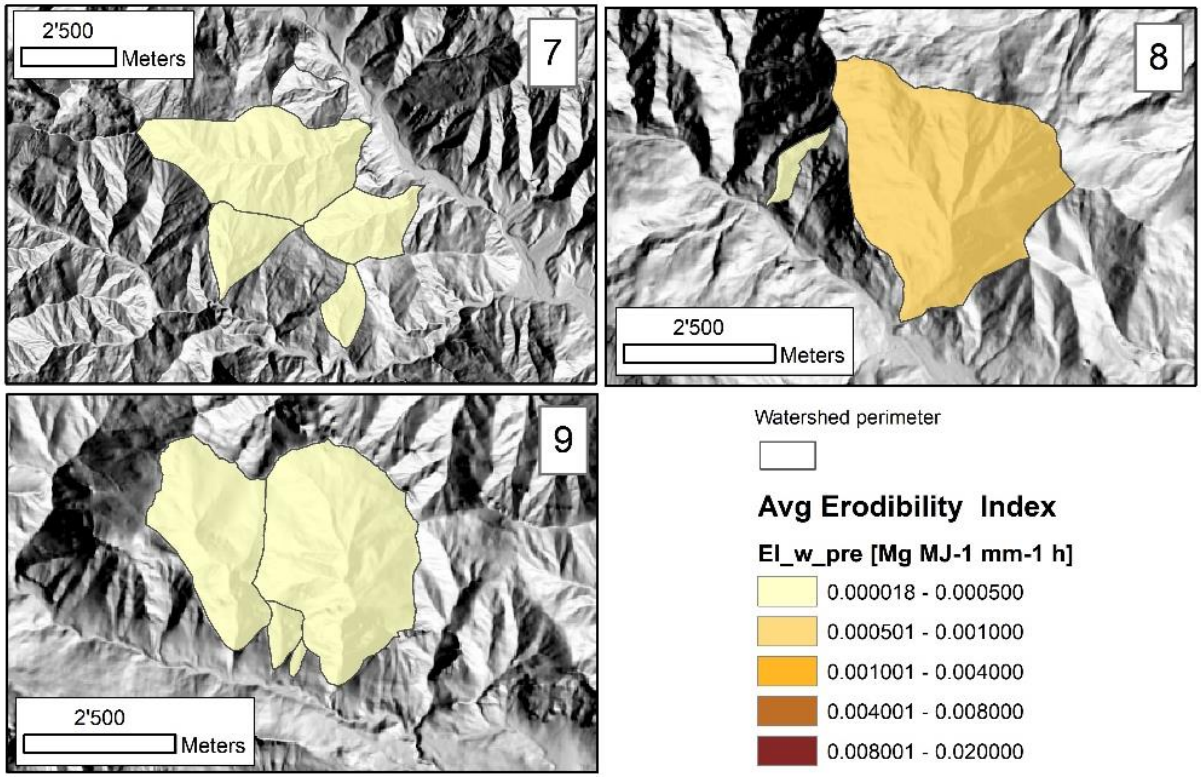


*Figure 7.25 - Pre-fire spatially averaged value of the Erodibility Index, $EI_{w\_pre}$, for the watersheds affected by the Roure/Perrero (7), Traversella (8) and Demonte (9) wildfires.*

The average annual soil loss caused by surface water erosion $A_{pre}$, in pre-fire condition has been calculated by using a 500m resolution raster grid for R value (fig A4.16, A4.17 and A4.18, Appendix 4) and a P value set to 1.

In fig. 7.26, 7.27 and 7.28 the spatially averaged value $A_{\_w\_pre}$ [Mg $ha^{-1}$ $y^{-1}$] of the average annual soil loss $A_{pre}$ calculated for every watershed is given.

The results describing averaged soil loss $A_{\_w\_pre}$ is consistent with the Erodibility Index distribution over the 49 watersheds, and the overall mean value is 1.05 Mg $ha^{-1}$ $y^{-1}$. The 83 % of the watersheds has an average annual soil loss value below 1.00 Mg $ha^{-1}$ $y^{-1}$, the 93% being less than 5.00 Mg $ha^{-1}$ $y^{-1}$. Again, higher values are registered for the Rocciamelone, rio Prebech and Crosiglione watersheds.

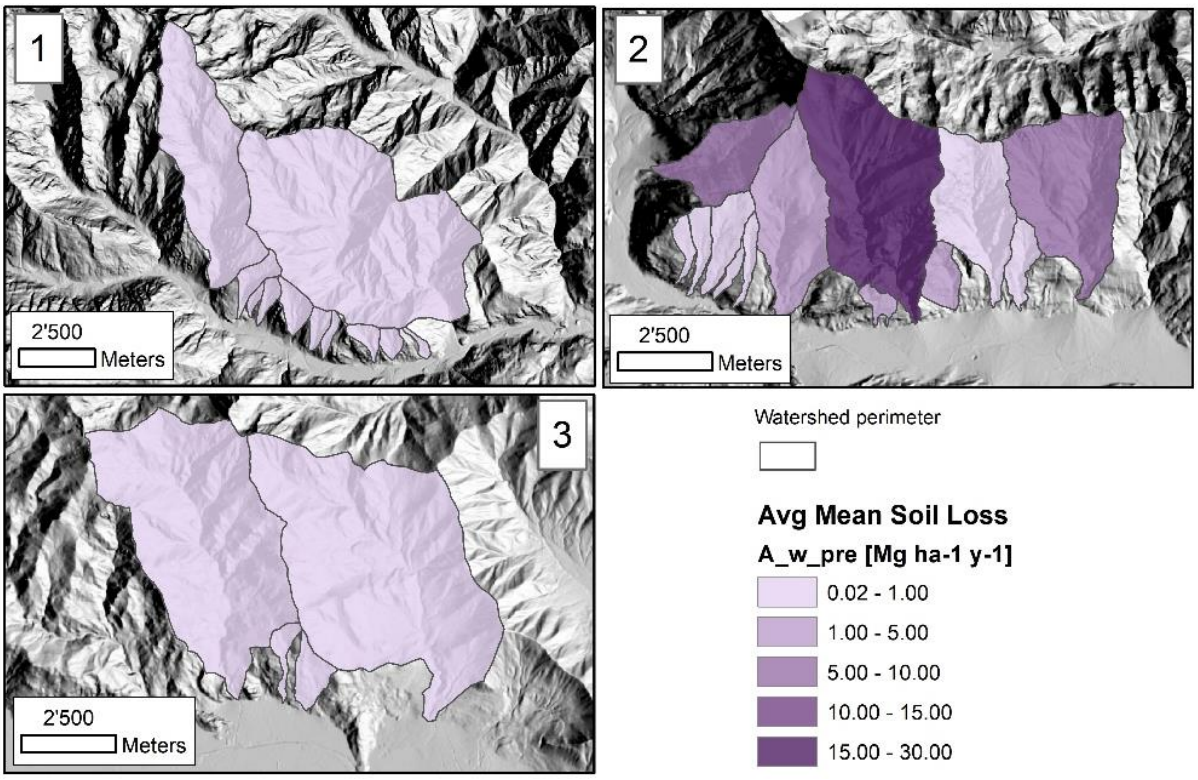


*Figure 7.26 - Pre-fire spatially averaged value of the annual soil loss, $A_{pre\_w}$, for the watersheds affected by the Locana/Ribordone (1), Bussoleno/Mompantero (2) and Caprie/Rubiana (3) wildfires.*

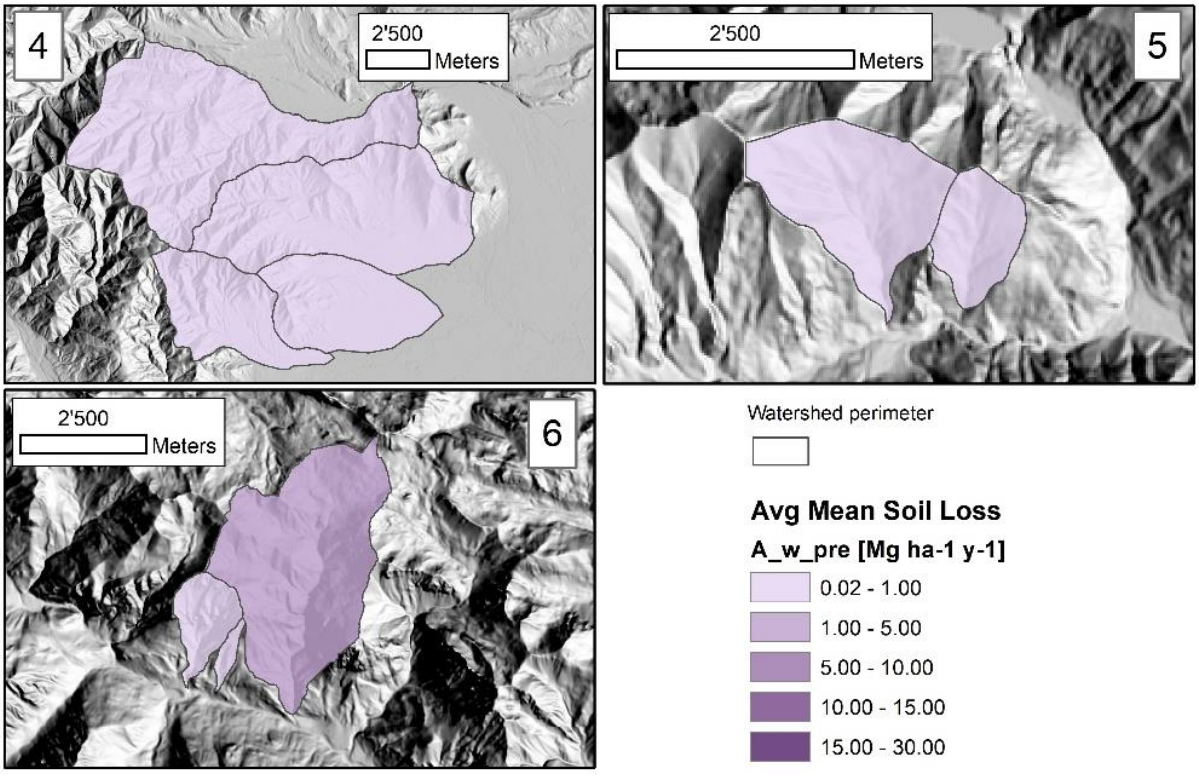


*Figure 7.27 - Pre-fire spatially averaged value of the annual soil loss, $A_{pre\_w}$, for the watersheds affected by the Cumiana/Cantalupa (4), Bellino/Casteldelfino (5) and Sambuco/Pietraporzio (6) wildfires.*

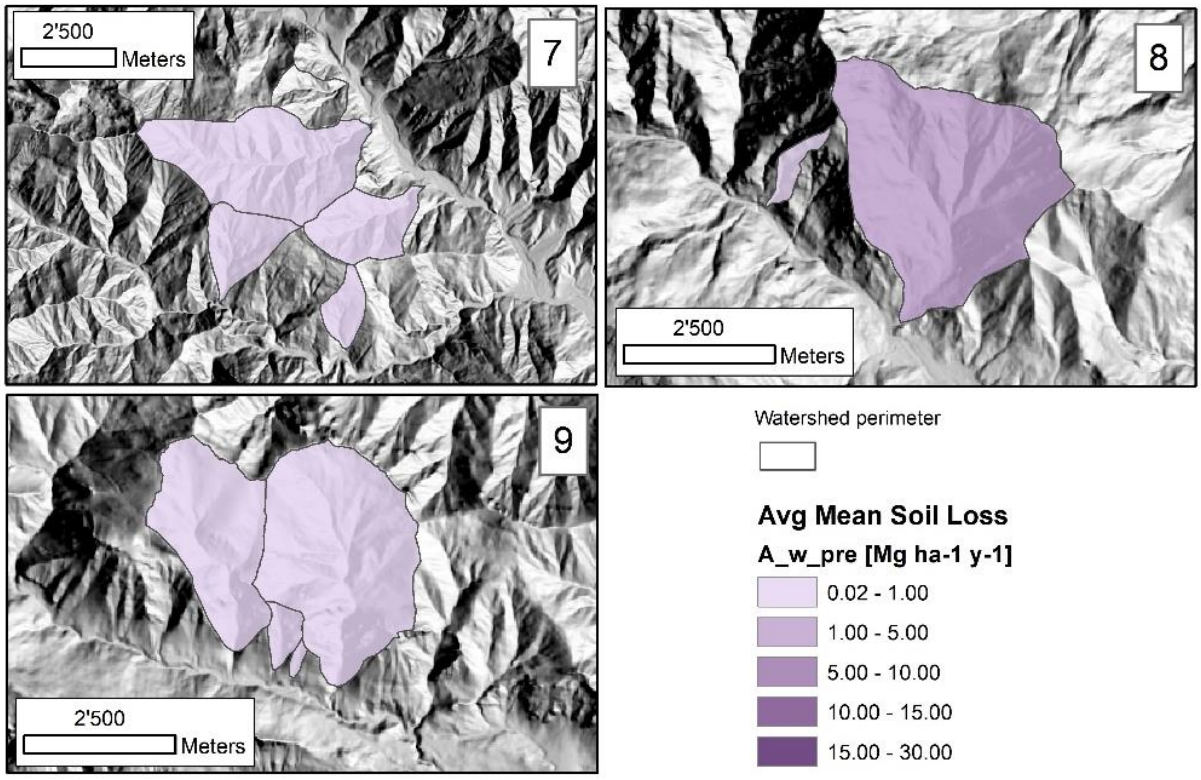


*Figure 7.28 - Pre-fire spatially averaged value of the annual soil loss, $A_{pre\_w}$, for the watersheds affected by the Roure/Perrero (7), Traversella (8) and Demonte (9) wildfires.*

The value of sediment loss $SL_{pre}$ [Mg $y^{-1}$] for each watershed is presented in figg. A4.19, A4.20 and A4.21 (appendix 4). Mean Sediment loss over the 49 watersheds is 1130 Mg $y^{-1}$. Again, higher values are found for the rio Prebech, Crosiglione and especially Rocciamelone watersheds, the latter reaching values a value above 27000 Mg $y^{-1}$.

### 7.2.4.2 Post-fire

Post-fire condition has been modeled for both the initial and the extended assessment by calculating mean soil loss per year $A_{ini}$ and $A_{ext}$ and Erodibility Index $EI_{ini}$ and $EI_{ext}$ following the procedure of par 6.2.4. Parameters $C_{ini}$, $C_{ext}$, $K_{ini}$, $K_{ext}$, $LS_{ini}$ and $LS_{ext}$ has been adjusted as a function of fire severity (unburned, low, moderate or high). R factor has been maintained equal to pre-fire condition. Spatial distribution of C, K, LS, EI and A can be found in Appendix 4 for both the initial and extended assessment.

Spatially averaged values of EI [Mg $MJ^{-1}$ $mm^{-1}$ h] and A [Mg $ha^{-1}$ $y^{-1}$] for the initial assessment ($EI_{w\_ini}$ and $A_{w\_ini}$) are given in fig. 7.29, 7.30, 7.31, 7.32, 7.33 and 7.34, whereas EI and A values for the extended assessment are given in fig A4.49, A4.50, A4.51, A4.55, A4.56, and A4.57 (appendix 4).

For the initial assessment the averaged value of the Erodibility Index at the watershed scale ranges from a minimum value of 1.82E$^{-05}$ to a maximum of 1.69E$^{-02}$, the mean value raising to 4.27E$^{-03}$ Mg MJ$^{-1}$ mm$^{-1}$ h. The percentage of the watersheds having a value below 1.00E$^{-03}$ Mg MJ$^{-1}$ mm$^{-1}$ h decrease to 24%, the 46% shoving values above 4.00 E$^{-03}$ Mg MJ-1 mm$^{-1}$ h. As expected, the watershed affected by the Locana/Ribordone and the Bussoleno/Mompantero wildfires, as a consequence of their generally higher fire severity, shows the higher values of Erodibility Index. For the other wildfires-affected areas, the raise in the Erodibility Index values is less marked, except some singularities (i.e. Cumbal della Comu and Valle Chiara Primo) (fig. 7.35).

For the extended assessment, the averaged value of the Erodibility Index at the watershed scale ranges from a minimum value of 1.77E$^{-05}$ to a maximum of 1.40E$^{-02}$, the mean value being equal to 3.00E$^{-03}$ Mg MJ$^{-1}$ mm$^{-1}$ h. The percentage of the watersheds having a value below 1.00E$^{-03}$ Mg MJ$^{-1}$ mm$^{-1}$ h is equal to 27%, the 27% shoving values above 4.00 E$^{-03}$ Mg MJ$^{-1}$ mm$^{-1}$ h. on average, the watershed affected by the Locana/Ribordone and the Bussoleno/Mompantero wildfires, again, shows the higher values of Erodibility Index (fig. 7.34).

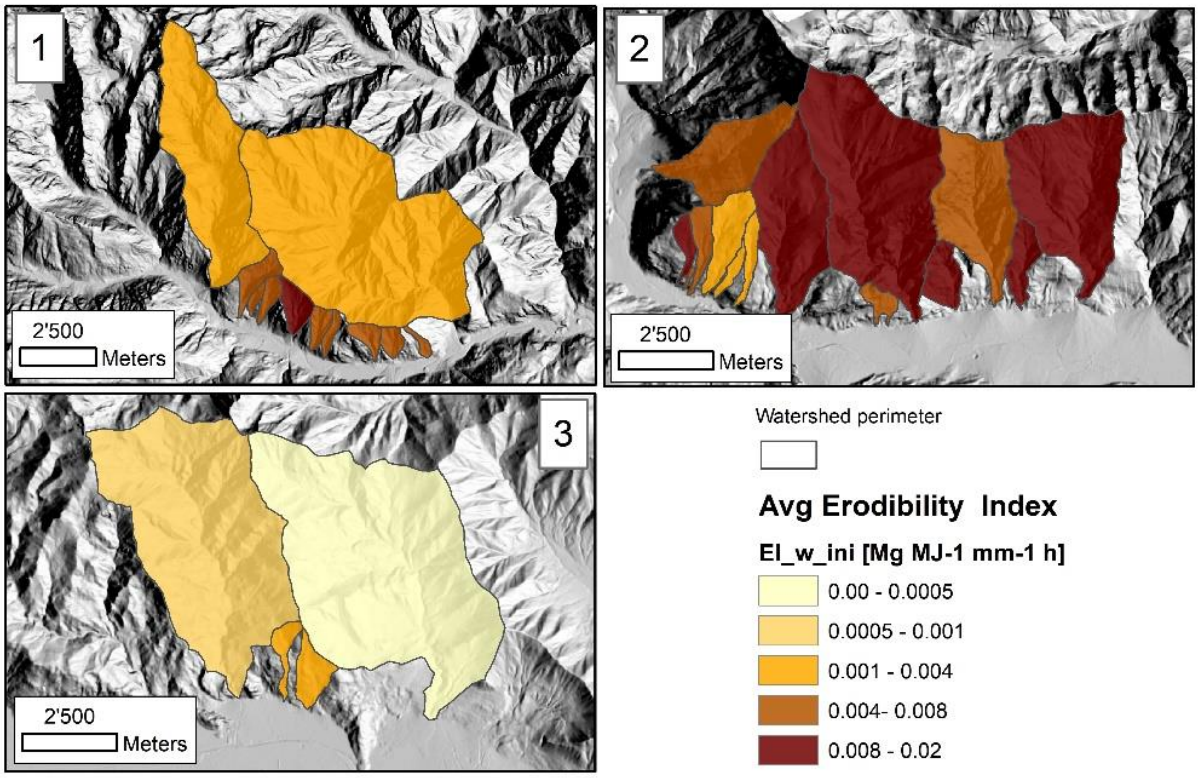


*Figure 7.29 - Spatially averaged value of the Erodibility Index, $EI_{w\_ini}$, for the watersheds affected by the Locana/Ribordone (1), Bussoleno/Mompantero (2) and Caprie/Rubiana (3) wildfires; post-fire condition, initial assessment.*

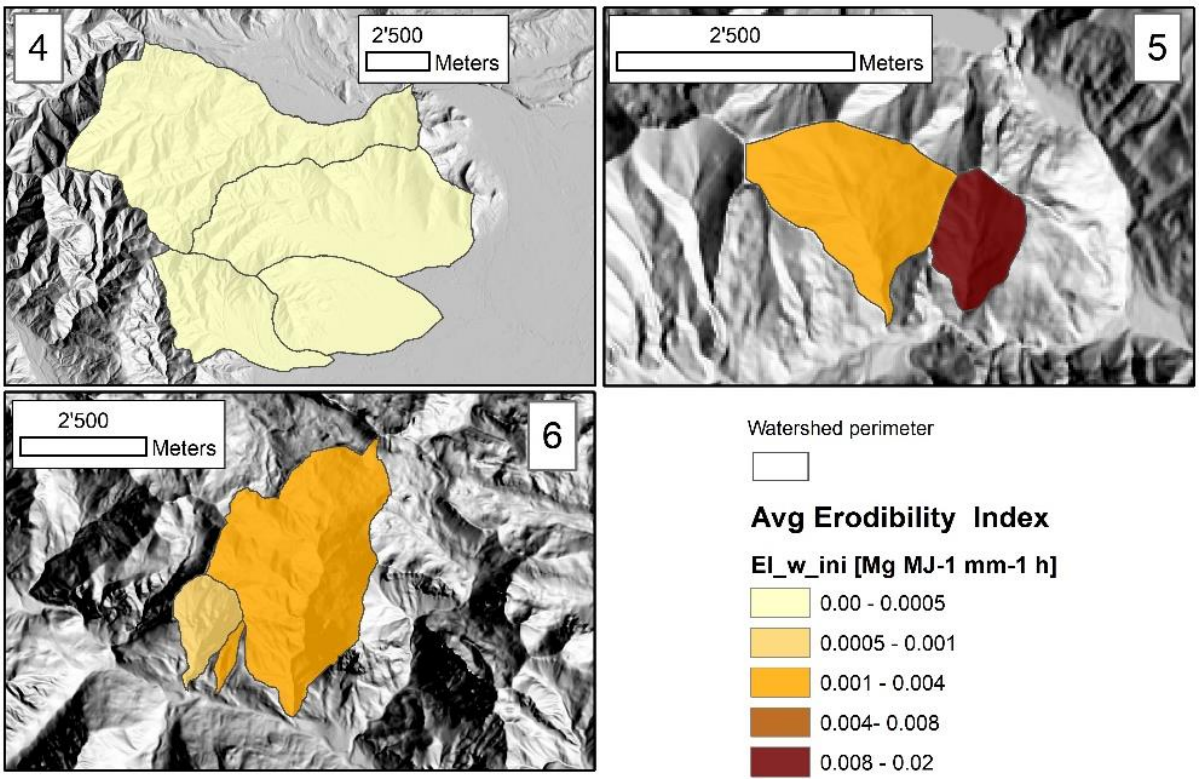


*Figure 7.30 - Spatially averaged value of the Erodibility Index, $EI_{w\_ini}$, for the watersheds affected by the Cumiana/Cantalupa (4), Bellino/Casteldelfino (5) and Sambuco/Pietraporzio (6) wildfires; post-fire condition, initial assessment.*

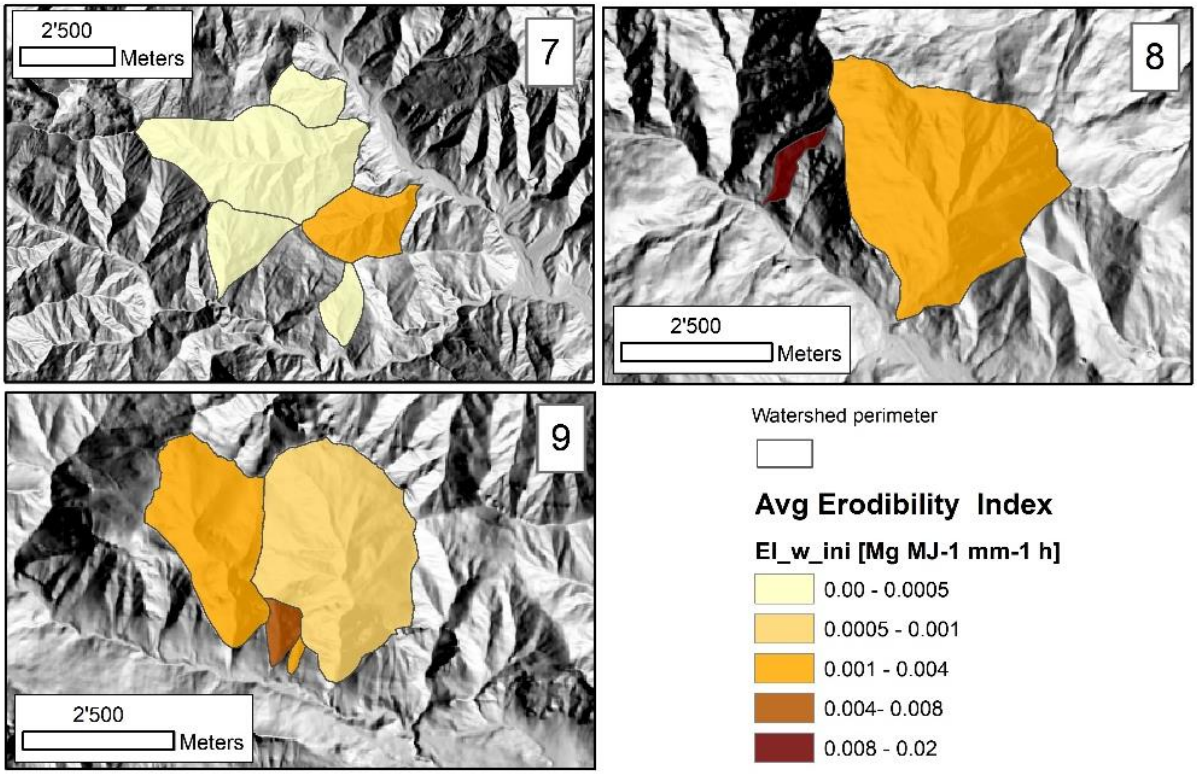


*Figure 7.31 - Spatially averaged value of the Erodibility Index, $EI_{w\_ini}$, for the watersheds affected by the Roure/Perrero (7), Traversella (8) and Demonte (9) wildfires; post-fire condition, initial assessment.*

The results describing averaged soil loss $A_{w\_ini}$ are consistent with the Erodibility Index distribution over the 49 watersheds, and the mean value is 5.65 Mg ha$^{-1}$ y$^{-1}$. The 20 % of the watersheds has an average annual soil loss value below 1.00 Mg ha$^{-1}$ y$^{-1}$, the 44% being more than 5.00 Mg ha$^{-1}$ y$^{-1}$. Higher values are registered for the Valle Chiara Primo, Rocciamelone, and Rio Bocchetta watersheds (fig. 7.36).

Considering the extended assessment, the 24% of the watersheds has an average annual soil loss value below 1.00 Mg ha$^{-1}$ y$^{-1}$, the 27% being more than 5.00 Mg ha$^{-1}$ y$^{-1}$. The overall mean value is 3.84 Mg ha$^{-1}$ y$^{-1}$(fig. 7.35).

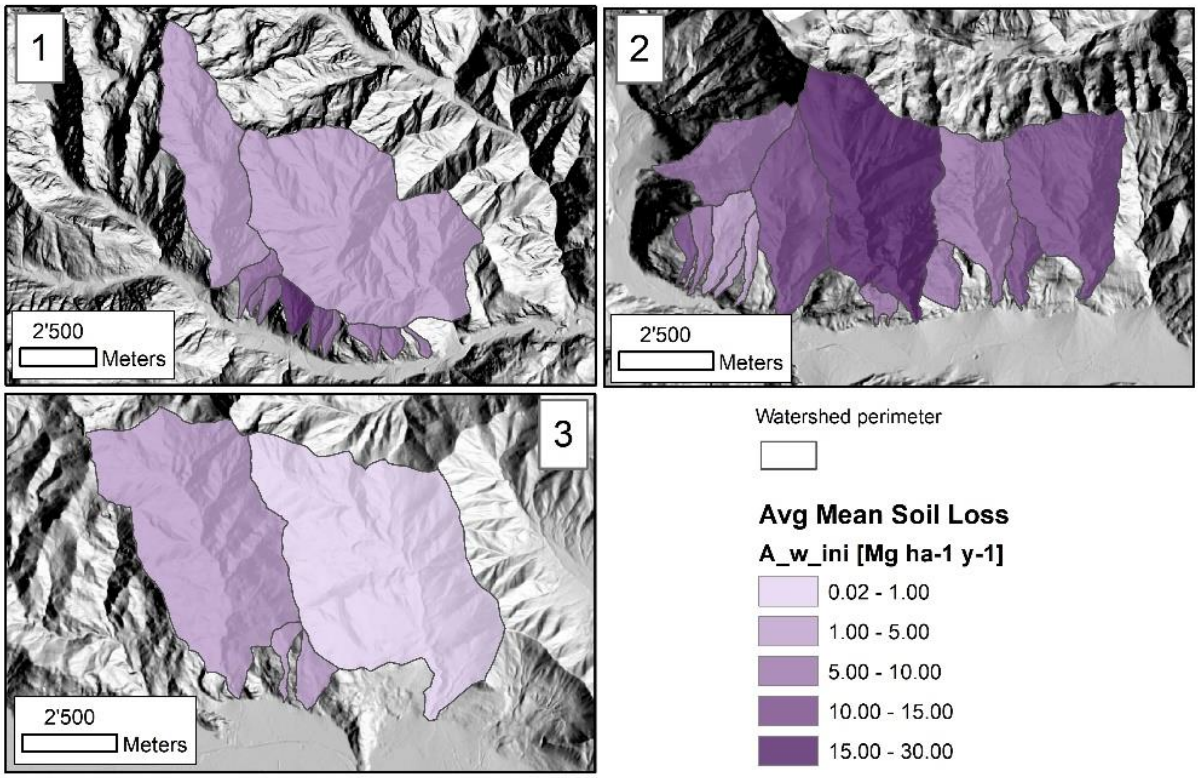


*Figure 7.32 - Spatially averaged value of the annual soil loss, Aw_ini, for the watersheds affected by the Locana/Ribordone (1), Bussoleno/Mompantero (2) and Caprie/Rubiana (3) wildfires; post-fire condition, initial assessment.*

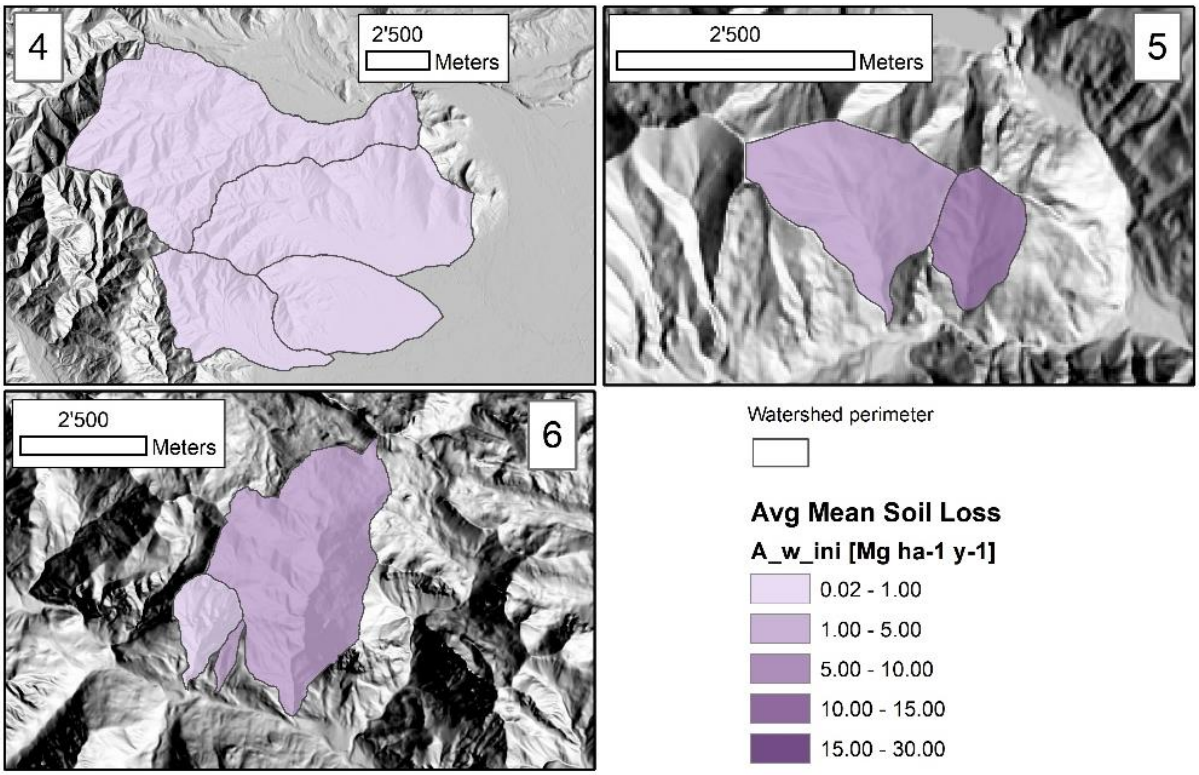


*Figure 7.33 - Spatially averaged value of the annual soil loss, Aw_ini, for the watersheds affected by the Cumiana/Cantalupa (4), Bellino/Casteldelfino (5) and Sambuco/Pietraporzio (6) wildfires; post-fire condition, initial assessment.*

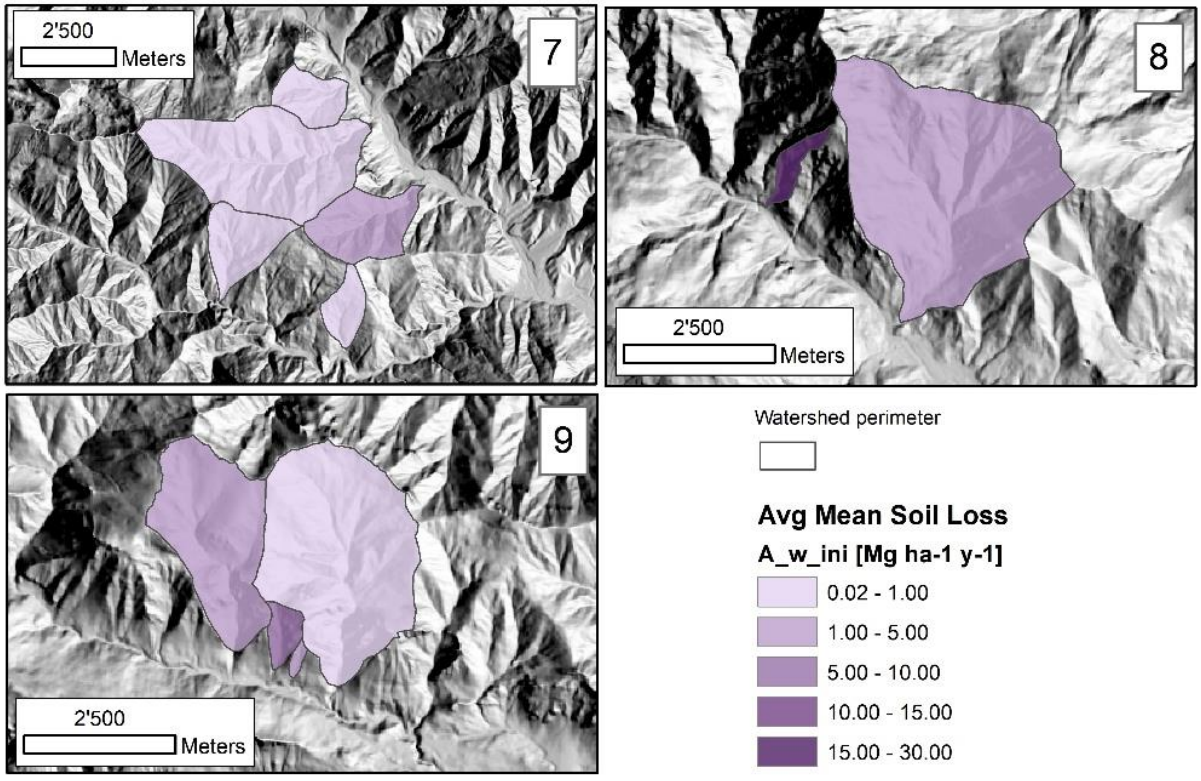


*Figure 7.34 - Spatially averaged value of the annual soil loss, Aw_ini, for the watersheds affected by the Roure/Perrero (7), Traversella (8) and Demonte (9) wildfires; post-fire condition, initial assessment.*

Finally, $SL_{ini}$ and $SL_{ext}$ [Mg $y^{-1}$] have been then calculated repeating the pre-fire procedure. For the initial assessment, mean value of sediment loss is 2244 Mg $y^{-1}$, while for the extended assessment the mean value is 1764 Mg $y^{-1}$. Higher values for both the initial and the extended assessment are found for the Rio Prebech, Giandula and Rocciamelone watersheds (fig. 7.37). Maps for this parameter are given in Appendix 4 (figg. A4.37, A4.38, A4.39, A4.58, A4.59 and A4.60).

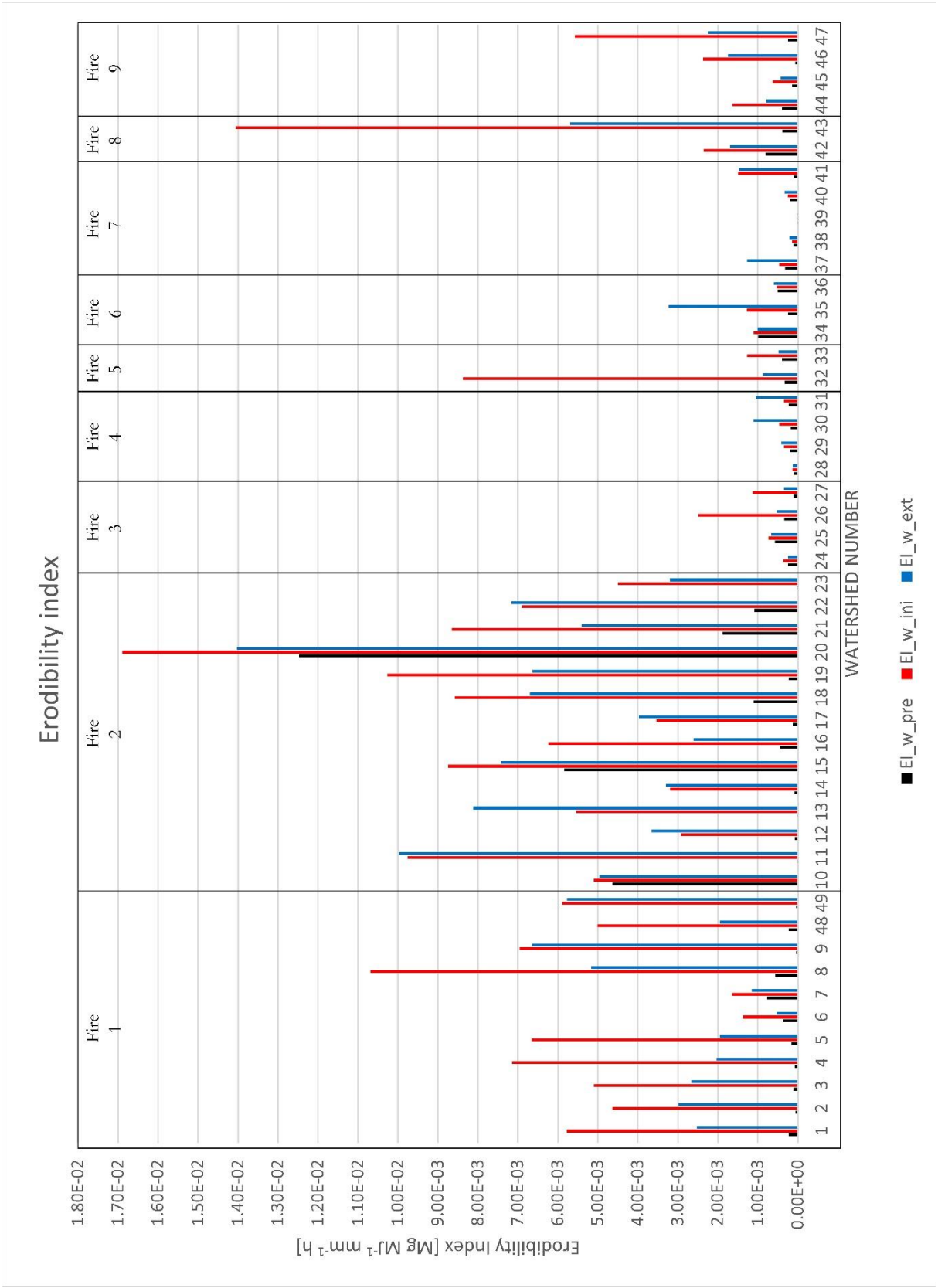


*Figure 7.35 – Values of Erodibility Index, EI, for the 49 watershed in the pre-fire condition and for the post-fire initial and extended assessment.*

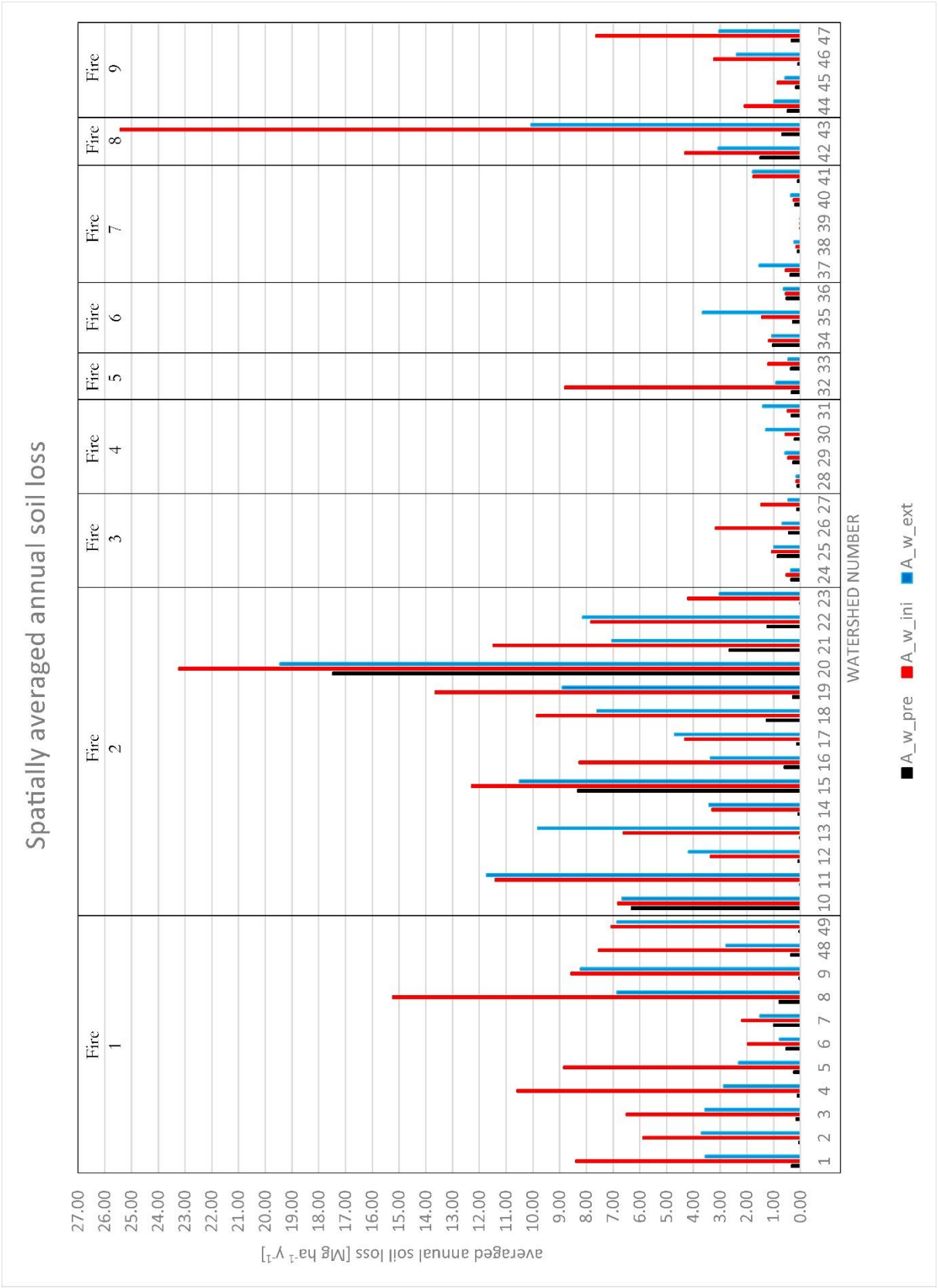


*Figure 7.36 – Values of Average Annual Soil Loss, A, for the 49 watershed in the pre-fire condition and for the post-fire initial and extended assessment.*

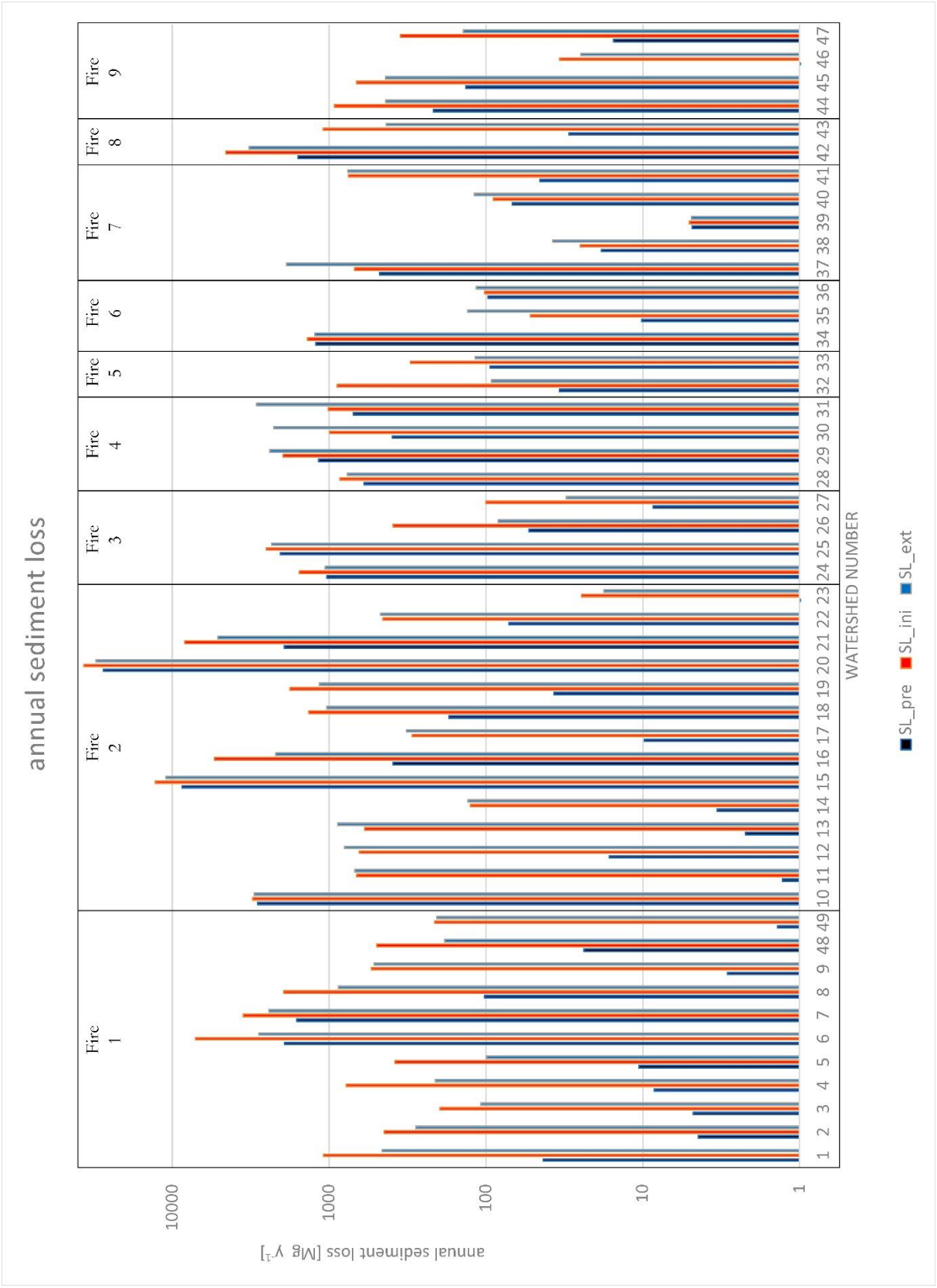


*Figure 7.37 – Values of Annual Sediment Loss, SL, for the 49 watershed in the pre-fire condition and for the post-fire initial and extended assessment.*

#### 7.2.4.3 Pre-fire vs post-fire

EI values calculated for the pre-fire situation $EI_{w\_pre}$, for the post-fire initial assessment $EI_{w\_ini}$ and for the post-fire extended assessment $EI_{w\_ext}$ have been compared by calculating their relative ratios (R_EI_ini_pre and R_EI_ext_pre and R_EI_ext_ini) for assessing the effect of wildfires with respect to pre-fire condition. Results of the initial vs pre-fire comparison are given fig 7.38, while related maps and detailed tables are reported in appendix 4.

Overall results show a general increase in the EI values for the post fire condition, the ratio between initial and pre-fire assessment having a mean value of 43.56 and the ratio between extended and pre-fire assessment averaging 38.66. It is moreover evident a dichotomy between fire number 1 and 2 (Locana/Ribordone and Bussoleno/Mompantero) and the other seven wildfires: the mean value of the EI ratios (initial assessment vs pre-fire) of the first two fires is equal to 77.49 (63,54 and 88.45 respectively), while the mean value of the remaining is 8.22. Maximum EI ratios are observed for the Bussoleno/Mompantero fire, in which watersheds no. 11, 13 and 23 are characterized by values of 513.79, 388.96 and 197.12 respectively (for the extended assessment with respect to pre-fire condition).

The comparison between the post-fire extended and initial assessment shows a general reduction of the EI ratios, the first being on average the 91% of the second. The decrease in the extended assessment is consistent between watershed for the fire no. 1 (mean value 0.55), while in the Bussoleno/Mompantero fire some watersheds (nos. 11, 12 and 13) are subjected to an increase of the EI values for the extended assessment, the ratio being equal to 1.24. For fires nos. 3, 4, 5, 6, 7, 8 and 9 the Erodibility Index ratio between extended and initial assessment is on average equal to 1.07, showing a slight increase.

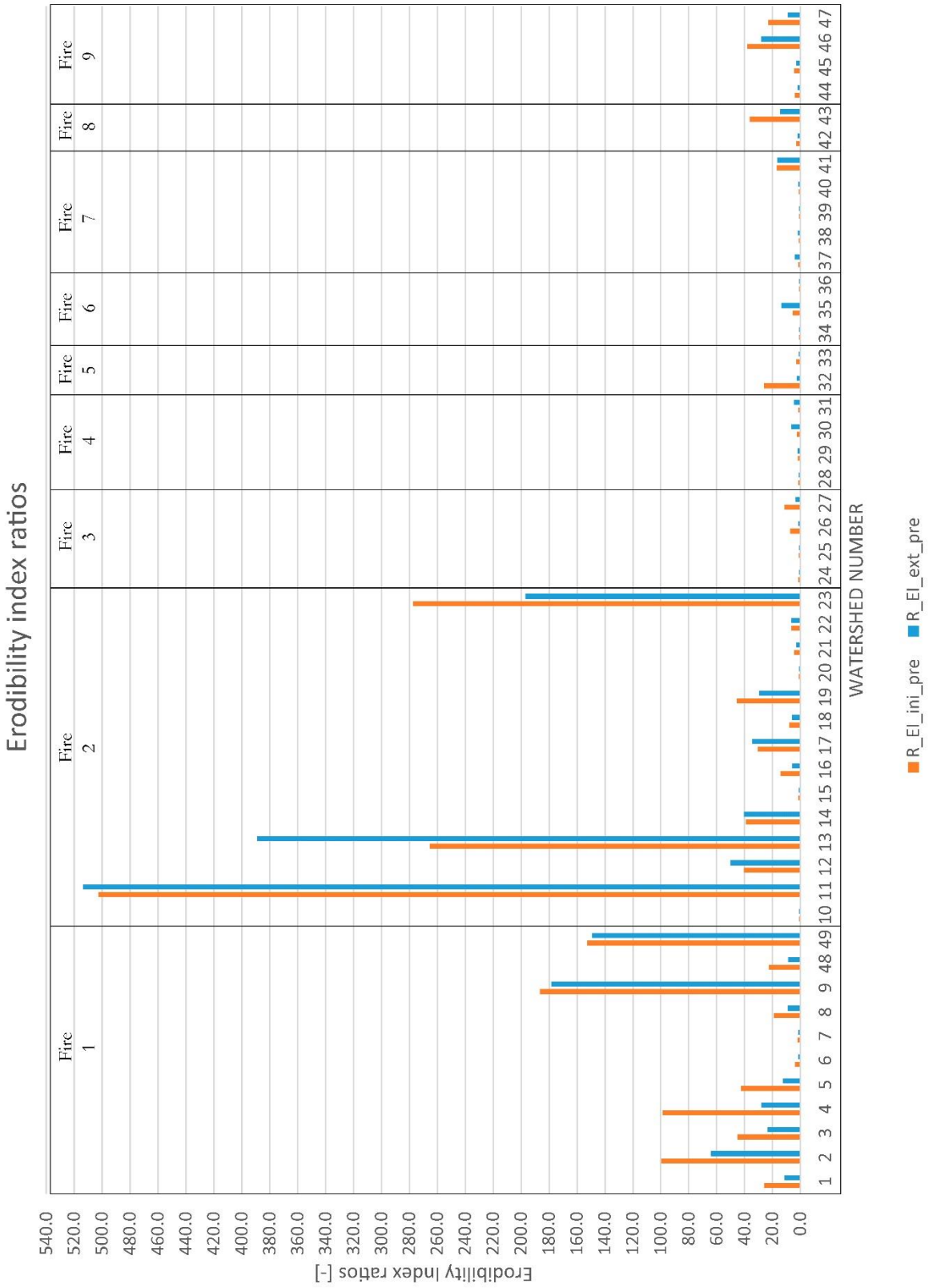


*Figure 7.38 – Erodibility Index relative ratios R_EI_ini_pre and R_EI_ext_pre.*

Spatially averaged annual soil loss (A) values calculated for the pre-fire situation $A_{w\_pre}$, for the post-fire initial assessment $A_{w\_ini}$ and for the post-fire extended assessment $A_{w\_ext}$ have been compared by calculating their relative ratios (R_A_ini_pre and R_A_ext_pre). Results of the initial vs pre-fire comparison are given fig 7.39, while related maps are reported in appendix 4.

Overall results show a tendency very similar to the overall EI ratios over the 49 watershed, suggesting a homogeneously distributed contribution of the rainfall erosivity factor R. A general increase in the A ratios for the post fire condition is registered, the ratio between initial and pre-fire assessment having a mean value of 43.42 and the ratio between extended and pre-fire assessment averaging 38.87. Again, strong differences affect fire number 1 and 2 (Locana/Ribordone and Bussoleno/Mompantero) and the other seven wildfires: the mean value of the A ratios (initial assessment vs pre-fire) of the first two fires is equal to 77.28 (61,87 and 89.39 respectively), while the mean value of the remaining is 8.16. Maximum A ratios are observed for the Bussoleno/Mompantero fire, in which watersheds n. 11, 13 and 23 are characterized by values of 532.09, 400.03 and 195.92, respectively (for the extended assessment with respect to pre-fire condition).

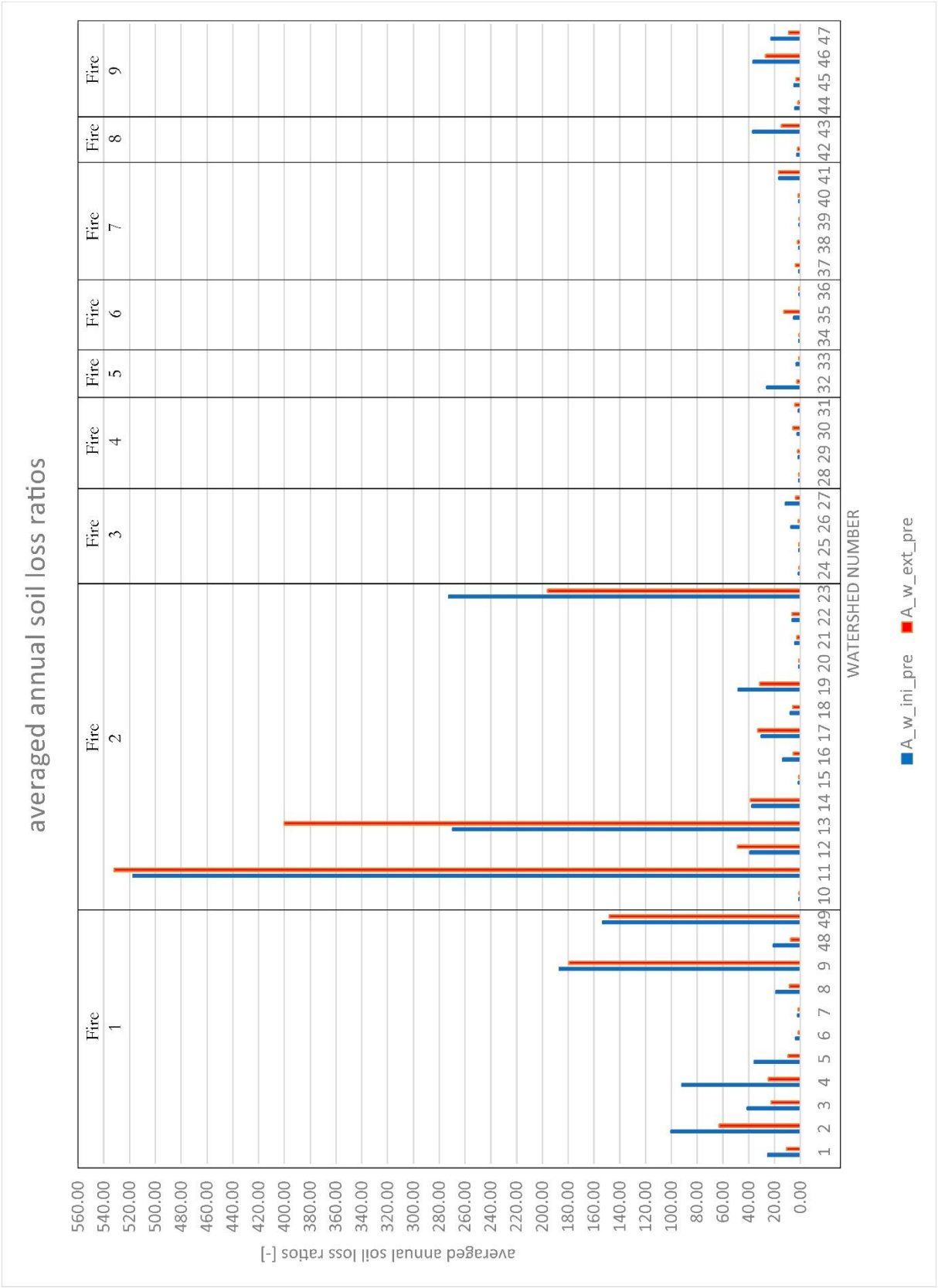


*Figure 7.39 – Spatially averaged annual soil loss relative ratios A_w_ini_pre and A_w_ext_pre.*

## 7.2.5 Fire-related runoff model

### 7.2.5.1 Pre-fire

*CN* values for the watersheds affected by 2017 wildfires have been computed as described in the paragraph 6.2.5. The area weighted $CN_{w\_pre}$ values for the 49 watersheds and the detailed map of the CN values calculated for homogeneous sub-areas are reported in figg. A5.1 – A5.6 (appendix 5). Results for the pre-fire conditions show, for all the 49 watersheds, averaged CN ranging from 50.89 to 84.77, with mean value of 62.43. Maximum values (over 80 or slightly below) are reached in four watersheds interested by the Locana/Ribordone fire, namely the nos. 1, 3, 7 and 48.

Excess runoff values $Q_{pre}$ for the chosen design 24h precipitation are given in figg. 7.40, 7.41 and 7.42. The results describing averaged soil loss ($Q_{w\_pre}$) for the pre-fire situation over the 49 watersheds show a mean runoff excess equal to 40.22 mm, with a range from 5.71 to 123.60 mm. The higher values are registered for the Locana/Ribordone area (mean = 78.43 mm), while lower ones characterize the Bussoleno/Mompantero and Bellino/Casteldelfino areas (mean equal to 18.49 and 6.03 mm respectively).

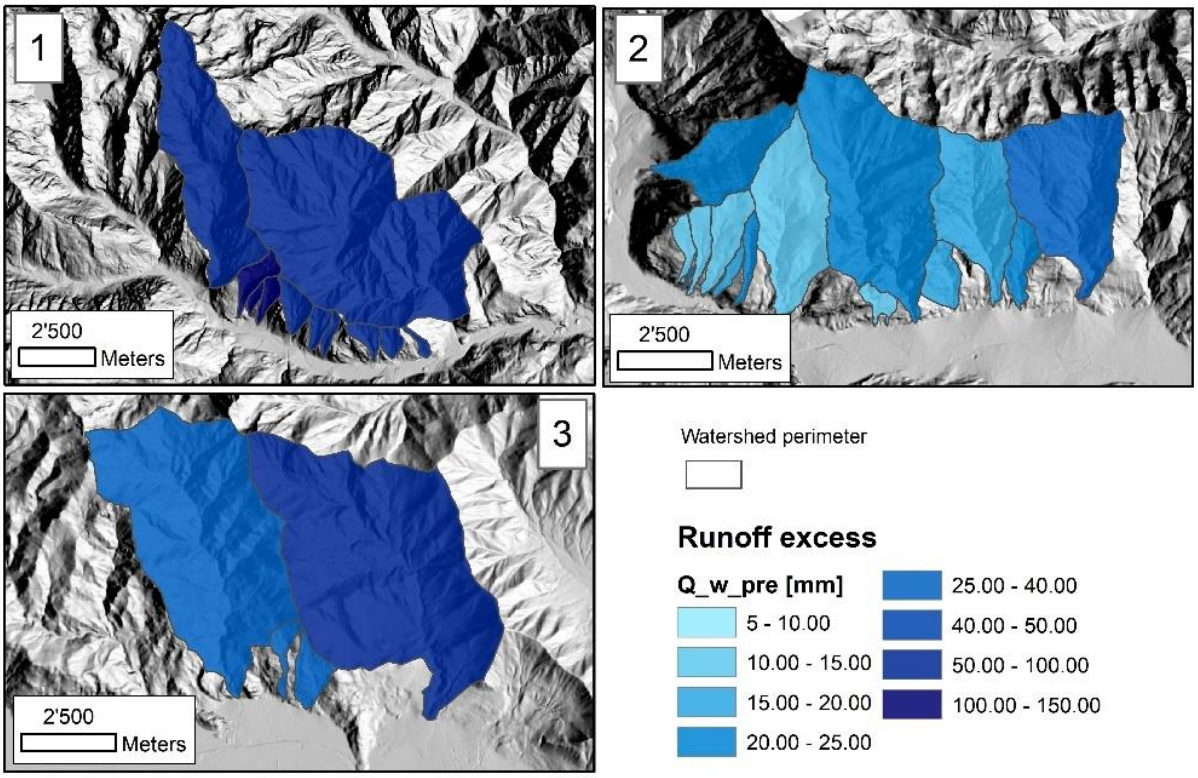


*Figure 7.40 - Pre-fire runoff excess, $Q_{w\_pre}$, for the watersheds affected by the Locana/Ribordone (1), Bussoleno/Mompantero (2) and Caprie/Rubiana (3) wildfires.*

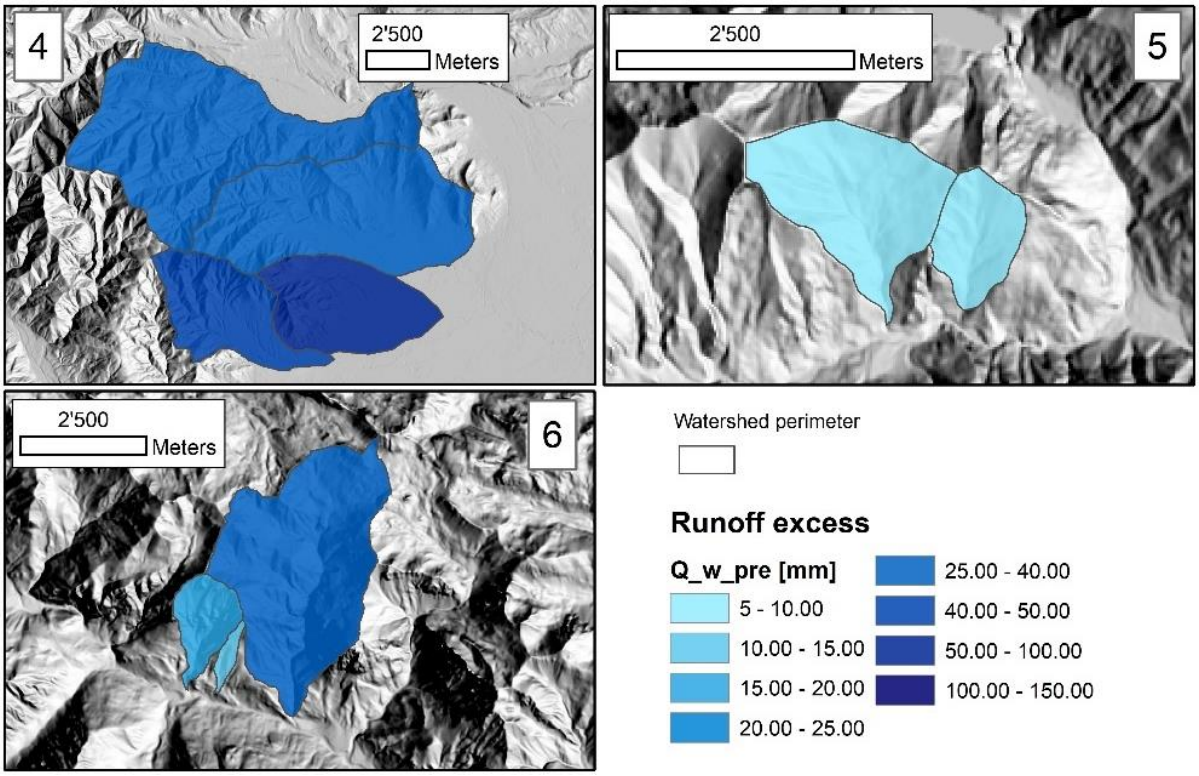


*Figure 7.41 - Pre-fire runoff excess, $Q_{w\_pre}$, for the watersheds affected by the Cumiana/Cantalupa (4), Bellino/Casteldelfino (5) and Sambuco/Pietraporzio (6) wildfires.*

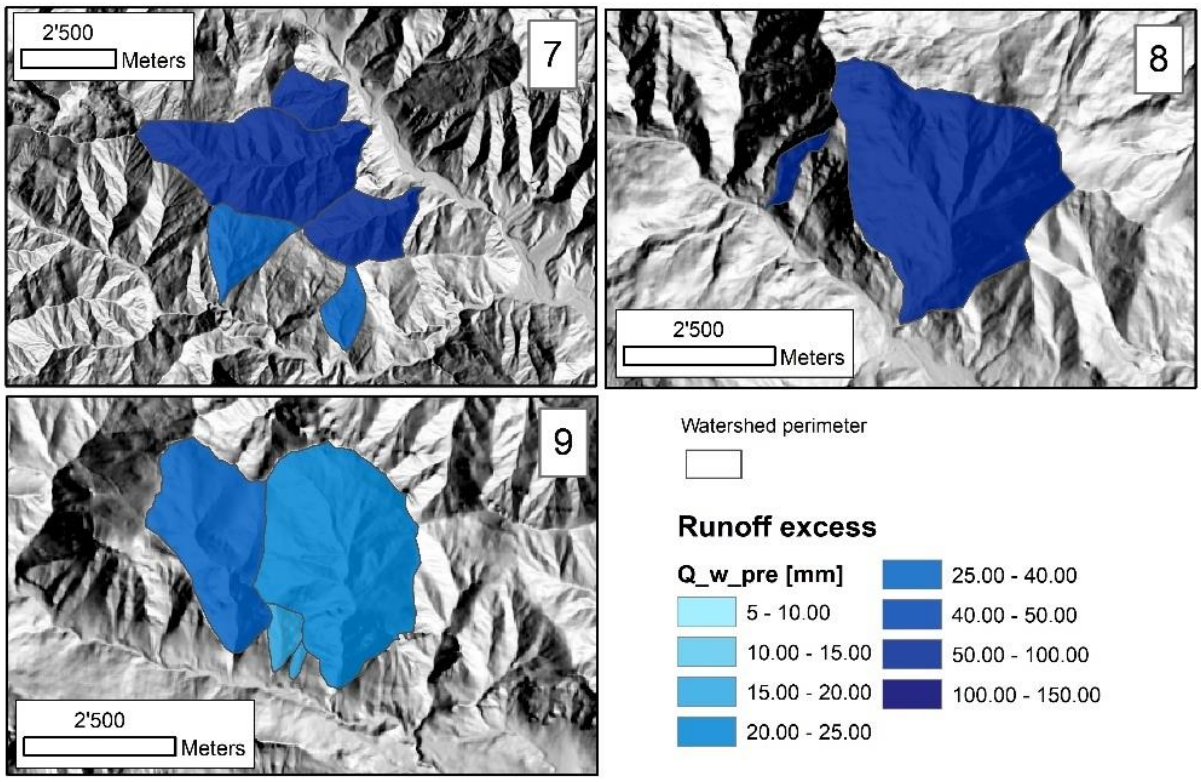


*Figure 7.42 - Pre-fire runoff excess, $Q_{w\_pre}$, for the watersheds affected by the Roure/Perrero (7), Traversella (8) and Demonte (9) wildfires.*

#### 7.2.5.2 Post-fire

Post-fire condition has been modeled by computing post-fire *CN* values as a function of fire severity (unburned, low, moderate or high) following the empirical adjustment factors described in par. 6.2.5. All maps describing the CN values ($CN_{ini}$ and $CN_{ext}$) calculated for homogeneous sub-areas and the spatially averaged CN values ($CN_{w\_ini}$ and $CN_{w\_ext}$) are reported in figg. A5.7 – A5.18 (appendix 5). The graph summarizing the CN values for the 49 watersheds in the pre- and post-fire situation is reported in fig. 7.43. Excess runoff values $Q_{w\_ini}$ for the chosen design 24h precipitation are reported in figg. 7.44, 7.45 and 7.46, while the extended assessment results $Q_{w\_ext}$ are reported in figg. A5.19, A5.20 and A5.21 (Appendix 5).

Results for the post-fire conditions, initial assessment, show averaged CN ranging from 55.85 to 87.37, having a mean value of 72.53. A marked increase is registered in the watersheds affected by the Locana/Ribordone and the Bussoleno/Mompantero wildfires. For the extended assessment values span from 51.89 to 87.30. averaging 69.59, showing thereof a very slight decrease.

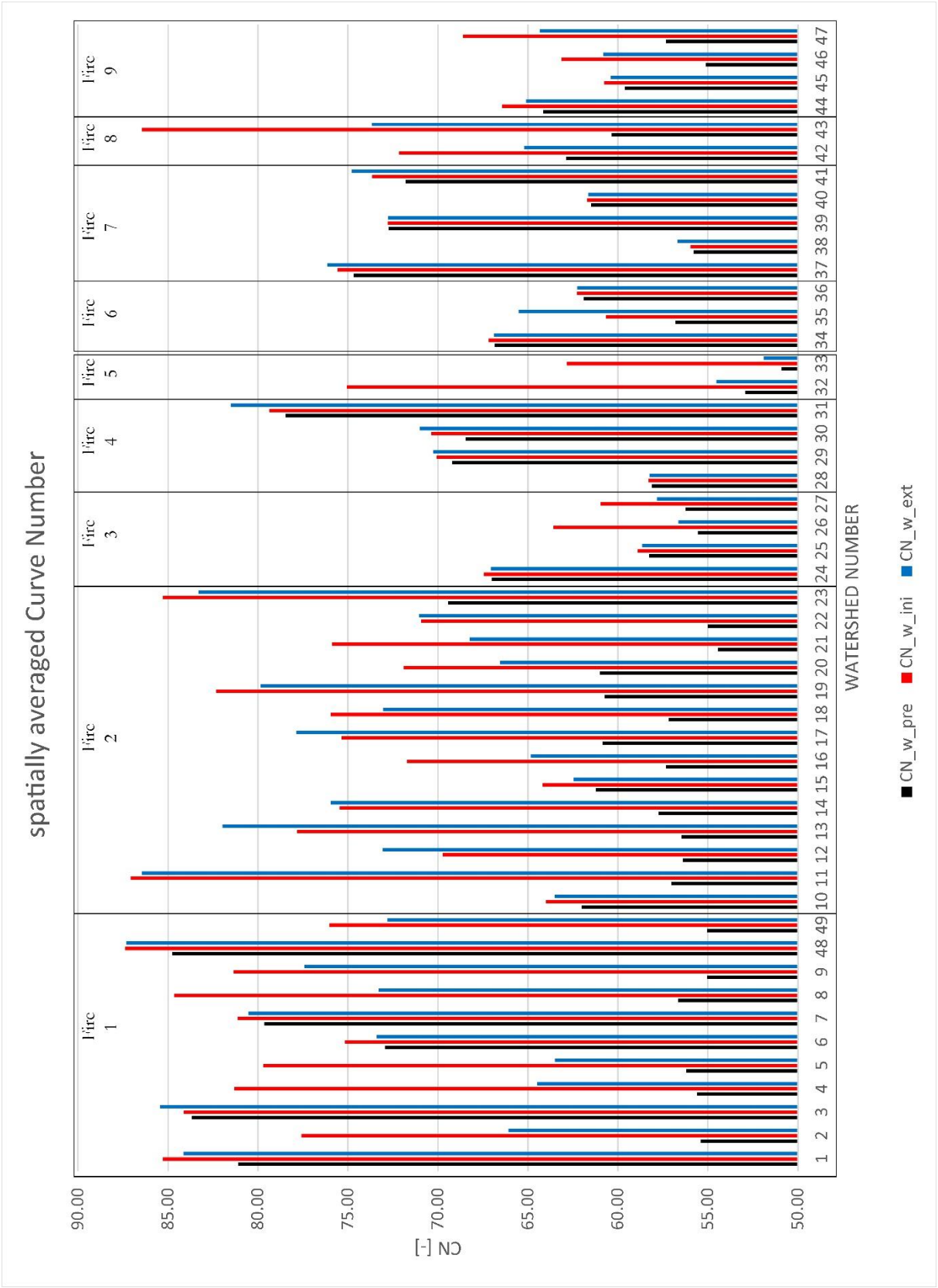


*Figure 7.43 – Values of the Curve Number, CN, for the 49 watershed in the pre-fire condition and for the post-fire initial and extended assessment.*

The results regarding the averaged soil loss ($Q_{w\_ini}$) for the initial assessment over the 49 watersheds show a mean runoff excess equal to 59.71 mm, with a range from 16.55 to 136.67 m. The higher values are registered for the Locana/Ribordone and Traversella areas (mean equal to 115.62 mm and 109.17), while lower ones characterize the Bellino/Casteldelfino and Sambuco/Pietraporzio areas (mean equal to 24.10 mm and 21.13 mm, respectively)(fig. 7.47).

For the extended assessment, the averaged soil loss ($Q_{w\_ext}$) show a mean runoff excess equal to 53.43 mm, with a range from 6.44 to 130.67 m over the 49 watersheds. The higher values are registered for the Locana/Ribordone and Traversella areas (mean equal to 99.66 mm and 82.94), while lower ones characterize the Bellino/Casteldelfino and Sambuco/Pietraporzio areas (mean equal to 7.01 mm and 22.96 mm, respectively) (fig. 7.47).

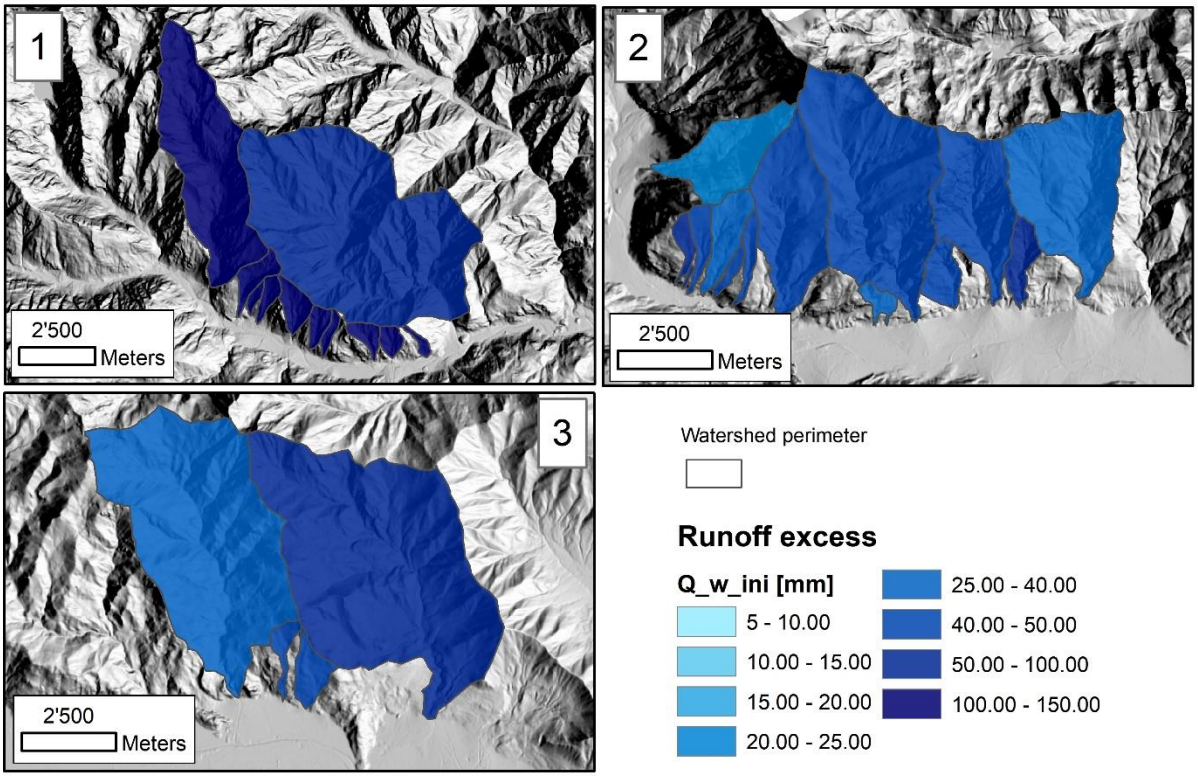


*Figure 7.44 – Runof excess, $Q_{w\_ini}$, for the watersheds affected by the Locana/Ribordone (1), Bussoleno/Mompantero (2) and Caprie/Rubiana (3) wildfires; post-fire, initial assessment.*

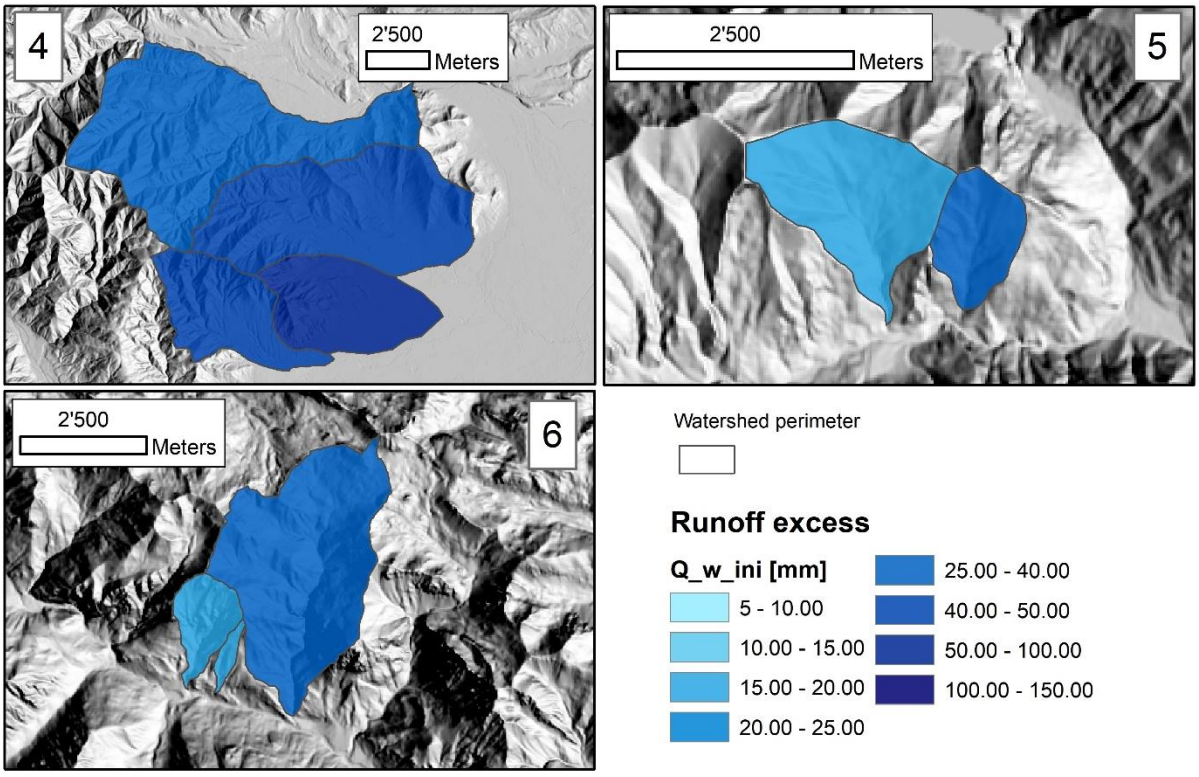


*Figure 7.45 - Runof excess, $Q_{w\_ini}$, for the watersheds affected by the Cumiana/Cantalupa (4), Bellino/Casteldelfino (5) and Sambuco/Pietraporzio (6) wildfires; post-fire, initial assessment.*

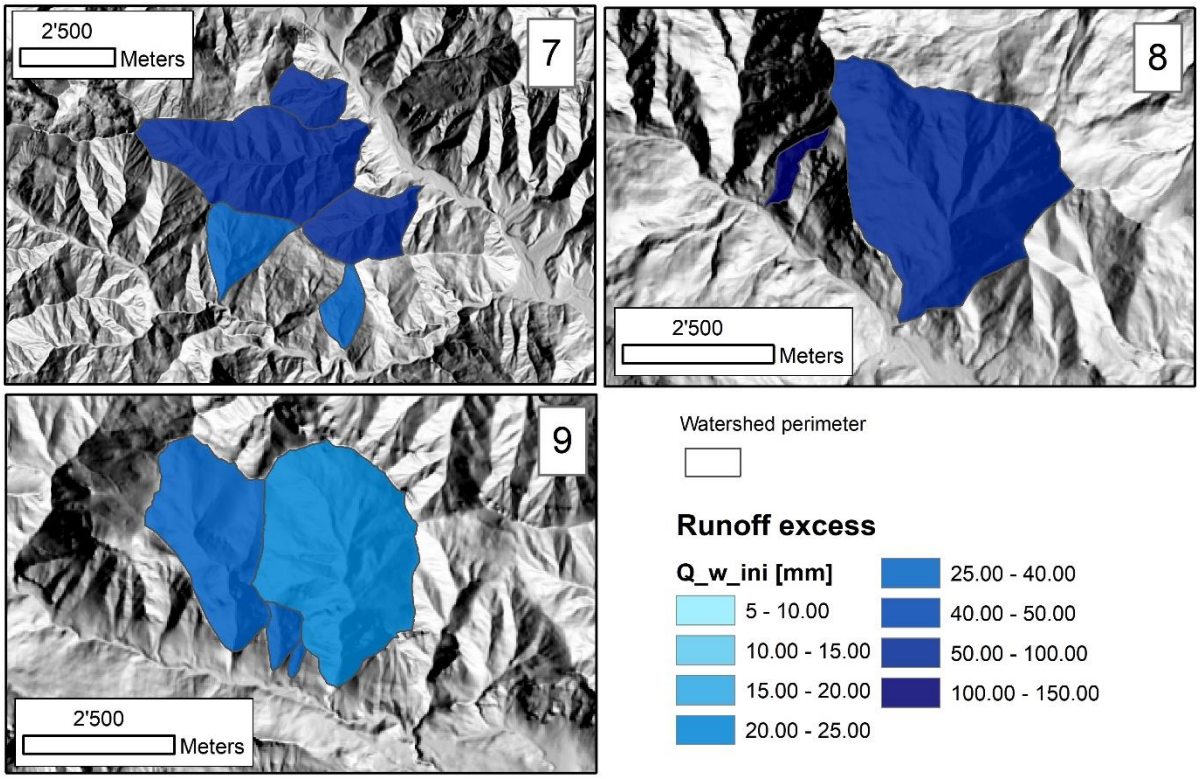


*Figure 7.46 - Runof excess, $Q_{w\_ini}$, for the watersheds affected by the Roure/Perrero (7), Traversella (8) and Demonte (9) wildfires; post-fire, initial assessment.*

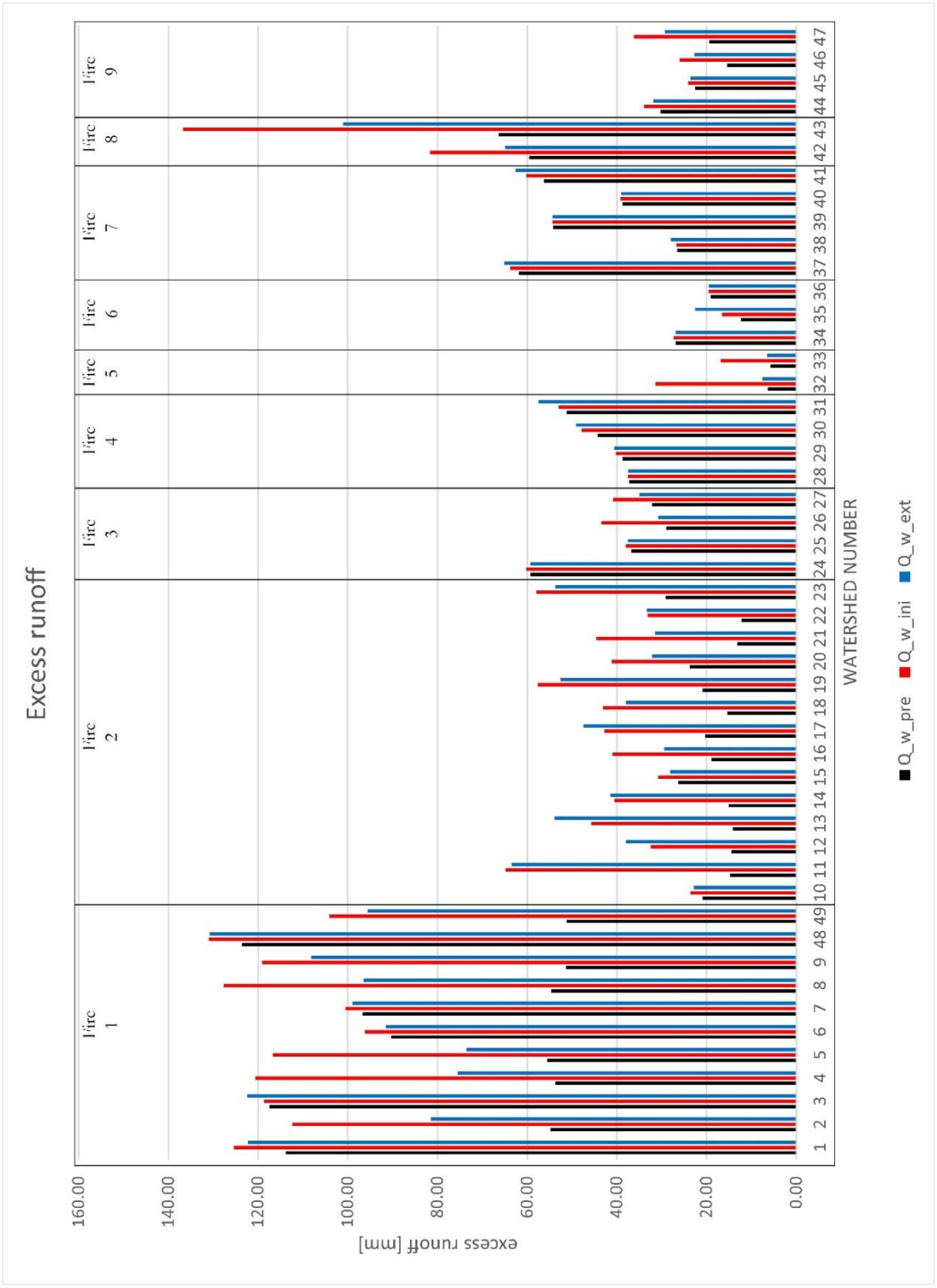


*Figure 7.47 – Values of the excess runoff depth, Q, for the 49 watershed in the pre-fire condition and for the post-fire initial and extended assessment.*

#### 7.2.5.3 Pre-fire vs post-fire

Excess runoff depth ratio comparing pre-fire and post-fire conditions are given in fig 7.48 in which $R\_Q_{ini\_pre}$, and $R\_Q_{ext\_pre}$ are reported. Figures 7.49, 7.50 and 7.51 report the map for $R\_Q_{ini\_pre}$, and shows in a graphical way the increase in runoff for the analyzed watersheds. Detailed tables are reported in appendix 5, in which also the maps of $R\_Q_{ext\_pre}$ and $R\_Q_{ext\_ini}$ are given.

Overall statistics for the 49 watersheds report an average initial assessment vs pre-fire ratio of 1.79, values ranging from 1.00 to 4.94. The ratio between the extended assessment and the pre-fire condition has an average value of 1.54, with a range between 1.00 and 4.33. The mean extended assessment to initial assessment ratio has a value equal to 0.91, varying from 0.24 to 1.36.

Maximum values of the $R\_Q_{ini\_pre}$ are recorded for the Bellino/Casteldelfino and Bussoleno/Mompantero fires, for which the mean values are 3.94 and 2.47, respectively; for the $R\_Q_{ext\_ini}$ the maximum values are found for the Bussoleno/Mompantero areas, mean value being 2.35. Looking at the $R\_Q_{ext\_pre}$ values, three wildfire affected areas show an increase over 9, namely Cumiana/Cantalupa, Sambuco/Pietraporzio and Roure/Perrero, mean values being 1.03, 1.11 and 1.02, respectively.

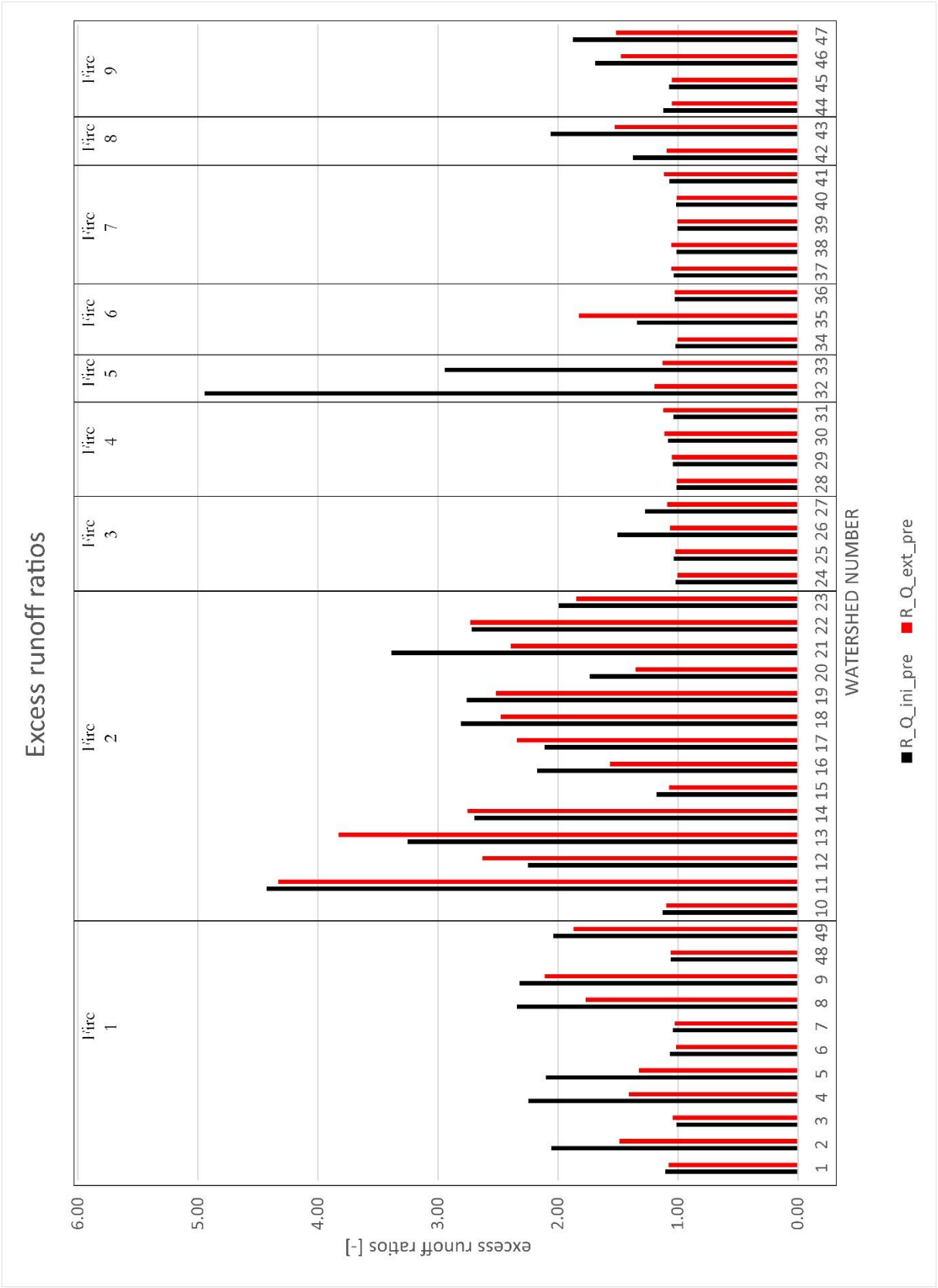


*Figure 7.48 - Excess runoff depth ratio comparing pre-fire and post-fire conditions $R\_Q_{ini\_pre}$, and $R\_Q_{ext\_pre}$..*

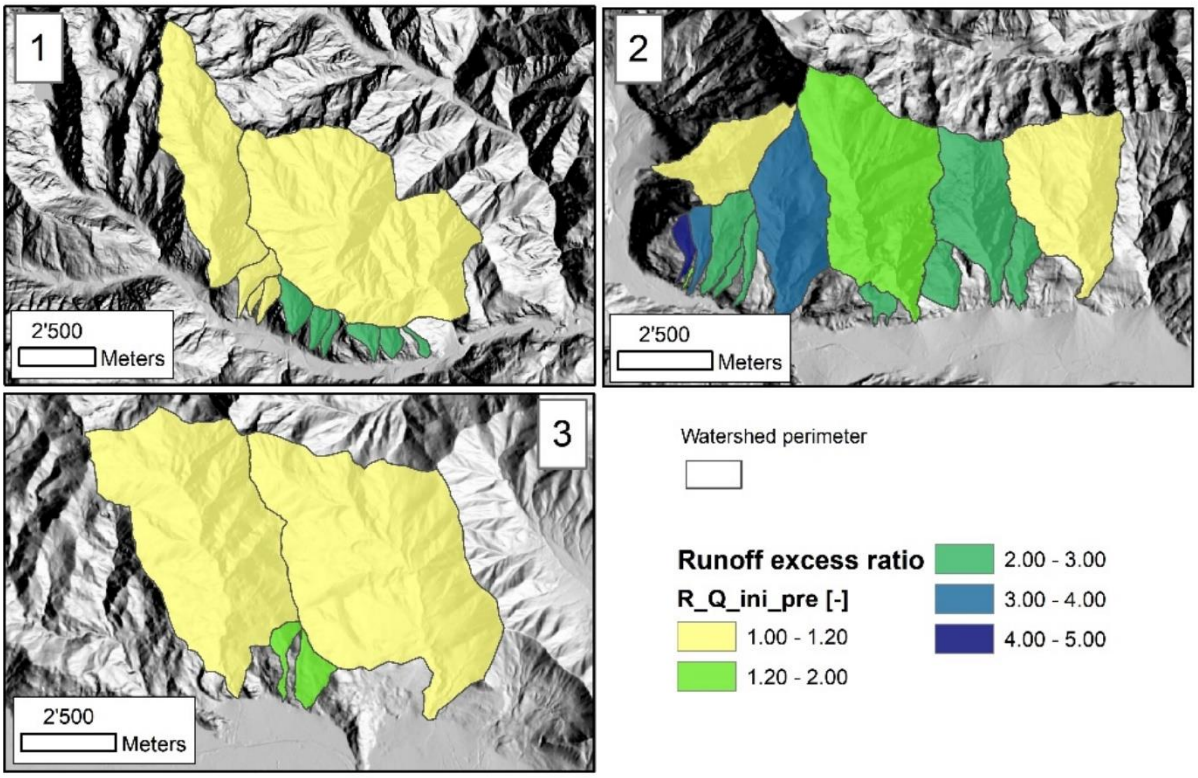


*Figure 7.49 – Runoff excess ratio, R_Q_ini_pre, between post-fire (initial assessment) and pre-fire situation for the watersheds affected by the Locana/Ribordone (1), Bussoleno/Mompantero (2) and Caprie/Rubiana (3) wildfires.*

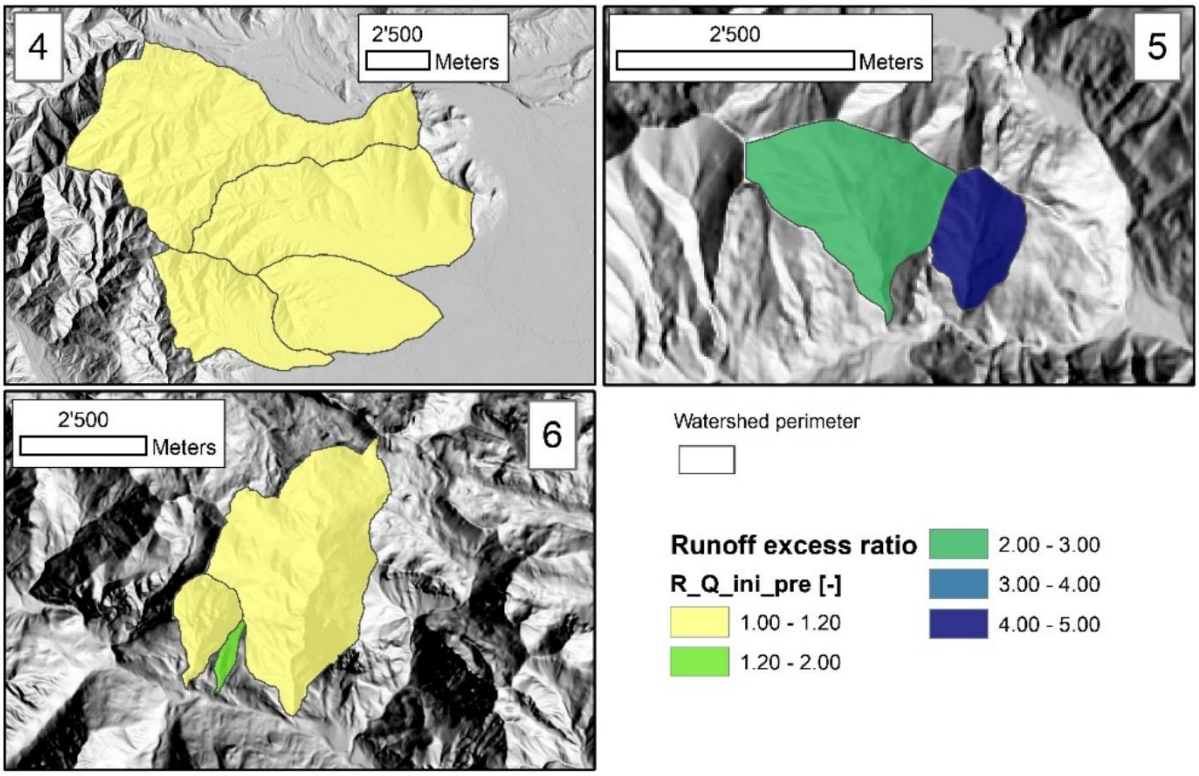


*Figure 7.50 - Runoff excess ratio, R_Q_ini_pre, between post-fire (initial assessment) and pre-fire situation for the watersheds affected by the Cumiana/Cantalupa (4), Bellino/Casteldelfino (5) and Sambuco/Pietraporzio (6) wildfires.*

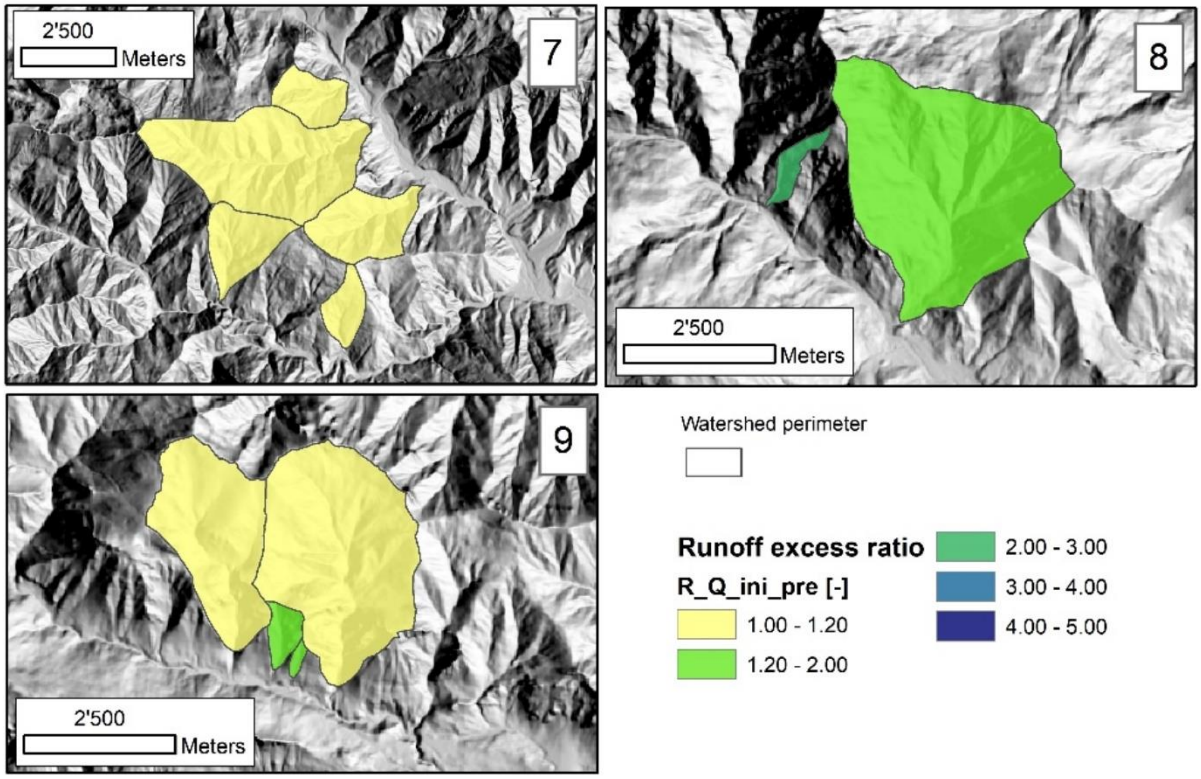


*Figure 7.51 - Runoff excess ratio, R_Q_ini_pre, between post-fire (initial assessment) and pre-fire situation for the watersheds affected by the Roure/Perrero (7), Traversella (8) and Demonte (9) wildfires.*

## 7.3 The Comba delle Foglie Case Study

The Comba delle Foglie watershed experienced in May and June 2018 consecutive (either mud-flows and debris-flows) flow events, reaching the outlet and striking the uppermost part of the village, especially at the San Lorenzo locality. The date and type of the flows are reported in table 7.22.

*Table 7-22 – date of occurrence, type and damages related to the events registered at the Comba delle Foglie outlet.*

| Date (dd/mm/yy) | Type | Damages |
|---|---|---|
| **29/04/18** | debris/mud-flow | Few roads, water pipeline |
| **02/05/18** | Flood | - |
| **09/05/18** | Flood | - |
| **13/05/18** | Flood | - |
| **07/06/18** | Debris/mud-flow | Roads, houses, lifelines |

### 7.3.1 Field surveys and post-fire watershed response

The watershed suffered a fire in 2003, in addition to that of 2017. Fire severity maps for both the wildfires are reported in fig. 7.52.

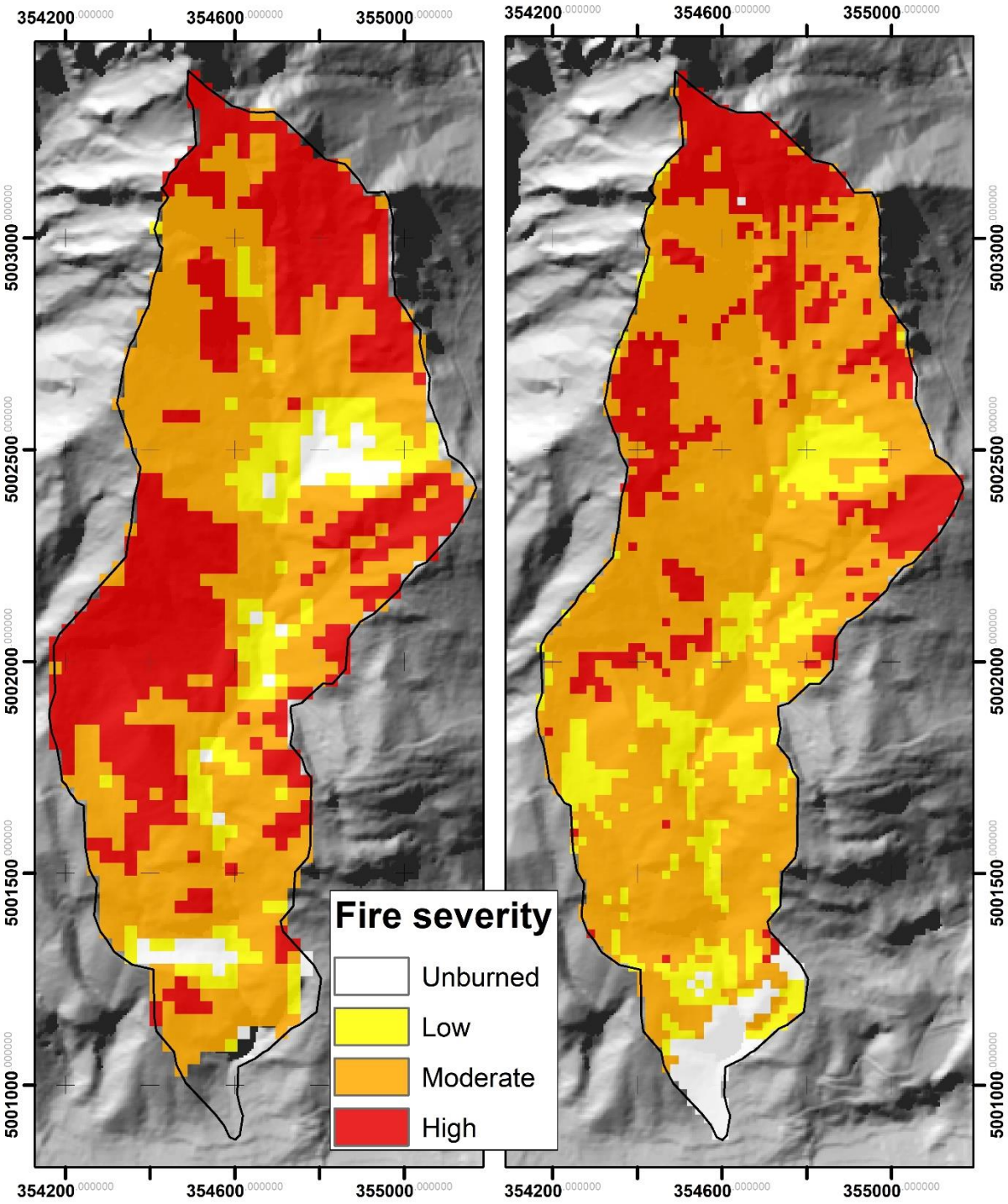


*Figure 7.52 – Fire severity maps related to the 2003 (left) and 2017 (right) wildfires.*

Survey conducted in the watershed, starting from the uppermost portion revealed evident traces of overland flow coalescing into rills, and then into the main drainage line at the watershed bottom (fig. 7.53). Zero and first order streams showed evidence of increased erosion and sediment transport, since the very beginning close to the divide of the catchment (Fig 7.54 a). On open slopes the dominant

erosional process was found to be the sheetflow erosion, occasionally associated with rill dominated sectors where the tree vegetation was denser (fig 7.54 b). In the lower part of the basin, characterized by a generally higher percentage of residual vegetation cover, rill and little gullies were detected. Also, some pathway showed signs of erosional processes due to overland flow.

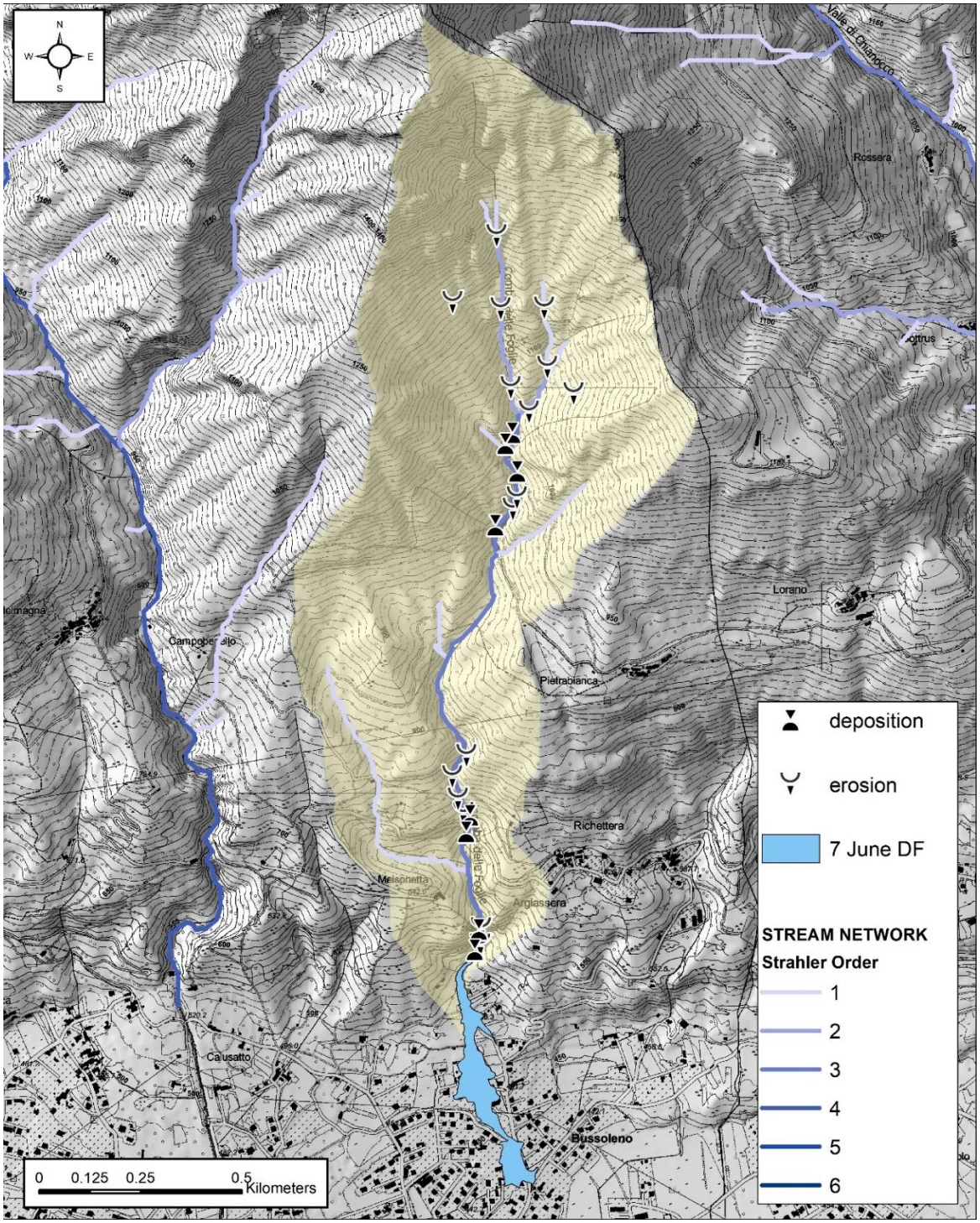


*Figure 7.53 – erosional and depositional feature surveyed in the watershed.*

In the main channel the erosion, increasing proceeding downstream, was marked by channel incision with steep banks and frequently exposed bedrock (fig 7.54 c). At 1000 m a.s.l., where two second-order drainages converge, localized debris-flow levees were found in flat areas and behind obstacles: these well sorted deposits were constituted by cobbles and boulders up to 500 mm in a poor silt and sandy matrix. Other deposits were found between 1000 m a.s.l. and 900 m a.s.l., alternated with erosion dominated sectors.

Down the channel, sorting of the deposit decreased while the amount of matrix increased. At 900 m a.s.l., where the slope is flattened due to a road crossing, a bigger deposition area was found, with cobble and small boulders, in chaotic disposition, supported by a gravelly-sandy matrix.

Below the road cut, the erosion level increased again. At 650 m a.s.l. two small lobes, made of cobbles mixed with abundant sandy-silty matrix and floated materials (wood, char...) were found in a flat area above a road cut (fig 7.54 d). After this point, the channel is again very incised and reaches a steep jump just above the fan (570 m a.s.l.).

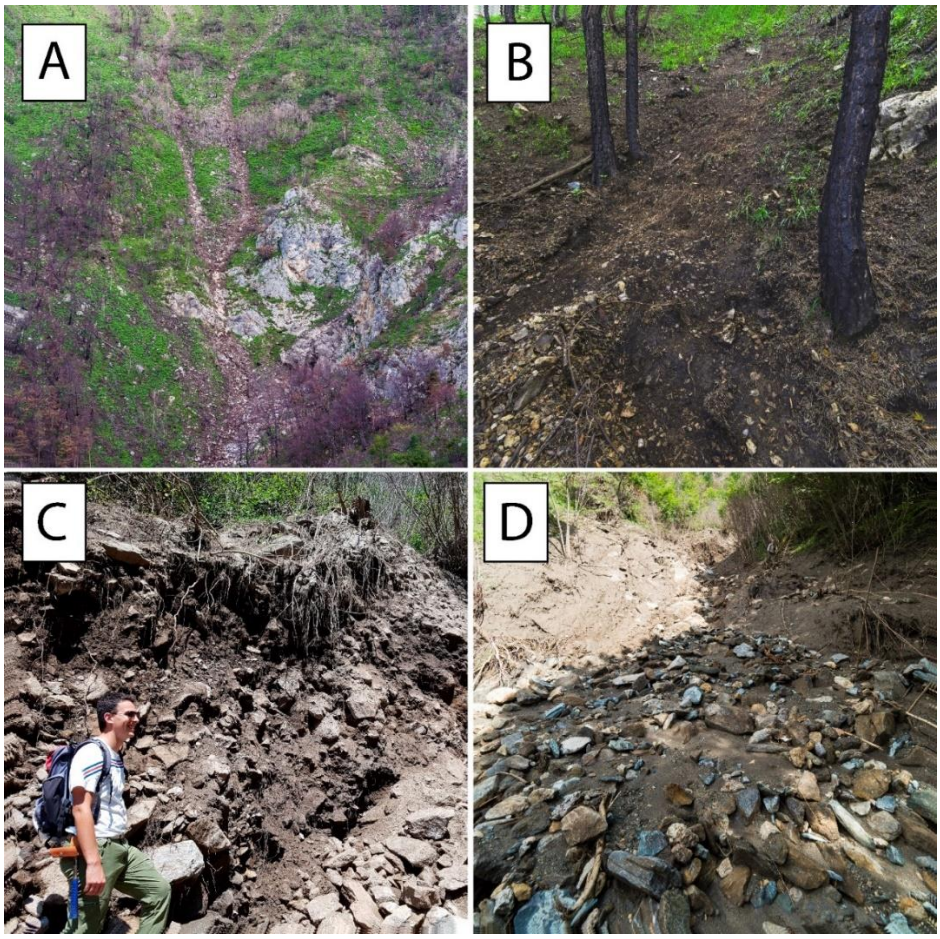


*Figure 7.54 – increased erosion in the zero and first-order streams (a), sheetflow erosion (b), deep main channel incision (c) and flow deposits in the intermediate sector of the main channel.*

With respect to a survey conducted on June 5 (two days before the main debris-flow occurrence) a massive amount of debris and material previously accumulated in the channel, especially at the bottom of the last cliff overhanging the fan apex, was lacking. The erosion undergone in this sector can be easily inferred by comparing the pre-and post-event images (fig 7.55 a and b).

Below this point the signs of the flow path were clearly visible: the bedrock was exposed and polished, and the flow splash signs could be found some meters above the valley bottom on the trees (fig 7.55 c). At 500 m a.s.l., the gorge ends and reaches the fan apex. In main deposition zone, deposits made of gravels and cobbles were mixed in an abundant sandy silty matrix was found. The original channel incision, covered by a road pavement, was exhumated (Fig 7.55 d).

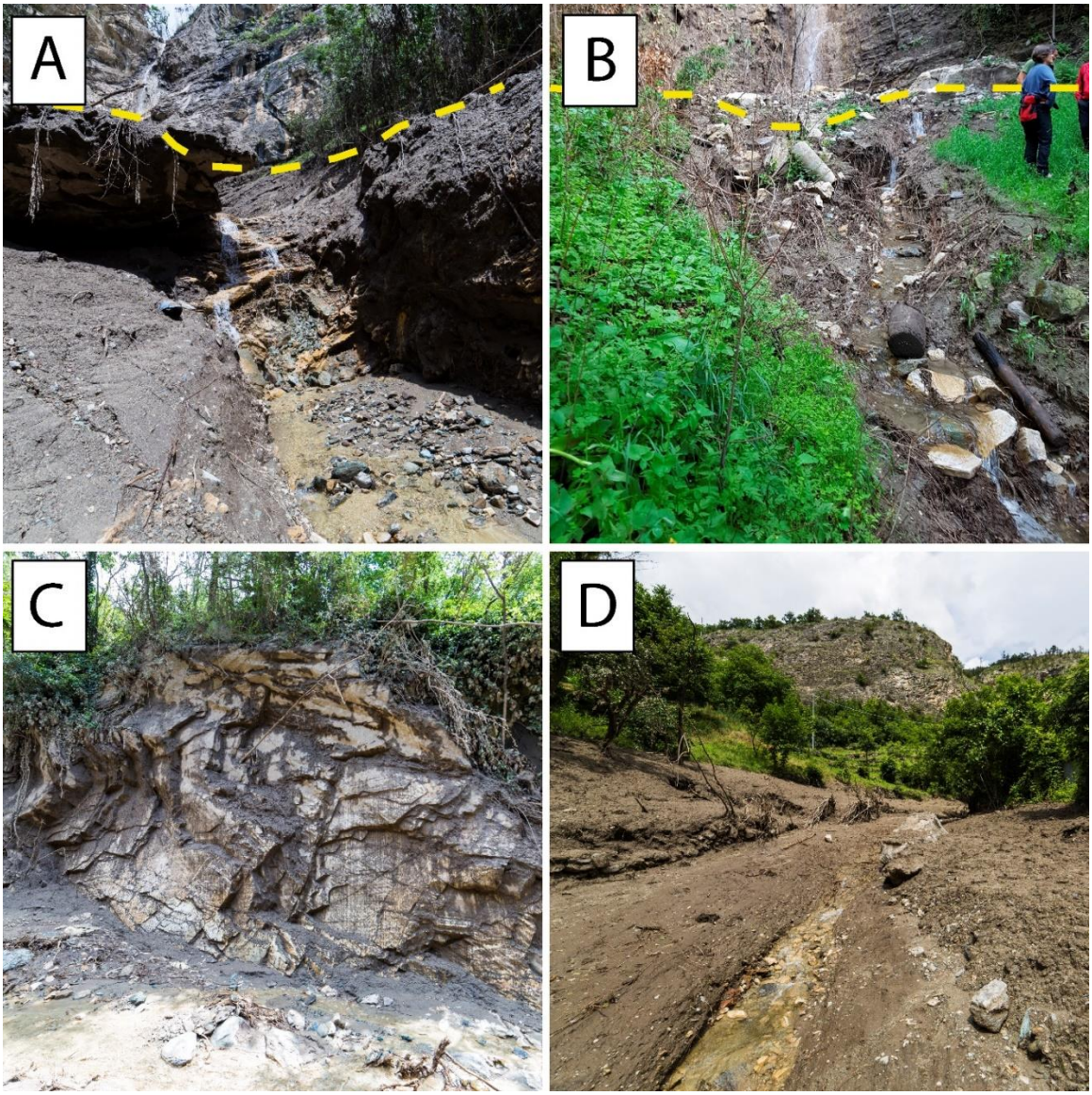


*Figure 7.55 – post-fire (a) and pre-fire (b) channel depth in the lower part of the watershed, polished rock outcrop at the watershed outlet (c) and exumation of the old channel path in the fan (d).*

The maximum deposit thickness reconstructed via photogrammetric modelling was approximatively 2 m, over a surface of about 26000 m². The coarser fraction was concentrated in the central part of the deposit and was approx. 600 m in length, while the fluid fraction had propagated for a longer distance (900 m from the apex). The volume of the coarser fraction of the deposit, estimated from photogrammetry is about 5000 m³, while Arpa estimates of the total event volume is about 20000 m³ (ARPA Piemonte 2018b).

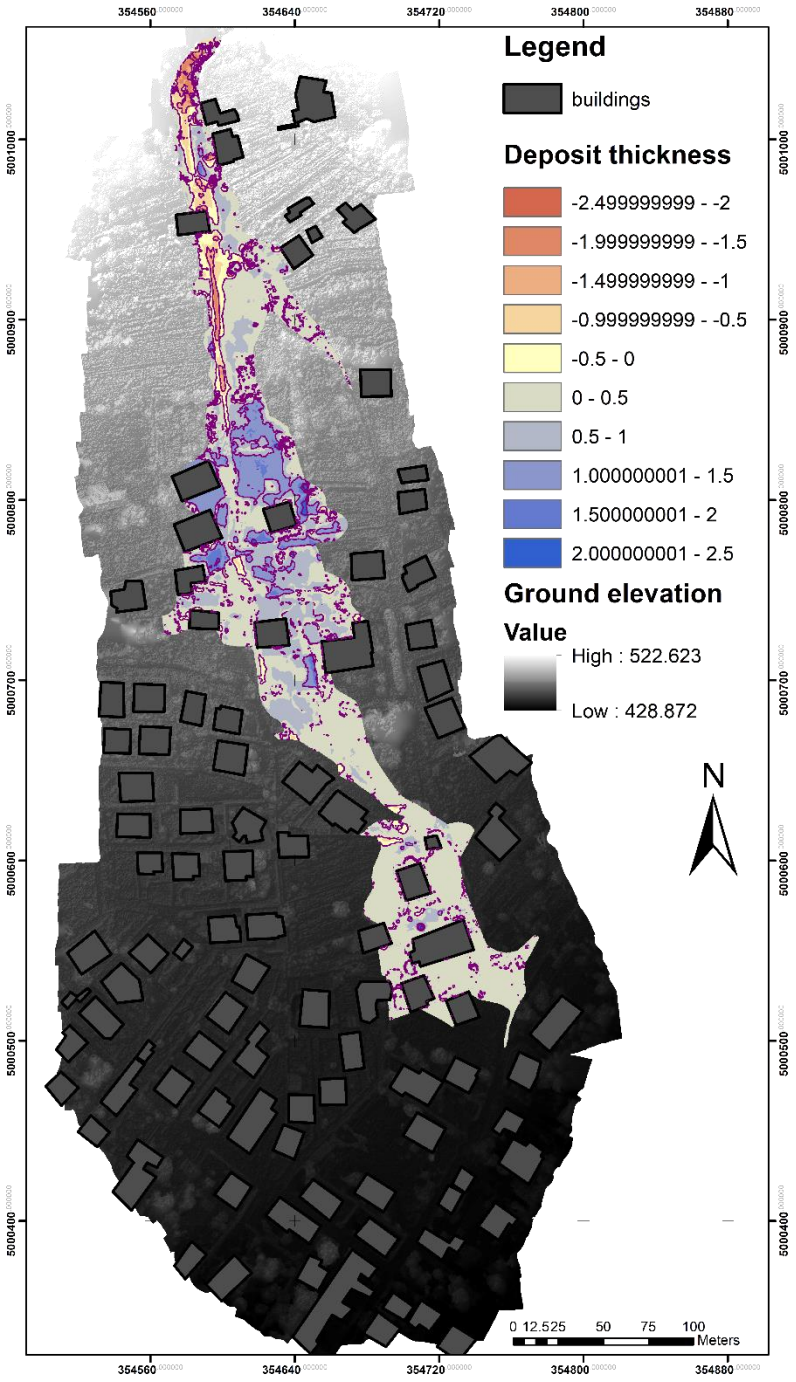


*Figure 7.56 – deposit thickness reconstruction at the watershed outlet*

### 7.3.2 Monthly erosion calculation

Sediment erosion has been assessed implementing the RUSLE model at a monthly scale. Monthly R factors from September 2017 to August 2018 have been quantified by calculating the summation of the parameter $EI_{30}$ of every single erosive event for each considered month at each of the three selected rain gauges located in the surrounding of the Comba delle Foglie watershed. Single R factor has been then averaged for assessing the representative rainfall erosive power at the watershed scale. Single erosive rainfall events for each station are given in table 7.23, 7.24 and 7.25, while calculated monthly R factors are given in table 7.26.

For the Prarotto, Borgone and Malciaussia rain gauges have been identified 22, 24 and 22 erosive rainfall events. For the Prarotto rain gauge the selected storms are characterized by a mean precipitation value of 30.94 mm, duration of 23.23 h and EI30 of 95.99 MJ mm $ha^{-1}$ $h^{-1}$. For the Borgone rain gauge mean precipitation, duration and EI30 values are 27.67mm, 20.19 h and 73.06 MJ mm $ha^{-1}$ $h^{-1}$. At the Malciaussia station mean value recorded are 29.20 mm, 16.02 h and 55.40 MJ mm $ha^{-1}$ $h^{-1}$, for precipitation, duration and EI30.

Monthly R factor maximum values are reached in May, April and March 2018, and are, on contrary, equal to zero for September and October 2017 (table 7-26 and fig. 7.57). R factor distribution over time is consistent with Piedmont meteorological data descripted in chapter 5, reporting an extremely dry end of 2017 and very wet month of January, April and May 2018. In fact, erosive events registered in these months represents approximatively the 75% of the entire annual R factor, and in particular the month of May reaching almost the 40%.

*Table 7-23 – Single erosive storms registered at the Prarotto rain gauge (Sep 2017 – Aug 2018).*

| Date | Precip | Duration | Max 5 | Max10 | Max15 | Max30 | Max60 | EI30 |
|---|---|---|---|---|---|---|---|---|
| | | | | | | | | |
| **MO/DA/YR** | mm | h | mm/h | mm/h | mm/h | mm/h | mm/h | MJ*mm/ha*h |
| **11/04/2017** | 14.37 | 19.17 | 3.6 | 3.6 | 3.6 | 3.6 | 3 | 5.895 |
| **12/30/2017** | 28.02 | 26.5 | 4.8 | 4.8 | 4.8 | 4.436 | 4.4 | 14.413 |
| **01/04/2018** | 15.39 | 10 | 3.6 | 3.6 | 3.6 | 3.2 | 2.8 | 5.654 |
| **01/06/2018** | 125.27 | 66.67 | 12.003 | 12.003 | 10.494 | 9.603 | 9.213 | 172.666 |
| **01/21/2018** | 14.8 | 7.83 | 6 | 6 | 5.72 | 5.26 | 5.03 | 10.633 |
| **03/10/2018** | 19.36 | 53.67 | 4.761 | 4.761 | 4.374 | 3.987 | 3.594 | 8.91 |
| **04/03/2018** | 21.81 | 41.83 | 3.6 | 3.6 | 3.6 | 3.2 | 2.594 | 7.432 |
| **04/10/2018** | 23.2 | 51.33 | 3.6 | 3.6 | 3.32 | 2.86 | 2.43 | 7.048 |
| **04/28/2018** | 61.52 | 24.67 | 43.549 | 43.549 | 40.7 | 32.674 | 21.045 | 436.959 |
| **05/01/2018** | 44.35 | 5 | 9.002 | 9.002 | 8.367 | 7.256 | 6.628 | 40.685 |
| **05/07/2018** | 4.23 | 20.83 | 14.406 | 14.406 | 11.812 | 7.517 | 6.04 | 15.318 |
| **05/12/2018** | 45.23 | 3.67 | 49.194 | 49.194 | 46.265 | 45.082 | 33.27 | 505.926 |
| **05/13/2018** | 32.32 | 16.5 | 29.207 | 29.207 | 27.818 | 22.849 | 16.148 | 146.24 |
| **05/19/2018** | 31 | 42.33 | 14.4 | 14.4 | 9.6 | 8.813 | 7.599 | 40.629 |
| **05/26/2018** | 12.93 | 3 | 35.136 | 35.136 | 33.878 | 22.584 | 12.33 | 72.276 |
| **05/27/2018** | 17.79 | 6.67 | 15.583 | 15.583 | 11.189 | 9.172 | 6.401 | 25.281 |
| **05/28/2018** | 14 | 14.17 | 9.641 | 9.641 | 8.707 | 6.38 | 5.197 | 11.69 |
| **05/30/2018** | 46.94 | 12.5 | 43.404 | 43.404 | 36.76 | 22.91 | 17.771 | 232.186 |
| **06/03/2018** | 24.51 | 17.33 | 19.333 | 19.333 | 18.99 | 17.533 | 9.306 | 77.639 |
| **06/06/2018** | 30.59 | 38.17 | 23.096 | 23.096 | 20.85 | 16.54 | 11.281 | 88.431 |
| **06/11/2018** | 18.18 | 22.17 | 27.6 | 27.6 | 19.68 | 10.827 | 5.571 | 37.224 |
| **08/16/2018** | 24.96 | 7 | 40.778 | 40.778 | 35.428 | 26.718 | 20.075 | 148.656 |
| **mean** | 30.49 | 23.23 | 18.92 | 18.92 | 16.80 | 13.32 | 9.62 | 95.99 |
| **max** | 125.27 | 66.67 | 49.19 | 49.19 | 46.27 | 45.08 | 33.27 | 505.93 |
| **min** | 4.23 | 3.00 | 3.60 | 3.60 | 3.32 | 2.86 | 2.43 | 5.65 |

*Table 7-24 - Single erosive storms registered at the Borgone rain gauge (Sep 2017 – Aug 2018).*

| Date | Precip | Duration | Max 5 | Max10 | Max15 | Max30 | Max60 | EI30 |
|---|---|---|---|---|---|---|---|---|
| **MO/DA/YR** | mm | h | mm/h | mm/h | mm/h | mm/h | mm/h | MJ*mm/ha*h |
| **11/04/2017** | 14.21 | 17 | 4.821 | 4.821 | 4.552 | 4.007 | 3.406 | 6.706 |
| **12/29/2017** | 13 | 14.83 | 3.6 | 3.6 | 3.6 | 3.236 | 3 | 4.826 |
| **01/03/2018** | 13.4 | 17.5 | 3.636 | 3.636 | 3.352 | 2.8 | 2.406 | 4.192 |
| **01/06/2018** | 188.63 | 63.83 | 25.29 | 25.29 | 23.494 | 19.309 | 13.454 | 604.73 |
| **02/23/2018** | 13.19 | 19.33 | 3.716 | 3.716 | 3.312 | 2.403 | 2.2 | 3.464 |
| **03/11/2018** | 17.23 | 13.67 | 3.621 | 3.621 | 3.32 | 2.86 | 2.441 | 5.479 |
| **03/15/2018** | 14.39 | 12 | 3.6 | 3.6 | 3.272 | 3.2 | 3 | 5.198 |
| **04/03/2018** | 13 | 25.67 | 2.421 | 2.421 | 2.4 | 2 | 1.6 | 2.719 |
| **04/08/2018** | 14.18 | 24.5 | 3.6 | 3.6 | 3.6 | 3.2 | 2.396 | 5.023 |
| **04/10/2018** | 36.41 | 35.67 | 7.23 | 7.23 | 6.62 | 5.319 | 4.488 | 23.906 |
| **04/12/2018** | 19.02 | 18 | 9.6 | 9.6 | 9.6 | 9.265 | 7.645 | 25.106 |
| **04/29/2018** | 53.02 | 17.67 | 45.561 | 45.561 | 36.037 | 23.271 | 17.363 | 281.605 |
| **05/01/2018** | 35.22 | 74.67 | 6 | 6 | 6 | 5.6 | 4.64 | 23.533 |
| **05/07/2018** | 23.2 | 10.33 | 23.303 | 23.303 | 20.889 | 16.478 | 12.186 | 73.577 |
| **05/12/2018** | 32.56 | 3.83 | 36.231 | 36.231 | 31.977 | 26.013 | 24.078 | 197.493 |
| **05/13/2018** | 24.7 | 14.5 | 25.38 | 25.38 | 21.413 | 13.856 | 9.148 | 62.326 |
| **05/27/2018** | 13.99 | 7.17 | 9.02 | 9.02 | 8.417 | 6.805 | 4.774 | 13.332 |
| **05/28/2018** | 13 | 13.17 | 4.8 | 4.8 | 4.8 | 4.4 | 4.014 | 6.855 |
| **05/30/2018** | 40.81 | 23.5 | 36.322 | 36.322 | 32.181 | 21.046 | 18.649 | 178.349 |
| **06/03/2018** | 18.24 | 22 | 12 | 12 | 8.76 | 7.57 | 5.243 | 20.229 |
| **06/06/2018** | 11.44 | 19.33 | 35.035 | 35.035 | 29.075 | 16.498 | 8.249 | 41.981 |
| **06/07/2018** | 14.82 | 5.67 | 16.868 | 16.868 | 14.237 | 10.882 | 7.606 | 25.928 |
| **07/16/2018** | 18.34 | 7.5 | 29.139 | 29.139 | 26.68 | 25.511 | 13.356 | 105.051 |
| **08/07/2018** | 7.99 | 3.33 | 41.974 | 41.974 | 28.383 | 15.191 | 7.786 | 31.768 |
| **mean** | 27.67 | 20.19 | 16.37 | 16.37 | 14.00 | 10.45 | 7.63 | 73.06 |
| **max** | 188.63 | 74.67 | 45.56 | 45.56 | 36.04 | 26.01 | 24.08 | 604.73 |
| **min** | 7.99 | 3.33 | 2.42 | 2.42 | 2.40 | 2.00 | 1.60 | 2.72 |

*Table 7-25 - Single erosive storms registered at the Malciaussia rain gauge (Sep 2017 – Aug 2018).*

| Date | Precip. | Duration | Max 5 | Max10 | Max15 | Max30 | Max60 | EI30 |
|---|---|---|---|---|---|---|---|---|
| **MO/DA/YR** | mm | h | mm/h | mm/h | mm/h | mm/h | mm/h | MJ*mm/ha*h |
| **11/04/2017** | 22.2 | 25.17 | 3.6 | 3.6 | 3.28 | 2.84 | 2.62 | 6.914 |
| **11/07/2017** | 16.8 | 6.17 | 6 | 6 | 6 | 5.668 | 5.43 | 13.239 |
| **12/30/2017** | 22.8 | 6 | 9.6 | 9.6 | 9.6 | 8.82 | 7.654 | 31.968 |
| **01/04/2018** | 25 | 9.33 | 7.23 | 7.23 | 6.774 | 6.387 | 5.992 | 23.816 |
| **03/03/2018** | 13.21 | 5.17 | 4.8 | 4.8 | 4.8 | 4.425 | 4 | 7.544 |
| **03/12/2018** | 14.6 | 4 | 6 | 6 | 5.6 | 5.2 | 5 | 10.677 |
| **03/16/2018** | 15.98 | 4.17 | 10.937 | 10.937 | 9.291 | 7.646 | 6.623 | 18.954 |
| **03/17/2018** | 15.6 | 5.5 | 10.8 | 10.8 | 9.912 | 8.405 | 7.009 | 19.449 |
| **04/09/2018** | 37.8 | 33.33 | 6 | 6 | 6 | 5.6 | 5.008 | 27.082 |
| **04/13/2018** | 30.76 | 8.17 | 9.624 | 9.624 | 9.232 | 9.187 | 8.621 | 47.771 |
| **04/29/2018** | 65.41 | 16.67 | 19.695 | 19.695 | 18.192 | 14.135 | 11.227 | 173.685 |
| **05/02/2018** | 86.3 | 55.67 | 17.227 | 17.227 | 15.441 | 9.533 | 7.205 | 117.228 |
| **05/13/2018** | 63.65 | 38.17 | 8.43 | 8.43 | 7.772 | 6.8 | 5.798 | 59.677 |
| **05/27/2018** | 40.51 | 35.83 | 31.165 | 31.165 | 21.881 | 12.404 | 11.369 | 78.842 |
| **05/30/2018** | 33.85 | 13.17 | 23.763 | 23.763 | 17.842 | 13.894 | 10.044 | 85.434 |
| **06/04/2018** | 21.36 | 20 | 12.06 | 12.06 | 10.603 | 8.555 | 5.792 | 25.88 |
| **06/07/2018** | 23.81 | 12.33 | 20.393 | 20.393 | 18.694 | 15.246 | 10.839 | 65.122 |
| **06/11/2018** | 19.33 | 3.5 | 37.588 | 37.588 | 32.097 | 24.545 | 13.042 | 117.592 |
| **06/12/2018** | 19.62 | 6.67 | 29.17 | 29.17 | 27.282 | 18.669 | 14.542 | 82.918 |
| **07/20/2018** | 15.36 | 11 | 38.707 | 38.707 | 33.908 | 21.905 | 13.408 | 74.938 |
| **07/22/2018** | 14.66 | 10.67 | 41.992 | 41.992 | 31.675 | 20.037 | 12.08 | 61.289 |
| **08/07/2018** | 23.82 | 21.83 | 34.643 | 34.643 | 24.695 | 16.367 | 9.583 | 68.808 |
| **mean** | 29.20 | 16.02 | 17.70 | 17.70 | 15.03 | 11.19 | 8.31 | 55.40 |
| **max** | 86.30 | 55.67 | 41.99 | 41.99 | 33.91 | 24.55 | 14.54 | 173.69 |
| **min** | 13.21 | 3.50 | 3.60 | 3.60 | 3.28 | 2.84 | 2.62 | 6.91 |

*Table 7-26 - Monthly R factors calculated for the Borgone, Prarotto and Malciaussia rain gauges.*

| Month | BORGONE | PRAROTTO | MALCIAUSSIA | Average | Annual ratio |
|---|---|---|---|---|---|
| | [MJ mmh$^{-1}$ha$^{-1}$m$^{-1}$] | [MJ mmh$^{-1}$ha$^{-1}$m$^{-1}$] | [MJ mmh$^{-1}$ha$^{-1}$m$^{-1}$] | [MJ mmh$^{-1}$ha$^{-1}$m$^{-1}$] | [%] |
| **SEP '17** | 0.00 | 0.00 | 0.00 | 0.00 | 0.00 |
| **OCT '17** | 0.00 | 0.00 | 0.00 | 0.00 | 0.00 |
| **NOV '17** | 6.71 | 5.90 | 20.15 | 10.92 | 0.64 |
| **DEC '17** | 4.83 | 14.41 | 31.97 | 17.07 | 1.01 |
| **JAN '18** | 608.92 | 188.95 | 23.82 | 273.90 | 16.16 |
| **FEB '18** | 3.46 | 0.00 | 0.00 | 1.15 | 0.07 |
| **MAR '18** | 10.68 | 8.91 | 56.62 | 25.40 | 1.50 |
| **APR '18** | 338.36 | 451.44 | 248.54 | 346.11 | 20.42 |
| **MAY '18** | 555.47 | 1090.23 | 341.18 | 662.29 | 39.08 |
| **JUN '18** | 88.14 | 203.29 | 291.51 | 194.31 | 11.47 |
| **JUL '18** | 105.05 | 0.00 | 136.23 | 80.43 | 4.75 |
| **AUG '18** | 31.77 | 148.66 | 68.81 | 83.08 | 4.90 |
| **TOTAL** | 1753.37 | 2111.79 | 1218.83 | 1694.66 | 100.00 |

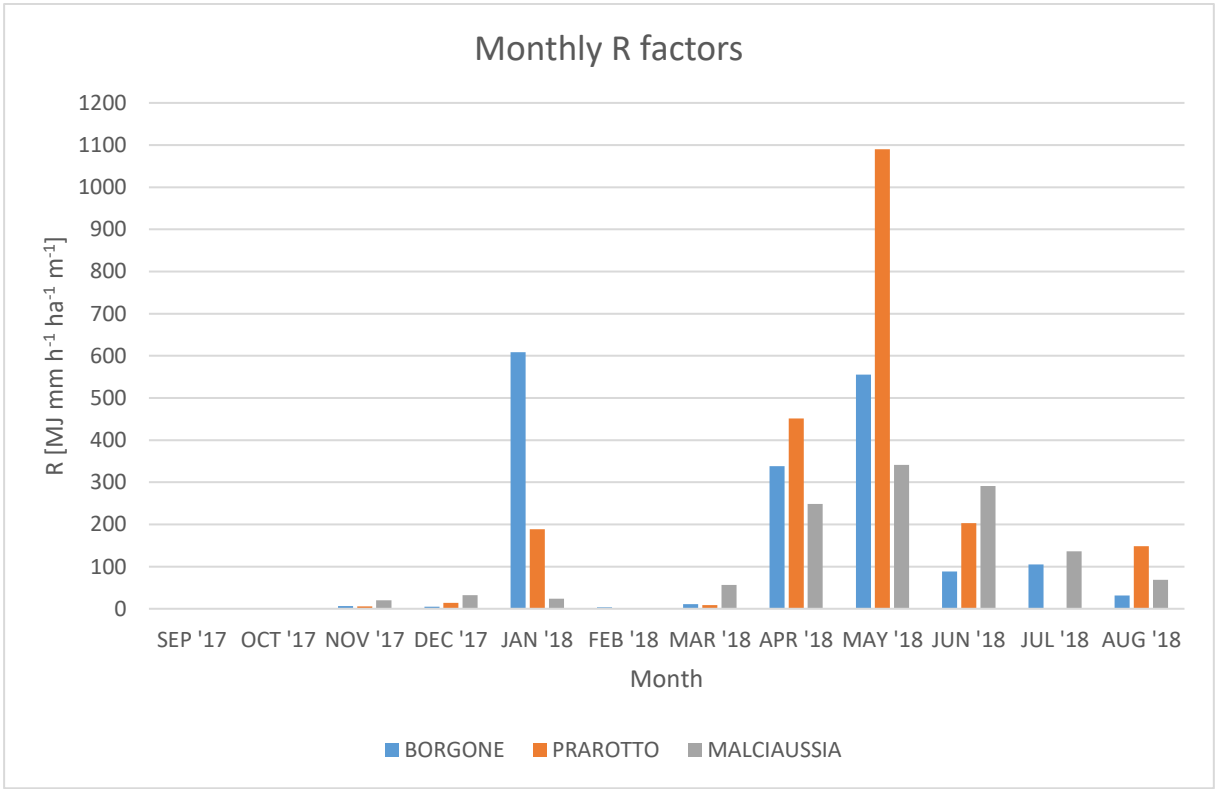


*Figure 7.57 - Monthly R factors calculated for the Borgone, Prarotto and Malciaussia rain gauges.*

Retrieved R factors have been compared to average monthly rainfall erosivity calculated at European scale analyzing >17 years of rainfall data by Ballabio et al (2017) reported in fig 7.58 and table 7-27.

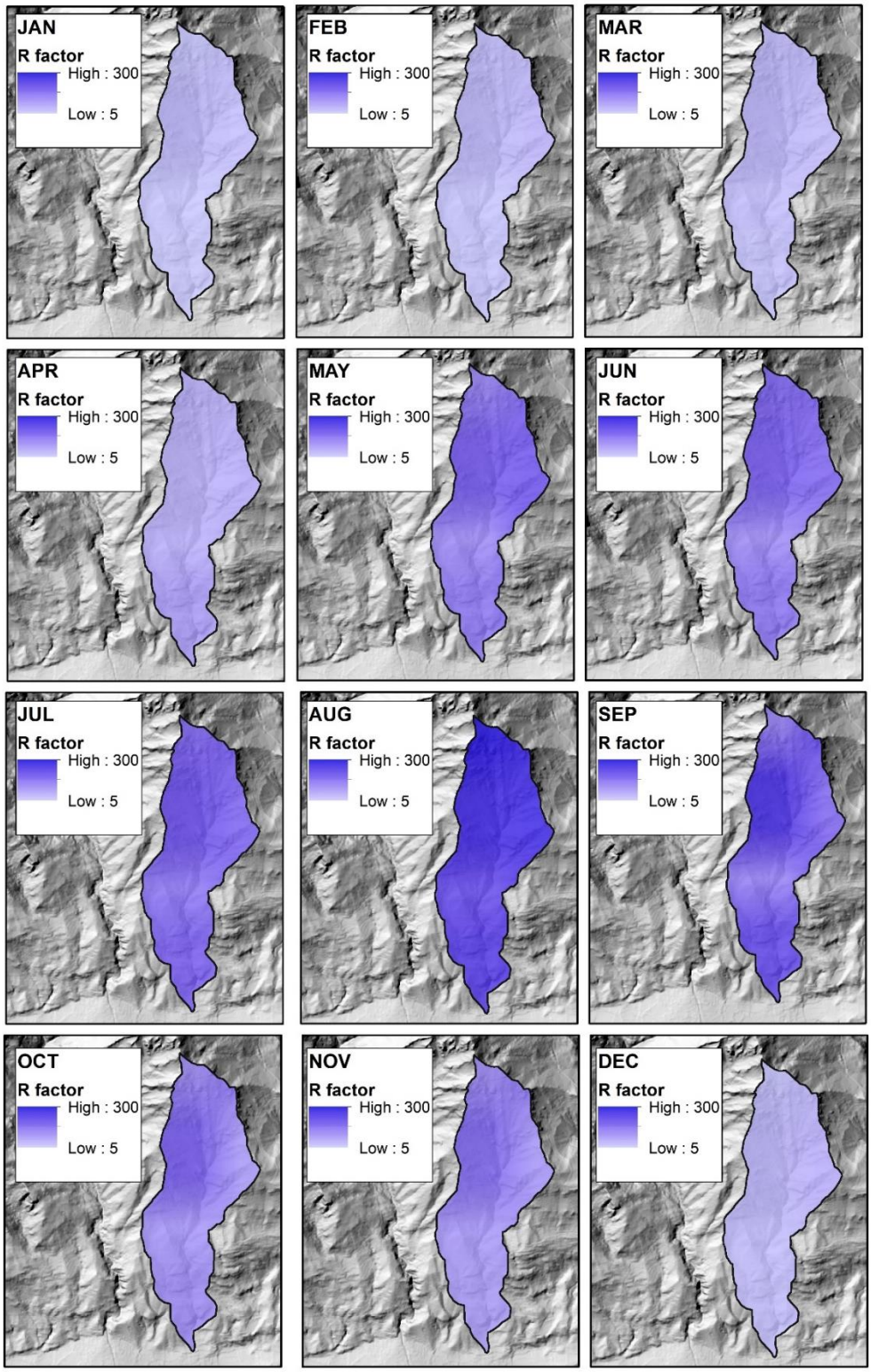


*Figure 7.58 – Long term monthly R factors (redrawn after Ballabio et al. 2017).*

The Month of January, April and May show values eleven times, eight times and four times greater than the long time series data, respectively. On opposite, from September to December 2017, the cumulated R factor barely reaches the 6% of the normal value (fig. 7.59).

*Table 7-27 - Long term monthly R factors and inter annual distribution (Ballabio et al., 2017)*

| Month | Ballabio et al 2017 | Annual ratio |
|---|---|---|
| | [MJ mm $h^{-1}$ $ha^{-1}$ $m^{-1}$] | [%] |
| **SEP** | 181.97 | 14.36 |
| **OCT** | 115.16 | 9.09 |
| **NOV** | 110.50 | 8.72 |
| **DEC** | 36.89 | 2.91 |
| **JAN** | 24.09 | 1.90 |
| **FEB** | 28.72 | 2.27 |
| **MAR** | 28.63 | 2.26 |
| **APR** | 40.67 | 3.21 |
| **MAY** | 155.31 | 12.25 |
| **JUN** | 144.89 | 11.43 |
| **JUL** | 161.83 | 12.77 |
| **AUG** | 238.72 | 18.84 |
| **TOTAL** | 1267.39 | 100.00 |

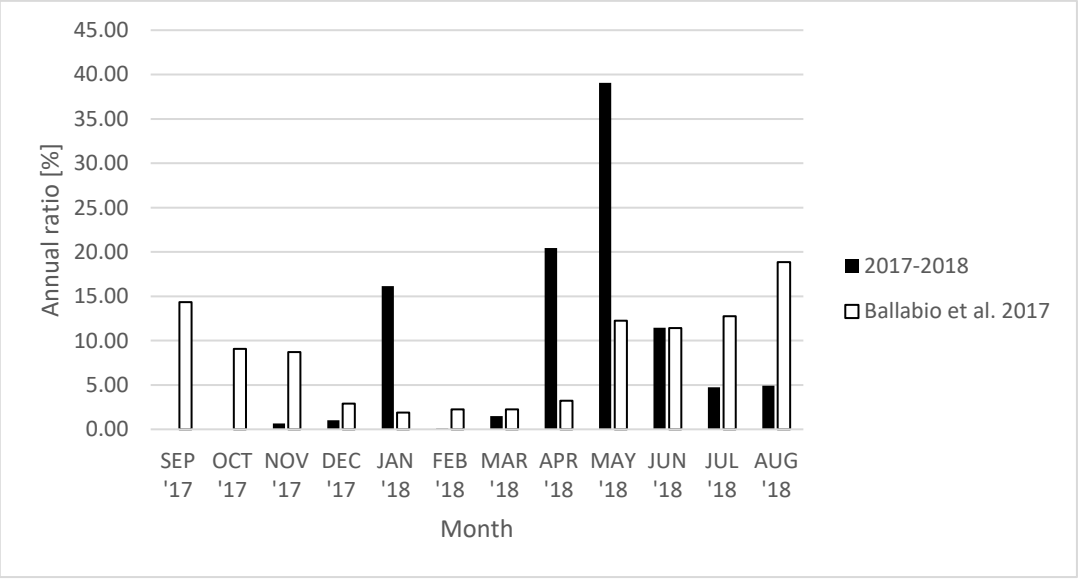


*Figure 7.59 – comparison between calculated and long term inter annual R-factor.*

Erodibility K factor representative of the pre-fire condition has been determined based on soil textural data. The post-fire adjusted K values have been then calculated by applying the correction procedure

described in par. 6.2.4. Laboratory analysis reports for each sample are given in appendix 6, while spatialized pre-fire and post-fire K values are reported in fig 7.60.

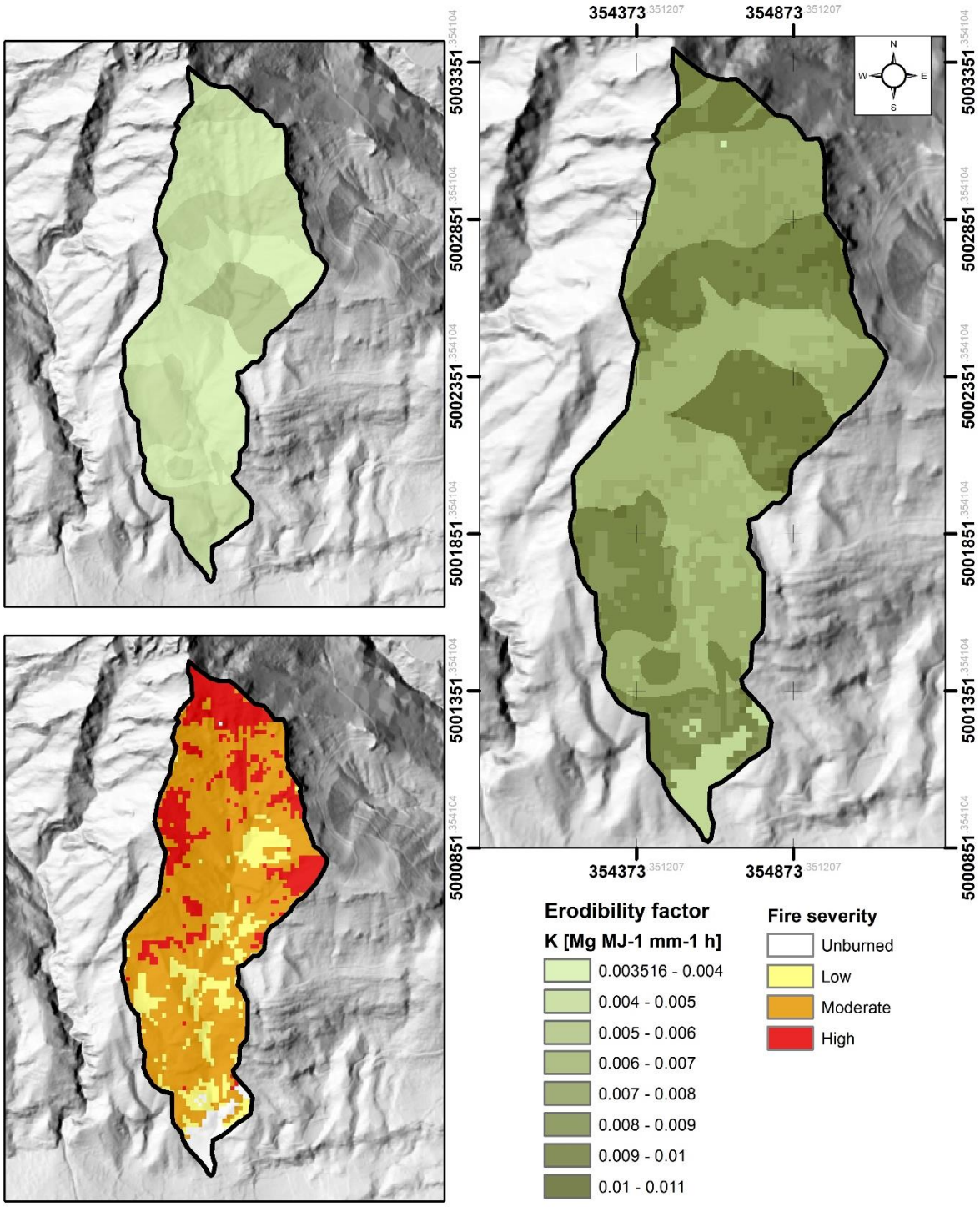


*Figure 7.60 – Pre-fire (top left) and post-fire (top right) erodibility factor distribution over the watershed; Post-fire erodibility has been calculated based on fire severity maps (bottom left).*

LS and C factor (fig 7.61 a and b) has been calculated as described in Par 6.2.4, whereas P value has been set to 1.

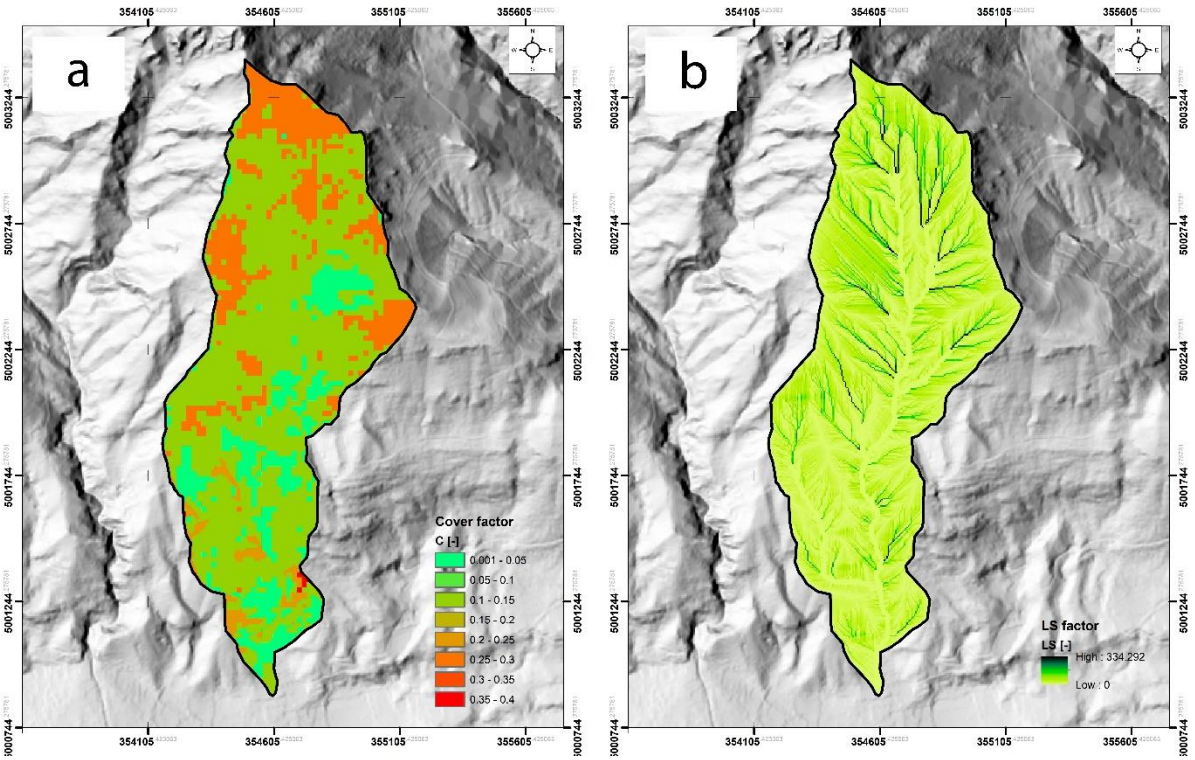


*Figure 7.61 – LS and C factors calculated for the post-fire condition.*

Erodibility Index values for the pre-fire and post-fire situation (table 7-28) has been calculated following equation given in par 6.2.4, and finally monthly mean soil loss A [Mg $ha^{-1}$ $m^{-1}$] and averaged monthly sediment loss SL [Mg $m^{-1}$] for the entire watershed have been computed for both the burned and unburned condition (fig. 7.62 and table 7-29).

The post-fire mean Erodibility Index is more than one order of magnitude higher than the pre-fire one, having a pre-fire value of 4.58E-04 Mg MJ-1 mm-1 h and a post fire value of 1.97E-02 Mg MJ-1 mm-1 h; the comparison with Erodibility Index calculated in the par xx show similar values (2.24E-04 for the pre-fire and 1.03E-02 for the initial assessment).

*Table 7-28 –post-fire vs pre-fire Erodibility Index values over the Comba delle Foglie watershed.*

| **EI [Mg $MJ^{-1}$ $mm^{-1}$ h]** | **MIN** | **MAX** | **RANGE** | **MEAN** | **STD** |
|---|---|---|---|---|---|
| | | | | | |
| **Pre-fire** | 0.00E+00 | 2.78E-02 | 2.78E-02 | 4.58E-04 | 1.61E-03 |
| **Post-fire** | 0.00E+00 | 5.93E-01 | 5.93E-01 | 1.97E-02 | 3.26E-02 |

Monthly mean soil loss A [Mg ha$^{-1}$ m$^{-1}$] and averaged monthly sediment loss SL [Mg m$^{-1}$] comparison for the pre and post-fire conditions results in a post-fire increase of both the indicators of more than 40 times with respect to pre-fire. Maximum pre-fire values occur in May, being 0.30 Mg ha-1 m-1 and 39.40 Mg m-1 for monthly mean soil loss and monthly sediment loss respectively; for the post-fire, these parameters reach values of 13.07 Mg ha-1 m-1 and 1698.92 Mg m-1.

*Table 7-29 – Spatially averaged mean soil loss A and averaged monthly sediment loss SL comparison for the burned and unburned situation.*

| | **Burned (initial ass.t)** | | **Unburned** | |
|---|---|---|---|---|
| **Month** | A | SL | A | SL |
| | [Mg ha-1 m-1] | [Mg m-1] | [Mg ha-1 m-1] | [Mg m-1] |
| **sep '17** | 0.00 | 0.00 | 0.000 | 0.00 |
| **ott-17** | 0.00 | 0.00 | 0.000 | 0.00 |
| **nov-17** | 0.22 | 28.01 | 0.005 | 0.65 |
| **dic-17** | 0.34 | 43.79 | 0.008 | 1.02 |
| **gen-18** | 5.41 | 702.59 | 0.125 | 16.30 |
| **feb-18** | 0.02 | 2.95 | 0.001 | 0.07 |
| **mar-18** | 0.50 | 65.16 | 0.012 | 1.51 |
| **apr-18** | 6.83 | 887.85 | 0.158 | 20.59 |
| **mag-18** | 13.07 | 1698.92 | 0.303 | 39.40 |
| **giu-18** | 3.83 | 498.45 | 0.089 | 11.56 |
| **lug-18** | 1.59 | 206.30 | 0.037 | 4.79 |
| **ago-18** | 1.64 | 213.12 | 0.038 | 4.94 |
| **TOTAL** | 33.45 | 4347.19 | 0.776 | 100.83 |

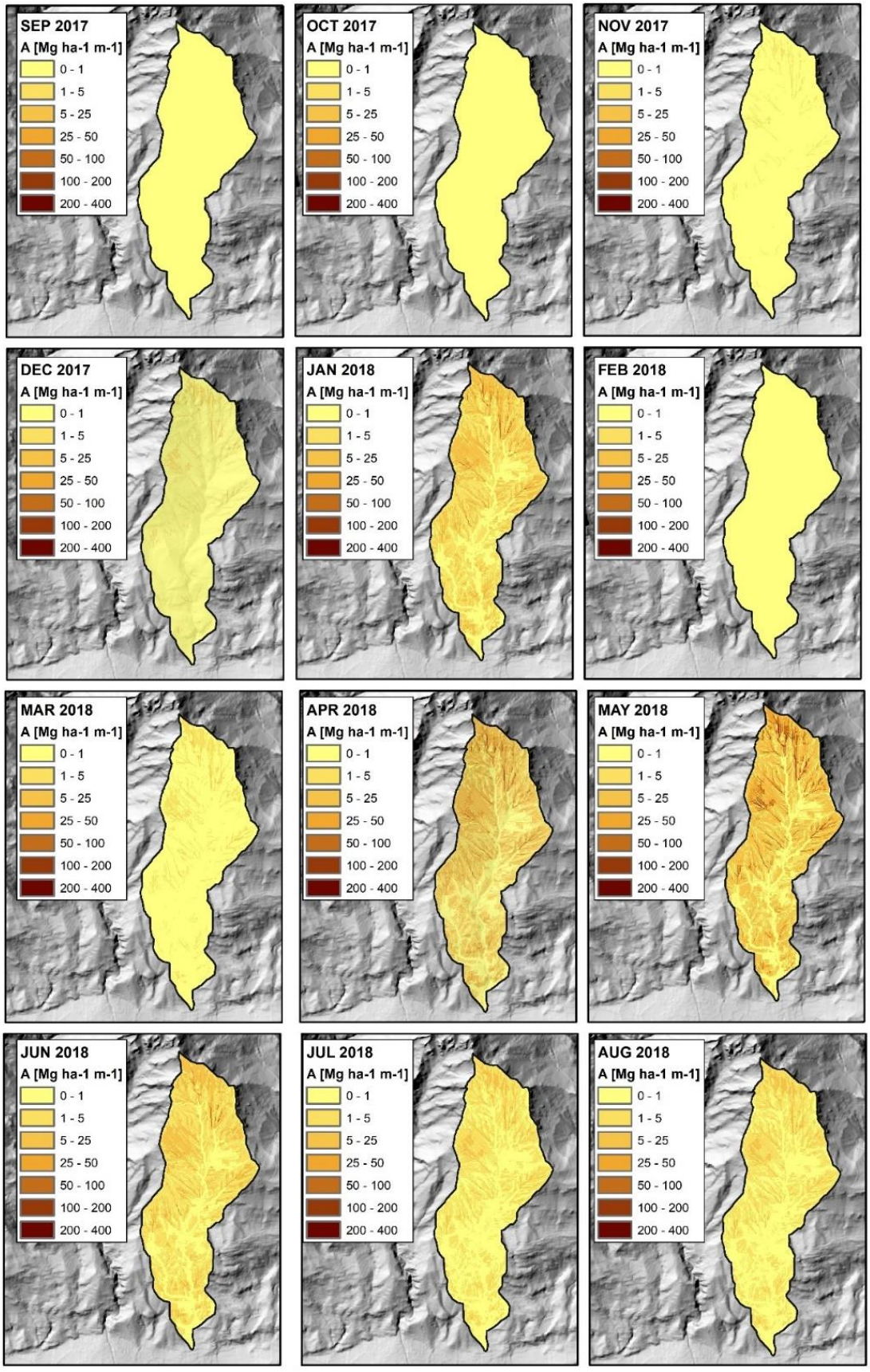


*Figure 7.62 - monthly mean soil loss.*

### 7.3.3 Peak discharge calculation

The SCS-CN Graphical Peak Discharge method has been applied for computing peak discharge for pre-fire and post-fire conditions (initial and extended assessment) by assuming a Type I rainfall distribution (see SCS-USDA 1986). Watershed area $A_w$ is given in table A2.1, A2.2 and A2.3 (Appendix 2), 5-year return period 24h rainfall depth (P) for the Comba delle Foglie watershed is given in table 6-12 (see par 6.2.5) and the watershed Curve Number ($CN_w$) and excess runoff ($Q_w$) have been calculated for the pre-fire and post-fire initial and extended assessment in par. 7.2.5. The watershed $CN_w$ (par 7.2.5) has been used to determine the initial abstraction ($I_a$), and then the $I_a/P$ ratio.

Time of concentration Tc has been calculated by using the Kirpich equation while coefficient C0, C1 and C2 has been retrieved by interpolation of the ones provided, for each $I_a/P$ ratio, in table 6-23. These values have been used for determining the unit peak discharge $q_u$ and finally the peak discharge $q_p$.

Results are summarized in table 7-30: peak discharge raise from 2.8 $m^3/s$ to 13.58 $m^3/s$ and 12.06 $m^3/s$ for the initial and extended assessment respectively, thus showing approximatively a fourfold value.

*Table 7-30 – Peak discharge calculation for the pre-fire and post-fire (initial and extended assessment).*

| **Parameters** | | | |
|---|---|---|---|
| **P [mm]** | 102.8 | | |
| **$A_w$ [km²]** | 1.29 | | |
| **$T_c$ [h]** | 0.17 | | |
| | **pre-fire** | **initial assessment** | **extended assessment** |
| **$CN_w$ [-]** | 60.71 | 82.3 | 79.84 |
| **$Q_w$ [mm]** | 20.89 | 57.62 | 52.54 |
| **Fp [-]** | 1 | 1 | 1 |
| **Ia/P [-]** | 0.32 | 0.106 | 0.129 |
| **$C_0$** | 2.44695 | 2.55047 | 2.54234 |
| **$C_1$** | -0.61994 | -0.61535 | -0.61604 |
| **$C_2$** | -0.10533 | -0.16254 | -0.15815 |
| **$q_u$ [m³/s/km²/mm]** | 0.107 | 0.183 | 0.178 |
| **$q_p$ [m³/s]** | **2.8** | **13.58** | **12.063** |

## 7.4 Field tests

In the following table the mean thermal conductivity values and the relative temperature for each experiment are reported.

*Table 7-31 – mean thermal conductivity values for the conducted test.*

| | **Test 1** | **Test 2** | **Test 3** |
|---|---|---|---|
| **λ [W m$^{-1}$ k$^{-1}$]** | 1.32 | 0.855 | 0.764 |
| **T [°C]** | 21.4 | 16.9 | 9.8 |

The temperature profiles in the subsoil plotted vs time for each thermocouple for the three experiments are reported in fig 7.63, 7.64 and 7.65, while in tables 7-32, 7-33 and 7-34 main experimental results are summarized.

Test 1, conducted with a fuel load of 9.37 kg/m$^2$, results in a maximum temperature registered at the soil surface of 135.9 °C, corresponding to a maximum value registered at -2 cm depth of 61 °C; the temperature delta between maximum value and pre-fire condition (reached at 60 min from start) is equal to 38.3 °C. Maximum temperatures registered at 4, 6 and 8 cm from the surface are 40.4 °C, 37.0 °C and 33.5 °C respectively.

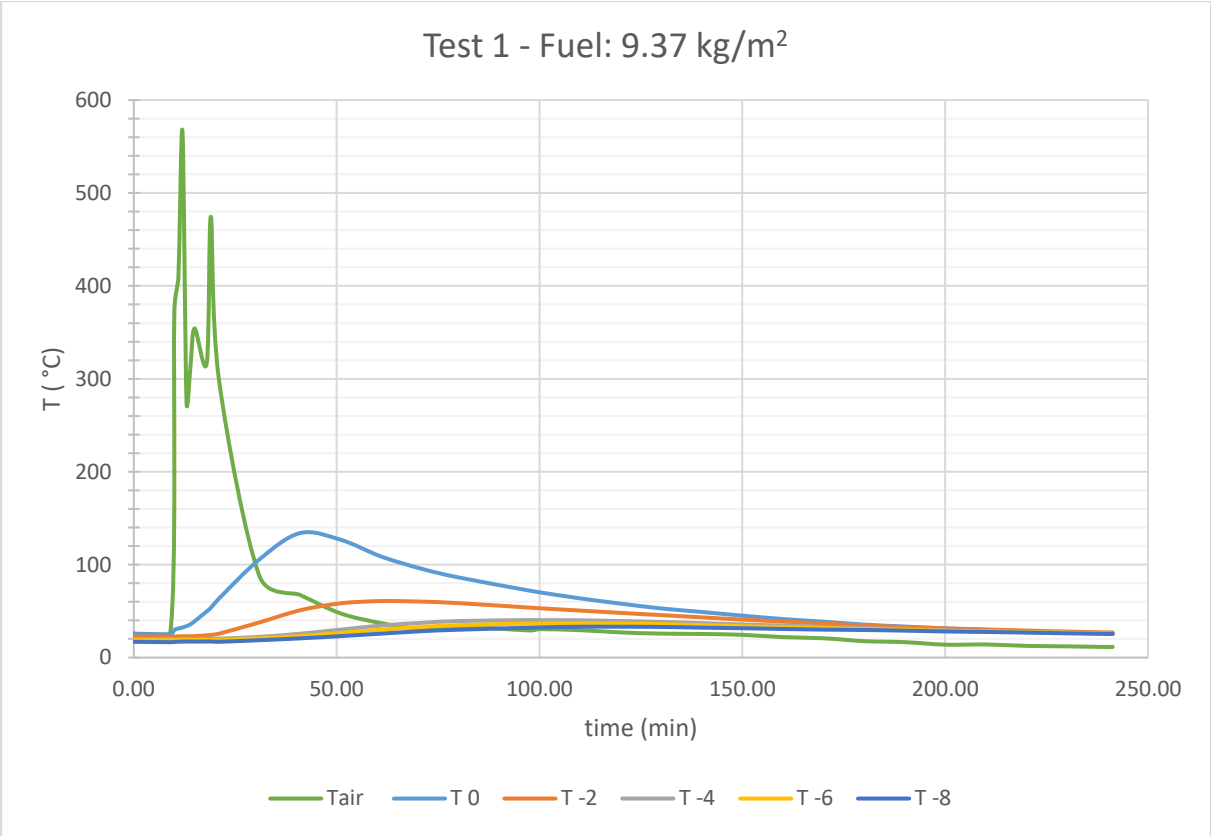


*Figure 7.63 – temperature over time for the six thermocouples (test 1)*

*Table 7-32 – Main experimental results (test 1).*

| | Tair | T 0 | T -2 | T -4 | T -6 | T -8 |
|---|---|---|---|---|---|---|
| **start** | 26.0 | 25.7 | 22.7 | 20.0 | 18.8 | 17.0 |
| **end** | 11.5 | 25.7 | 27.0 | 26.2 | 25.8 | 25.4 |
| **min** | 11.1 | 25.3 | 22.6 | 19.9 | 18.6 | 16.4 |
| **max** | 702.3 | 135.9 | 61.0 | 40.4 | 37.0 | 33.5 |
| **ΔT max** | 676.3 | 110.2 | 38.3 | 20.4 | 18.2 | 16.5 |

Test 2, conducted with a fuel load of 21.87 kg/m², results in a maximum temperature registered at the soil surface of 165.5 °C, corresponding to a maximum value registered at -2 cm depth of 69.7° C; the temperature delta between maximum value and pre-fire condition (reached at 140 min from start) is equal to 53.3° C. Maximum temperatures registered at 4, 6 and 8 cm from the surface are 66.3° C, 65.4° C and 51.0° C respectively.

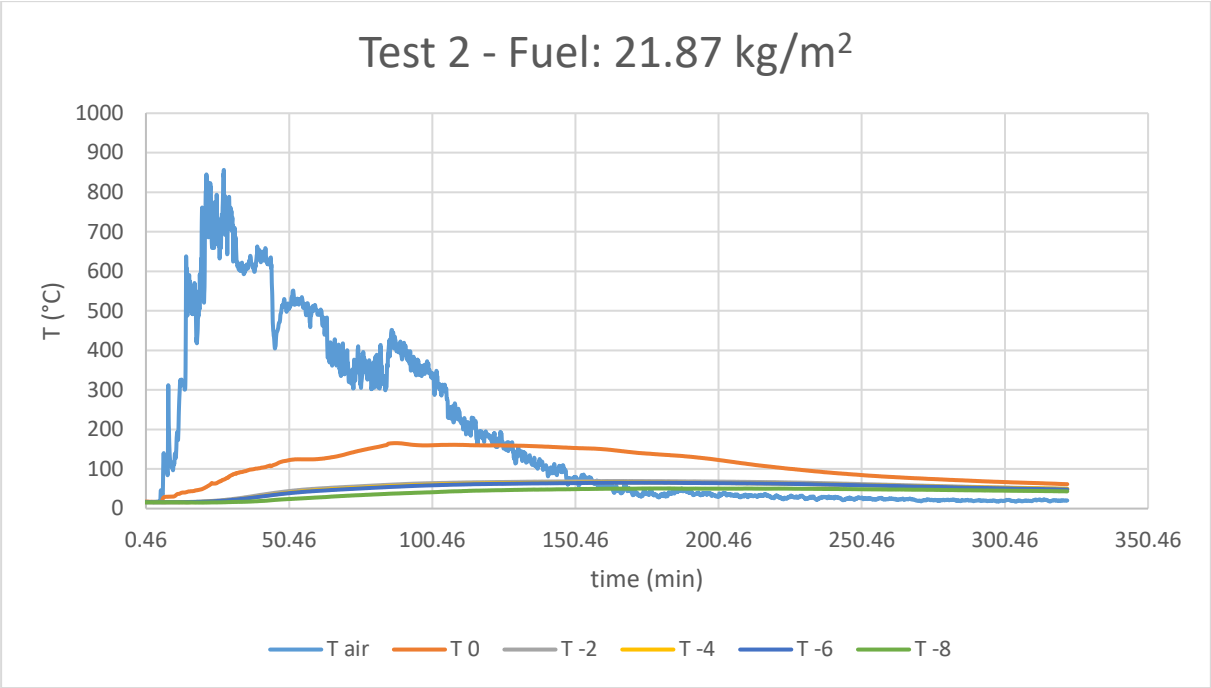


*Figure 7.64 - temperature over time for the six thermocouples (test 2).*

*Table 7-33 - Main experimental results (test 2).*

| | Tair | T 0 | T -2 | T -4 | T -6 | T -8 |
|---|---|---|---|---|---|---|
| **start** | 16.7 | 17.7 | 16.4 | 16.3 | 16.2 | 16.0 |
| **end** | 20.4 | 61.7 | 50.1 | 49.8 | 48.2 | 43.7 |
| **min** | 16.6 | 16.8 | 16.2 | 16.0 | 16.0 | 15.1 |
| **max** | 856.5 | 165.5 | 69.7 | 66.3 | 65.4 | 51.0 |
| **ΔT max** | 839.8 | 147.8 | 53.3 | 50 | 49.2 | 35.0 |

Test 3, conducted with a fuel load of 28.12 kg/m², results in a maximum temperature registered at the soil surface of 528.5° C, corresponding to a maximum value registered at -2 cm depth of 68.8° C; the temperature delta between maximum value and pre-fire condition (reached at 160 min from start) is equal to 59.5 °C. Maximum temperatures registered at 4, 6 and 8 cm from the surface are 58.6 °C, 47.3 °C and 39.4 °C respectively.

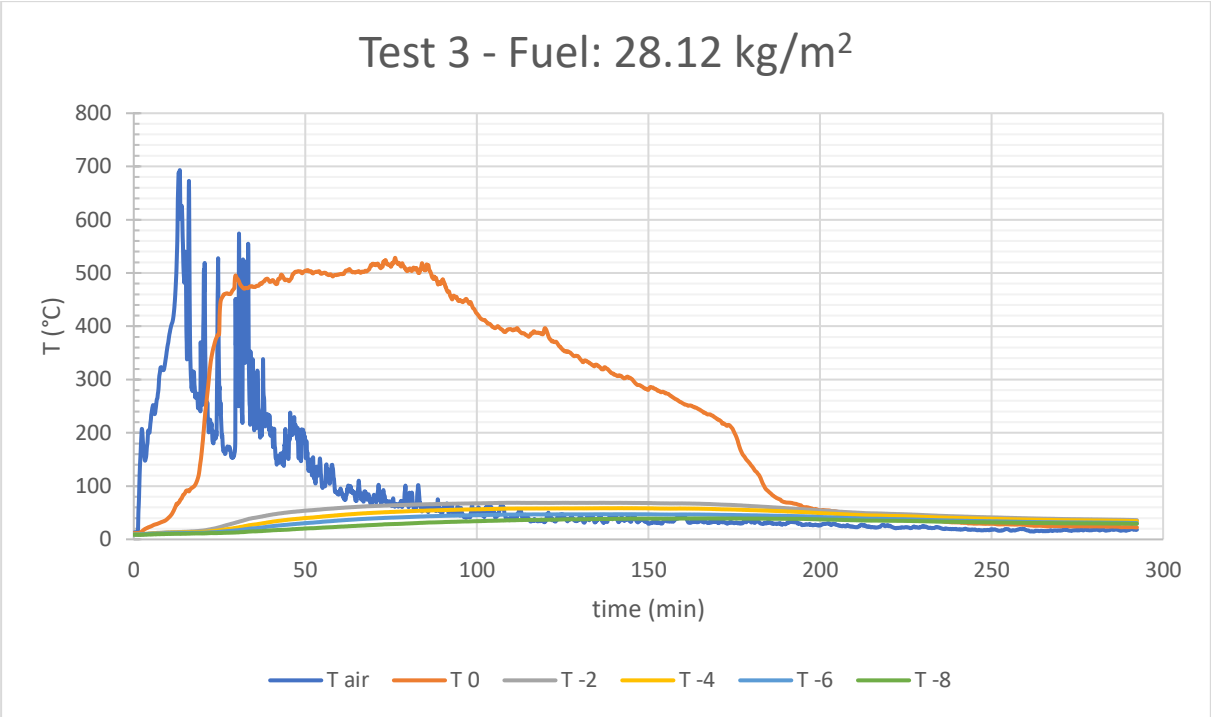


*Figure 7.65 - temperature over time for the six thermocouples (test 3).*

*Table 7-34 - Main experimental results (test 3).*

| | Tair | T 0 | T -2 | T -4 | T -6 | T -8 |
|---|---|---|---|---|---|---|
| **start** | 12.7 | 11.9 | 9.3 | 9.5 | 9.3 | 8.9 |
| **end** | 18.2 | 22.6 | 36.2 | 34.3 | 30.6 | 29.3 |
| **min** | 12.6 | 11.8 | 9.2 | 9.4 | 9.2 | 8.6 |
| **max** | 693.1 | 528.5 | 68.8 | 58.6 | 47.3 | 39.4 |
| **ΔT max** | 680.4 | 516.6 | 59.5 | 49.1 | 38.0 | 30.5 |

The simulation results (figg. 7.66 and 7.67) show a satisfactory agreement with the experimental data, reproducing correctly the shape of the measured curves, especially for the first 200 min of simulation. Despite this, the experimental temperatures registered at -2, -4 and -6 cm appear closer one to each other with respect to the simulated temperatures; a possible explanation could lie in the not precise positioning of the thermocouples at the various depths, especially for the second and third sensors which would seem to be placed a little more superficially than expected. Despite these problems and the lack of refinement in the treatment of data and simulation results, it can be said that it is possible to model the analyzed phenomena with sufficient accuracy, adapting a software that uses algorithms dedicated to the modeling of heat flows in conditions of significantly lower gradients.

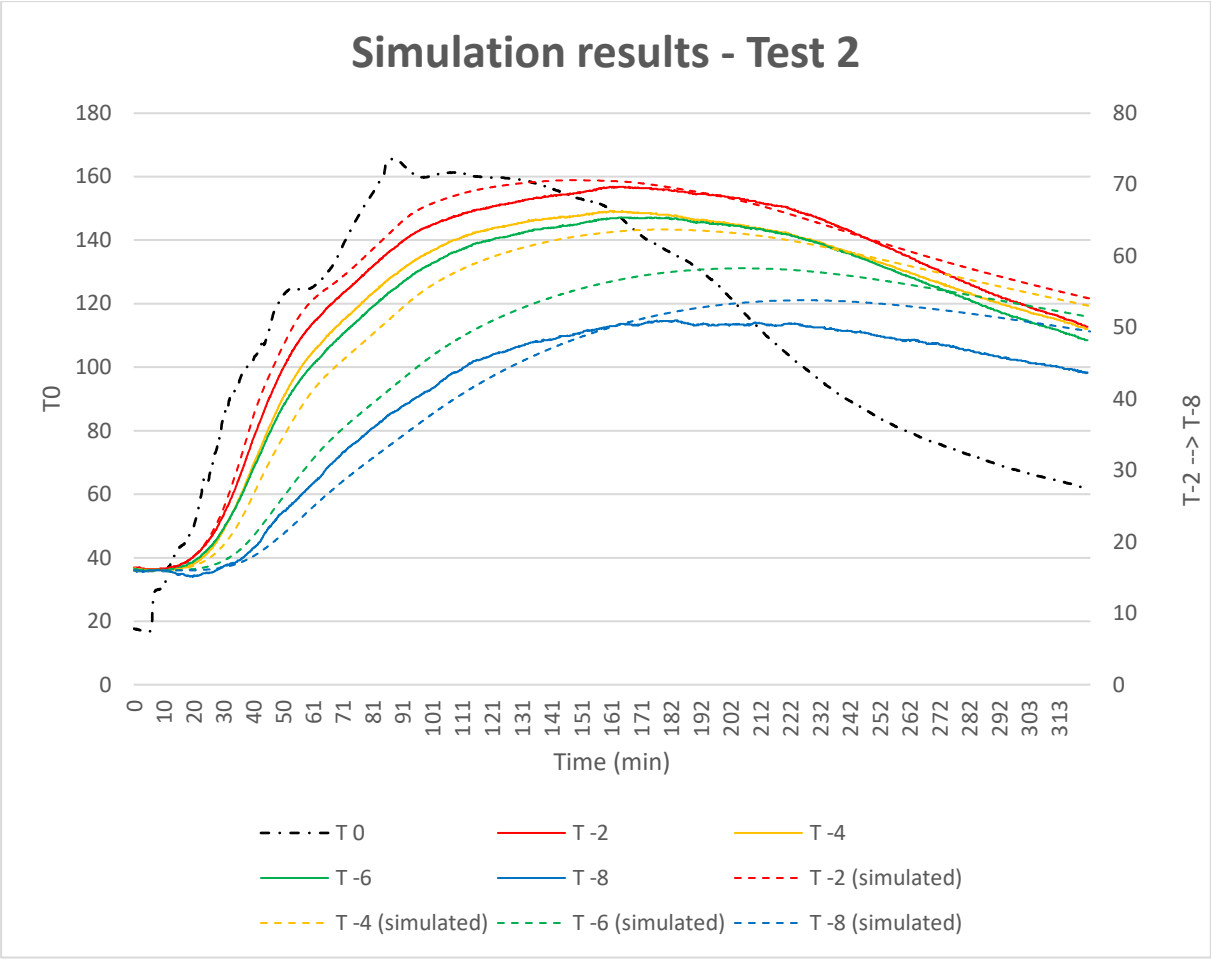


*Figure 7.66 – simulated vs measured temperature values for the six thermopcouples.*

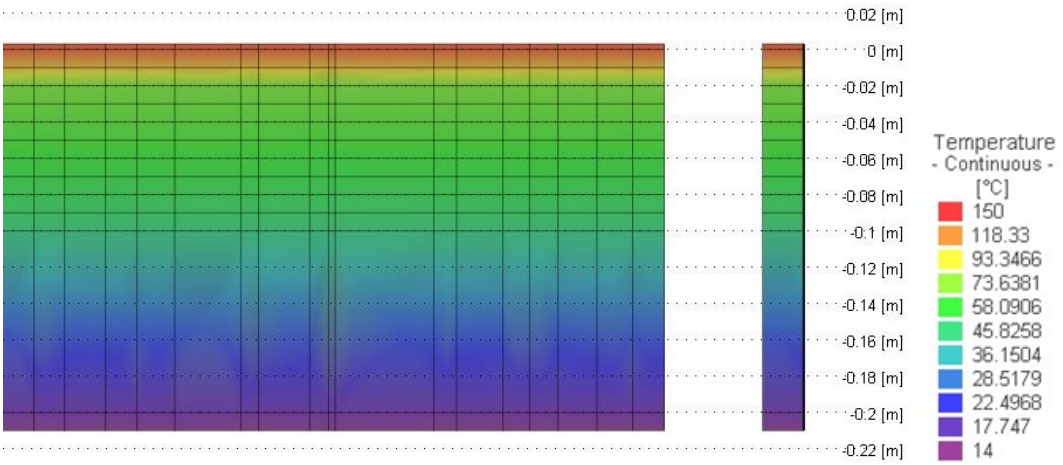


*Figure 7.67 – simulated soil temperature profile at depth, time = 150 min from start.*

# 8 Discussion

The wildfires and landslides databases cross-comparison at regional scale has resulted in 7 possibly correlated events (either landslides or debris/mud flows). Of this, only for one event (Pallanzeno) was it possible to find detailed information to justify a causal link between the occurrence of the fire and the triggering of the landslide event. Unfortunately, the temporal coverage of the data on fires only reaches up to 1997, which greatly reduces the accuracy of this survey. Furthermore, given the lack of awareness of the role of fires in favoring phenomena such as flows or landslides, it may have caused a general neglect in reporting events which, although minor, could have an important statistical significance. In spite of this, even if it was not possible to perform statistical analyses, it is still useful to be aware of possible correlations on which to base future investigations and in-depth analyses.

The study of the 2017 fires, conducted both using an integrated approach consisting of field surveys, the use of remote sensing data and the application of models for the estimation of erosion and runoff, produced some useful results in terms of hierarchization and classification of the impact of fires at the various sites, and the role of this impact on the debris and mud-flows generation.

After the field surveys, the most critical areas from a hydrogeological perspective have been found to be that of the Bussoleno/Mompantero Fire and that of the Locana/Ribordone fire. In the other seven wildfire sites, no particular clues that would suggest a condition of increased hazard were found.

The analysis of the satellite multispectral images proved the aforementioned critical area to be those more severely affected by the fires, with some watersheds experiencing moderate or high fire severity for almost all of their areal extension: for example, in the initial assessment, watershed nos. 4, 8, 9, 11, 19 and 23 experienced more than the 80% of their surface burned with higher severity; overall, in the Locana/Ribordone fire and Bussoleno Mompantero fire the 63.56% and 51.52% of the watershed area belongs to these 2 class of fire severity. For the extended assessment, probably as a consequence of the vegetation re-growth (exceeding delayed mortality), also medium and high severity area percentages decrease: some watersheds, all of them encompassed in the Bussoleno/Mompantero fire, shows nevertheless values above the 70% (nos. 11, 13, 19, 23) (fig. 8.1).
Regarding the fire severity data of the watersheds that have been affected by the mud and debris flow phenomena, which are no. 1 (Rio Fura), 4 (Carlevaria), 48 (Locana Est), 49 (Apparè), 11 (Rio della Ravoire) and 19 (Comba delle Foglie), values of areal incidence of moderate and high severity class (initial assessment) are 78.02%, 82.97%, 72.18%, 64.31%, 94.20% and 83.22%, respectively. Values related to the extended assessment are 35.67%, 21.20%, 39.52%, 53.25%, 90.33% and 73.54%, respectively.

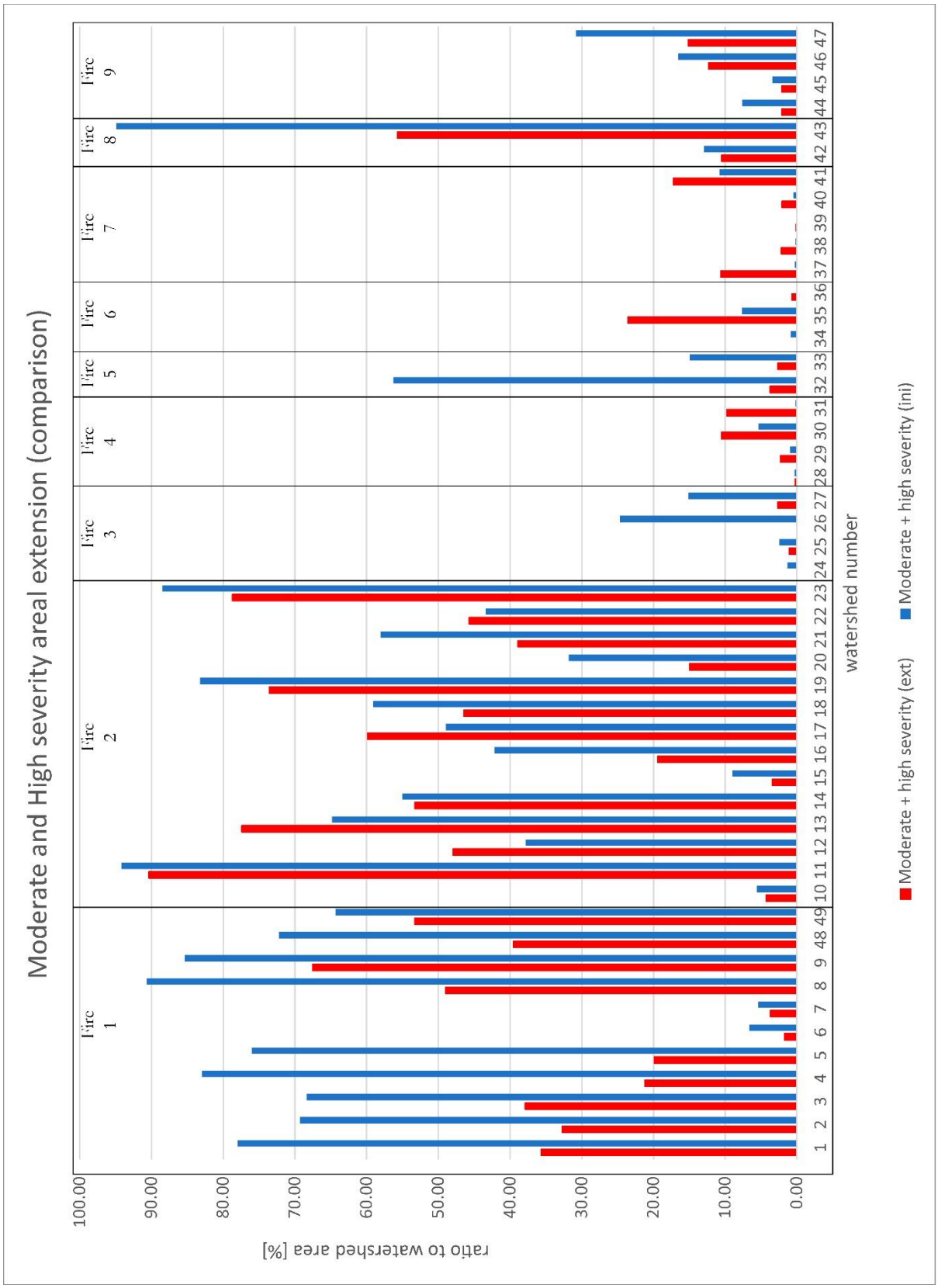


*Figure 8.1 – moderate + high severity areal percentages over the 49 watersheds for the initial and extended assessment.*

The fields surveys, in addition to allowing a validation of the remote sensing data, confirmed the evidence highlighted in the most recent bibliography: the erosive processes following fires, favored by an increase in surface runoff, contribute substantially to the availability of mobilizable material that can be conveyed to the drainage network and give rise to mass transport phenomena, impacting from the point of view of the off-site hazard and risk. Following these considerations, a modeling approach was chosen aimed at quantifying, at the watershed scale, the impact of fires on erodibility and runoff rates.

The results of the application of the RUSLE model, whose coefficients have been corrected to simulate post-fire conditions, show how the average increase in the erodibility index, compared with unburned situation, is consistent both immediately following the fire and one year after it (initial and extended evaluation); the values reached immediately after fires in Locana/Ribordone and Bussoleno/Mompantero are on average 60 and 80 times higher than those of the unburned situation (fig. 8.2). The slight decrease of the erodibility index in the long term (extended assessment) with respect to the initial assessment is generalized, with the only exception represented by the Bussoleno/Mompantero fire area where an increase is registered, which mimics the rising trend in fire severity, probably due to a significant contribution from vegetation delayed mortality.

If we focus on the watersheds from where the flows originated (nos. 1, 4, 48, 49 11 and 19 for reminder) the ratio between the erodibility index for the initial assessment and the pre-fire is 25.90, 98.61, 22.75, 152.64 502.59 and 45.80 respectively. Similarly, the ratio for the extended assessment assumes values of 11.30, 27.96, 8.86, 149.38, 513.79 and 29.62. Comparable values were recorded in watershed that did not experienced debris or mud- flows, such as the nos. 2, 9, 13 and 23, which show R_EI_ini_pre values of 99.51, 186.63, 265.55 and 277.20.

Overall results for the average annual soil loss ratios show a tendency very similar to the overall EI ratios over the 49 watersheds (fig. 8.3): this is due to the spatial distribution of the 24h rainfall values over the watersheds location; in fact, given that there are no significant differences in rainfall with 5 years return period, the range of variability of the R index values of the RUSLE model does not bring substantial changes in the mutual relationships between the various watersheds. As a consequence, a general increase in the A ratios for the post fire condition is registered, the extended assessment condition showing lower values; again, fire number 1 and 2 are characterized by much higher values than the others.

Finally, SL values, which depend on average sediment loss and watershed area, are subject to the same rate of increase as the value of A (fig. 8.4); highest values, registered for watersheds nos. 6, 15, 20 and 21 are due to the larger surface of these watersheds compared to the others. SL results for watershed affected by the debris and mud flows are for the initial assessment 1087 Mg $y^{-1}$, 777 Mg $y^{-1}$, 498 Mg $y^{-1}$, 208 Mg $y^{-1}$, 665 Mg $y^{-1}$ and 1774 Mg $y^{-1}$ (for watershed nos. 1, 4, 48, 49, 11 and 19, respectively). Similarly, values for the extended assessment are 460 Mg $y^{-1}$, 210 Mg $y^{-1}$, 183 Mg $y^{-1}$, 205 Mg $y^{-1}$, 683 Mg $y^{-1}$ and 1156 Mg $y^{-1}$.

The hypothesis made about the post-fire increase in erosion and runoff, confirmed albeit empirically through the application of the RUSLE model, are also reflected in the results deriving from the implementation of the SCS-CN runoff model on the analyzed watersheds. The post-fire watershed averaged Curve Number (which in turn mimics the decrease in soil roughness and infiltration) increases by about 30% for the initial assessment, and by 23% for the extended assessment for the watersheds affected by the post-fire events (fig. 8.6). A similar rise in post-fire CN is also recorded in watersheds that have not been affected by sediment-laden flows. Also looking at the excess runoff ratios, Q, it can be seen that in almost all the basins affected by debris and mud flow events the model estimates significant increases in runoff (Q value for the initial assessment is on average more than doubled), and that this increase is also observed in other basins (especially in those affected by Bussoleno/Mompantero fire) (fig. 8.7).

By comparing the outcomes from the RUSLE and the SCS-CN it can be noted that, despite the not negligible uncertainties of both models, the Locana/Ribordone and, even more, the Bussoleno/Mompantero fire have suffered by the most significant impact. The two used models are able to classify the increase in erosion and runoff rates with reasonable accuracy, taking into account that for the application of the two procedures open source or easily available input data were used. Moreover, an acceptable estimate of the quantity of material that can be mobilized is given, and the increased debris and mud-flow susceptibility under the 5-years return period rainfall scenario is assessed. Of course, these models are subject to considerable limitations, being designed to be implemented through the use of large-scale spatialized data, which might result in under- or over-estimation for some specific site conditions. In addition, it was not possible to accurately validate the erosion or runoff estimates in the field, although as a first approximation it is possible to use the occurrence of sediment-laden phenomena as a rough estimator of the goodness of the results.

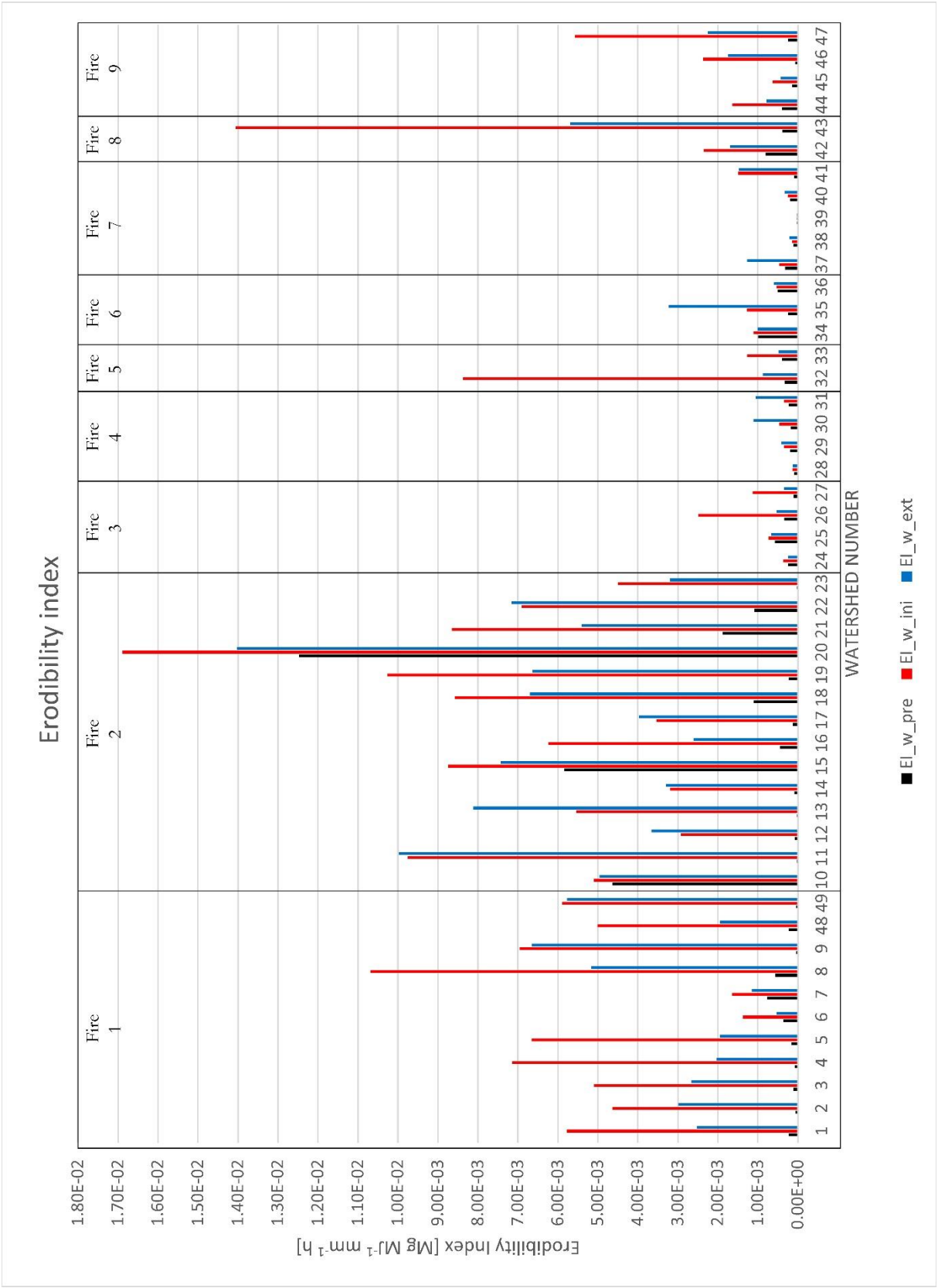


*Figure 8.2 – Erodibility Index comparison for the pre-fire situation and the post-fire initial and extended assessment.*

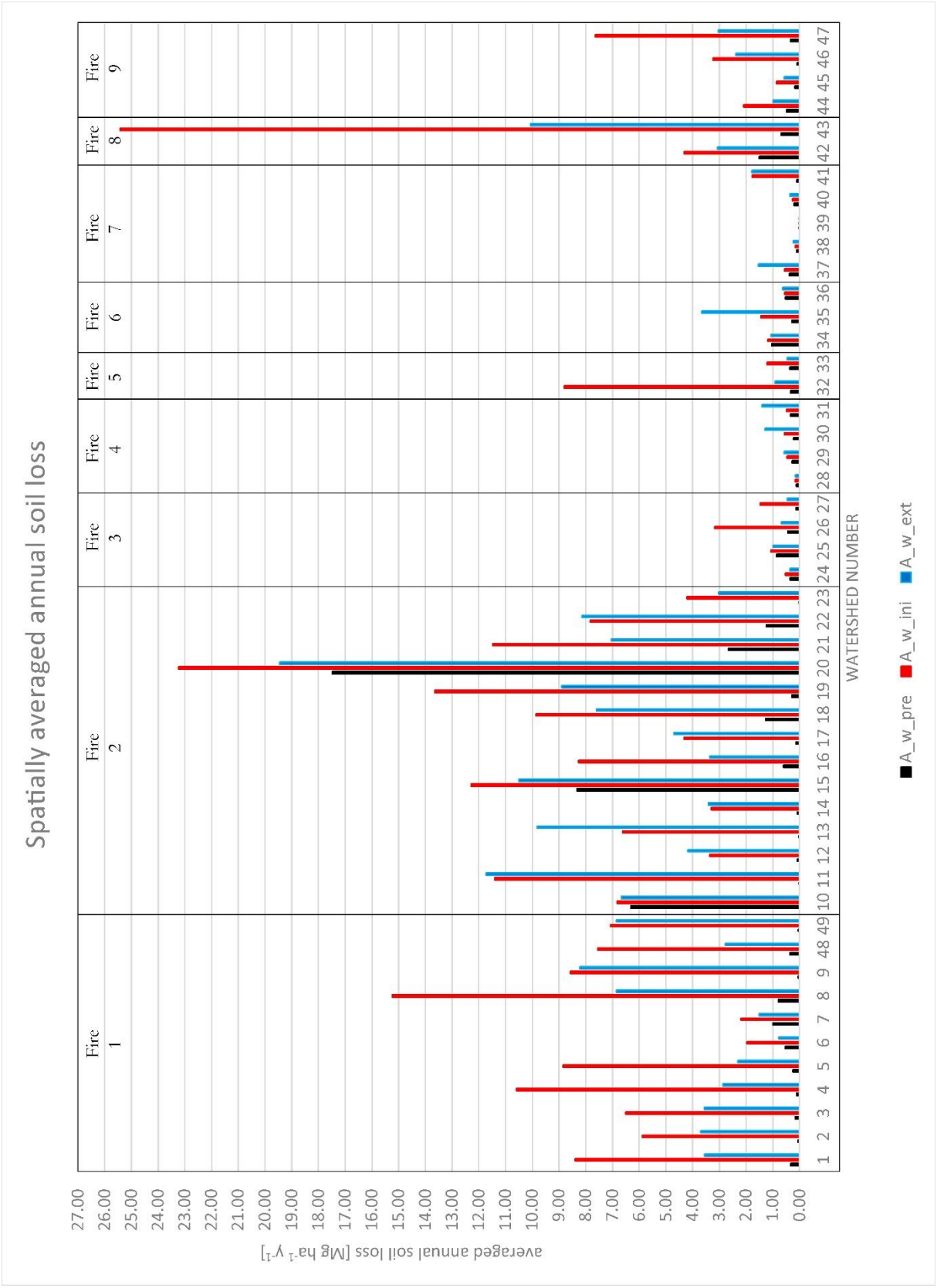


*Figure 8.3 – Average Annual Soil Loss comparison for the pre-fire situation and the post-fire initial and extended assessment.*

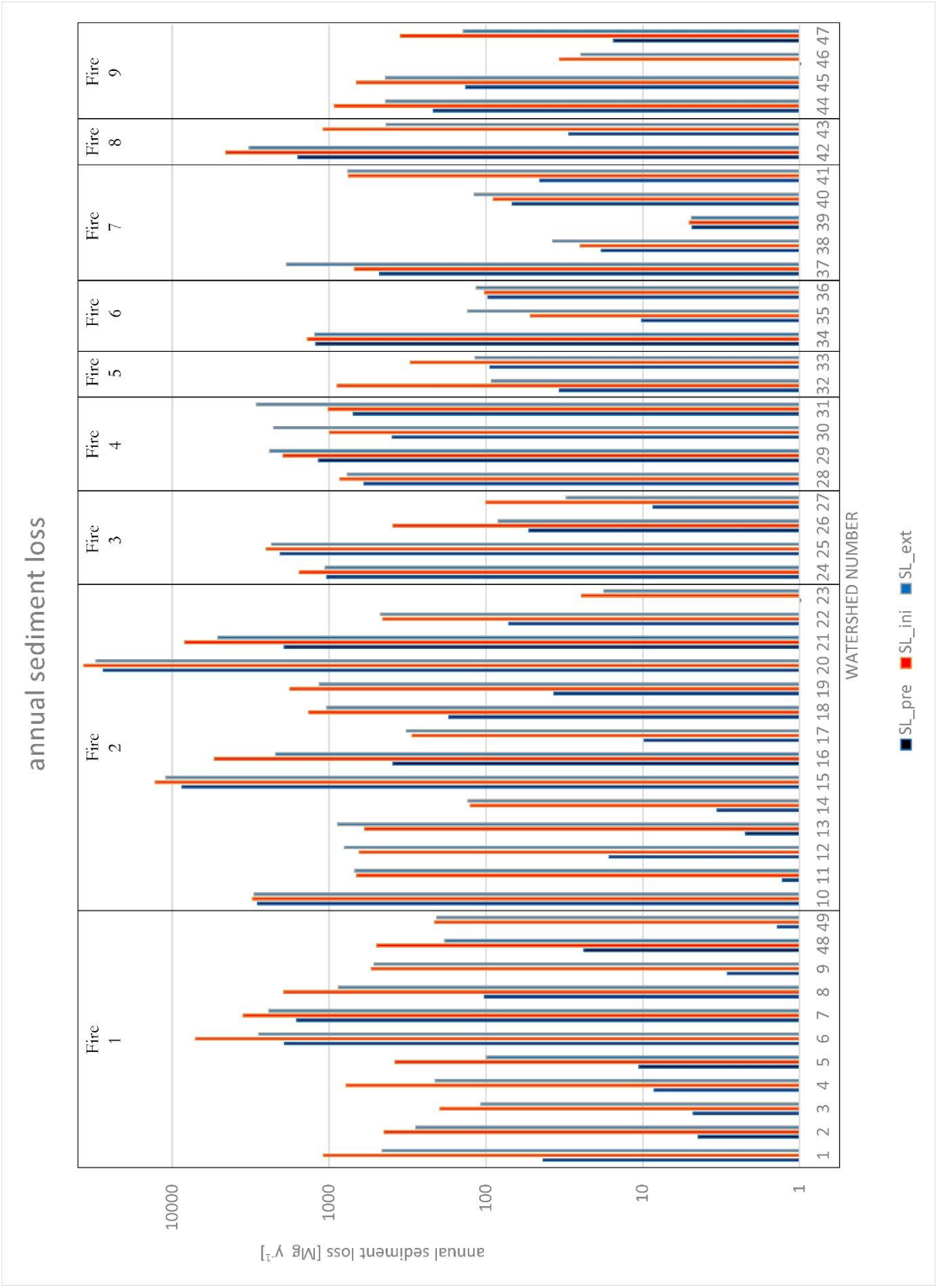


*Figure 8.4 – Annual sediment loss comparison for the pre-fire situation and the post-fire initial and extended assessment.*

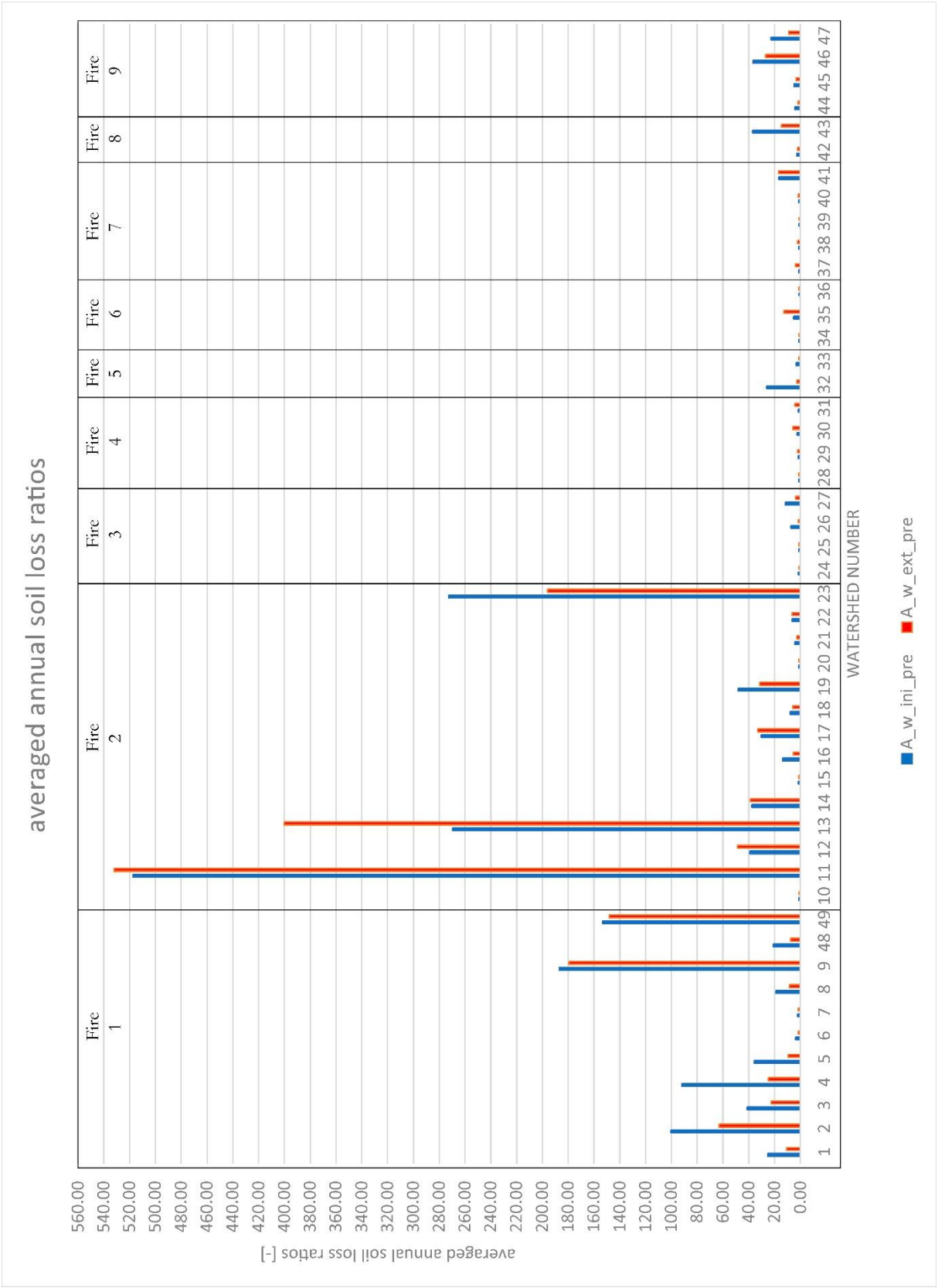


*Figure 8.5 – Average Annual Soil Loss ratios between pre and post fire situation.*

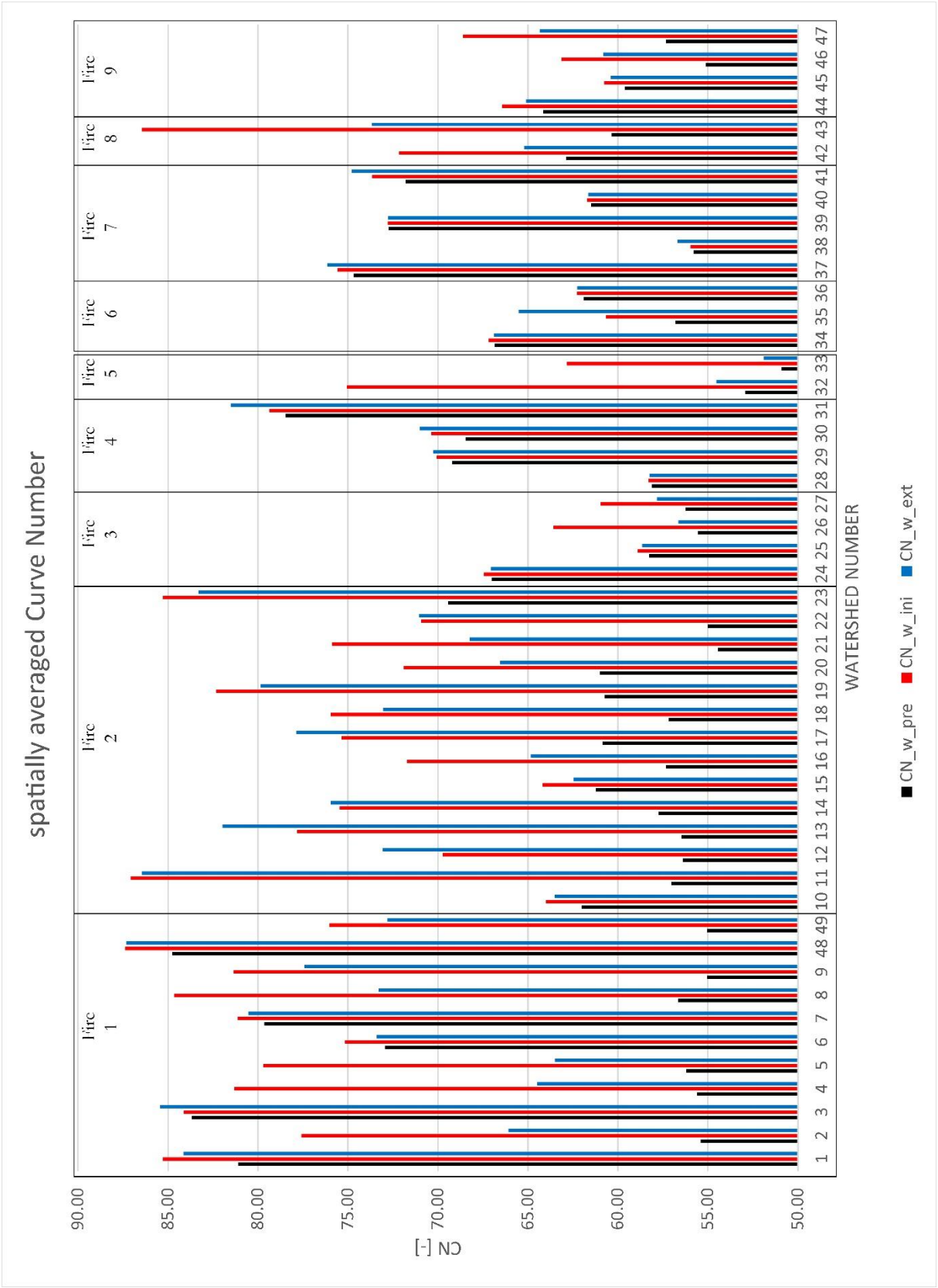


*Figure 8.6 – Curve Number comparison for the pre-fire situation and the post-fire initial and extended assessment.*

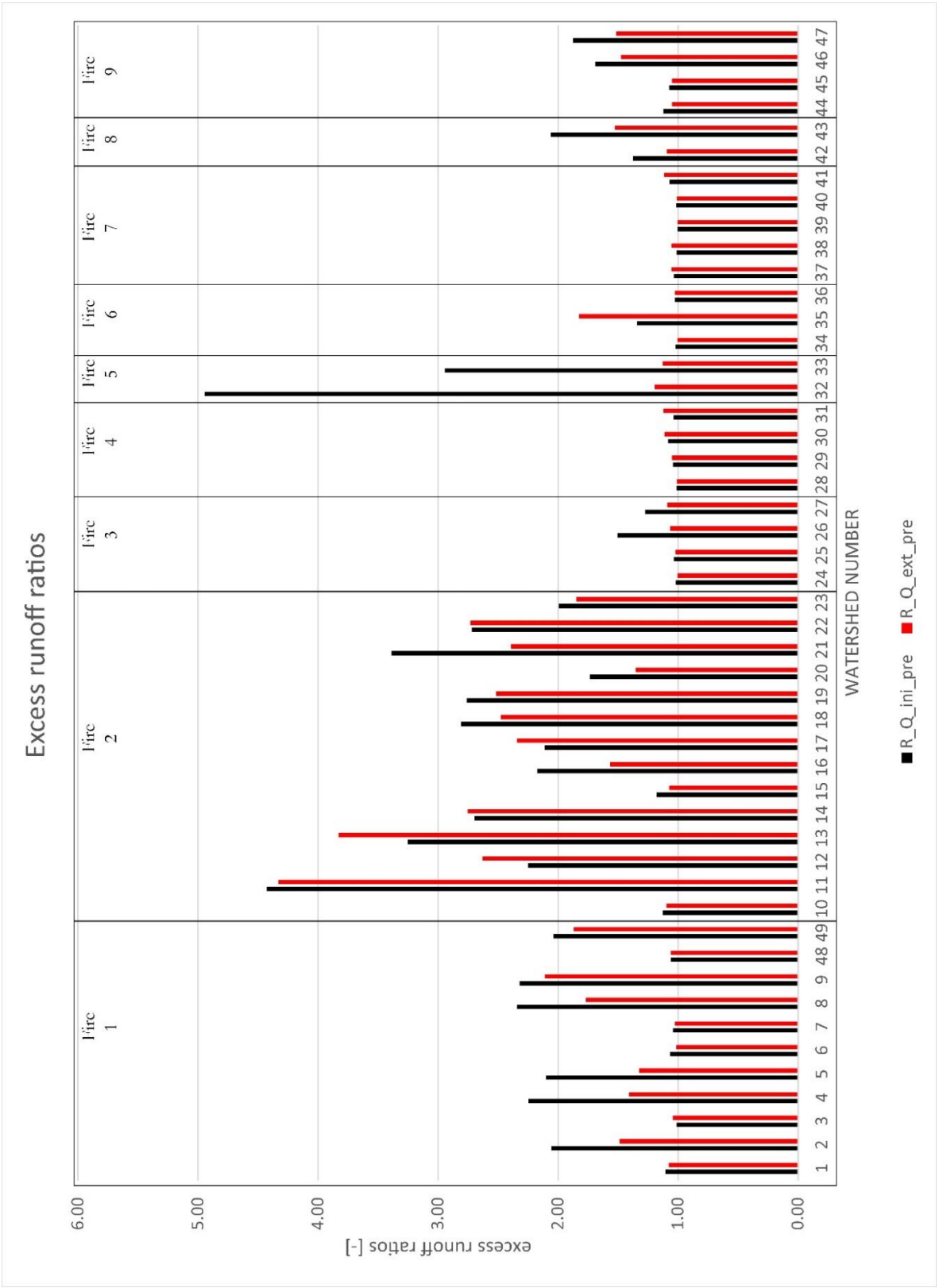


*Figure 8.7- Excess runoff ratios comparing post-fire initial and extended assessment with respect to pre-fire situation.*

Regarding the evaluation of the accuracy of the modeling carried out, some insights can be taken from the analysis of the case study of Comba delle Foglie, for which the analysis was conducted with greater spatial and temporal resolution. Sediment erosion has been assessed implementing the RUSLE model at a monthly scale, by considering a more detailed erodibility map and calculating the erosive power of every significant rainfall event. Monthly mean soil loss A [Mg $ha^{-1}$ $m^{-1}$] and averaged monthly sediment loss SL [Mg $m^{-1}$] reflect the remarkably exceptional R values recorded in the months of January, April and May; these three months in fact contribute for about 75% to the annual erosion recorded in the watershed. The RUSLE model estimates a SL of approximatively 4000 Mg from the extinction of the fire to June, when the most significant event occurred. The maximum deposit thickness of the 7 June debris-flow reconstructed via photogrammetric modelling was approximatively 2 m, over a surface of about 26000 $m^2$. The coarser fraction volume estimate is about 5000 $m^3$. By applying a simple rule of thumb, considering a bulk density of 1500 $Kg/m^3$, the deposit mass can be estimated in 7500 Mg. Taking into account the remarkable erosion exerted by the flow along its path, which may have increased its volume greatly, the results of the model can be considered a reasonable estimator of the amount of material ready to be taken over by the flow.

Following these arguments, it seems reasonable to hypothesize how the considerable amount of sediment mobilized from the date of the fire may have been delivered to the bottom of the slopes and inside the stream network on the occasion of the repeated downpours of rain that occurred on the basin. In occasion of some of them, smaller mud-flows and hyper-concentrated flows have originated. The progressive increase of sediments then reached a critical threshold in conjunction with which a rainy event of a certain intensity caused the triggering of the most destructive debris-flow on 7 June. This hypothesis is supported by the field evidence: during the inspections prior to 7 June a considerable amount of sediments and combustion residues had been observed inside the channels, especially in the terminal part of the watershed and at the apex of the fan. The investigations carried out following the event revealed evident traces of areal and channeled erosion, starting from the upper part of the slopes and into the lower-order channels. It is clear how all this mass of sediments has gone to constitute the load of the debris-flow during its transit.

A detailed analysis of the post-fire conditions for the Comba delle Foglie allows to evaluate not only the increased erosion, but also the increase in excess runoff and peak discharge at the watershed outlet; given the reduced time of concentration, the peak discharge is almost five times higher in post-fire conditions than in pre-fire conditions. This data confirms that in the case analyzed, the fire favored a significant increase in surface runoff on the occasion of a rainy events that was little more than ordinary, which in turn caused exceptional flood waves which undermined the inefficient drainage system at the valley outlet.

Alongside the analyzes concerning the erosion rates and the changes to the hydrological conditions of the watersheds, the tests conducted through simulation of small-scale fires made it possible to confirm, albeit

empirically, the results of the surveys in the field. In fact, a fire simulated using a fuel load similar to that measured in the Mompantero area results in a temperature increase at 2 cm depth of just 53 °C. Even a fuel load greater than 30% gives a temperature rise of a few more degrees. At the maximum depth investigated during the simulations, given the experimental conditions, the maximum temperature increase is around 35° C. These results confirm how the low thermal conductivity of the soil limits the propagation of the heat wave in depth, with thermal increases not so significant as to distort the geotechnical characteristics of the soil (except for a very pellicular portion close to the soil-air interface). Clearly, these results derive from the simulation performed on a soil different from that of the burned areas, in which the component of organic litter and duff can be present in a much greater amount in the first horizons. In this case, the temperatures recorded in the subsoil following the combustion of these substances could be much higher. The literature data, however, agree that it is unlikely that below the first 10 cm of depth the effects of the temperature rise can have significant effects on the physical-mechanical characteristics of the soil.

# 9 Conclusion

The study was devoted to analyzing the geological hazards occurring after wildfires in Piedmont, a region in the Western Italian Alps; following the 2017 exceptional wildfire season which led to the 2018 sediment-laden flow and floods hitting the Susa Valley, the focus was centered in studying the spatial, temporal and causal correlations between the wildfire impact on the landscape and the generation of multi-hazard processes.

Through the review of the historical series of landslides and fires, the analysis and modeling of the areas burned in 2017 and the execution of tests in the field, it was possible to deepen the understanding of the phenomena involved, at the same time verifying how the evidence emerged in the scientific literature, from other parts of the world, are also reflected in the area examined. The examination of the historical series proved to be useful in bringing to light 7 landslide events, possibly correlated with the fires that occurred previously in the same areas. While on the one hand the scarcity of information to strengthen the genetic constraints of these events represents a limiting factor, on the other hand it allows to highlight the need to improve the methodologies and to increase the efforts to catalog and classify landslides and phenomena that they grow in burned areas. In fact, it is necessary to increase the consideration given to the role of fires as a predisposing factor for the triggering of these sudden and destructive geological phenomena.

The study of the areas burned in 2017 and the processes that occurred in the affected areas made it possible to highlight the close link between the effects of the fires and the increased susceptibility to failure. In particular, it emerged that the removal of the vegetation cover, both herbaceous and arboreal, as a function of the fire severity, is one of the most important factors in determining an increase in erosive phenomena and runoff rates. This fact, widely recognized in areas other than the one analysed, is also confirmed for a region characterized by temperate sub-continental climatic conditions. In fact, in a context of significant climatic fluctuation, a hot and dry year (2017) was followed by a particularly rainy season (2018); all this led to the occurrence of conditions in which the rainy events favoured the washout of the slopes no longer protected by the vegetation cover and the accumulation of large quantities of sediments at their bottom and in the drainage network. Through the application of erosion and runoff models it was possible to numerically quantify the effect of the fires on the affected watersheds and made it possible to classify situations with increasing susceptibility. The results of these models are in agreement with the conditions found in the field and depict the actual scenario with good approximation: in fact, the watersheds affected by the Locana/Ribordone and, above all, the Bussoleno/Mompantero wildfires, are those that have revealed the greatest criticalities both after the field surveys and in the results of the models. In particular, some of them showed a marked increase in both the Erodibility Index and the

annual sediment loss, reflecting on average high fire severity conditions. For these watersheds, moreover, the increased Curve Number in the post-fire situation results also in a rise in the excess runoff depth, which is in some cases more than doubled. It is worth underlining that these values derive from the use of predetermined erosivity and precipitation quantities (average rainfall erosivity and 5-year return time precipitation respectively); in the case of thunderstorm type localized events, the combined effects of marked erodibility and increased surface runoff can lead to situations where the propensity to originate flow or flood phenomena is further increased.

An example of this is the case of Comba delle Foglie, a watershed for which it was possible to carry out a more detailed analysis as regards the parameters of erodibility and the erosive factors linked to precipitation. In fact, in the face of an insubstantial increase in the Erodibility Index (refined after a granulometric characterization of the soil surface horizons), the results of annual sediment loss and peak discharge are considerably greater than an evaluation carried out with the average precipitation values. Indeed, the different interannual distribution of precipitation events compared to the norm has meant that the erosion of the slopes, and therefore the progressive sediment bulking, was concentrated in the two months preceding the flow and flood events of May and June 2018.

Therefore, it seems quite evident that the most impacting process on a slope scale, in the time frame analysed (from 2017/2020) was the increase in runoff-related erosion rates; in fact, in the same period of time, no discrete landslide failures was observed. The latter are usually infiltration-triggered phenomena which respond to long duration rainstorms. However, it is not certain that these events cannot develop later, in response to a decreased evapotranspiration of the soil or decay of regolith-anchoring roots. For this reason, it will be necessary to monitor the situation also in the coming years.

Some considerations also need to be made on field tests: the small-scale fire simulations have allowed to verify how the depth affected by significant increases in temperatures, during combustion, is truly pellicular. This is certainly true under experimental conditions; however it is possible that in situations where the quantity of organic matter present within the first soil horizons is greater, the temperatures developed are considerably higher. Regarding this, future investigations need to be conducted.

Evaluating the proposed approach, it can be stated that the workflow used, although it can be improved and calibrated with greater accuracy, can be used on a regional scale as a tool for assessing in a relative way situations with different susceptibility to instability. In fact, the use of opensource data and the possibility of tailoring the input data according to needs make it easily implementable for civil protection purposes and in decision-making.

In spite of this, it is also necessary to evaluate the weaknesses of the proposed work scheme: the use of spatialized data on a large scale involves considerable simplifications and an inevitable loss of resolution. Furthermore, the models used are empirical models calibrated on data obtained in different contexts

(USA). Therefore, although the results can be considered reasonably correct, a modification of the constitutive equations on the basis of a larger database of experimental data could allow for further improvement. Finally, since it was not possible to verify the quantities of mobilized material and the runoff rates in the field, the relative uncertainties must be taken into consideration.

Future research developments in this area derive from the need to overcome the limitations characterizing the study just described, and the necessity to deepen the research topic is justified by the fact that future climate scenarios predict an increase in both the forest fires and extreme rainfall events occurrence. If we consider this, it seems right to continue working on these lines of research, with a view to reaching a more complete understanding of the phenomena, a quantitative characterization of the parameters involved and of the risk, and the definition of rainfall thresholds to be used for early warning purpose.

# 10 References

Abernethy B (1999) - On the role of woody vegetation in riverbank stability. Ph.D. thesis, Monash Univ., Melbourne, Victoria, Australia.

Abney RB and Berhe AA (2018) - Pyrogenic Carbon Erosion: Implications for Stock and Persistence of Pyrogenic Carbon in Soil. Front. Earth Sci. 6:26.

Abramowitz M and IA Stegun (1972) - Handbook of mathematical functions. Dover Publications, Inc., New York.

Agee J (2007) - Fire severity. In: FireWords: Fire Science Glossary [electronic]. U.S. Department of Agriculture, Forest Service, Rocky Mountain Research Station, Fire Sciences Laboratory (Producer). Available: http://www.firewords.net/.

Arndt N, Vacik H, Koch V, Arpaci A and Gossow H (2013) - Modeling human-caused forest fire ignition for assessing forest fire danger in Austria. IForest 6:315–325.

Arpa Piemonte (2005) – Il "trasporto in massa" a Pallanzeno (VB) del 18 Luglio 2005. Available online at http://www.arpa.piemonte.it/pubblicazioni-2/relazioni-tecniche/analisi-eventi/eventi-2005/pdf-trasporto-massa-2005/at_download/file.

Arpa Piemonte (2018) – Il Clima in Piemonte 2017. Available online at https://www.arpa.piemonte.it/rischinaturali/tematismi/clima/rapporti-di-analisi/annuale.html.

Arpa Piemonte (2018b) – Rapporto di evento del 07/06/2018. Colata detritica nel comune di Bussoleno.

Arpa Piemonte (2019) – Il Clima in Piemonte 2018. Available online at https://www.arpa.piemonte.it/rischinaturali/tematismi/clima/rapporti-di-analisi/annuale.html.

Ascoli D, Castagneri D, Valsecchi C, Conedera M and Bovio G (2013) - Post-fire restoration of beech stands in the Southern Alps by natural regeneration. Ecological Engineering, 54, 210-217.

ASTM D5334 (2014) - Standard Test Method for Determination of Thermal Conductivity of Soil and Soft Rock by Thermal Needle Probe Procedure. ASTM: West Conshohocken, PA, USA, 2014.

Badia D and Marti C (2003) - Plant ash and heat intensity effects on chemical and physical properties of two contrasting soils. Arid Land Res Manage 17:23-41.

Balfour VN, (2013) - Variations in wildfire ash properties and implications for post-fire hydrological response within Western North American ecosystems. Graduate Student Theses, Dissertations, & Professional Papers. 10742.

Balfour VN and Woods SW (2013) - The hydrological properties and the effects of hydration on vegetative ash from the Northern Rockies, USA. Catena 111, 9–24.

Ballabio C, Borrelli P, Spinoni J, Meusburger K, Michaelides S, Beguería S, Klik A, Petan S, Janecek M, Olsen P, Aalto J, Lakatos M, Rymszewicz A, Dumitrescu A, Tadić MP, Nazzareno D, Kostalova J, Rousseva S, Banasik KL, Alewell C and Panagos P (2017) - Mapping monthly rainfall erosivity in Europe. *Sci Total Environ. 579*: 1298-1315.

Bathurst JC, Moretti G, El-Hames A, Beguería S and García-Ruiz JM (2007) - Modelling the impact of forest loss on shallow landslide sediment yield, Ijuez river catchment, Spanish Pyrenees. Hydrology and Earth System Sciences Discussions, European Geosciences Union, 2007, 11 (1), pp.569-583.

Blake WH, Theocharopoulos SP, Skoulikidis N, Clark P, Tountas P, Hartley R and Amaxidis Y (2010) - Wildfire impacts on hillslope sediment and phosphorus yields. J Soils Sediments (2010) 10:671–682.

Byram GM (1959) - Combustion of forest fuels. In 'Forest Fire: Control and Use'. (Ed. KP Davis) pp. 61–89. (McGraw-Hill: NewYork).

Bodi MB, Martin DA, Balfour VN, Santin C, Doerr SH, Pereira P and Mataix-Solera J (2014) - Wildland fire ash: Production, composition and eco-hydro-geomorphic effects. Earth-Science Reviews,130,103–127.

Bowman DMJS, Balch JK, Artaxo P, Bond WJ, Carlson JM, Cochrane MA, D'Antonio CM, DeFries RS, Doyle JC, Harrison SP, Johnston FH, Keeley JE, Krawchuk MA, Kull CA, Marston JB, Moritz MA, Prentice IC, Roos CI, Scott AC, Swetnam TV, van der Wer GR and Pyne SJ (2009) - Fire in the earth system. Science 324:481–484.

Bradstock RA and Auld TD (1995) - Soil temperatures during experimental bushfires in relation to fire intensity: consequences for legume germination and fire management in south-eastern Australia. Journal of Applied Ecology 32, 76–84.

Bristow KL (1998) - Measurement of thermal properties and water content of unsaturated sandy soil using dual-probe heat pulse probes. Agr Forest Meteorol. 89: 75–84.

Brown LC and Foster GR (1987) - Storm erosivity using idealized intensity distributions. Trans. Am. Soc. Agric. Eng. 30, 379–386.

Buckley AJ (1993) - Fuel reducing regrowth forests with a wiregrass fuel type: fire behaviour guide and prescriptions. Department of Conservation and Environment, Research Report No. 40. (Melbourne).

Calcaterra D, Parise M, Palma B and Pelella L (2000) - Multiple debris flows in volcaniclastic materials mantling carbonate slopes. In: Wieczorek GF, Naeser ND (eds) Proceedings of 2nd international

conference "Debris-flow hazards mitigation: mechanics, prediction, and assessment". Taiwan, pp 99–107.

Cannon SH, Bigio ER and Mine E (2001) - A process for fire-related debris flow initiation, Cerro Grande fire, New Mexico. Hydrol. Process. 15, 3011–3023.

Cannon SH, Kirkham RM, Parise M (2001) - Wildfire-related debris-flow initiation processes, Storm King Mountain, Colorado. Geomorphology 39, 171–188.

Cannon SH, Gartner JE, Parrett C, Parise M (2003) - Wildfire-related debris flow generation through episodic progressive sediment bulking processes, western USA. In: Rickenmann D, Chen CL (eds) Proceedings of 3rd international conference "Debris-flow hazards mitigation— mechanics, prediction, and assessment". Davos, Switzerland, pp 71–82.

Cannon SH, Gartner JE (2005) - Wildfire-related debris flow from a hazards perspective. In: Jakob M, Hungr O (eds) Debris-flow hazards and related phenomena. Praxis, pp 363–385.

Campbell G S, Jungbauer J D, Bidlake W R, Hungerford R D. (1994) - Predicting the effect of temperature on soil thermal conductivity. Soil Sci. 158: 307–313.

Carraro F, Cadoppi P, Baggio P, Bellino L, Castelletto M, Giraud V and Mensio L (2002) - Foglio 154 Susa, Carta Geologica d'Italia, scala 1:50.000. Carta Geol - Serv Geol D'Italia Coord CARRARO F 126.

Catchpole W (2000) - The international scene and its impact on Australia. In 'National Academies Forum Proceedings of the 1999 Seminar: Fire! The Australian Experience', 30 September–1 October 1999, University of Adelaide, Australia. pp. 137–148. Australian Academy of Technological Sciences and Engineering Limited. (National Academies Forum: Canberra, ACT).

Jane G, Cawson A, Nymanb P, Smith HG, Lane NJP, Sheridan GJ (2016) - How soil temperatures during prescribed burning affect soil water repellency, infiltration and erosion. Geoderma 278 (2016) 12–22.

Camerano P, Giannetti F, Terzuolo PG, Guiot E (2017) - La Carta Forestale del Piemonte – Aggiornamento 2016. IPLA S.p.A. – Regione Piemonte.

Carslaw HS and Jaeger JC (1959) - Conduction of Heat in Solids. 2nd Ed. Oxford University Press, London.

Cerdà A (1998) - Changes in overland flow and infiltration after a rangeland fire in a Mediterranean scrubland. Hydrol. Process. 12, 1031–1042.

Cerdà A and Doerr SH (2008) - The effect of ash and needle cover on surface runoff and erosion in the immediate post-fire period. Catena 74, 256–263.

Certini G (2005) - Effects of fire on properties of forest soils: a review. Oecologia 143, 1–10.

Chafer CJ, Noonan M and Mcnaught E (2004) - The post-fire measurement of fire severity and intensity in the Christmas 2001 Sydney wildfires. International Journal ofWildland Fire 13, 227–240.

Chappell CB and Agee JK (1996) - Fire severity and tree seedling establishment in Abies magnifica forests, southern Cascades, Oregon. Ecological Applications 6, 628–640.

Chatto K and Tolhurst KG (2004) - A review of the relationship between fireline intensity and the ecological and economic effects of fire, and methods currently used to collect fire data. Department of Sustainability and Environment, Fire Management Branch, Research Report No. 67. (Melbourne).

Chow VT, Maidment DR and Mays LW (1988) - Applied Hydrology. New York: McGraw-Hill.

Chuvieco E, Riano D, Danson FM and Martin P (2006) - Use of a radiative transfer model to simulate the post-fire spectral response to burn severity. Journal of Geophysical Research 111, G04S09.

Clauser C and Huenges E (1995) - Thermal conductivity of rocks and minerals. In American Geophysical Union (ed.) Rock Physics and Phase Relations: A Handbook of Physical Constants. American Geophysical Union, Washington, D.C. pp. 105– 126.

Cocke AE, Fule PZ and Crouse JE (2005) - Comparison of burn severity assessments using Differenced Normalized Burn Ratio and ground data. International Journal of Wildland Fire 14, 189–198.

Conard SG, Sukhinin AI, Stocks BJ, Cahoon DR, Davidenko EP and Ivanova GA (2002) - Determining effects of area burned and fire severity on carbon cycling and emissions in Siberia. Climatic Change 55, 197–211.

Conedera M, Cesti G, Pezzatti G, Zumbrunnen T and Spinedi F (2006) - Lightning-induced fires in the Alpine region: An increasing problem. Forest Ecology and Management - FOREST ECOL MANAGE. 234.

Coschignano G, Nicolaci A, Ferrari E, Cruscomagno F and Iovino F (2019) - Evaluation of hydrological and erosive effects at the basin scale in relation to the severity of forest fires. iForest 12: 427-434.

Cram DS, Baker TT and Boren J (2006) - Wildland fire effects in silviculturally treated vs. untreated stands of New Mexico and Arizona. USDS Forest Service, Rocky Mountain Research Station, Research Paper RMRS-RP- 55. (Fort Collins, CO).

Cruden DM and Varnes DJ (1996) - Landslide types and processes. In Landslides: Investigation and Mitigation, Special Report 247, 36-75. Washington: Transportation Research Board.

DeBano LF, Mann LD and Hamilton DA (1970) - Translocation of hydrophobic substances into soil by burning organic litter. Proceedings- Soil Science Society of America 34, 130– 133.

DeBano LF, Neary DG and Ffolliott PF (1998) - Fire's Effects on Ecosystems. New York: John Wiley & Sons, Inc.; p. 333.

DeBano LF (2000) - Water repellency in soils: a historical overview. Journal of Hydrology 231–232, 4–32.

DeBano LF (2000b) - The role of fire and soil heating on water repellency in wildland environments: a review. J. Hydrol. 231-232, 195–206.

DellaSala DA and Hanson CT (2015) - The Ecological Importance of Mixed-Severity Fires. Edited by Flannigan MD, Krawchuk MA, De Groot WJ, et al (2009) Implications of changing climate for global wildland fire. International Journal of Wildland Fire 18:483–507.

DiNenno PJ, Drysdale D, Beyler CL, Douglas Walton W, Custer RLP, Hall JR, John JR and Watts J (2002) - SFPE Handbook of Fire Protection Engineering. Third Edition, Philip J. DiNenno (ed) National Fire Protection Association, Inc. ISBN: 087765-451-4.

Dennison PE, Charoensiri K, Roberts DA, Peterson SH, Green RO (2006) - Wildfire temperature and land cover modeling using hyperspectral data. Remote Sensing of Environment 100, 212–222.

Dickinson MB and Johnson EA (2001) - Fire effects on trees. In 'Forest Fires: Behavior and Ecological Effects'. (Eds EA Johnson, K Miyanishi) pp. 477–525. (Academic Press: San Francisco, CA).

Doerr SH, Shakesby RA and Walsh RPD (2000) - Soil water repellency: its causes, characteristics and hydro-geomorphological significance. Earth-Sci. Rev. 51, 33–65.

Doerr SH, Blake WH, Shakesby RA, Stagnitti F, Vuurens SH, Humphreys GS and Wallbrink, PJ (2004) - Heating effects on water repellency in Australian eucalypt forest soils and their value in estimating wildfire soil temperatures. Int. J.Wildland Fire 13, 157–163.

Doerr SH, Shakesby RA, Blake WH, Chafer CJ, Humphreys GS and Wallbrink PJ (2006) - Effects of differing wildfire severities on soil wettability and implications for hydrological response. Journal of Hydrology 319, 295–311.

Doerr SH and Santın C (2016) - Global trends in wildfire and its impacts: perceptions versus realities in a changing world. Phil. Trans. R. Soc. B 371: 20150345.

Dupire S, Curt T, Bigot S and Fréjaville T (2019) - Vulnerability of forest ecosystems to fire in the French Alps. European Journal of Forest Research (2019) 138:813–830.

Durgin PB (1985) - Burning changes the erodibility in forests soils. J. Soil Water Conserv. 40, 299–301.

Efthimiou N, Psomiadis E and Panagos P (2020) - Fire severity and soil erosion susceptibility mapping using multi-temporal Earth Observation data: The case of Mati fatal wildfire in Eastern Attica, Greece. Catena 187 (2020) 104320.

Epting J, Verbyla D and Sorbel B (2005) - Evaluation of remotely sensed indices for assessing burn severity in interior Alaska using Landsat TM and ETM+. Remote Sensing of Environment 96, 328–339.

Etiégni L and Campbell AG (1991) - Physical and chemical characteristics of wood ash. Bioresour. Technol. 37:173–178.

Flannigan M, Krawchuk M, de Groot W, Wotton B and Gowman L (2009) - Implications of changing climate for global wildland fire. Int. J. Wildl. Fire 18, 483–507.

Foltz RB, Robichaud PR and Rhee H (2009) - A synthesis of post-fire road treatments for BAER teams: methods, treatment effectiveness, and decision making tools for rehabilitation. Gen. Tech. Rep. RMRS-GTR-228, Rocky Mountain Research Station, USDA Forest Service, Fort Collins, CO, USA, pp. 152.

Foster GR, Toy TJ and Renard KG (2003) - Comparison of the USLE, RUSLE1.06c, and RUSLE2 for application to highly disturbed lands. Proceedings of the First Interagency Conference on Research in the Watersheds. USDA—Agricultural Research Service, Washington, DC, pp. 154–160.

Gasco I, Gattiglio M and Borghi A (2011) - Lithostratigraphic setting and P-T metamorphic evolution for the Dora Maira Massif along the Piedmont Zone boundary (middle Susa Valley, NW Alps). Int J Earth Sci 100:1065–1085.

Gehring E, Conedera M, Maringer J, Giadrossich F, Guastini E and Schwarz M (2019) - Shallow landslide disposition in burnt European beech (Fagus sylvatica L.) forests. Scientific Reports 9, 8538.

Georg J, Spessa A, Van Der Werf GR and Thonicke K (2013) - Vegetation Fires and Global Change – Challenges for Concerted International Action. Kessel Publishing House Eifelweg 37 53424 Remagen-Oberwinter Germany.

Giampani C, Girelli C, Marco F, Moletta G, Bellardone G (2013) - Inventario Dei Conoidi Alluvionali In Piemonte, Attivita' B4 – C4 – Piene E Lave Torrentizie, Progetto Strategico Tranfrontaliero Risknat. Arpa Piemonte, Regione Piemonte.

Giglio L, Randerson JT and Van Der Werf GR (2013) - Analysis of daily, monthly, and annual burned area using the fourth-generation global fire emissions database (GFED4). J. Geophys. Res. Biogeosci. 118, 317–328.

Giovannini G (1994) - The effect of fire on soil quality. In: Sala, M., Rubio, J.L. (Eds.), Soil Erosion as a Consequence of Forest Fires. Geoforma Ediciones, Logrono, Spain, pp. 15– 27.

Giovannini G and Lucchesi S (1983) - Effect of fire on hydrophobic and cementing substances of soil aggregates. Soil Science 136, 231–236.

Giovannini G, Lucchesi S and Giachetti M (1988) - Effects of heating on some physical and chemical parameters related to soil aggregation and erodibility. Soil Sei 146:255-261.

Goldammer J., Mitsopoulos I, Mallinis G, Woolf M (2017) - Words into action guidelines: National disaster risk assessment - UNISDR.

González-Pelayo O, Andreu V, Campo J, Gimeno-García E and Rubio JL (2006) - Hydrological properties of a Mediterranean soil burned with different fire intensities. Catena 68, 186–193.

Gravelius H (1914) -Grundrifi der gesamten Gewcisserkunde. Band I: Flufikunde (Compendium of Hydrology, vol. I. Rivers, in German). Germany: Goschen, Berlin.

Guerrero C, Mataix-Solera J, Garcia-Orenes F, Gomez I and Navarro-Pedreno J (2001) - Different patterns of aggregate stability in burned and restored soils. Arid Land Resour Manag 15:163–171.

Guilinger JJ, Gray AB, Barth NC and Fong BT (2020) - The evolution of sediment sources over a sequence of postfire sediment-laden flows revealed through repeat high-resolution change detection. Journal of Geophysical Research: Earth Surface, 125, e2020JF005527.

Hammill KA and Bradstock RA (2006) - Remote sensing of fire severity in the Blue Mountains: influence of vegetation type and inferring fire intensity. International Journal of Wildland Fire 15, 213–226. doi:10.1071/ WF05051.

Hanshaw MN, Schmidt KM and Stock JD (2009) - The role of vegetation canopy removal on post-fire debris-flow rainfall intensity-duration thresholds. Geol Soc Abs Pro.

Horton RE (1932) - Drainage-basin characteristics, Eos, Transactions American Geophysical Union; 13: 350-361.

Hubbert KR, Wohlgemuth PM, Preisler HK and Graham RC (2002) - Effects of prescribed burning on selected soil properties in steep chaparral, southern California. Geol Soc Abs Pro.

Hubbert KR, Preisler HK, Wohlgemuth PM, Graham RC and Narog MG (2006) - Prescribed burning effects on soil physical properties and soil water repellency in a steep chaparral watershed, southern California, USA. Geoderma 130, 284–298.

Hungr O, Leroueil S and Picarelli L (2014) - The Varnes classification of landslide types, an update. Landslides 11, 167–194.

Hutchinson JN (1988) - General Report: Morphological and geotechnical parameters of landslides in relation to geology and hydrogeology. Proceedings, Fifth International Symposium on Landslides (Ed: Bonnard, C.), 1, 3-35. Rotterdam: Balkema.

IEEE 442 (1981) - IEEE Guide for Soil Thermal Resistivity Measurements. C25W/P442_WG—Working Group for Guide for Soil Thermal Resistivity Measurements—IEEE 442 1981.

Jain T, Pilliod D and Graham R (2004) - Tongue-tied. Wildfire 4, 22–36.

Jenson SK and Domingue JO (1988) - Extracting Topographic Structure from Digital Elevation Data for Geographic Information System Analysis. Photogrammetric Engineering and Remote Sensing 54 (11): 1593–1600.

Keeley JE (2009) - Fire intensity, fire severity and burn severity: A brief review and suggested usage. International Journal of Wildland Fire. 18, 116–126. DOI: 10.1071/WF07049.

Ketterings QM, Bigham JM and Laperche V (2000) - Changes in soil mineralogy and texture caused by slash-and-burn fires in Sumatra, Indonesia. Soil Sei Soc Am J 64:1108-1117.

Key (2006) - Ecological and sampling constraints on defining landscape fire severity Fire Ecology, Vol. 2, No. 2, 2006.

Key CH and Benson NC (2006) - Landscape Assessment (LA). In 'FIREMON: Fire Effects Monitoring and Inventory System'. (Eds DC Lutes, RE Keane, JF Caratti, CH Key, NC Benson, S Sutherland, LJ Gangi) USDA Forest Service, Rocky Mountain Research Station, General Technical Report RMRS-GTR-164-CD, p. LA-1-55. (Fort Collins, CO).

Kinnell PIA, CJ Chartres and CL Watson (1990) - The effects of fire on the soil in a degraded semi-arid woodland: II. Susceptibility of the soil to erosion by shallow rain-impacted flow. Aust. J. Soil Res. 28:779–794.

Kirpich ZP (1940) - Time of concentration of small agricultural watersheds. Civil Engineering, 10 (6), 362.

Ice GG, Neary DG and Adams PW (2004) - Effects of wildfire on soils and watershed processes. Journal of Forestry 102, 16–20.

Kluitenberg GJ, Ham JM and Bristow KL (1993) - Error analysis of the heat pulse method for measuring soil volumetric heat capacity. Soil Sci Soc Am J. 57: 1444–1451.

Kreith F and Black WZ (1980) - Basic Heat Transfer. New York, NY: Harpers and RowPubl.

Larsen IJ, MacDonald LH, Brown E, Rough D, Welsh MJ, Pietraszek JH, Libohova Z, Benavides-Solorio JdD and Schaffrath K (2009) - Causes of post-fire runoff and erosion: water repellency, cover, or soil sealing? Soil Sci. Soc. Am. J. 73, 1393–1407.

Larson AJ and Franklin JF (2005) - Patterns of conifer tree regeneration following an autumn wildfire event in the western Oregon Cascade Range, USA. Forest Ecology and Management 218, 25–36.

Le houerou HN (1992) - Vegetation and land-use in the Mediterranean Basin by the year 2050: A prospecive study. In: L. Jeeftic, Milliman JD, Sestini G (eds) Climate Change and the Mediterranean-Environmental and Societal Impacts of Climatic change and Sea-level Rise in the Mediterranean Region. Edward Arnold, London, pp 175–232.

Leopardi M and Scorzini AR (2015) - Effects of wildfires on peak discharges in watersheds. iForest 8: 302-307.

Lewis SA, Wu JQ and Robichaud PR (2006) - Assessing burn severity and comparing soil water repellency, Hayman Fire, Colorado. Hydrological Processes 20, 1–16.

Liu Y, Stanturf J and Goodrick S (2010) - Trends in global wildfire potential in a changing climate. Forest Ecology and Management 259:685–697.

Loaiciga HA, Pederos D and Roberts D (2001) - Wildfire-stream flow interactions in a chaparral watershed. Adv Environ Res 5:295–305.

Mallik AU, Gimingham C and Rahman AA (1984) - Ecological effects of heather burning: I. Water infiltration, moisture retention, and porosity of surface soil. J. Ecol. 72:767–776.

Marchi L, Pasuto A and Tecca PR (1993) - Flow processes on alluvial fans in the Eastern Italian Alps. Zeitschrift für Geomorphologie, 37(4), 447-458.

Marchi L and Brochot S (2000) - Les cônes de déjection torrentiels dans les Alpes françaises, morphométrie et processus de transport solide torrentiel. Journal of Alpine Research | Revue de géographie alpine, Vol n°88-3, pp. 23-38.

Maringer J, Ascoli D, Dorren L, Bebi P and Conedera M (2016) - Temporal trends in the protective capacity of burnt beech forests (Fagus sylvatica L.) against rockfall. European Journal of Forest Research, 135(4), 657-673.

Marquardt DW (1963) - An algorithm for least-squares estimation of nonlinear parameters J. Soc. Indust. Appl. Math. 11:431-441.

Mataix-Solera J and Doerr SH (2004) - Hydrophobicity and aggregate stability in calcareous topsoils from fire-affected pine forests in south-eastern Spain. Geoderma 118, 77–88.

Mataix-Solera J, Cerdà A, Arcenegui V, Jordán A and Zavala LM (2011) - Fire effects on soil aggregation: A review.Earth-Sci. Rev.2011,109, 44–60.

May CL and Gresswell RE (2003) - Processes and rates of sediment and wood accumulation in headwater streams of the Oregon Coast Range, USA. Earth Surf Proc Landf 28:409–424.

McCaw WL, Smith RH and Neal JE (1997) - Prescribed burning of thinning slash in regrowth stands of karri (Eucalyptus diversicolor). 1. Fire characteristics, fuel consumption and tree damage. International Journal of Wildland Fire 7, 29–40.

McCuen RH (2009) - Uncertainty analyses of watershed time parameters. Journal of Hydrologic Engineering, 14 (5), 490–498.

Megahan WF (1983) - Hydrologic effects of clearcutting and wildfire on steep granitic slopes in Idaho. Water Resou Res 19:811–819.

Melton MA (1965) - The geomorphic and paleoclimatic significance of alluvial deposits in Southern Arizona. J. Geol. 73:1-38.

Meyer GA and Wells SG (1997) - Fire-related sedimentation events on alluvial fans, Yellowstone National Park, USA. J Sed Res 67:776–791.

Meyer GA, Pierce JL, Wood SH and Jull AJT (2001) - Fire, storms, and erosional events in the Idaho batholith. Hydrol Process 15:3025–3038.

Midttømme K and Roaldset E (1998) - The effect of grain size on thermal conductivity of quartz sands and silts. Petrol. Geosci. 4: 165–172.

Miller VC A (1953) - Quantitative geomorphic study of drainage basin characteristics in the Clinch Mountain area Virginia and Tennessee. Columbia Univ. Tech Rept. N. 3, Contract N6 ONR 271-30.

Miller JD and Yool SR (2002) - Mapping forest post-fire canopy consumption in several overstory types using multi-temporal Landsat TM and ETM data. Remote Sensing of Environment 82, 481–496. doi:10.1016/S0034- 4257(02)00071-8.

Miller JD, Nyhan JW and Yool SR (2003) - Modeling potential erosion due to the Cerro Grande fire with a GIS-based implementation of the Revised Universal Soil Loss Equation. International Journal of Wildland Fire 12, 85–100.

Miller JD and Thode AE (2007) - Quantifying burn severity in a heterogeneous landscape with a relative version of the delta Normalized Burn Ratio (dNBR). Remote Sens. Environ. 2007, 109, 66–80.

Miller JD, Knapp EE, Key CH, Skinner CN, Isbell CJ, Creasy RM and Sherlock JW (2009) - Calibration and validation of the relative differenced Normalized Burn Ratio (RdNBR) to three measures of fire severity in the Sierra Nevada and Klamath Mountains, California, USA. Remote Sens. Environ. 2009, 113, 645–656.

Mitasova H, Hofierka J, Zlocha M and Iverson LR (1996) - Modeling topographic potential for erosion and deposition using GIS. International Journal of Geographical Information Science 10 (5), 629–641.

Moody JA and Martin PA (2001) - Initial hydrologic and geomorphic response following a wildfire in the Colorado front range. Earth Surface Processes and Landforms 26, 1049–1070.

Moody JA and Martin DA (2009) - Synthesis of sediment yields after wildland fire in different rainfall regimes in the western Unites States. Int J Wildl Fire 18:96–115.

Moreira F, Viedma O, Arianoutsou M, Curt T, Koutsias N, Rigolot E, Barbati A, Corona P, Vaz P, Xanthopoulos G, Mouillot F and Bilgili E (2011) - Landscape - wildfire interactions in southern Europe: Implications for landscape management. Journal of Environmental Management 92:2389–2402.

Moreno JM and Oechel WC (1989) - A simple method for estimating fire intensity after a burn in California chaparral. Acta Oecologica 10, 57–68.

Morin J and Benyamini Y. (1977) - Rainfall infiltration into bare soils. Water Resour. Res. 13:813–817.

Morresi D, Marzano R, Lingua E, Motta R and Garbarino M. (2021) - Mapping burn severity in the western Italian Alps through phenologically coherent reflectance composites derived from Sentinel-2 imagery. Remote Sensing of Environment, submitted for publication.

Morton DM (1989) - Distribution and frequency of storm-generated soil slips on burned and unburned slopes, San Timoteo Badlands, Southern California. In: Sadler PM, Morton DM (eds.), Landslides in a semiarid environment with emphasis on the Inland valleys of Southern California. Publications of the Inland Geological Society 2, pp 279–284.

Moss AJ and Watson CL. (1991) - Rain-impact soil crust: III. Eff ects of continuous and fl awed crusts on infi ltration, and the ability of plant covers to maintain crustal fl aws. Aust. J. Soil Res. 29:311–330.

Mouillot F, Ratte JP, Joffre R Mouillot D and Rambal S (2005) - Long-term forest dynamic after land abandonment in a fire prone Mediterranean landscape (central Corsica, France). Landscape Ecology 20:101–112.

Müller MM, Vilà-Vilardell L and Vacik H (2020) - Forest fires in the Alps – State of knowledge, future challenges and options for an integrated fire management. EUSALP Action Group 8.

Nearing MA, Jetten V, Baffaut C, Cerda O, Couturier A, Hernandez M, Le Bissonnais Y, Nichols MH, Nunes JP, Renschler CS, Souchère V and van Oost K (2005) - Modeling response of soil erosion and runoff to changes in precipitation and cover. Catena 61, 131–154.

Neary DG, Klopatek CC, DeBano LF and Ffolliott PF (1999) - Fire effects on belowground sustainability: a review and synthesis. Forest Ecology and Management 122, 51–71.

Neary DG, Ryan KC and DeBano LF (2005) - Wildland Fire in Ecosystems: Effects of Fire on Soil and Water. General Technical Report RMRSGTR- 42 Volume 4. Ogden, UT: U.S. Department of Agriculture, Forest Service, Rocky Mountain Research Station; 2005. p. 250.

Neary DG and Leonard JM (2019) - Physical Vulnerabilities from Wildfires: Flames, Floods, and Debris Flows. Natural Resources Management and Biological Sciences [Working Title] 1–17.

Neary DG and Leonard JM (2020) - Effects of Fire on Grassland Soils and Water: A Review. in: Kindomihou, Valentin Missiako, ed. Grasses and grassland aspects. IntechOpen.

NWCG (2006) - Glossary of wildland fire terminology. National Wildfire Coordinating Group, Incident Operations Standards Working Team.

Panagos P, Ballabio C, Borrelli P, Meusburger K, Klik A, Rousseva S, Tadic MP, Michaelides S, Hrabalíková M, Olsen P, Aalto J, Lakatos M, Rymszewicz A, Dumitrescu A, Beguería S and Alewell, C. (2015a) - Rainfall erosivity in Europe. Sci Total Environ. 511, pp. 801-814.

Panagos P, Borrelli P, Meusburger K, Alewell C, Lugato E, Montanarella L (2015b) - Estimating the soil erosion cover-management factor at the European scale. Land Use Policy 48 (2015) 38–50.

Parise M and Cannon SH (2008) - The effects of wildfires on erosion and debris-flow generation in Mediterranean climatic areas: a first database. Proceedings of 1st World Landslide Forum. Tokyo, Japan, pp 465–468.

Parise M and Cannon SH (2012) - Wildfire Impacts on the Processes that Generate Debris Flows in Burned Watersheds: Natural Hazards, v. 61.

Parson A, Robichaud P R, Lewis SA, Napper C and Clark JT (2010) - Field guide for mapping post-fire soil burn severity. Gen. Tech. Rep. RMRS-GTR-243. Fort Collins, CO: U.S. Department of Agriculture, Forest Service, Rocky Mountain Research Station. 49 p.

Parsons A (2003) - Burned Area Emergency Rehabilitation (BAER) soil burn severity definitions and mapping guidelines. Draft. USDA Forest Service, Rocky Mountain Research Station. (Missoula, MT).

Pereira P, Cerdà A, Úbeda X, Mataix-Solera J, Arcenegui V and Zavala LM (2013) - Modelling the impacts of wildfire on ash thickness in a short-term period. Land Degrad. Dev.

Pasquale V, Verdoya M, Chiozzi P (2015) - Measurements of rock thermal conductivity with a Transient Divided Bar. Geothermics 2015, 53, 183–189.

Pezzatti GB, Zumbrunnen T, Bürgi M, Ambrosetti P and Conedera M (2013) - Fire regime shifts as a consequence of fire policy and socio-economic development: an analysis based on the change point approach. Forest Policy and Economics, 29, 7-18.

Piana F, Fioraso G, Irace A, Mosca P, d'Atri A, Barale L, Falletti P, Monegato G, Morelli M, Tallone S and Vigna GB (2017) - Geology of Piemonte region (NW Italy, Alps–Apennines interference zone), Journal of Maps, 13:2, 395-405.

Poesen J (1986) - Surface sealing as infl uenced by slope angle and position of simulated stones in the top layer of loose sediments. Earth Surf. Processes Landforms 11:1–10.

Pollen N and Simon A (2005) - Estimating the mechanical effects of riparian vegetation on stream bank stability using a fiber bundle model, Water Resour. Res., 41, W07025.

Ravi S, D'Odorico P, Zobeck TM and Over TM (2009) - The effect of fire-induced soil hydrophobicity on wind erosion in a semiarid grassland: Experimental observations and theoretical framework. Geomorphology. 2009; 105:80-86.

Regione Piemonte (2010) - Land Cover Piemonte: Classificazione uso del suolo 2010 (vettoriale) – storico. Available at http://www.geoportale.piemonte.it/geocatalogorp/.

Regione Piemonte (2012) - Valutazione del rischio delle principali conoidi alluvionali in Piemonte-relazione illustrativa. Progetto Strategico Tranfrontaliero Risknat. Attivita' b4 – c4 – piene e lave torrentizie. http://www.risknet-alcotra.org/rna/allegati/conoidi-regione-pericolosita-afhe-rischio-918_918.pdf.

Renard KG, Foster GR, Weesies GA, McCool DK and Yoder DC (1997) - Predicting Soil Erosion by Water: A Guide to Conservation Planning with the Revised Universal Soil Loss Equation (RUSLE) (Agricultural Handbook 703). US Department of Agriculture, Washington, DC, p. 404.

Rengers FK, McGuire LA, Oakley NS, Kean JW, Staley DM and Tang H (2020) - Landslides after wildfire: initiation, magnitude, and mobility. Landslides (2020) 17:2631–2641. DOI 10.1007/s10346-020-01506-3.

Robichaud PR, Beyers JL and Neary DG (2000) - Evaluating the effectiveness of post-fire rehabilitation treatments. USDA Forest Service, Rocky Mountain Research Station, General Technical Report RMRS-GTR-63. (Ogden, UT).

Robichaud PR, Lewis SA, Laes DYM, Hudak AT, Kodaly RF and Zamudio JA (2007) - Post-fire soil burn severity mapping with hyperspectral image unmixing. Remote Sensing of Environment 108(4), 467–480.

Rogan J and Franklin J (2001) - Mapping wildfire burn severity in southern California forests and shrublands using Enhanced Thematic Mapper imagery. Geocarto International 16(4), 91–106.

Roldán-Zamarrón A, Merino-de-Miguel S, González-Alonso F, García- Gigorro S and Cuevas JM (2006) - Minas de Riotinto (south Spain) forest fire: Burned area assessment and fire severity mapping using Landsat 5-TM, Envisat-MERIS, and Terra-Modis post-fire images. Journal of Geophysical Research – Biogeosciences 111.

Ruan H, Ahuja LR, Green TR and Benjamin JG (2001) - Residue cover and surface sealing eff ects on infi ltration: Numerical simulations for fi eld applications. Soil Sci. Soc. Am. J. 65:853–861.

Ruiz-Gallardo JR, Castano S and Calera A (2004) - Application of remote sensing and GIS to locate priority intervention areas after wildland fires in Mediterranean systems: a case study from south-eastern Spain. International Journal ofWildland Fire 13, 241–252.

Ryan KC (2002) - Dynamic interactions between forest structure and fire behavior in boreal ecosystems. Silva Fennica 36, 13–39.

Ryan KC and Noste NV (1985) - Evaluating prescribed fires. In 'Proceedings, Symposium and Workshop on Wilderness Fire', 15–18 November 1983, Missoula, MT. (Eds JE Lotan, BM Kilgore, WC Fischer, RW Mutch) USDA Forest Service, Intermountain Forest and Range Experiment Station, General Technical Report INT-182, pp. 230–238. (Missoula, MT).

Sanchez-Castillo L, Kubota T, Cantu-Silva I, Yanez-Diaz M, Hasnawi R and Pequeno-Ledezma M (2017) - Comparisons of the Root Mechanical Properties of three Native Mexican Tree Species for Soil Bioengineering Practices. Botanical Sciences, 95(2), 259269.

Sankey JB, Kreitler J, Hawbaker TJ, McVay JL, Miller ME, Mueller ER, Vaillant NM, Lowe SE and Sankey TT (2017) - Climate, wildfire, and erosion ensemble foretells more sediment in western USA watersheds, Geophys. Res. Lett., 44, 8884–8892.

San-Miguel-Ayanz J and Camia A (2009) - Forest fires at a glance: facts, figures and trends in the EU. In: Yves Birot, editor. Living with Wildfires: What Science Can Tell Us. A Contribution to the Science-Policy Dialogue. Joensuu (Finland): European Forest Institute; 2009. p. 11-18. JRC5514.

San-Miguel-Ayanz J, Schulte E, Schmuck G, Camia A, Strobl P, Liberta G, Giovando C, Boca R, Sedano F, Kempeneers P, McInerney D, Withmore C, Santos de Oliveira S, Rodrigues M, Durrant T, Corti P, Oehler F, Vilar L and Amatulli G (2012) - Comprehensive Monitoring of Wildfires in Europe: The European Forest Fire Information System (EFFIS), Approaches to Managing Disaster - Assessing Hazards, Emergencies and Disaster Impacts, Prof. John Tiefenbacher (Ed.), ISBN: 978-953-51-0294-6.

San-Miguel-Ayanz J, Durrant T, Boca R, Maianti P, Libertà G, Artés-Vivancos T, Oom D, Branco A, de Rigo D, Ferrari D, Pfeiffer H, Grecchi R, Nuijten D, Leray T (2020) – Forest fires in Europe, Middle East and North Africa 2019, EUR 30402 EN, Publications Office of the European Union, Luxembourg, 2020, ISBN 978-92-76-23209-4, doi:10.2760/468688, JRC122115.

Santi PM, deWolfe VG, Higgins JD, Cannon SH and Gartner JE (2008) - Sources of debris flow material in burned areas. Geomorphology 96:310–321.

Schmidt MWI and Noack AG (2000) - Black carbon in soils and sediments: Analysis , distribution , implications , and current challenges. 14:777–793.

Schumm SA (1956) - Evolution of drainage systems and slopes in badlands at Perth Amboy. New Jersey, Geological society of America bulletin 1956; 67: 597-646.

Schwarz MA, Cohen RD, Giadrossich F, Egorov P, Stolz BD and M Thormann JJ (2015) - Root reinforcement of soils under compression. J. Geophys. Res. F Earth Surf. 120, 2103–2120.

SCS-USDA - Soil Conservation Service, United States Department of Agriculture (1986) - Urban Hydrology for Small Watersheds. Washington, D. C.: U. S. Government Printing Office.

Shakesby RA, Wallbrink PJ, Doerr SH, English PM, Chafer C, Humphreys GS, Blake WH and Tomkins KM (2007) - Distinctiveness of wildfire effects on soil erosion in south-east Australian eucalypt forests assessed in a global context. For. Ecol. Manag. 238, 347–364.

Shakesby RA and Doerr SH (2006) - Wildfire as a hydrological and geomorphological agent. Earth-Science Reviews 74:269–307.

Simard AJ (1991) - Fire severity, changing scales, and how things hang together. International Journal of Wildland Fire 1, 23–34.

Simon A and Collison AJC (2002) - Quantifying the mechanical and hydrologic effects of riparian vegetation on streambank stability, Earth Surf. Processes Landforms, 27, 527– 546.

Smith HG, Sheridan GJ, Nyman P, Child DP, Lane PNJ, Hotchkis MAC and Jacobsen GE (2012) - Quantifying sources of fine sediment supplied to post-fire debris flows using fallout radionuclide tracers. Geomorphology 139–140, 403–415.

Smith H, Cawson J, Sheridan G and Lane P (2011) - Desktop review–Impact of bushfires on water quality. Report for the Government Department of Sustainability, Environment, Water, Population and Communities, 18th March 2011.

Smits KM, Kirby E, Massman WJ and Baggett LS (2016) - Experimental and modeling study of forest fire effect on soil thermal conductivity. Pedosphere. 26(4): 462–473.

Stoof CR, Moore D, Ritsema CJ and Dekker LW (2011) - Natural and fire-induced soil water repellency in a Portuguese shrubland. Soil Sci. Soc. Am. J. 75 (6), 2283–2295.

Strahler AN (1957) - Quantitative analysis of watershed geomorphology. Eos, Transactions American Geophysical Union, 38, 913-920.

Strahler AN (1964) - Quantitative geomorphology of drainage basin and channel networks, Handbook of applied hydrology.

Stronach NH and McNaughton SJ (1989) - Grassland fire dynamics in the Serengeti ecosystem, and a potential method of retrospectively estimating fire energy. Journal of Applied Ecology 26, 1025–1033.

Swanson FJ (1981) - Fire and geomorphic processes. In: Mooney HA, Bonniksen TH, Christensen NL, Lotan JE, Reiners WA (eds.) Fire regimes and ecosystem properties. US Department of Agriculture, Forest Service general technical report WO-26, pp 401–420.

Tecle A and Neary D (2015) - Water Quality Impacts of Forest Fires. Journal of Pollution Effects and Control. 3:2.

Terranova O, Antronico L, Coscarelli R and Iaquinta P (2009) - Soil erosion risk scenarios in the Mediterranean environment using RUSLE and GIS:An application model for Calabria (southern Italy). Geomorphology 112 (2009) 228–245.

Thorne CR (1990) - Effects of vegetation on riverbank erosion and stability, in Vegetation and Erosion, edited by J. B. Thornes, pp. 125– 144, John Wiley, Hoboken, N. J.

Tolhurst KG (1995) - Fire from a flora, fauna and soil perspective: sensible heat measurement. CALM Science 4(Suppl.), 45–88.

Turner MG, Hargrove WW, Gardner RH and Romme WH (1994) - Effects of fire on landscape heterogeneity inYellowstone National Park,Wyoming. Journal of Vegetation Science 5, 731–742.

Úbeda X and Outeiro L (2009) - Physical and chemical effects of fire on soil. In: Cerdà, A., Robichaud, P.R. (Eds.), Fire Effects on Soils and Restoration Strategies. Science Publishers, Enfield, NH, pp. 105–133.

USDA – NRCS (1999) - Soil Taxonomy, 2nd Edition. Agricultural Handbook n. 436, 1999.

USDA (2014) - United States Department of Agriculture. Rainfall Intensity Summarization Tool (RIST). Accessed from, http://www.ars.usda.gov.

Vacchiano G, Foderi C, Berretti R, Marchi E and Motta R (2018) - Modeling anthropogenic and natural fire ignitions in an inner-alpine valley. Natural Hazards and Earth System Sciences, 18, 935–948.

Vadilonga T, Ubeda X, Germann PF and Lorca M (2008) - Effects of prescribed burnings on soil hydrological parameters. Hydrol. Process. 22, 4249–4256.

Van Wagner CE (1973) - Height of crown scorch in forest fires. Canadian Journal of Forest Research 3, 373–378.

Van Lierop P, Lindquist E, Sathyapala S and Franceschini G (2015) - Global forest area disturbance from fire, insect pests, diseases and severe weather events. For. Ecol. Manage. 352, 78–88.

Van Wagtendonk JW, Root RR and Key CH (2004) - Comparison of AVIRIS and Landsat ETM+ detection capabilities for burn severity. Remote Sensing of Environment 92, 397–408.

Varnes DJ (1978) - Slope movement types and processes. In: Special Report 176: Landslides: Analysis and Control (Eds: Schuster, R. L. & Krizek, R. J.). Transportation and Road Research Board, National Academy of Science, Washington D. C., 11-33.

Wade DD (1993) - Thinning young loblolly pine stands with fire. International Journal of Wildland Fire 3, 169–178.

Wastl C, Schunk C, Leuchner M, Pezzatti B and Menzel A (2012) - Recent climate change: Long-term trends in meteorological forest fire danger in the Alps. Agricultural and Forest Meteorology 162–163:1–13.

Wells CG, DeBano LF, Lewis CE, Fredriksen RL, Franklin EC, Froelich RC and Dunn PH (1979) - Effects of fire on soil. A state-of-knowledge review. USDA Forest Service, General Technical Report WO-7. (Washington, DC)

Wischmeier WH and Smith DD (1978) - Predicting rainfall erosion losses: a guide to conservation planning. Agriculture Handbook no. 537, USDA, Washington DC, USA, pp. 13-27.

White PS and Pickett STA (1985) - Natural disturbance and patch dynamics: an introduction. In 'The Ecology of Natural Disturbance and Patch Dynamics'. (Eds STA Pickett, PS White) pp. 1–13. (Academic Press: San Diego, CA).

White JD, Ryan KC, Key CC and Running SW (1996) - Remote sensing of forest fire severity and vegetation recovery. International Journal of Wildland Fire 6, 125–136.

Wright HA, Churchill FM and Stevens WC (1976) - Effect of prescribed burning on sediment, water yield, and water quality from juniper lands in Central Texas. Journal of Range Management; 29:294-298.

Williams RJ, Gill AM and Moore PHR (1998) - Seasonal changes in fire behaviour in a tropical savanna in northern Australia. International Journal of Wildland Fire 8, 227–239.

Wilson CJ, Carey JW, Beeson PC, Gard MO and Lane LJ (2001) - A GIS-based hillslope erosion and sediment delivery model and its application in the Cerro Grande burn area. Hydrological Processes 15, 2995–3010.

Woods SW and Balfour VN (2008) - The effect of ash on runoff and erosion after a severe forest fire, Montana, USA. Int J Wildl Fire 17:535–548.

Wooster MJ, Zhukov B and Oertel D (2003) - Fire radiative energy for quantitative study of biomass burning: derivation from the BIRD experimental satellite and comparison to MODIS fire products. Remote Sensing of Environment 86, 83–107.

Wondzell SM and King JG (2003) - Post-fire erosional processes in the Pacific Northwest and Rocky Mountains Regions. For Ecol Manag 178:75–87.

Wu TH, McKinnell III WP and DN Swanston (1979) - Strength of tree roots and landslides on Prince of Wales Island, Alaska, Can. Geotech. J., 16, 19– 33.

Zumbrunnen T, Bugmann H, Conedera M and Bürgi M (2009) - Linking forest fire regimes and climate - A historical analysis in a dry inner Alpine valley. Ecosystems 12:73–86.

# Appendix 1

| Cover description: Cover type and hydrologic condition | Average percent impervious area [2] | Curve numbers for hydrologic soil group: A | B | C | D |
|---|---|---|---|---|---|
| *Fully developed urban areas (vegetation established)* | | | | | |
| Open space (lawns, parks, golf courses, cemeteries, etc.) [3]: | | | | | |
| Poor condition (grass cover < 50%) | | 68 | 79 | 86 | 89 |
| Fair condition (grass cover 50% to 75%) | | 49 | 69 | 79 | 84 |
| Good condition (grass cover > 75%) | | 39 | 61 | 74 | 80 |
| Impervious areas: | | | | | |
| Paved parking lots, roofs, driveways, etc. (excluding right-of-way) | | 98 | 98 | 98 | 98 |
| Streets and roads: | | | | | |
| Paved; curbs and storm sewers (excluding right-of-way) | | 98 | 98 | 98 | 98 |
| Paved; open ditches (including right-of-way) | | 83 | 89 | 92 | 93 |
| Gravel (including right-of-way) | | 76 | 85 | 89 | 91 |
| Dirt (including right-of-way) | | 72 | 82 | 87 | 89 |
| Western desert urban areas: | | | | | |
| Natural desert landscaping (pervious areas only) [4] | | 63 | 77 | 85 | 88 |
| Artificial desert landscaping (impervious weed barrier, desert shrub with 1- to 2-inch sand or gravel mulch and basin borders) | | 96 | 96 | 96 | 96 |
| Urban districts: | | | | | |
| Commercial and business | 85 | 89 | 92 | 94 | 95 |
| Industrial | 72 | 81 | 88 | 91 | 93 |
| Residential districts by average lot size: | | | | | |
| 1/8 acre or less (town houses) | 65 | 77 | 85 | 90 | 92 |
| 1/4 acre | 38 | 61 | 75 | 83 | 87 |
| 1/3 acre | 30 | 57 | 72 | 81 | 86 |
| 1/2 acre | 25 | 54 | 70 | 80 | 85 |
| 1 acre | 20 | 51 | 68 | 79 | 84 |
| 2 acres | 12 | 46 | 65 | 77 | 82 |
| *Developing urban areas* | | | | | |
| Newly graded areas (pervious areas only, no vegetation) [5] | | 77 | 86 | 91 | 94 |
| Idle lands (CN's are determined using cover types similar to those in table 2-2c). | | | | | |

[1] Average runoff condition, and $I_a = 0.2S$.

[2] The average percent impervious area shown was used to develop the composite CN's. Other assumptions are as follows: impervious areas are directly connected to the drainage system, impervious areas have a CN of 98, and pervious areas are considered equivalent to open space in good hydrologic condition. CN's for other combinations of conditions may be computed using figure 2-3 or 2-4.

[3] CN's shown are equivalent to those of pasture. Composite CN's may be computed for other combinations of open space cover type.

[4] Composite CN's for natural desert landscaping should be computed using figures 2-3 or 2-4 based on the impervious area percentage (CN = 98) and the pervious area CN. The pervious area CN's are assumed equivalent to desert shrub in poor hydrologic condition.

[5] Composite CN's to use for the design of temporary measures during grading and construction should be computed using figure 2-3 or 2-4 based on the degree of development (impervious area percentage) and the CN's for the newly graded pervious areas.

*Figure A1.1 - Runoff Curve Number for urban areas (SCS-USDA, 1986)*

| Cover description | | | Curve numbers for hydrologic soil group | | | |
|---|---|---|---|---|---|---|
| Cover type | Treatment [2] | Hydrologic condition [3] | A | B | C | D |
| Fallow | Bare soil | — | 77 | 86 | 91 | 94 |
| | Crop residue cover (CR) | Poor | 76 | 85 | 90 | 93 |
| | | Good | 74 | 83 | 88 | 90 |
| Row crops | Straight row (SR) | Poor | 72 | 81 | 88 | 91 |
| | | Good | 67 | 78 | 85 | 89 |
| | SR + CR | Poor | 71 | 80 | 87 | 90 |
| | | Good | 64 | 75 | 82 | 85 |
| | Contoured (C) | Poor | 70 | 79 | 84 | 88 |
| | | Good | 65 | 75 | 82 | 86 |
| | C + CR | Poor | 69 | 78 | 83 | 87 |
| | | Good | 64 | 74 | 81 | 85 |
| | Contoured & terraced (C&T) | Poor | 66 | 74 | 80 | 82 |
| | | Good | 62 | 71 | 78 | 81 |
| | C&T+ CR | Poor | 65 | 73 | 79 | 81 |
| | | Good | 61 | 70 | 77 | 80 |
| Small grain | SR | Poor | 65 | 76 | 84 | 88 |
| | | Good | 63 | 75 | 83 | 87 |
| | SR + CR | Poor | 64 | 75 | 83 | 86 |
| | | Good | 60 | 72 | 80 | 84 |
| | C | Poor | 63 | 74 | 82 | 85 |
| | | Good | 61 | 73 | 81 | 84 |
| | C + CR | Poor | 62 | 73 | 81 | 84 |
| | | Good | 60 | 72 | 80 | 83 |
| | C&T | Poor | 61 | 72 | 79 | 82 |
| | | Good | 59 | 70 | 78 | 81 |
| | C&T+ CR | Poor | 60 | 71 | 78 | 81 |
| | | Good | 58 | 69 | 77 | 80 |
| Close-seeded or broadcast legumes or rotation meadow | SR | Poor | 66 | 77 | 85 | 89 |
| | | Good | 58 | 72 | 81 | 85 |
| | C | Poor | 64 | 75 | 83 | 85 |
| | | Good | 55 | 69 | 78 | 83 |
| | C&T | Poor | 63 | 73 | 80 | 83 |
| | | Good | 51 | 67 | 76 | 80 |

[1] Average runoff condition, and $I_a$=0.2S

[2] Crop residue cover applies only if residue is on at least 5% of the surface throughout the year.

[3] Hydraulic condition is based on combination factors that affect infiltration and runoff, including (a) density and canopy of vegetative areas, (b) amount of year-round cover, (c) amount of grass or close-seeded legumes, (d) percent of residue cover on the land surface (good ≥ 20%), and (e) degree of surface roughness.

Poor: Factors impair infiltration and tend to increase runoff.

Good: Factors encourage average and better than average infiltration and tend to decrease runoff.

*Figure A1.2 - Runoff Curve Number for cultivated agricultural lands (SCS-USDA, 1986)*

| Cover description | | Curve numbers for hydrologic soil group | | | |
|---|---|---|---|---|---|
| Cover type | Hydrologic condition | A | B | C | D |
| Pasture, grassland, or range—continuous forage for grazing. [2] | Poor | 68 | 79 | 86 | 89 |
| | Fair | 49 | 69 | 79 | 84 |
| | Good | 39 | 61 | 74 | 80 |
| Meadow—continuous grass, protected from grazing and generally mowed for hay. | — | 30 | 58 | 71 | 78 |
| Brush—brush-weed-grass mixture with brush the major element. [3] | Poor | 48 | 67 | 77 | 83 |
| | Fair | 35 | 56 | 70 | 77 |
| | Good | 30 [4] | 48 | 65 | 73 |
| Woods—grass combination (orchard or tree farm). [5] | Poor | 57 | 73 | 82 | 86 |
| | Fair | 43 | 65 | 76 | 82 |
| | Good | 32 | 58 | 72 | 79 |
| Woods. [6] | Poor | 45 | 66 | 77 | 83 |
| | Fair | 36 | 60 | 73 | 79 |
| | Good | 30 [4] | 55 | 70 | 77 |
| Farmsteads—buildings, lanes, driveways, and surrounding lots. | — | 59 | 74 | 82 | 86 |

1 Average runoff condition, and $I_a = 0.2S$.
2 *Poor:* <50%) ground cover or heavily grazed with no mulch.
*Fair:* 50 to 75% ground cover and not heavily grazed.
*Good:* > 75% ground cover and lightly or only occasionally grazed.
3 *Poor:* <50% ground cover.
*Fair:* 50 to 75% ground cover.
*Good:* >75% ground cover.
4 Actual curve number is less than 30; use CN = 30 for runoff computations.
5 CN's shown were computed for areas with 50% woods and 50% grass (pasture) cover. Other combinations of conditions may be computed from the CN's for woods and pasture.
6 *Poor:* Forest litter, small trees, and brush are destroyed by heavy grazing or regular burning.
*Fair:* Woods are grazed but not burned, and some forest litter covers the soil.
*Good:* Woods are protected from grazing, and litter and brush adequately cover the soil.

*Figure A1.3 - Runoff Curve Number for other agricultural lands (SCS-USDA, 1986)*

| Cover description | | Curve numbers for hydrologic soil group | | | |
|---|---|---|---|---|---|
| Cover type | Hydrologic condition [2/] | A [3/] | B | C | D |
| Herbaceous—mixture of grass, weeds, and low-growing brush, with brush the minor element. | Poor | | 80 | 87 | 93 |
| | Fair | | 71 | 81 | 89 |
| | Good | | 62 | 74 | 85 |
| Oak-aspen—mountain brush mixture of oak brush, aspen, mountain mahogany, bitter brush, maple, and other brush. | Poor | | 66 | 74 | 79 |
| | Fair | | 48 | 57 | 63 |
| | Good | | 30 | 41 | 48 |
| Pinyon-juniper—pinyon, juniper, or both; grass understory. | Poor | | 75 | 85 | 89 |
| | Fair | | 58 | 73 | 80 |
| | Good | | 41 | 61 | 71 |
| Sagebrush with grass understory. | Poor | | 67 | 80 | 85 |
| | Fair | | 51 | 63 | 70 |
| | Good | | 35 | 47 | 55 |
| Desert shrub—major plants include saltbush, greasewood, creosotebush, blackbrush, bursage, palo verde, mesquite, and cactus. | Poor | 63 | 77 | 85 | 88 |
| | Fair | 55 | 72 | 81 | 86 |
| | Good | 49 | 68 | 79 | 84 |

1 Average runoff condition, and $I_a = 0.2S$. For range in humid regions, use table 2-2c.
2 Poor: <30% ground cover (litter, grass, and brush overstory).
Fair: 30 to 70% ground cover.
Good: > 70% ground cover.
3 Curve numbers for group A have been developed only for desert shrub.

*Figure A1.4 - Runoff Curve Number for arid and semiarid rangelands (SCS-USDA, 1986)*

# Appendix 2

*Table A2.1– Geometric parameters of watersheds interested by the Locana/Ribordone wildfire*

| **Fire n. 1** | **LOCANA/RIBORDONE** | | | | | | | | | | |
|---|---|---|---|---|---|---|---|---|---|---|---|
| **Watershed** | **Aw** | **P** | **Lb** | **Emin** | **Emax** | **Eran** | **Emean** | **Smin** | **Smax** | **Sran** | **Smea** |
| | [km²] | [km] | [km] | [m a.s.l.] | [m a.s.l.] | [m] | [m a.s.l.] | [°] | [°] | [°] | [°] |
| **Rio Fura** | 1.29 | 6.17 | 2.66 | 669 | 1978 | 1309 | 1414 | 0.74 | 73.10 | 72.36 | 35.54 |
| **Rio Di Chioso Bosco** | 0.75 | 3.99 | 1.58 | 602 | 1510 | 908 | 1210 | 1.85 | 75.50 | 73.65 | 34.65 |
| **R. Montepiano** | 0.30 | 2.87 | 1.11 | 703 | 1506 | 802 | 1100 | 2.08 | 58.86 | 56.78 | 35.47 |
| **Carlevaria** | 0.73 | 3.85 | 1.62 | 613 | 1615 | 1002 | 1199 | 1.74 | 73.65 | 71.91 | 41.07 |
| **Rio Di Bardonetto Inferiore** | 0.43 | 3.70 | 1.78 | 580 | 1593 | 1012 | 1153 | 2.65 | 72.36 | 69.71 | 36.64 |
| **Ribordone** | 36.00 | 26.44 | 11.94 | 587 | 2839 | 2251 | 1580 | 0.00 | 82.25 | 82.25 | 33.63 |
| **Eugio** | 16.07 | 21.46 | 10.04 | 741 | 3261 | 2520 | 2205 | 0.00 | 83.35 | 83.35 | 32.45 |
| **Rio Bocchetta** | 1.28 | 5.07 | 1.83 | 677 | 1815 | 1139 | 1340 | 0.66 | 78.29 | 77.63 | 37.77 |
| **Rio Di Calsazio** | 0.63 | 3.14 | 1.12 | 608 | 1457 | 849 | 1058 | 1.37 | 70.60 | 69.23 | 40.68 |
| **Locana Est** | 0.66 | 4.16 | 1.92 | 638 | 1817 | 1178 | 1280 | 3.59 | 83.16 | 79.57 | 39.38 |
| **Apparè** | 0.30 | 3.05 | 1.34 | 530 | 1391 | 861 | 894 | 0.25 | 66.11 | 65.86 | 37.01 |
| **Mean** | **5.31** | **7.63** | **3.36** | **631.64** | **1889.27** | **1257.36** | **1312.09** | **1.36** | **74.29** | **72.94** | **36.75** |

*Table A2.2 - Geometric parameters of watersheds interested by the Bussoleno/Mompantero wildfire*

| **Fire n. 2** | **BUSSOLENO/MOMPANTERO** | | | | | | | | | | |
|---|---|---|---|---|---|---|---|---|---|---|---|
| **Watershed** | **Aw** | **P** | **Lb** | **Emin** | **Emax** | **Eran** | **Emean** | **Smin** | **Smax** | **Sran** | **Smea** |
| | [km²] | [km] | [km] | [m a.s.l.] | [m a.s.l.] | [m] | [m a.s.l.] | [°] | [°] | [°] | [°] |
| **Crosiglione** | 4.51 | 10.85 | 3.42 | 823 | 3051 | 2228 | 1790 | 0.06 | 79.16 | 79.10 | 32.93 |
| **Rio Della Ravoire** | 0.58 | 4.59 | 1.40 | 556 | 1670 | 1114 | 1272 | 3.61 | 62.88 | 59.27 | 28.26 |
| **Fogasso** | 1.90 | 7.36 | 3.22 | 526 | 1977 | 1451 | 1448 | 1.96 | 68.55 | 66.58 | 27.47 |
| **Rio Della Codrea** | 0.90 | 5.68 | 2.16 | 549 | 1778 | 1229 | 1313 | 1.81 | 64.48 | 62.67 | 28.89 |
| **Trinitâ** | 0.38 | 4.00 | 1.23 | 526 | 1600 | 1074 | 1076 | 8.57 | 68.22 | 59.65 | 29.25 |
| **Rio Prebech** | 10.41 | 15.10 | 5.99 | 556 | 2661 | 2106 | 1560 | 0.37 | 80.63 | 80.26 | 34.69 |
| **Moletta** | 6.54 | 12.94 | 5.10 | 524 | 2965 | 2441 | 1693 | 0.45 | 85.81 | 85.36 | 40.65 |
| **Rio Di Periere** | 0.68 | 5.84 | 2.56 | 528 | 1833 | 1305 | 1338 | 2.12 | 77.96 | 75.84 | 30.66 |
| **Ravera** | 1.36 | 5.07 | 1.73 | 489 | 1642 | 1153 | 972 | 0.98 | 79.73 | 78.75 | 36.51 |
| **Comba Delle Foglie** | 1.30 | 6.10 | 2.59 | 480 | 1747 | 1267 | 1035 | 1.50 | 74.82 | 73.32 | 35.01 |
| **Rocciamelone** | 15.71 | 19.27 | 7.98 | 496 | 3536 | 3040 | 1983 | 0.15 | 85.72 | 85.57 | 36.09 |
| **Giandula** | 7.27 | 13.70 | 5.74 | 561 | 3048 | 2487 | 1677 | 0.10 | 75.61 | 75.51 | 29.87 |
| **I Piani** | 0.58 | 4.31 | 1.46 | 478 | 1326 | 849 | 879 | 3.76 | 73.52 | 69.76 | 34.15 |
| **San Giuseppe** | 0.06 | 1.43 | 0.71 | 563 | 991 | 428 | 814 | 8.59 | 56.62 | 48.03 | 32.33 |
| **Mean** | **3.73** | **8.30** | **3.24** | **546.79** | **2130.36** | **1583.71** | **1346.43** | **2.43** | **73.84** | **71.41** | **32.63** |

*Table A2.3 - Geometric parameters of watersheds interested by the Caprie/Rubiana wildfire*

| **Fire n. 3** | | | | | **CAPRIE/RUBIANA** | | | | | | |
|---|---|---|---|---|---|---|---|---|---|---|---|
| **Watershed** | **Aw** | **P** | **Lb** | **Emin** | **Emax** | **Eran** | **Emean** | **Smin** | **Smax** | **Sran** | **Smea** |
| | [km²] | [km] | [km] | [m a.s.l.] | [m a.s.l.] | [m] | [m a.s.l.] | [°] | [°] | [°] | [°] |
| **Messa** | 29.16 | 25.42 | 10.14 | 366 | 2233 | 1867 | 1042 | 0.00 | 76.34 | 76.34 | 24.93 |
| **Sessi** | 23.48 | 22.92 | 9.47 | 388 | 2270 | 1883 | 1353 | 0.08 | 80.85 | 80.77 | 28.66 |
| **Novaretto** | 1.23 | 5.34 | 1.31 | 368 | 1442 | 1074 | 800 | 0.52 | 59.67 | 59.15 | 28.04 |
| **Fra Barbe** | 0.68 | 5.27 | 1.59 | 372 | 1493 | 1122 | 1044 | 0.51 | 67.21 | 66.70 | 26.78 |
| **Mean** | **13.64** | **14.74** | **5.63** | **373.50** | **1859.50** | **1486.50** | **1059.75** | **0.28** | **71.02** | **70.74** | **27.10** |

*Table A2.4 - Geometric parameters of watersheds interested by the Cumiana/Cantalupa wildfire*

| **Fire n. 4** | | | | | **CUMIANA/CANTALUPA** | | | | | | |
|---|---|---|---|---|---|---|---|---|---|---|---|
| **Watershed** | **Aw** | **P** | **Lb** | **Emin** | **Emax** | **Eran** | **Emean** | **Smin** | **Smax** | **Sran** | **Smea** |
| | [km²] | [km] | [km] | [m a.s.l.] | [m a.s.l.] | [m] | [m a.s.l.] | [°] | [°] | [°] | [°] |
| **1*Int. Dx. Sangone** | 50.74 | 40.35 | 16.95 | 368 | 2057 | 1689 | 888 | 0.00 | 81.93 | 81.93 | 24.76 |
| **T. Chisola** | 41.65 | 29.52 | 11.73 | 269 | 1440 | 1171 | 542 | 0.00 | 74.91 | 74.91 | 17.94 |
| **T. Noce** | 17.56 | 21.39 | 9.27 | 306 | 1455 | 1149 | 731 | 0.00 | 84.08 | 84.08 | 23.61 |
| **Chisola Pianura** | 20.54 | 18.76 | 8.09 | 270 | 1224 | 954 | 396 | 0.00 | 64.41 | 64.41 | 11.05 |
| **Mean** | **32.62** | **27.51** | **11.51** | **303.25** | **1544.00** | **1240.75** | **639.25** | **0.00** | **76.33** | **76.33** | **19.34** |

*Table A2.5 - Geometric parameters of watersheds interested by the Bellino/Casteldelfino wildfire*

| **Fire n. 5** | **BELLINO/CASTELDELFINO** | | | | | | | | | | |
|---|---|---|---|---|---|---|---|---|---|---|---|
| **Watershed** | **Aw** | **P** | **Lb** | **Emin** | **Emax** | **Eran** | **Emean** | **Smin** | **Smax** | **Sran** | **Smea** |
| | [km²] | [km] | [km] | [m a.s.l.] | [m a.s.l.] | [m] | [m a.s.l.] | [°] | [°] | [°] | [°] |
| **Cumbal Della Comu** | 1.01 | 3.94 | 0.94 | 1417 | 2271 | 854 | 1860 | 1.35 | 74.12 | 72.77 | 34.58 |
| **T. Mas Del Bernard** | 2.51 | 6.99 | 2.31 | 1468 | 2728 | 1260 | 2095 | 0.63 | 75.34 | 74.71 | 31.43 |
| **Mean** | **1.76** | **5.47** | **1.63** | **1442.50** | **2499.50** | **1057.00** | **1977.50** | **0.99** | **74.73** | **73.74** | **33.01** |

*Table A2.6 - Geometric parameters of watersheds interested by the Sambuco/Pietraporzio wildfire*

| **Fire n. 6** | **SAMBUCO/PIETRAPORZIO** | | | | | | | | | | |
|---|---|---|---|---|---|---|---|---|---|---|---|
| **Watershed** | **Aw** | **P** | **Lb** | **Emin** | **Emax** | **Eran** | **Emean** | **Smin** | **Smax** | **Sran** | **Smea** |
| | [km²] | [km] | [km] | [m a.s.l.] | [m a.s.l.] | [m] | [m a.s.l.] | [°] | [°] | [°] | [°] |
| **R. Bianco** | 11.60 | 16.07 | 5.78 | 1185 | 2759 | 1574 | 2113 | 0.00 | 82.54 | 82.54 | 30.49 |
| **Sn** | 0.36 | 3.34 | 1.33 | 1263 | 2206 | 943 | 1674 | 4.14 | 67.53 | 63.39 | 34.81 |
| **Rio Di Castello Pietraporzio** | 1.82 | 6.04 | 2.50 | 1259 | 2554 | 1295 | 1939 | 0.13 | 81.01 | 80.88 | 40.20 |
| **Mean** | **4.59** | **8.48** | **3.20** | **1235.67** | **2506.33** | **1270.67** | **1908.67** | **1.42** | **77.03** | **75.60** | **35.17** |

*Table A2.7 - Geometric parameters of watersheds interested by the Roure/Perrero wildfire*

| **Fire n. 7** | | | | | **ROURE/PERRERO** | | | | | | |
|---|---|---|---|---|---|---|---|---|---|---|---|
| **Watershed** | **Aw** | **P** | **Lb** | **Emin** | **Emax** | **Eran** | **Emean** | **Smin** | **Smax** | **Sran** | **Smea** |
| | [km²] | [km] | [km] | [m a.s.l.] | [m a.s.l.] | [m] | [m a.s.l.] | [°] | [°] | [°] | [°] |
| **V.Ne Di Borsetto** | 12.12 | 15.86 | 6.90 | 861 | 2809 | 1948 | 1756 | 0.26 | 85.23 | 84.97 | 34.69 |
| **S. Martino Sud** | 1.61 | 5.43 | 1.65 | 813 | 1825 | 1011 | 1331 | 0.22 | 62.05 | 61.83 | 27.87 |
| **Colet** | 2.29 | 6.09 | 2.17 | 896 | 1975 | 1078 | 1423 | 0.19 | 68.11 | 67.92 | 35.43 |
| **Molotta** | 3.30 | 8.24 | 2.53 | 1007 | 2208 | 1201 | 1736 | 0.18 | 74.33 | 74.15 | 30.88 |
| **Gernier** | 4.24 | 9.05 | 3.76 | 779 | 2193 | 1414 | 1468 | 0.52 | 76.82 | 76.30 | 34.65 |
| **Mean** | **4.71** | **8.93** | **3.40** | **871.20** | **2202.00** | **1330.40** | **1542.80** | **0.27** | **73.31** | **73.03** | **32.70** |

*Table A2.8 - Geometric parameters of watersheds interested by the Traversella wildfire*

| **Fire n. 8** | | | | | **TRAVERSELLA** | | | | | | |
|---|---|---|---|---|---|---|---|---|---|---|---|
| **Watershed** | **Aw** | **P** | **Lb** | **Emin** | **Emax** | **Eran** | **Emean** | **Smin** | **Smax** | **Sran** | **Smea** |
| | [km²] | [km] | [km] | [m a.s.l.] | [m a.s.l.] | [m] | [m a.s.l.] | [°] | [°] | [°] | [°] |
| **T. Bersella** | 10.52 | 13.95 | 4.94 | 727 | 2352 | 1625 | 1459 | 0.06 | 76.52 | 76.46 | 30.37 |
| **Valle Chiara Primo** | 0.43 | 3.86 | 1.47 | 866 | 2049 | 1183 | 1396 | 0.64 | 71.67 | 71.03 | 38.30 |
| **Mean** | **5.48** | **8.91** | **3.21** | **796.50** | **2200.50** | **1404.00** | **1427.50** | **0.35** | **74.10** | **73.75** | **34.34** |

*Table A2.9 - Geometric parameters of watersheds interested by the Demonte wildfire*

| **Fire n. 9** | | | | | **DEMONTE** | | | | | | |
|---|---|---|---|---|---|---|---|---|---|---|---|
| **Watershed** | **Aw** | **P** | **Lb** | **Emin** | **Emax** | **Eran** | **Emean** | **Smin** | **Smax** | **Sran** | **Smea** |
| | [km²] | [km] | [km] | [m a.s.l.] | [m a.s.l.] | [m] | [m a.s.l.] | [°] | [°] | [°] | [°] |
| **V. Del Saut** | 4.41 | 9.51 | 3.72 | 1110 | 2308 | 1198 | 1883 | 0.20 | 76.95 | 76.76 | 27.25 |
| **Valle Di Monfreis** | 7.64 | 11.42 | 4.11 | 962 | 2200 | 1238 | 1612 | 0.29 | 80.52 | 80.23 | 30.17 |
| **Sn 2** | 0.10 | 1.54 | 1.33 | 1052 | 1476 | 424 | 1254 | 10.70 | 45.95 | 35.25 | 33.83 |
| **Rio Di Prafioret C.** | 0.46 | 3.01 | 0.66 | 1066 | 1767 | 701 | 1447 | 0.85 | 72.79 | 71.94 | 36.51 |
| **Mean** | **3.15** | **6.37** | **2.46** | **1047.50** | **1937.75** | **890.25** | **1549.00** | **3.01** | **69.05** | **66.05** | **31.94** |

*Table A2.10 - Hydrological parameters of watersheds interested by the Locana/Ribordone wildfire*

| **Fire n. 1** | **LOCANA/RIBORDONE** | | |
|---|---|---|---|
| **Watershed** | **Lp [km]** | **LpS [°]** | **L [km]** |
| **Rio Fura** | 2.51 | 35.63 | 5.02 |
| **Rio Di Chioso Bosco** | 1.43 | 34.52 | 2.65 |
| **R. Montepiano** | 0.96 | 36.18 | 1.16 |
| **Carlevaria** | 1.47 | 40.54 | 2.49 |
| **Rio Di Bardonetto Inferiore** | 1.63 | 34.65 | 1.50 |
| **Ribordone** | 11.79 | 19.48 | 125.03 |
| **Eugio** | 9.89 | 21.82 | 66.03 |
| **Rio Bocchetta** | 1.68 | 40.31 | 4.40 |
| **Rio Di Calsazio** | 0.97 | 37.72 | 2.20 |
| **Locana Est** | 1.77 | 32.61 | 2.86 |
| **Apparè** | 0.54 | 39.21 | 0.90 |
| **Mean** | **3.15** | **33.88** | **19.48** |

*Table A2.11 - Hydrological parameters of watersheds interested by the Bussoleno/Mompantero wildfire*

| **Fire n. 2** | **BUSSOLENO/MOMPANTERO** | | |
|---|---|---|---|
| **Watershed** | **Lp [km]** | **LpS [°]** | **L [km]** |
| **Crosiglione** | 3.27 | 32.19 | 21.65 |
| **Rio Della Ravoire** | 1.25 | 29.98 | 3.00 |
| **Fogasso** | 3.07 | 28.86 | 8.08 |
| **Rio Della Codrea** | 2.01 | 27.85 | 4.01 |
| **Trinitâ** | 1.08 | 29.40 | 1.85 |
| **Rio Prebech** | 5.84 | 27.57 | 40.95 |
| **Moletta** | **4.95** | **34.92** | **24.63** |
| **Rio Di Periere** | 2.41 | 32.69 | 2.49 |
| **Ravera** | 1.58 | 31.74 | 4.52 |
| **Comba Delle Foglie** | 2.44 | 32.22 | 4.14 |
| **Rocciamelone** | 7.83 | 38.47 | 54.48 |
| **Giandula** | 5.59 | 28.22 | 25.11 |
| **I Piani** | 1.31 | 32.61 | 2.11 |
| **San Giuseppe** | 0.56 | 33.08 | 0.06 |
| **Mean** | **3.09** | **31.41** | **14.08** |

*Table A2.12 - Hydrological parameters of watersheds interested by the Caprie/Rubiana wildfire*

| **Fire n. 3** | **CAPRIE/RUBIANA** | | |
|---|---|---|---|
| **Watershed** | **Lp [km]** | **LpS [°]** | **L [km]** |
| **Messa** | 9.99 | 22.97 | 108.08 |
| **Sessi** | 9.32 | 17.28 | 77.55 |
| **Novaretto** | 1.16 | 23.88 | 5.06 |
| **Fra Barbe** | 1.44 | 28.86 | 2.60 |
| **Mean** | **5.48** | **23.25** | **48.32** |

*Table A2.13 - Hydrological parameters of watersheds interested by the Cumiana/Cantalupa wildfire*

| **Fire n. 4** | **CUMIANA/CANTALUPA** | | |
|---|---|---|---|
| **Watershed** | **Lp [km]** | **LpS [°]** | **L [km]** |
| **1*Int. Dx. Sangone** | 16.80 | 14.90 | 168.67 |
| **T. Chisola** | 11.58 | 14.41 | 167.56 |
| **T. Noce** | 9.12 | 18.31 | 68.54 |
| **Chisola Pianura** | 7.94 | 8.26 | 98.89 |
| **Mean** | **11.36** | **13.97** | **125.92** |

*Table A2.14 - Hydrological parameters of watersheds interested by the Bellino/Casteldelfino wildfire*

| **Fire n. 5** | **BELLINO/CASTELDELFINO** | | |
|---|---|---|---|
| **Watershed** | **Lp [km]** | **LpS [°]** | **L [km]** |
| **Cumbal Della Comu** | 0.79 | 28.91 | 3.34 |
| **T. Mas Del Bernard** | 2.16 | 28.84 | 8.87 |
| **Mean** | **1.48** | **28.88** | **6.11** |

*Table A2.15 - Hydrological parameters of watersheds interested by the Sambuco/Pietraporzio wildfire*

| **Fire n. 6** | **SAMBUCO/PIETRAPORZIO** | | |
|---|---|---|---|
| **Watershed** | **Lp [km]** | **LpS [°]** | **L [km]** |
| **R. Bianco** | 5.63 | 27.38 | 40.81 |
| **Sn** | 1.18 | 30.66 | 1.79 |
| **Rio Di Castello Pietraporzio** | 2.35 | 35.39 | 6.82 |
| **Mean** | **3.05** | **31.14** | **16.47** |

*Table A2.16 - Hydrological parameters of watersheds interested by the Roure/Perrero wildfire*

| **Fire n. 7** | | **ROURE/PERRERO** | |
|---|---|---|---|
| **Watershed** | **Lp** | **LpS** | **L** |
| | **[km]** | **[°]** | **[km]** |
| **V.Ne Di Borsetto** | 6.75 | 29.91 | 35.55 |
| **S. Martino Sud** | 1.50 | 33.05 | 5.76 |
| **Colet** | 2.02 | 36.47 | 6.80 |
| **Molotta** | 2.38 | 33.53 | 11.41 |
| **Gernier** | 3.61 | 32.50 | 11.91 |
| **Mean** | **3.25** | **33.09** | **14.29** |

*Table A2.17 - Hydrological parameters of watersheds interested by the Traversella wildfire*

| **Fire n. 8** | | **TRAVERSELLA** | |
|---|---|---|---|
| **Watershed** | **Lp** | **LpS** | **L** |
| | **[km]** | **[°]** | **[km]** |
| **T. Bersella** | 4.79 | 22.26 | 41.33 |
| **Valle Chiara Primo** | 1.32 | 37.85 | 1.36 |
| **Mean** | **3.06** | **30.06** | **21.35** |

*Table A2.18 - Hydrological parameters of watersheds interested by the Demonte wildfire*

| **Fire n. 9** | | **DEMONTE** | |
|---|---|---|---|
| **Watershed** | **Lp [km]** | **LpS [°]** | **L [km]** |
| **V. Del Saut** | 3.57 | 26.64 | 10.94 |
| **Valle Di Monfreis** | 3.96 | 26.80 | 24.39 |
| **Sn 2** | 1.18 | 33.31 | 0.29 |
| **Rio Di Prafioret C.** | 0.51 | 29.67 | 1.56 |
| **Mean** | **2.31** | **29.11** | **9.30** |

*Table A2.19 - morphometric parameters of watersheds interested by the Locana/Ribordone wildfire*

| **Fire n. 1** | **LOCANA/RIBORDONE** | | | | | | |
|---|---|---|---|---|---|---|---|
| **Watershed** | **Af_Aw** | **Ff** | **Rc** | **Re** | **Me** | **Dd** | **Tc** |
| | **[-]** | **[-]** | **[-]** | **[-]** | **[-]** | **[km/km²]** | **[h]** |
| **Rio Fura** | 5.36 | 0.20 | 0.43 | 0.51 | 1.14 | 3.87 | 0.18 |
| **Rio Di Chioso Bosco** | 5.39 | 0.37 | 0.60 | 0.69 | 1.02 | 3.51 | 0.11 |
| **R. Montepiano** | 42.46 | 0.33 | 0.46 | 0.65 | 1.47 | 3.84 | 0.08 |
| **Carlevaria** | 3.24 | 0.34 | 0.62 | 0.66 | 1.16 | 3.39 | 0.11 |
| **Rio Di Bardonetto Inferiore** | 0.83 | 0.16 | 0.39 | 0.45 | 1.51 | 3.50 | 0.12 |
| **Ribordone** | 1.24 | 0.26 | 0.65 | 0.57 | 0.38 | 3.47 | 0.81 |
| **Eugio** | 1.53 | 0.16 | 0.44 | 0.46 | 0.63 | 4.11 | 0.64 |
| **Rio Bocchetta** | 6.26 | 0.45 | 0.62 | 0.76 | 1.00 | 3.45 | 0.12 |
| **Rio Di Calsazio** | 3.82 | 0.67 | 0.80 | 0.92 | 1.06 | 3.51 | 0.08 |
| **Locana Est** | 0.02 | 0.21 | 0.48 | 0.52 | 1.45 | 4.33 | 0.13 |
| **Apparè** | 0.06 | 0.21 | 0.40 | 0.52 | 1.57 | 2.99 | 0.09 |
| **Mean** | **6.38** | **0.31** | **0.54** | **0.61** | **1.13** | **3.63** | **0.22** |

*Table A2.20 - morphometric parameters of watersheds interested by the Bussoleno/Mompantero wildfire*

| **Fire n. 2** | **BUSSOLENO/MOMPANTERO** | | | | | | |
|---|---|---|---|---|---|---|---|
| **Watershed** | **Af_Aw** | **Ff** | **Rc** | **Re** | **Me** | **Dd** | **Tc** |
| | **[-]** | **[-]** | **[-]** | **[-]** | **[-]** | **[km/km²]** | **[h]** |
| **Crosiglione** | 20.43 | 0.42 | 0.48 | 0.73 | 1.02 | 4.80 | 0.22 |
| **Rio Della Ravoire** | 2.31 | 0.37 | 0.35 | 0.69 | 1.41 | 5.15 | 0.10 |
| **Fogasso** | 0.34 | 0.20 | 0.44 | 0.51 | 1.10 | 4.26 | 0.22 |
| **Rio Della Codrea** | 1.46 | 0.22 | 0.35 | 0.53 | 1.29 | 4.45 | 0.15 |
| **Trinitâ** | 1.51 | 0.33 | 0.30 | 0.65 | 1.34 | 4.88 | 0.09 |
| **Rio Prebech** | 19.50 | 0.31 | 0.57 | 0.62 | 0.64 | 3.93 | 0.38 |
| **Moletta** | 17.45 | 0.27 | 0.49 | 0.58 | 0.95 | 3.77 | 0.30 |
| **Rio Di Periere** | 9.82 | 0.12 | 0.25 | 0.39 | 1.52 | 3.64 | 0.17 |
| **Ravera** | 7.77 | 0.55 | 0.67 | 0.84 | 0.97 | 3.31 | 0.13 |
| **Comba Delle Foglie** | 8.14 | 0.22 | 0.44 | 0.53 | 1.02 | 3.19 | 0.18 |
| **Rocciamelone** | 6.69 | 0.26 | 0.53 | 0.57 | 0.76 | 3.47 | 0.44 |
| **Giandula** | 2.75 | 0.23 | 0.49 | 0.55 | 0.91 | 3.46 | 0.37 |
| **I Piani** | 9.39 | 0.34 | 0.39 | 0.66 | 1.18 | 3.66 | 0.10 |
| **San Giuseppe** | 23.54 | 0.19 | 0.36 | 0.49 | 1.74 | 1.06 | 0.05 |
| **Mean** | **9.36** | **0.29** | **0.44** | **0.60** | **1.13** | **3.79** | **0.21** |

*Table A2.21 - morphometric parameters of watersheds interested by the Caprie/Rubiana wildfire*

| **Fire n. 3** | | | | **CAPRIE/RUBIANA** | | | |
|---|---|---|---|---|---|---|---|
| **Watershed** | **Af_Aw** | **Ff** | **Rc** | **Re** | **Me** | **Dd** | **Tc** |
| | **[-]** | **[-]** | **[-]** | **[-]** | **[-]** | **[km/km²]** | **[h]** |
| **Messa** | 5.75 | 0.29 | 0.57 | 0.61 | 0.35 | 3.71 | 0.67 |
| **Sessi** | 7.24 | 0.27 | 0.56 | 0.59 | 0.39 | 3.30 | 0.69 |
| **Novaretto** | 3.16 | 0.92 | 0.54 | 1.08 | 0.97 | 4.12 | 0.11 |
| **Fra Barbe** | 6.01 | 0.33 | 0.31 | 0.65 | 1.36 | 3.83 | 0.12 |
| **Mean** | **5.54** | **0.45** | **0.50** | **0.73** | **0.77** | **3.74** | **0.40** |

*Table A2.22 - morphometric parameters of watersheds interested by the Cumiana/Cantalupa wildfire*

| **Fire n. 4** | | | | **CUMIANA/CANTALUPA** | | | |
|---|---|---|---|---|---|---|---|
| **Watershed** | **Af_Aw** | **Ff** | **Rc** | **Re** | **Me** | **Dd** | **Tc** |
| | **[-]** | **[-]** | **[-]** | **[-]** | **[-]** | **[km/km²]** | **[h]** |
| **1*Int. Dx. Sangone** | - | 0.18 | 0.39 | 0.48 | 0.24 | 3.32 | 1.24 |
| **T. Chisola** | - | 0.31 | 0.60 | 0.63 | 0.18 | 4.02 | 0.99 |
| **T. Noce** | - | 0.21 | 0.48 | 0.52 | 0.27 | 3.90 | 0.75 |
| **Chisola Pianura** | - | 0.33 | 0.73 | 0.65 | 0.21 | 4.81 | 0.77 |
| **Mean** | - | **0.26** | **0.55** | **0.57** | **0.23** | **4.01** | **0.94** |

*Table A2.23 - morphometric parameters of watersheds interested by the Bellino/Casteldelfino wildfire*

| **Fire n. 5** | **BELLINO/CASTELDELFINO** | | | | | | |
|---|---|---|---|---|---|---|---|
| **Watershed** | **Af_Aw** | **Ff** | **Rc** | **Re** | **Me** | **Dd** | **Tc** |
| | **[-]** | **[-]** | **[-]** | **[-]** | **[-]** | **[km/km²]** | **[h]** |
| **Cumbal Della Comu** | 1.59 | 1.62 | 0.81 | 1.44 | 0.84 | 3.32 | 0.08 |
| **T. Mas Del Bernard** | 0.77 | 0.54 | 0.64 | 0.83 | 0.79 | 3.54 | 0.17 |
| **Mean** | **1.18** | **1.08** | **0.73** | **1.14** | **0.82** | **3.43** | **0.13** |

*Table A2.24 - morphometric parameters of watersheds interested by the Sambuco/Pietraporzio wildfire*

| **Fire n. 6** | **SAMBUCO/PIETRAPORZIO** | | | | | | |
|---|---|---|---|---|---|---|---|
| **Watershed** | **Af_Aw** | **Ff** | **Rc** | **Re** | **Me** | **Dd** | **Tc** |
| | **[-]** | **[-]** | **[-]** | **[-]** | **[-]** | **[km/km²]** | **[h]** |
| **R. Bianco** | 0.56 | 0.37 | 0.56 | 0.68 | 0.47 | 3.52 | 0.41 |
| **Sn** | 5.67 | 0.26 | 0.40 | 0.58 | 1.54 | 4.98 | 0.10 |
| **Rio Di Castello Pietraporzio** | 0.96 | 0.33 | 0.63 | 0.65 | 0.96 | 3.74 | 0.17 |
| **Mean** | **2.40** | **0.32** | **0.53** | **0.64** | **0.99** | **4.08** | **0.23** |

*Table A2.25 - morphometric parameters of watersheds interested by the Roure/Perrero wildfire*

| **Fire n. 7** | | | | **ROURE/PERRERO** | | | |
|---|---|---|---|---|---|---|---|
| **Watershed** | **Af_Aw** | **Ff** | **Rc** | **Re** | **Me** | **Dd** | **Tc** |
| | **[-]** | **[-]** | **[-]** | **[-]** | **[-]** | **[km/km²]** | **[h]** |
| **V.Ne Di Borsetto** | 0.34 | 0.27 | 0.61 | 0.58 | 0.55 | 2.93 | 0.45 |
| **S. Martino Sud** | 0.99 | 0.72 | 0.69 | 0.96 | 0.79 | 3.57 | 0.12 |
| **Colet** | 1.28 | 0.56 | 0.78 | 0.85 | 0.70 | 2.97 | 0.15 |
| **Molotta** | 0.09 | 0.58 | 0.61 | 0.86 | 0.66 | 3.46 | 0.18 |
| **Gernier** | 1.03 | 0.33 | 0.65 | 0.65 | 0.68 | 2.81 | 0.26 |
| **Mean** | **0.75** | **0.49** | **0.67** | **0.78** | **0.68** | **3.15** | **0.23** |

*Table A2.26 - morphometric parameters of watersheds interested by the Traversella wildfire*

| **Fire n. 8** | | | | **TRAVERSELLA** | | | |
|---|---|---|---|---|---|---|---|
| **Watershed** | **Af_Aw** | **Ff** | **Rc** | **Re** | **Me** | **Dd** | **Tc** |
| | **[-]** | **[-]** | **[-]** | **[-]** | **[-]** | **[km/km²]** | **[h]** |
| **T. Bersella** | 0.33 | 0.46 | 0.68 | 0.76 | 0.50 | 3.93 | 0.36 |
| **Valle Chiara Primo** | 1.30 | 0.25 | 0.36 | 0.56 | 1.79 | 3.17 | 0.10 |
| **Mean** | **0.82** | **0.36** | **0.52** | **0.66** | **1.15** | **3.55** | **0.23** |

*Table A2.27 - morphometric parameters of watersheds interested by the Demonte wildfire*

| **Fire n. 9** | **DEMONTE** | | | | | | |
|---|---|---|---|---|---|---|---|
| **Watershed** | **Af_Aw** | **Ff** | **Rc** | **Re** | **Me** | **Dd** | **Tc** |
| | **[-]** | **[-]** | **[-]** | **[-]** | **[-]** | **[km/km²]** | **[h]** |
| **V. Del Saut** | 3.31 | 0.35 | 0.61 | 0.66 | 0.57 | 2.48 | 0.28 |
| **Valle Di Monfreis** | 0.54 | 0.49 | 0.74 | 0.79 | 0.44 | 3.19 | 0.31 |
| **Sn 2** | 13.01 | 0.08 | 0.55 | 0.31 | 1.33 | 2.76 | 0.09 |
| **Rio Di Prafioret C.** | 7.66 | 1.79 | 0.64 | 1.51 | 1.00 | 3.42 | 0.05 |
| **Mean** | **6.13** | **0.68** | **0.64** | **0.82** | **0.84** | **2.96** | **0.18** |

# Appendix 3

*Table A3.1 – Land cover percentages for the watersheds affected by the Locana/Ribordone wildfire*

| **Fire n. 1** | **LOCANA/RIBORDONE** | | | | | | | | | | | | | | | | | | | | | |
|---|---|---|---|---|---|---|---|---|---|---|---|---|---|---|---|---|---|---|---|---|---|---|
| ***Watershed*** | *Land Cover type* | | | | | | | | | | | | | | | | | | | | | |
| | *112* | *131* | *211* | *221* | *222* | *231* | *242* | *243* | *311* | *312* | *313* | *322* | *324* | *332* | *333* | *311b* | *312b* | *313b* | *3211* | *3212* | *322b* | *0* |
| | *%* | *%* | *%* | *%* | *%* | *%* | *%* | *%* | *%* | *%* | *%* | *%* | *%* | *%* | *%* | *%* | *%* | *%* | *%* | *%* | *%* | *%* |
| ***Rio Fura*** | - | - | - | - | - | - | - | - | *46.0* | *10.9* | *0.4* | *7.1* | *0.3* | - | - | - | - | - | - | *35.3* | - | - |
| ***Rio Di Chioso Bosco*** | - | - | - | - | - | - | - | - | *86.8* | *9.8* | - | - | *3.4* | - | - | - | - | - | - | - | - | - |
| ***R. Montepiano*** | - | - | - | - | - | - | - | - | *56.9* | *27.6* | *0.1* | *5.7* | *9.7* | - | - | - | - | - | - | - | - | - |
| ***Carlevaria*** | - | - | - | - | - | - | - | - | *93.1* | *1.8* | *0.0* | - | *0.3* | - | - | - | - | - | - | *4.8* | - | - |
| ***Rio Di Bardonetto Inferiore*** | - | - | - | - | - | - | - | - | *82.4* | *1.6* | *0.1* | *3.3* | *3.0* | - | - | - | - | - | - | *9.5* | - | - |
| ***Ribordone*** | *0.1* | - | - | - | *0.0* | - | - | *0.6* | *41.4* | *6.1* | *0.2* | *12.3* | *0.3* | *4.9* | *0.4* | - | *0.3* | - | *12.4* | *20.9* | - | - |
| ***Eugio*** | - | - | - | - | - | - | - | - | *7.7* | *0.3* | - | *17.5* | - | *31.1* | *9.8* | - | - | - | *11.3* | *22.4* | - | - |
| ***Rio Bocchetta*** | - | - | - | - | - | - | - | - | *47.7* | *0.3* | *0.2* | *30.6* | *3.4* | - | - | - | - | - | - | *17.8* | - | - |
| ***Locana Est*** | *0.0* | - | - | - | - | - | - | - | *29.7* | *27.6* | *1.5* | *12.3* | *21.4* | - | - | - | - | - | - | *7.5* | - | - |
| ***Apparè*** | - | - | - | - | - | - | - | - | *100.0* | - | - | - | - | - | - | - | - | - | - | - | - | - |

*Table A3.2 - Land cover percentages for the watersheds affected by the Bussoleno/Mompantero wildfire*

| **Fire n. 2** | **BUSSOLENO/MOMPANTERO** | | | | | | | | | | | | | | | | | | | | | |
|---|---|---|---|---|---|---|---|---|---|---|---|---|---|---|---|---|---|---|---|---|---|---|
| ***Watershed*** | *Land Cover type* | | | | | | | | | | | | | | | | | | | | | |
| | *112* | *131* | *211* | *221* | *222* | *231* | *242* | *243* | *311* | *312* | *313* | *322* | *324* | *332* | *333* | *311b* | *312b* | *313b* | *3211* | *3212* | *322b* | *0* |
| | *%* | *%* | *%* | *%* | *%* | *%* | *%* | *%* | *%* | *%* | *%* | *%* | *%* | *%* | *%* | *%* | *%* | *%* | *%* | *%* | *%* | *%* |
| ***Rio Di Calsazio*** | - | - | - | - | - | - | - | - | 100.0 | - | - | - | - | - | - | - | - | - | - | - | - | - |
| ***Crosiglione*** | - | - | - | - | 0.6 | - | - | - | 9.9 | 39.4 | 8.6 | - | 9.6 | 9.4 | - | - | 2.6 | 1.5 | 3.7 | 14.2 | - | 0.4 |
| ***Rio Della Ravoire*** | - | - | - | - | - | - | - | - | 37.7 | 54.2 | 8.1 | - | - | - | - | - | - | - | - | - | - | - |
| ***Fogasso*** | - | - | - | - | - | - | - | 0.0 | 31.1 | 41.3 | 14.7 | - | 7.3 | - | - | - | - | - | 5.6 | - | - | - |
| ***Rio Della Codrea*** | - | - | - | - | - | - | - | 0.0 | 26.9 | 39.4 | 33.8 | - | - | - | - | - | - | - | - | - | - | - |
| ***Trinitâ*** | - | - | - | - | - | - | - | - | 46.0 | 4.9 | 33.4 | - | 15.8 | - | - | - | - | - | - | - | - | - |
| ***Rio Prebech*** | - | - | - | - | - | - | - | 0.2 | 30.3 | 15.5 | 11.8 | - | 3.5 | - | 3.6 | - | - | 0.7 | - | 33.7 | - | 0.6 |
| ***Moletta*** | - | - | - | - | - | - | - | 0.8 | 27.0 | 3.4 | 20.0 | - | 2.1 | 0.8 | - | 0.4 | - | 0.5 | 22.7 | 22.4 | - | - |
| ***Rio Di Periere*** | - | - | - | - | - | - | - | - | 20.5 | 5.8 | 37.8 | - | 26.3 | - | - | 8.9 | - | - | 0.7 | - | - | - |
| ***Ravera*** | - | - | - | - | - | - | - | 2.0 | 58.7 | 1.0 | 4.8 | 18.8 | 5.4 | - | 9.4 | - | - | - | - | - | - | - |
| ***Comba Delle Foglie*** | - | - | - | - | - | - | - | 5.5 | 24.5 | - | 38.2 | - | 4.2 | - | - | 0.6 | - | 26.1 | - | 0.9 | - | - |
| ***Rocciamelone*** | - | - | - | - | - | - | - | - | 8.2 | 16.0 | 13.3 | 0.0 | 7.0 | 13.4 | 0.5 | - | 1.1 | - | 34.6 | 4.2 | - | 1.6 |
| ***Giandula*** | 0.1 | - | - | - | - | - | - | - | 18.6 | 14.9 | 24.6 | - | 2.7 | 0.7 | - | - | 1.5 | - | 31.7 | 5.0 | - | 0.3 |
| ***I Piani*** | - | - | - | - | - | - | - | - | 11.0 | 0.0 | 7.7 | 51.1 | - | - | - | - | - | - | - | 30.2 | - | - |
| ***San Giuseppe*** | - | - | - | - | - | - | - | - | 98.4 | - | 1.3 | - | - | - | - | - | - | - | - | - | - | - |

*Table A3.3 - Land cover percentages for the watersheds affected by the Caprie/Rubiana wildfire*

| **Fire n. 3** | **CAPRIE/RUBIANA** | | | | | | | | | | | | | | | | | | | | | |
|---|---|---|---|---|---|---|---|---|---|---|---|---|---|---|---|---|---|---|---|---|---|---|
| ***Watershed*** | *Land Cover type* | | | | | | | | | | | | | | | | | | | | | |
| | *112* | *131* | *211* | *221* | *222* | *231* | *242* | *243* | *311* | *312* | *313* | *322* | *324* | *332* | *333* | *311b* | *312b* | *313b* | *3211* | *3212* | *322b* | *0* |
| | *%* | *%* | *%* | *%* | *%* | *%* | *%* | *%* | *%* | *%* | *%* | *%* | *%* | *%* | *%* | *%* | *%* | *%* | *%* | *%* | *%* | *%* |
| ***Messa*** | *3.5* | *-* | *-* | *-* | *-* | *0.0* | *-* | *0.6* | *55.7* | *26.2* | *3.2* | *-* | *4.4* | *0.0* | *3.2* | *0.0* | *-* | *-* | *-* | *3.1* | *-* | *-* |
| ***Sessi*** | *0.0* | *-* | *-* | *-* | *-* | *-* | *-* | *1.5* | *61.1* | *0.6* | *5.2* | *1.2* | *8.7* | *3.1* | *6.1* | *-* | *-* | *-* | *12.1* | *0.4* | *-* | *-* |
| ***Novaretto*** | *0.4* | *-* | *-* | *-* | *-* | *10.1* | *-* | *-* | *88.7* | *-* | *0.2* | *-* | *0.6* | *-* | *-* | *-* | *-* | *-* | *-* | *-* | *-* | *-* |
| ***Fra Barbe*** | *-* | *-* | *-* | *-* | *-* | *-* | *-* | *0.1* | *87.7* | *-* | *1.3* | *-* | *10.8* | *-* | *-* | *-* | *-* | *-* | *-* | *-* | *-* | *-* |

*Table A3.4 - Land cover percentages for the watersheds affected by the Cumiana/Cantalupa wildfire*

| **Fire n. 4** | **CUMIANA/CANTALUPA** | | | | | | | | | | | | | | | | | | | | | |
|---|---|---|---|---|---|---|---|---|---|---|---|---|---|---|---|---|---|---|---|---|---|---|
| ***Watershed*** | *Land Cover type* | | | | | | | | | | | | | | | | | | | | | |
| | *112* | *131* | *211* | *221* | *222* | *231* | *242* | *243* | *311* | *312* | *313* | *322* | *324* | *332* | *333* | *311b* | *312b* | *313b* | *3211* | *3212* | *322b* | *0* |
| | *%* | *%* | *%* | *%* | *%* | *%* | *%* | *%* | *%* | *%* | *%* | *%* | *%* | *%* | *%* | *%* | *%* | *%* | *%* | *%* | *%* | *%* |
| ***1*Int. Dx. Sangone*** | *0.2* | *0.2* | *-* | *-* | *-* | *-* | *0.1* | *3.0* | *77.7* | *4.4* | *6.7* | *2.7* | *0.2* | *-* | *-* | *-* | *-* | *0.3* | *-* | *4.5* | *-* | *-* |
| ***T. Chisola*** | *3.3* | *-* | *-* | *-* | *-* | *1.0* | *11.6* | *10.6* | *71.5* | *1.5* | *-* | *-* | *0.6* | *-* | *-* | *-* | *-* | *-* | *-* | *-* | *-* | *-* |
| ***T. Noce*** | *9.5* | *-* | *-* | *1.7* | *-* | *0.0* | *2.7* | *5.6* | *76.9* | *1.4* | *1.3* | *-* | *1.0* | *-* | *-* | *-* | *-* | *-* | *-* | *-* | *-* | *-* |
| ***Chisola Pianura*** | *0.0* | *-* | *12.2* | *0.1* | *-* | *-* | *23.1* | *21.0* | *43.6* | *-* | *-* | *-* | *-* | *-* | *-* | *-* | *-* | *-* | *-* | *-* | *-* | *-* |

*Table A3.5 - Land cover percentages for the watersheds affected by the Bellino/Casteldelfino wildfire*

| **Fire n. 5** | **BELLINO/CASTELDELFINO** | | | | | | | | | | | | | | | | | | | | | |
|---|---|---|---|---|---|---|---|---|---|---|---|---|---|---|---|---|---|---|---|---|---|---|
| ***Watershed*** | *Land Cover type* | | | | | | | | | | | | | | | | | | | | | |
| | *112* | *131* | *211* | *221* | *222* | *231* | *242* | *243* | *311* | *312* | *313* | *322* | *324* | *332* | *333* | *311b* | *312b* | *313b* | *3211* | *3212* | *322b* | *0* |
| | *%* | *%* | *%* | *%* | *%* | *%* | *%* | *%* | *%* | *%* | *%* | *%* | *%* | *%* | *%* | *%* | *%* | *%* | *%* | *%* | *%* | *%* |
| ***Cumbal Della Comu*** | *-* | *-* | *-* | *-* | *-* | *0.0* | *-* | *-* | *5.0* | *61.7* | *0.5* | *-* | *0.2* | *-* | *-* | *-* | *-* | *-* | *32.6* | *-* | *-* | *-* |
| ***T. Mas Del Bernard*** | *-* | *-* | *-* | *-* | *-* | *-* | *-* | *-* | *2.3* | *9.7* | *-* | *0.1* | *4.9* | *0.3* | *-* | *1.2* | *0.5* | *-* | *79.5* | *1.5* | *-* | *-* |

*Table A3.6 - Land cover percentages for the watersheds affected by the Sambuco/Pietraporzio wildfire*

| **Fire n. 6** | **SAMBUCO/PIETRAPORZIO** | | | | | | | | | | | | | | | | | | | | | |
|---|---|---|---|---|---|---|---|---|---|---|---|---|---|---|---|---|---|---|---|---|---|---|
| ***Watershed*** | *Land Cover type* | | | | | | | | | | | | | | | | | | | | | |
| | *112* | *131* | *211* | *221* | *222* | *231* | *242* | *243* | *311* | *312* | *313* | *322* | *324* | *332* | *333* | *311b* | *312b* | *313b* | *3211* | *3212* | *322b* | *0* |
| | *%* | *%* | *%* | *%* | *%* | *%* | *%* | *%* | *%* | *%* | *%* | *%* | *%* | *%* | *%* | *%* | *%* | *%* | *%* | *%* | *%* | *%* |
| ***R. Bianco*** | - | - | - | - | - | - | - | - | 2.9 | 5.6 | - | 0.1 | 7.0 | 6.2 | 5.2 | - | 0.8 | - | 40.6 | 31.6 | - | - |
| ***Sn*** | - | - | - | - | - | - | - | - | - | 75.5 | - | 6.2 | 10.2 | - | - | - | 4.5 | - | - | 3.5 | - | - |
| ***Rio Di Castello Pietraporzio*** | - | - | - | - | - | 1.2 | - | - | 0.4 | 35.0 | - | - | 23.0 | - | - | - | 0.9 | - | 0.7 | 38.9 | - | - |

*Table A3.7 - Land cover percentages for the watersheds affected by the Roure/Perrero wildfire*

| **Fire n. 7** | **ROURE/PERRERO** | | | | | | | | | | | | | | | | | | | | | |
|---|---|---|---|---|---|---|---|---|---|---|---|---|---|---|---|---|---|---|---|---|---|---|
| ***Watershed*** | *Land Cover type* | | | | | | | | | | | | | | | | | | | | | |
| | *112* | *131* | *211* | *221* | *222* | *231* | *242* | *243* | *311* | *312* | *313* | *322* | *324* | *332* | *333* | *311b* | *312b* | *313b* | *3211* | *3212* | *322b* | *0* |
| | *%* | *%* | *%* | *%* | *%* | *%* | *%* | *%* | *%* | *%* | *%* | *%* | *%* | *%* | *%* | *%* | *%* | *%* | *%* | *%* | *%* | *%* |
| ***V.Ne Di Borsetto*** | - | - | - | - | - | - | - | - | 11.9 | 38.6 | 6.5 | 6.0 | 10.8 | 0.0 | - | - | 0.6 | - | 7.0 | 18.6 | 0.1 | - |
| ***S. Martino Sud*** | - | - | - | - | - | 5.1 | - | - | 16.5 | 74.2 | 0.0 | - | 0.3 | - | - | 0.7 | 3.1 | - | - | - | - | - |
| ***Colet*** | - | - | - | - | - | - | - | - | 4.9 | 27.9 | 66.8 | - | - | - | - | - | - | - | 0.3 | - | 0.1 | - |
| ***Molotta*** | - | - | - | - | - | - | - | - | 18.3 | 33.3 | 12.2 | - | 3.7 | - | - | - | 10.8 | - | - | 21.7 | - | - |
| ***Gernier*** | - | - | - | - | - | - | - | - | 30.4 | 51.3 | 10.8 | 2.7 | - | - | - | - | 0.2 | - | - | 4.7 | - | - |

*Table A3.8 - Land cover percentages for the watersheds affected by the Traversella wildfire*

| **Fire n. 8** | **TRAVERSELLA** | | | | | | | | | | | | | | | | | | | | | |
|---|---|---|---|---|---|---|---|---|---|---|---|---|---|---|---|---|---|---|---|---|---|---|
| ***Watershed*** | *Land Cover type* | | | | | | | | | | | | | | | | | | | | | |
| | *112* | *131* | *211* | *221* | *222* | *231* | *242* | *243* | *311* | *312* | *313* | *322* | *324* | *332* | *333* | *311b* | *312b* | *313b* | *3211* | *3212* | *322b* | *0* |
| | *%* | *%* | *%* | *%* | *%* | *%* | *%* | *%* | *%* | *%* | *%* | *%* | *%* | *%* | *%* | *%* | *%* | *%* | *%* | *%* | *%* | *%* |
| ***T. Bersella*** | - | - | - | - | - | - | - | 8.9 | 24.6 | 0.4 | 3.0 | 4.7 | - | - | 7.8 | 1.1 | - | - | 7.6 | 42.1 | - | - |
| ***Valle Chiara Primo*** | - | - | - | - | - | - | - | - | 15.1 | - | 36.2 | - | - | - | - | - | - | - | 0.1 | 48.7 | - | - |

*Table A3.9 - Land cover percentages for the watersheds affected by the Demonte wildfire*

| **Fire n. 9** | **DEMONTE** | | | | | | | | | | | | | | | | | | | | | |
|---|---|---|---|---|---|---|---|---|---|---|---|---|---|---|---|---|---|---|---|---|---|---|
| ***Watershed*** | *Land Cover type* | | | | | | | | | | | | | | | | | | | | | |
| | *112* | *131* | *211* | *221* | *222* | *231* | *242* | *243* | *311* | *312* | *313* | *322* | *324* | *332* | *333* | *311b* | *312b* | *313b* | *3211* | *3212* | *322b* | *0* |
| | *%* | *%* | *%* | *%* | *%* | *%* | *%* | *%* | *%* | *%* | *%* | *%* | *%* | *%* | *%* | *%* | *%* | *%* | *%* | *%* | *%* | *%* |
| ***V. Del Saut*** | - | - | - | - | - | 1.4 | - | - | 10.2 | 2.4 | 2.0 | 0.5 | 4.6 | - | - | - | - | - | 0.0 | 78.9 | - | - |
| ***Valle Di Monfreis*** | - | - | - | - | - | - | - | - | 49.6 | 6.9 | 0.5 | 1.0 | 10.4 | - | - | 1.8 | - | - | - | 29.5 | 0.3 | - |
| ***Sn 2*** | - | - | - | - | - | - | - | - | 93.8 | 5.7 | - | - | 0.7 | - | - | - | - | - | - | - | - | - |
| ***Rio Di Prafioret C.*** | - | - | - | - | - | - | - | - | 72.8 | 6.1 | - | - | 4.0 | - | - | - | - | - | - | 17.1 | - | - |

# Appendix 4

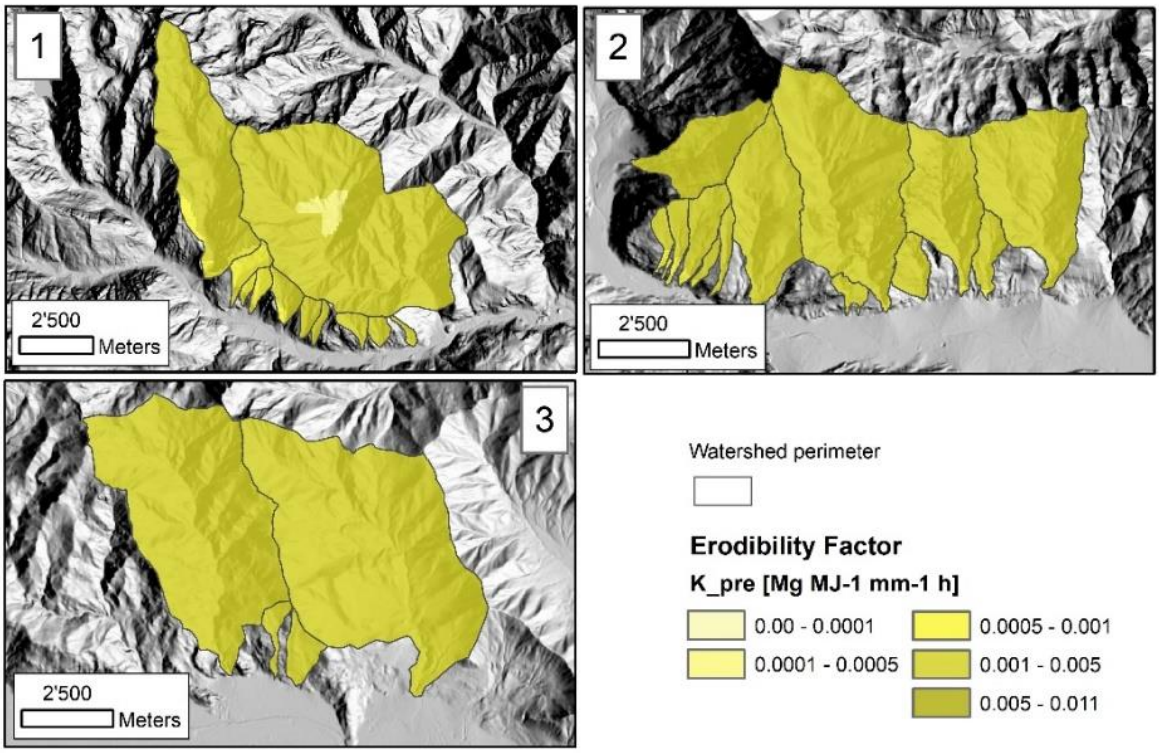


*Figure A4.1 - Erodibility Factor in the pre-fire situation for the watersheds affected by the Locana/Ribordone (1), Bussoleno/Mompantero (2) and Caprie/Rubiana (3) wildfires.*

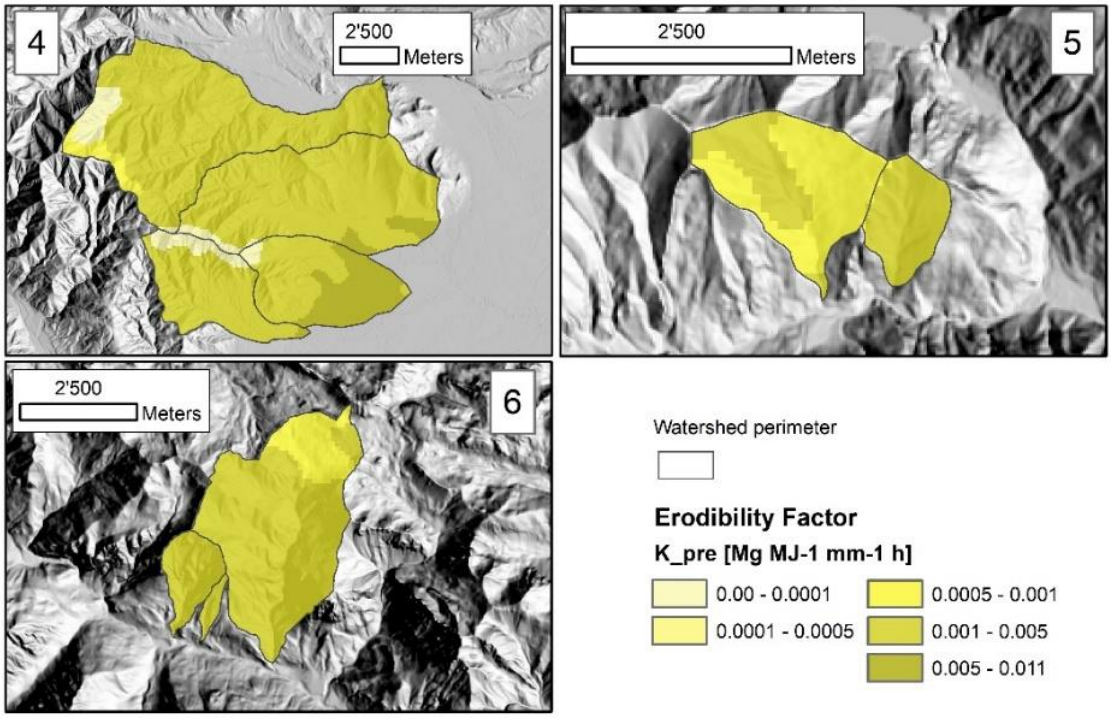


*Figure A4.2 - Erodibility Factor in the pre-fire situation for the watersheds affected by the Cumiana/Cantalupa (4), Bellino/Casteldelfino (5) and Sambuco/Pietraporzio (6) wildfires.*

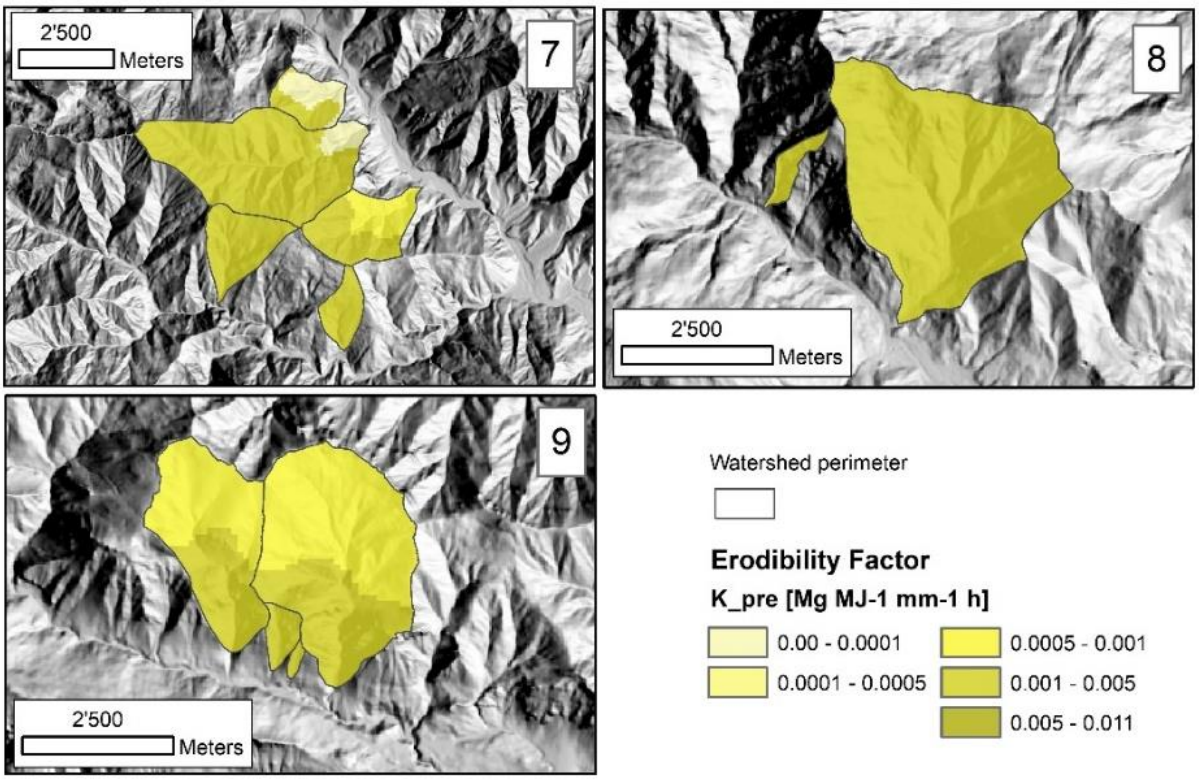


*Figure A4.3 - Erodibility Factor in the pre-fire situation for the watersheds affected by the Roure/Perrero (7), Traversella (8) and Demonte (9) wildfires.*

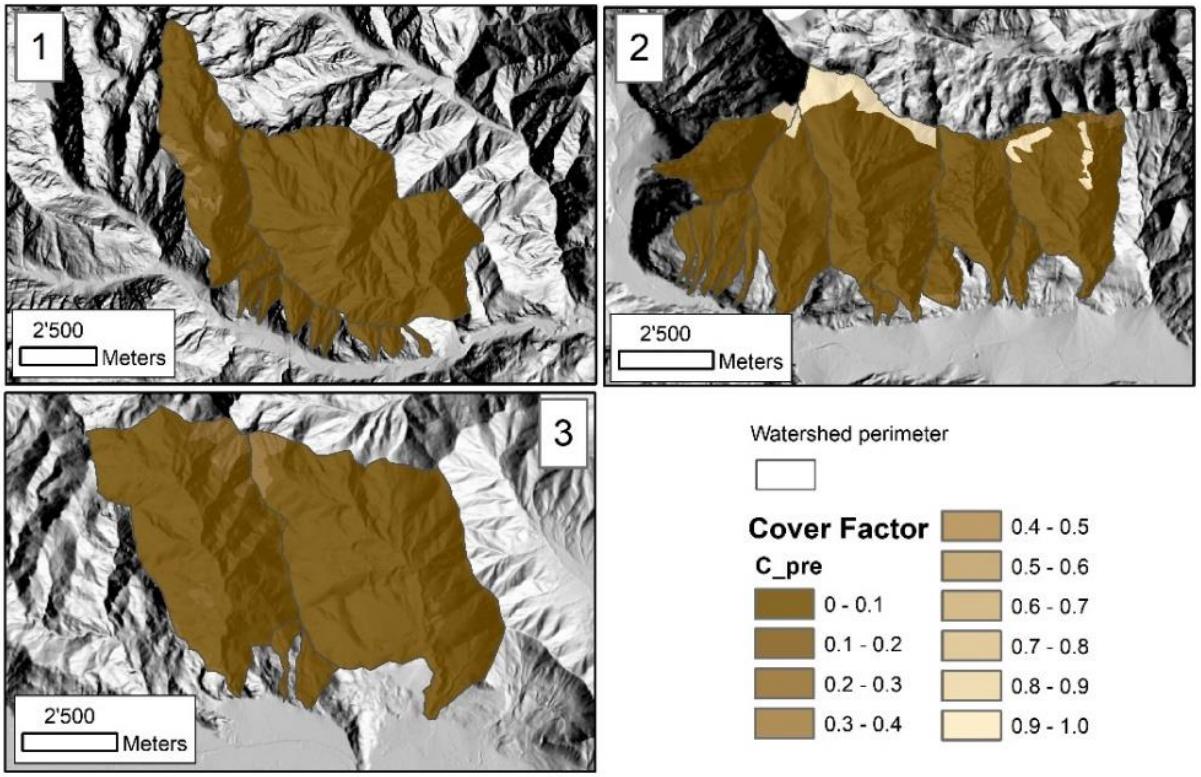


*Figure A4.4 - Cover Factor in the pre-fire situation for the watersheds affected by the Locana/Ribordone (1), Bussoleno/Mompantero (2) and Caprie/Rubiana (3) wildfires.*

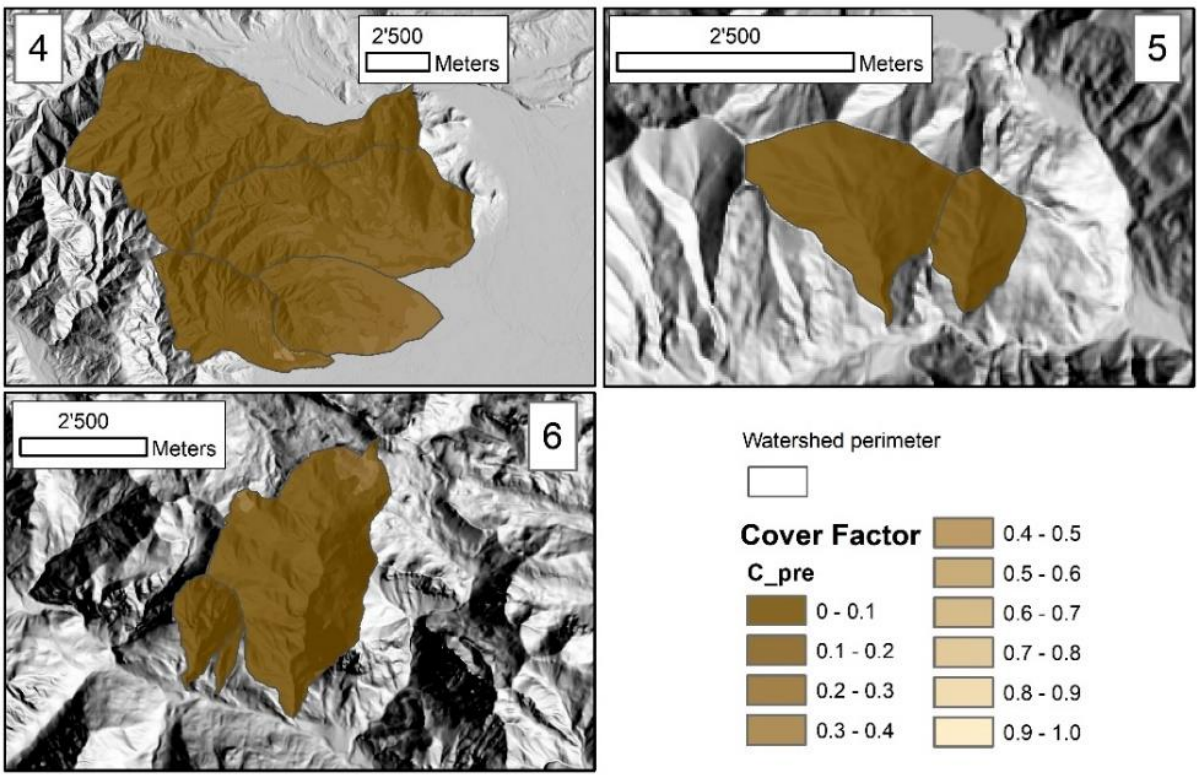


*Figure A4.5 - Cover Factor in the pre-fire situation for the watersheds affected by the Cumiana/Cantalupa (4), Bellino/Casteldelfino (5) and Sambuco/Pietraporzio (6) wildfires.*

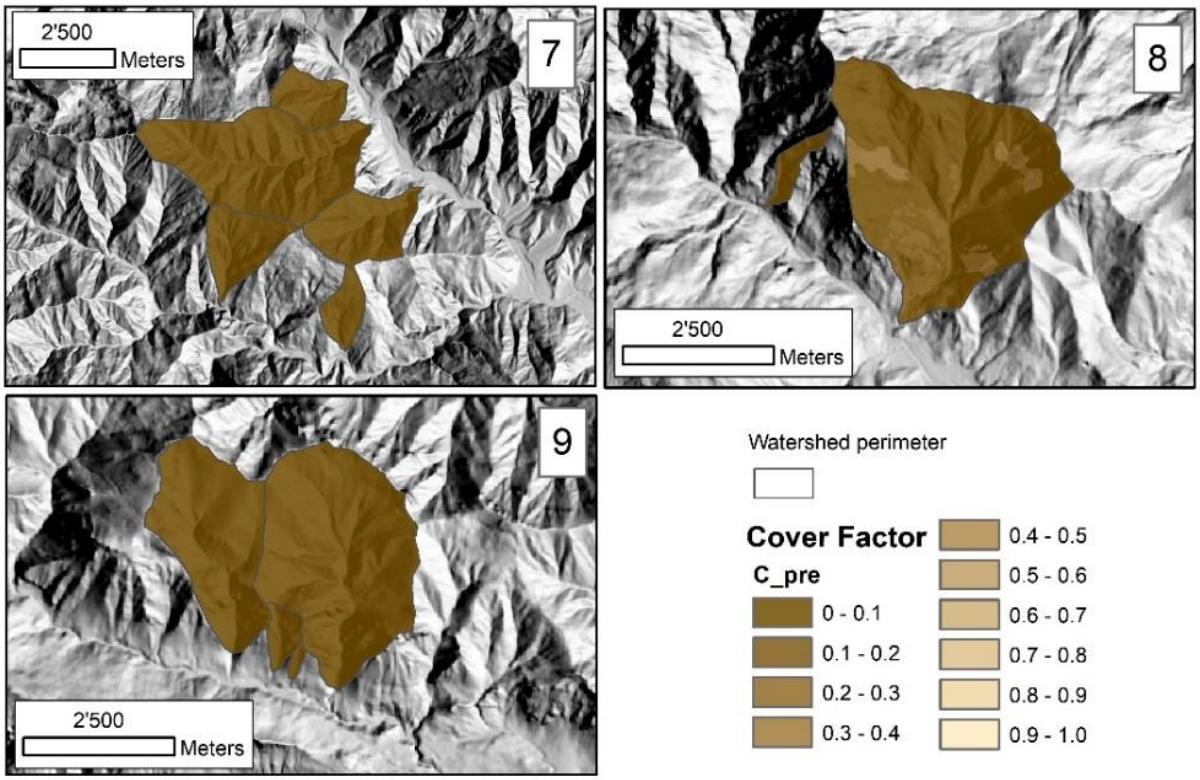


*Figure A4.6 - Cover Factor in the pre-fire situation for the watersheds affected by the Roure/Perrero (7), Traversella (8) and Demonte (9) wildfires.*

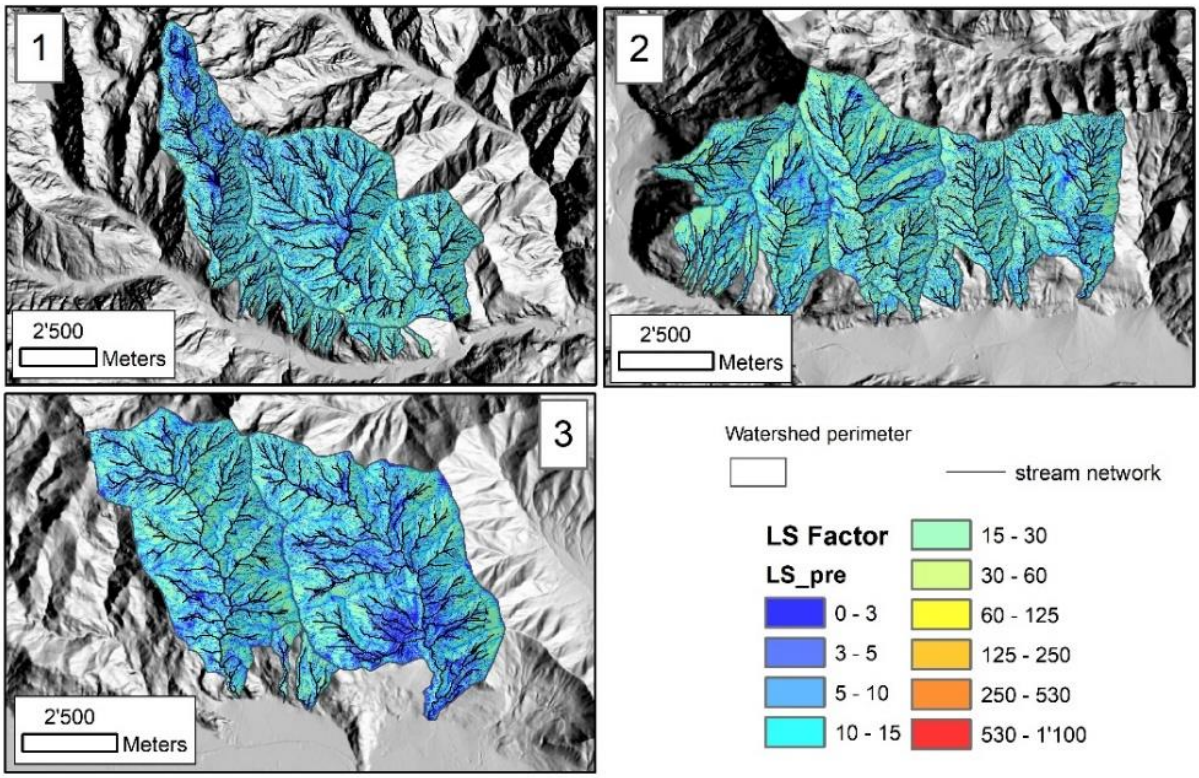


*Figure A4.7 - LS Factor in the pre-fire situation for the watersheds affected by the Locana/Ribordone (1), Bussoleno/Mompantero (2) and Caprie/Rubiana (3) wildfires.*

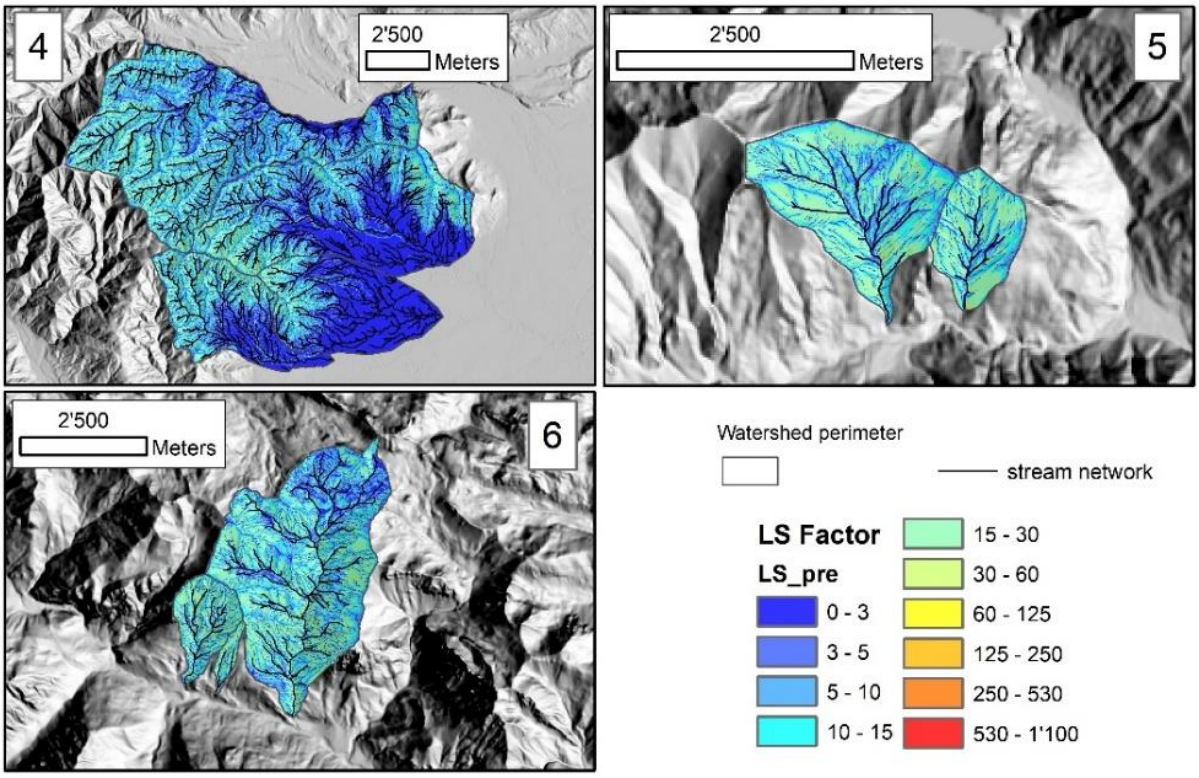


*Figure A4.8 - LS Factor in the pre-fire situation for the watersheds affected by Cumiana/Cantalupa (4), Bellino/Casteldelfino (5) and Sambuco/Pietraporzio (6) wildfires.*

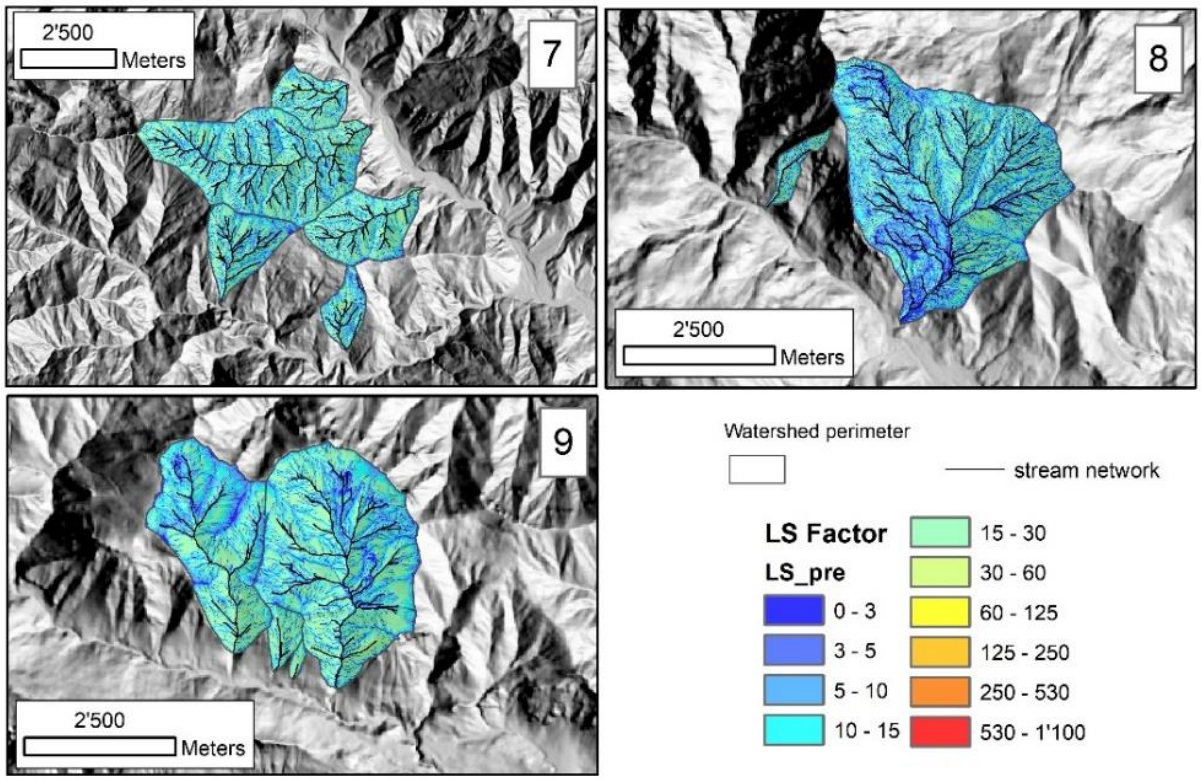


*Figure A4.9 - LS Factor in the pre-fire situation for the watersheds affected by the Roure/Perrero (7), Traversella (8) and Demonte (9) wildfires.*

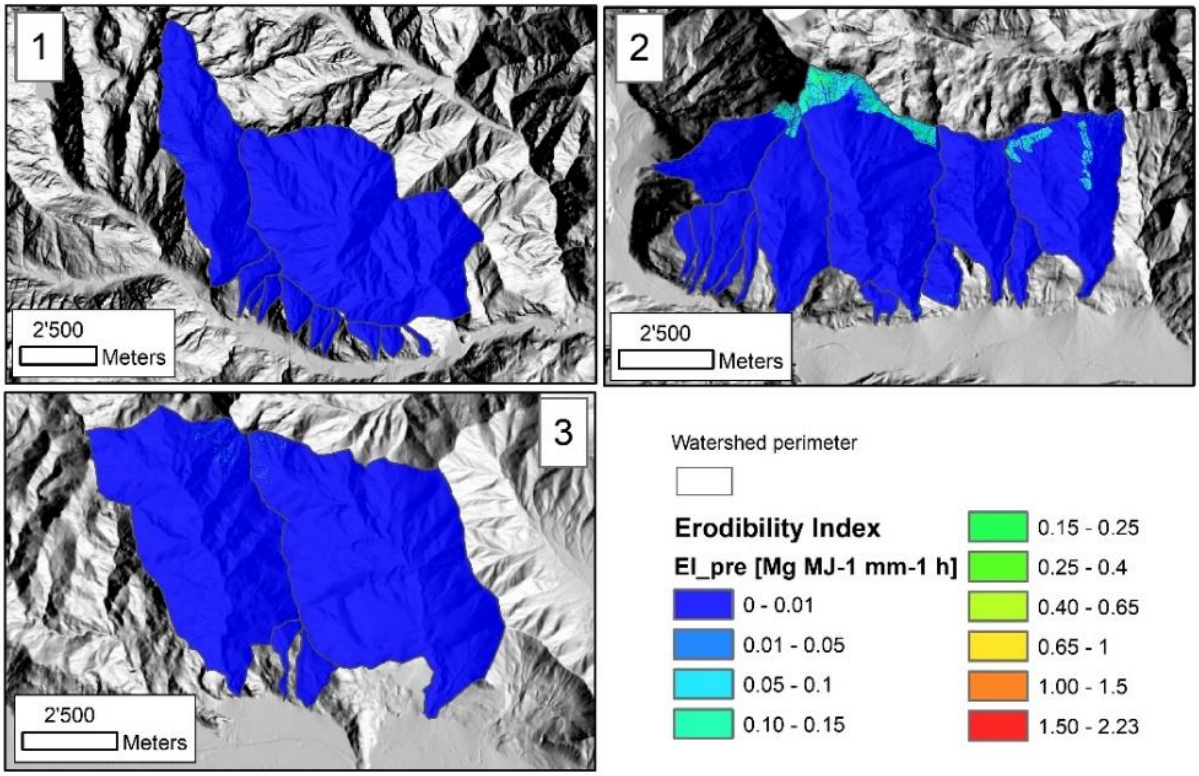


*Figure A4.10 – Erodibility Index in the pre-fire situation for the watersheds affected by the Locana/Ribordone (1), Bussoleno/Mompantero (2) and Caprie/Rubiana (3) wildfires.*

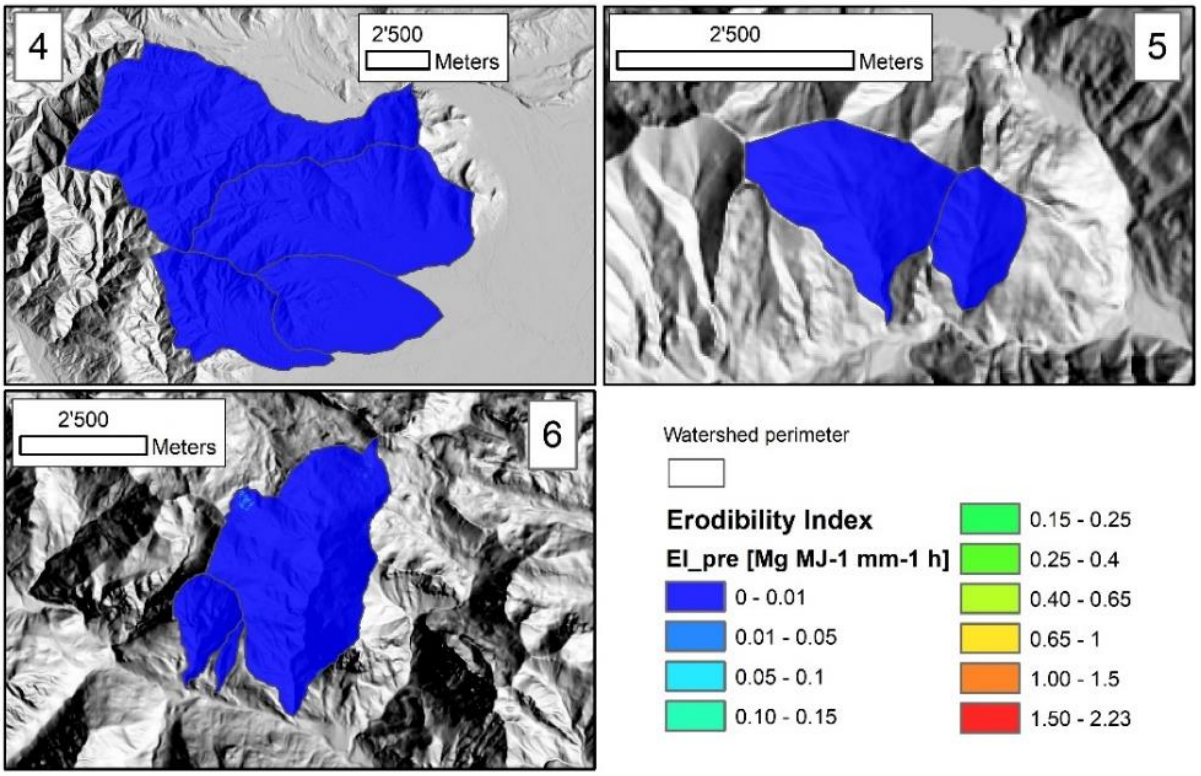


*Figure A4.11 – Erodibility Index in the pre-fire situation for the watersheds affected by the Cumiana/Cantalupa (4), Bellino/Casteldelfino (5) and Sambuco/Pietraporzio (6) wildfires.*

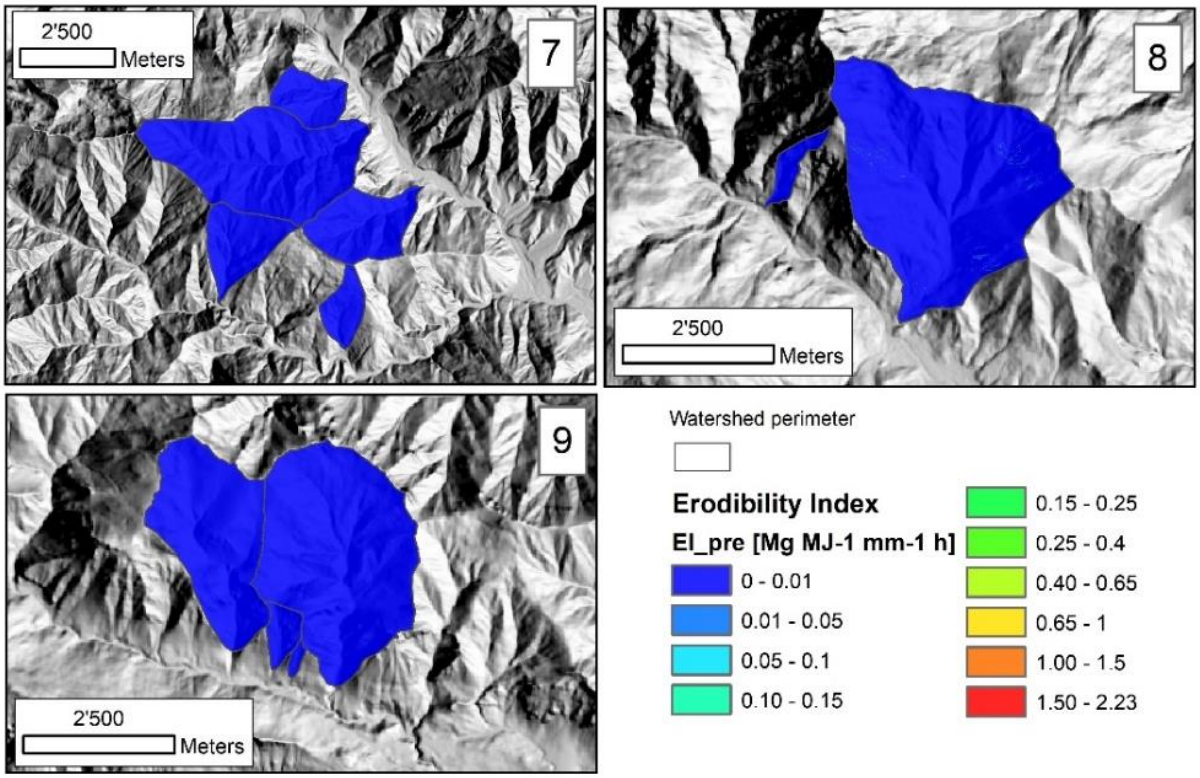


*Figure A4.12 – Erodibility Index in the pre-fire situation for the watersheds affected by the Roure/Perrero (7), Traversella (8) and Demonte (9) wildfires.*

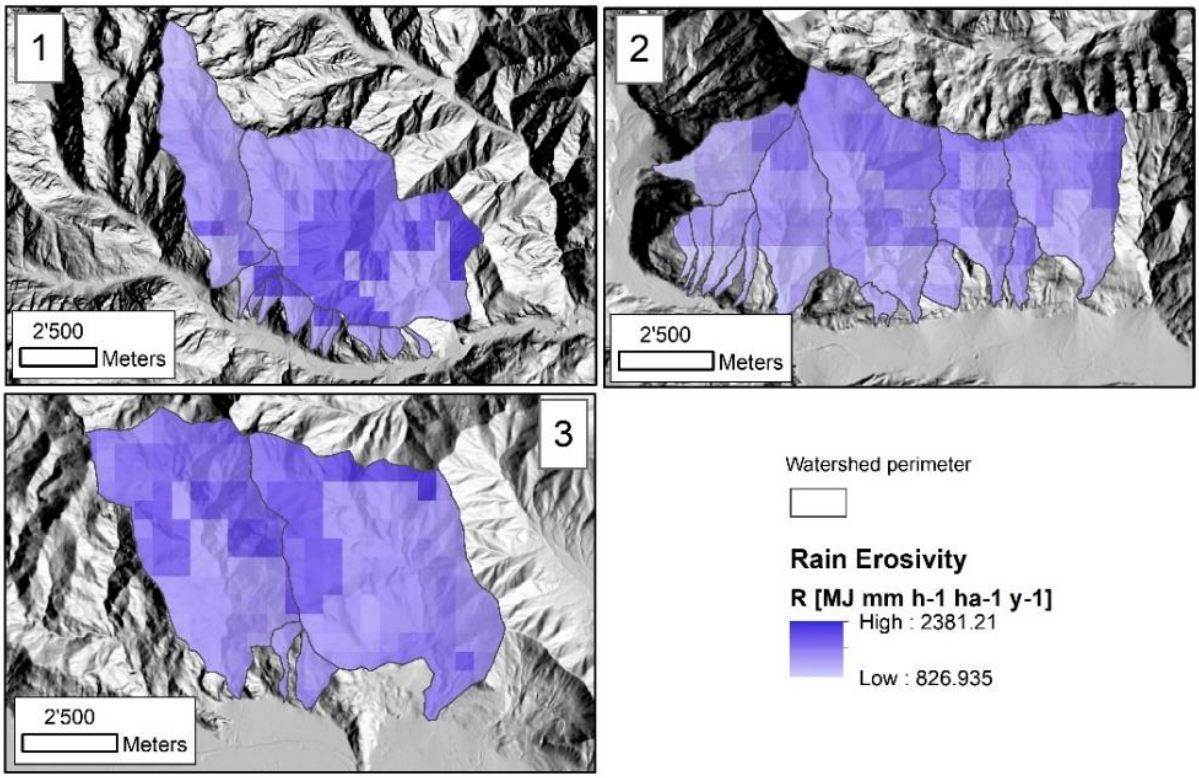


*Figure A4.13 – Rainfall Erosivity for the watersheds affected by the Locana/Ribordone (1), Bussoleno/Mompantero (2) and Caprie/Rubiana (3) wildfires.*

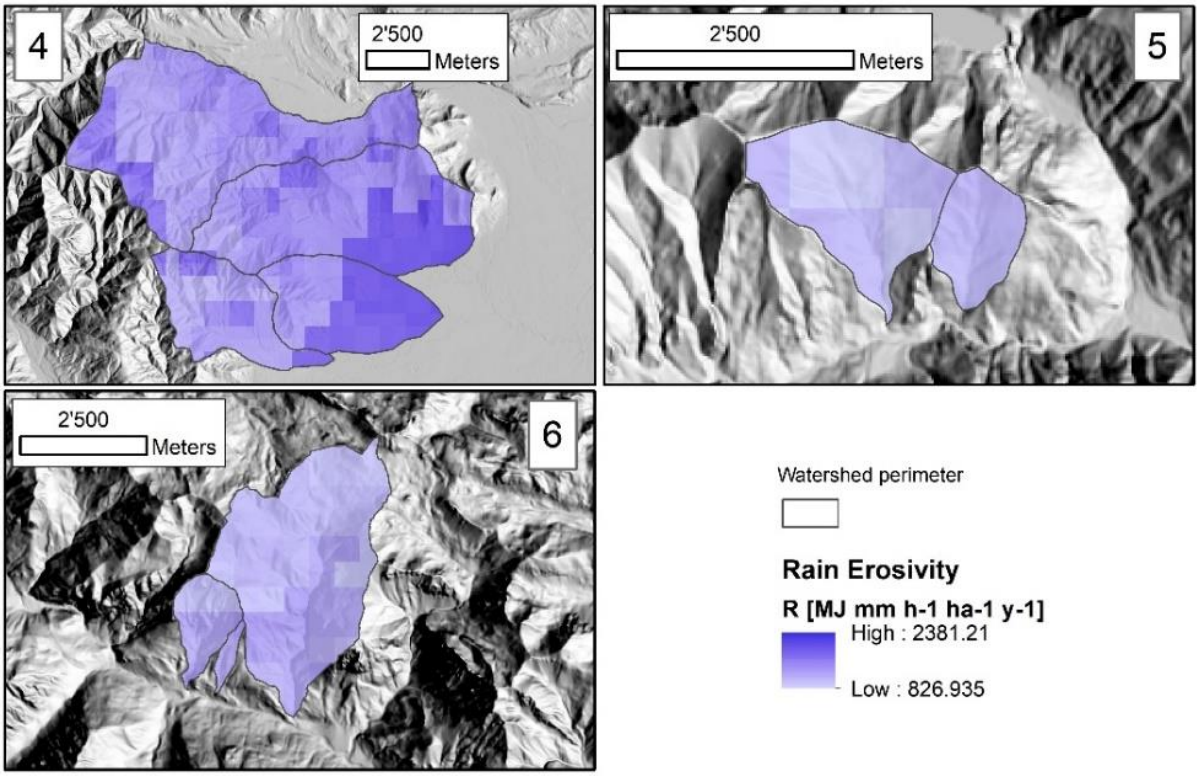


*Figure A4.14 – Rainfall Erosivity for the watersheds affected by the Cumiana/Cantalupa (4), Bellino/Casteldelfino (5) and Sambuco/Pietraporzio (6) wildfires.*

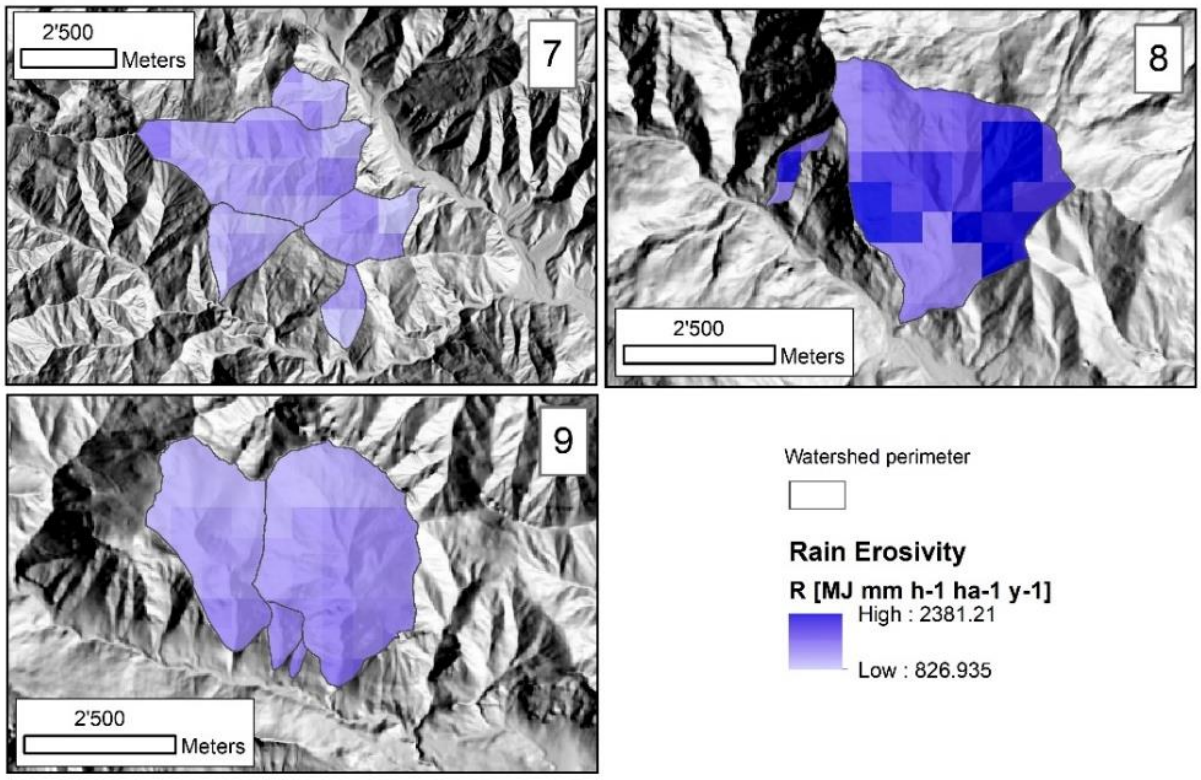


*Figure A4.15 – Rainfall Erosivity for the watersheds affected by the Roure/Perrero (7), Traversella (8) and Demonte (9) wildfires.*

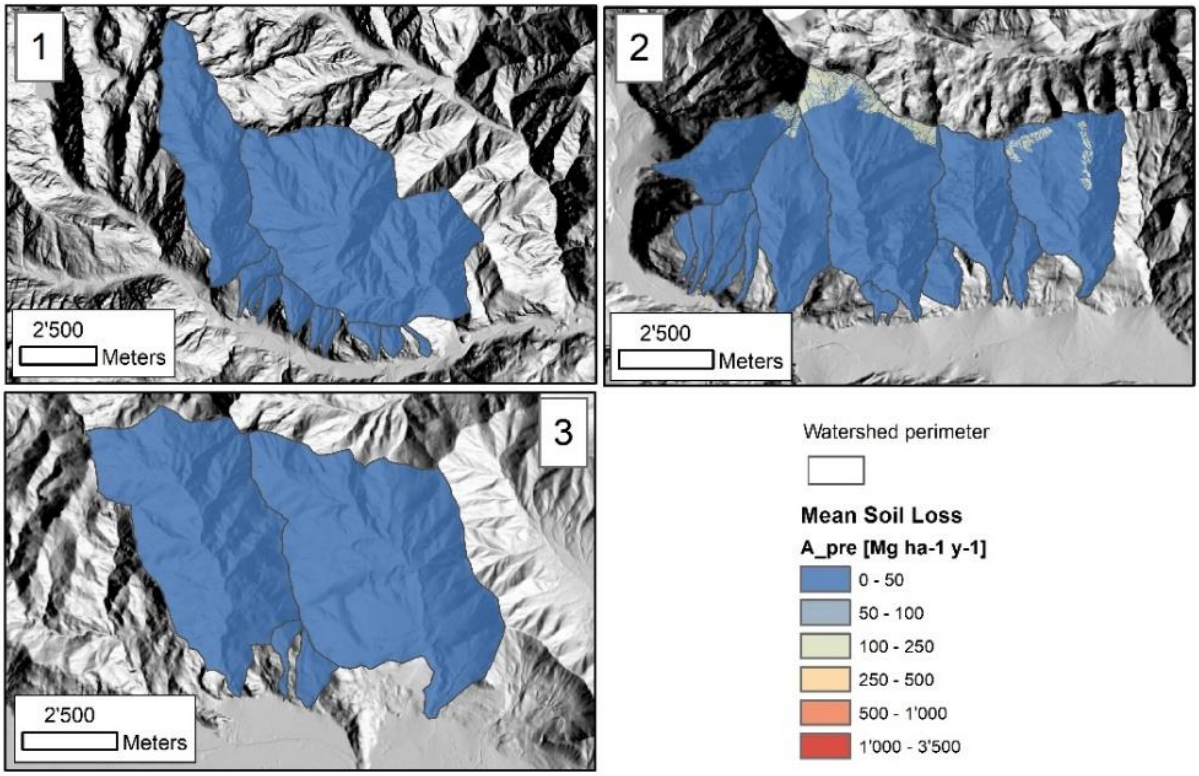


*Figure A4.16 – Mean Soil Loss in the pre-fire situation for the watersheds affected by the Locana/Ribordone (1), Bussoleno/Mompantero (2) and Caprie/Rubiana (3) wildfires.*

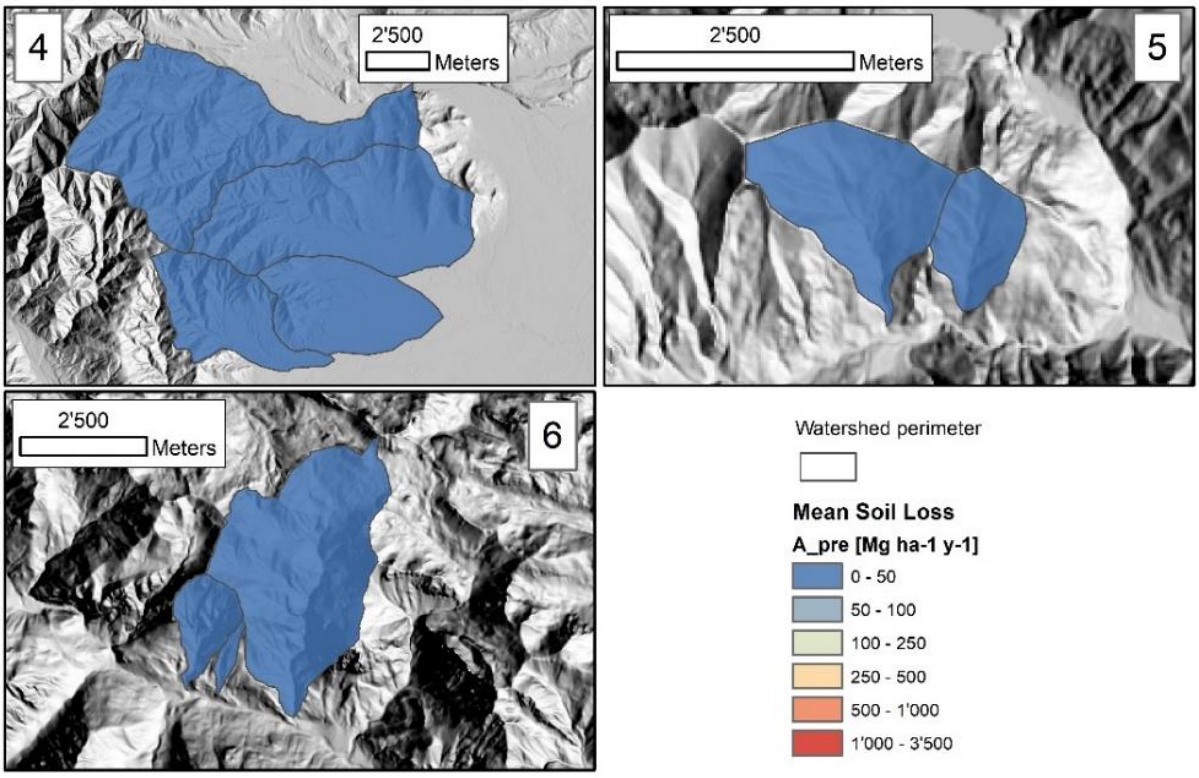


*Figure A4.17 – Mean Soil Loss in the pre-fire situation for the watersheds affected by the Cumiana/Cantalupa (4), Bellino/Casteldelfino (5) and Sambuco/Pietraporzio (6)) wildfires.*

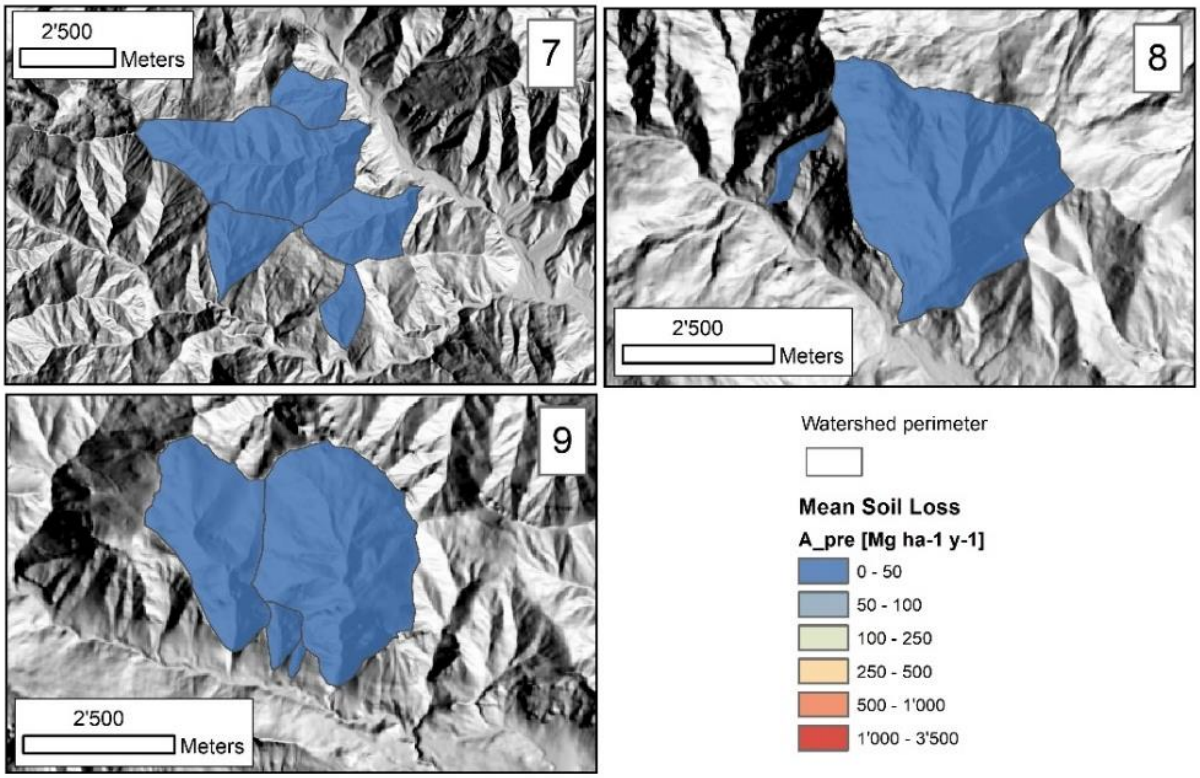


*Figure A4.18 – Mean Soil Loss in the pre-fire situation for the watersheds affected by the Roure/Perrero (7), Traversella (8) and Demonte (9) wildfires.*

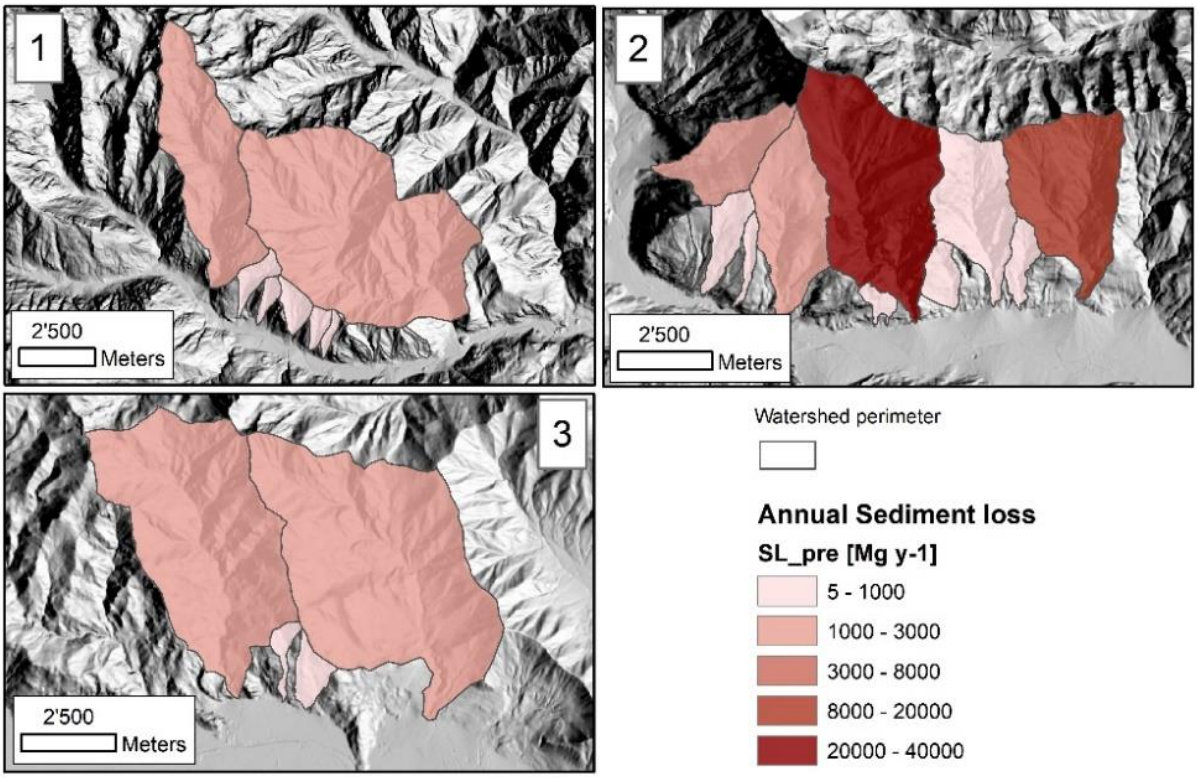


*Figure A4.19- Annual Sediment Loss in the pre-fire situation for the watersheds affected by the Locana/Ribordone (1), Bussoleno/Mompantero (2) and Caprie/Rubiana (3) wildfires.*

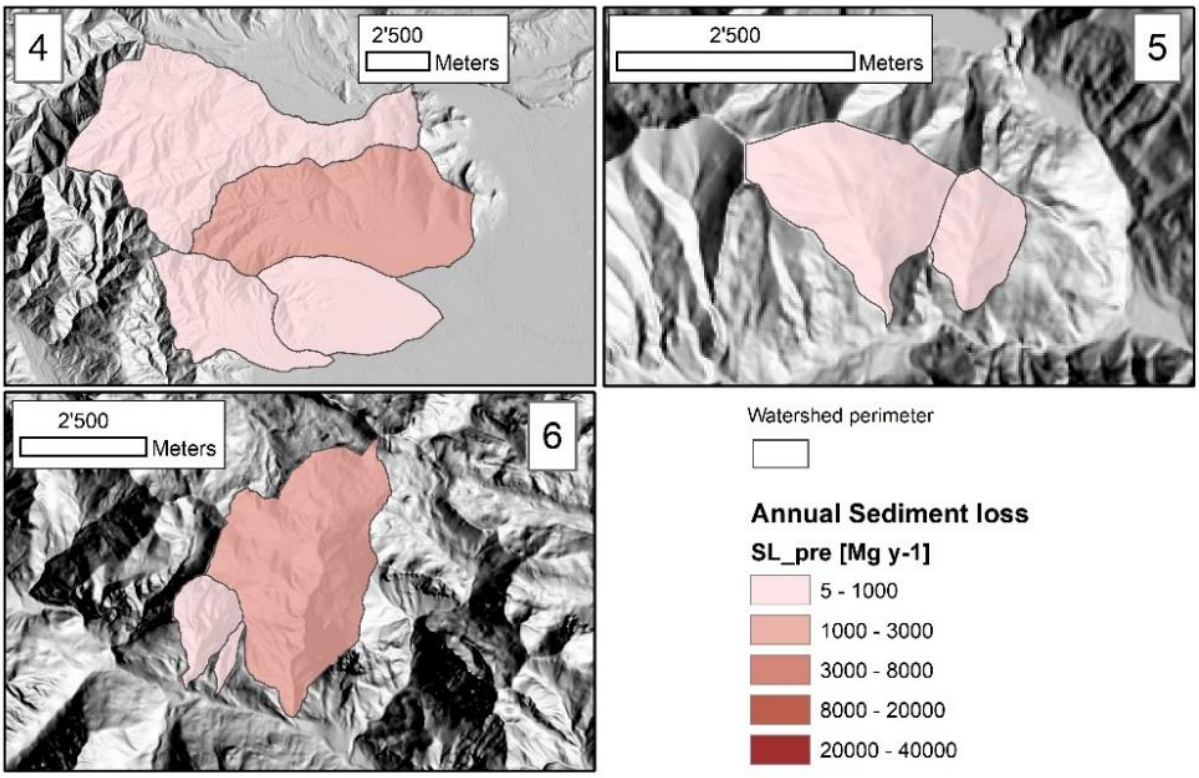


*Figure A4.20- Annual Sediment Loss in the pre-fire situation for the watersheds affected by the Cumiana/Cantalupa (4), Bellino/Casteldelfino (5) and Sambuco/Pietraporzio (6)) wildfires.*

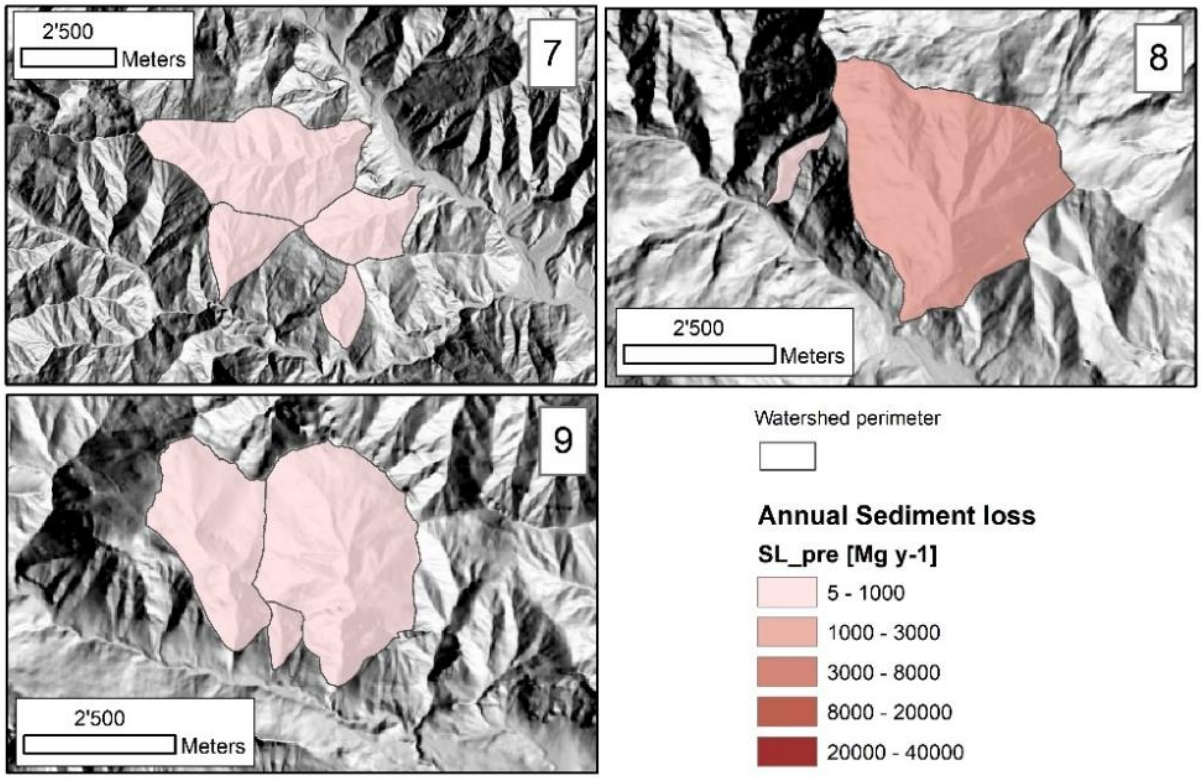


*Figure A4.21- Annual Sediment Loss in the pre-fire situation for the watersheds affected by the Roure/Perrero (7), Traversella (8) and Demonte (9) wildfires.*

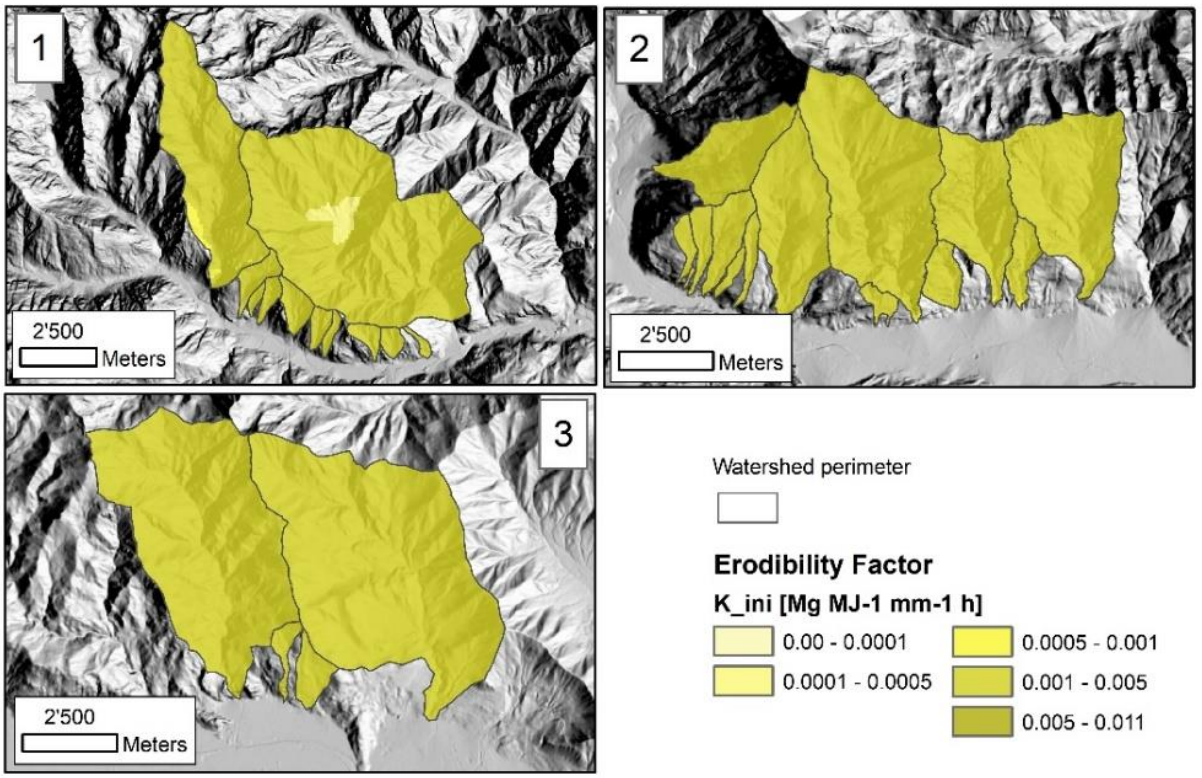


*Figure A4.22 - Erodibility Factor in the post-fire situation – initial assessment, for the watersheds affected by the Locana/Ribordone (1), Bussoleno/Mompantero (2) and Caprie/Rubiana (3) wildfires.*

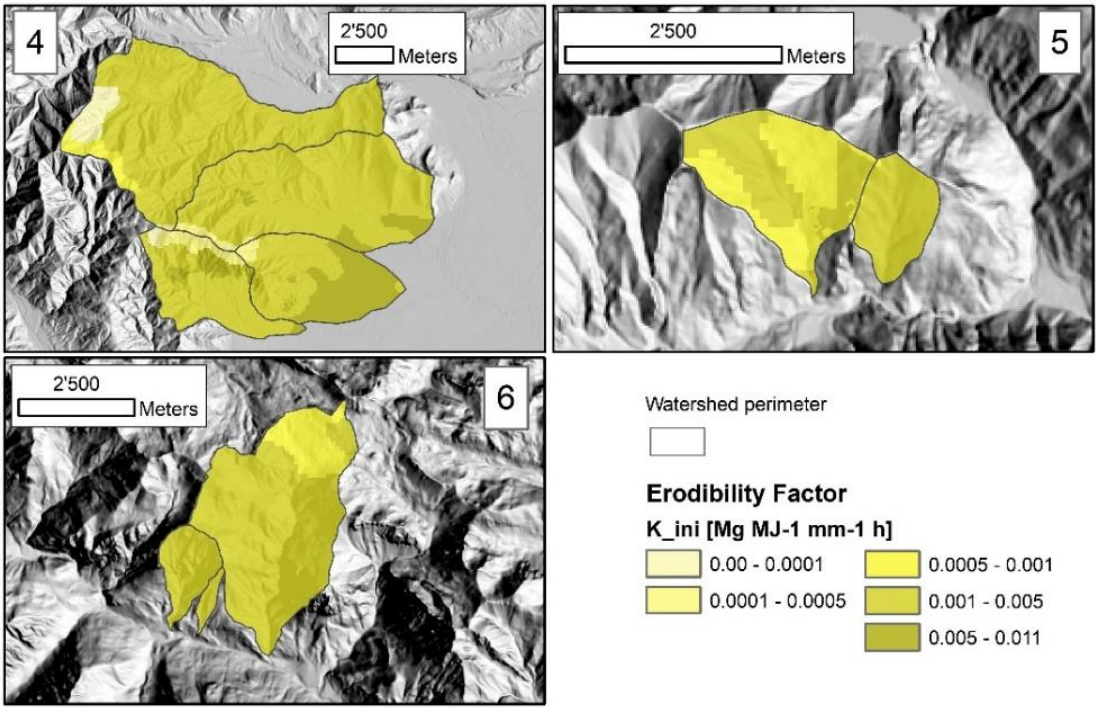


*Figure A4.23 - Erodibility Factor in the post-fire situation – initial assessment, for the watersheds affected by the Cumiana/Cantalupa (4), Bellino/Casteldelfino (5) and Sambuco/Pietraporzio (6) wildfires.*

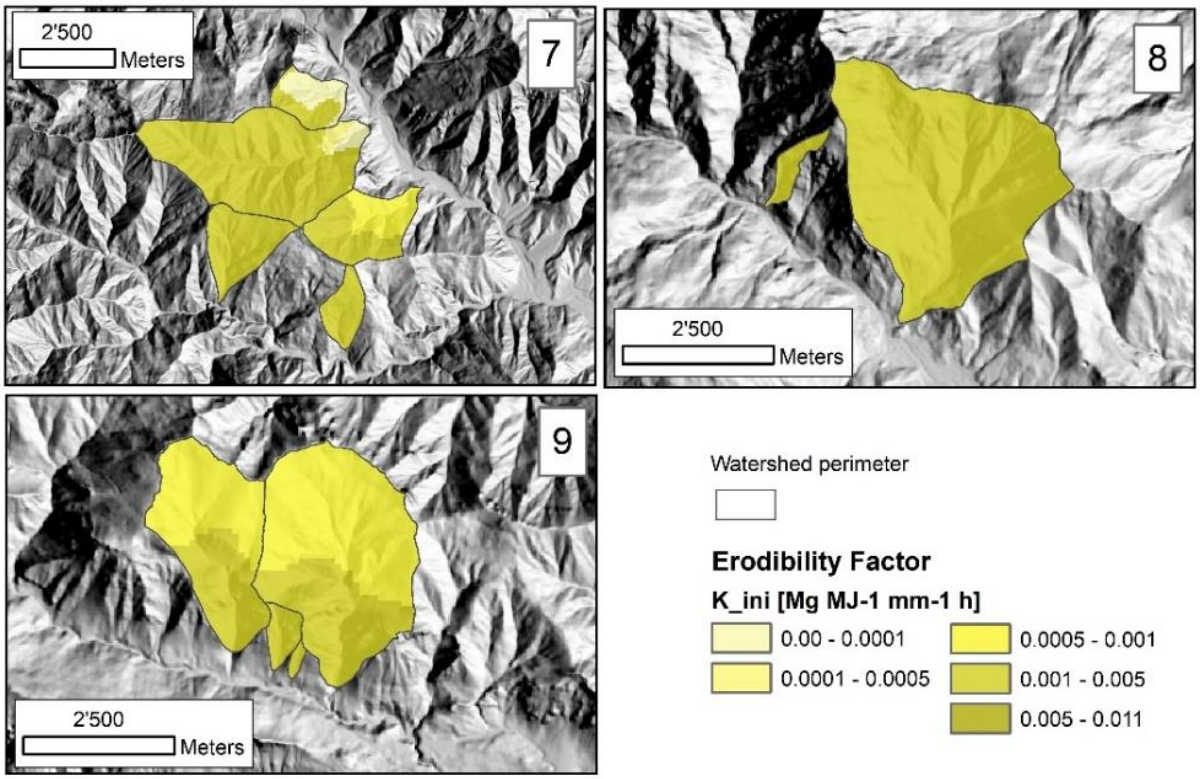


*Figure A4.24 - Erodibility Factor in the post-fire situation – initial assessment, for the watersheds affected by the Roure/Perrero (7), Traversella (8) and Demonte (9) wildfires.*

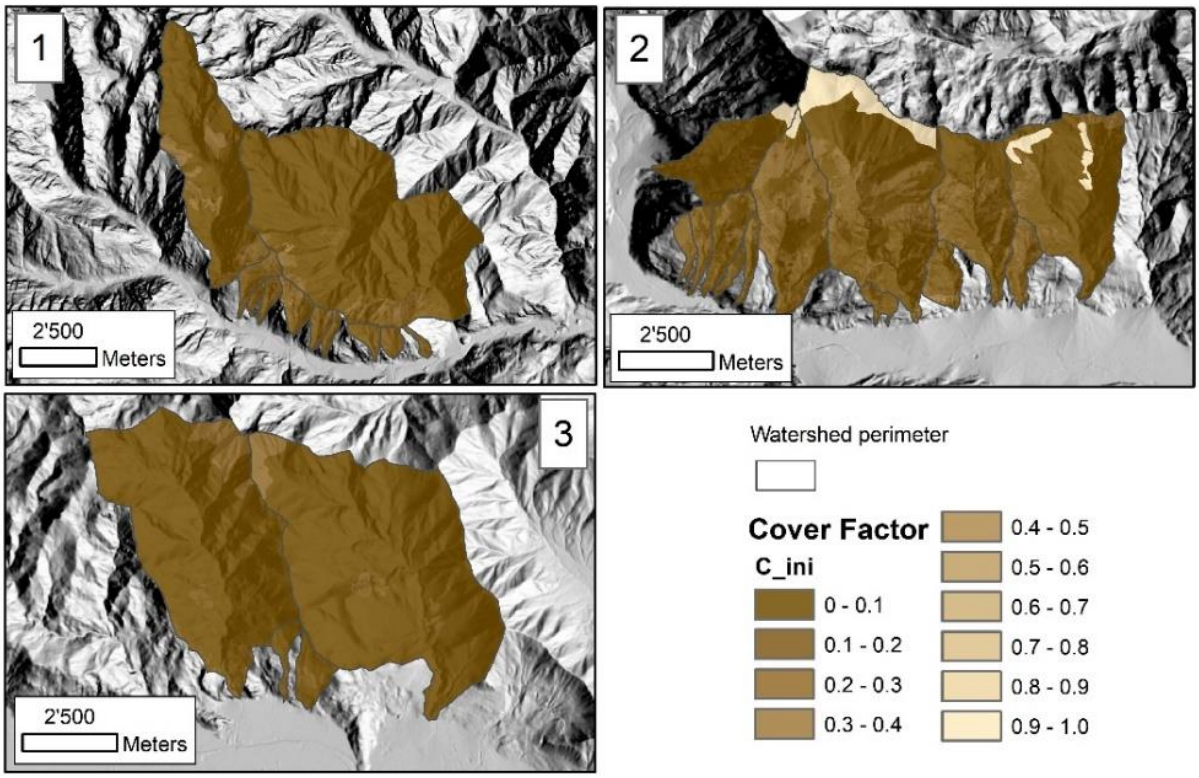


*Figure A4.25 - Cover Factor in the post-fire situation – initial assessment, for the watersheds affected by the Locana/Ribordone (1), Bussoleno/Mompantero (2) and Caprie/Rubiana (3) wildfires.*

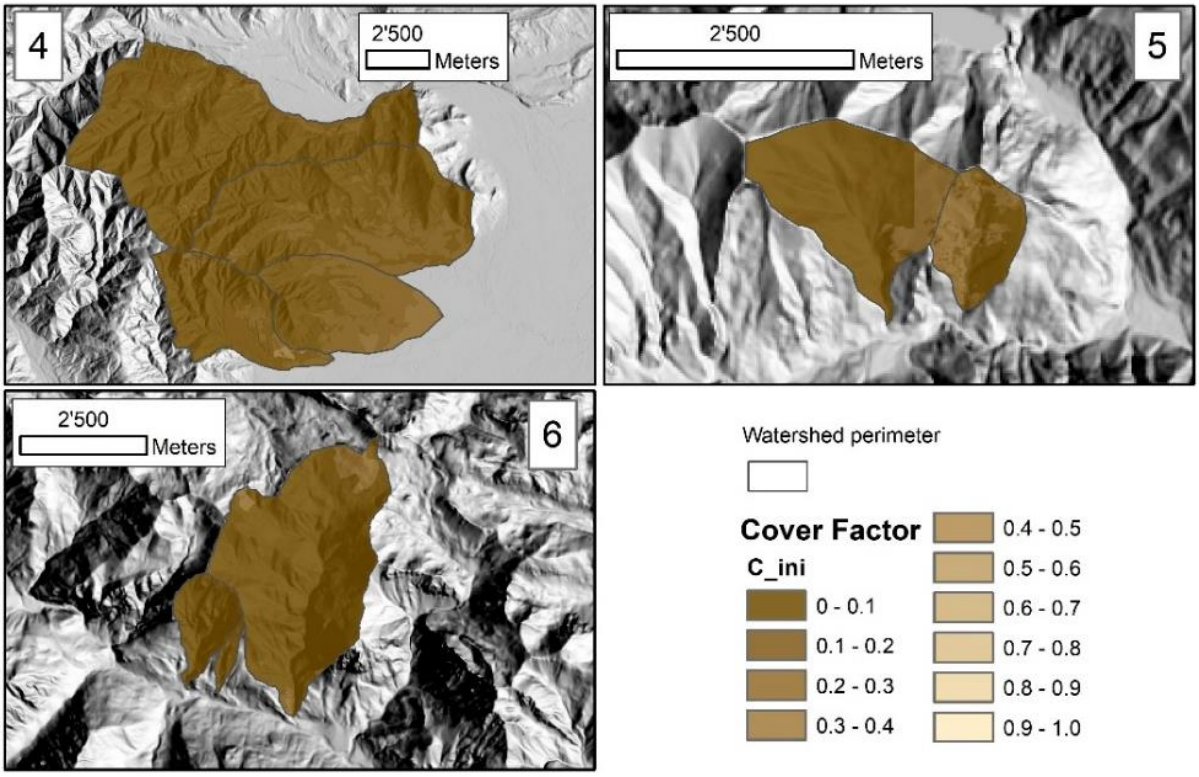


*Figure A4.26 - Cover Factor in the post-fire situation – initial assessment, for the watersheds affected by the Cumiana/Cantalupa (4), Bellino/Casteldelfino (5) and Sambuco/Pietraporzio (6) wildfires.*

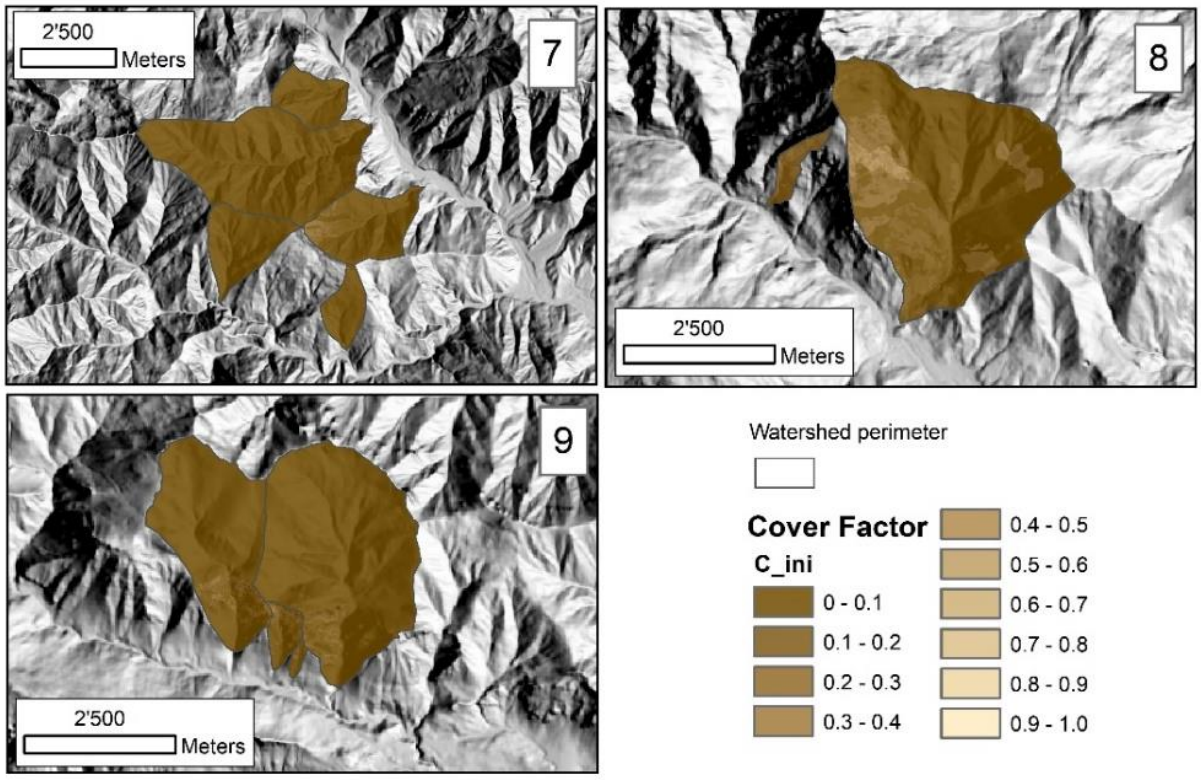


*Figure A4.27 - Cover Factor in the post-fire situation – initial assessment, for the watersheds affected by the Roure/Perrero (7), Traversella (8) and Demonte (9) wildfires.*

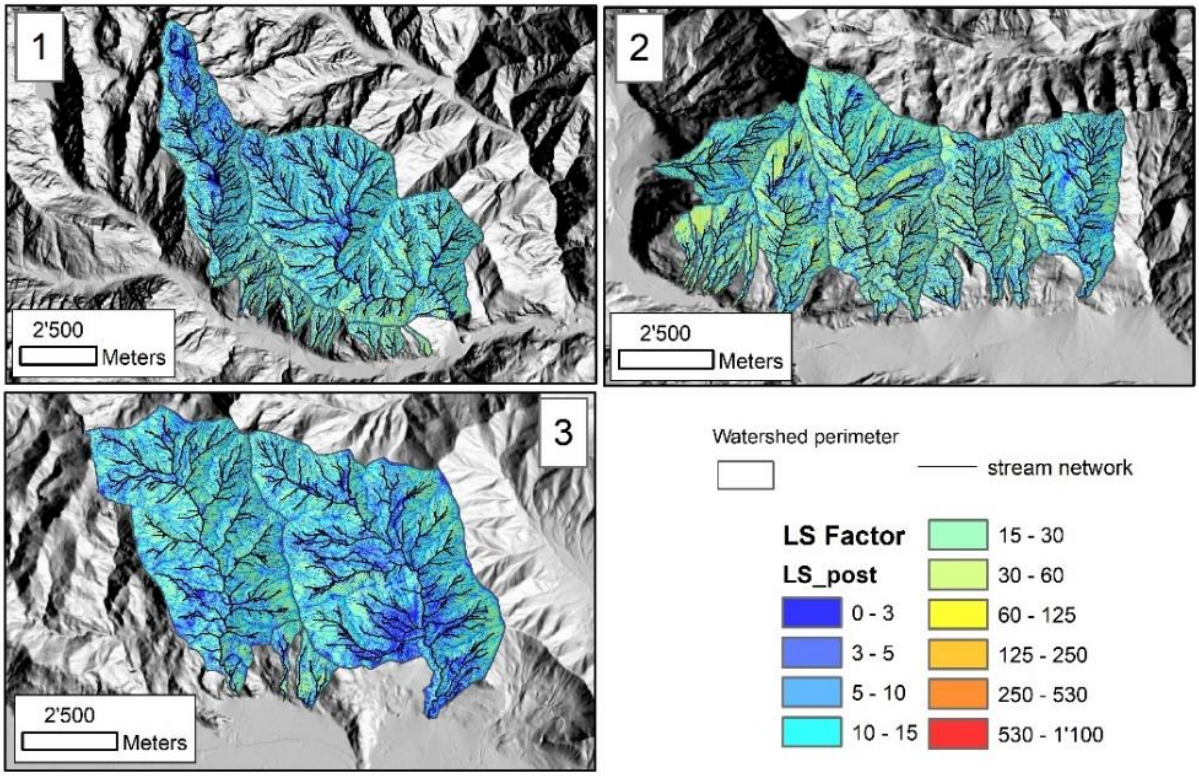


*Figure A4.28 - LS Factor in the post-fire situation – initial assessment, for the watersheds affected by the Locana/Ribordone (1), Bussoleno/Mompantero (2) and Caprie/Rubiana (3) wildfires.*

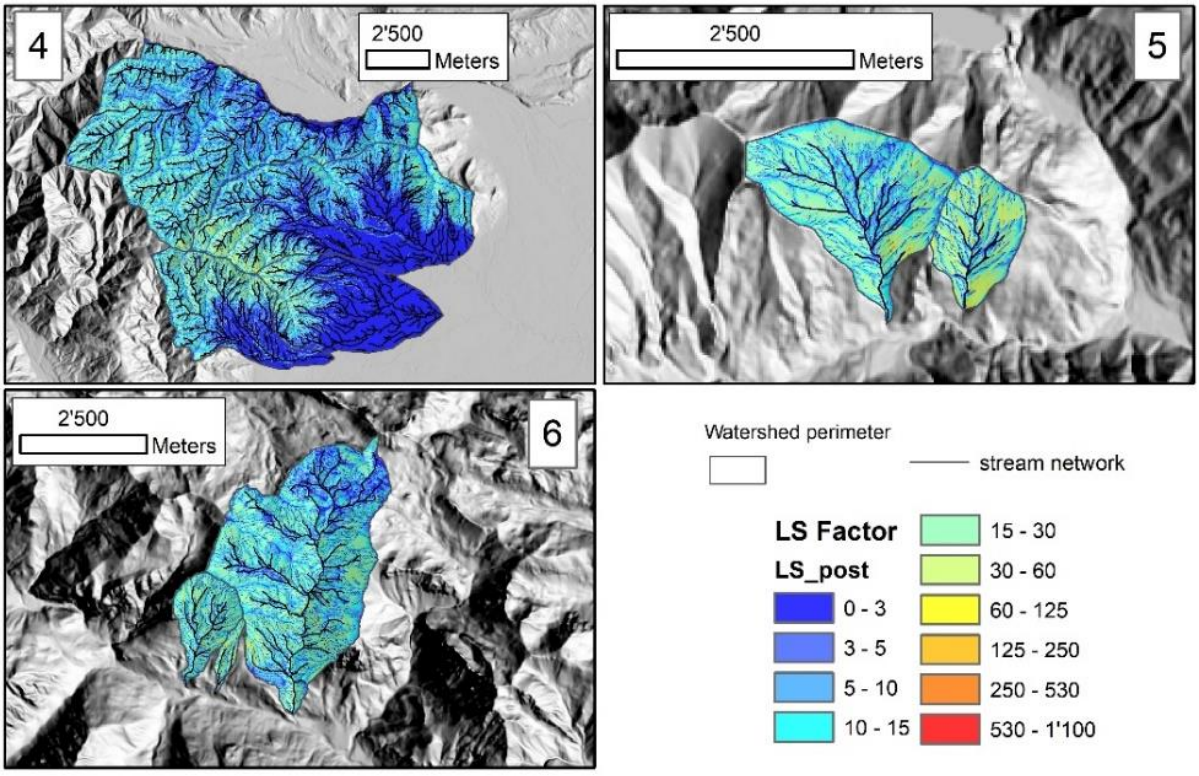


*Figure A4.29 - LS Factor in the post-fire situation – initial assessment, for the watersheds affected by Cumiana/Cantalupa (4), Bellino/Casteldelfino (5) and Sambuco/Pietraporzio (6) wildfires.*

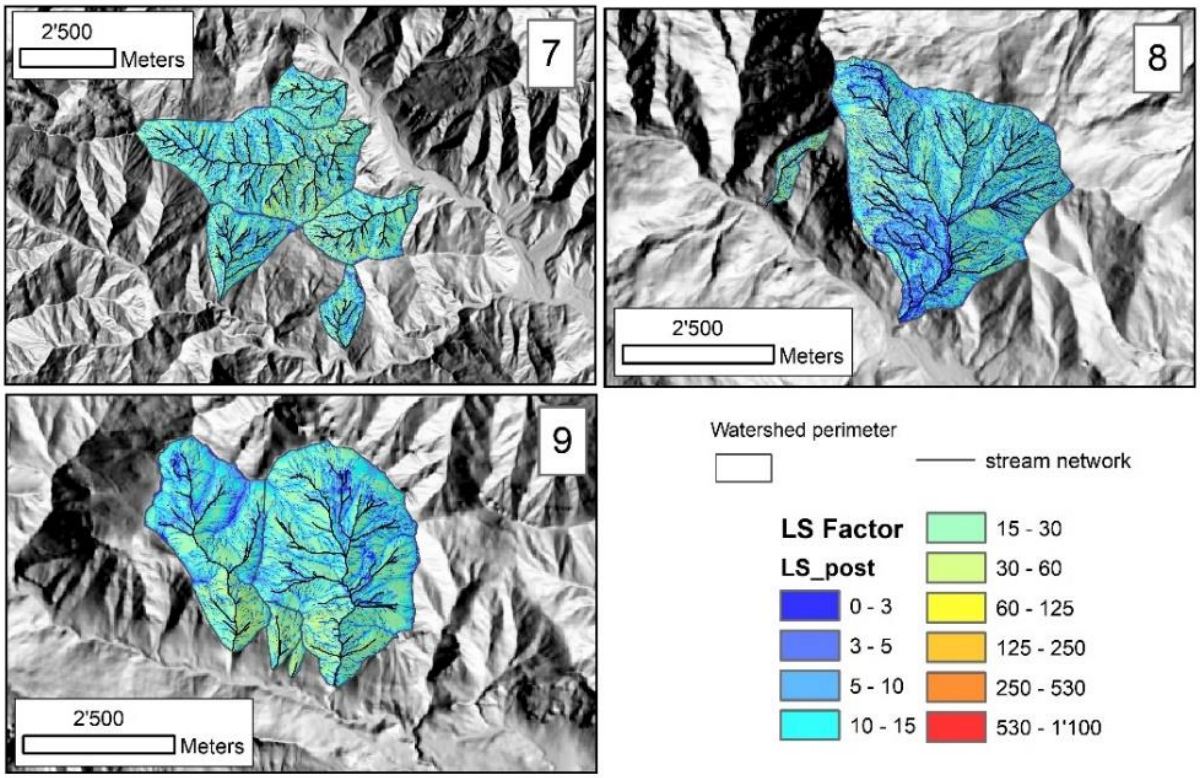


*Figure A4.30 - LS Factor in the post-fire situation – initial assessment, for the watersheds affected by the Roure/Perrero (7), Traversella (8) and Demonte (9) wildfires.*

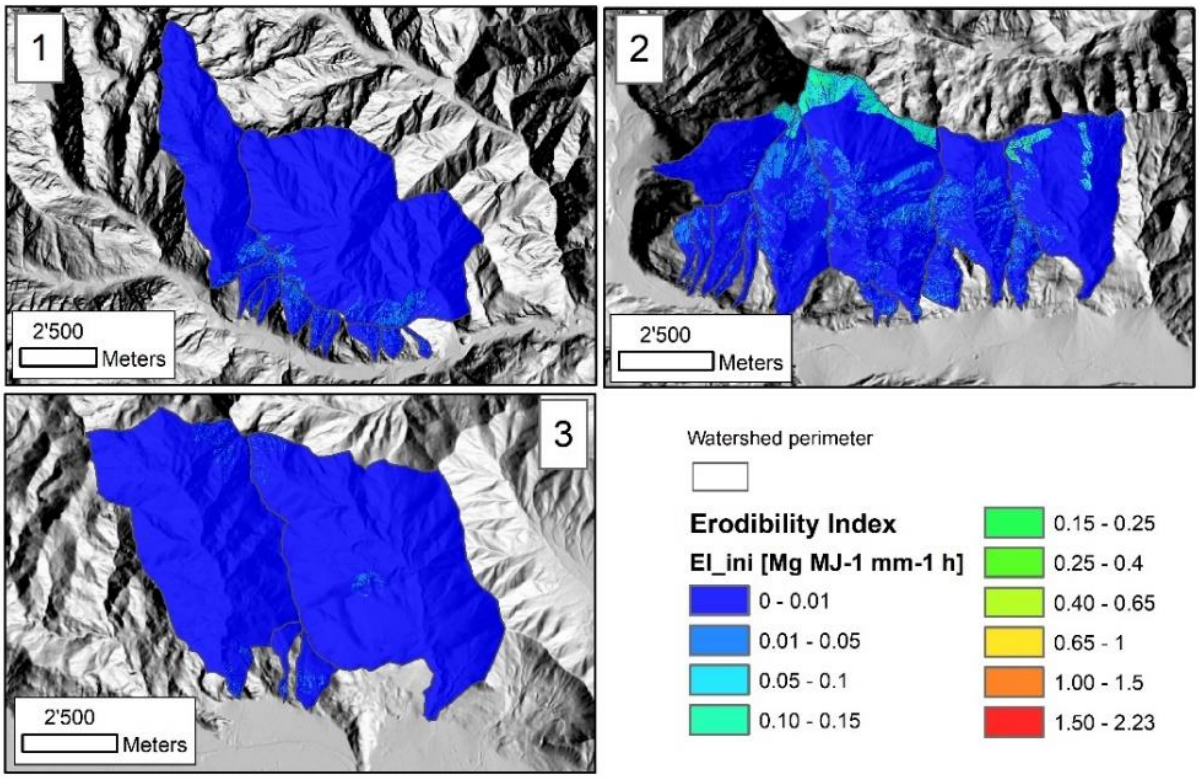


*Figure A4.31 - Erodibility Index in the post-fire situation – initial assessment, for the watersheds affected by the Locana/Ribordone (1), Bussoleno/Mompantero (2) and Caprie/Rubiana (3) wildfires.*

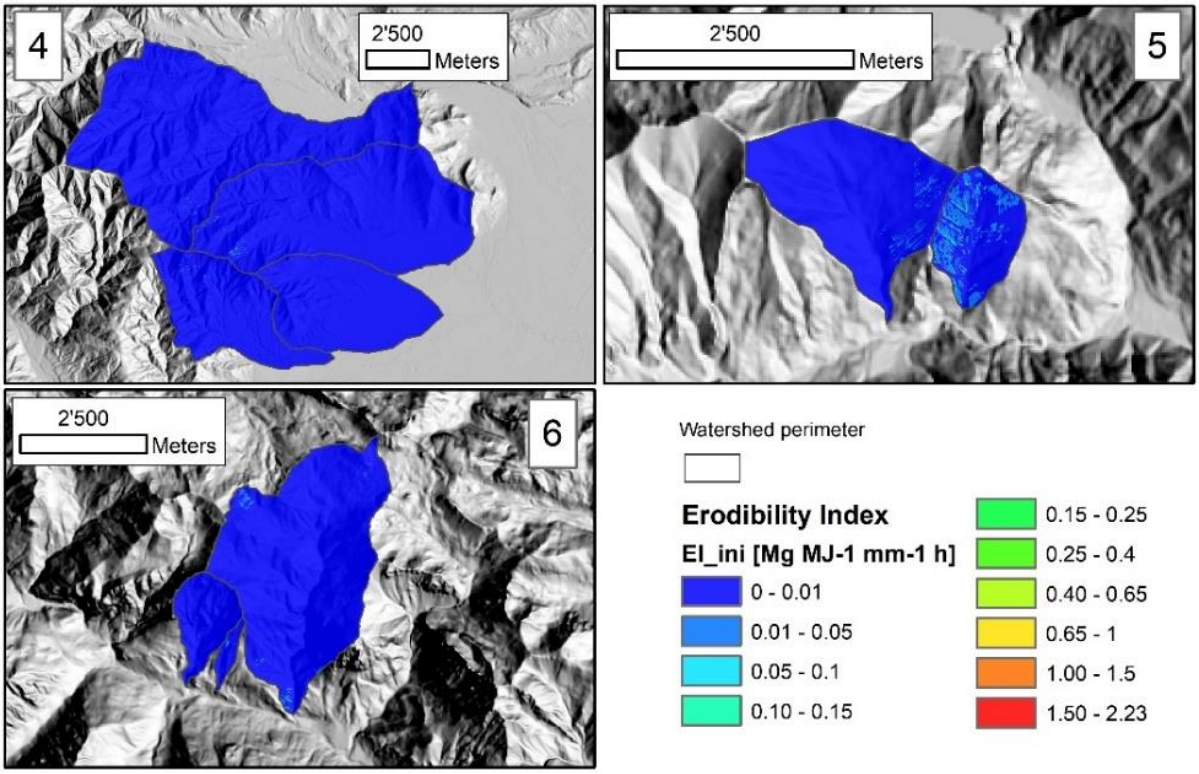


*Figure A4.32 - Erodibility Index in the post-fire situation – initial assessment, for the watersheds affected by the Cumiana/Cantalupa (4), Bellino/Casteldelfino (5) and Sambuco/Pietraporzio (6) wildfires.*

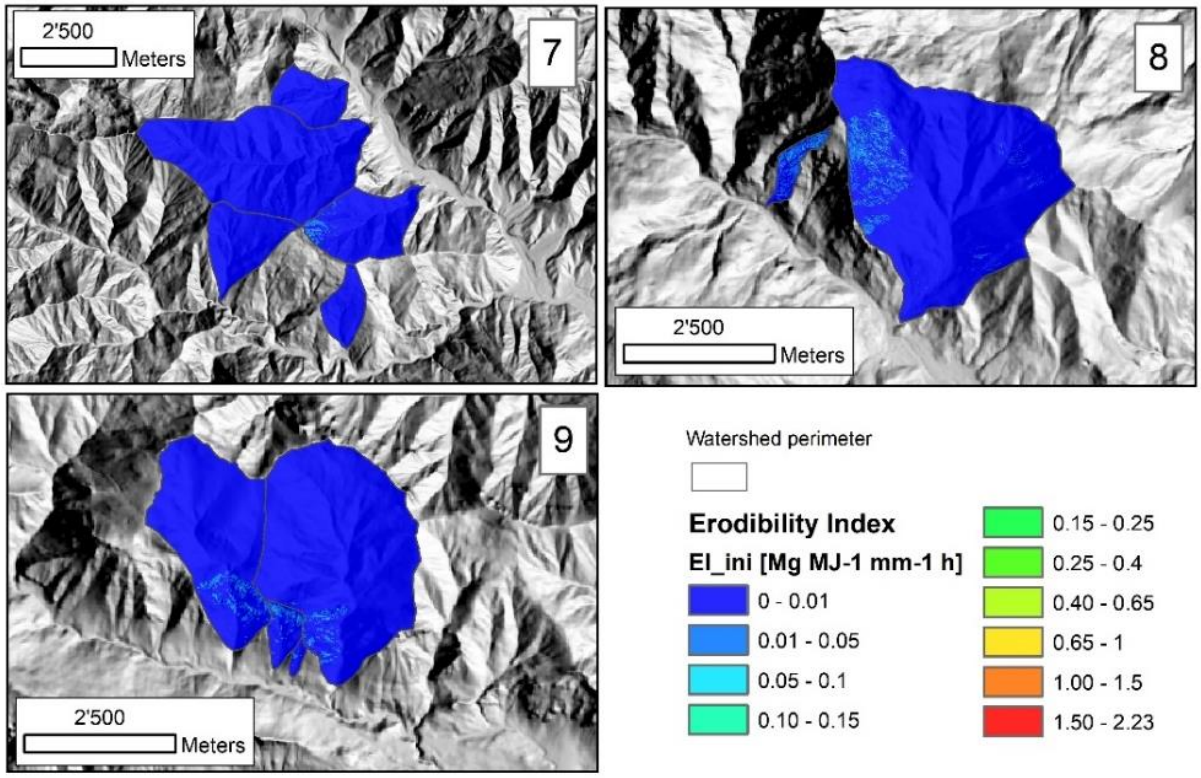


*Figure A4.33 - Erodibility Index in the post-fire situation – initial assessment, for the watersheds affected by the Roure/Perrero (7), Traversella (8) and Demonte (9) wildfires.*

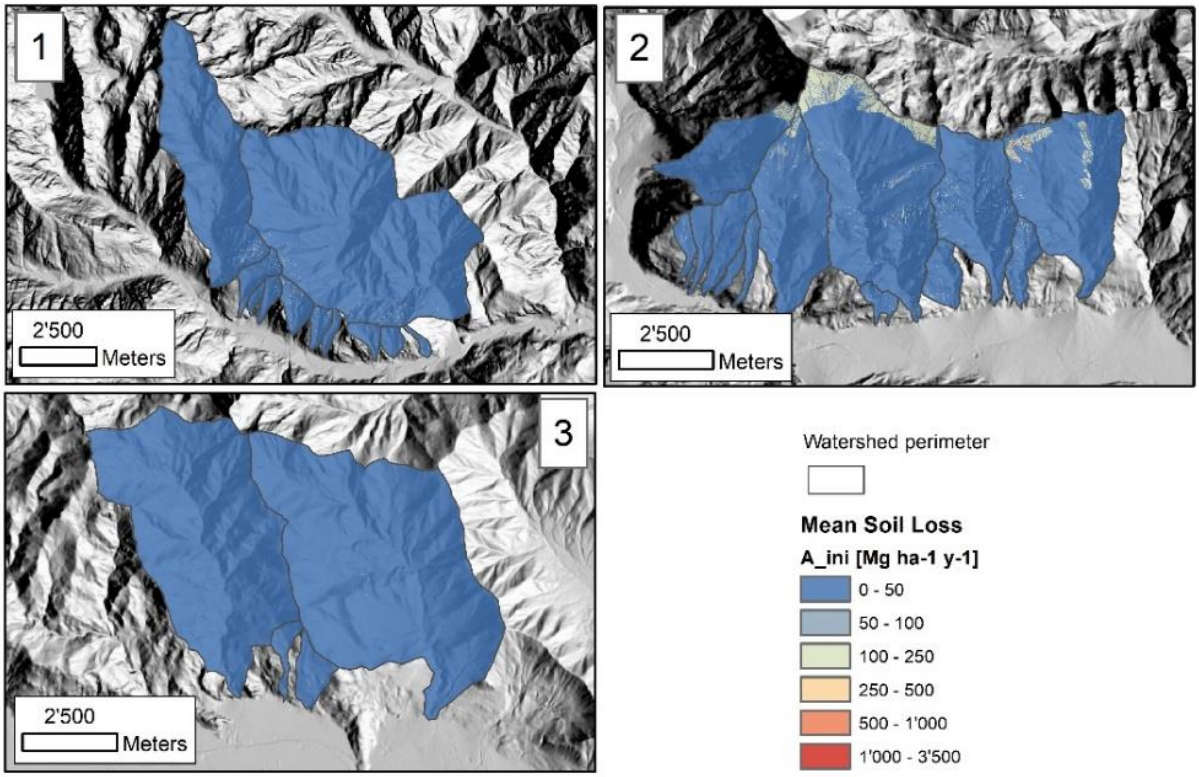


*Figure A4.34 – Mean Soil Loss in the post-fire situation – initial assessment, for the watersheds affected by the Locana/Ribordone (1), Bussoleno/Mompantero (2) and Caprie/Rubiana (3) wildfires.*

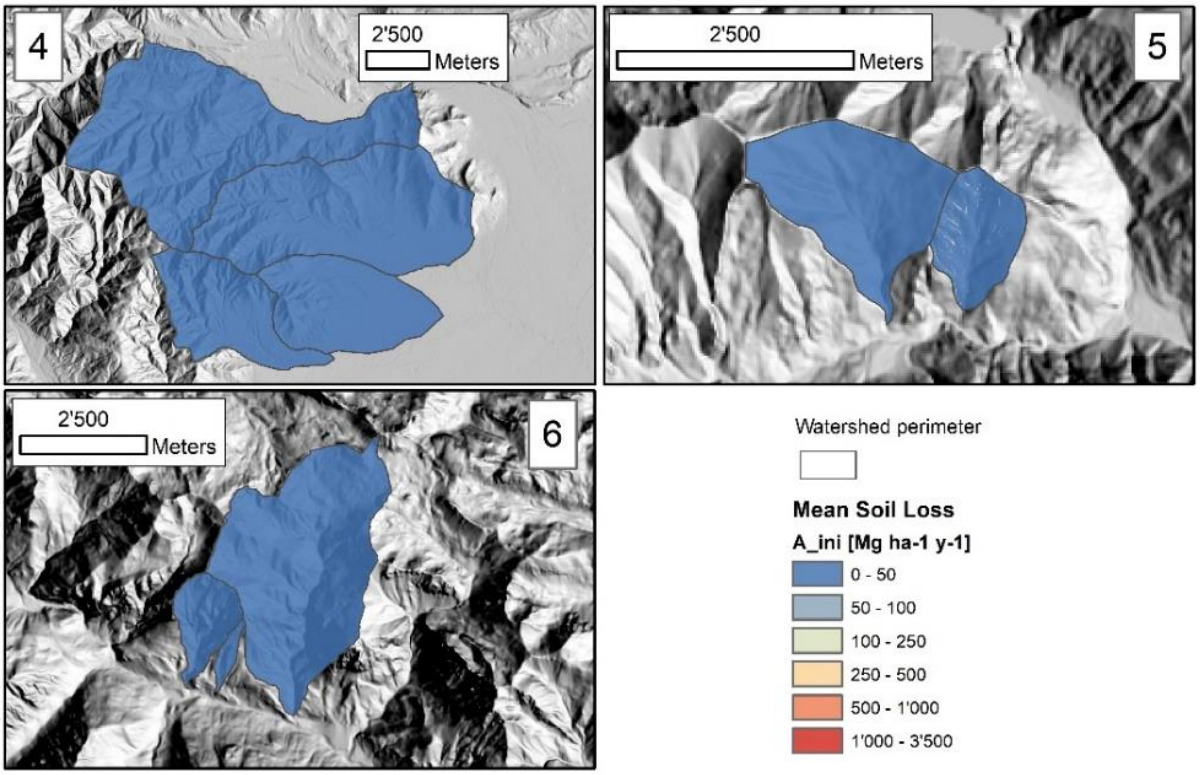


*Figure A4.35 – Mean Soil Loss in the post-fire situation – initial assessment, for the watersheds affected by the Cumiana/Cantalupa (4), Bellino/Casteldelfino (5) and Sambuco/Pietraporzio (6) wildfires.*

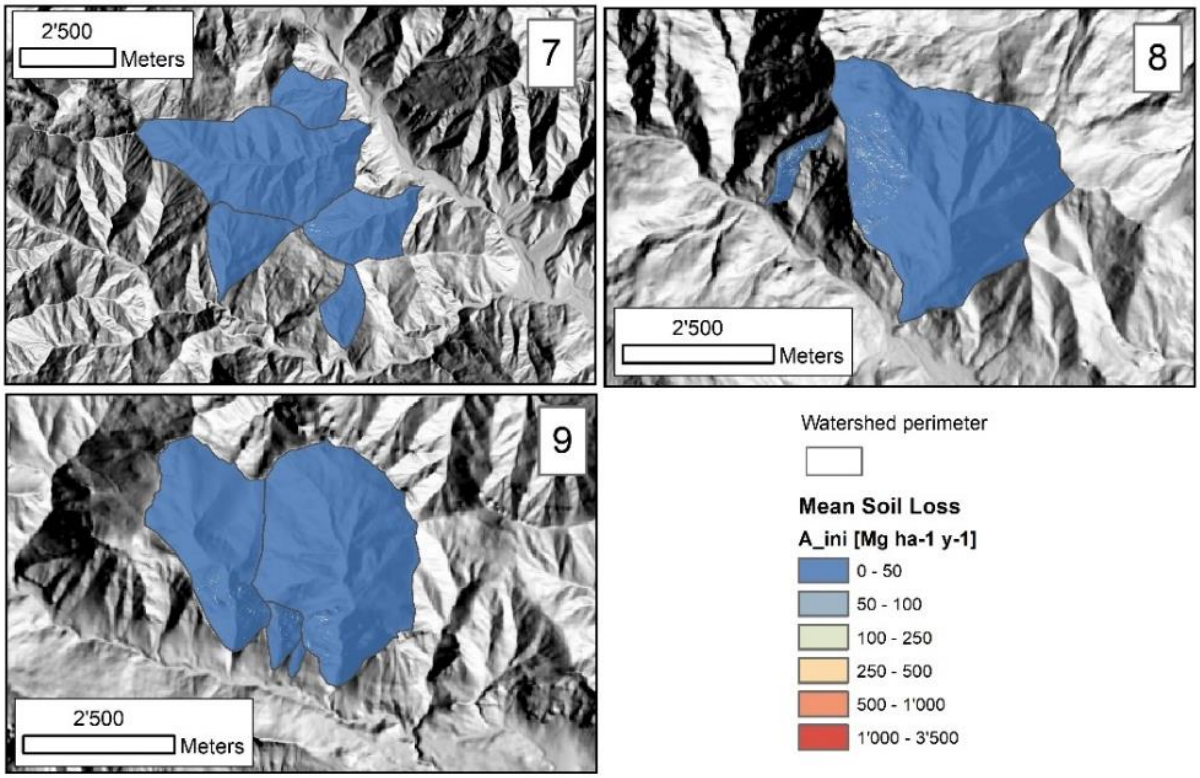


*Figure A4.36 – Mean Soil Loss in the post-fire situation – initial assessment, for the watersheds affected by the Roure/Perrero (7), Traversella (8) and Demonte (9) wildfires.*

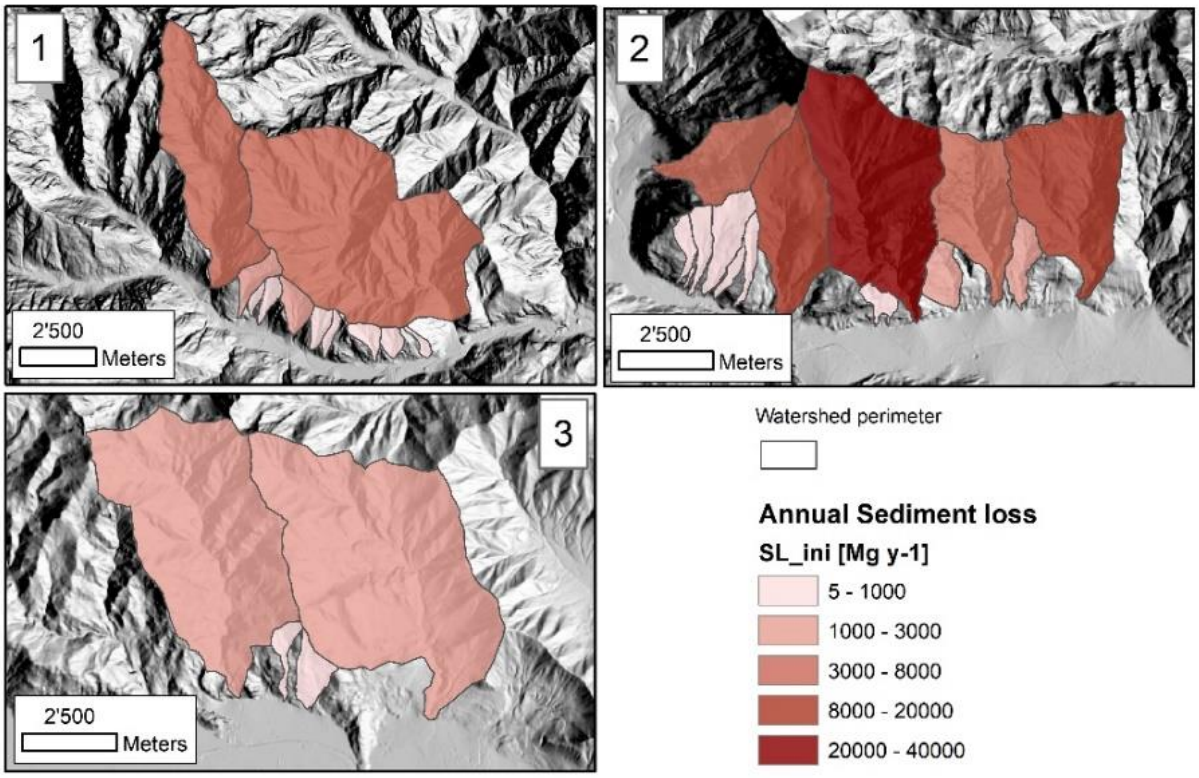


*Figure A4.37 – Annual Sediment Loss in the post-fire situation – initial assessment, for the watersheds affected by the Locana/Ribordone (1), Bussoleno/Mompantero (2) and Caprie/Rubiana (3) wildfires.*

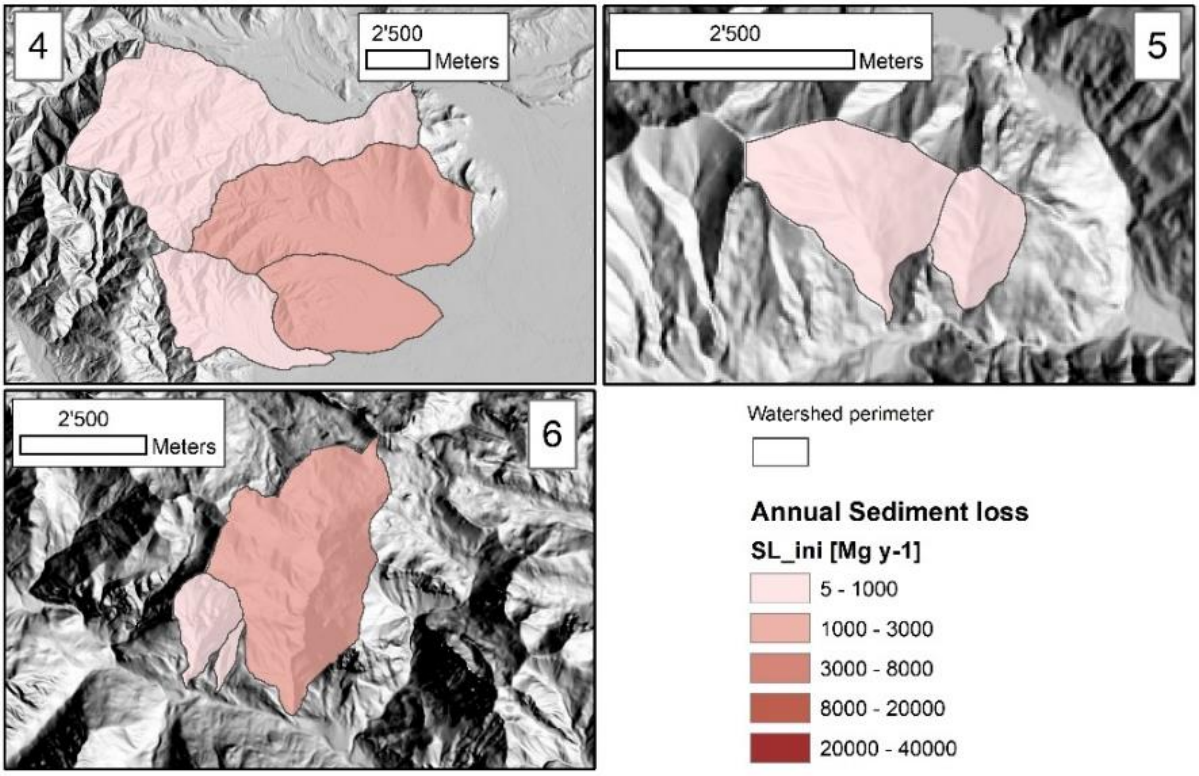


*Figure A4.38 – Annual Sediment Loss in the post-fire situation – initial assessment, for the watersheds affected by the Cumiana/Cantalupa (4), Bellino/Casteldelfino (5) and Sambuco/Pietraporzio (6) wildfires.*

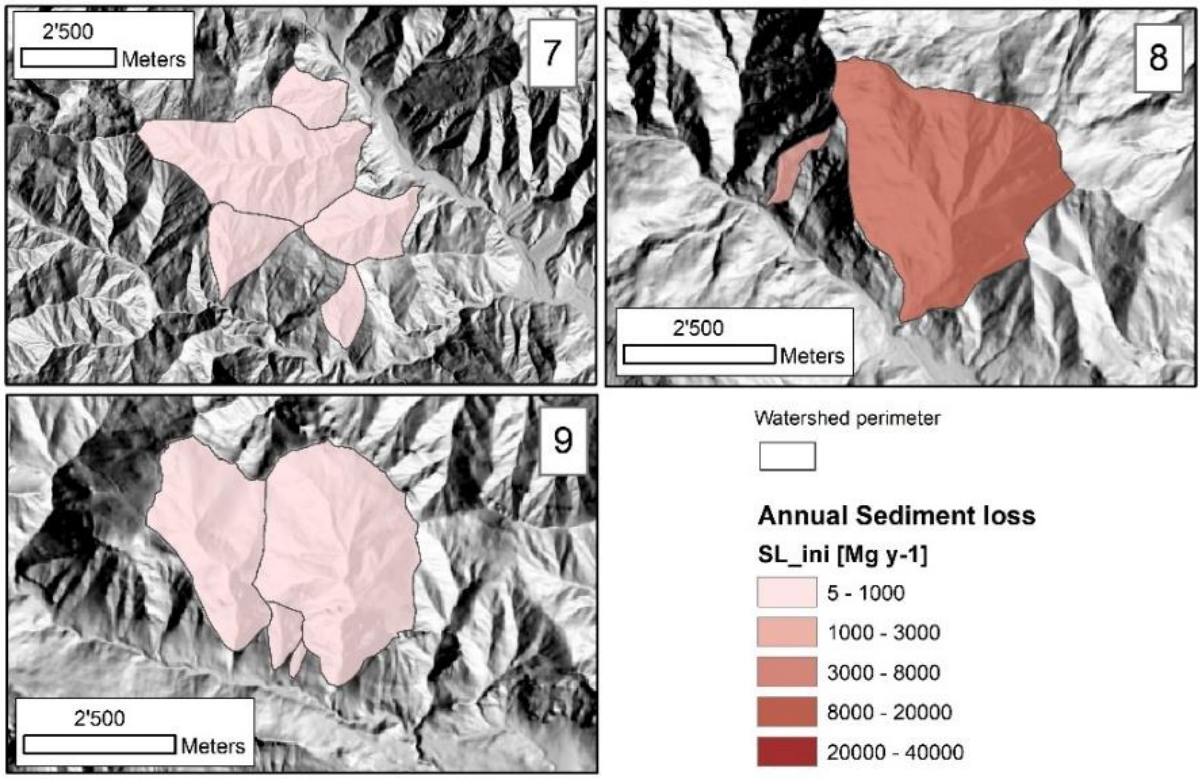


*Figure A4.39 – Annual Sediment Loss in the post-fire situation – initial assessment, for the watersheds affected by the Roure/Perrero (7), Traversella (8) and Demonte (9) wildfires.*

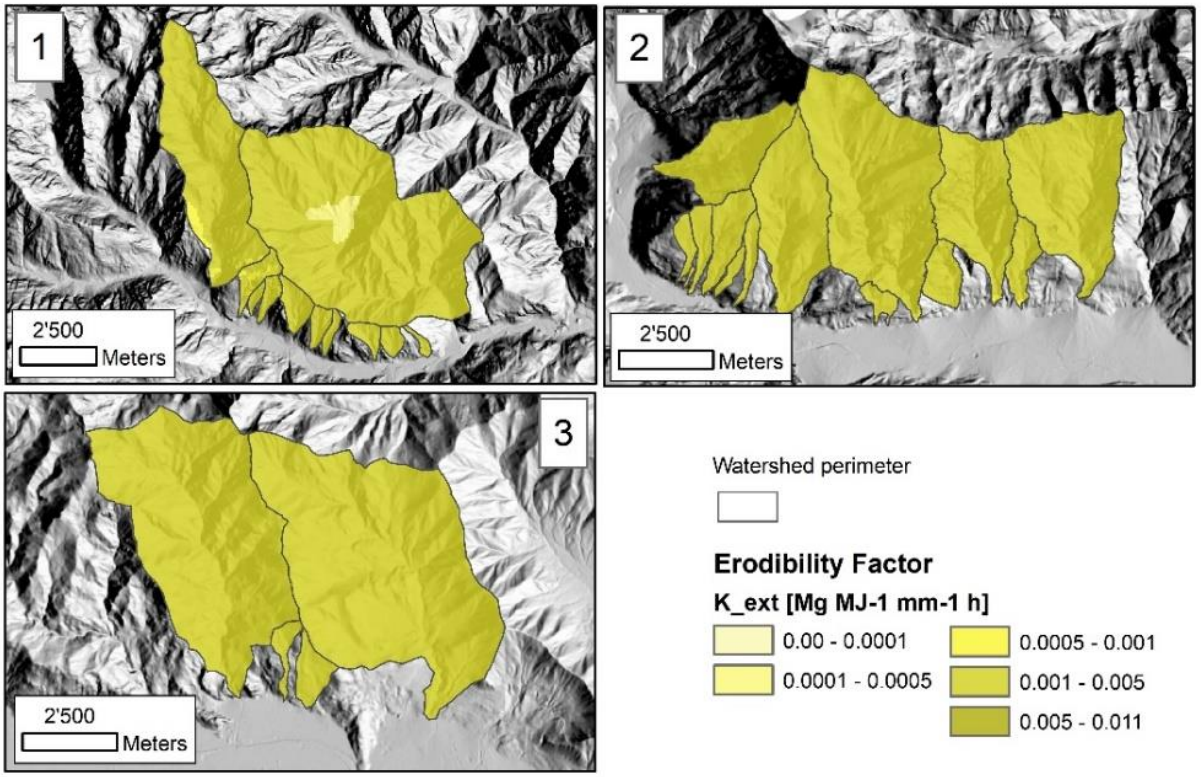


*Figure A4.40 - Erodibility Factor in the post-fire situation – extended assessment, for the watersheds affected by the Locana/Ribordone (1), Bussoleno/Mompantero (2) and Caprie/Rubiana (3) wildfires.*

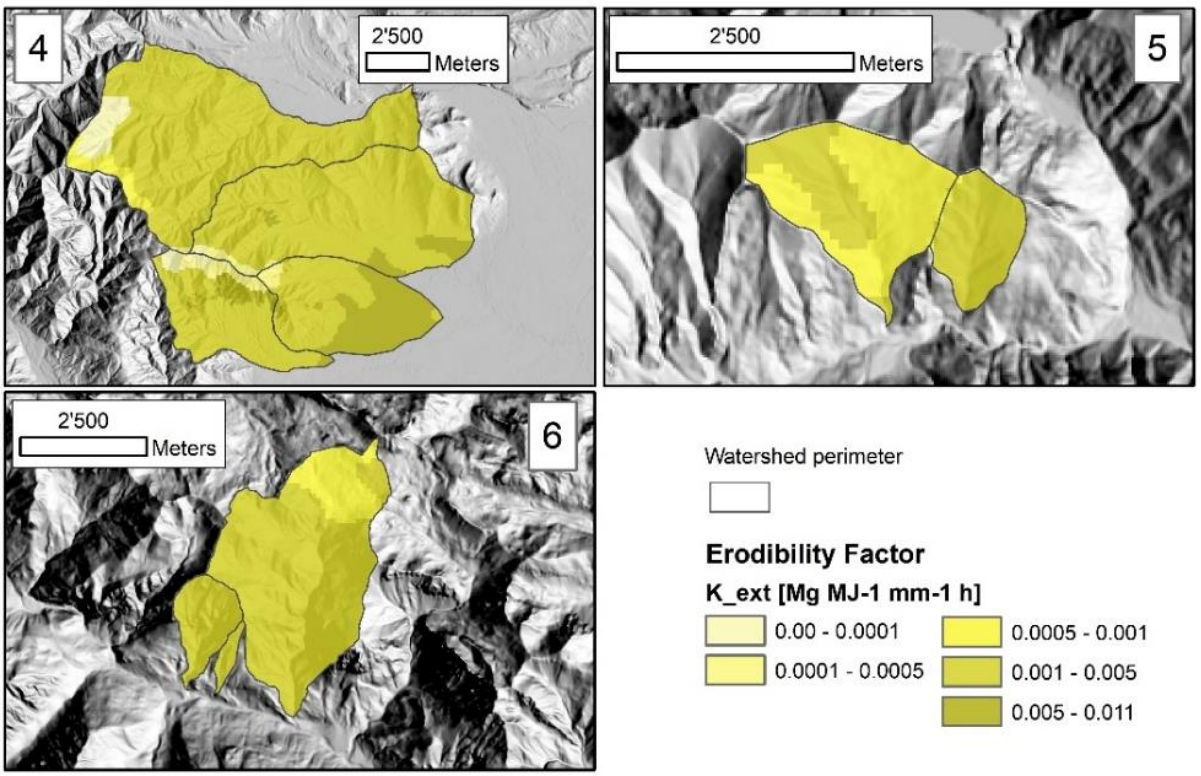


*Figure A4.41 - Erodibility Factor in the post-fire situation – extended assessment, for the watersheds affected by the Cumiana/Cantalupa (4), Bellino/Casteldelfino (5) and Sambuco/Pietraporzio (6) wildfires.*

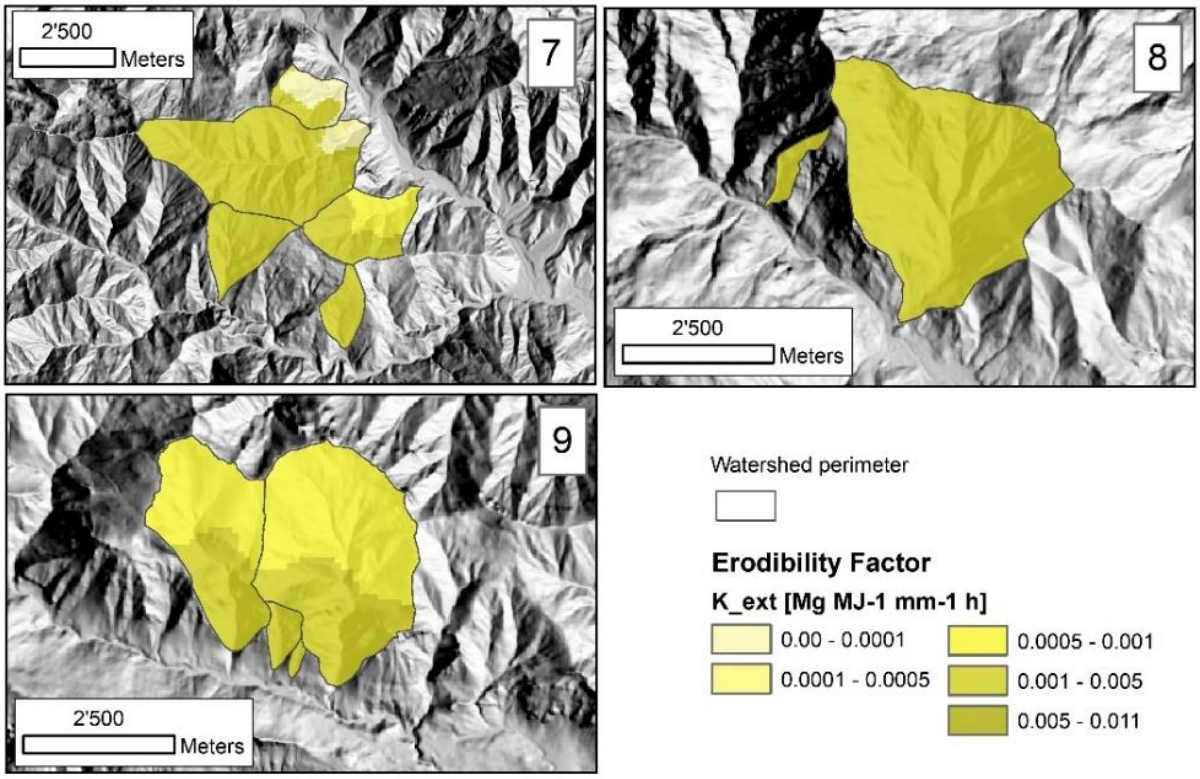


*Figure A4.42 - Erodibility Factor in the post-fire situation – extended assessment, for the watersheds affected by the Roure/Perrero (7), Traversella (8) and Demonte (9) wildfires.*

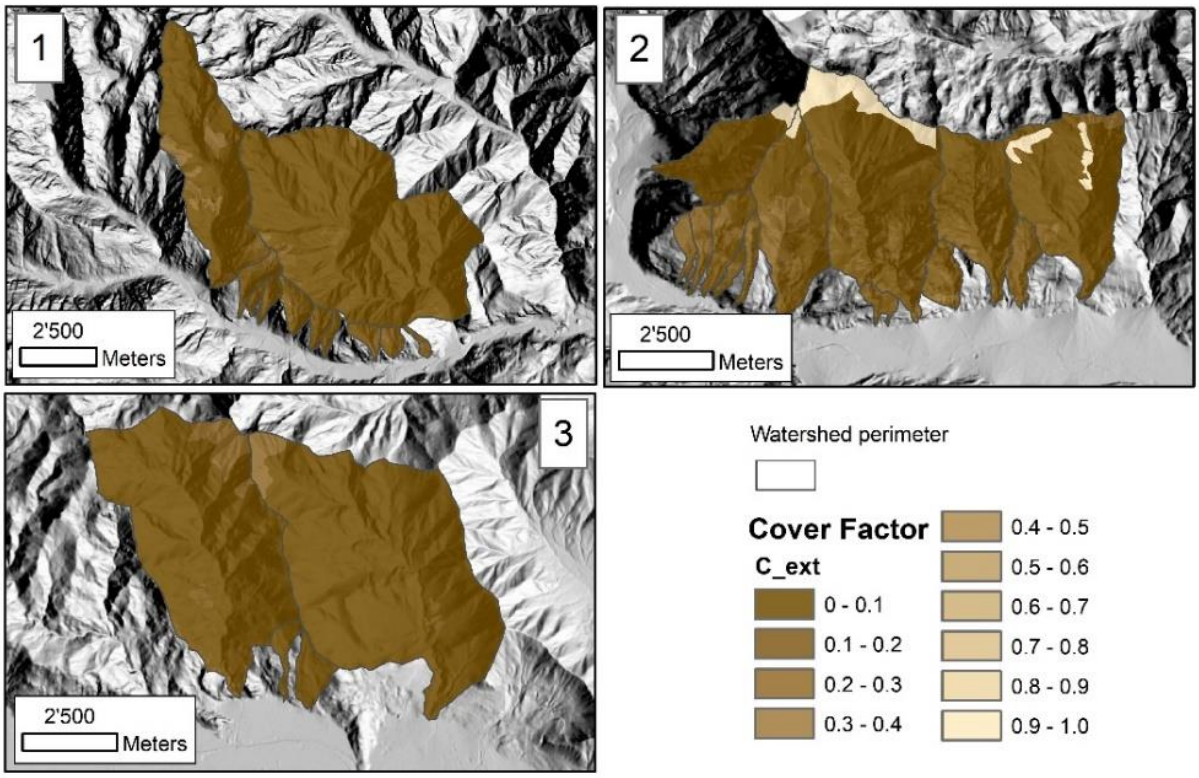


*Figure A4.43 - Cover Factor in the post-fire situation – extended assessment, for the watersheds affected by the Locana/Ribordone (1), Bussoleno/Mompantero (2) and Caprie/Rubiana (3) wildfires.*

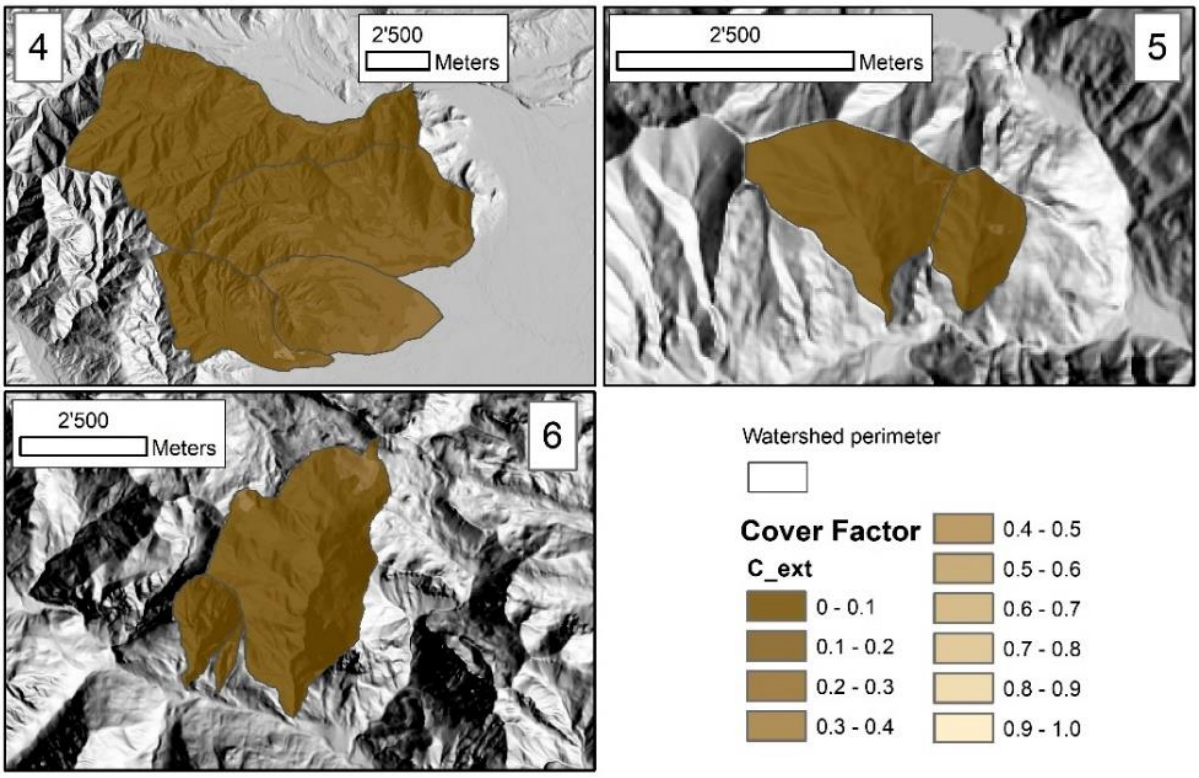


*Figure A4.44 - Cover Factor in the post-fire situation – extended assessment, for the watersheds affected by the Cumiana/Cantalupa (4), Bellino/Casteldelfino (5) and Sambuco/Pietraporzio (6) wildfires.*

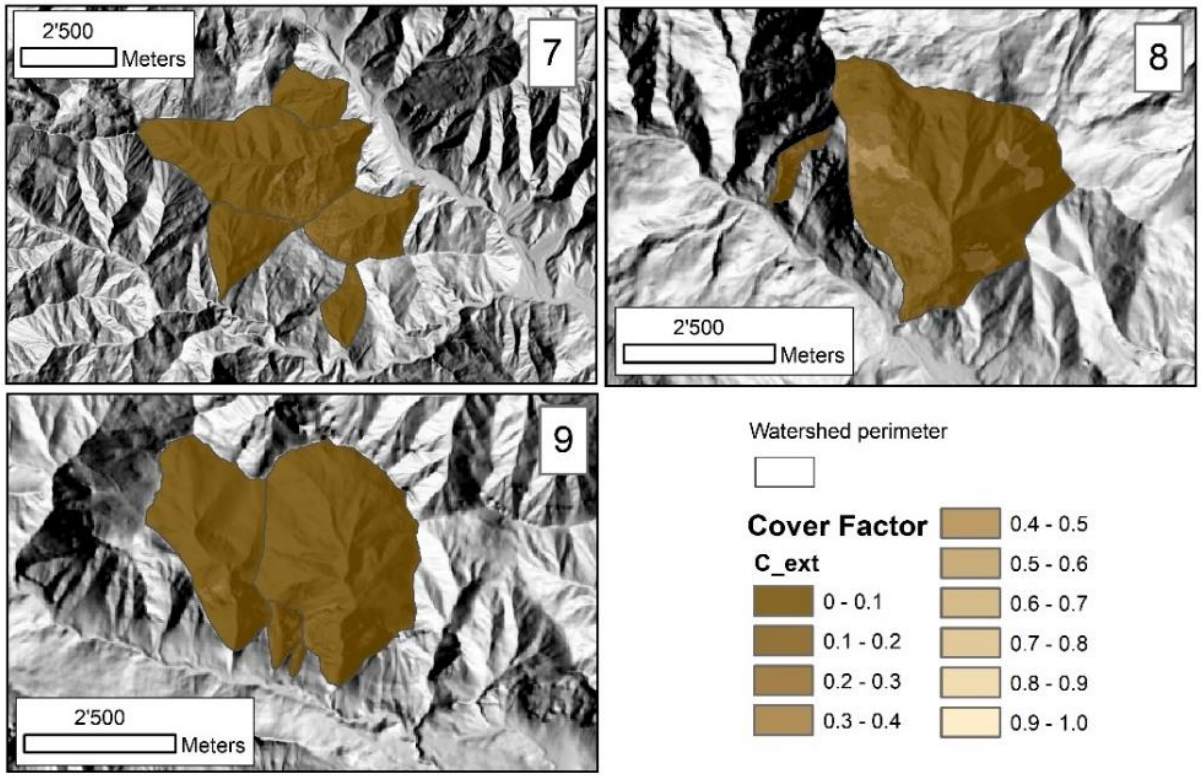


*Figure A4.45 - Cover Factor in the post-fire situation – extended assessment, for the watersheds affected by the Roure/Perrero (7), Traversella (8) and Demonte (9) wildfires.*

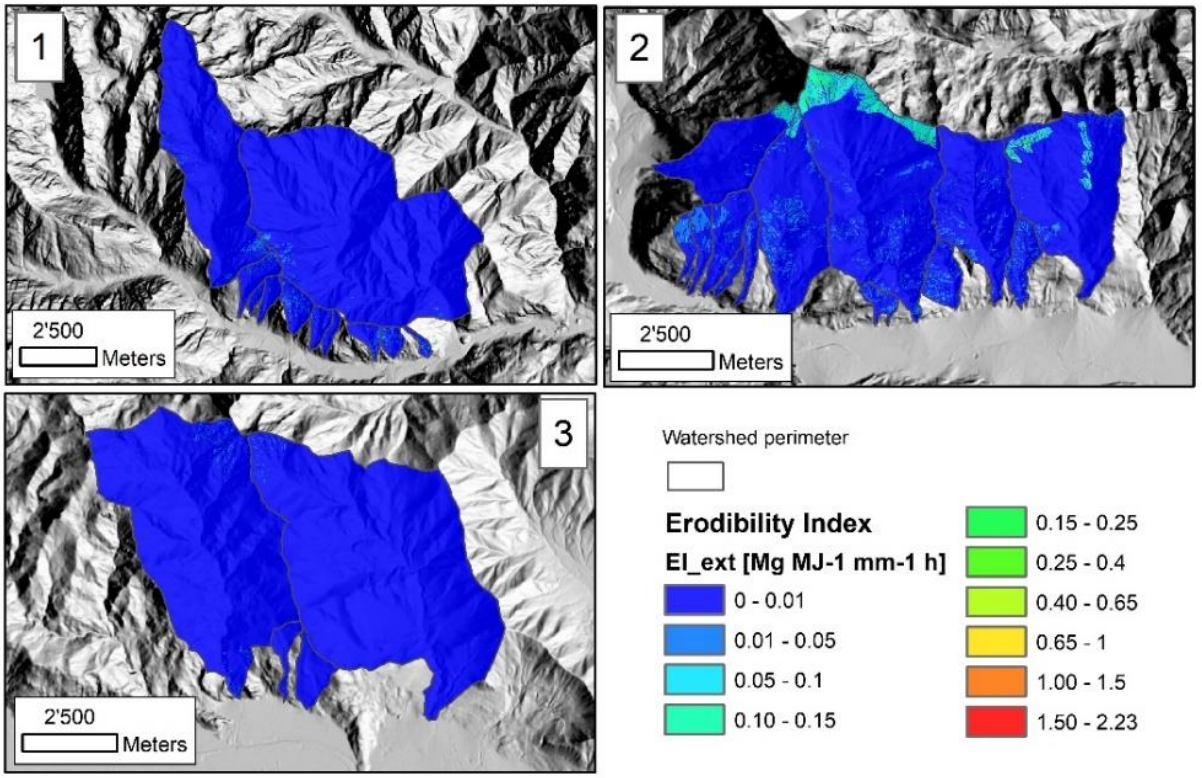


*Figure A4.46 - Erodibility Index in the post-fire situation – extended assessment, for the watersheds affected by the Locana/Ribordone (1), Bussoleno/Mompantero (2) and Caprie/Rubiana (3) wildfires.*

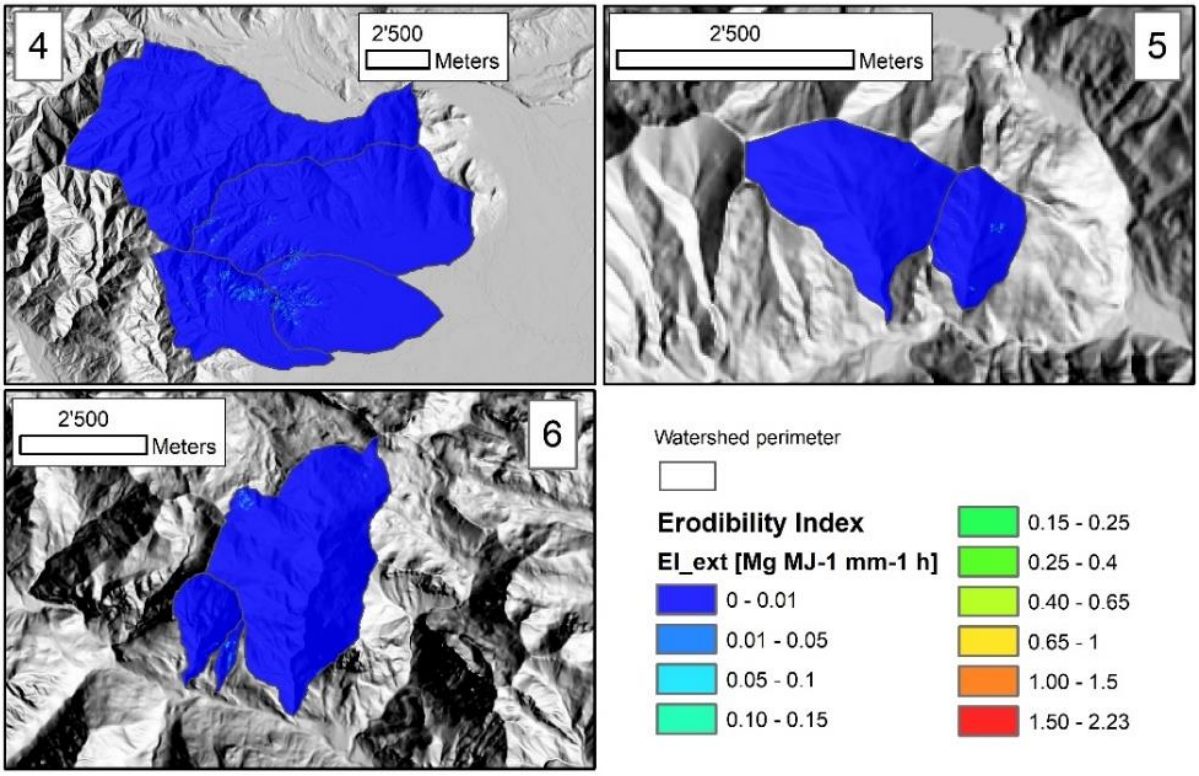


*Figure A4.47 - Erodibility Index in the post-fire situation – extended assessment, for the watersheds affected by the Cumiana/Cantalupa (4), Bellino/Casteldelfino (5) and Sambuco/Pietraporzio (6) wildfires.*

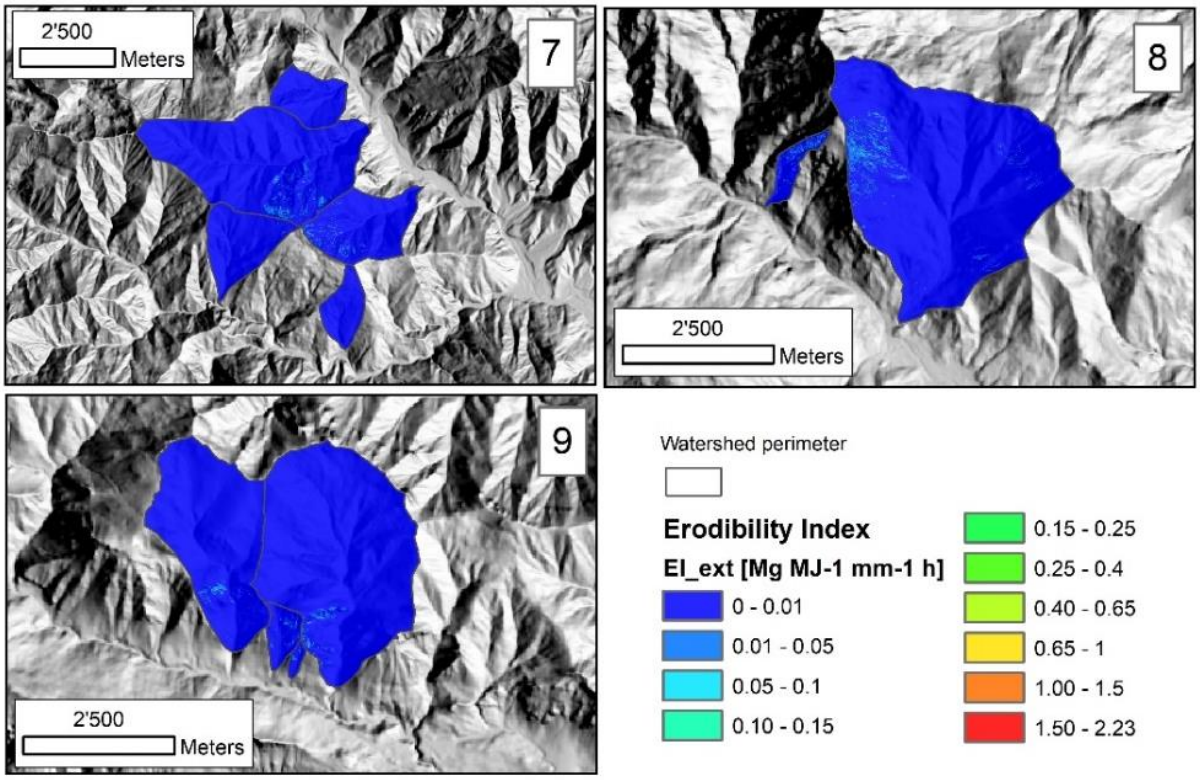


*Figure A4.48 - Erodibility Index in the post-fire situation – extended assessment, for the watersheds affected by the Roure/Perrero (7), Traversella (8) and Demonte (9) wildfires.*

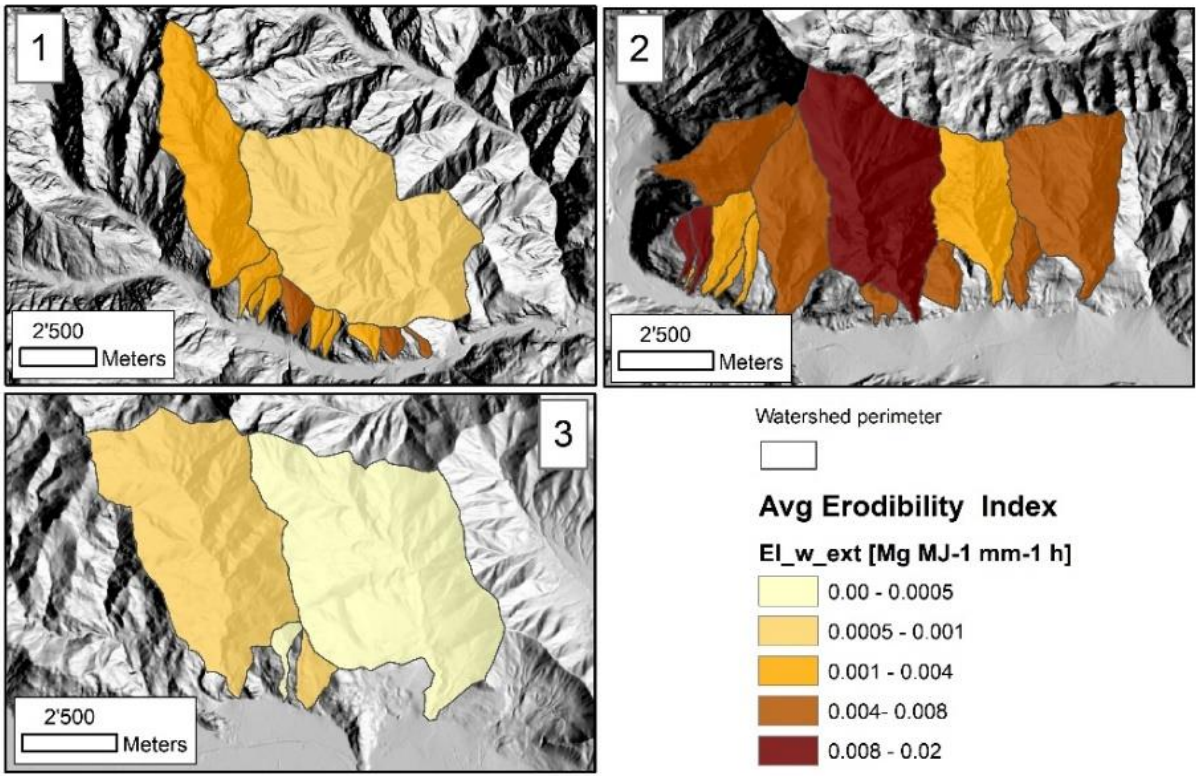


*Figure A4.49 – Spatially averaged Erodibility Index in the post-fire situation – extended assessment, for the watersheds affected by the Locana/Ribordone (1), Bussoleno/Mompantero (2) and Caprie/Rubiana (3)) wildfires.*

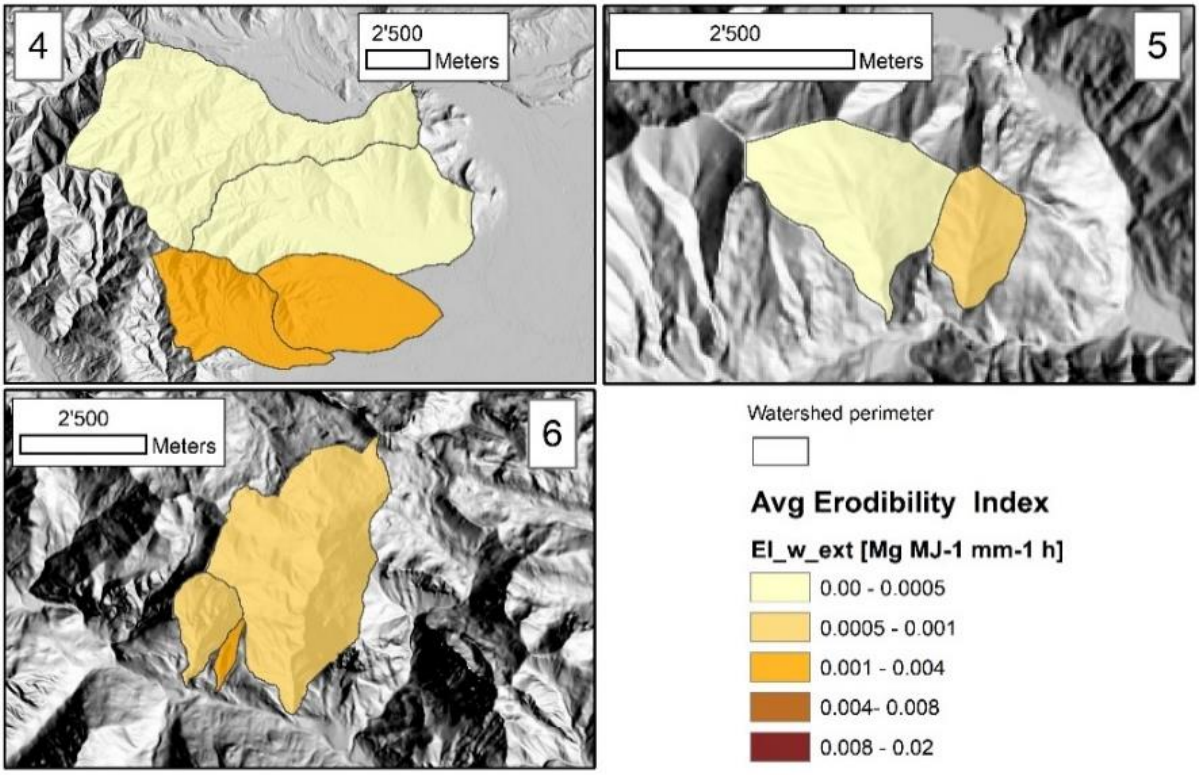


*Figure A4.50 – Spatially averaged Erodibility Index in the post-fire situation – extended assessment, for the watersheds affected by the Cumiana/Cantalupa (4), Bellino/Casteldelfino (5) and Sambuco/Pietraporzio (6) wildfires.*

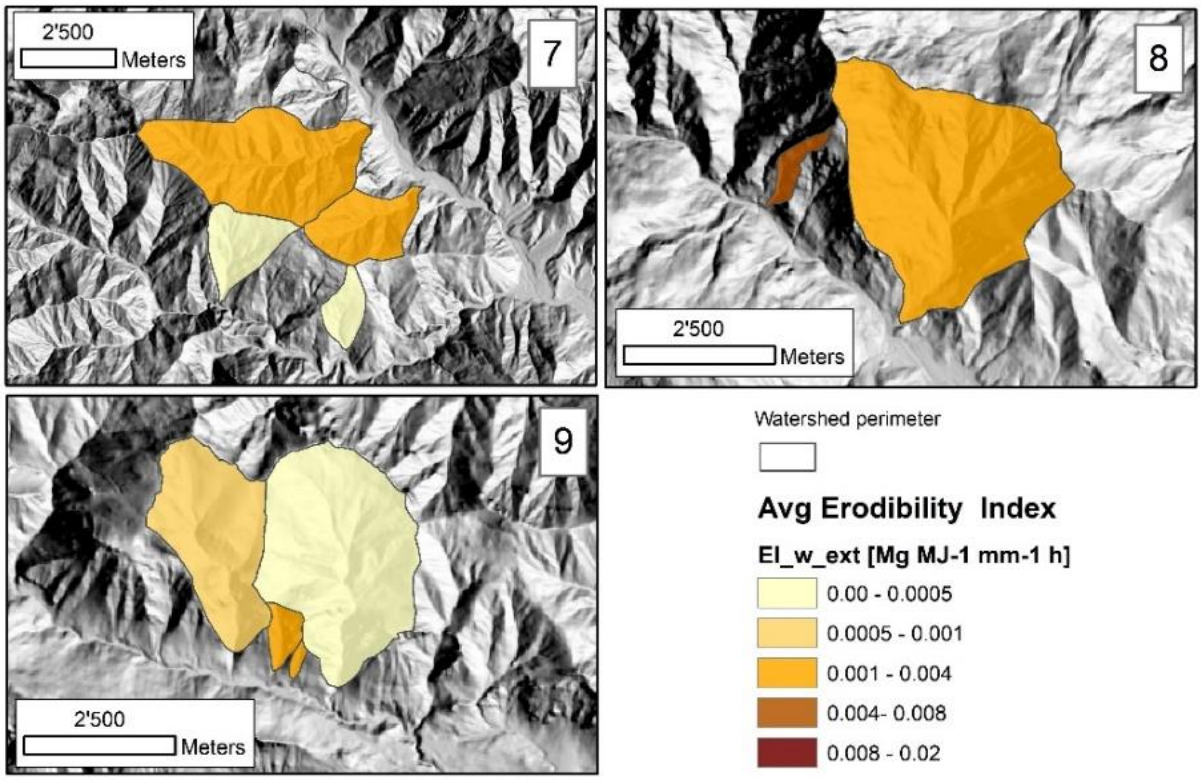


*Figure A4.51 – Spatially averaged Erodibility Index in the post-fire situation – extended assessment, for the watersheds affected by the Roure/Perrero (7), Traversella (8) and Demonte (9) wildfires.*

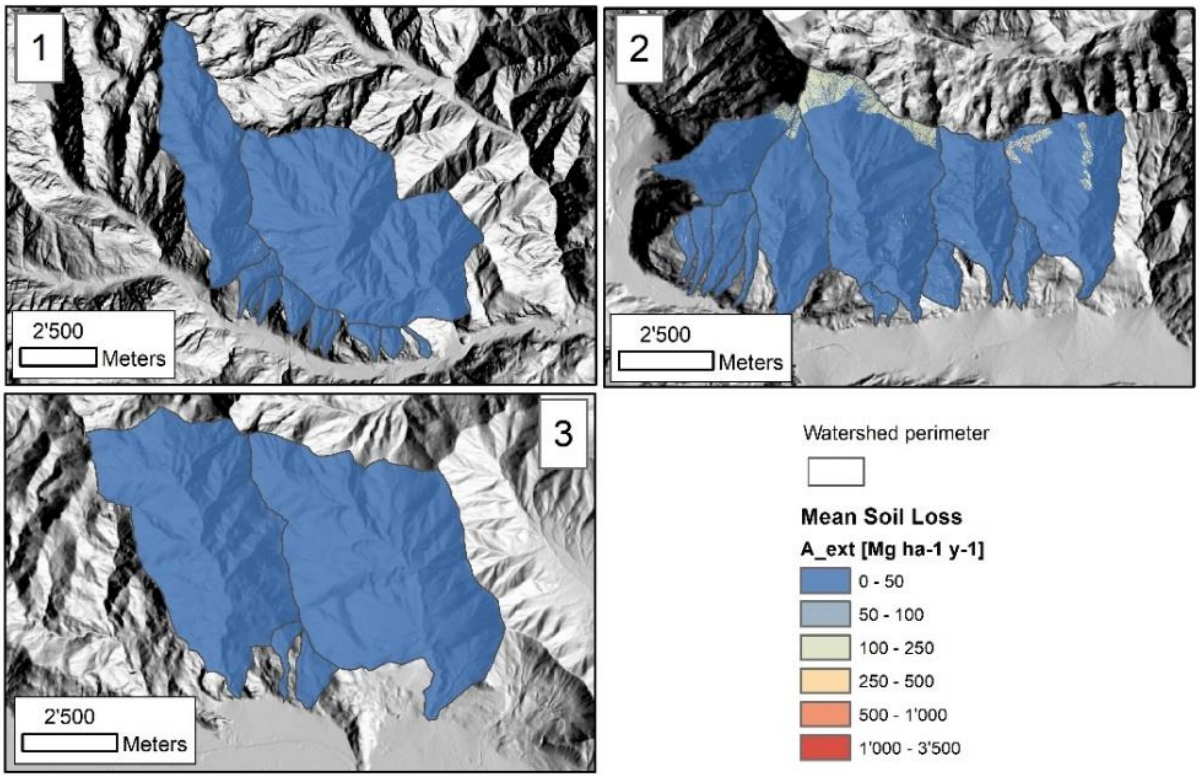


*Figure A4.52 – Mean Soil Loss in the post-fire situation – extended assessment, for the watersheds affected by the Locana/Ribordone (1), Bussoleno/Mompantero (2) and Caprie/Rubiana (3) wildfires.*

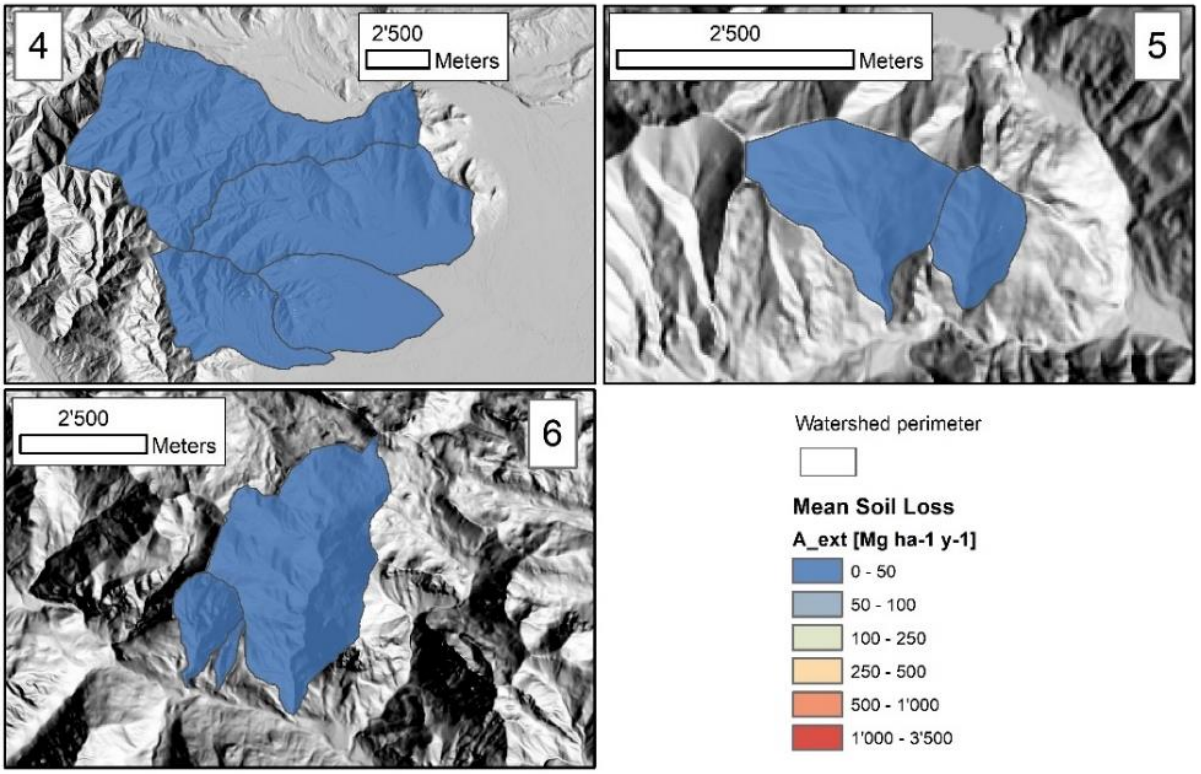


*Figure A4.53 – Mean Soil Loss in the post-fire situation – extended assessment, for the watersheds affected by the Cumiana/Cantalupa (4), Bellino/Casteldelfino (5) and Sambuco/Pietraporzio (6) wildfires.*

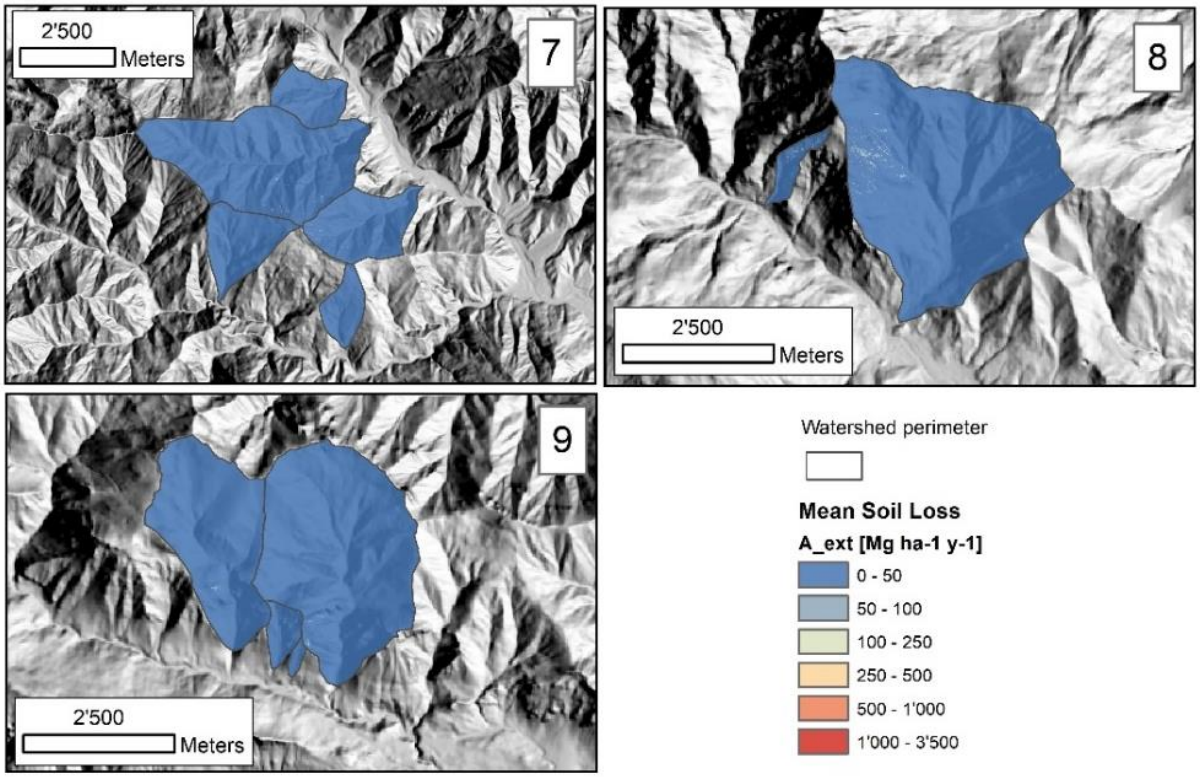


*Figure A4.54 – Mean Soil Loss in the post-fire situation – extended assessment, for the watersheds affected by the Roure/Perrero (7), Traversella (8) and Demonte (9) wildfires.*

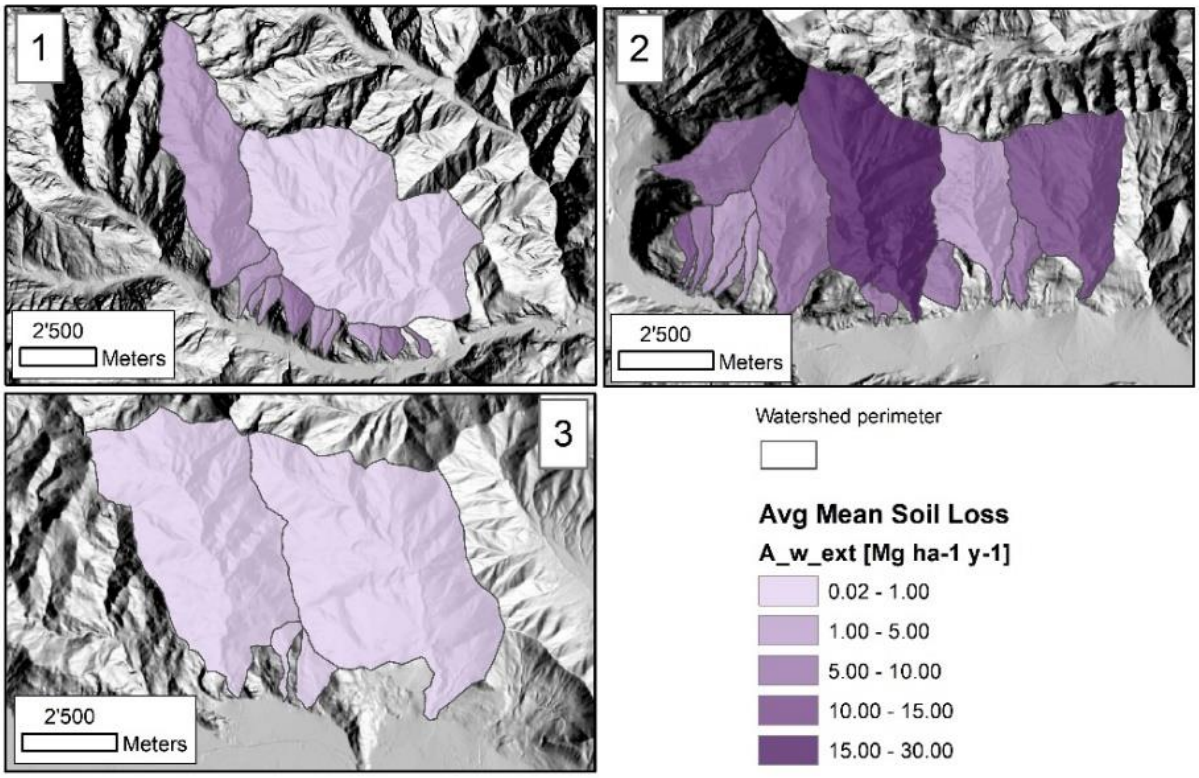


*Figure A4.55 – Spatially averaged Mean Soil Loss in the post-fire situation – extended assessment, for the watersheds affected by the Locana/Ribordone (1), Bussoleno/Mompantero (2) and Caprie/Rubiana (3) wildfires.*

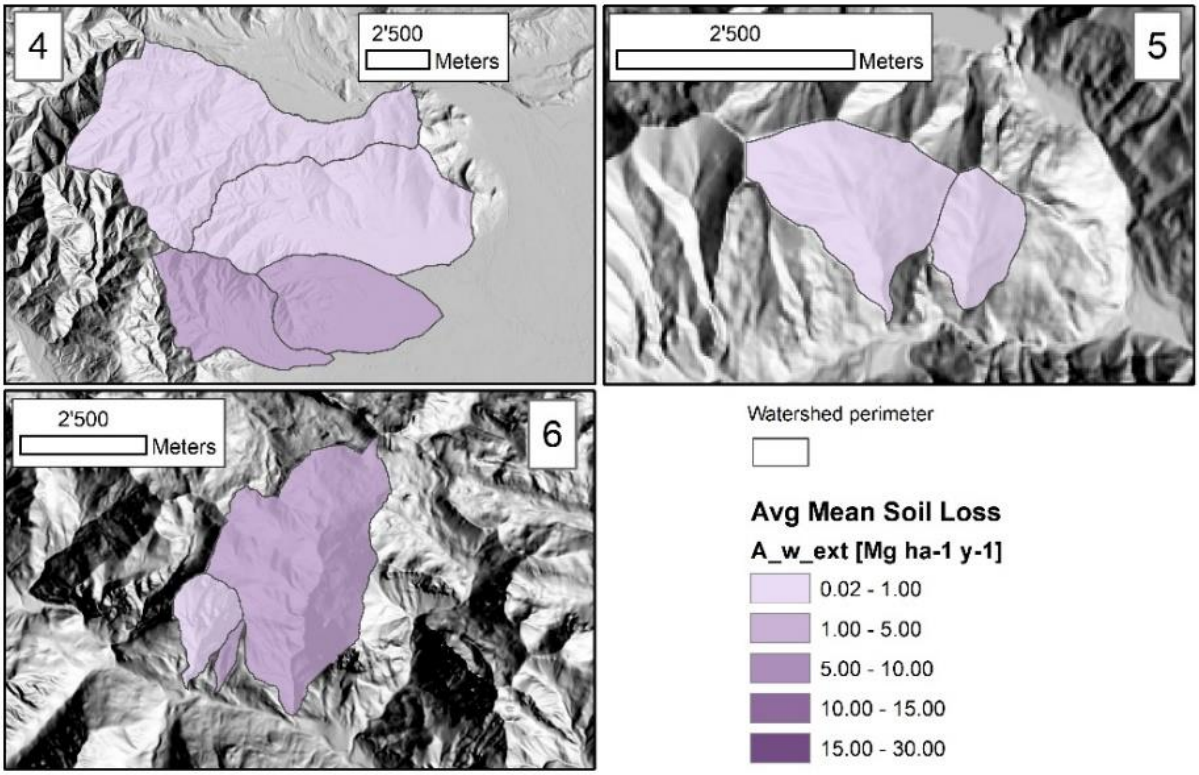


*Figure A4.56 – Spatially averaged Mean Soil Loss in the post-fire situation – extended assessment, for the watersheds affected by the Cumiana/Cantalupa (4), Bellino/Casteldelfino (5) and Sambuco/Pietraporzio (6) wildfires.*

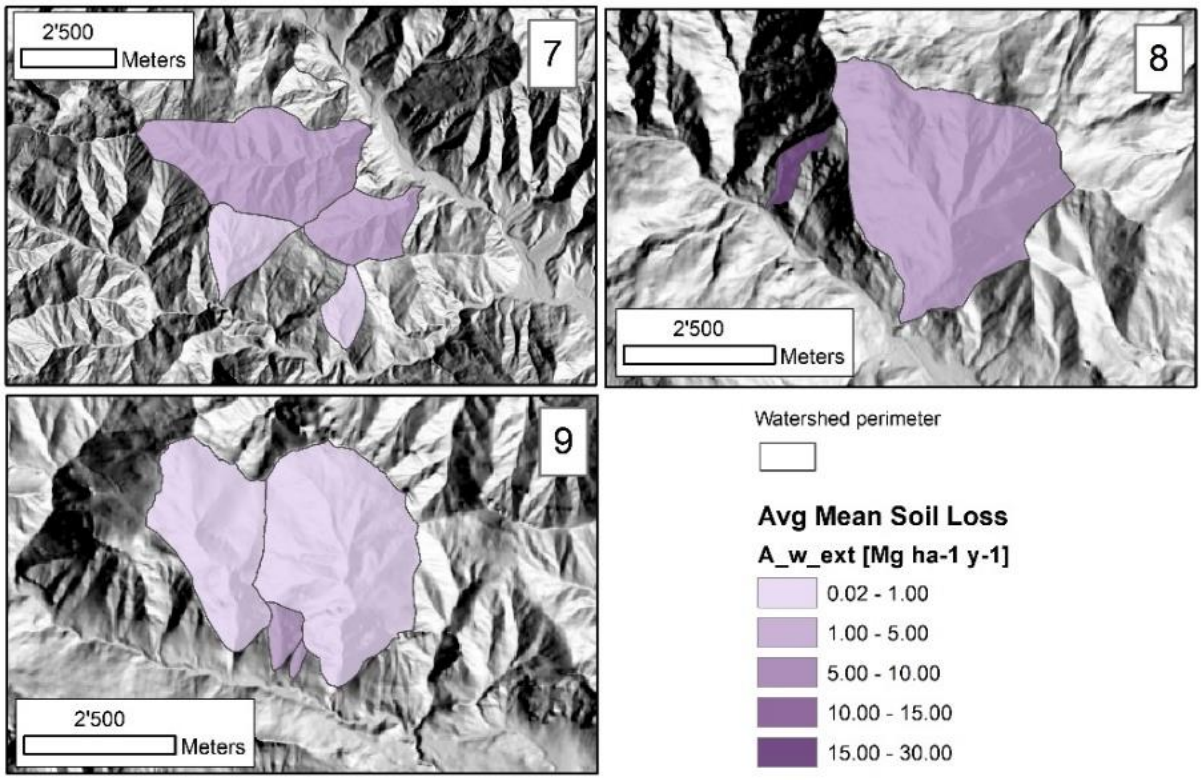


*Figure A4.57 – Spatially averaged Mean Soil Loss in the post-fire situation – extended assessment, for the watersheds affected by the Roure/Perrero (7), Traversella (8) and Demonte (9) wildfires.*

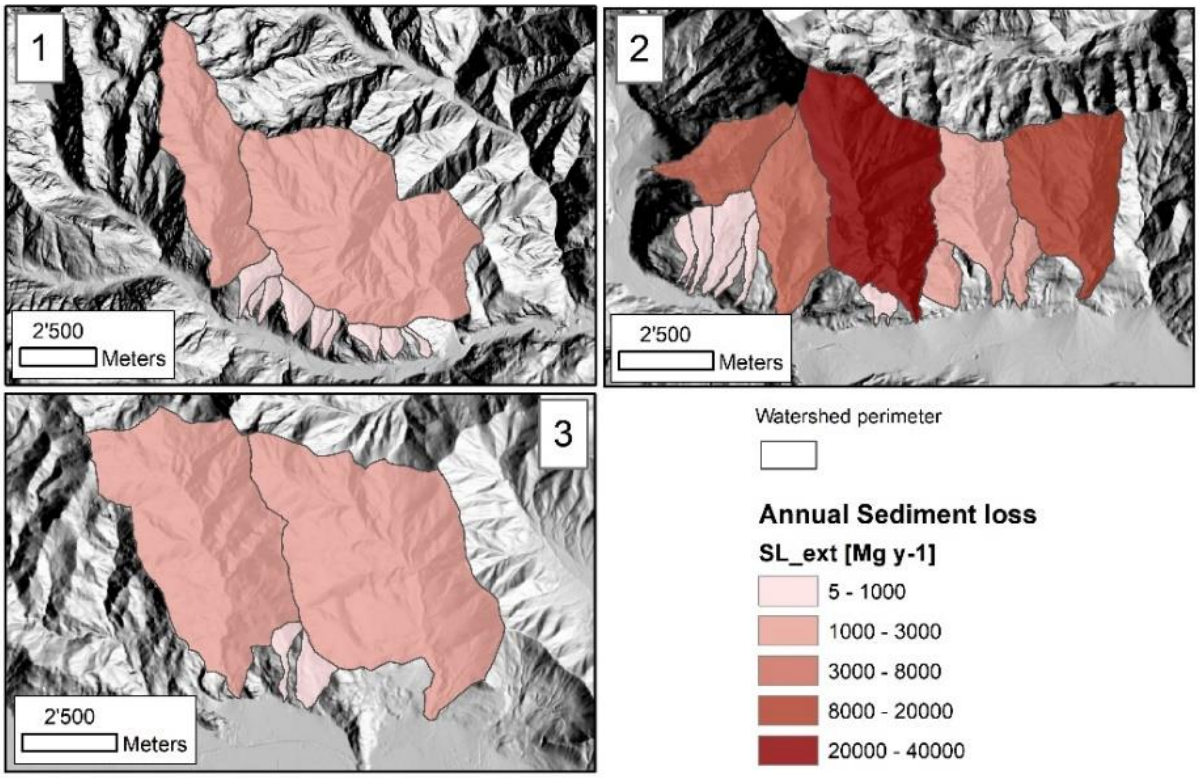


*Figure A4.58 – Annual Sediment Loss in the post-fire situation – extended assessment, for the watersheds affected by the Locana/Ribordone (1), Bussoleno/Mompantero (2) and Caprie/Rubiana (3) wildfires.*

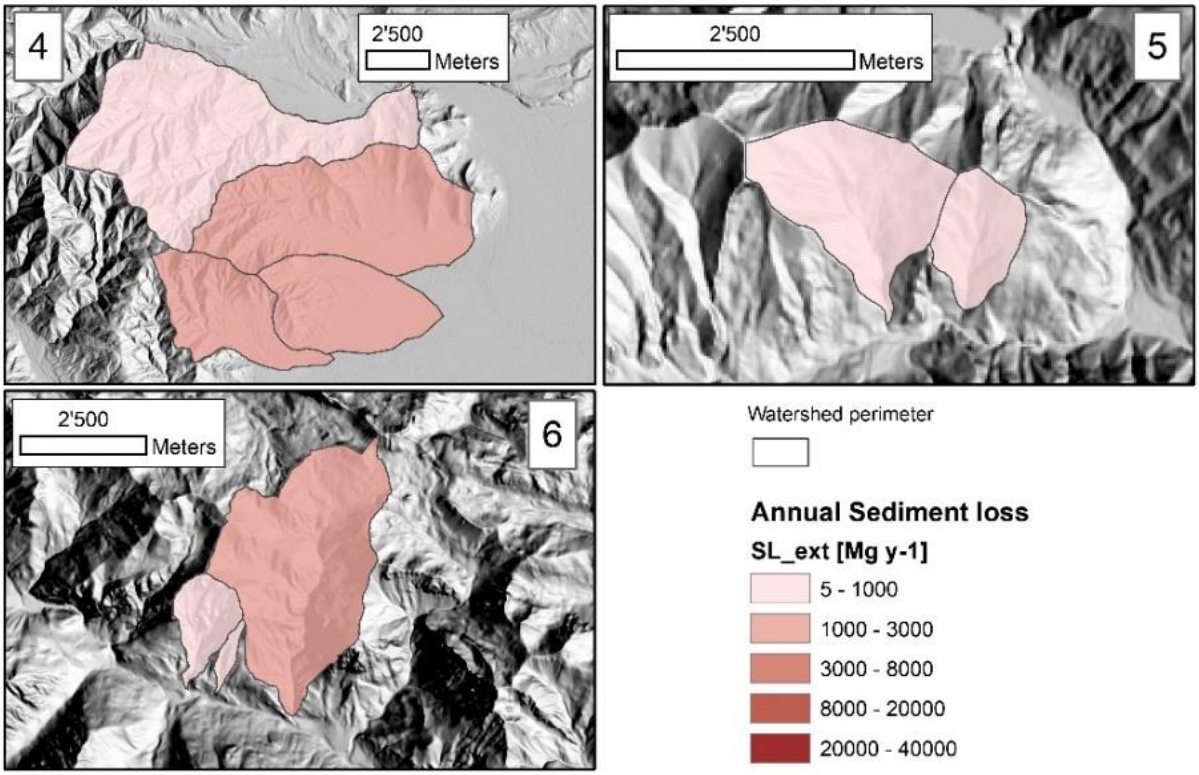


*Figure A4.59 – Annual Sediment Loss in the post-fire situation – extended assessment, for the watersheds affected by the Cumiana/Cantalupa (4), Bellino/Casteldelfino (5) and Sambuco/Pietraporzio (6) wildfires.*

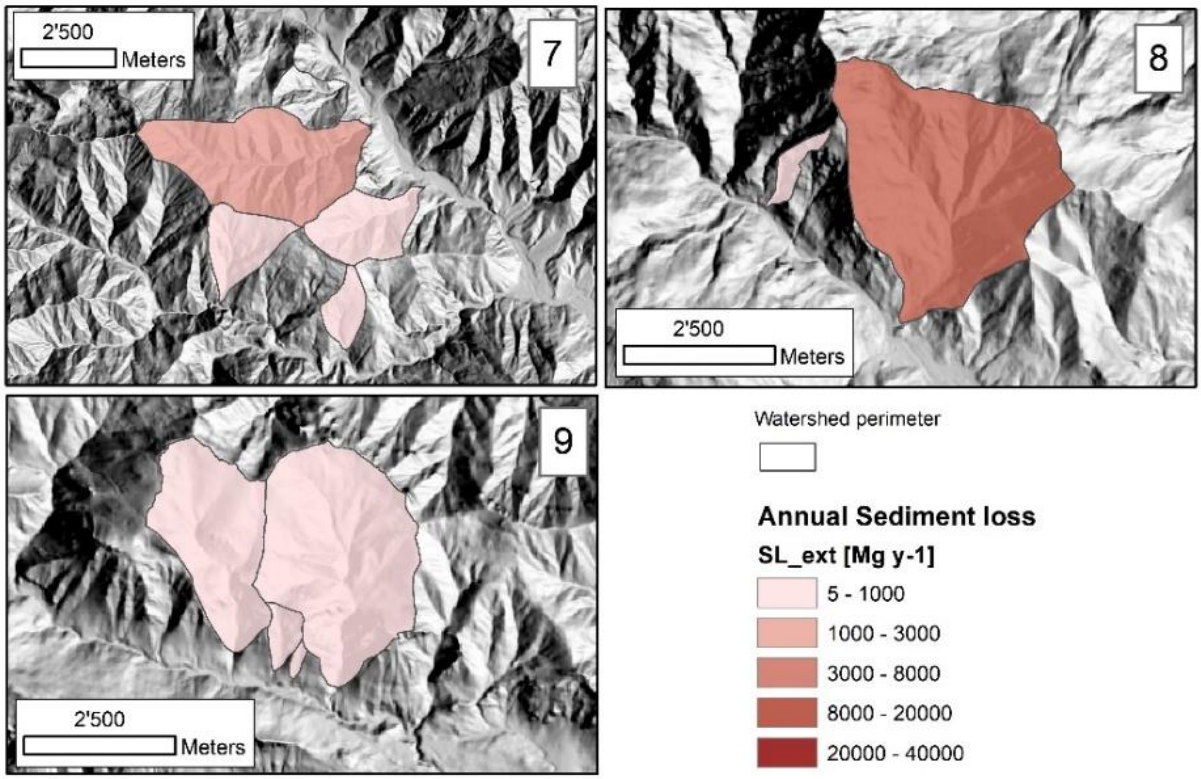


*Figure A4.60 – Annual Sediment Loss in the post-fire situation – extended assessment, for the watersheds affected by the Roure/Perrero (7), Traversella (8) and Demonte (9) wildfires.*

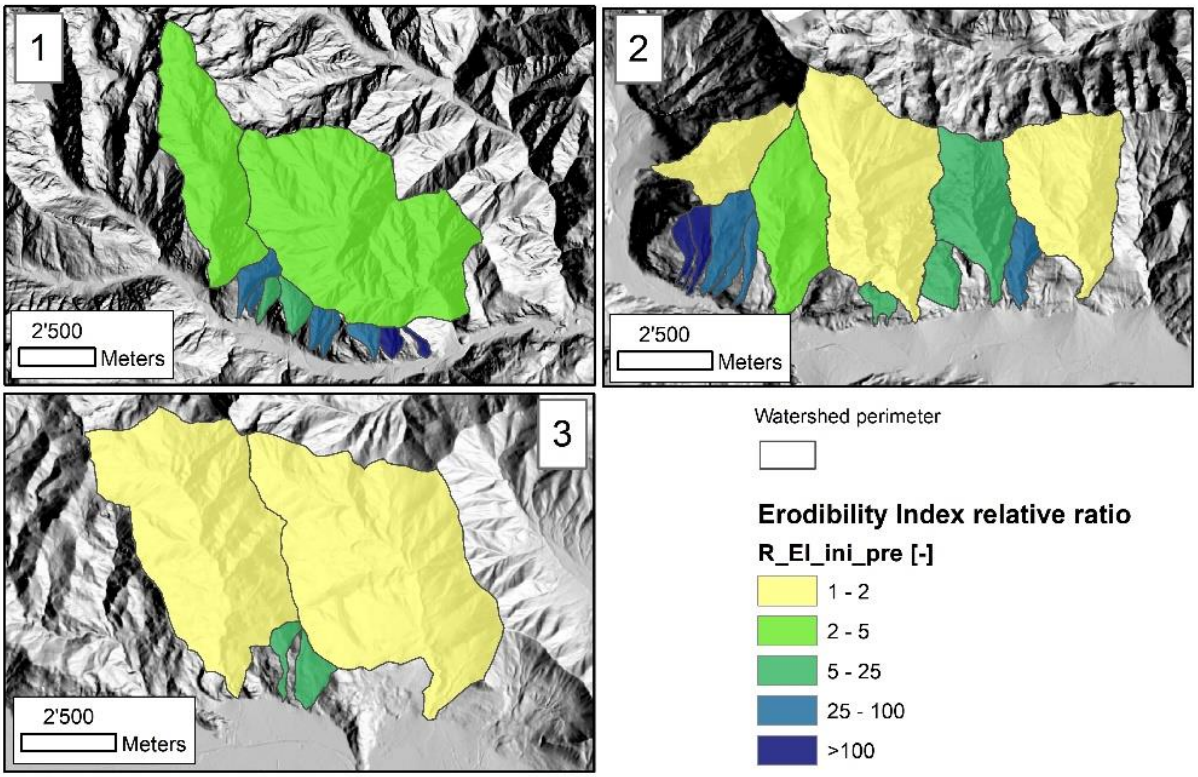


*Figure A4.61 – Erodibility Index relative ratio, R_EI_ini_pre, between post-fire (initial assessment) and pre-fire situation for the watersheds affected by the Locana/Ribordone (1), Bussoleno/Mompantero (2) and Caprie/Rubiana (3) wildfires.*

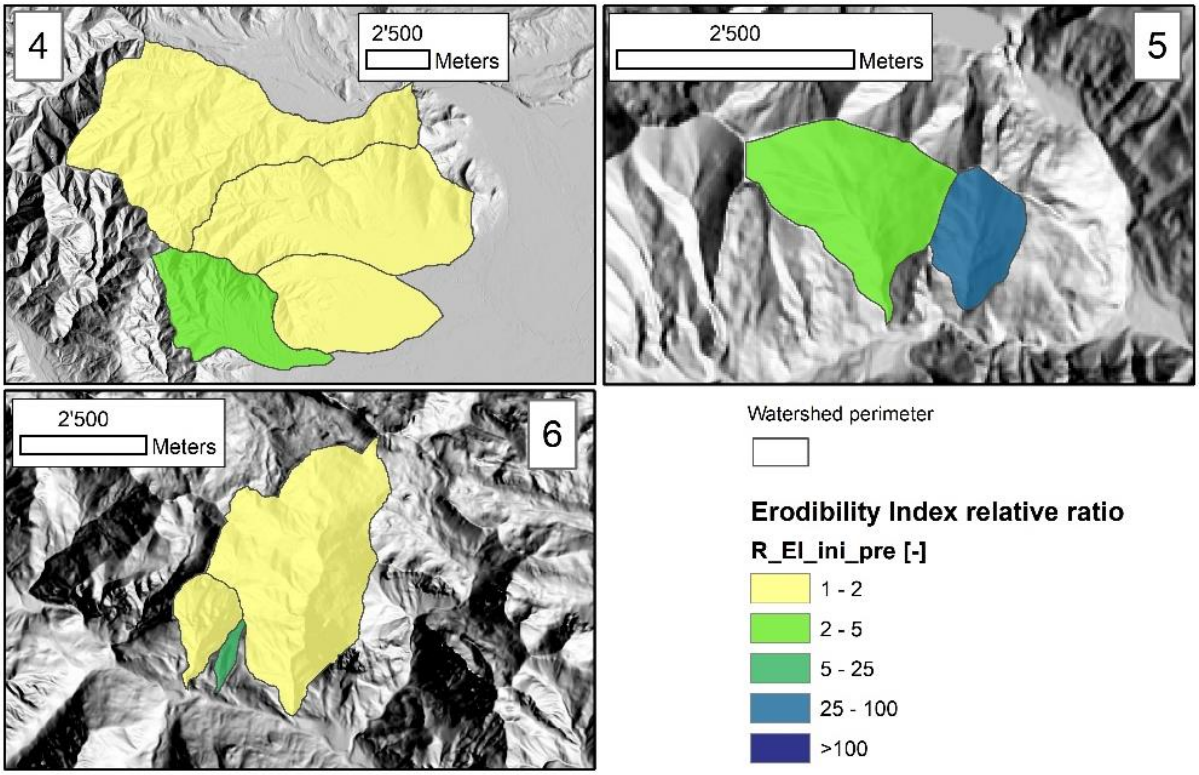


*Figure A4.62 – Erodibility Index relative ratio, R_EI_ini_pre, between post-fire (initial assessment) and pre-fire situation for the watersheds affected by the Cumiana/Cantalupa (4), Bellino/Casteldelfino (5) and Sambuco/Pietraporzio (6) wildfires.*

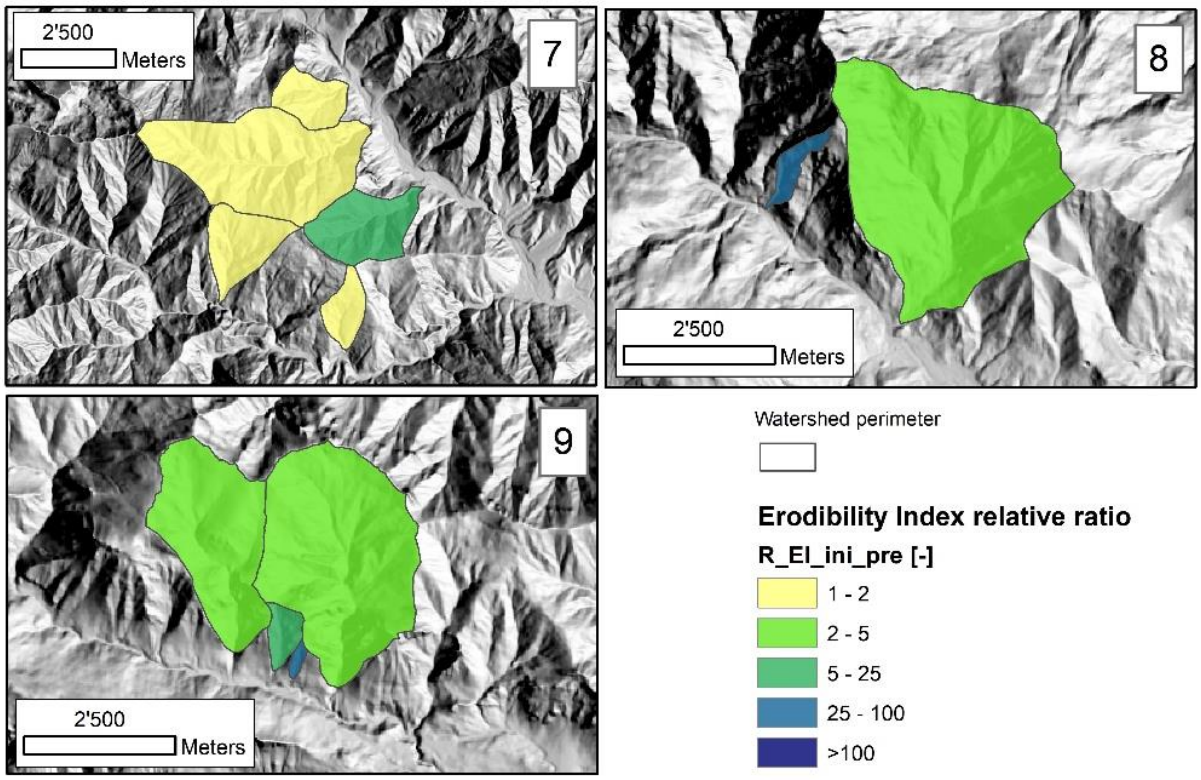


*Figure A4.63 – Erodibility Index relative ratio, R_EI_ini_pre, between post-fire (initial assessment) and pre-fire situation for the watersheds affected by the Roure/Perrero (7), Traversella (8) and Demonte (9) wildfires.*

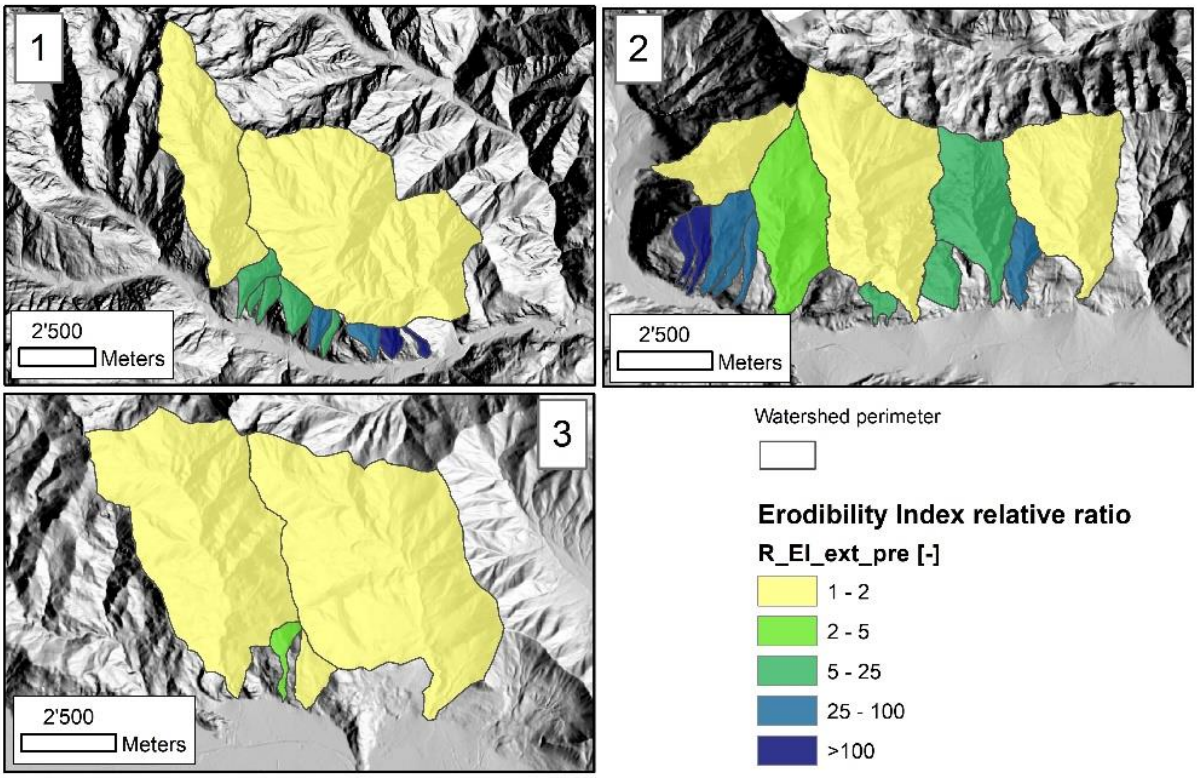


*Figure A4.64 – Erodibility Index relative ratio, R_EI_ext_pre, between post-fire (extended assessment) and pre-fire situation for the watersheds affected by the Locana/Ribordone (1), Bussoleno/Mompantero (2) and Caprie/Rubiana (3) wildfires.*

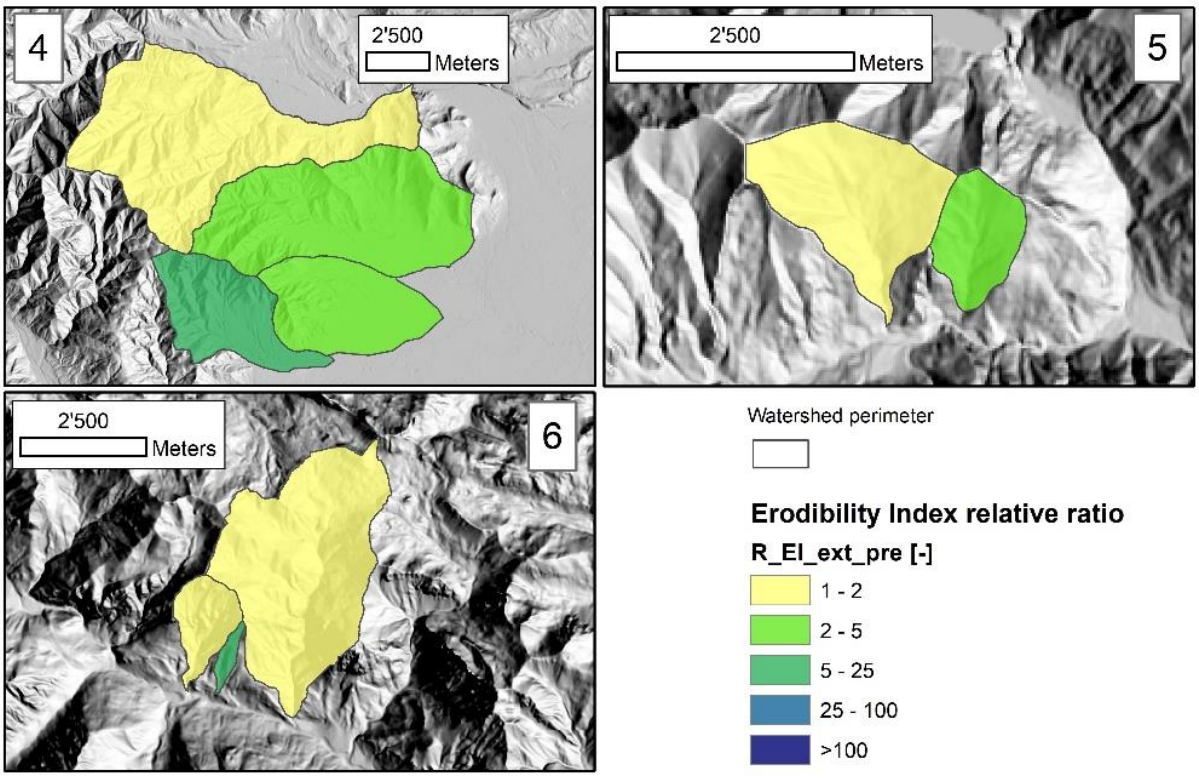


*Figure A4.65 – Erodibility Index relative ratio, R_EI_ext_pre, between post-fire (extended assessment) and pre-fire situation for the watersheds affected by the Cumiana/Cantalupa (4), Bellino/Casteldelfino (5) and Sambuco/Pietraporzio (6) wildfires.*

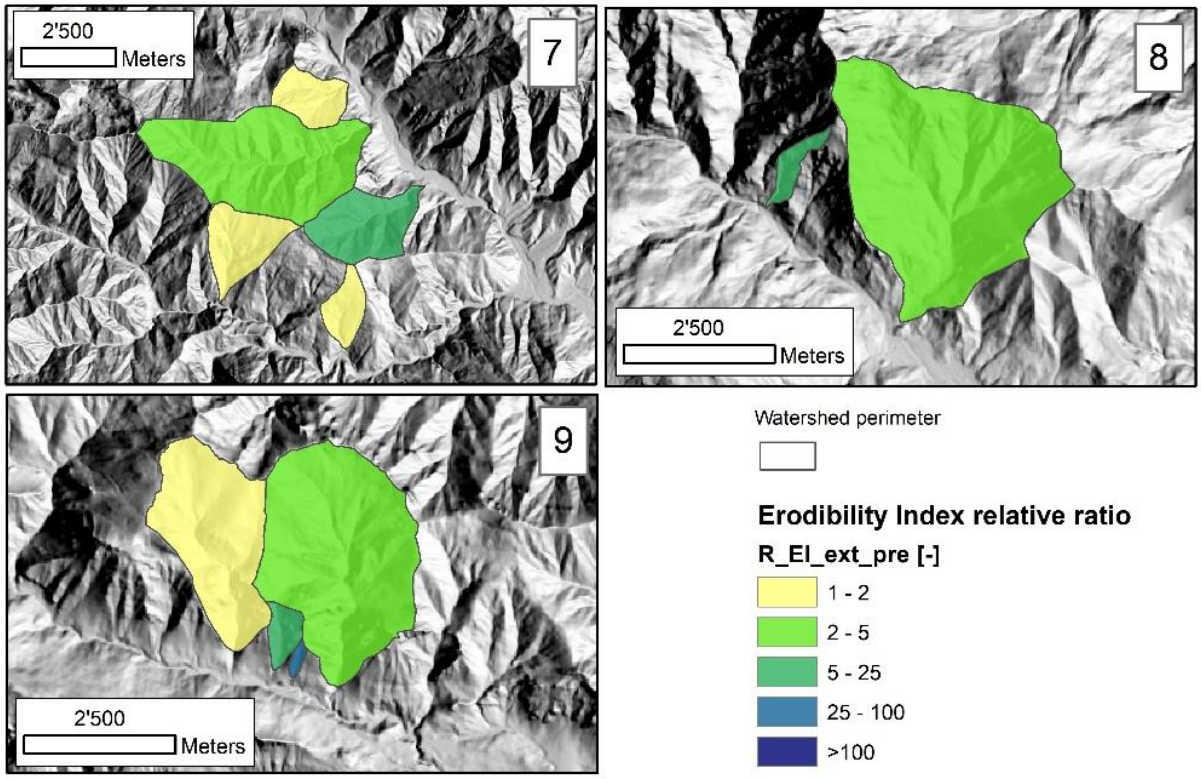


*Figure A4.66 – Erodibility Index relative ratio, R_EI_ext_pre, between post-fire (extended assessment) and pre-fire situation for the watersheds affected by the Roure/Perrero (7), Traversella (8) and Demonte (9) wildfires.*

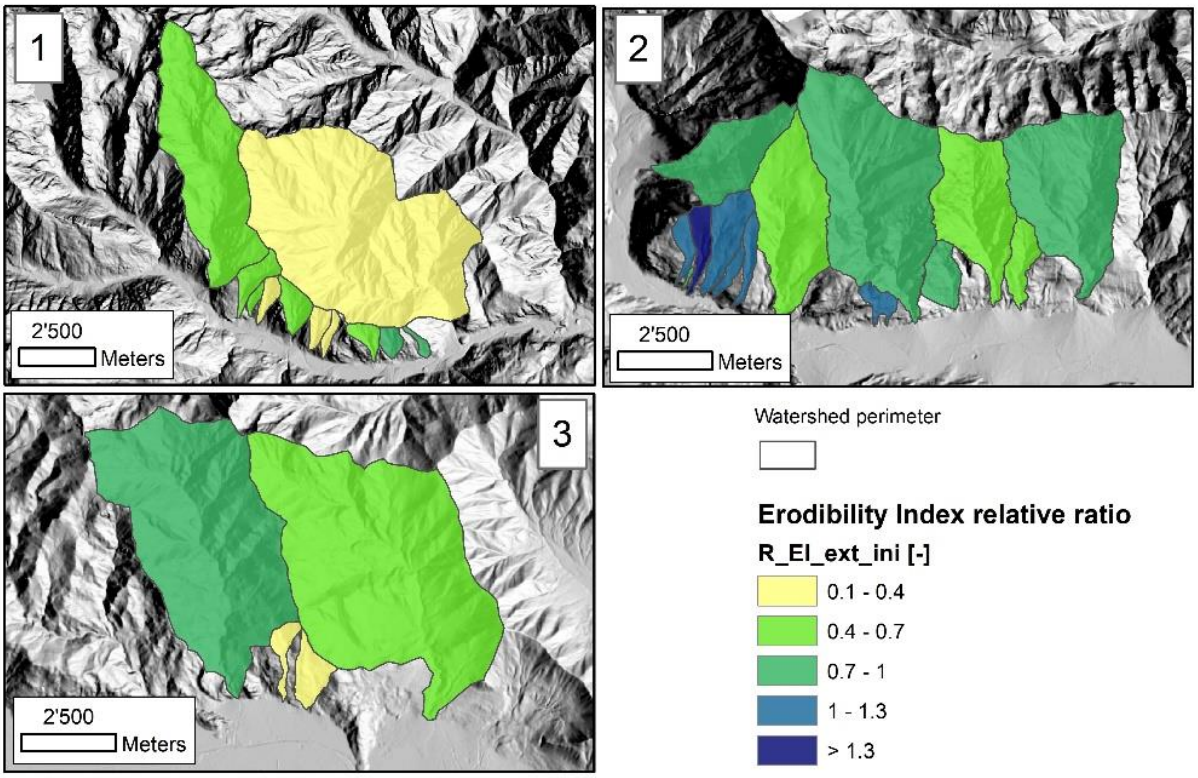


*Figure A4.67 – Erodibility Index relative ratio, R_EI_ext_ini, between extended assessment and initial assessment for the watersheds affected by the Locana/Ribordone (1), Bussoleno/Mompantero (2) and Caprie/Rubiana (3) wildfires.*

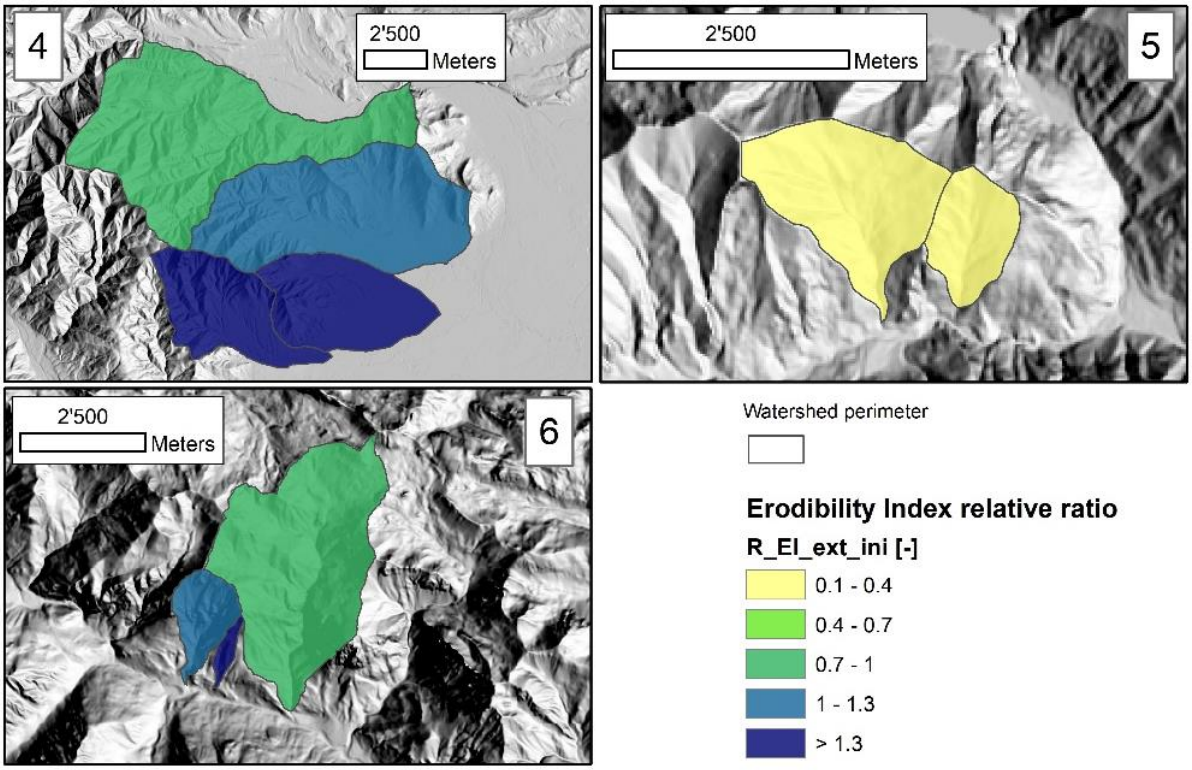


*Figure A4.68 – Erodibility Index relative ratio, R_EI_ext_ini, between extended assessment and initial assessment situation for the watersheds affected by the Cumiana/Cantalupa (4), Bellino/Casteldelfino (5) and Sambuco/Pietraporzio (6) wildfires.*

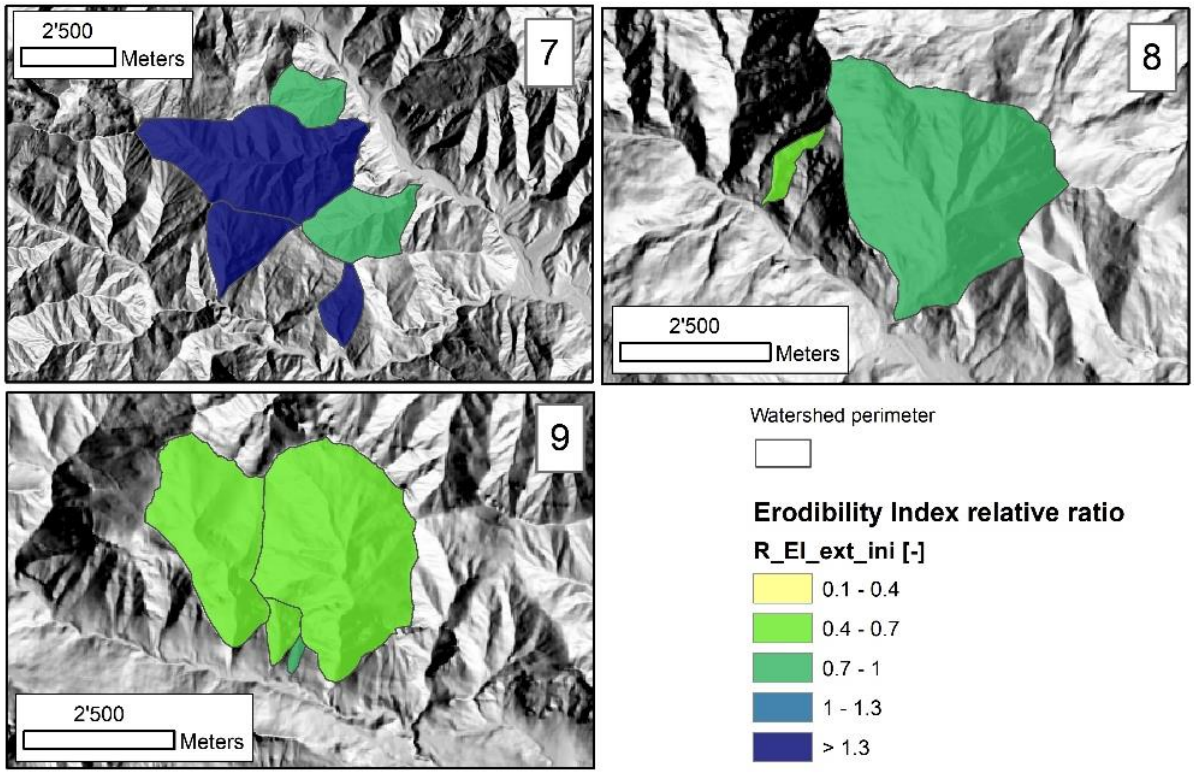


*Figure A4.69 – Erodibility Index relative ratio, R_EI_ext_ini, between extended assessment and initial assessment for the watersheds affected by the Roure/Perrero (7), Traversella (8) and Demonte (9) wildfires.*

*Table A4.1– Spatially averaged Erodibility Index and pre/post-fire relative ratios for the watersheds affected by the Locana/Ribordone wildfire.*

| **Fire n. 1** | **LOCANA/RIBORDONE** | | | | | |
|---|---|---|---|---|---|---|
| **Watershed** | EI_w_pre [Mg MJ$^{-1}$ mm$^{-1}$ h] | EI_w_ini [Mg MJ$^{-1}$ mm$^{-1}$ h] | EI_w_ext [Mg MJ$^{-1}$ mm$^{-1}$ h] | R_EI_ini_pre [-] | R_EI_ext_pre [-] | R_EI_ext_ini [-] |
| **Rio Fura** | 2.23E-04 | 5.78E-03 | 2.52E-03 | 25.9 | 11.3 | 0.4 |
| **Rio Di Chioso Bosco** | 4.65E-05 | 4.63E-03 | 2.98E-03 | 99.5 | 64.0 | 0.6 |
| **R. Montepiano** | 1.13E-04 | 5.09E-03 | 2.66E-03 | 45.1 | 23.6 | 0.5 |
| **Carlevaria** | 7.25E-05 | 7.15E-03 | 2.03E-03 | 98.6 | 28.0 | 0.3 |
| **Rio Di Bardonetto Inferiore** | 1.56E-04 | 6.66E-03 | 1.95E-03 | 42.7 | 12.5 | 0.3 |
| **Ribordone** | 3.57E-04 | 1.37E-03 | 5.27E-04 | 3.8 | 1.5 | 0.4 |
| **Eugio** | 7.68E-04 | 1.64E-03 | 1.15E-03 | 2.1 | 1.5 | 0.7 |
| **Rio Bocchetta** | 5.58E-04 | 1.07E-02 | 5.16E-03 | 19.1 | 9.2 | 0.5 |
| **Rio Di Calsazio** | 3.72E-05 | 6.95E-03 | 6.65E-03 | 186.6 | 178.5 | 1.0 |
| **Locana Est** | 2.20E-04 | 5.00E-03 | 1.95E-03 | 22.8 | 8.9 | 0.4 |
| **Apparè** | 3.86E-05 | 5.89E-03 | 5.76E-03 | 152.6 | 149.4 | 1.0 |
| **Mean** | **2.35E-04** | **5.53E-03** | **3.03E-03** | **63.54** | **44.39** | **0.55** |

*Table A4.2- Spatially averaged Erodibility Index and pre/post-fire relative ratios for the watersheds affected by the Bussoleno/Mompantero wildfire.*

| Fire n. 2 | BUSSOLENO/MOMPANTERO | | | | | |
|---|---|---|---|---|---|---|
| **Watershed** | EI_w_pre | EI_w_ini | EI_w_ext | R_EI_ini_pre | R_EI_ext_pre | R_EI_ext_ini |
| | [Mg MJ$^{-1}$ mm$^{-1}$ h] | [Mg MJ$^{-1}$ mm$^{-1}$ h] | [Mg MJ$^{-1}$ mm$^{-1}$ h] | [-] | [-] | [-] |
| **Crosiglione** | 4.64E-03 | 5.10E-03 | 4.95E-03 | 1.1 | 1.1 | 1.0 |
| **Rio Della Ravoire** | 1.94E-05 | 9.75E-03 | 9.97E-03 | 502.6 | 513.8 | 1.0 |
| **Fogasso** | 7.25E-05 | 2.93E-03 | 3.65E-03 | 40.4 | 50.4 | 1.2 |
| **Rio Della Codrea** | 2.09E-05 | 5.54E-03 | 8.11E-03 | 265.5 | 389.0 | 1.5 |
| **Trinitâ** | 8.14E-05 | 3.19E-03 | 3.29E-03 | 39.1 | 40.4 | 1.0 |
| **Rio Prebech** | 5.84E-03 | 8.74E-03 | 7.43E-03 | 1.5 | 1.3 | 0.8 |
| **Moletta** | 4.37E-04 | 6.24E-03 | 2.60E-03 | 14.3 | 5.9 | 0.4 |
| **Rio Di Periere** | 1.15E-04 | 3.53E-03 | 3.97E-03 | 30.6 | 34.5 | 1.1 |
| **Ravera** | 1.10E-03 | 8.56E-03 | 6.69E-03 | 7.8 | 6.1 | 0.8 |
| **Comba Delle Foglie** | 2.24E-04 | 1.03E-02 | 6.63E-03 | 45.8 | 29.6 | 0.6 |
| **Rocciamelone** | 1.25E-02 | 1.69E-02 | 1.40E-02 | 1.4 | 1.1 | 0.8 |
| **Giandula** | 1.88E-03 | 8.65E-03 | 5.40E-03 | 4.6 | 2.9 | 0.6 |
| **I Piani** | 1.08E-03 | 6.89E-03 | 7.15E-03 | 6.4 | 6.6 | 1.0 |
| **San Giuseppe** | 1.62E-05 | 4.50E-03 | 3.20E-03 | 277.2 | 197.1 | 0.7 |
| **Mean** | **2.00E-03** | **7.20E-03** | **6.22E-03** | **88.45** | **91.41** | **0.91** |

*Table A4 3- Spatially averaged Erodibility Index and pre/post-fire relative ratios for the watersheds affected by the Caprie/Rubiana wildfire.*

| Fire n. 3 | CAPRIE/RUBIANA | | | | | |
|---|---|---|---|---|---|---|
| **Watershed** | EI_w_pre | EI_w_ini | EI_w_ext | R_EI_ini_pre | R_EI_ext_pre | R_EI_ext_ini |
| | [Mg MJ$^{-1}$ mm$^{-1}$ h] | [Mg MJ$^{-1}$ mm$^{-1}$ h] | [Mg MJ$^{-1}$ mm$^{-1}$ h] | [-] | [-] | [-] |
| **Messa** | 2.33E-04 | 3.64E-04 | 2.39E-04 | 1.6 | 1.0 | 0.7 |
| **Sessi** | 5.71E-04 | 7.26E-04 | 6.61E-04 | 1.3 | 1.2 | 0.9 |
| **Novaretto** | 3.35E-04 | 2.49E-03 | 5.28E-04 | 7.4 | 1.6 | 0.2 |
| **Fra Barbe** | 9.90E-05 | 1.13E-03 | 3.46E-04 | 11.4 | 3.5 | 0.3 |
| **Mean** | **3.09E-04** | **1.18E-03** | **4.44E-04** | **5.41** | **1.82** | **0.52** |

*Table A4.4- Spatially averaged Erodibility Index and pre/post-fire relative ratios for the watersheds affected by the Cumiana/Cantalupa wildfire.*

| Fire n. 4 | CUMIANA/CANTALUPA | | | | | |
|---|---|---|---|---|---|---|
| **Watershed** | EI_w_pre | EI_w_ini | EI_w_ext | R_EI_ini_pre | R_EI_ext_pre | R_EI_ext_ini |
| | [Mg MJ$^{-1}$ mm$^{-1}$ h] | [Mg MJ$^{-1}$ mm$^{-1}$ h] | [Mg MJ$^{-1}$ mm$^{-1}$ h] | [-] | [-] | [-] |
| **1*Int. Dx. Sangone** | 8.78E-05 | 1.29E-04 | 1.15E-04 | 1.5 | 1.3 | 0.9 |
| **T. Chisola** | 1.86E-04 | 3.43E-04 | 4.16E-04 | 1.8 | 2.2 | 1.2 |
| **T. Noce** | 1.73E-04 | 4.59E-04 | 1.11E-03 | 2.7 | 6.4 | 2.4 |
| **Chisola Pianura** | 2.20E-04 | 3.38E-04 | 1.05E-03 | 1.5 | 4.8 | 3.1 |
| **Mean** | **1.67E-04** | **3.17E-04** | **6.71E-04** | **1.88** | **3.68** | **1.90** |

*Table A4.5- Spatially averaged Erodibility Index and pre/post-fire relative ratios for the watersheds affected by the Bellino/Casteldelfino wildfire.*

| Fire n. 5 | BELLINO/CASTELDELFINO | | | | | |
|---|---|---|---|---|---|---|
| **Watershed** | EI_w_pre | EI_w_ini | EI_w_ext | R_EI_ini_pre | R_EI_ext_pre | R_EI_ext_ini |
| | [Mg MJ$^{-1}$ mm$^{-1}$ h] | [Mg MJ$^{-1}$ mm$^{-1}$ h] | [Mg MJ$^{-1}$ mm$^{-1}$ h] | [-] | [-] | [-] |
| **Cumbal Della Comu** | 3.21E-04 | 8.38E-03 | 8.69E-04 | 26.1 | 2.7 | 0.1 |
| **T. Mas Del Bernard** | 3.95E-04 | 1.26E-03 | 4.85E-04 | 3.2 | 1.2 | 0.4 |
| **Mean** | **3.58E-04** | **4.82E-03** | **6.77E-04** | **14.62** | **1.97** | **0.24** |

*Table A4.6 - Spatially averaged Erodibility Index and pre/post-fire relative ratios for the watersheds affected by the Sambuco/Pietraporzio wildfire.*

| Fire n. 6 | SAMBUCO/PIETRAPORZIO | | | | | |
|---|---|---|---|---|---|---|
| **Watershed** | EI_w_pre | EI_w_ini | EI_w_ext | R_EI_ini_pre | R_EI_ext_pre | R_EI_ext_ini |
| | [Mg MJ$^{-1}$ mm$^{-1}$ h] | [Mg MJ$^{-1}$ mm$^{-1}$ h] | [Mg MJ$^{-1}$ mm$^{-1}$ h] | [-] | [-] | [-] |
| **R. Bianco** | 9.89E-04 | 1.11E-03 | 1.00E-03 | 1.1 | 1.0 | 0.9 |
| **Sn** | 2.35E-04 | 1.27E-03 | 3.23E-03 | 5.4 | 13.8 | 2.5 |
| **Rio Di Castello Pietraporzio** | 5.02E-04 | 5.27E-04 | 5.92E-04 | 1.0 | 1.2 | 1.1 |
| **Mean** | **5.75E-04** | **9.70E-04** | **1.61E-03** | **2.53** | **5.32** | **1.52** |

*Table A4.7 - Spatially averaged Erodibility Index and pre/post-fire relative ratios for the watersheds affected by the Roure/Perrero wildfire.*

| Fire n. 7 | ROURE/PERRERO | | | | | |
|---|---|---|---|---|---|---|
| **Watershed** | EI_w_pre | EI_w_ini | EI_w_ext | R_EI_ini_pre | R_EI_ext_pre | R_EI_ext_ini |
| | [Mg MJ$^{-1}$ mm$^{-1}$ h] | [Mg MJ$^{-1}$ mm$^{-1}$ h] | [Mg MJ$^{-1}$ mm$^{-1}$ h] | [-] | [-] | [-] |
| **V.Ne Di Borsetto** | 3.18E-04 | 4.60E-04 | 1.26E-03 | 1.4 | 4.0 | 2.7 |
| **S. Martino Sud** | 1.11E-04 | 1.43E-04 | 2.06E-04 | 1.3 | 1.9 | 1.4 |
| **Colet** | 1.75E-05 | 1.82E-05 | 1.77E-05 | 1.0 | 1.0 | 1.0 |
| **Molotta** | 1.88E-04 | 2.48E-04 | 3.27E-04 | 1.3 | 1.7 | 1.3 |
| **Gernier** | 8.83E-05 | 1.49E-03 | 1.47E-03 | 16.9 | 16.7 | 1.0 |
| **Mean** | **1.44E-04** | **4.73E-04** | **6.57E-04** | **4.40** | **5.05** | **1.49** |

*Table A4.8 - Spatially averaged Erodibility Index and pre/post-fire relative ratios for the watersheds affected by the Traversella wildfire.*

| **Fire n. 8** | | | **TRAVERSELLA** | | | |
|---|---|---|---|---|---|---|
| **Watershed** | EI_w_pre | EI_w_ini | EI_w_ext | R_EI_ini_pre | R_EI_ext_pre | R_EI_ext_ini |
| | [Mg MJ$^{-1}$ mm$^{-1}$ h] | [Mg MJ$^{-1}$ mm$^{-1}$ h] | [Mg MJ$^{-1}$ mm$^{-1}$ h] | [-] | [-] | [-] |
| **T. Bersella** | 8.02E-04 | 2.35E-03 | 1.70E-03 | 2.9 | 2.1 | 0.7 |
| **Valle Chiara Primo** | 3.86E-04 | 1.41E-02 | 5.69E-03 | 36.4 | 14.7 | 0.4 |
| **Mean** | **5.94E-04** | **8.20E-03** | **3.69E-03** | **19.69** | **8.43** | **0.56** |

*Table A4.9 - Spatially averaged Erodibility Index and pre/post-fire relative ratios for the watersheds affected by the Demonte wildfire.*

| **Fire n. 9** | | | **DEMONTE** | | | |
|---|---|---|---|---|---|---|
| **Watershed** | EI_w_pre | EI_w_ini | EI_w_ext | R_EI_ini_pre | R_EI_ext_pre | R_EI_ext_ini |
| | [Mg MJ$^{-1}$ mm$^{-1}$ h] | [Mg MJ$^{-1}$ mm$^{-1}$ h] | [Mg MJ$^{-1}$ mm$^{-1}$ h] | [-] | [-] | [-] |
| **V. Del Saut** | 3.96E-04 | 1.63E-03 | 7.84E-04 | 4.1 | 2.0 | 0.5 |
| **Valle Di Monfreis** | 1.39E-04 | 6.32E-04 | 4.20E-04 | 4.6 | 3.0 | 0.7 |
| **Sn 2** | 6.17E-05 | 2.36E-03 | 1.74E-03 | 38.3 | 28.3 | 0.7 |
| **Rio Di Prafioret C.** | 2.42E-04 | 5.56E-03 | 2.24E-03 | 23.0 | 9.3 | 0.4 |
| **Mean** | **2.10E-04** | **2.55E-03** | **1.30E-03** | **17.49** | **10.63** | **0.57** |

# Appendix 5

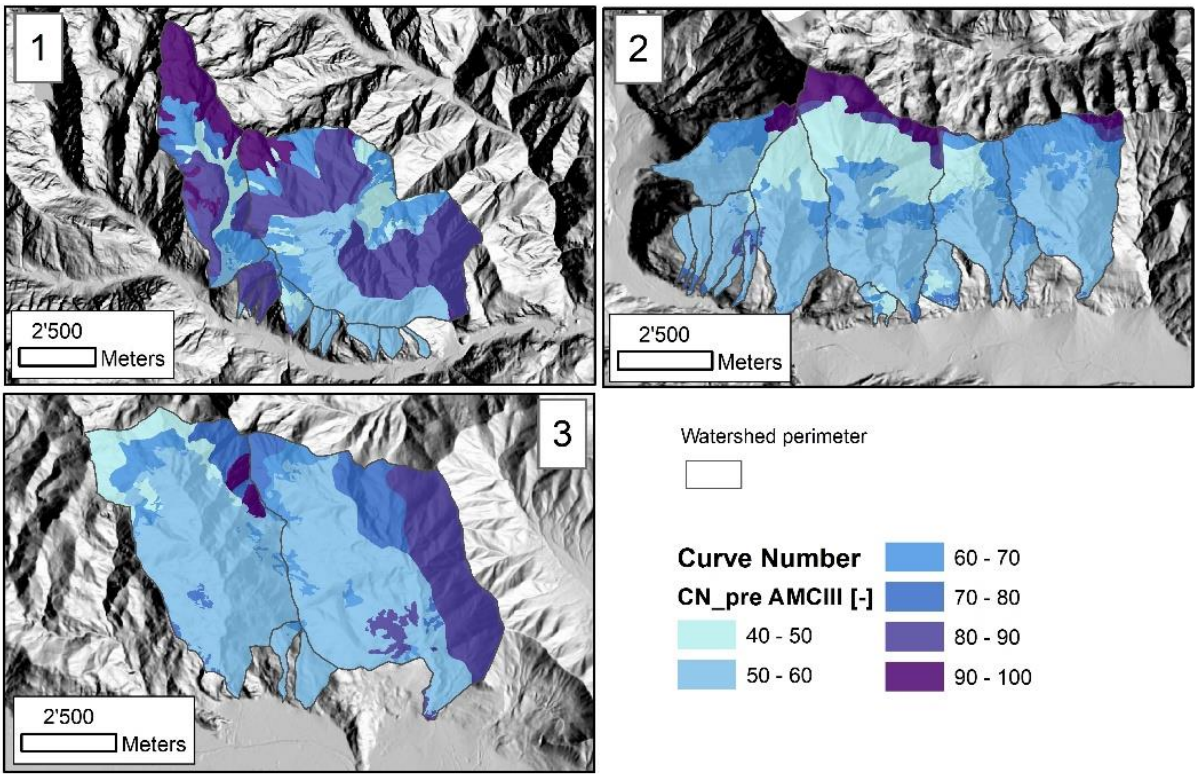


*Figure A5.1- Pre-fire value of the Curve Number, $CN_{pre}$, for the watersheds affected by the Locana/Ribordone (1), Bussoleno/Mompantero (2) and Caprie/Rubiana (3) wildfires.*

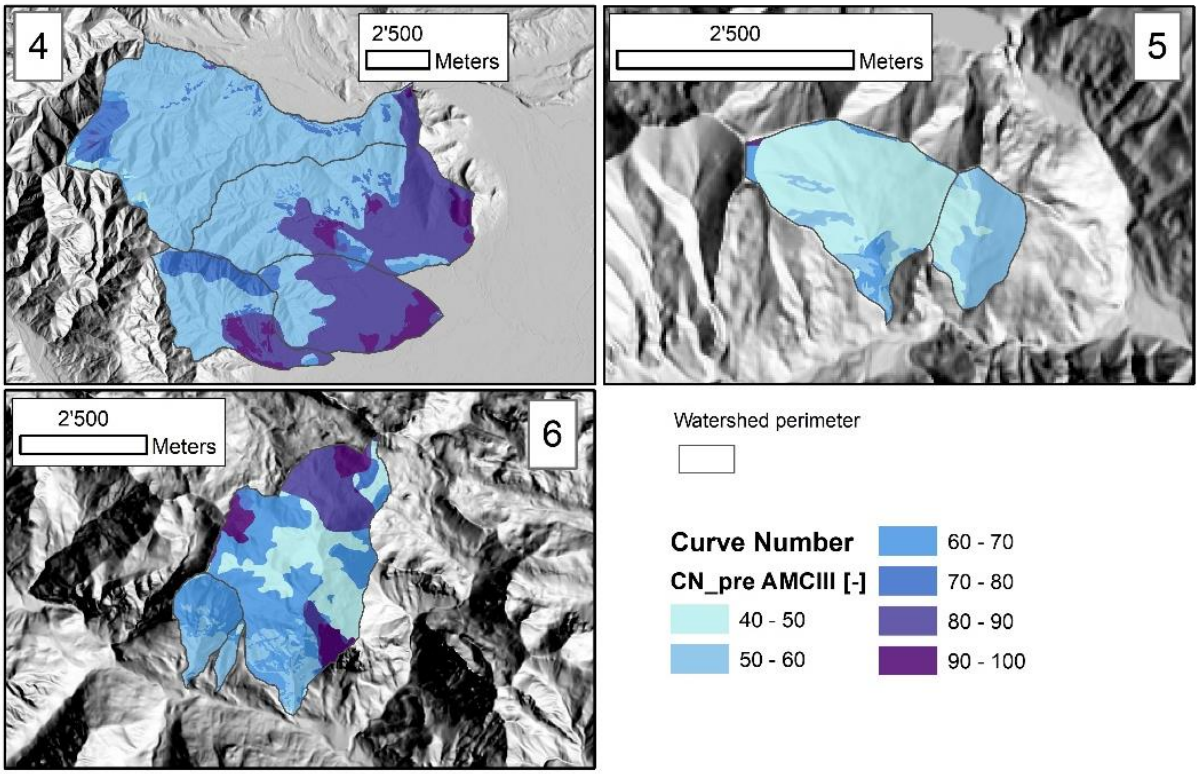


*Figure A5.2 - Pre-fire value of the Curve Number, $CN_{pre}$, for the watersheds affected by the Cumiana/Cantalupa (4), Bellino/Casteldelfino (5) and Sambuco/Pietraporzio (6) wildfires.*

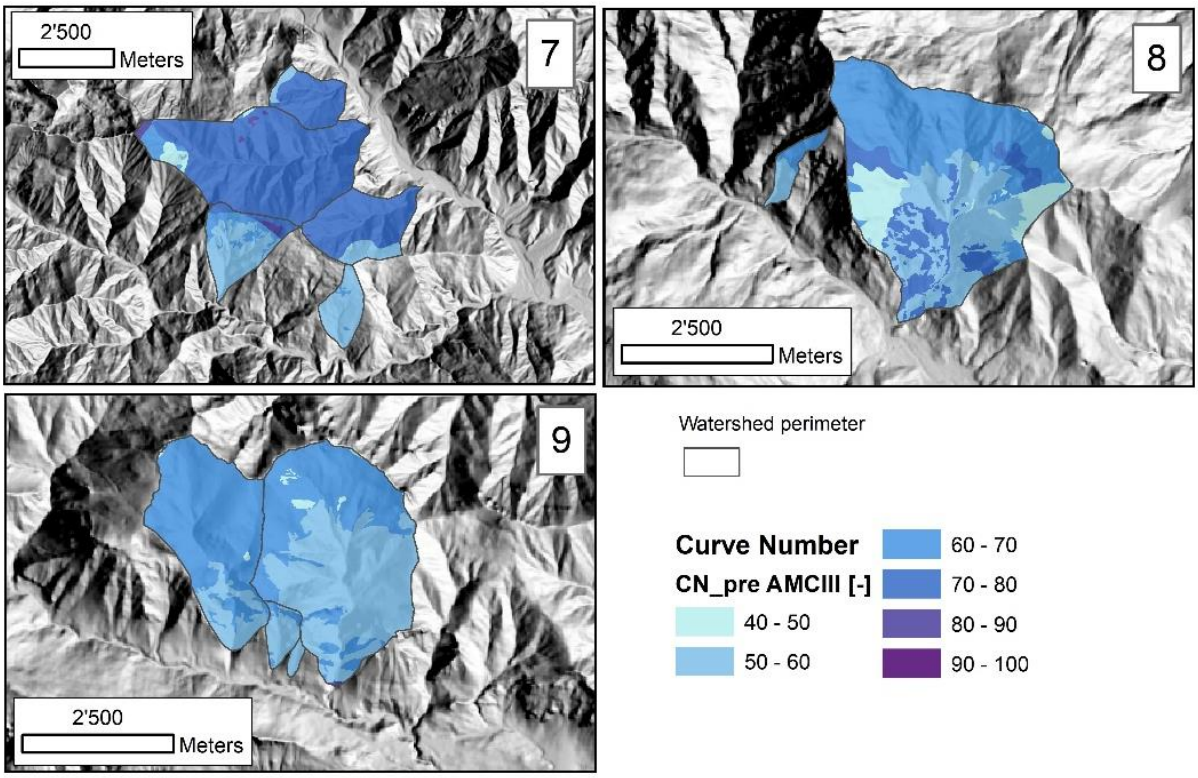


*Figure A5.3 - Pre-fire value of the Curve Number, $CN_{pre}$, for the watersheds affected by the Roure/Perrero (7), Traversella (8) and Demonte (9) wildfires.*

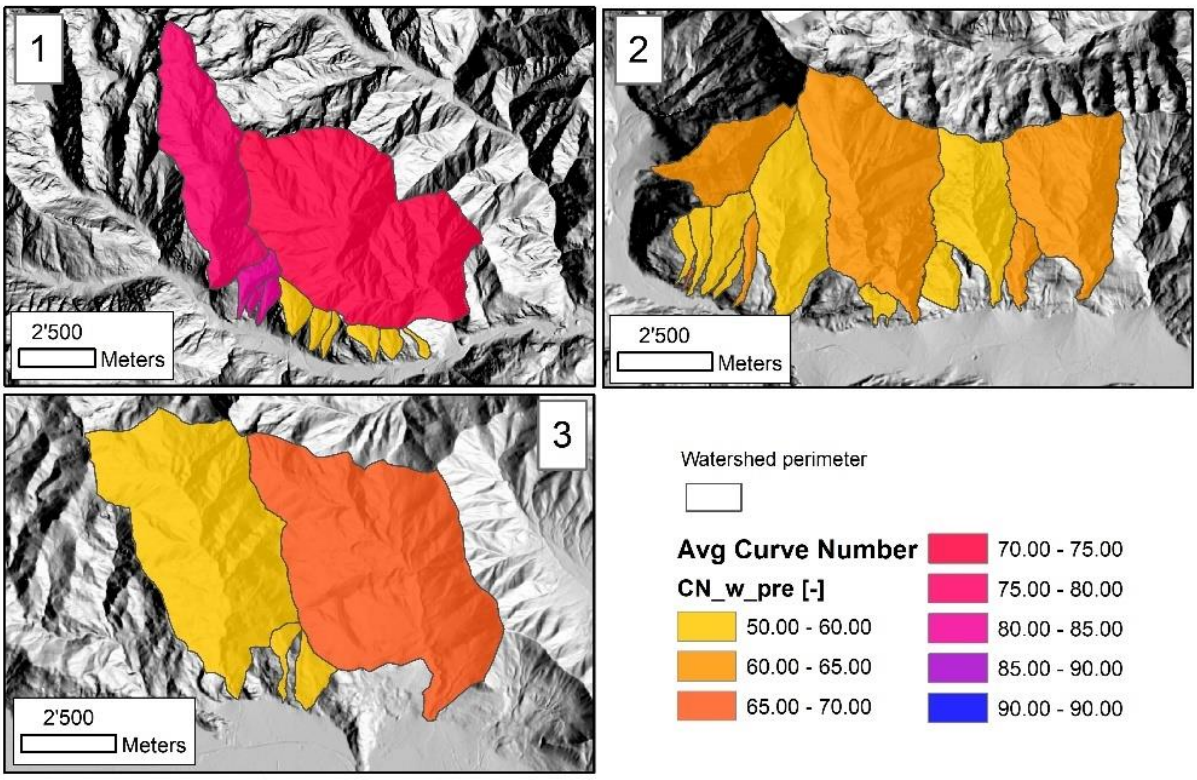


*Figure A5.4 - Pre-fire spatially averaged value of the Curve Number, $CN_{w\_pre}$, for the watersheds affected by the Locana/Ribordone (1), Bussoleno/Mompantero (2) and Caprie/Rubiana (3) wildfires.*

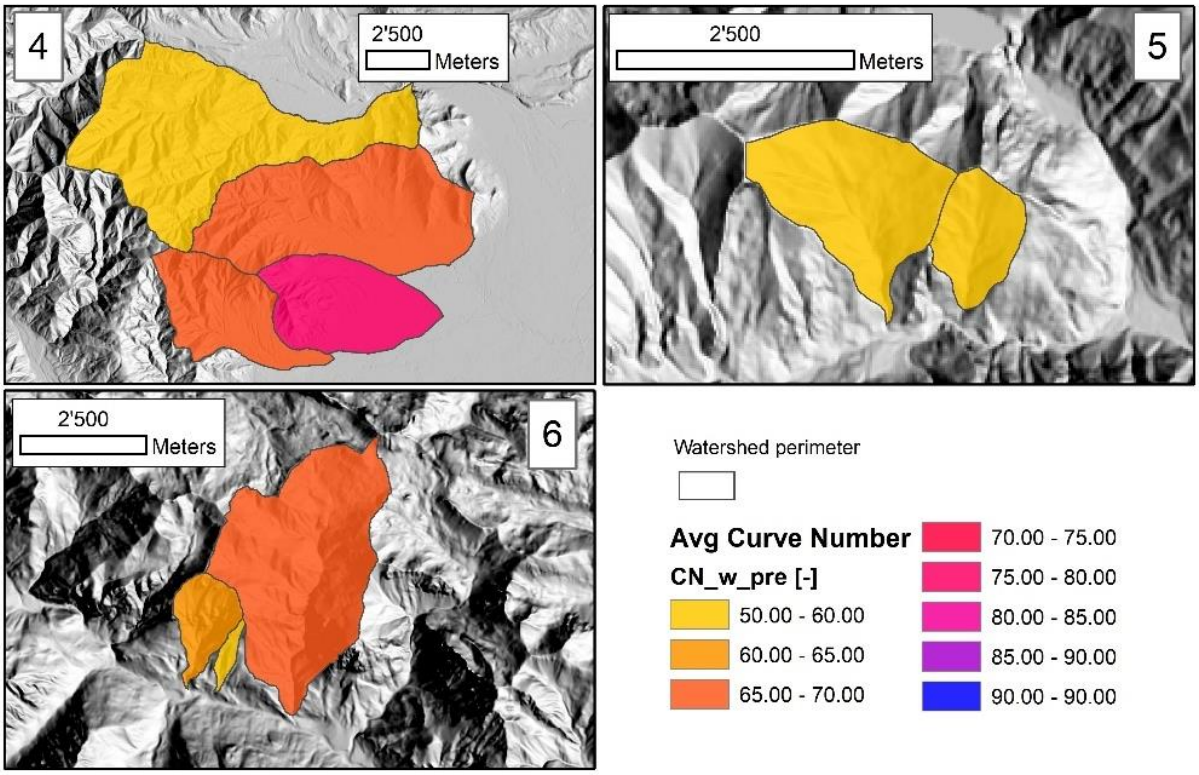


*Figure A5.5 - Pre-fire spatially averaged value of the Curve Number, $CN_{\_w\_pre}$, for the watersheds affected by the Cumiana/Cantalupa (4), Bellino/Casteldelfino (5) and Sambuco/Pietraporzio (6) wildfires.*

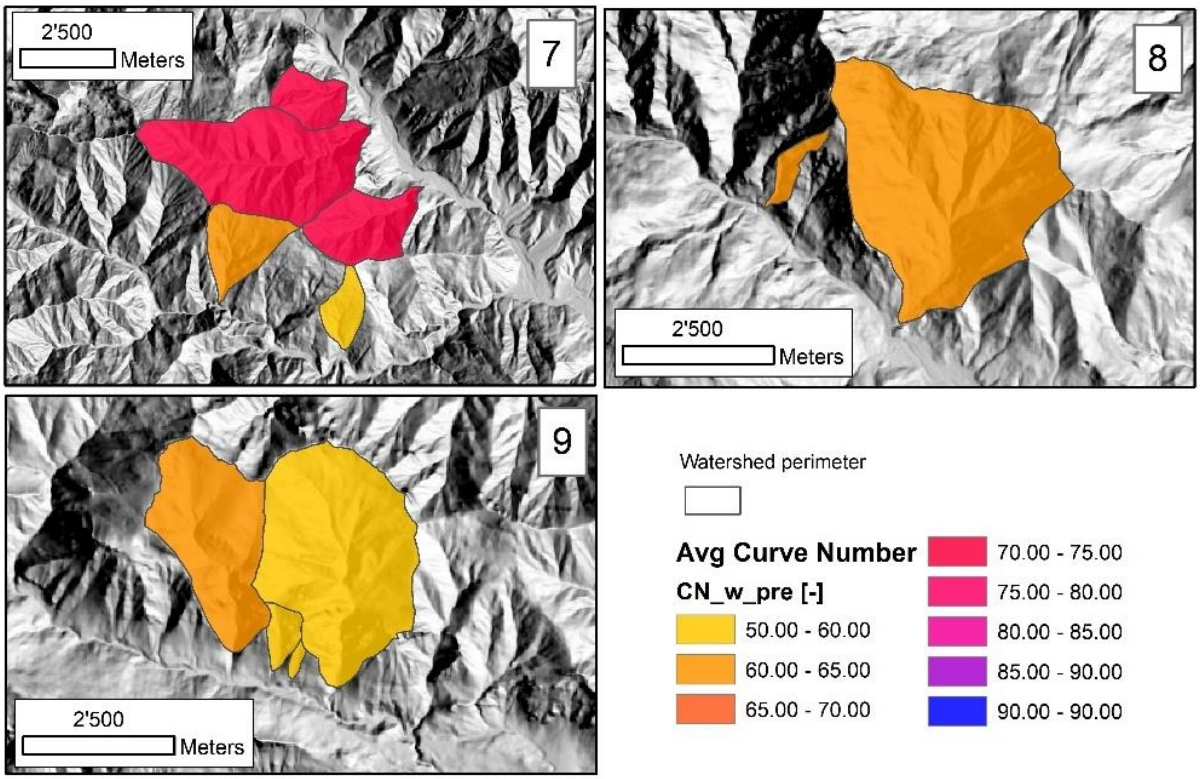


*Figure A5.6 - Pre-fire spatially averaged value of the Curve Number, $CN_{\_w\_pre}$, for the watersheds affected by the Roure/Perrero (7), Traversella (8) and Demonte (9) wildfires.*

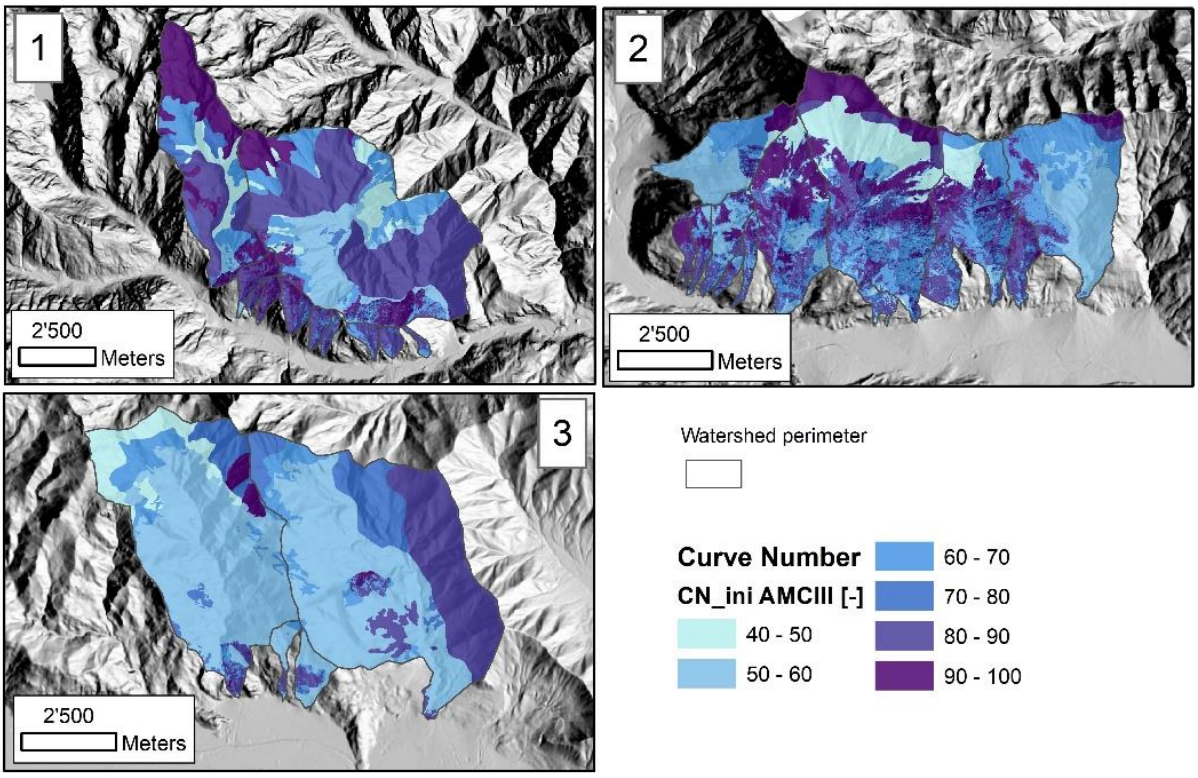


*Figure A5.7 - Value of the Curve Number, $CN_{ini}$, for the watersheds affected by the Locana/Ribordone (1), Bussoleno/Mompantero (2) and Caprie/Rubiana (3) wildfires; post-fire, initial assessment.*

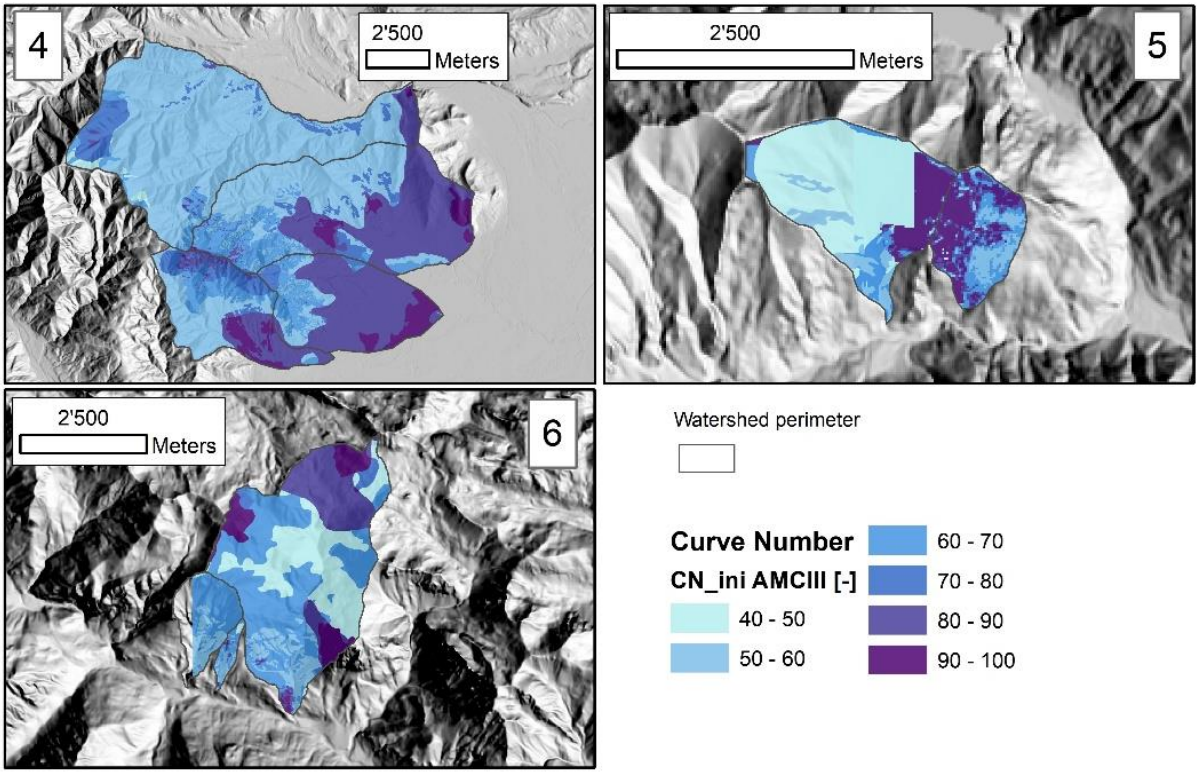


*Figure A5.8 - Value of the Curve Number, $CN_{ini}$, for the watersheds affected by the Cumiana/Cantalupa (4), Bellino/Casteldelfino (5) and Sambuco/Pietraporzio (6) wildfires; post-fire, initial assessment.*

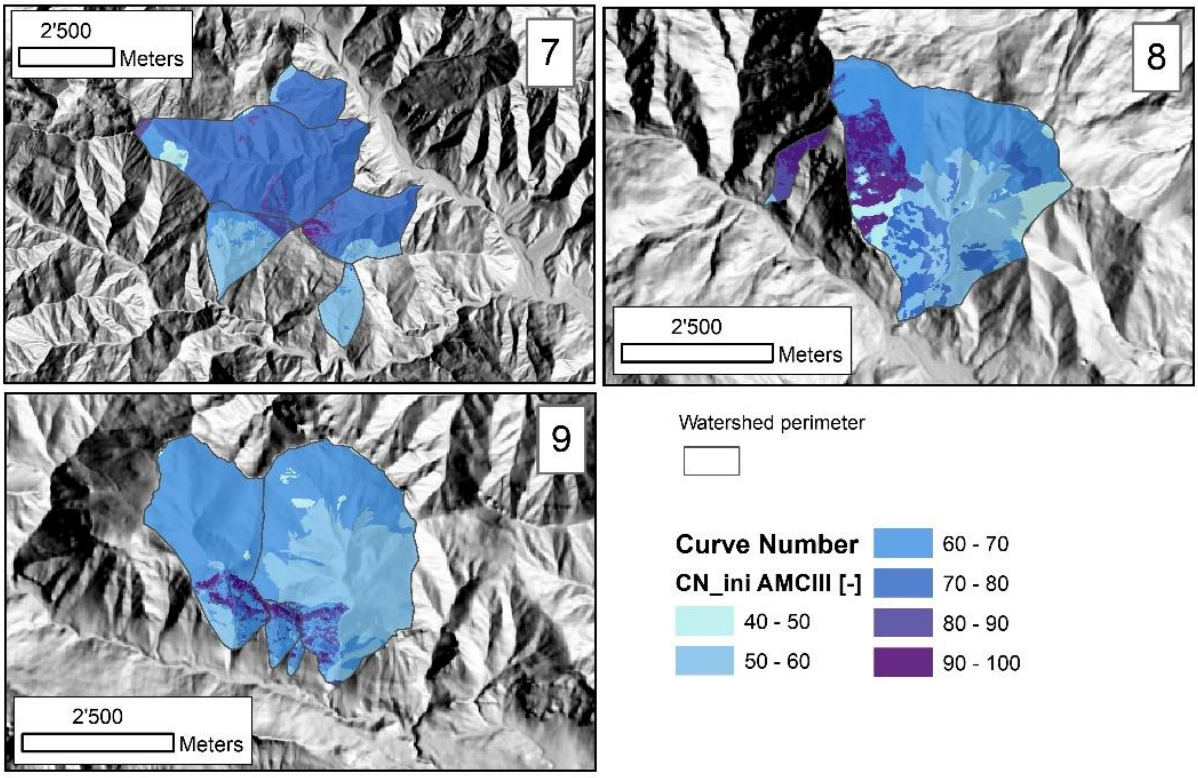


*Figure A5. 9 - Value of the Curve Number, $CN_{ini}$, for the watersheds affected by the Roure/Perrero (7), Traversella (8) and Demonte (9) wildfires; post-fire, initial assessment.*

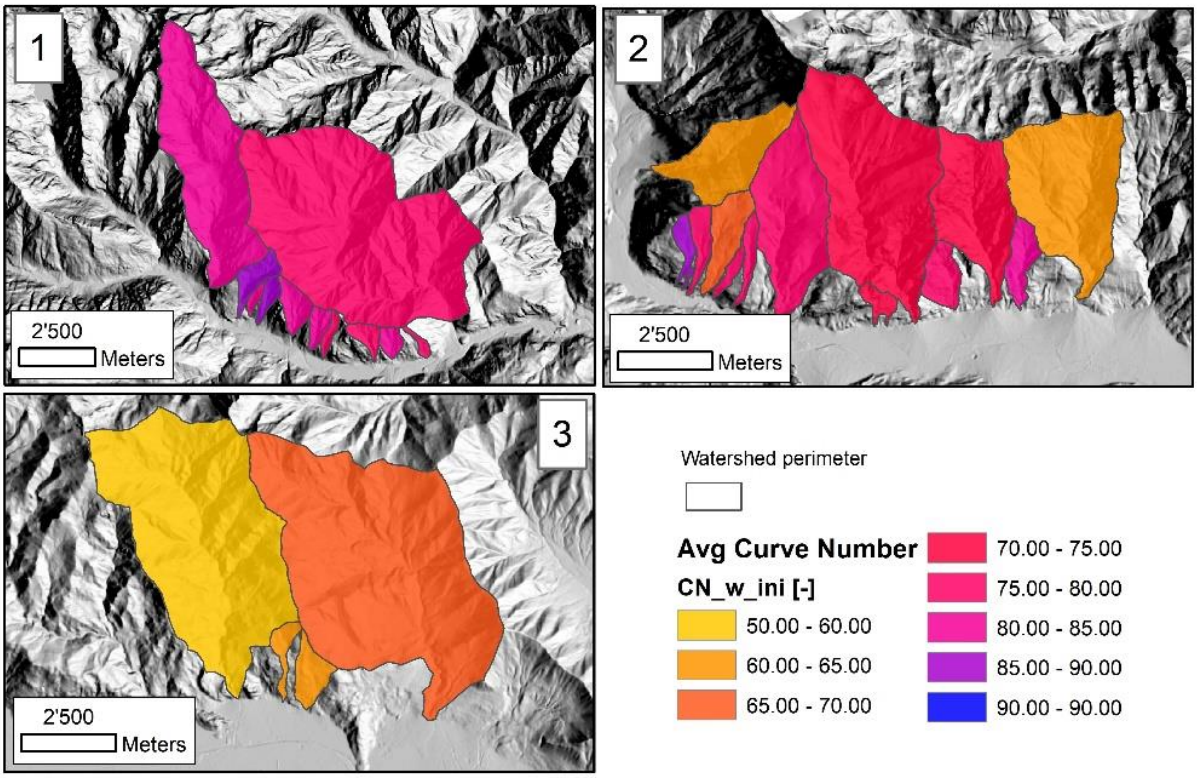


*Figure A5.10 - Spatially averaged value of the Curve Number, $CN_{w\_ini}$, for the watersheds affected by the Locana/Ribordone (1), Bussoleno/Mompantero (2) and Caprie/Rubiana (3) wildfires; post-fire, initial assessment.*

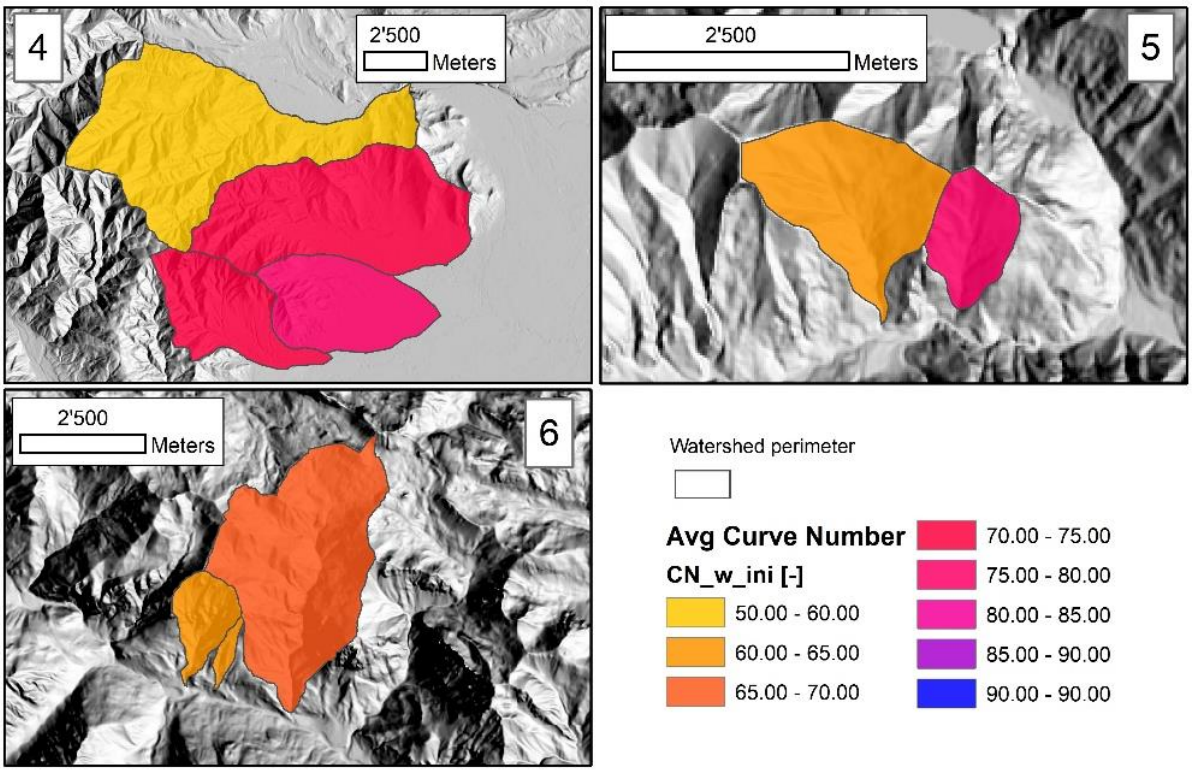


*Figure A5.11 - Spatially averaged value of the Curve Number, $CN_{w\_ini}$, for the watersheds affected by the Cumiana/Cantalupa (4), Bellino/Casteldelfino (5) and Sambuco/Pietraporzio (6) wildfires; post-fire, initial assessment.*

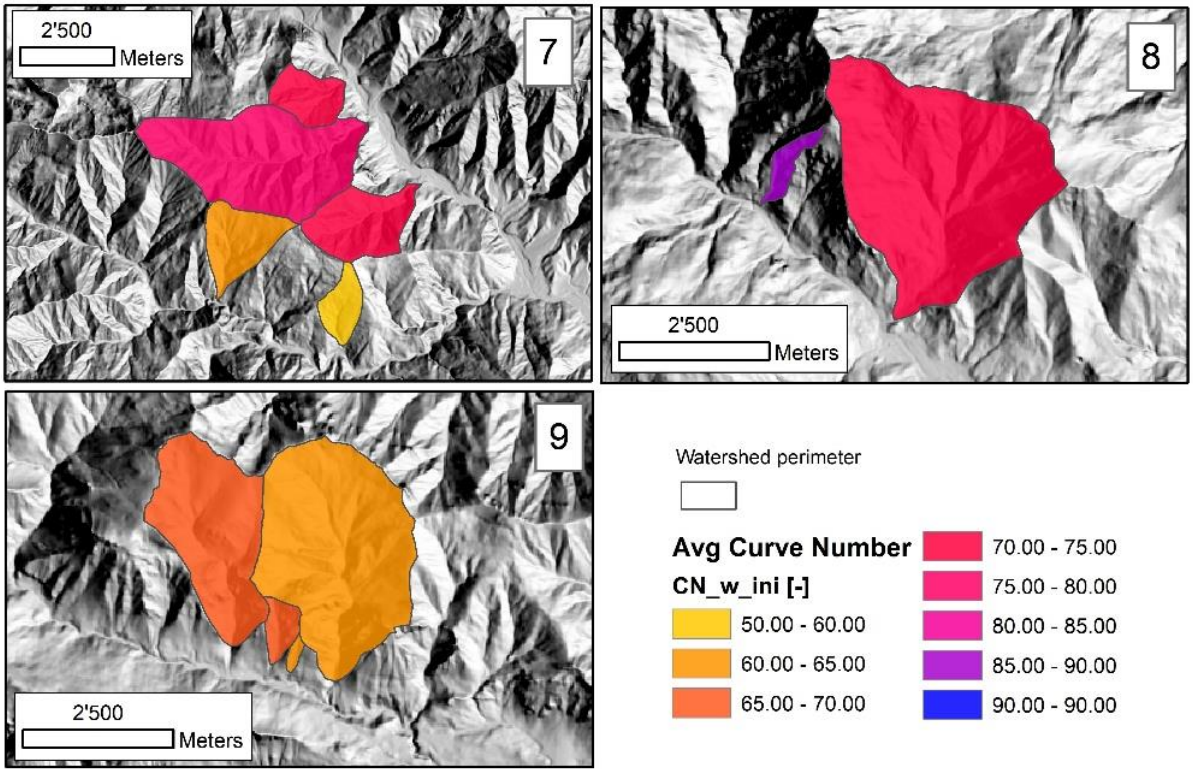


*Figure A5.12 - Spatially averaged value of the Curve Number, $CN_{w\_ini}$, for the watersheds affected by the Roure/Perrero (7), Traversella (8) and Demonte (9) wildfires; post-fire, initial assessment.*

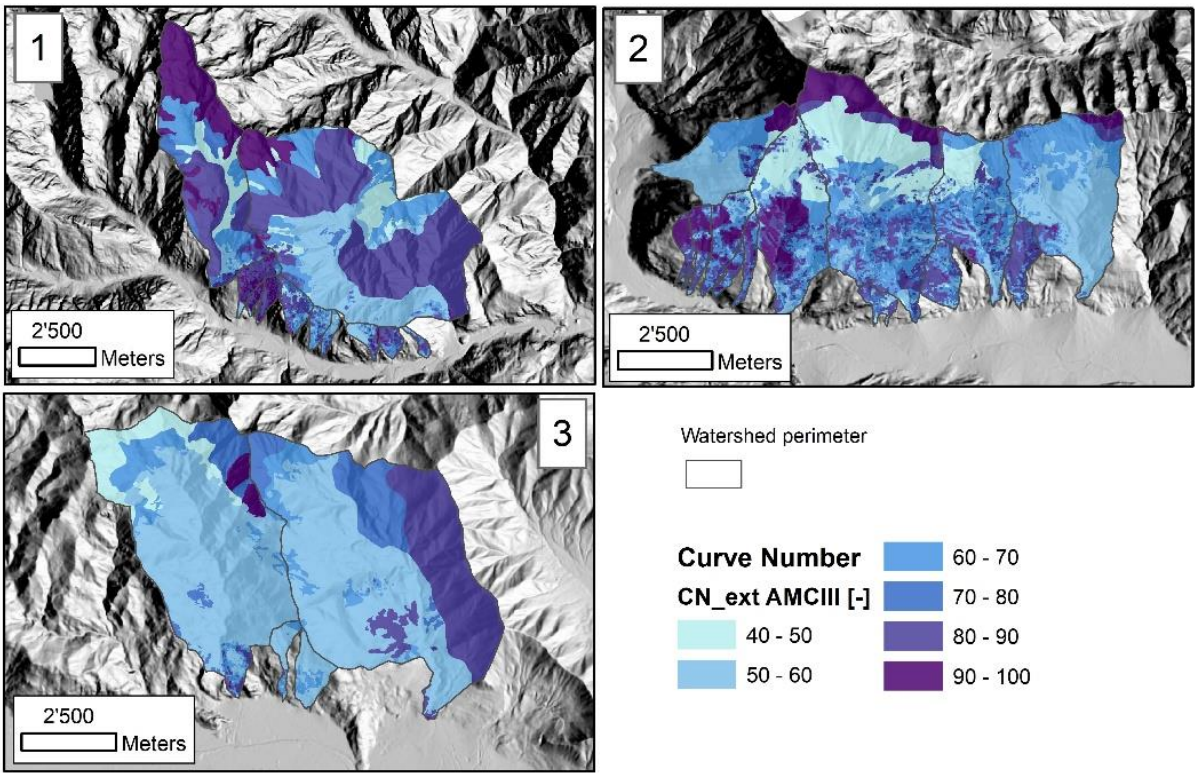


*Figure A5.13 - Value of the Curve Number, $CN_{ext}$, for the watersheds affected by the Locana/Ribordone (1), Bussoleno/Mompantero (2) and Caprie/Rubiana (3) wildfires; post-fire, extended assessment.*

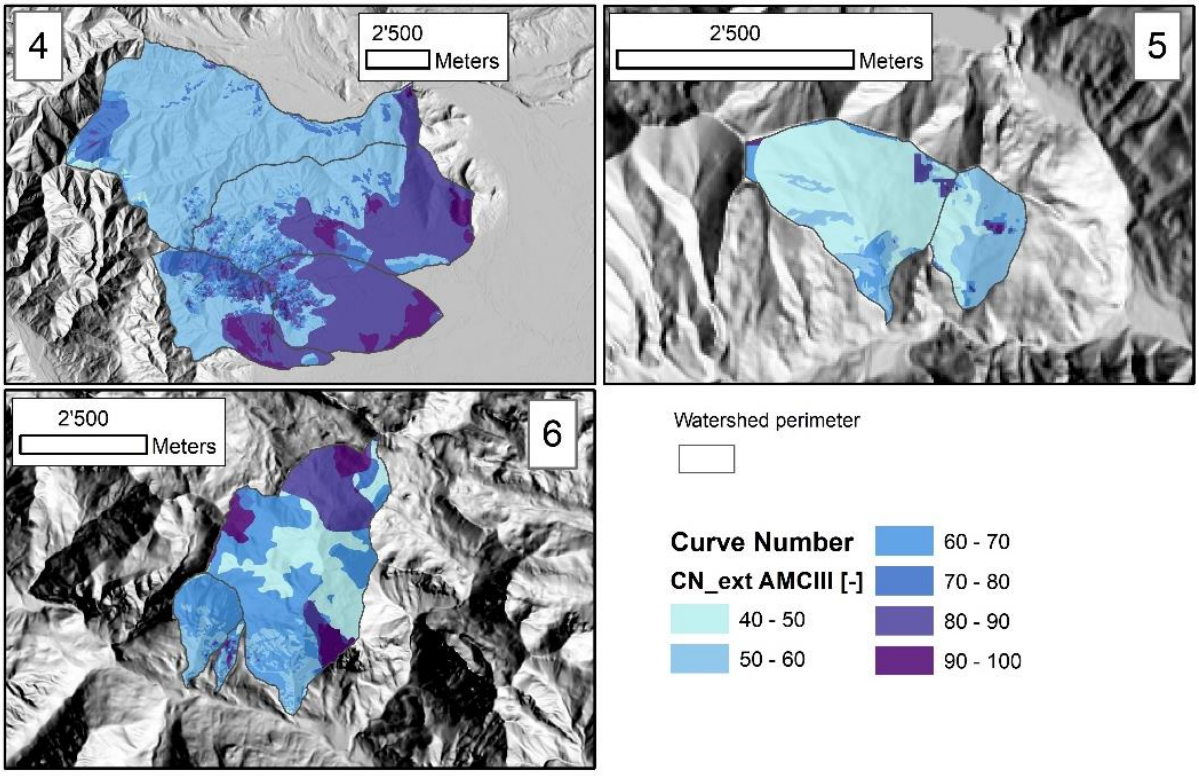


*Figure A5.14 - Value of the Curve Number, $CN_{ext}$, for the watersheds affected by the Cumiana/Cantalupa (4), Bellino/Casteldelfino (5) and Sambuco/Pietraporzio (6) wildfires; post-fire, extended assessment.*

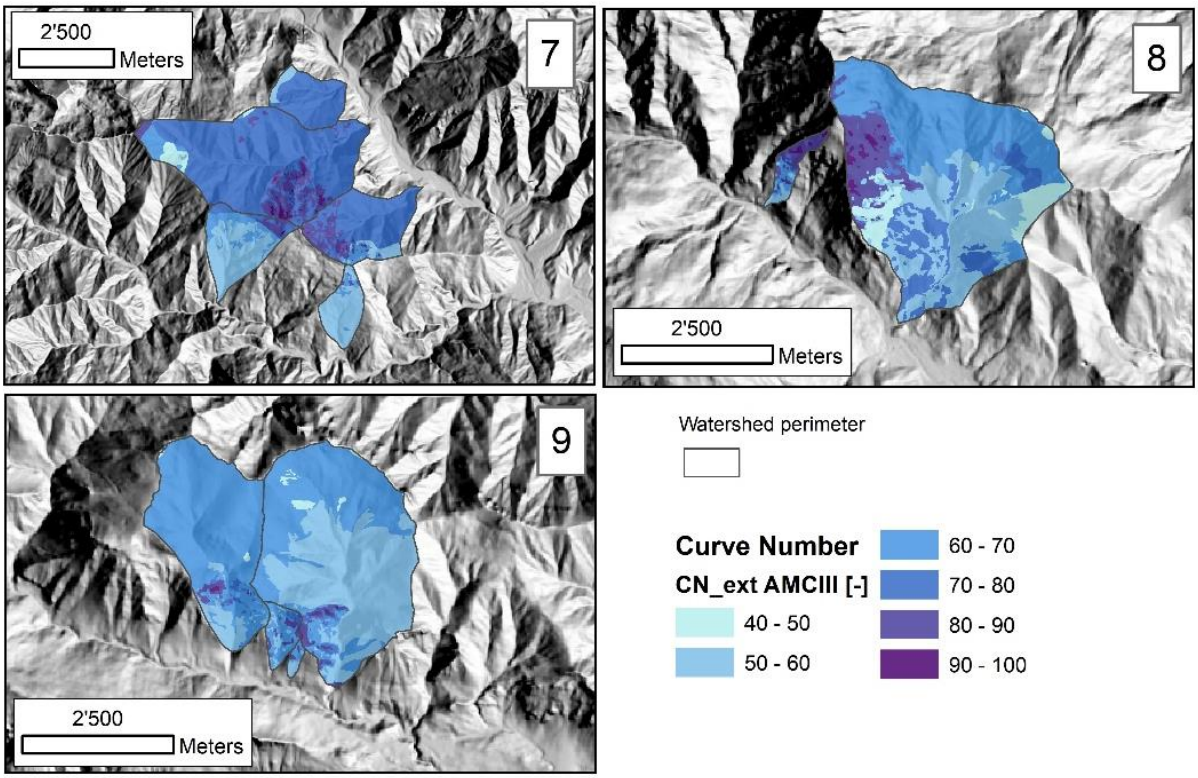


*Figure A5.15 - Value of the Curve Number, $CN_{ext}$, for the watersheds affected by the Roure/Perrero (7), Traversella (8) and Demonte (9) wildfires; post-fire, extended assessment.*

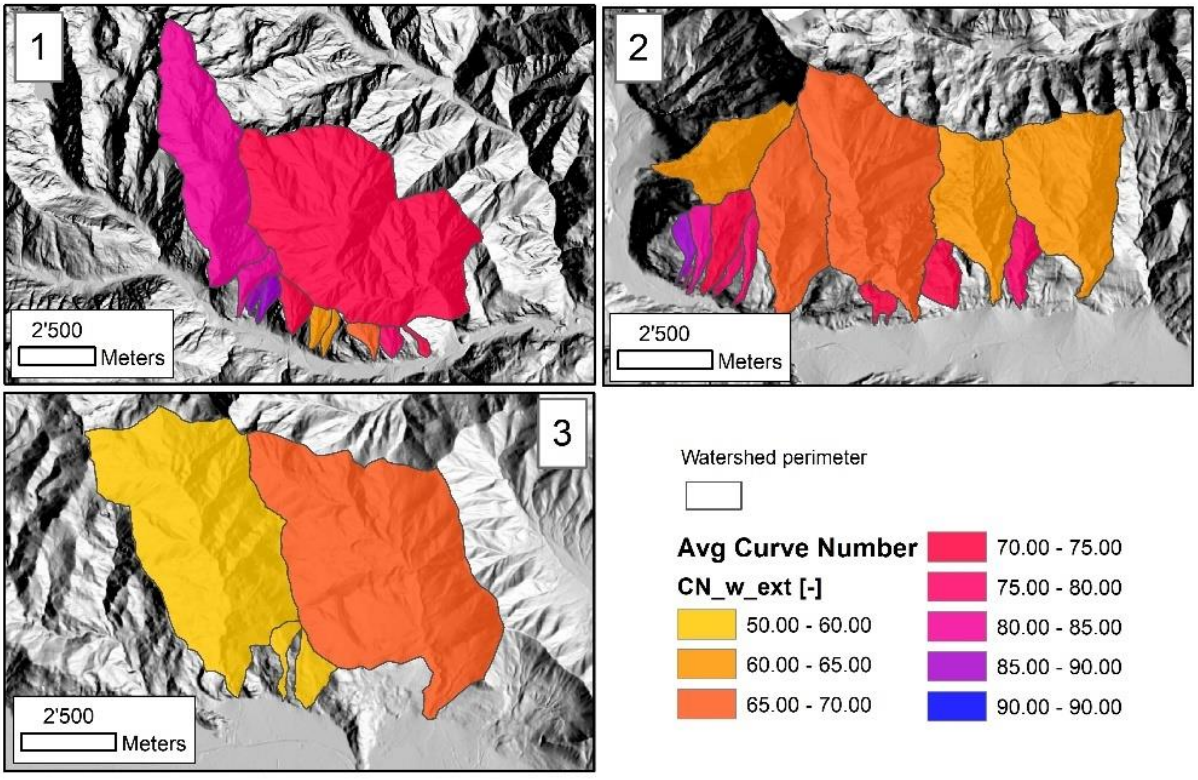


*Figure A5.16 – Spatially averaged value of the Curve Number, $CN_{w\_ext}$, for the watersheds affected by the Locana/Ribordone (1), Bussoleno/Mompantero (2) and Caprie/Rubiana (3) wildfires; post-fire, extended assessment.*

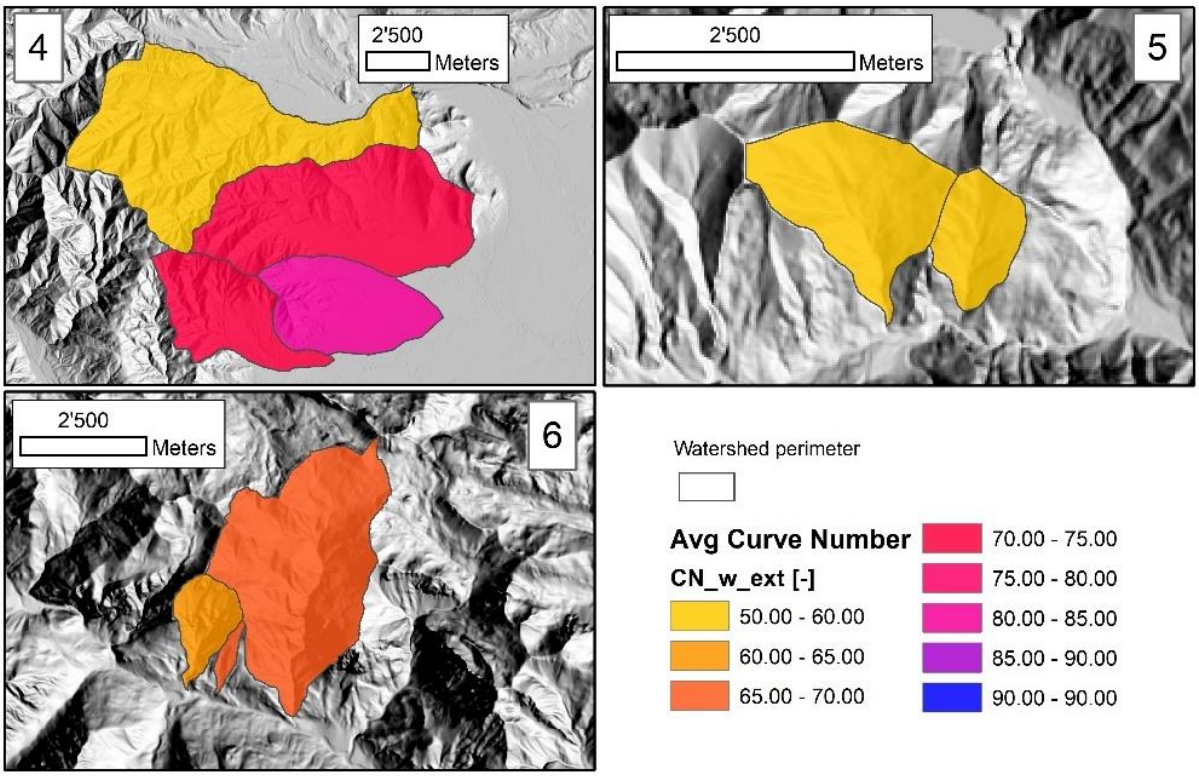


*Figure A5.17 – Spatially averaged value of the Curve Number, $CN_{\_w\_ext}$, for the watersheds affected by the Cumiana/Cantalupa (4), Bellino/Casteldelfino (5) and Sambuco/Pietraporzio (6) wildfires; post-fire, extended assessment.*

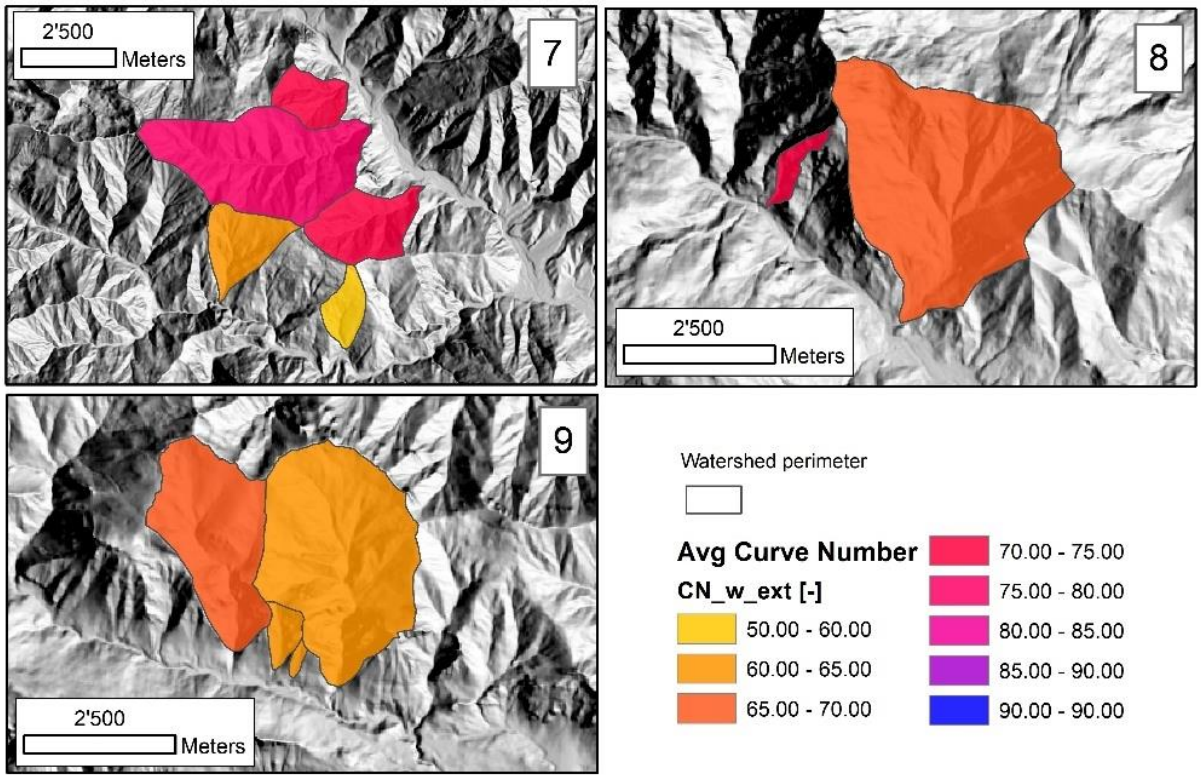


*Figure A5.18 – Spatially averaged value of the Curve Number, $CN_{\_w\_ext}$, for the watersheds affected by the Roure/Perrero (7), Traversella (8) and Demonte (9) wildfires; post-fire, extended assessment.*

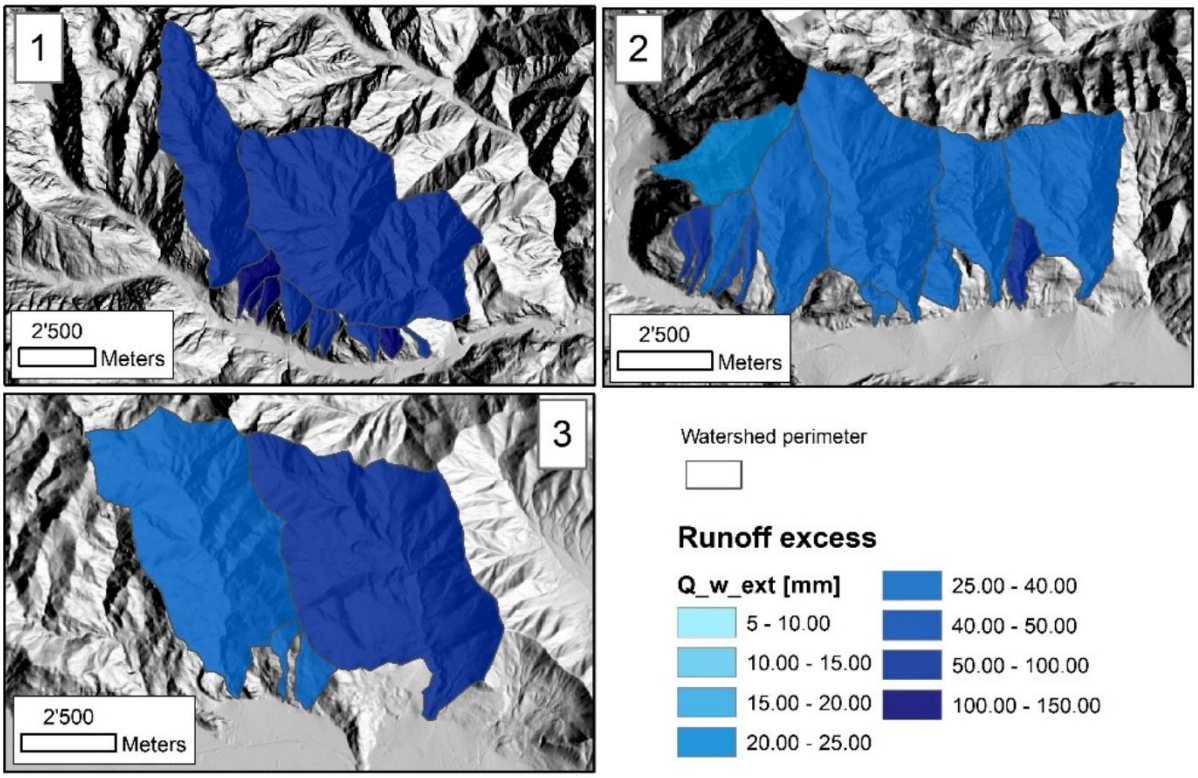


*Figure A5.19 – Excess runoff depth $Q_{w\_ext}$ for the watersheds affected by the Locana/Ribordone (1), Bussoleno/Mompantero (2) and Caprie/Rubiana (3) wildfires; post-fire, extended assessment.*

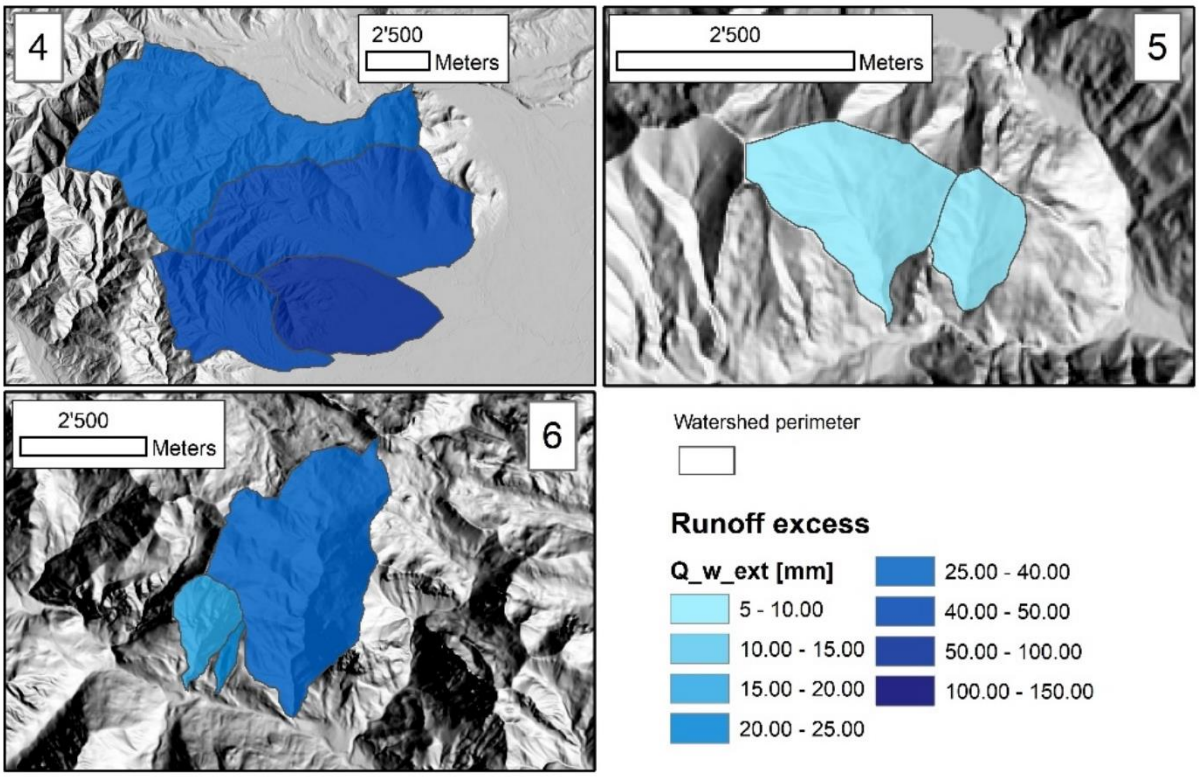


*Figure A5.20 – Excess runoff depth $Q_{w\_ext}$ for the watersheds affected by the Cumiana/Cantalupa (4), Bellino/Casteldelfino (5) and Sambuco/Pietraporzio (6) wildfires; post-fire, extended assessment.*

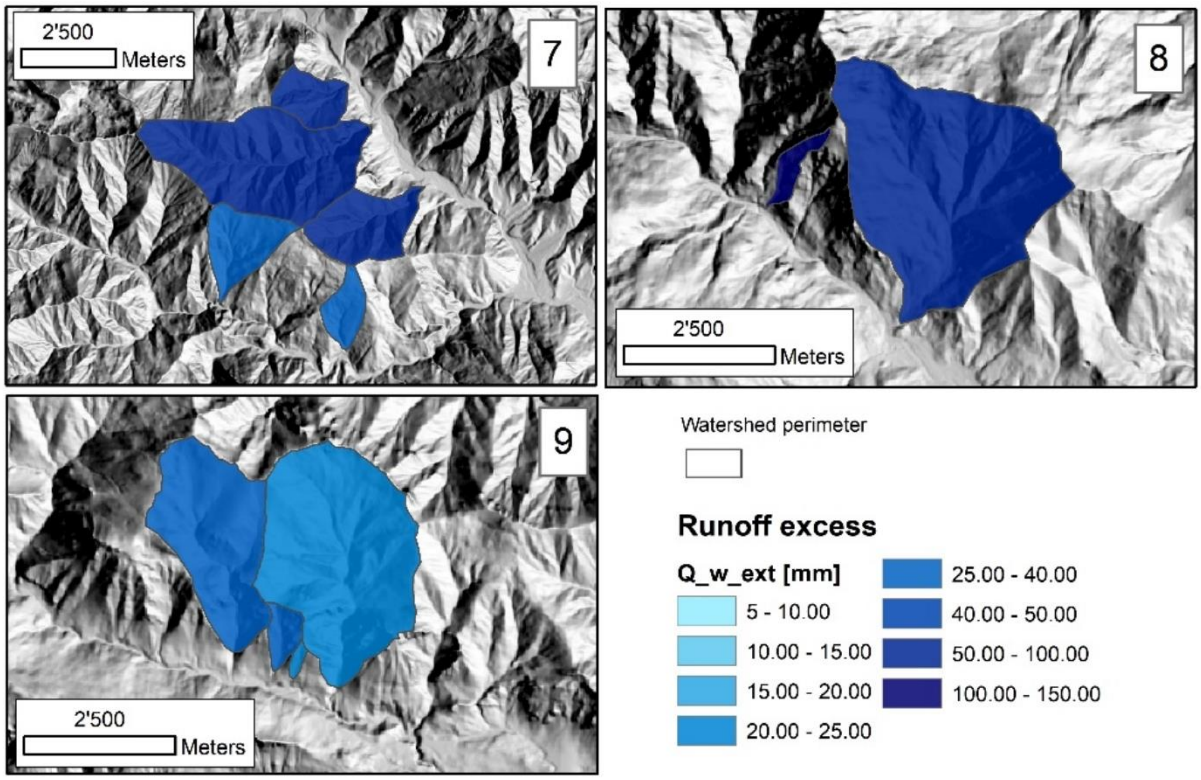


*Figure A5.21 – Excess runoff depth $Q_{w\_ext}$ for the watersheds affected by the Roure/Perrero (7), Traversella (8) and Demonte (9) wildfires; post-fire, extended assessment.*

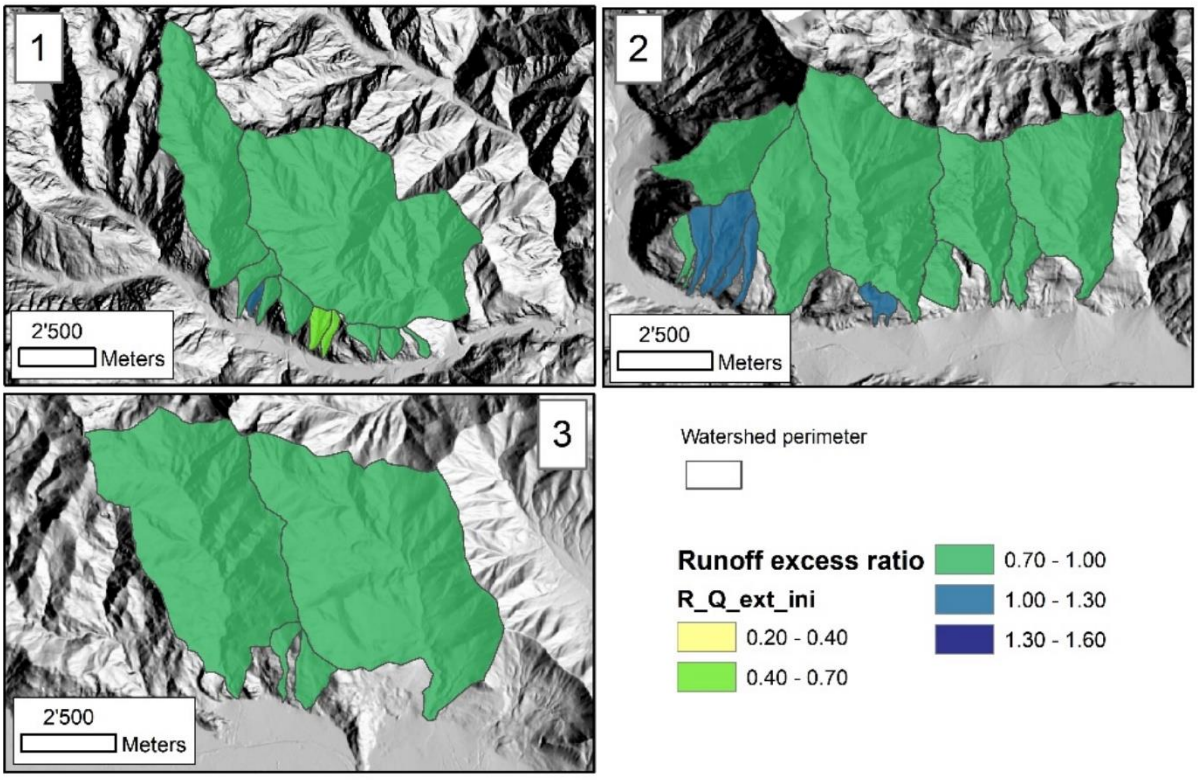


*Figure A5.22 – Runoff excess relative ratio, R_Q_ext_ini, between extended assessment and initial assessment for the watersheds affected by the Locana/Ribordone (1), Bussoleno/Mompantero (2) and Caprie/Rubiana (3) wildfires.*

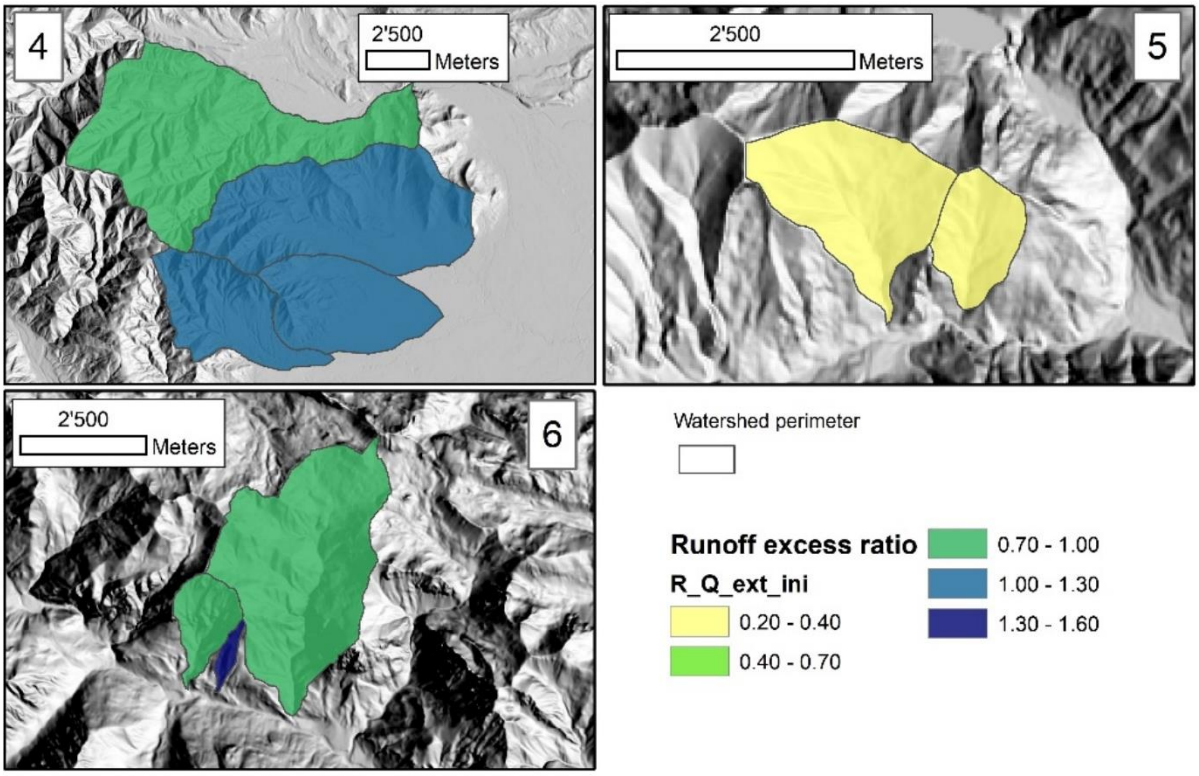


*Figure A5.23 – Runoff excess relative ratio, R_Q_ext_ini, between extended assessment and initial assessment situation for the watersheds affected by the Cumiana/Cantalupa (4), Bellino/Casteldelfino (5) and Sambuco/Pietraporzio (6) wildfires.*

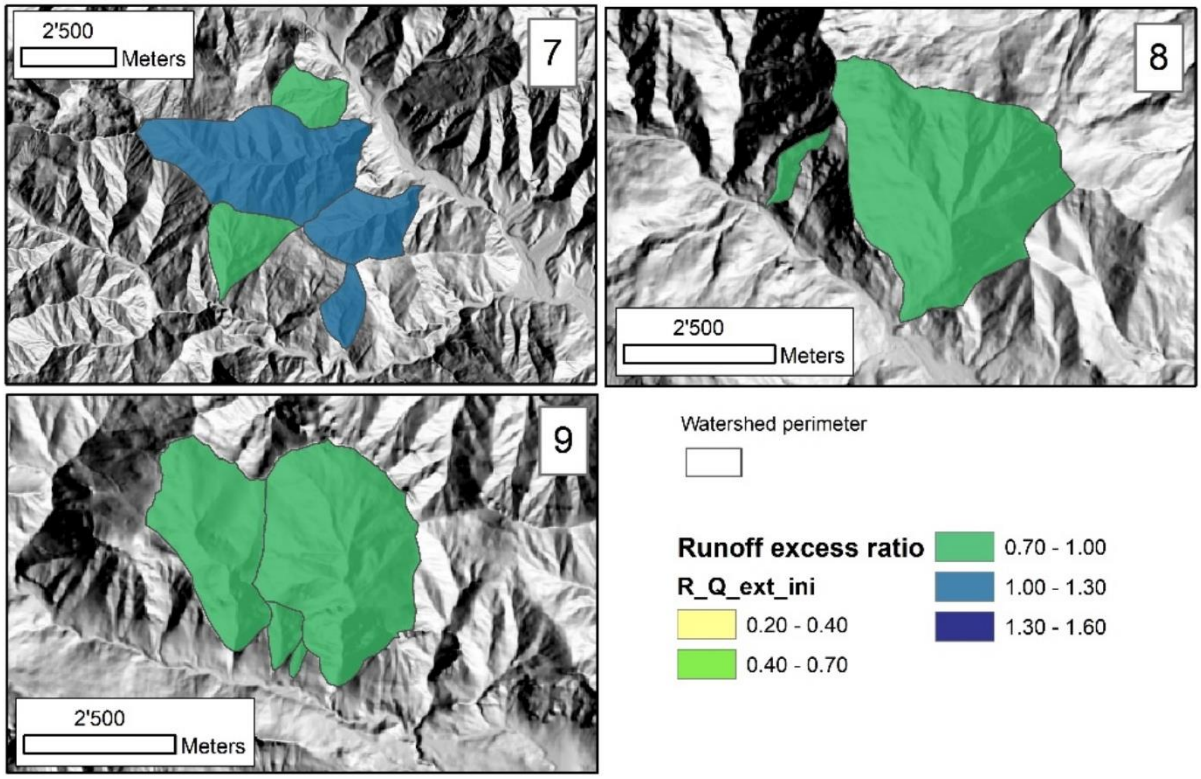


*Figure A5.24 – Runoff excess relative ratio, R_Q_ext_ini, between extended assessment and initial assessment for the watersheds affected by the Roure/Perrero (7), Traversella (8) and Demonte (9) wildfires.*

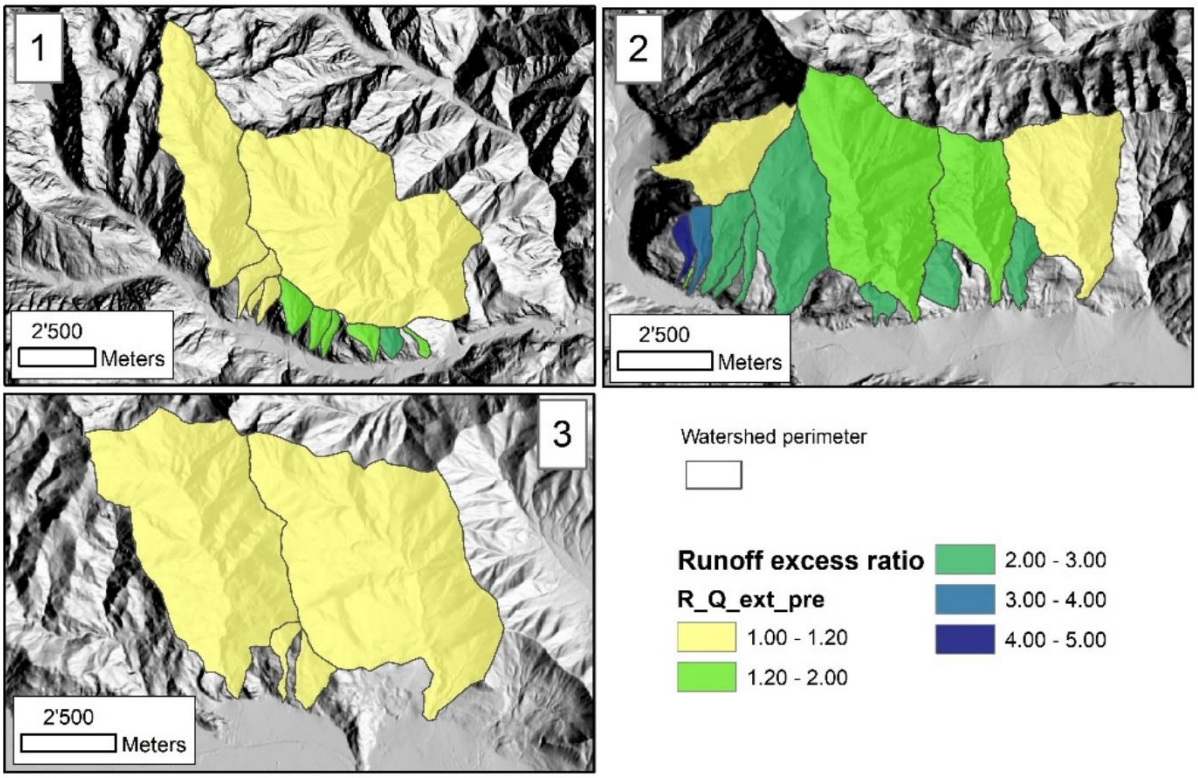


*Figure A5.25 – Runoff excess relative ratio, R_Q_ext_pre, between post-fire (extended assessment) and pre-fire situation for the watersheds affected by the Locana/Ribordone (1), Bussoleno/Mompantero (2) and Caprie/Rubiana (3) wildfires.*

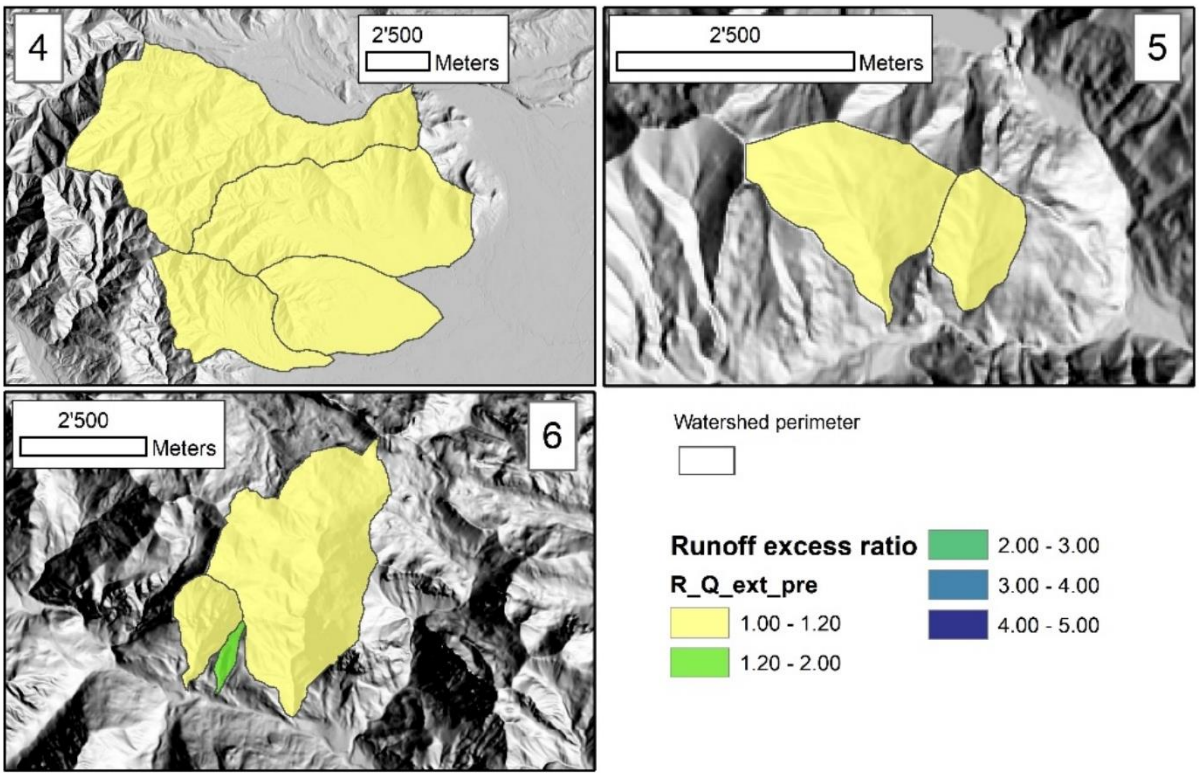


*Figure A5.26 – Runoff excess relative ratio, R_Q_ext_pre, between post-fire (extended assessment) and pre-fire situation for the watersheds affected by the Cumiana/Cantalupa (4), Bellino/Casteldelfino (5) and Sambuco/Pietraporzio (6) wildfires.*

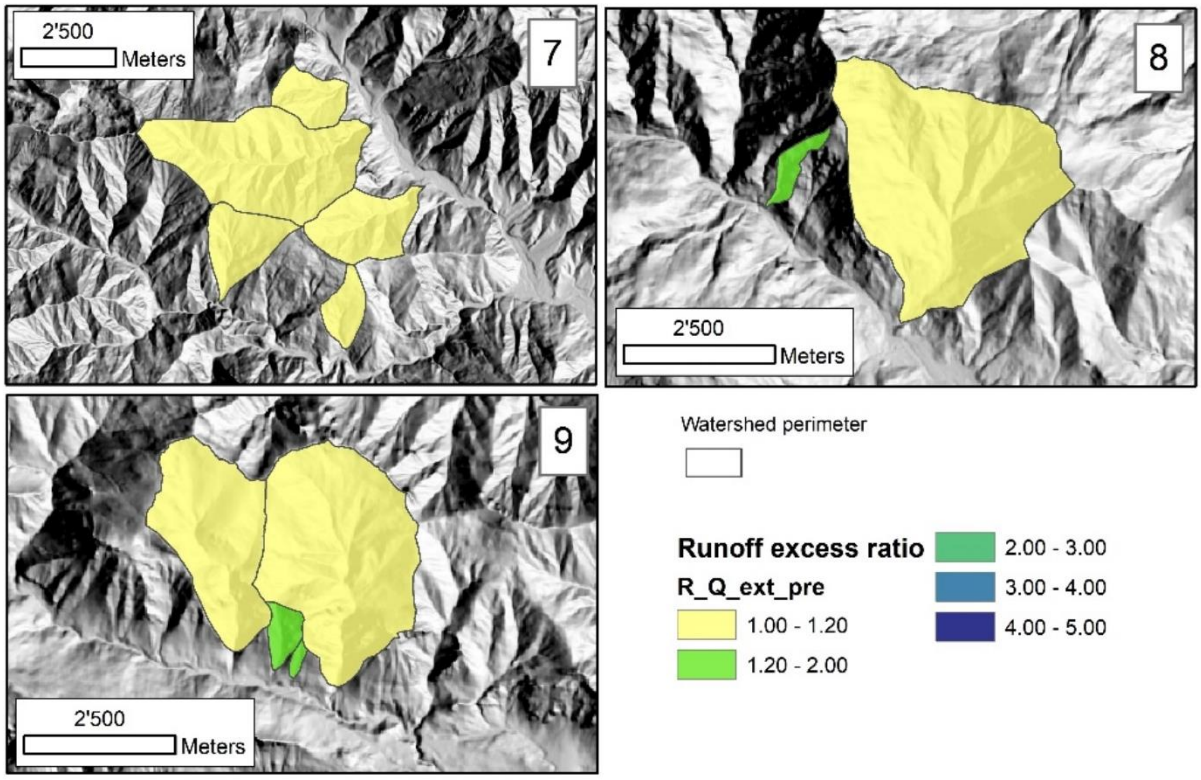


*Figure A5.27 – Runoff excess relative ratio, R_Q_ext_pre, between post-fire (extended assessment) and pre-fire situation for the watersheds affected by the Roure/Perrero (7), Traversella (8) and Demonte (9) wildfires.*

*Table A5.1 – Excess runoff depth and pre/post-fire relative ratios for the watersheds affected by the Locana/Ribordone wildfire.*

| **Fire n. 1** | **LOCANA/RIBORDONE** | | | | | |
|---|---|---|---|---|---|---|
| **Watershed** | **Q_w_pre** | **Q_w_ini** | **Q_w_ext** | **R_Q_ini_pre** | **R_Q_ext_pre** | **R_Q_ext_ini** |
| | **[mm]** | **[mm]** | **[mm]** | **[-]** | **[-]** | **[-]** |
| **Rio Fura** | 113.78 | 125.39 | 122.22 | 1.10 | 1.07 | 0.97 |
| **Rio Di Chioso Bosco** | 54.75 | 112.29 | 81.41 | 2.05 | 1.49 | 0.73 |
| **R. Montepiano** | 117.42 | 118.65 | 122.33 | 1.01 | 1.04 | 1.03 |
| **Carlevaria** | 53.66 | 120.51 | 75.50 | 2.25 | 1.41 | 0.63 |
| **Rio Di Bardonetto Inferiore** | 55.55 | 116.62 | 73.48 | 2.10 | 1.32 | 0.63 |
| **Ribordone** | 90.27 | 96.13 | 91.48 | 1.06 | 1.01 | 0.95 |
| **Eugio** | 96.64 | 100.50 | 98.94 | 1.04 | 1.02 | 0.98 |
| **Rio Bocchetta** | 54.59 | 127.67 | 96.43 | 2.34 | 1.77 | 0.76 |
| **Rio Di Calsazio** | 51.31 | 119.03 | 108.16 | 2.32 | 2.11 | 0.91 |
| **Locana Est** | 123.60 | 130.95 | 130.76 | 1.06 | 1.06 | 1.00 |
| **Apparè** | 51.12 | 104.09 | 95.49 | 2.04 | 1.87 | 0.92 |
| **Mean** | **78.43** | **115.62** | **99.65** | **1.67** | **1.38** | **0.86** |

*Table A5.2 - Excess runoff depth and pre/post-fire relative ratios for the watersheds affected by the Bussoleno/Mompantero wildfire.*

| Fire n. 2 | BUSSOLENO/MOMPANTERO | | | | | |
|---|---|---|---|---|---|---|
| **Watershed** | **Q_w_pre** | **Q_w_ini** | **Q_w_ext** | **R_Q_ini_pre** | **R_Q_ext_pre** | **R_Q_ext_ini** |
| | **[mm]** | **[mm]** | **[mm]** | **[-]** | **[-]** | **[-]** |
| **Crosiglione** | 20.88 | 23.51 | 22.87 | 1.13 | 1.09 | 0.97 |
| **Rio Della Ravoire** | 14.65 | 64.82 | 63.41 | 4.42 | 4.33 | 0.98 |
| **Fogasso** | 14.45 | 32.46 | 37.98 | 2.25 | 2.63 | 1.17 |
| **Rio Della Codrea** | 14.06 | 45.70 | 53.83 | 3.25 | 3.83 | 1.18 |
| **Trinitâ** | 15.04 | 40.52 | 41.39 | 2.69 | 2.75 | 1.02 |
| **Rio Prebech** | 26.22 | 30.81 | 28.11 | 1.17 | 1.07 | 0.91 |
| **Moletta** | 18.84 | 40.90 | 29.46 | 2.17 | 1.56 | 0.72 |
| **Rio Di Periere** | 20.27 | 42.75 | 47.42 | 2.11 | 2.34 | 1.11 |
| **Ravera** | 15.33 | 43.06 | 37.93 | 2.81 | 2.47 | 0.88 |
| **Comba Delle Foglie** | 20.90 | 57.63 | 52.54 | 2.76 | 2.51 | 0.91 |
| **Rocciamelone** | 23.73 | 41.14 | 32.08 | 1.73 | 1.35 | 0.78 |
| **Giandula** | 13.16 | 44.56 | 31.45 | 3.39 | 2.39 | 0.71 |
| **I Piani** | 12.20 | 33.12 | 33.29 | 2.72 | 2.73 | 1.01 |
| **San Giuseppe** | 29.09 | 57.90 | 53.64 | 1.99 | 1.84 | 0.93 |
| **Mean** | **18.49** | **42.78** | **40.39** | **2.47** | **2.35** | **0.95** |

*Table A5.3 - Excess runoff depth and pre/post-fire relative ratios for the watersheds affected by the Caprie/Rubiana wildfire.*

| Fire n. 3 | CAPRIE/RUBIANA | | | | | |
|---|---|---|---|---|---|---|
| **Watershed** | **Q_w_pre** | **Q_w_ini** | **Q_w_ext** | **R_Q_ini_pre** | **R_Q_ext_pre** | **R_Q_ext_ini** |
| | **[mm]** | **[mm]** | **[mm]** | **[-]** | **[-]** | **[-]** |
| **Messa** | 59.19 | 60.14 | 59.27 | 1.02 | 1.00 | 0.99 |
| **Sessi** | 36.80 | 38.00 | 37.53 | 1.03 | 1.02 | 0.99 |
| **Novaretto** | 28.93 | 43.41 | 30.78 | 1.50 | 1.06 | 0.71 |
| **Fra Barbe** | 32.11 | 40.77 | 34.97 | 1.27 | 1.09 | 0.86 |
| **Mean** | **39.26** | **45.58** | **40.64** | **1.21** | **1.04** | **0.89** |

*Table A5.4 - Excess runoff depth and pre/post-fire relative ratios for the watersheds affected by the Cumiana/Cantalupa wildfire.*

| Fire n. 4 | CUMIANA/CANTALUPA | | | | | |
|---|---|---|---|---|---|---|
| **Watershed** | **Q_w_pre** | **Q_w_ini** | **Q_w_ext** | **R_Q_ini_pre** | **R_Q_ext_pre** | **R_Q_ext_ini** |
| | **[mm]** | **[mm]** | **[mm]** | **[-]** | **[-]** | **[-]** |
| **1*Int. Dx. Sangone** | 37.17 | 37.55 | 37.41 | 1.01 | 1.01 | 1.00 |
| **T. Chisola** | 38.69 | 40.22 | 40.58 | 1.04 | 1.05 | 1.01 |
| **T. Noce** | 44.22 | 47.86 | 49.12 | 1.08 | 1.11 | 1.03 |
| **Chisola Pianura** | 51.15 | 52.95 | 57.40 | 1.04 | 1.12 | 1.08 |
| **Mean** | **42.81** | **44.65** | **46.13** | **1.04** | **1.07** | **1.03** |

*Table A5.5 - Excess runoff depth and pre/post-fire relative ratios for the watersheds affected by the Bellino/Casteldelfino wildfire.*

| Fire n. 5 | BELLINO/CASTELDELFINO | | | | | |
|---|---|---|---|---|---|---|
| **Watershed** | **Q_w_pre** | **Q_w_ini** | **Q_w_ext** | **R_Q_ini_pre** | **R_Q_ext_pre** | **R_Q_ext_ini** |
| | **[mm]** | **[mm]** | **[mm]** | **[-]** | **[-]** | **[-]** |
| **Cumbal Della Comu** | 6.35 | 31.40 | 7.57 | 4.94 | 1.19 | 0.24 |
| **T. Mas Del Bernard** | 5.71 | 16.80 | 6.44 | 2.94 | 1.13 | 0.38 |
| **Mean** | **6.03** | **24.10** | **7.01** | **3.94** | **1.16** | **0.31** |

*Table A5.6 - Excess runoff depth and pre/post-fire relative ratios for the watersheds affected by the Sambuco/Pietraporzio wildfire.*

| Fire n. 6 | SAMBUCO/PIETRAPORZIO | | | | | |
|---|---|---|---|---|---|---|
| **Watershed** | **Q_w_pre** | **Q_w_ini** | **Q_w_ext** | **R_Q_ini_pre** | **R_Q_ext_pre** | **R_Q_ext_ini** |
| | **[mm]** | **[mm]** | **[mm]** | **[-]** | **[-]** | **[-]** |
| **R. Bianco** | 26.81 | 27.33 | 26.87 | 1.02 | 1.00 | 0.98 |
| **Sn** | 12.36 | 16.55 | 22.55 | 1.34 | 1.82 | 1.36 |
| **Rio Di Castello Pietraporzio** | 19.04 | 19.51 | 19.48 | 1.02 | 1.02 | 1.00 |
| **Mean** | **19.40** | **21.13** | **22.97** | **1.13** | **1.28** | **1.11** |

*Table A5.7 - Excess runoff depth and pre/post-fire relative ratios for the watersheds affected by the Roure/Perrero wildfire.*

| Fire n. 7 | ROURE/PERRERO | | | | | |
|---|---|---|---|---|---|---|
| **Watershed** | **Q_w_pre** | **Q_w_ini** | **Q_w_ext** | **R_Q_ini_pre** | **R_Q_ext_pre** | **R_Q_ext_ini** |
| | **[mm]** | **[mm]** | **[mm]** | **[-]** | **[-]** | **[-]** |
| **V.Ne Di Borsetto** | 61.81 | 63.78 | 65.05 | 1.03 | 1.05 | 1.02 |
| **S. Martino Sud** | 26.48 | 26.74 | 27.92 | 1.01 | 1.05 | 1.04 |
| **Colet** | 54.20 | 54.26 | 54.25 | 1.00 | 1.00 | 1.00 |
| **Molotta** | 38.69 | 39.13 | 39.00 | 1.01 | 1.01 | 1.00 |
| **Gernier** | 56.20 | 60.16 | 62.59 | 1.07 | 1.11 | 1.04 |
| **Mean** | **47.48** | **48.81** | **49.76** | **1.02** | **1.04** | **1.02** |

*Table A5.8 - Excess runoff depth and pre/post-fire relative ratios for the watersheds affected by the Traversella wildfire.*

| Fire n. 8 | TRAVERSELLA | | | | | |
|---|---|---|---|---|---|---|
| **Watershed** | **Q_w_pre** | **Q_w_ini** | **Q_w_ext** | **R_Q_ini_pre** | **R_Q_ext_pre** | **R_Q_ext_ini** |
| | **[mm]** | **[mm]** | **[mm]** | **[-]** | **[-]** | **[-]** |
| **T. Bersella** | 59.48 | 81.67 | 64.90 | 1.37 | 1.09 | 0.79 |
| **Valle Chiara Primo** | 66.33 | 136.67 | 100.99 | 2.06 | 1.52 | 0.74 |
| **Mean** | **62.91** | **109.17** | **82.95** | **1.72** | **1.31** | **0.77** |

*Table A5.9 - Excess runoff depth and pre/post-fire relative ratios for the watersheds affected by the Demonte wildfire.*

| **Fire n. 9** | **DEMONTE** | | | | | |
|---|---|---|---|---|---|---|
| **Watershed** | **Q_w_pre** | **Q_w_ini** | **Q_w_ext** | **R_Q_ini_pre** | **R_Q_ext_pre** | **R_Q_ext_ini** |
| | **[mm]** | **[mm]** | **[mm]** | **[-]** | **[-]** | **[-]** |
| **V. Del Saut** | 30.26 | 33.95 | 31.77 | 1.12 | 1.05 | 0.94 |
| **Valle Di Monfreis** | 22.48 | 24.10 | 23.58 | 1.07 | 1.05 | 0.98 |
| **Sn 2** | 15.37 | 25.94 | 22.62 | 1.69 | 1.47 | 0.87 |
| **Rio Di Prafioret C.** | 19.33 | 36.18 | 29.29 | 1.87 | 1.52 | 0.81 |
| **Mean** | **21.86** | **30.04** | **26.82** | **1.44** | **1.27** | **0.90** |

# Appendix 6

Place: BUSSOLENO
Sample: **A00**

| **Sieve analysis** | | | | | | **Hydrometer analysis** | | | | |
|---|---|---|---|---|---|---|---|---|---|---|
| Sieve | Diameter | Mass | Fraction | Fraction % | Perc. Finer | | | | | |
| ASTM | D(mm) | P (g) | P/S | P/S*100 | % | Dispersing Agent Corr. | | Cd = | | **-2.5534** |
| | | | | | | Meniscus Corr. | | Cm = | | **0.5** |
| 3-in. | (75-mm) | | 0 | 0 | 100 | Temperature Corr. | | **Ct = 0,2207 T - 3,1141** | | |
| 2-in. | (50-mm) | | 0 | 0 | 100 | | | | | |
| 11/2-in. | (37.5-mm) | | 0 | 0 | 100 | | | | | |
| 1-in. | (25.0-mm) | 0.0 | 0 | 0 | 100 | Dry Sample fraction | | Csp | **40** | g |
| | (5.00-mm) | 160.0 | 0.12568735 | 12.5687353 | 87.4312647 | Sp. Weight < 0,074 | | Gs | **2.7** | g/cm3 |
| No. 10 | (2.00-mm) | 128.0 | 0.10054988 | 10.0549882 | 77.3762765 | SP. Weight water | | Gw | 1 | g/cm3 |
| No. 18 | (1.00-mm) | 108.0 | 0.08483896 | 8.48389631 | 68.8923802 | Cost.: Gs/(Gs-1) *100 / Csp | | = K | | **3.9705882** |
| No. 40 | (425-µm) | 242.0 | 0.19010212 | 19.0102121 | 49.8821681 | | | | | |
| No. 80 | (180-µm) | 387.0 | 0.30400628 | 30.4006284 | 19.4815397 | | | | | |
| No. 200 | (75-µm) | 157.0 | 0.12333071 | 12.3330715 | 7.14846819 | | | | | |
| | <75 µm | 91.0 | 0.07148468 | 7.14846819 | 0 | | | | | |
| Total mass S | (g) | 1273 | | | | | | | | |

| Day | Hour | Time | Temperature | Hydrometer read | Corrected read | Temperature correction | Grain diameter | Reduced read | % fraction | % sum |
|---|---|---|---|---|---|---|---|---|---|---|
| | | dt | T°C | R | R'=R+Cm | Ct | D (mm) | R"=R'+Cd+Ct | KR" | KR"X |
| | | 0.5 | 18.7 | 24.00 | 24.5 | 1.0 | 0.0604 | 23.0 | 91.16308 | 6.516764 |
| | | 1 | 18.7 | 19.00 | 19.5 | 1.0 | 0.0452 | 18.0 | 71.31014 | 5.097582 |
| | | 2 | 18.7 | 16.50 | 17.0 | 1.0 | 0.0329 | 15.5 | 61.38367 | 4.387992 |
| | | 4 | 18.7 | 15.00 | 15.5 | 1.0 | 0.0236 | 14.0 | 55.42778 | 3.962237 |
| | | 8 | 18.7 | 13.00 | 13.5 | 1.0 | 0.0170 | 12.0 | 47.48661 | 3.394565 |
| | | 15 | 18.7 | 11.00 | 11.5 | 1.0 | 0.0127 | 10.0 | 39.54543 | 2.826893 |
| | | 30 | 18.7 | 10.00 | 10.5 | 1.0 | 0.0090 | 9.0 | 35.57484 | 2.543056 |
| | | 62 | 18.7 | 9.00 | 9.5 | 1.0 | 0.0063 | 8.0 | 31.60425 | 2.25922 |
| | | 120 | 18.7 | 8.00 | 8.5 | 1.0 | 0.0046 | 7.0 | 27.63367 | 1.975384 |
| | | 240 | 19.8 | 6.80 | 7.3 | 1.3 | 0.0032 | 6.0 | 23.8329 | 1.703687 |
| | | 478 | 19.6 | 5.90 | 6.4 | 1.2 | 0.0023 | 5.1 | 20.08411 | 1.435706 |
| | | 1440 | 17.8 | 5.00 | 5.5 | 0.8 | 0.0014 | 3.8 | 14.93322 | 1.067497 |

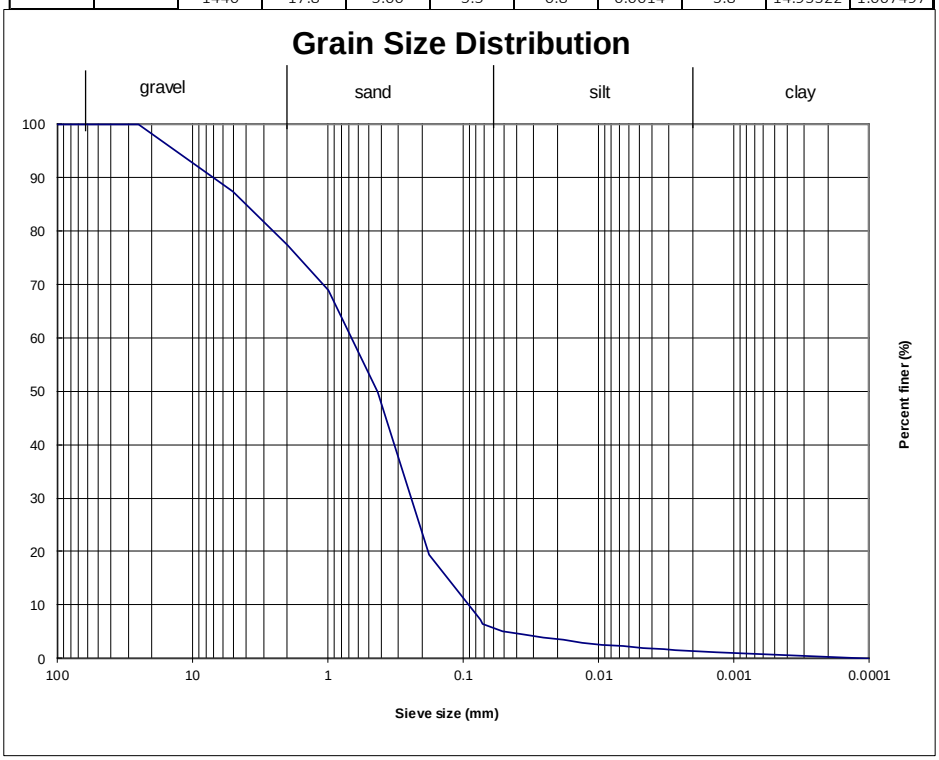


| Gravel | % | Sand | % | Silt | % | Clay | % |
|---|---|---|---|---|---|---|---|
| | 22.62372 | | 70.85951 | | 5.081057 | | 1.435706 |

| Dg | = | 1.686849 |
|---|---|---|

| K factor | = | 0.00459 |
|---|---|---|

*Dataset A6.1 – Grain size distribution and Erodibility Factor – Sample n. A00*

Place: BUSSOLENO
Sample: **A01**

| **Sieve analysis** | | | | | | **Hydrometer analysis** | | | | |
|---|---|---|---|---|---|---|---|---|---|---|
| Sieve | Diameter | Mass | Fraction | Fraction % | Perc. Finer | | | | Cilindro N. ... | nn |
| ASTM | D(mm) | P (g) | P/S | P/S*100 | % | Dispersing Agent Corr. | | Cd = | | -2.5534 |
| | | | | | | Meniscus Corr. | | Cm = | | 0.5 |
| 3-in. | (75-mm) | | 0 | 0 | 100 | Temperature Corr. | | **Ct = 0,2207 T - 3,1141** | | |
| 2-in. | (50-mm) | | 0 | 0 | 100 | | | | | |
| 11/2-in. | (37.5-mm) | | 0 | 0 | 100 | | | | | |
| 1-in. | (25.0-mm) | 0.0 | 0 | 0 | 100 | Dry Sample fraction | | Csp | 40 | g |
| | (5.00-mm) | 681.0 | 0.29028133 | 29.028133 | 70.971867 | Sp. Weight < 0,074 | | Gs | 2.7 | g/cm3 |
| No. 10 | (2.00-mm) | 386.0 | 0.16453538 | 16.4535379 | 54.5183291 | SP. Weight water | | Gw | 1 | g/cm3 |
| No. 18 | (1.00-mm) | 253.0 | 0.10784314 | 10.7843137 | 43.7340153 | Cost.: Gs/(Gs-1) *100 / Csp | | = K | | 3.97058824 |
| No. 40 | (425-µm) | 388.0 | 0.16538789 | 16.5387894 | 27.1952259 | | | | | |
| No. 80 | (180-µm) | 409.0 | 0.1743393 | 17.4339301 | 9.76129582 | | | | | |
| No. 200 | (75-µm) | 148 | 0.0630861 | 6.3086104 | 3.45268542 | | | | | |
| | <75 µm | 81.0 | 0.03452685 | 3.45268542 | 0 | | | | | |
| | | | | | | | | | | |
| Total mass S | (g) | 2346 | | | | | | | | |

| Day | Hour | Time | Temperature | Hydrometer read | Corrected read | Temperature correction | Grain diameter | Reduced read | % fraction | % sum |
|---|---|---|---|---|---|---|---|---|---|---|
| | | dt | T°C | R | R'=R+Cm | Ct | D (mm) | R"=R'+Cd+Ct | KR" | KR"X |
| | | 0.5 | 18.7 | 25.00 | 25.5 | 1.0 | 0.0596 | 24.0 | 95.13367 | 3.284666 |
| | | 1 | 18.7 | 21.00 | 21.5 | 1.0 | 0.0442 | 20.0 | 79.25131 | 2.736299 |
| | | 2 | 18.7 | 18.00 | 18.5 | 1.0 | 0.0323 | 17.0 | 67.33955 | 2.325023 |
| | | 4 | 18.7 | 16.00 | 16.5 | 1.0 | 0.0234 | 15.0 | 59.39837 | 2.050839 |
| | | 8 | 18.7 | 14.00 | 14.5 | 1.0 | 0.0169 | 13.0 | 51.4572 | 1.776655 |
| | | 15 | 18.7 | 13.00 | 13.5 | 1.0 | 0.0124 | 12.0 | 47.48661 | 1.639563 |
| | | 30 | 18.7 | 12.00 | 12.5 | 1.0 | 0.0089 | 11.0 | 43.51602 | 1.502471 |
| | | 55 | 18.7 | 10.80 | 11.3 | 1.0 | 0.0066 | 9.8 | 38.75131 | 1.337961 |
| | | 120 | 18.7 | 9.00 | 9.5 | 1.0 | 0.0046 | 8.0 | 31.60425 | 1.091195 |
| | | 240 | 19.4 | 6.60 | 7.1 | 1.2 | 0.0033 | 5.7 | 22.68826 | 0.783354 |
| | | 469 | 19.1 | 5.50 | 6 | 1.1 | 0.0024 | 4.5 | 18.05772 | 0.623476 |
| | | 1440 | 17.8 | 4.30 | 4.8 | 0.8 | 0.0014 | 3.1 | 12.15381 | 0.419633 |

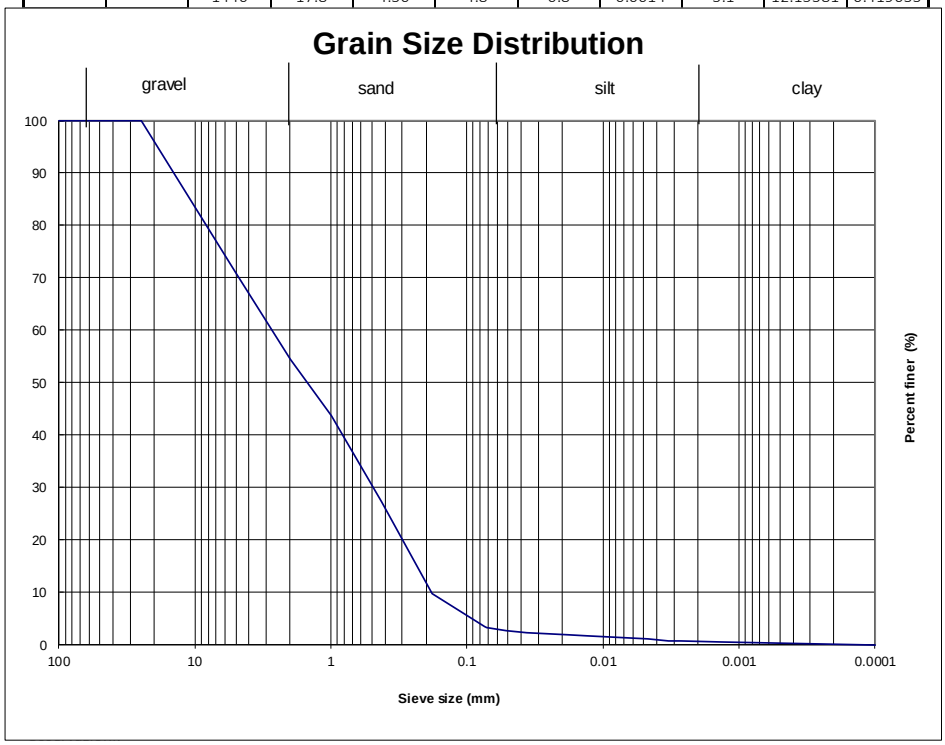


| Gravel % | Sand % | Silt % | Clay % |
|---|---|---|---|
| 45.48167 | 51.23366 | 2.66119 | 0.623476 |

| Dg = | 4.228178 | K factor = | 0.003628 |
|---|---|---|---|

*Dataset A6. 2 – Grain size distribution and Erodibility Factor – Sample n. A01*

Place: BUSSOLENO
Sample: **A02**

| **Sieve analysis** | | | | | | **Hydrometer analysis** | | | | |
|---|---|---|---|---|---|---|---|---|---|---|
| Sieve | Diameter | Mass | Fraction | Fraction % | Perc. Finer | | | | Cilindro N. ... | nn |
| ASTM | D(mm) | P (g) | P/S | P/S*100 | % | Dispersing Agent Corr. | | Cd = | | -2.5534 |
| | | | | | | Meniscus Corr. | | Cm = | | 0.5 |
| 3-in. | (75-mm) | | 0 | 0 | 100 | Temperature Corr. | | **Ct = 0,2207 T - 3,1141** | | |
| 2-in. | (50-mm) | | 0 | 0 | 100 | | | | | |
| 11/2-in. | (37.5-mm) | | 0 | 0 | 100 | | | | | |
| 1-in. | (25.0-mm) | 0.0 | 0 | 0 | 100 | Dry Sample fraction | | Csp | 40 | g |
| | (5.00-mm) | 180.0 | 0.097244733 | 9.72447326 | 90.27552674 | Sp. Weight < 0,074 | | Gs | 2.7 | g/cm3 |
| No. 10 | (2.00-mm) | 190.0 | 0.102647218 | 10.2647218 | 80.01080497 | SP. Weight water | | Gw | 1 | g/cm3 |
| No. 18 | (1.00-mm) | 198.0 | 0.106969206 | 10.6969206 | 69.31388439 | Cost.: Gs/(Gs-1) *100 / Csp = K | | | | 3.970588235 |
| No. 40 | (425-µm) | 292.0 | 0.157752566 | 15.7752566 | 53.53862777 | | | | | |
| No. 80 | (180-µm) | 478.0 | 0.25823879 | 25.823879 | 27.71474878 | | | | | |
| No. 200 | (75-µm) | 370 | 0.19989195 | 19.989195 | 7.725553755 | | | | | |
| | <75 µm | 143.0 | 0.077255538 | 7.72555375 | 0 | | | | | |
| | | | | | | | | | | |
| Total mass S (g) | | 1851 | | | | | | | | |

| Day | Hour | Time | Temperature | Hydrometer read | Corrected read | Temperature correction | Grain diameter | Reduced read | % fraction | % sum |
|---|---|---|---|---|---|---|---|---|---|---|
| | | dt | T°C | R | R'=R+Cm | Ct | D (mm) | R"=R'+Cd+Ct | KR" | KR"X |
| | | 0.5 | 18.4 | 24.00 | 24.50 | 0.9 | 0.0606 | 22.9 | 90.90019 | 7.022543 |
| | | 1 | 18.4 | 22.00 | 22.50 | 0.9 | 0.0439 | 20.9 | 82.95901 | 6.409043 |
| | | 2 | 18.4 | 19.00 | 19.50 | 0.9 | 0.0321 | 17.9 | 71.04724 | 5.488793 |
| | | 4 | 18.5 | 17.00 | 17.50 | 1.0 | 0.0232 | 15.9 | 63.1937 | 4.882063 |
| | | 8 | 18.5 | 14.40 | 14.90 | 1.0 | 0.0168 | 13.3 | 52.87017 | 4.084513 |
| | | 16 | 18.5 | 12.50 | 13.00 | 1.0 | 0.0121 | 11.4 | 45.32605 | 3.501688 |
| | | 30 | 18.8 | 10.30 | 10.80 | 1.0 | 0.0090 | 9.3 | 36.85365 | 2.847149 |
| | | 61 | 19.0 | 8.80 | 9.30 | 1.1 | 0.0064 | 7.8 | 31.07303 | 2.400564 |
| | | 131 | 19.1 | 7.50 | 8.00 | 1.1 | 0.0044 | 6.5 | 25.9989 | 2.008559 |
| | | 240 | 18.7 | 6.40 | 6.90 | 1.0 | 0.0033 | 5.4 | 21.28073 | 1.644054 |
| | | 440 | 18.6 | 5.50 | 6.00 | 1.0 | 0.0025 | 4.4 | 17.61956 | 1.361209 |
| | | 1440 | 19.0 | 4.00 | 4.50 | 1.1 | 0.0014 | 3.0 | 12.01421 | 0.928164 |

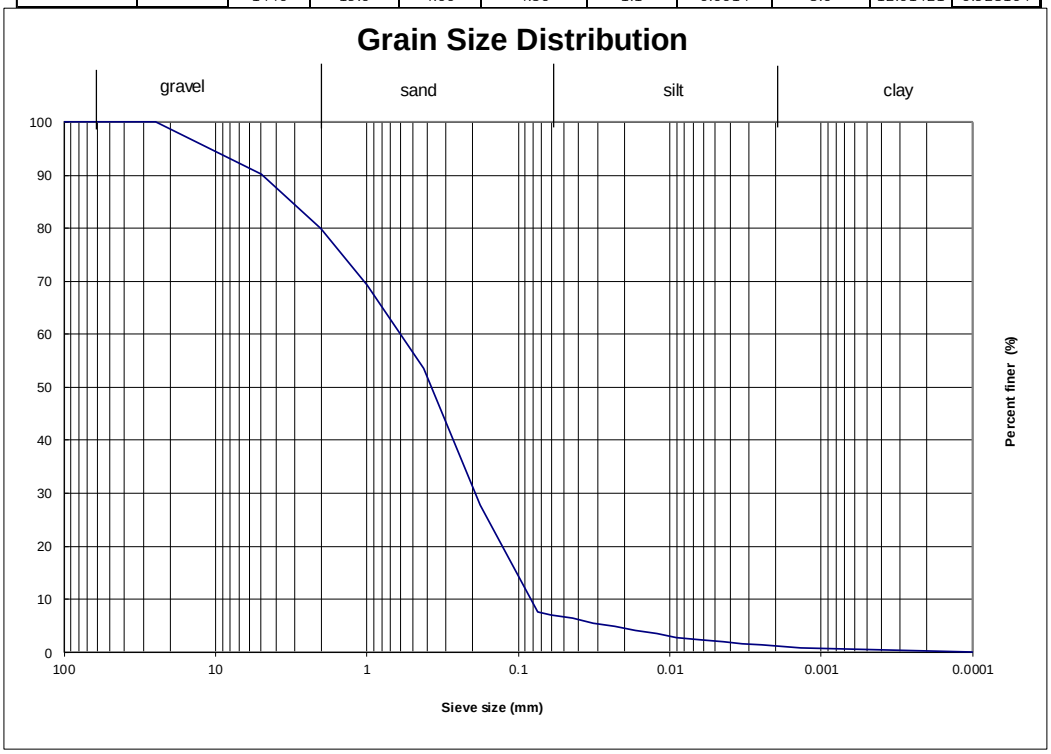


| Gravel | % | Sand | % | Silt | % | Clay | % |
|---|---|---|---|---|---|---|---|
| | 19.989195 | | 72.98826 | | 5.6613337 | | 1.361209 |

| Dg | = | 1.518882 | K factor | = | 0.0048081 |
|---|---|---|---|---|---|

*Dataset A6. 3 – Grain size distribution and Erodibility Factor – Sample n. A02*

Place: BUSSOLENO
Sample: **A03**

| Sieve analysis | | | | | | Hydrometer analysis | | | | |
|---|---|---|---|---|---|---|---|---|---|---|
| Sieve | Diameter | Mass | Fraction | Fraction % | Perc. Finer | | | | Cilindro N. ... | nn |
| ASTM | D(mm) | P (g) | P/S | P/S*100 | % | Dispersing Agent Corr. | | Cd = | | -2.5534 |
| | | | | | | Meniscus Corr. | | Cm = | | 0.5 |
| 3-in. | (75-mm) | | 0 | 0 | 100 | Temperature Corr. | | **Ct = 0,2207 T - 3,1141** | | |
| 2-in. | (50-mm) | | 0 | 0 | 100 | | | | | |
| 11/2-in. | (37.5-mm) | | 0 | 0 | 100 | | | | | |
| 1-in. | (25.0-mm) | 0.0 | 0 | 0 | 100 | Dry Sample fraction | | Csp | 40 | g |
| | (5.00-mm) | 35.0 | 0.02857143 | 2.85714286 | 97.1428571 | Sp. Weight < 0,074 | | Gs | 2.7 | g/cm3 |
| No. 10 | (2.00-mm) | 189.0 | 0.15428571 | 15.4285714 | 81.7142857 | SP. Weight water | | Gw | 1 | g/cm3 |
| No. 18 | (1.00-mm) | 136.0 | 0.11102041 | 11.1020408 | 70.6122449 | Cost.: Gs/(Gs-1) *100 / Csp | | = K | | 3.97058824 |
| No. 40 | (425-µm) | 144.0 | 0.11755102 | 11.755102 | 58.8571429 | | | | | |
| No. 80 | (180-µm) | 408.0 | 0.33306122 | 33.3061224 | 25.5510204 | | | | | |
| No. 200 | (75-µm) | 201.0 | 0.16408163 | 16.4081633 | 9.14285714 | | | | | |
| | <75 µm | 112.0 | 0.09142857 | 9.14285714 | 0 | | | | | |
| Total mass S | (g) | 1225 | | | | | | | | |

| Day | Hour | Time | Temperature | Hydrometer | Corrected | Temperature | Grain | Reduced | % fraction | % sum |
|---|---|---|---|---|---|---|---|---|---|---|
| | | | | read | read | correction | diameter | read | | |
| | | dt | T°C | R | R'=R+Cm | Ct | D (mm) | R"=R'+Cd+Ct | KR" | KR"X |
| | | 0.5 | 18.3 | 24.00 | 24.5 | 0.9 | 0.0607 | 22.9 | 90.81255 | 8.302862 |
| | | 1 | 18.3 | 13.00 | 13.5 | 0.9 | 0.0484 | 11.9 | 47.13608 | 4.309585 |
| | | 2 | 18.3 | 10.00 | 10.5 | 0.9 | 0.0352 | 8.9 | 35.22432 | 3.220509 |
| | | 4 | 18.3 | 8.00 | 8.5 | 0.9 | 0.0253 | 6.9 | 27.28314 | 2.494459 |
| | | 8 | 18.3 | 6.00 | 6.5 | 0.9 | 0.0182 | 4.9 | 19.34197 | 1.768408 |
| | | 15 | 18.3 | 5.00 | 5.5 | 0.9 | 0.0134 | 3.9 | 15.37138 | 1.405383 |
| | | 30 | 18.3 | 4.00 | 4.5 | 0.9 | 0.0096 | 2.9 | 11.40079 | 1.042358 |
| | | 60 | 18.3 | 3.30 | 3.8 | 0.9 | 0.0068 | 2.2 | 8.621378 | 0.78824 |
| | | 120 | 18.3 | 3.00 | 3.5 | 0.9 | 0.0048 | 1.9 | 7.430201 | 0.679333 |
| | | 240 | 19.6 | 2.60 | 3.1 | 1.2 | 0.0034 | 1.8 | 6.981168 | 0.638278 |
| | | 464 | 19.0 | 2.50 | 3 | 1.1 | 0.0024 | 1.5 | 6.058324 | 0.553904 |
| | | 1440 | 17.8 | 2.40 | 2.9 | 0.8 | 0.0014 | 1.2 | 4.609694 | 0.421458 |

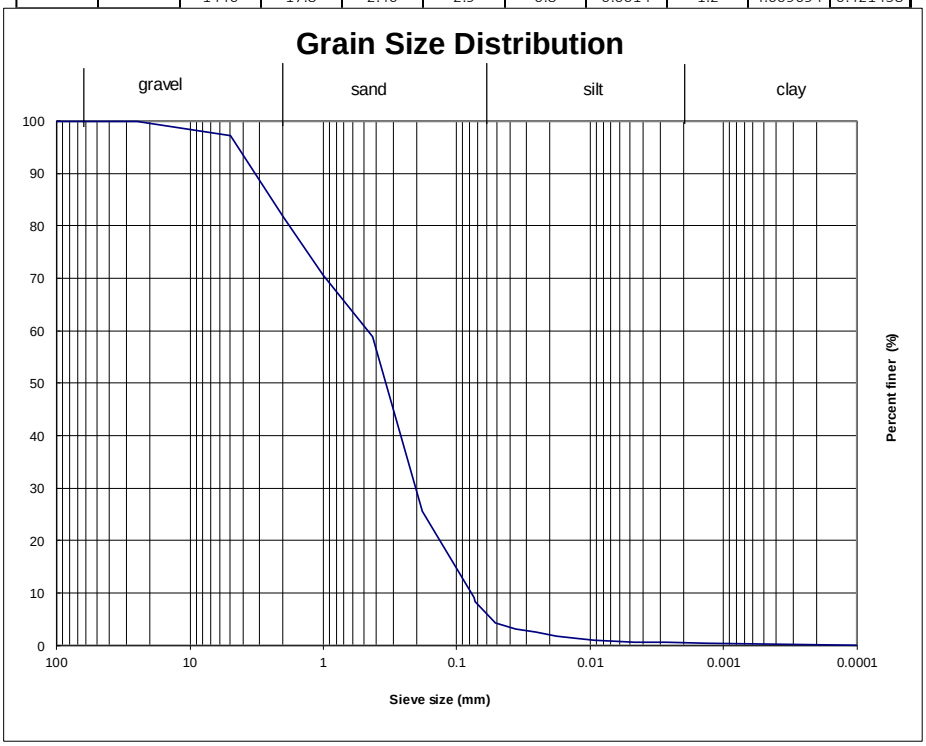


| Gravel | % | Sand | % | Silt | % | Clay | % |
|---|---|---|---|---|---|---|---|
| | 18.28571 | | 73.41142 | | 7.748958 | | 0.553904 |

| Dg | = | 1.408402 |
|---|---|---|

| K factor | = | 0.004986 |
|---|---|---|

*Dataset A6. 4 – Grain size distribution and Erodibility Factor – Sample n. A03*

Place: BUSSOLENO
Sample: **A04**

| **Sieve analysis** | | | | | | **Hydrometer analysis** | | | | |
|---|---|---|---|---|---|---|---|---|---|---|
| Sieve | Diameter | Mass | Fraction | Fraction % | Perc. Finer | | | | Cilindro N. ... | nn |
| ASTM | D(mm) | P (g) | P/S | P/S*100 | % | Dispersing Agent Corr. | | Cd = | | -2.5534 |
| | | | | | | Meniscus Corr. | | Cm = | | 0.5 |
| 3-in. | (75-mm) | | 0 | 0 | 100 | Temperature Corr. | | **Ct = 0,2207 T - 3,1141** | | |
| 2-in. | (50-mm) | | 0 | 0 | 100 | | | | | |
| 11/2-in. | (37.5-mm) | | 0 | 0 | 100 | | | | | |
| 1-in. | (25.0-mm) | 226.0 | 0.09920983 | 9.92098332 | 90.0790167 | Dry Sample fraction | | Csp | 40 | g |
| | (5.00-mm) | 820.0 | 0.35996488 | 35.9964881 | 54.0825285 | Sp. Weight < 0,074 | | Gs | 2.7 | g/cm3 |
| No. 10 | (2.00-mm) | 227.0 | 0.09964881 | 9.96488147 | 44.1176471 | SP. Weight water | | Gw | 1 | g/cm3 |
| No. 18 | (1.00-mm) | 149.0 | 0.06540825 | 6.54082529 | 37.5768218 | Cost.: Gs/(Gs-1) *100 / Csp | = | K | | 3.97058824 |
| No. 40 | (425-µm) | 278.0 | 0.12203687 | 12.2036874 | 25.3731343 | | | | | |
| No. 80 | (180-µm) | 298.0 | 0.13081651 | 13.0816506 | 12.2914838 | | | | | |
| No. 200 | (75-µm) | 178.0 | 0.07813872 | 7.81387182 | 4.47761194 | | | | | |
| | <75 µm | 102.0 | 0.04477612 | 4.47761194 | 0 | | | | | |
| Total mass S | (g) | 2278 | | | | | | | | |

| Day | Hour | Time | Temperature | Hydrometer read | Corrected read | Temperature correction | Grain diameter | Reduced read | % fraction | % sum |
|---|---|---|---|---|---|---|---|---|---|---|
| | | dt | T°C | R | R'=R+Cm | Ct | D (mm) | R"=R'+Cd+Ct | KR" | KR"X |
| | | 0.5 | 17.8 | 24.00 | 24.5 | 0.8 | 0.0610 | 22.8 | 90.3744 | 4.046615 |
| | | 1 | 17.8 | 19.00 | 19.5 | 0.8 | 0.0458 | 17.8 | 70.52146 | 3.157677 |
| | | 2 | 17.8 | 15.00 | 15.5 | 0.8 | 0.0337 | 13.8 | 54.63911 | 2.446527 |
| | | 4 | 17.8 | 12.00 | 12.5 | 0.8 | 0.0246 | 10.8 | 42.72734 | 1.913165 |
| | | 8 | 17.8 | 9.90 | 10.4 | 0.8 | 0.0177 | 8.7 | 34.38911 | 1.539811 |
| | | 15 | 17.8 | 8.60 | 9.1 | 0.8 | 0.0131 | 7.4 | 29.22734 | 1.308687 |
| | | 30 | 17.8 | 7.00 | 7.5 | 0.8 | 0.0094 | 5.8 | 22.8744 | 1.024227 |
| | | 60 | 18.0 | 5.50 | 6 | 0.9 | 0.0067 | 4.3 | 17.09378 | 0.765393 |
| | | 120 | 19.0 | 4.50 | 5 | 1.1 | 0.0047 | 3.5 | 13.9995 | 0.626843 |
| | | 240 | 19.9 | 3.60 | 4.1 | 1.3 | 0.0033 | 2.8 | 11.21465 | 0.502148 |
| | | 471 | 20.0 | 3.30 | 3.8 | 1.3 | 0.0024 | 2.5 | 10.1111 | 0.452736 |
| | | 1440 | 21.2 | 2.80 | 3.3 | 1.6 | 0.0013 | 2.3 | 9.177379 | 0.410927 |

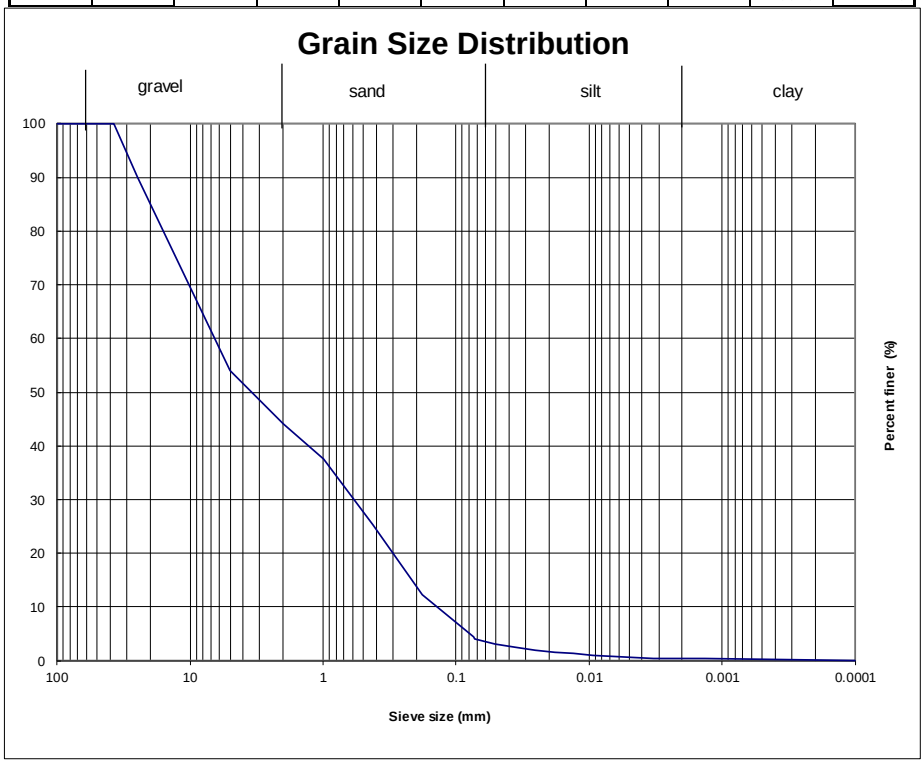


| Gravel | % | Sand | % | Silt | % | Clay | % |
|---|---|---|---|---|---|---|---|
| | 55.88235 | | 40.07103 | | 3.593879 | | 0.452736 |

| Dg | = | 5.899935 |
|---|---|---|

| K factor | = | 0.003516 |
|---|---|---|

*Dataset A6. 5 – Grain size distribution and Erodibility Factor – Sample n. A04*

Place: BUSSOLENO
Sample: **A05**

| **Sieve analysis** | | | | | | **Hydrometer analysis** | | | | |
|---|---|---|---|---|---|---|---|---|---|---|
| Sieve | Diameter | Mass | Fraction | Fraction % | Perc. Finer | | | | Cilindro N. ... | nn |
| ASTM | D(mm) | P (g) | P/S | P/S*100 | % | Dispersing Agent Corr. | | Cd = | | -2.5534 |
| | | | | | | Meniscus Corr. | | Cm = | | 0.5 |
| 3-in. | (75-mm) | | 0 | 0 | 100 | Temperature Corr. | | **Ct = 0,2207 T - 3,1141** | | |
| 2-in. | (50-mm) | | 0 | 0 | 100 | | | | | |
| 11/2-in. | (37.5-mm) | | 0 | 0 | 100 | | | | | |
| 1-in. | (25.0-mm) | 0.0 | 0 | 0 | 100 | Dry Sample fraction | | Csp | 40 | g |
| | (5.00-mm) | 136.0 | 0.11305071 | 11.3050707 | 88.6949293 | Sp. Weight < 0,074 | | Gs | 2.7 | g/cm3 |
| No. 10 | (2.00-mm) | 187.0 | 0.15544472 | 15.5444722 | 73.1504572 | SP. Weight water | | Gw | 1 | g/cm3 |
| No. 18 | (1.00-mm) | 198.0 | 0.16458853 | 16.4588529 | 56.6916043 | Cost.: Gs/(Gs-1) *100 / Csp | = | K | | 3.97058824 |
| No. 40 | (425-µm) | 218.0 | 0.18121363 | 18.1213633 | 38.5702411 | | | | | |
| No. 80 | (180-µm) | 284.0 | 0.23607648 | 23.6076475 | 14.9625935 | | | | | |
| No. 200 | (75-µm) | 106.0 | 0.08811305 | 8.81130507 | 6.15128845 | | | | | |
| | <75 µm | 74.0 | 0.06151288 | 6.15128845 | 0 | | | | | |
| Total mass S | (g) | 1203 | | | | | | | | |

| Day | Hour | Time | Temperature | Hydrometer read | Corrected read | Temperature correction | Grain diameter | Reduced read | % fraction | % sum |
|---|---|---|---|---|---|---|---|---|---|---|
| | | dt | T°C | R | R'=R+Cm | Ct | D (mm) | R"=R'+Cd+Ct | KR" | KR"X |
| | | 0.5 | 18.2 | 24.00 | 24.5 | 0.9 | 0.0607 | 22.8 | 90.72492 | 5.580752 |
| | | 1 | 18.2 | 19.00 | 19.5 | 0.9 | 0.0455 | 17.8 | 70.87198 | 4.35954 |
| | | 2 | 18.2 | 17.30 | 17.8 | 0.9 | 0.0328 | 16.1 | 64.12198 | 3.944328 |
| | | 4 | 18.2 | 15.00 | 15.5 | 0.9 | 0.0237 | 13.8 | 54.98963 | 3.382571 |
| | | 8 | 18.2 | 12.20 | 12.7 | 0.9 | 0.0173 | 11.0 | 43.87198 | 2.698692 |
| | | 15 | 18.2 | 10.80 | 11.3 | 0.9 | 0.0128 | 9.6 | 38.31316 | 2.356753 |
| | | 30 | 18.2 | 9.20 | 9.7 | 0.9 | 0.0092 | 8.0 | 31.96022 | 1.965965 |
| | | 60 | 19.0 | 8.30 | 8.8 | 1.1 | 0.0065 | 7.3 | 29.08774 | 1.789271 |
| | | 120 | 19.5 | 7.40 | 7.9 | 1.2 | 0.0046 | 6.5 | 25.95236 | 1.596405 |
| | | 300 | 20.1 | 5.80 | 6.3 | 1.3 | 0.0029 | 5.1 | 20.1252 | 1.237959 |
| | | 463 | 20.8 | 5.00 | 5.5 | 1.5 | 0.0023 | 4.4 | 17.56215 | 1.080299 |
| | | 1440 | 20.9 | 4.50 | 5 | 1.5 | 0.0013 | 3.9 | 15.66449 | 0.963568 |

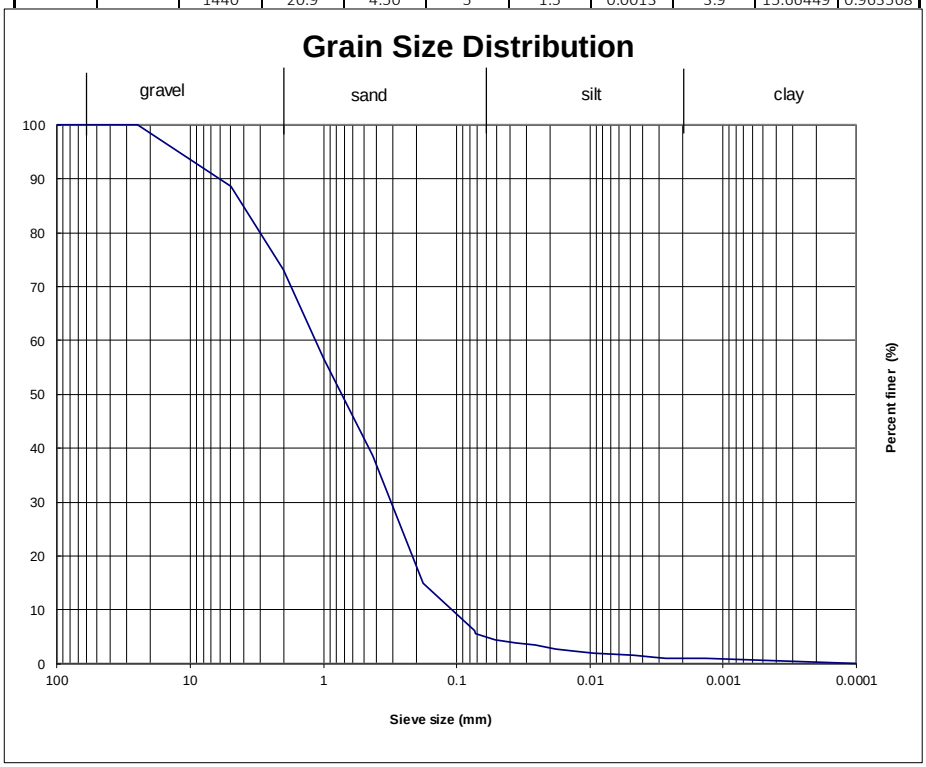


| Gravel % | Sand % | Silt % | Clay % |
|---|---|---|---|
| 26.84954 | 67.56971 | 4.500453 | 1.080299 |

| Dg = | 2.037147 |
|---|---|

| K factor = | 0.00427 |
|---|---|

*Dataset A6. 6 – Grain size distribution and Erodibility Factor – Sample n. A05*

Place: BUSSOLENO
Sample: **A07**

| **Sieve analysis** | | | | | | **Hydrometer analysis** | | | | |
|---|---|---|---|---|---|---|---|---|---|---|
| Sieve | Diameter | Mass | Fraction | Fraction % | Perc. Finer | | | | Cilindro N. ... | nn |
| ASTM | D(mm) | P (g) | P/S | P/S*100 | % | Dispersing Agent Corr. | | Cd = | | -2.5534 |
| | | | | | | Meniscus Corr. | | Cm = | | 0.5 |
| 3-in. | (75-mm) | | 0 | 0 | 100 | Temperature Corr. | | **Ct = 0,2207 T - 3,1141** | | |
| 2-in. | (50-mm) | | 0 | 0 | 100 | | | | | |
| 11/2-in. | (37.5-mm) | | 0 | 0 | 100 | | | | | |
| 1-in. | (25.0-mm) | 5.0 | 0.00413907 | 0.41390728 | 99.5860927 | Dry Sample fraction | | Csp | 40 | g |
| | (5.00-mm) | 142.0 | 0.11754967 | 11.7549669 | 87.8311258 | Sp. Weight < 0,074 | Gs | | 2.7 | g/cm3 |
| No. 10 | (2.00-mm) | 83.0 | 0.06870861 | 6.87086093 | 80.9602649 | SP. Weight water | Gw | | 1 | g/cm3 |
| No. 18 | (1.00-mm) | 68.0 | 0.05629139 | 5.62913907 | 75.3311258 | Cost.: Gs/(Gs-1) *100 / Csp | = | K | | 3.97058824 |
| No. 40 | (425-µm) | 195.0 | 0.16142384 | 16.1423841 | 59.1887417 | | | | | |
| No. 80 | (180-µm) | 438.0 | 0.36258278 | 36.2582781 | 22.9304636 | | | | | |
| No. 200 | (75-µm) | 167.0 | 0.13824503 | 13.8245033 | 9.10596026 | | | | | |
| | <75 µm | 110.0 | 0.0910596 | 9.10596026 | 0 | | | | | |
| Total mass S | (g) | 1208 | | | | | | | | |

| Day | Hour | Time | Temperature | Hydrometer read | Corrected read | Temperature correction | Grain diameter | Reduced read | % fraction | % sum |
|---|---|---|---|---|---|---|---|---|---|---|
| | | dt | T°C | R | R'=R+Cm | Ct | D (mm) | R"=R'+Cd+Ct | KR" | KR"X |
| | | 0.5 | 18.6 | 25.00 | 25.5 | 1.0 | 0.0597 | 23.9 | 95.04604 | 8.654854 |
| | | 1 | 18.6 | 21.00 | 21.5 | 1.0 | 0.0443 | 19.9 | 79.16368 | 7.208613 |
| | | 2 | 18.6 | 18.50 | 19 | 1.0 | 0.0322 | 17.4 | 69.23721 | 6.304713 |
| | | 4 | 18.6 | 14.60 | 15.1 | 1.0 | 0.0237 | 13.5 | 53.75192 | 4.894628 |
| | | 8 | 18.6 | 12.50 | 13 | 1.0 | 0.0171 | 11.4 | 45.41368 | 4.135352 |
| | | 15 | 18.6 | 10.50 | 11 | 1.0 | 0.0127 | 9.4 | 37.47251 | 3.412231 |
| | | 30 | 18.6 | 8.50 | 9 | 1.0 | 0.0092 | 7.4 | 29.53133 | 2.689111 |
| | | 60 | 18.6 | 7.30 | 7.8 | 1.0 | 0.0066 | 6.2 | 24.76662 | 2.255239 |
| | | 120 | 18.9 | 6.20 | 6.7 | 1.1 | 0.0047 | 5.2 | 20.66187 | 1.881462 |
| | | 240 | 18.7 | 5.00 | 5.5 | 1.0 | 0.0033 | 4.0 | 15.7219 | 1.43163 |
| | | 453 | 19.7 | 4.00 | 4.5 | 1.2 | 0.0024 | 3.2 | 12.62762 | 1.149866 |
| | | 1440 | 20.4 | 3.50 | 4 | 1.4 | 0.0014 | 2.8 | 11.25574 | 1.024944 |

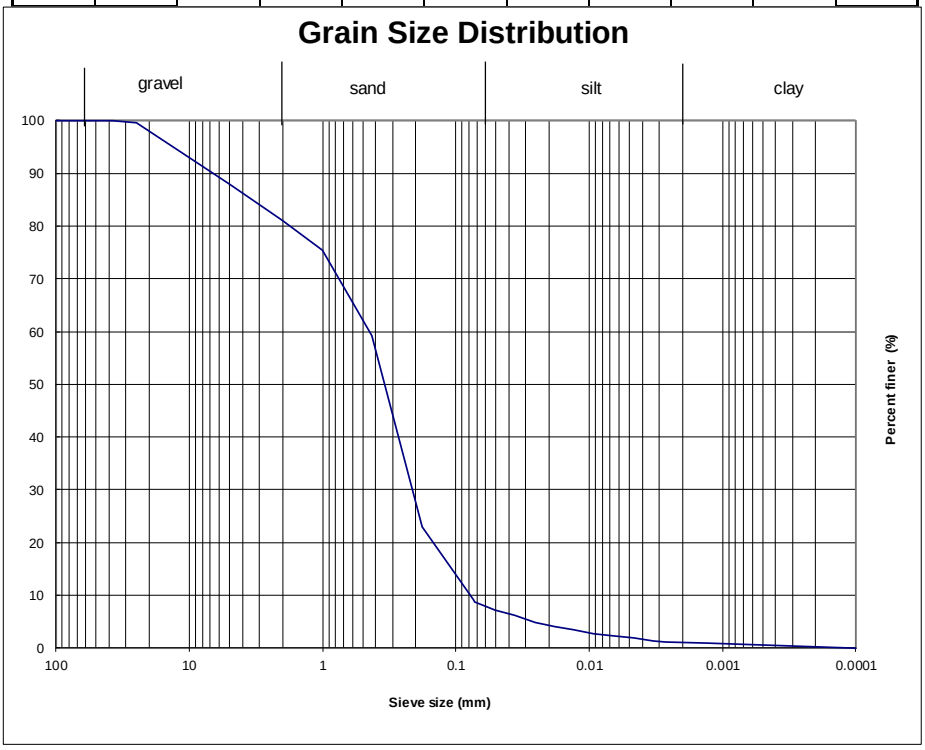


| Gravel % | Sand % | Silt % | Clay % |
|---|---|---|---|
| 19.03974 | 72.30541 | 7.504988 | 1.149866 |

| Dg = | 1.398807 |
|---|---|

| K factor = | 0.005002 |
|---|---|

*Dataset A6. 7 – Grain size distribution and Erodibility Factor – Sample n. A07*

Place: BUSSOLENO
Sample: **A08**

| **Sieve analysis** | | | | | | **Hydrometer analysis** | | | | |
|---|---|---|---|---|---|---|---|---|---|---|
| Sieve | Diameter | Mass | Fraction | Fraction % | Perc. Finer | | | | Cilindro N. ... | nn |
| ASTM | D(mm) | P (g) | P/S | P/S*100 | % | Dispersing Agent Corr. | | Cd = | | -2.5534 |
| | | | | | | Meniscus Corr. | | Cm = | | 0.5 |
| 3-in. | (75-mm) | | 0 | 0 | 100 | Temperature Corr. | | **Ct = 0,2207 T - 3,1141** | | |
| 2-in. | (50-mm) | | 0 | 0 | 100 | | | | | |
| 11/2-in. | (37.5-mm) | | 0 | 0 | 100 | | | | | |
| 1-in. | (25.0-mm) | 115.0 | 0.05695889 | 5.69588905 | 94.3041109 | Dry Sample fraction | | Csp | 40 | g |
| | (5.00-mm) | 623.0 | 0.3085686 | 30.8568598 | 63.4472511 | Sp. Weight < 0,074 | | Gs | 2.7 | g/cm3 |
| No. 10 | (2.00-mm) | 265.0 | 0.1312531 | 13.1253096 | 50.3219416 | SP. Weight water | | Gw | 1 | g/cm3 |
| No. 18 | (1.00-mm) | 135.0 | 0.06686478 | 6.68647845 | 43.6354631 | Cost.: Gs/(Gs-1) *100 / Csp | = | K | | 3.97058824 |
| No. 40 | (425-µm) | 220.0 | 0.10896483 | 10.8964834 | 32.7389797 | | | | | |
| No. 80 | (180-µm) | 381.0 | 0.18870728 | 18.8707281 | 13.8682516 | | | | | |
| No. 200 | (75-µm) | 181.0 | 0.08964834 | 8.96483408 | 4.90341753 | | | | | |
| | <75 µm | 99.0 | 0.04903418 | 4.90341753 | 0 | | | | | |
| Total mass S | (g) | 2019 | | | | | | | | |

| Day | Hour | Time | Temperature | Hydrometer read | Corrected read | Temperature correction | Grain diameter | Reduced read | % fraction | % sum |
|---|---|---|---|---|---|---|---|---|---|---|
| | | dt | T°C | R | R'=R+Cm | Ct | D (mm) | R"=R'+Cd+Ct | KR" | KR"X |
| | | 0.5 | 18.5 | 25.00 | 25.5 | 1.0 | 0.0598 | 23.9 | 94.9584 | 4.656207 |
| | | 1 | 18.5 | 20.50 | 21 | 1.0 | 0.0446 | 19.4 | 77.09076 | 3.780082 |
| | | 2 | 18.5 | 17.50 | 18 | 1.0 | 0.0326 | 16.4 | 65.17899 | 3.195998 |
| | | 4 | 18.5 | 15.50 | 16 | 1.0 | 0.0235 | 14.4 | 57.23782 | 2.806609 |
| | | 8 | 18.5 | 13.00 | 13.5 | 1.0 | 0.0171 | 11.9 | 47.31135 | 2.319873 |
| | | 15 | 18.5 | 11.50 | 12 | 1.0 | 0.0126 | 10.4 | 41.35546 | 2.027831 |
| | | 30 | 18.5 | 9.80 | 10.3 | 1.0 | 0.0091 | 8.7 | 34.60546 | 1.69685 |
| | | 60 | 18.5 | 8.00 | 8.5 | 1.0 | 0.0065 | 6.9 | 27.4584 | 1.3464 |
| | | 120 | 19.0 | 7.00 | 7.5 | 1.1 | 0.0046 | 6.0 | 23.92597 | 1.17319 |
| | | 240 | 19.3 | 6.00 | 6.5 | 1.1 | 0.0033 | 5.1 | 20.21828 | 0.991386 |
| | | 444 | 19.6 | 5.00 | 5.5 | 1.2 | 0.0024 | 4.2 | 16.51058 | 0.809583 |
| | | 1440 | 20.5 | 4.00 | 4.5 | 1.4 | 0.0013 | 3.4 | 13.32867 | 0.65356 |

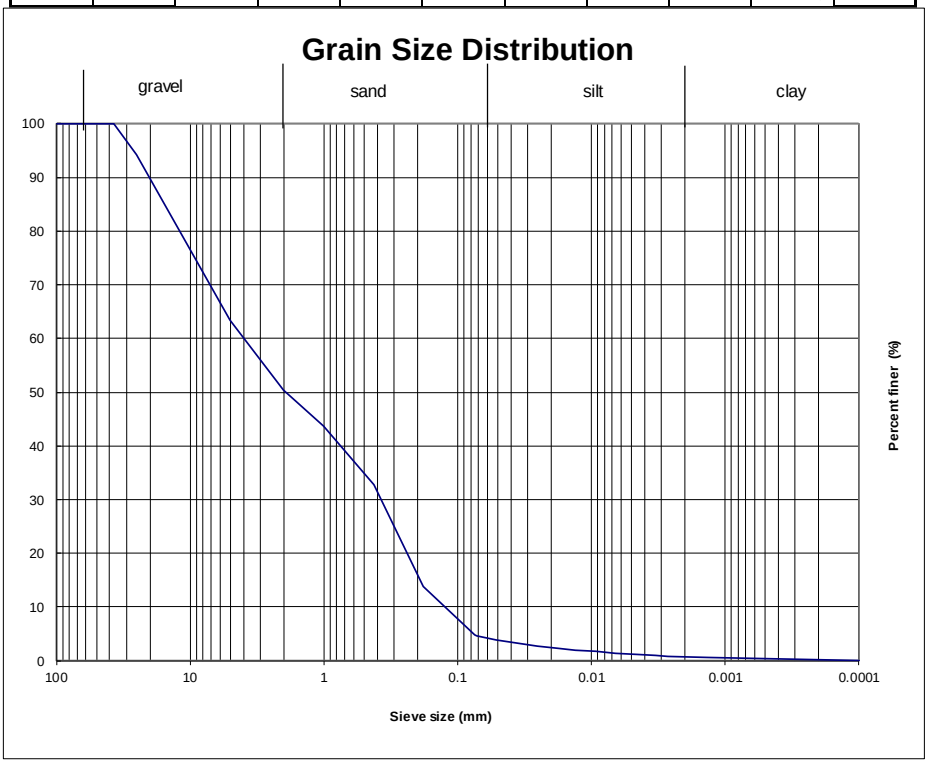


| Gravel % | Sand % | Silt % | Clay % |
|---|---|---|---|
| 49.67806 | 45.66573 | 3.846624 | 0.809583 |

| Dg = | 4.619491 |
|---|---|

| K factor = | 0.003592 |
|---|---|

*Dataset A6. 8 – Grain size distribution and Erodibility Factor – Sample n. A08*

Place: BUSSOLENO
Sample: **A09**

| **Sieve analysis** | | | | | | **Hydrometer analysis** | | | | |
|---|---|---|---|---|---|---|---|---|---|---|
| Sieve | Diameter | Mass | Fraction | Fraction % | Perc. Finer | | | | Cilindro N. ... | nn |
| ASTM | D(mm) | P (g) | P/S | P/S*100 | % | Dispersing Agent Corr. | | Cd = | | -2.5534 |
| | | | | | | Meniscus Corr. | | Cm = | | 0.5 |
| 3-in. | (75-mm) | | 0 | 0 | 100 | Temperature Corr. | | **Ct = 0,2207 T - 3,1141** | | |
| 2-in. | (50-mm) | | 0 | 0 | 100 | | | | | |
| 11/2-in. | (37.5-mm) | | 0 | 0 | 100 | | | | | |
| 1-in. | (25.0-mm) | 19.0 | 0.00900901 | 0.9009009 | 99.0990991 | Dry Sample fraction | | Csp | 40 | g |
| | (5.00-mm) | 615.0 | 0.2916074 | 29.1607397 | 69.9383594 | Sp. Weight < 0,074 | | Gs | 2.7 | g/cm3 |
| No. 10 | (2.00-mm) | 307.0 | 0.14556662 | 14.5566619 | 55.3816975 | SP. Weight water | | Gw | 1 | g/cm3 |
| No. 18 | (1.00-mm) | 150.0 | 0.07112376 | 7.11237553 | 48.269322 | Cost.: Gs/(Gs-1) *100 / Csp | = | K | | 3.97058824 |
| No. 40 | (425-µm) | 195.0 | 0.09246088 | 9.24608819 | 39.0232338 | | | | | |
| No. 80 | (180-µm) | 421.0 | 0.19962067 | 19.9620673 | 19.0611664 | | | | | |
| No. 200 | (75-µm) | 284.0 | 0.13466098 | 13.4660977 | 5.59506875 | | | | | |
| | <75 µm | 118.0 | 0.05595069 | 5.59506875 | 0 | | | | | |
| Total mass S | (g) | 2109 | | | | | | | | |

| Day | Hour | Time | Temperature | Hydrometer read | Corrected read | Temperature correction | Grain diameter | Reduced read | % fraction | % sum |
|---|---|---|---|---|---|---|---|---|---|---|
| | | dt | T°C | R | R'=R+Cm | Ct | D (mm) | R"=R'+Cd+Ct | KR" | KR"X |
| | | 0.5 | 18.7 | 24.00 | 24.5 | 1.0 | 0.0604 | 23.0 | 91.16308 | 5.100637 |
| | | 1 | 18.7 | 22.50 | 23 | 1.0 | 0.0435 | 21.5 | 85.2072 | 4.767401 |
| | | 2 | 18.7 | 20.00 | 20.5 | 1.0 | 0.0316 | 19.0 | 75.28073 | 4.212008 |
| | | 4 | 18.7 | 16.00 | 16.5 | 1.0 | 0.0234 | 15.0 | 59.39837 | 3.32338 |
| | | 8 | 18.7 | 12.50 | 13 | 1.0 | 0.0171 | 11.5 | 45.50131 | 2.54583 |
| | | 15 | 18.7 | 10.70 | 11.2 | 1.0 | 0.0127 | 9.7 | 38.35425 | 2.145947 |
| | | 30 | 18.7 | 8.50 | 9 | 1.0 | 0.0092 | 7.5 | 29.61896 | 1.657201 |
| | | 60 | 18.6 | 7.30 | 7.8 | 1.0 | 0.0066 | 6.2 | 24.76662 | 1.38571 |
| | | 120 | 19.2 | 6.30 | 6.8 | 1.1 | 0.0046 | 5.4 | 21.32182 | 1.192971 |
| | | 240 | 20.3 | 5.40 | 5.9 | 1.4 | 0.0033 | 4.7 | 18.71223 | 1.046962 |
| | | 460 | 19.6 | 4.90 | 5.4 | 1.2 | 0.0024 | 4.1 | 16.11352 | 0.901563 |
| | | 1440 | 19.8 | 3.90 | 4.4 | 1.3 | 0.0014 | 3.1 | 12.31819 | 0.689211 |

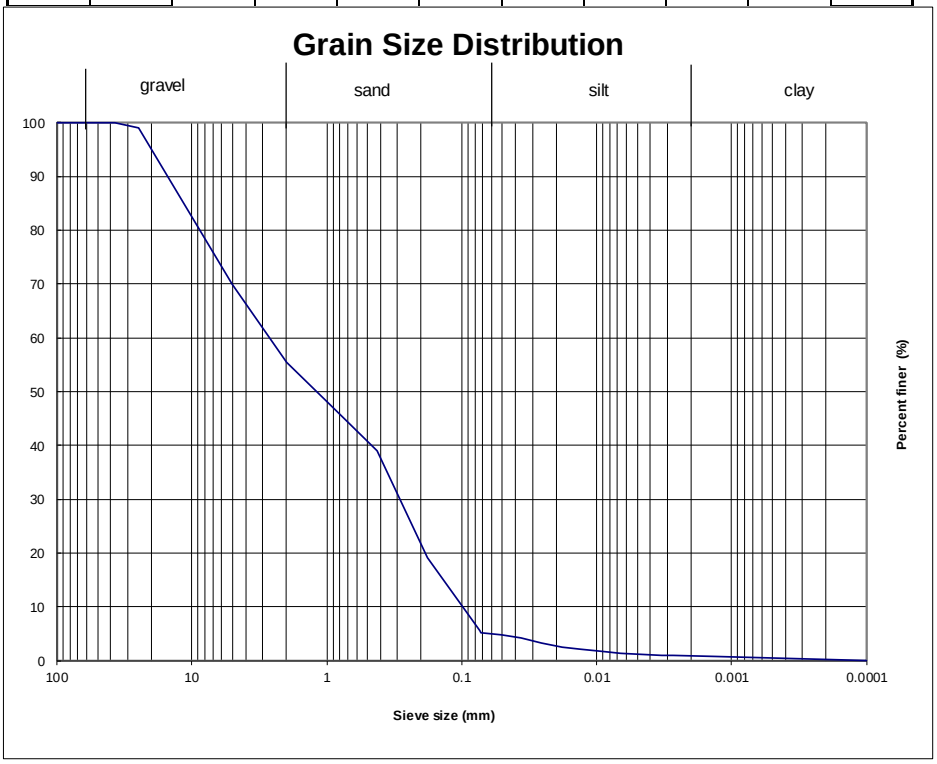


| Gravel | % | Sand | % | Silt | % | Clay | % |
|---|---|---|---|---|---|---|---|
| | 44.6183 | | 50.28106 | | 4.199074 | | 0.901563 |

| Dg | = | 3.816544 |
|---|---|---|

| K factor | = | 0.003679 |
|---|---|---|

*Dataset A6. 9 – Grain size distribution and Erodibility Factor – Sample n. A09*

Place: BUSSOLENO
Sample: **A10**

Temperature Corr. **Ct = 0,2207 T - 3,1141**

**Sieve analysis**

| Sieve | Diameter | Mass | Fraction | Fraction % | Perc. Finer |
|---|---|---|---|---|---|
| ASTM | D(mm) | P (g) | P/S | P/S*100 | % |
| | | | | | |
| 3-in. | (75-mm) | | 0 | 0 | 100 |
| 2-in. | (50-mm) | | 0 | 0 | 100 |
| 11/2-in. | (37.5-mm) | | 0 | 0 | 100 |
| 1-in. | (25.0-mm) | 217.0 | 0.06849747 | 6.84974747 | 93.1502525 |
| | (5.00-mm) | 1315.0 | 0.41508838 | 41.5088384 | 51.6414141 |
| No. 10 | (2.00-mm) | 352.0 | 0.11111111 | 11.1111111 | 40.530303 |
| No. 18 | (1.00-mm) | 221.0 | 0.0697601 | 6.9760101 | 33.5542929 |
| No. 40 | (425-µm) | 437.0 | 0.13794192 | 13.7941919 | 19.760101 |
| No. 80 | (180-µm) | 363.0 | 0.11458333 | 11.4583333 | 8.30176768 |
| No. 200 | (75-µm) | 183.0 | 0.05776515 | 5.77651515 | 2.52525253 |
| | <75 µm | 80.0 | 0.02525253 | 2.52525253 | 0 |
| | | | | | |
| Total mass S (g) | | 3168 | | | |

| | | | | |
|---|---|---|---|---|
| Dry Sample fraction | Csp | | Cilindro N. ... | nn |
| Sp. Weight < 0,074 | Gs | | | -2.5534 |
| SP. Weight water | Gw | | | 0.5 |
| Cost.: Gs/(Gs-1) *100 / Csp | = K | | | |
| | | | | |
| | | 40 | g | |
| | | 2.7 | g/cm3 | |
| | | 1 | g/cm3 | |
| Cost.: Gs/(Gs-1) *100 / Csp | = K | | | 3.97058824 |

| Day | Hour | Time | Temperature | Hydrometer read | Corrected read | Temperature correction | Grain diameter | Reduced read | % fraction | % sum |
|---|---|---|---|---|---|---|---|---|---|---|
| | | dt | T°C | R | R'=R+Cm | Ct | D (mm) | R"=R'+Cd+Ct | KR" | KR"X |
| | | 0.5 | 18.2 | 24.00 | 24.5 | 0.9 | 0.0607 | 22.8 | 90.72492 | 2.291033 |
| | | 1 | 18.2 | 22.00 | 22.5 | 0.9 | 0.0440 | 20.8 | 82.78375 | 2.090499 |
| | | 2 | 18.2 | 19.00 | 19.5 | 0.9 | 0.0322 | 17.8 | 70.87198 | 1.789697 |
| | | 4 | 18.2 | 16.00 | 16.5 | 0.9 | 0.0235 | 14.8 | 58.96022 | 1.488894 |
| | | 8 | 18.2 | 13.00 | 13.5 | 0.9 | 0.0171 | 11.8 | 47.04845 | 1.188092 |
| | | 15 | 18.6 | 11.00 | 11.5 | 1.0 | 0.0127 | 9.9 | 39.4578 | 0.996409 |
| | | 30 | 18.6 | 8.80 | 9.3 | 1.0 | 0.0092 | 7.7 | 30.72251 | 0.775821 |
| | | 64 | 19.0 | 7.50 | 8 | 1.1 | 0.0063 | 6.5 | 25.91126 | 0.654325 |
| | | 122 | 19.3 | 6.50 | 7 | 1.1 | 0.0046 | 5.6 | 22.20357 | 0.560696 |
| | | 240 | 19.7 | 5.60 | 6.1 | 1.2 | 0.0033 | 4.8 | 18.98056 | 0.479307 |
| | | 450 | 19.3 | 4.80 | 5.3 | 1.1 | 0.0024 | 3.9 | 15.45357 | 0.390242 |
| | | 1440 | 19.7 | 3.40 | 3.9 | 1.2 | 0.0014 | 2.6 | 10.24527 | 0.258719 |

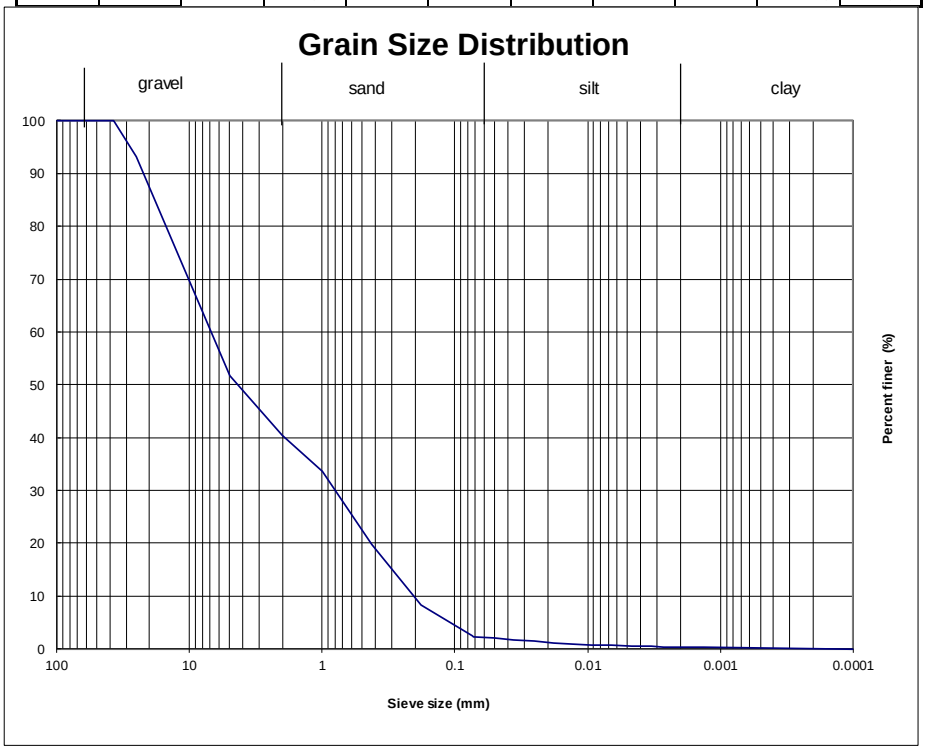


| Gravel | % | Sand | % | Silt | % | Clay | % |
|---|---|---|---|---|---|---|---|
| | 59.4697 | | 38.23927 | | 1.900792 | | 0.390242 |

| Dg | = | 7.104222 |
|---|---|---|

| K factor | = | 0.003478 |
|---|---|---|

*Dataset A6. 10 – Grain size distribution and Erodibility Factor – Sample n. A10*

Place: BUSSOLENO
Sample: **A11**

| **Sieve analysis** | | | | | | **Hydrometer analysis** | | | | |
|---|---|---|---|---|---|---|---|---|---|---|
| Sieve | Diameter | Mass | Fraction | Fraction % | Perc. Finer | | | | Cilindro N. ... | nn |
| ASTM | D(mm) | P (g) | P/S | P/S*100 | % | Dispersing Agent Corr. | | Cd = | | -2.5534 |
| | | | | | | Meniscus Corr. | | Cm = | | 0.5 |
| 3-in. | (75-mm) | | 0 | 0 | 100 | Temperature Corr. | | **Ct = 0,2207 T - 3,1141** | | |
| 2-in. | (50-mm) | | 0 | 0 | 100 | | | | | |
| 11/2-in. | (37.5-mm) | | 0 | 0 | 100 | | | | | |
| 1-in. | (25.0-mm) | 0.0 | 0 | 0 | 100 | Dry Sample fraction | | Csp | 40 | g |
| | (5.00-mm) | 180.0 | 0.098306936 | 9.83069361 | 90.16930639 | Sp. Weight < 0,074 | | Gs | 2.7 | g/cm3 |
| No. 10 | (2.00-mm) | 170.0 | 0.09284544 | 9.28454397 | 80.88476242 | SP. Weight water | | Gw | 1 | g/cm3 |
| No. 18 | (1.00-mm) | 178.0 | 0.097214637 | 9.72146368 | 71.16329874 | Cost.: Gs/(Gs-1) *100 / Csp | = | K | | 3.970588235 |
| No. 40 | (425-µm) | 312.0 | 0.170398689 | 17.0398689 | 54.12342982 | | | | | |
| No. 80 | (180-µm) | 478.0 | 0.26105953 | 26.105953 | 28.01747679 | | | | | |
| No. 200 | (75-µm) | 370 | 0.202075369 | 20.2075369 | 7.809939924 | | | | | |
| | <75 µm | 143.0 | 0.078099399 | 7.80993992 | 0 | | | | | |
| | | | | | | | | | | |
| Total mass S (g) | | 1831 | | | | | | | | |

| Day | Hour | Time | Temperature | Hydrometer | Corrected | Temperature | Grain | Reduced | % fraction | % sum |
|---|---|---|---|---|---|---|---|---|---|---|
| | | | | read | read | correction | diameter | read | | |
| | | dt | T°C | R | R'=R+Cm | Ct | D (mm) | R"=R'+Cd+Ct | KR" | KR"X |
| | | 0.5 | 18.4 | 24.00 | 24.50 | 0.9 | 0.0606 | 22.9 | 90.90019 | 7.09925 |
| | | 1 | 18.4 | 22.00 | 22.50 | 0.9 | 0.0439 | 20.9 | 82.95901 | 6.479049 |
| | | 2 | 18.4 | 19.00 | 19.50 | 0.9 | 0.0321 | 17.9 | 71.04724 | 5.548747 |
| | | 4 | 18.5 | 17.00 | 17.50 | 1.0 | 0.0232 | 15.9 | 63.1937 | 4.93539 |
| | | 8 | 18.5 | 14.40 | 14.90 | 1.0 | 0.0168 | 13.3 | 52.87017 | 4.129128 |
| | | 16 | 18.5 | 12.50 | 13.00 | 1.0 | 0.0121 | 11.4 | 45.32605 | 3.539937 |
| | | 30 | 18.8 | 10.30 | 10.80 | 1.0 | 0.0090 | 9.3 | 36.85365 | 2.878248 |
| | | 61 | 19.0 | 8.80 | 9.30 | 1.1 | 0.0064 | 7.8 | 31.07303 | 2.426785 |
| | | 131 | 19.1 | 7.50 | 8.00 | 1.1 | 0.0044 | 6.5 | 25.9989 | 2.030498 |
| | | 240 | 18.7 | 6.40 | 6.90 | 1.0 | 0.0033 | 5.4 | 21.28073 | 1.662012 |
| | | 440 | 18.6 | 5.50 | 6.00 | 1.0 | 0.0025 | 4.4 | 17.61956 | 1.376077 |
| | | 1440 | 19.0 | 4.00 | 4.50 | 1.1 | 0.0014 | 3.0 | 12.01421 | 0.938302 |

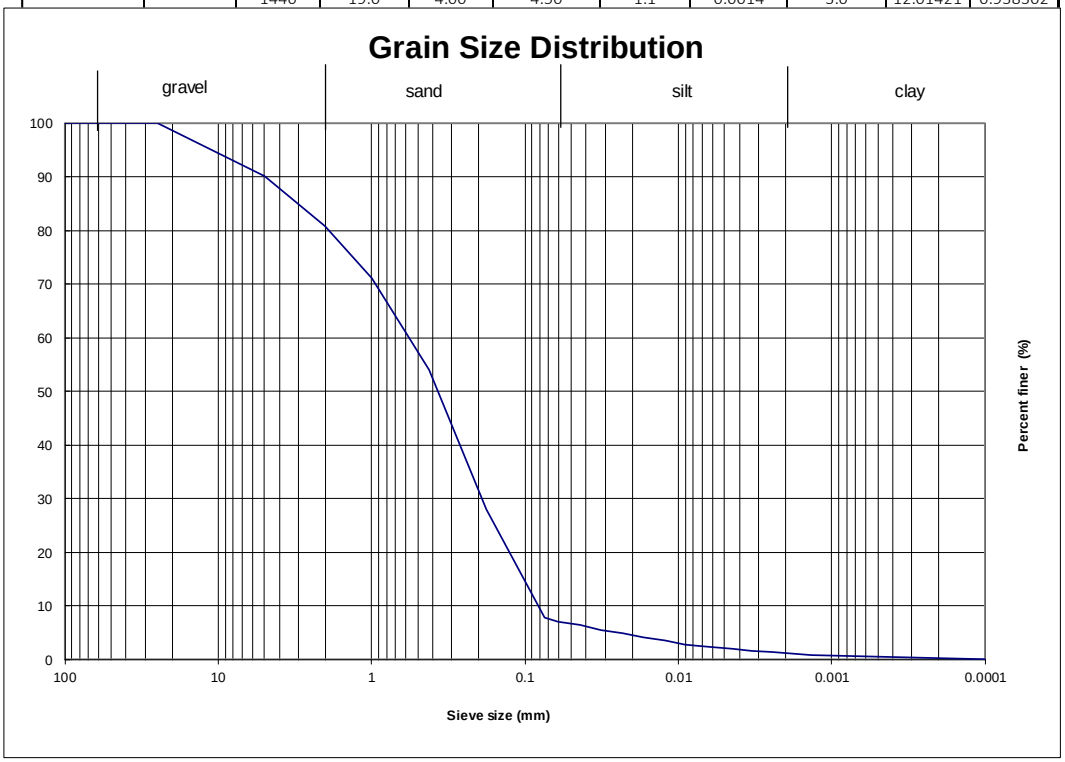


| Gravel | % | Sand | % | Silt | % | Clay | % |
|---|---|---|---|---|---|---|---|
| | 19.115238 | | 19.11524 | | 5.7231724 | | 1.376077 |

| Dg | = | 1.469659 |
|---|---|---|

| K factor | = | 0.0048833 |
|---|---|---|

*Dataset A6. 11 – Grain size distribution and Erodibility Factor – Sample n. A11*

# Acknowledgements

I would like to give special thanks to Prof. Giuseppe Mandrone for his guidance, support, patience and comprehension, as well as encouragement throughout this process.

I would also like to thank Prof. Mario Parise and Prof. Claudia Meisina, the members of my thesis committee, for their beneficial insight and comments towards the completion of this degree.

My deepest gratitude goes out to Prof. Matteo Garbarino, Prof. Raffaella Marzano and Dr. Donato Morresi for their support and insight in the field of forestry and fire dynamics.

I would also like to give acknowledgement to Dr. Daniele Drago for the involvement in the technical table and for the precious suggestions.

I would like to thank Arpa Piemonte and IPLA for sharing their data, as well as the Provincial Command of the Fire Brigade of Turin for accessing their aerial shots.

The field surveys and the days in the office would not have been nearly as enjoyable without the company and help of Jessica Chicco, thank you.

Thanks to my family for always being there, and for making me who I am today.

*"Try to learn something about everything and everything about something"*

*Thomas H. Huxley*